Five-dimensional Perspective on Higgs Physics and the $b \to s\gamma$ Transition in a Warped Extra Dimension

Dissertation
zur Erlangung des Grades "Doktor der Naturwissenschaften"
am Fachbereich Physik, Mathematik und Informatik
der Johannes Gutenberg-Universität
in Mainz

Raoul Christopher Malm

geb. in Mainz
Mainz, den 02.05.2016

Erster Berichterstatter: Prof. Dr. Matthias Neubert
Zweiter Berichterstatter: Prof. Dr. Marc Vanderhaeghen

Contents

Abstract

This thesis studies the Higgs-boson production and decay processes as well as the flavor-changing neutral current $b \to s\gamma$ in models with one warped extra dimension, where the gauge bosons and fermions propagate into the bulk and the Higgs sector is localized on or near the infra-red brane. These so-called Randall-Sundrum models present attractive scenarios beyond the Standard Model of particle physics that can address the disparity between the electroweak and the Planck scale. Furthermore, these models provide a natural explanation for the hierarchical pattern observed in the flavor sector and the smallness of flavor-changing neutral currents.

In order to search for hints of a warped extra dimension this work mainly focuses on loop-induced processes, which can receive significant contributions from the exchange of heavy Kaluza-Klein resonances in the loops. Working in the five-dimensional (5D) framework, the Feynman amplitudes of the Higgs-production process via gluon fusion $gg \to h$, the Higgs decay into two photons $h \to \gamma\gamma$ and the electromagnetic dipole transition $b \to s\gamma$ are expressed in terms of integrals over fermion and gauge-boson 5D propagators. Using 5D propagators avoids the notion of infinite sums over Kaluza-Klein states and allows to obtain analytically closed expressions valid to all orders in an expansion of $v^2/M_{\rm KK}^2$. The fermion 5D propagator is derived by retaining the full dependence of the Yukawa matrices and by regularizing the profile of the Higgs vacuum expectation value by a square box of width η and height $1/\eta$ with $\eta \ll v|Y_q|/M_{\rm KK}$.

It is shown that the amplitude of the fermion triangle diagram that contributes to $gg \to h$ and $h \to \gamma\gamma$ depends on the localization of the Higgs sector on or near the infra-red brane. This leads to a classification of different Randall-Sundrum models according to the parametric relation of the characteristic width of the Higgs-boson profile with respect to the two ratios $v|Y_q|/M_{\rm KK}$ and $v|Y_q|/\Lambda_{\rm TeV}$, where $\Lambda_{\rm TeV}$ is the ultra-violet cutoff near the infra-red brane. In the phenomenological part of this thesis corrections to the tree-level $c_W, c_Z, c_t, c_b, c_\tau$ and loop-induced effective $c_g^{\rm eff}, c_\gamma^{\rm eff}$ Higgs couplings are compared with fit results of experimental data from the Large Hadron Collider. Furthermore, modifications of the signal rates of the processes $pp \to h \to b\bar{b}$,$\tau^+\tau^-$,WW^*,ZZ^*,$\gamma\gamma$ are analyzed, which can exclude large fractions of the Randall-Sundrum parameter space.

Finally, the loop-induced electro- and chromomagnetic dipole coefficients $C_{7\gamma,8g}$ and their chirality-flipped counterparts $\tilde{C}_{7\gamma,8g}$ are investigated at one-loop order. The main corrections from virtual Kaluza-Klein modes arise from the scalar part of the W-boson penguin diagrams, which includes the contributions from the fifth component of the 5D gauge boson and from the charged Nambu-Goldstone bosons in the Higgs sector. For the phenomenological analysis the dipole coefficients are renormalization-group evolved to the B-meson scale while taking into account the mixing effects between the electro- and chromomagnetic dipole operators. The branching ratio for the inclusive decay $\bar{B} \to X_s\gamma$ and the time-dependent CP asymmetry in $\bar{B}_d^0 \to \bar{K}^{*0}\gamma$ are studied, showing that sizeable corrections can only occur for large values of the entries of the anarchic 5D Yukawa matrices.

Zusammenfassung

Die vorliegende Arbeit befasst sich mit den Produktions- und Zerfallsprozessen des Higgs-Bosons sowie dem Flavor-ändernden neutralen Strom $b \to s\gamma$ in Modellen mit einer gekrümmten Extradimension, in denen die Eichbosonen und Fermionen im Bulk propagieren, während der Higgs-Sektor auf oder nahe der infraroten Brane lokalisiert ist. Diese sogenannten Randall-Sundrum Modelle stellen vielversprechende Szenarien dar, die über die Physik des Standardmodells hinausgehen und den Größenunterschied zwischen der elektroschwachen und der Planck Skala erklären können. Weiterhin bieten diese Modelle eine natürliche Erklärung für das hierarchische Muster im Flavor-Sektor und für die Unterdrückung von Flavor-ändernden neutralen Strömen.

Der Schwerpunkt dieser Arbeit liegt auf der Suche nach Hinweisen für eine gekrümmte Extradimension mittels Schleifen-induzierter Prozesse, die signifikante Beiträge durch den Austausch von virtuellen Kaluza-Klein Resonanzen erhalten. In der fünfdimensionalen (5D) Analyse werden die Feynman-Amplituden der Higgs-Produktion über Gluonfusion $gg \to h$, des Higgs-Zerfalls in zwei Photonen $h \to \gamma\gamma$ und des elektromagnetischen Dipolübergangs $b \to s\gamma$ mit fermionischen und bosonischen 5D Propagatoren ausgedrückt. Die Verwendung von 5D Propagatoren vermeidet das Auftreten unendlicher Summen von Kaluza-Klein Zuständen und erlaubt es analytisch geschlossene Ausdrücke zu erhalten, die exakt in allen Ordnungen von $v^2/M_{\rm KK}^2$ sind. Der fermionische 5D Propagator wird hergeleitet, unter Beibehaltung der vollen Abhängigkeit der Yukawa-Matrizen und indem das Profil des Higgs-Vakuumerwartungswertes durch eine rechteckige Funktion der Breite η und Höhe $1/\eta$, mit $\eta \ll v|Y_q|/M_{\rm KK}$, regularisiert wird.

Es wird gezeigt, dass die Amplitude des fermionischen Dreiecksdiagramms, welches zu $gg \to h$ und $h \to \gamma\gamma$ beiträgt, von der Lokalisierung des Higgs-Sektors auf oder nahe der infraroten Brane abhängt. Dieses Ergebnis führt zu einer Klassifikation verschiedener Randall-Sundrum Modelle, die anhand der charakteristischen Breite des Higgs-Boson Profils in Bezug zu den beiden Verhältnissen $v|Y_q|/M_{\rm KK}$ und $v|Y_q|/\Lambda_{\rm TeV}$ unterschieden werden können. Hierbei wird der ultraviolette Cutoff nahe der infraroten Brane mit $\Lambda_{\rm TeV}$ bezeichnet. Im phänomenologischen Abschnitt dieser Arbeit werden Korrekturen zu den Higgs-Kopplungen auf Baumgraphen-Niveau $c_W, c_Z, c_t, c_b, c_\tau$ und auf Schleifen-Niveau $c_g^{\rm eff}, c_\gamma^{\rm eff}$ mit Fit-Resultaten von experimentellen Daten des Large Hadron Colliders verglichen. Weiterhin werden Modifizierungen der Signalraten für die Prozesse $pp \to h \to b\bar{b}, \tau^+\tau^-, WW^*, ZZ^*, \gamma\gamma$ analysiert, die es erlauben signifikante Bereiche des Parameterraumes im Randall-Sundrum Modell auszuschließen.

Zum Schluss werden die Schleifen-induzierten elektro- und chromomagnetischen Dipol-Koeffizienten $C_{7\gamma,8g}$ und die zugehörigen Koeffizienten mit umgedrehter Chiralität $\tilde{C}_{7\gamma,8g}$ auf Ein-Schleifen-Niveau untersucht. Es wird gezeigt, dass die wichtigsten Korrekturen der virtuellen Kaluza-Klein Moden von den skalaren W-Boson Pinguin-Diagrammen stammen, welche die Beiträge der fünften Komponente des 5D Eichbosons und der geladenen Nambu-Goldstone-Bosonen im Higgs-Sektor umfassen. Für die phänomenologische Analyse werden die Dipol-Koeffizienten mittels der Renormierungsgruppe zur B-Meson Skala, unter Berücksichtigung der Mischungseffekte zwischen den elektro- und chromomagnetischen Dipoloperatoren, laufen gelassen. Es werden das Verzweigungsverhältnis des inklusiven Zerfalls $\bar{B} \to X_s\gamma$ und die zeitabhängige CP-Asymmetrie in $\bar{B}_d^0 \to \bar{K}^{*0}\gamma$ studiert, mit dem Ergebnis, dass signifikante Korrekturen nur für große Einträge der anarchischen 5D Yukawa-Matrizen möglich sind.

Preface

The *Standard Model* (SM) of particle physics is a mathematical description of elementary particles and their interactions via the strong, weak and electromagnetic forces. So far, the SM has successfully passed all experimental tests performed at collider experiments up to the multiple TeV energy scale, which is currently probed by the *Large Hadron Collider* (LHC). The discovery of the Higgs boson, the last missing piece of the SM, at the LHC in July 2012 with a mass of roughly 125 GeV raises the question about the mechanism that stabilizes the Higgs mass near the electroweak scale. In principle, the scope of the SM can be extended up to the Planck mass[1] $M_{\rm Pl} = \sqrt{\hbar c/G} \approx 1.22 \times 10^{19}\,\mathrm{GeV}/c^2$ [1], where the gravitational force becomes so strong that it cannot be neglected in the description of elementary particles.[2] Since decades the disparity between the electroweak and the Planck scale has been used as a guideline to construct new-physics models beyond the SM. One of them is the so-called *Randall-Sundrum* (RS) model which supplements four-dimensional space-time with one warped extra dimension. Remarkably, this model does not only explain the separation of the electroweak and Planck scale but also provides a natural explanation for the hierarchical pattern of the quark masses and mixings, and the smallness of flavor-changing neutral currents. In order to find hints for the existence of a warped extra dimension one can search directly for heavy *Kaluza-Klein* (KK) resonances, which are massive copies of the SM particles with approximately equidistant mass gaps, predicted by RS models. Unfortunately, none of these particles have been observed yet, and electroweak precision measurements indicate that their masses could be too large for direct detection at the LHC. Therefore, we will consider indirect searches and comprehensively study the predictions of the RS models for the Higgs-boson production and decay processes as well as the flavor-changing neutral current $b \to s\gamma$. In particular, we will focus on loop-induced processes since they can be very sensitive on the exchange of heavy KK modes in the loops.

The first chapter introduces the fundamentals of this thesis. After briefly recapitulating the SM in the context of an effective field theory description we will motivate the search for new physics beyond the SM, and discuss in more detail the gauge-hierarchy problem and the flavor puzzle. Afterwards, we will present several new-physics ideas: supersymmetry, the pseudo Nambu-Goldstone Higgs and warped extra dimensions. In the latter case we will cover the basic ingredients of extra-dimensional models where the Higgs sector is localized on or near one of the boundaries of the fifth dimension. The chapter will end with a discussion of the Higgs-sector implementation where we will distinguish between the so-called *brane-localized* and *narrow bulk-Higgs* scenarios.

[1] Here, $\hbar$ denotes the reduced Planck constant, c is the speed of light in vacuum and G is the gravitational constant. For the remainder of this thesis we will use natural units and set $c = \hbar = 1$.

[2] While one can work with a perturbative quantum-gravity theory at low energies, where perturbations around non-dynamical (metric) backgrounds are assumed to be small, such an approach loses its validity for energies above the Planck mass $E \gtrsim M_{\rm Pl}$ because the effective graviton coupling grows like $g_G \sim E/M_{\rm Pl}$.

The subject of Chapter 2 is to present the phenomenological RS models our calculations and analyses in the subsequent chapters will be based on. At first, we will discuss the *minimal RS model* which is based on the SM gauge group and presents the simplest extension of the SM in the context of warped extra dimensions. Since this version is in tension with a tree-level analysis of the Peskin-Takeuchi parameters, we will also discuss the *custodial RS model* which is based on an enlarged gauge group in order to protect the T parameter from large corrections. We will then discuss the parameter space of the models under consideration and explain our procedure to generate RS points, which will be required for the phenomenological implications of our results in Chapters 4 and 5.

The loop-induced processes considered in this work will be calculated in the five-dimensional (5D) framework, where the corresponding Feynman amplitudes are expressed in terms of integrals over 5D propagators. The advantage of using 5D propagators is that sums over infinitely many KK resonances can be replaced by analytically closed expressions. Therefore, Chapter 3 is being dedicated to the derivation of solutions for the Higgs, gauge-boson and fermion 5D propagators in both the minimal and custodial RS models. The final results will be valid to all orders in an expansion of the new-physics scale. Especially extensive will be the calculation of the 5D fermion propagator where we keep the full dependence of the 5D Yukawa matrices, and which is sensitive on the details of the localization of the Higgs sector. The last section of this chapter analyzes the ultra-violet behavior of the 5D propagators.

The fourth chapter studies the Higgs-boson production and decay processes in the minimal and custodial RS models. In the first two sections we will study the loop-induced processes of Higgs production via two gluons ($gg \to h$) and the Higgs decay into two photons ($h \to \gamma\gamma$). The main conceptual result will be that the contribution of virtual KK-fermion modes depends on the concrete implementation of the Higgs sector. This leads to different results for the brane-localized and narrow bulk-Higgs scenarios, which cannot be smoothly connected to each other. Besides the loop-induced processes we will discuss the tree-level Higgs couplings to fermions and massive gauge bosons. In order to search for hints of a warped extra dimension we will compare the tree-level and loop-induced Higgs couplings with fit results obtained from current experimental data of the LHC and elucidate the potential of future measurements at high-luminosity proton and lepton colliders. Furthermore, we will analyze the signal rates for the processes $pp \to h \to b\bar{b}$,$\tau^+\tau^-$,WW^*,ZZ^*,$\gamma\gamma$ with the latest LHC data, which can significantly cut into the RS parameter space.

In the last chapter we will study the loop-induced $b \to s\gamma$ and $b \to sg$ transitions in the minimal RS model. We will derive integral expressions for the corresponding electro- and chromomagnetic (quark) dipole Wilson coefficients and discuss the origin of the main corrections. For the phenomenological analysis we will renormalization-group evolve the dipole Wilson coefficients from the new-physics scale down to the B-meson scale, where we will include the mixing between the electro- and chromomagnetic operators. We will then compare the RS predictions with experimental measurements of the branching ratio of the inclusive decay $\bar{B} \to X_s\gamma$ and the time-dependent CP asymmetry in $\bar{B}_d^0 \to \bar{K}^{*0}\gamma$.

1 Introduction

This chapter lays out the foundation for the subject of this thesis. After briefly recapitulating the Standard Model of particle physics in the first section, we will discuss the gauge-hierarchy problem and the flavor puzzle as motivations for new physics in Section 1.2. We will then review two popular extensions of the SM, namely supersymmetry and the pseudo Nambu-Goldstone Higgs in Section 1.3. Subsequently we will explain the Randall-Sundrum idea and introduce the basic concepts of models with one warped extra dimension. At the end of Section 1.4 we will discuss the implementation of the Higgs sector in warped extra-dimensional models which plays an important role for the remainder of this work.

Since this chapter serves as an introduction into the topic of my work, the concepts and ideas presented here are not my own but are based on the references given in the text below. The only exception is Section 1.4.5 where I present some of the results that I have derived in our publication [2].

1.1 The Standard Model as an effective field theory

As mentioned in the preface, the Standard Model (SM) should be considered as an *effective field theory*[1] (EFT), representing a low-energy description of a more fundamental *ultra-violet* (UV) theory. We denote the SM cutoff scale, i.e. the energy where non-SM particles and interactions emerge, as Λ with $\Lambda \lesssim M_{\rm Pl}$. The effective SM Lagrangian consists of an infinite series of local Lorentz and gauge-invariant operators of arbitrary mass dimension, where the corresponding Wilson coefficients are properly rescaled by powers of the cutoff Λ such that each term of the Lagrangian has mass dimension four. Phenomenological viability requires the following SM gauge group

$$\mathcal{G}_{\rm SM} = SU(3)_c \times SU(2)_L \times U(1)_Y \,, \tag{1.1}$$

where the associated gauge bosons form the force mediating particles of the strong and electroweak interactions. The matter content of the SM includes spin 0 and spin 1/2 particles, which are assigned quantum numbers under the SM gauge group. More details will be presented below. Here, it is sufficient to remark that the Higgs and the three Nambu-Goldstone bosons (NGBs) form a $SU(2)_L$ doublet Φ transforming as a $(1, \mathbf{2}, \frac{1}{2})$ under $\mathcal{G}_{\rm SM}$, such that the $SU(2)_L \times U(1)_Y$ gauge symmetry is a linearly realized symmetry in the scalar sector.[2] Then, before *electroweak symmetry breaking* (EWSB) in

[1] It is assumed that the reader is familiar with the concepts of effective (quantum) field theories and the renormalization-group evolution. A selection of readable introductions is given by [3–7].

[2] This assumption yields the simplest and most direct interpretation of the LEP, Tevatron and LHC data. Another (more general) alternative is the non-linearly realized $SU(2)_L \times U(1)_Y$ gauge symmetry with a light Higgs scalar, see e.g. [8].

the Higgs sector the effective SM Lagrangian can be expressed by

$$\mathcal{L}_{\text{eff}} = c_0\,\Lambda^4 + c_2\,\Lambda^2\Phi^\dagger\Phi + \sum_i c_4^{(i)} Q_4^{(i)} + \sum_i \frac{c_5^{(i)}}{\Lambda} Q_5^{(i)} + \sum_i \frac{c_6^{(i)}}{\Lambda^2} Q_6^{(i)} + \dots\,, \tag{1.2}$$

where c_0, c_2 and $c_{4,5,6}^{(i)}$ are dimensionless Wilson coefficients. The canonical mass dimension of the operators is indicated by their subscripts. Operators of mass dimension one and three violate the gauge symmetry and are therefore absent in (1.2). The contribution of a given operator $Q_n^{(i)}$ to a process with a typical energy scale $E \ll \Lambda$ can be estimated by $(E/\Lambda)^{n-4}$. Operators with mass dimensions greater than four yield cutoff-suppressed contributions and are called *irrelevant* operators. Dimension-four operators are termed *marginal* and the ones with mass dimensions lower than four are called *relevant* operators. The Higgs mass operator along with all marginal operators forms the renormalizable part of the effective SM Lagrangian, which will be referred to as the SM Lagrangian $\mathcal{L}_{\text{SM}}$.

The first term in (1.2) is sensitive to the fourth power of the cutoff scale and contributes to the energy density of the vacuum of space, which presents the simplest description of *dark energy*[3] in terms of a cosmological constant. Based on the standard model of cosmology[4] (the ΛCDM model) the observed dark energy contributes roughly 68.5% [12] of the total energy in the present-day observable universe which implies that $c_0 \sim (10^{-12}\text{GeV})^4/\Lambda^4$. If we assume $\Lambda \sim M_{\text{Pl}}$ the dimensional coefficient must take an extremely small value $c_0 \sim 10^{-120}$, which is referred to as the *cosmological constant problem*. However, since the cosmological constant is irrelevant to the physics of elementary particles in the SM we will not dwell on this problem here. Let us continue with the quadratic Higgs-mass term, which is the only relevant operator in the SM. In order to spontaneously break the $SU(2)_L \times U(1)_Y$ symmetry at the electroweak scale $M_{\text{EW}} \sim 100\,\text{GeV}$ the Higgs-mass coefficient has to take the value $c_2 \sim M_{\text{EW}}^2/\Lambda^2$. Again, if $\Lambda \sim M_{\text{Pl}}$ this leads to a large hierarchy and forms the *gauge-hierarchy problem*, which will be further discussed in Section 1.2.

The Wilson coefficients of the irrelevant operators in (1.2) contain the effects of the underlying UV theory when integrating out the additional degrees of freedom, i.e. heavy particles of the more fundamental theory. Interestingly, there exists only one five-dimensional operator consistent with the symmetries, the Weinberg operator[5] $c_5^{(ij)} \frac{1}{\Lambda} L_L^{iT} \epsilon \Phi C \Phi^T \epsilon L_L^j$ [13] and its hermitian conjugate, which after EWSB in the scalar sector gives rise to a Majorana mass term for the left-chiral neutrinos. At the level of dimension-six operators the first systematic classification can be found in [14]. Preserving baryon and lepton number, and barring the flavor structure, there are 59 independent dimension-six operators.[6] In Chapters 4 and 5 of this thesis, we will calculate the Wilson coefficients of some of those dimension-six operators after EWSB and for different extensions of the SM that incorporate one warped extra dimension. For instance, we will deal

[3] Dark energy is a hypothesis to explain the expansion of the universe at an accelerating rate [9, 10].

[4] This model is based upon a spatially-flat, expanding universe whose dynamics are governed by General Relativity and whose constituents are dominated by cold dark matter and a cosmological constant at late times. An introduction to cosmology can be found, e.g. in [11].

[5] Here, L_L^i denotes the lepton doublet of the i^{th} generation, C is the charge conjugation matrix and ϵ is the two-dimensional Levi-Civita symbol.

[6] In fact, when accounting for the flavor indices for three generations, there are 2499 hermitian operators and real parameters (1350 CP-even and 1149 CP-odd parameters) [15].

spin	field	$SU(3)_c$	$SU(2)_L$	$U(1)_Y$
1	G	**8**	**1**	0
	W	**1**	**3**	0
	B	**1**	**1**	0
1/2	$Q_L^i = \begin{pmatrix} u_L \\ d_L \end{pmatrix}, \begin{pmatrix} c_L \\ s_L \end{pmatrix}, \begin{pmatrix} t_L \\ b_L \end{pmatrix}$	**3**	**2**	1/6
	$L_L^i = \begin{pmatrix} \nu_{eL} \\ e_L \end{pmatrix}, \begin{pmatrix} \nu_{\mu L} \\ \mu_L \end{pmatrix}, \begin{pmatrix} \nu_{\tau L} \\ \tau_L \end{pmatrix}$	**1**	**2**	$-1/2$
	$u_R^i = u_R,\, c_R,\, t_R$	**3**	**1**	2/3
	$d_R^i = d_R,\, s_R,\, b_R$	**3**	**1**	$-1/3$
	$e_R^i = e_R,\, \mu_R,\, \tau_R$	**1**	**1**	-1
0	Φ	**1**	**2**	1/2

Table 1.1: Representations of the fields in the SM. Fermion $SU(2)_L$ doublets and singlets come in three generations with $i = 1, 2, 3$. The electromagnetic charge is given by $Q = T^3 + Y$, where T^3 denotes the third component of weak isospin and Y is the weak hypercharge.

with the effective operators[7] $hG^a_{\mu\nu}G^{a,\mu\nu}$, $hF_{\mu\nu}F^{\mu\nu}$ and $\bar{s}_L\sigma_{\mu\nu}F^{\mu\nu}b_R$ that contribute to Higgs production via gluon fusion $gg \to h$, to the Higgs decay into two photons $h \to \gamma\gamma$, and to the neutral flavor-changing $b \to s\gamma$ transition. This will allow us to search for indirect hints of new physics effects in existing measurements of collider experiments, and to probe the parameter space of the warped extra-dimensional models.

The renormalizable part of the effective SM Lagrangian

The historic development of the SM started in the 1960s with the unification of the electromagnetic and weak interactions by Glashow, Weinberg and Salam [16–18], culminating in the Glashow-Weinberg-Salam (GWS) theory. Later, the renormalizability of the (spontaneously broken) theory was proven by 't Hooft and Veltman [19], which was back in that time a necessary condition any realistic theory had to fulfill. In 1964 the quark model was proposed independently by Gell-Mann [20] and Zweig [21]. Gross, Wilczek and Politzer discovered that non-abelian gauge theories have the remarkable property of asymptotic freedom [22–25]. Some of the important experimental results were the discovery of the W and Z vector-bosons [26], the τ lepton [27], the bottom [28] and top quarks [29], and recently the Higgs boson [30, 31]. More historic details about the making of the SM are contained in the readable summary [32].

In the following we will briefly recapitulate the structure of the SM Lagrangian, see e.g. [4, 5] for comprehensive descriptions. As already mentioned, experimental evidence led to the SM gauge group $SU(3)_c \times SU(2)_L \times U(1)_Y$. The associated gauge bosons are the gluons $G^{1,\dots,8}$, the mediators of the strong $SU(3)_c$ interactions, and the $W^{1,2,3}$ and B bosons which are the mediators of the electroweak $SU(2)_L \times U(1)_Y$ interactions. Table 1.1 summarizes the representations of the fields in the SM including fermions (spin-1/2 particles) and bosons (spin-0 Higgs field and spin-1 gauge bosons). The SM is a chiral theory, i.e. left- and right-chiral components of a Dirac spinor that can be

[7] They originate from the dimension-six operators $\Phi^\dagger\Phi G^a_{\mu\nu}G^{a,\mu\nu}$, $\Phi^\dagger\Phi F_{\mu\nu}F^{\mu\nu}$ and $\bar{Q}^2_L\Phi\sigma_{\mu\nu}F^{\mu\nu}b_R$ after applying EWSB in the scalar sector, and are therefore suppressed by two powers of Λ. Here, $G_{\mu\nu}$ and $F_{\mu\nu}$ denote the chromo- and electromagnetic field strength tensors, and Q^2_L is the quark $SU(2)_L$ doublet of the 2$^{\text{nd}}$ generation.

distinguished by the projection operator $P_{L,R} = (1 \mp \gamma_5)/2$ transform differently under the SM gauge group $\mathcal{G}_{\rm SM}$. Left-chiral fermions transform as $SU(2)_L$ doublets Q_L^i, L_L^i while right-chiral fermions are $SU(2)_L$ singlets u_R^i, d_R^i, e_R^i, with generation (family) index $i = 1, 2, 3$. Right-chiral neutrinos are not included in the original formulation of the SM, since they would transform as singlets under the entire SM gauge group.[8] Based on the SM field content the Lagrangian can be constructed from local operators which respect the Lorentz and gauge symmetry including the principle of renormalizability. It is convenient to decompose the SM Lagrangian into the form

$$\mathcal{L}_{\rm SM} = \mathcal{L}_{\rm Ferm} + \mathcal{L}_{\rm Gauge} + \mathcal{L}_{\rm Higgs} + \mathcal{L}_{\rm Yuk} + \mathcal{L}_{\rm GF} + \mathcal{L}_{\rm FPG}\,. \tag{1.3}$$

The first term contains the kinetic terms for the fermions and reads

$$\mathcal{L}_{\rm Ferm} = \bar{Q}_L^i i\not{D} Q_L^i + \bar{u}_R^i i\not{D} u_R^i + \bar{d}_R^i i\not{D} d_R^i + \bar{L}_L i\not{D} L_L^i + \bar{e}_R^i i\not{D} e_R^i\,, \tag{1.4}$$

where $\not{D} \equiv \gamma^\mu D_\mu$. In order to obtain gauge invariant operators we introduced the covariant derivative $D_\mu = \partial_\mu - i g_s\, G_\mu^a\, \frac{t^a}{2} - i g\, W_\mu^i\, \frac{\sigma^i}{2} - i g'\, B_\mu\, Y$ where g_s, g and g' are the gauge couplings of $SU(3)_c$, $SU(2)_L$ and $U(1)_Y$. The corresponding generators are given by the Gell-Mann matrices t^a $(a = 1, 2, ..., 8)$, the Pauli matrices σ^i $(i = 1, 2, 3)$ and the hypercharge Y. Next, we consider the kinetic terms for the gauge bosons

$$\mathcal{L}_{\rm Gauge} = -\frac{1}{4} G_{\mu\nu}^a G^{a,\mu\nu} - \frac{1}{4} W_{\mu\nu}^i W^{i,\mu\nu} - \frac{1}{4} B_{\mu\nu} B^{\mu\nu}\,, \tag{1.5}$$

with the field strength tensors $G_{\mu\nu}^a \equiv \partial_\mu G_\nu^a - \partial_\nu G_\mu^a + g_s\, f^{abc} G_\mu^b G_\nu^c$, $W_{\mu\nu}^i \equiv \partial_\mu W_\nu^i - \partial_\nu W_\mu^i + g\, \epsilon^{ijk}\, W_\mu^j\, W_\nu^k$ and $B_{\mu\nu} \equiv \partial_\mu B_\nu - \partial_\nu B_\mu$. The tensors f^{abc} and ϵ^{ijk} are the structure constants of the non-abelian $SU(3)_c$ and $SU(2)_L$ groups. For a proper quantization of the gauge fields two further Lagrangians $\mathcal{L}_{\rm GF}$ and $\mathcal{L}_{\rm FPG}$ are required, which include gauge-fixing terms and Faddeev-Popov ghosts, but which are not relevant for further discussion in this section. Up to this stage, all fermions and gauge bosons are massless. Explicit mass terms are forbidden by the chiral structure of the SM and the requirement of gauge invariance. In order to obtain massive fermions and gauge bosons the $SU(2)_L \times U(1)_Y$ gauge symmetry gets spontaneously broken at the electroweak scale, often summarily referred to as the *Higgs mechanism* [33–36], while keeping the SM Lagrangian gauge invariant. One introduces a scalar $SU(2)_L$ doublet Φ transforming as a $(1, \mathbf{2}, \frac{1}{2})$ under the SM gauge group. The most general scalar Lagrangian consistent with the symmetries reads

$$\mathcal{L}_{\rm Higgs} = \big(D_\mu \Phi\big)^\dagger \big(D^\mu \Phi\big) - V(\Phi)\,, \qquad V(\Phi) = -\mu^2 \Phi^\dagger \Phi + \lambda \big(\Phi^\dagger \Phi\big)^2\,, \tag{1.6}$$

where $V(\Phi)$ denotes the Higgs potential. Stability of the electroweak vacuum requires that the potential $V(\Phi)$ is bounded from below, which implies a positive value for the quartic coupling, $\lambda > 0$. If the squared mass $\mu^2 > 0$ is positive, the local minimum of the potential, i.e. the ground state $\langle 0|\Phi|0\rangle$, breaks the electroweak symmetry via the symmetry breaking pattern $SU(2)_L \times U(1)_Y \to U(1)_{\rm EM}$. The field fluctuations around this ground state can be parametrized by

$$\Phi(x) = \frac{1}{\sqrt{2}} \begin{pmatrix} -i\sqrt{2}\varphi^+(x) \\ v + h(x) + i\varphi^3(x) \end{pmatrix}\,, \tag{1.7}$$

[8] Right-chiral neutrinos are also called *sterile* neutrinos to distinguish them from the *active* neutrinos in the SM that are charged under the electroweak gauge group.

where $v = \mu/\sqrt{\lambda}$ is the *vacuum expectation value* (vev) minimizing the Higgs potential. The scalars $\varphi^\pm$ and φ^3 are the three NGBs arising from the global breaking of $SU(2)_L \times U(1)_Y \to U(1)_{\rm EM}$. Since the electroweak symmetry group is gauged they provide the longitudinal degrees of freedom of the massive W^+, W^- and Z bosons. The remaining degree of freedom in (1.7) is the famous Higgs boson h with the tree-level mass $m_h = \sqrt{2\lambda}v$. Mass terms for the gauge bosons arise from the kinetic term in the Higgs Lagrangian (1.6). Fermions obtain their masses from the Yukawa interactions that are given prior to EWSB by

$$\mathcal{L}_{\rm Yuk} = -\bar{Q}_L^i \Phi \boldsymbol{Y}_d^{ij} d_R^j - \bar{Q}_L^i i\sigma^2 \Phi^\dagger \boldsymbol{Y}_u^{ij} u_R^j - \bar{L}_L^i \Phi \boldsymbol{Y}_e^{ij} e_R^j + \text{h.c.}\,, \tag{1.8}$$

where $\boldsymbol{Y}_{u,d,l}$ are complex 3×3 Yukawa matrices in generation space. In the interaction basis those matrices are in general non-diagonal. To obtain the physical mass eigenstates one can diagonalize the Yukawa interactions via bi-unitary transformations, e.g. the up-quark masses are given by $\text{diag}(m_u, m_c, m_t) = \frac{v}{\sqrt{2}} \boldsymbol{U}_u^\dagger \boldsymbol{Y}_u \boldsymbol{W}_u$, where $\boldsymbol{U}_u$ and $\boldsymbol{W}_u$ are unitary 3×3 matrices diagonalizing $\boldsymbol{Y}_u$. Analogous transformations can be performed for the down-type quarks and the charged leptons. The fermion mass eigenstates can be obtained by rescaling the fields $f_L \to \boldsymbol{U}_f f_L$ and $f_R \to \boldsymbol{W}_f f_R$ with $f = u, d, e$. The lepton interactions and the interactions of the quarks with the neutral gauge bosons (gluon, photon, Z boson) stay invariant when switching from the interaction to the mass eigenstates. This circumstance implies that there are no *flavor-changing neutral currents* (FCNCs) in the SM at tree-level. We will come back to this point in Section 1.2.2. However, in the mass eigenstate basis the interactions of the quarks to the $W^\pm$ bosons are given by $\mathcal{L}_{\rm Ferm} \ni \frac{g}{\sqrt{2}} \bar{u}_L \gamma^\mu W_\mu^+ \boldsymbol{V}_{\rm CKM}\, d_L + \text{h.c.}$, where $\boldsymbol{V}_{\rm CKM} \equiv \boldsymbol{U}_u^\dagger \boldsymbol{U}_d$ is the *Cabibbo-Kobayashi-Maskawa* (CKM) matrix [37, 38]. The CKM matrix is unitary and has in general three rotation angles and six complex phases. Five phases are unphysical and can be rotated away by redefining the quark fields. One physical complex phase remains, which is responsible for CP violation in the electroweak sector of the SM.

Flavor and custodial symmetry

In the absence of Yukawa interactions the SM fermions are invariant under the global symmetry group $U(3)_{Q_L} \times U(3)_{u_R} \times U(3)_{d_R} \times U(3)_{L_L} \times U(3)_{e_R}$ acting in generation space, whose fundamental representation has 45 generators. The Yukawa interactions break this symmetry group to the subgroup $U(1)_B \times U(1)_e \times U(1)_\mu \times U(1)_\tau$, which represents baryon (B) and leptonic family (L_e, L_μ, L_τ) number conservation. The $45 - 4 = 41$ broken generators yield symmetry transformations that can be used to remove unphysical parameters of the 54 real parameters of the Yukawa matrices $\boldsymbol{Y}_u$, $\boldsymbol{Y}_d$ and $\boldsymbol{Y}_e$. The remaining $54 - 41 = 13$ physical parameters distribute among the 6 quark masses, 3 charged lepton masses and the 3 angles and one CP-violating phase of the CKM matrix. The conservation of baryon and leptonic family number are accidental symmetries in the sense that they have not been imposed a priori, but follow from the particle content of the SM, the gauge principle and the renormalizability condition.[9]

In the limit $g' \to 0$ the Higgs Lagrangian (1.6) is globally invariant under $SO(4) \sim SU(2)_L \times SU(2)_R$, where $SU(2)_L$ is just the global version of the gauge symmetry. The vev breaks the global symmetry in the pattern $SU(2)_L \times SU(2)_R \to SU(2)_{L+R}$. The

[9] The observation of neutrino oscillations [39] violates the leptonic family number conservation, but still allows for the total lepton number conservation $L = L_e + L_\mu + L_\tau$. Moreover, baryon or lepton number alone are broken by (chiral) anomalies at the quantum level, only the quantum number $B - L$ is free from anomalies [40–42].

remaining so-called *custodial symmetry* [43] of the Higgs sector implies that the W^+, W^- and Z bosons transform as a triplet under $SU(2)_{L+R}$, implying that $m_W = m_Z$ in the limit $g' \to 0$. For instance, one implication in the SM is that the relation $\rho \equiv m_W^2/(m_Z^2 \cos^2\theta_W) = 1$ [44, 45] with the Weinberg angle θ_W receives only (small) radiative electroweak corrections, which is experimentally satisfied to better than 1%. As a consequence, any extension of the SM must implement some mechanism to protect the ρ parameter from too large corrections. In Section 2.5.2 we will discuss the Peskin-Takeuchi parameters S, T, U [46], that parametrize contributions of electroweak vacuum-polarization diagrams to precision experiments. The T parameter measures deviations from the SM prediction of ρ, which imposes an important constraint on the warped extra-dimensional models discussed in this thesis.

1.2 Motivation for new physics beyond the Standard Model

In the beginning of this chapter we have mentioned that the SM does not include a quantum theory of gravity, which implies that the SM loses its validity at energies close to the Planck scale. Apart from this problem, one striking argument for physics beyond the SM is the existence of non-baryonic *dark matter* (DM) which is the dominant matter component of our universe, and which cannot be explained within the particle content of the SM [47].[10] Furthermore, the CP violation in the SM is insufficient to explain the observed baryon asymmetry in the universe that may have been dynamically created by *baryogenesis* from a matter-antimatter symmetric initial state.[11] At last, the observation of *neutrino oscillations* [39] implies that at least two neutrino flavors are massive, while in the SM all neutrinos are massless by construction.[12]

Moreover, there are some long-standing experimental deviations from the respective SM predictions. In this category belongs the anomalous magnetic moment of the muon $g_\mu - 2$ where the SM prediction results in a $3-4\sigma$ deviation from the experimental result of the Brookhaven E821 experiment [51].[13] Another severe problem is the proton radius puzzle which can be extracted from high-precision measurements of the Lamb shift ($2S - 2P$ atomic transitions) in muonic hydrogen atom [53, 54] and displays 7σ deviations from results determined from eH spectroscopy or $e-p$ elastic scattering [1]. So far, all observations at the LHC and at preceding high-energy experiments are in general consistent with the SM predictions, see [55] for a status report after the first run of the LHC. Still, we like to mention at least two recent reports from the ATLAS and CMS collaborations, where an excess of events in the $\sqrt{s} = 13\,\text{TeV}$ diphoton spectrum at a mass of about 750 GeV (ATLAS) and 760 GeV (CMS) with local significances of 3.6σ

[10] Weakly interacting massive particles around the TeV scale are considered as the leading DM candidates, since they would have the right annihilation cross section in the early universe to explain the present DM relic density.

[11] In principle, the SM fulfills the three Sakharov conditions [48]. First, the weak interaction violates P invariance maximally, while CP invariance is violated by the complex phase in the CKM matrix. Secondly, the expansion of the universe brings the primordial plasma out of thermal equilibrium. At last, baryon number conservation is violated due to a quantum anomaly [40–42].

[12] One possibility is to add right-chiral neutrinos to the SM which allows for a right-chiral Majorana mass term and a neutrino Dirac-mass term after EWSB. Then, a large Majorana mass scale might explain the tiny size of the observed neutrino masses through the *see-saw mechanism* [49, 50].

[13] To address this discrepancy one possibility is to consider a *dark photon*, which is a light vector-boson that couples to the SM photon via kinetic mixing. However, nowadays the $g_\mu - 2$ favored parameter region of the dark photon is severely constrained by experimental searches, see e.g. [52].

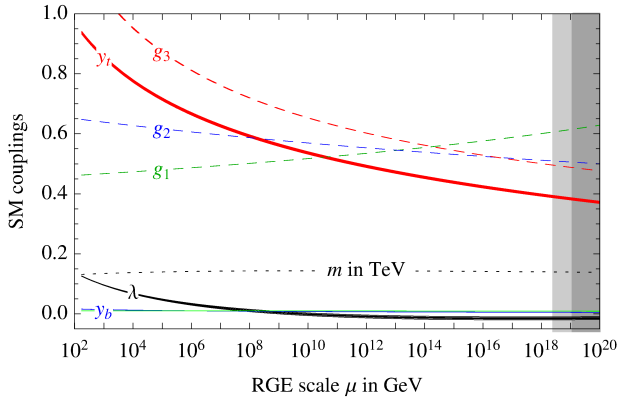

Figure 1.1: RG running of the SM couplings in the $\overline{\text{MS}}$ scheme. The gauge couplings are denoted by $g_1 = \sqrt{5/3}g'$, $g_2 = g$, $g_3 = g_s$, the top and bottom Yukawa couplings by y_t and y_b, the Higgs quartic coupling by λ and the parameter of the quadratic Higgs-mass term by m. The plot is taken from [62].

[56] (ATLAS) and 2.6σ [57] (CMS) was observed. Taking into account the look-elsewhere effect those numbers shrink to 2.0σ (ATLAS) and 1.2σ (CMS).[14]

The above-mentioned problems need a satisfactory explanation, and possibly require new physics beyond the SM. However, there are also "aesthetic" considerations, which have been used as a guideline for the construction of SM extensions. For instance, when we solve the renormalization-group (RG) equations for the three SM gauge couplings[15] $g_1 = \sqrt{5/3}g'$, $g_2 = g$ and $g_3 = g_s$ we observe that they do not exactly unify at some high-energy scale, see Figure 1.1. The lack of unification triggered the development of *grand unified theories* (GUTs) [63], where all forces are combined into a single force at the GUT scale $M_{\text{GUT}} \sim 10^{16}$ GeV. In the following, we will discuss two important issues in more detail that motivate new physics beyond the SM, namely the gauge-hierarchy problem and the flavor puzzle. Both are relevant for this thesis, since they can be addressed by models in warped 5D space-time.

1.2.1 The gauge-hierarchy problem

There are various approaches to the gauge-hierarchy problem, which in their entirety might clarify why this puzzle is one of the main guiding principles for the construction of extensions beyond the SM. We begin with the effective SM Lagrangian (1.2) containing the Higgs-mass operator $Q_2 = \Phi^\dagger\Phi$, which is the only relevant operator present. Based on the EFT approach and naive dimensional analysis, the corresponding Wilson coefficient μ^2 of Q_2 can be expressed by a dimensionless Wilson coefficient c_2 using the characteristic scale Λ, up to which the SM is supposed to be valid, such that $\mu^2 = c_2\,\Lambda^2$. If we assume that the SM is valid up to the Planck scale ($\Lambda \sim M_{\text{Pl}}$) the Wilson coefficient must take

[14] If the measured signal is interpreted as a new particle with a mass of 750 GeV that undergoes a two-body decay into two photons the Landau-Yang theorem [58, 59] forbids the new particle to have spin 1. One possibility would be to assume a new spin-0 particle which is produced in gluon fusion and decays into two photons via loops of new vector-like fermions. As an example, within the context of warped extra-dimensional models, there are proposals to identify the diphoton resonance with the lightest excitation of a new 5D scalar field, which is a singlet under the entire gauge group [60, 61].

[15] The factor $\sqrt{5/3}$ normalizes the gauge coupling g_1 such that the hypercharge generator is consistent with a $SU(5)$ or $SO(10)$ grand unified theory.

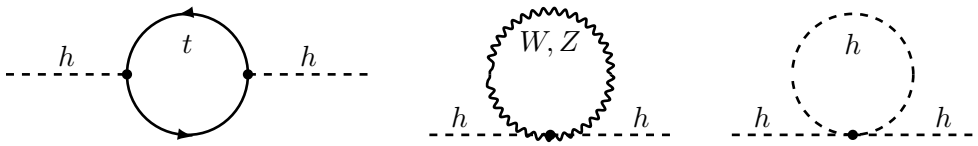

Figure 1.2: A subset of one-loop diagrams contributing to the Higgs-boson mass squared with fermions (left), spin-1 (middle) and spin-0 (right) bosons in the loop.

a tiny value

$$c_2 \sim \left(\frac{100\,\mathrm{GeV}}{10^{19}\,\mathrm{GeV}}\right)^2 \sim 10^{-34} \ll \mathcal{O}(1)\,, \tag{1.9}$$

in order to allow for $\mu \sim 100\,\mathrm{GeV}$ at the electroweak scale. But, since the Higgs mass operator is not protected by a symmetry a "natural" value for the dimensionless Wilson coefficient would be $c_2 \sim 1$. The hierarchy between (1.9) and what we expect from the EFT approach is regarded as being "unnatural". However, the *naturalness* principle is certainly not a necessary (physical) criterion for the internal consistency of the SM. It must be rather viewed as an aesthetic criterion which is the reason why there is no unique definition of a natural theory, see [64] for a general discussion about the naturalness concept. For example, Dirac's naturalness condition states that all dimensionless parameters are of order one and that dimensionful parameters must be of the same magnitude in size [65, 66]. A weaker naturalness condition is formulated by 't Hooft who says that one parameter is allowed to be much smaller than unity only if setting it to zero increases the symmetry of the theory [67]. Moreover, there exists the terminology of *technical naturalness*, which allows for hierarchies in the bare parameters of the Lagrangian but requires that radiative corrections do not exceed the corresponding bare parameters by many orders in magnitude.

In view of the last statement, we now consider radiative corrections to the bare Higgs mass. As an example, we calculate the contribution of the left one-loop diagram in Figure 1.2 that exchanges two virtual top quarks. Since the diagram is UV divergent we regularize the loop integral by imposing a sharp momentum cutoff Λ, i.e. after performing a Wick rotation of the loop four-momentum k to Euclidean momentum space we implement the condition $k_E \leq \Lambda$, where $k_E = \sqrt{-k^2}$. The correction to the squared Higgs mass is given by

$$\begin{aligned} \delta m_h^2\big|_t &= -iN_c\, y_t^2 \int^{\Lambda} \frac{d^4k}{(2\pi)^4}\, \mathrm{Tr}\left[\frac{1}{\not{k} - m_t + i0}\,\frac{1}{\not{k} - m_t + i0}\right] \\ &= \frac{3N_c\, y_t^2}{4\pi^2}\left[-\frac{\Lambda^2}{3} + m_t^2\left(\ln\frac{\Lambda^2}{m_t^2} - \frac{2}{3}\right) + \mathcal{O}\left(\frac{1}{\Lambda^2}\right)\right], \end{aligned} \tag{1.10}$$

where y_t is the Yukawa coupling of the top quark, and $N_c = 3$ is the color factor for quarks. The first term of the result shows the quadratic sensitivity on the cutoff. If the cutoff is set to the Planck scale ($\Lambda \sim M_{\mathrm{Pl}}$) the corresponding counter-term has to be finely tuned in order to cancel the term proportional to Λ^2 in (1.10) and obtain the renormalized Higgs mass at the electroweak scale. This is often referred to as the *fine-tuning problem* of the Higgs boson. Furthermore, we observe that m_h^2 is renormalized additively (as opposed to multiplicatively), so that quantum corrections are parametrically uncorrelated with the bare value of m_h^2 and can be numerically much larger. The additive renormalization comes from the fact that there is no symmetry enhancement

in the limit $m_h \to 0$, and consequently the principle of technical naturalness is violated.[16] In this context, we note that the gauge bosons and fermions in the SM are renormalized multiplicatively since their masses are protected by gauge and chiral symmetry. For instance, in the limit $m_f \to 0$ the left- and right-chiral components of the fermion spinors transform independently of each other, which forbids Dirac masses at all orders in perturbation theory. Consequently, chiral symmetry implies that radiative corrections to the fermion masses in the SM have only a logarithmic dependence on the cutoff $m_f \sim m_f \ln(\Lambda/m_f)$.[17]

One might object to the conclusions drawn from the quadratic sensitivity on Λ of the radiative corrections in (1.10), since this result depends on the regularization procedure. Therefore, it is instructive to repeat the calculation of the left one-loop diagram in Figure 1.2, implementing this time dimensional regularization [19, 68, 69]. Extending space-time to $d = 4 - 2\epsilon$ dimensions with $\epsilon > 0$ we obtain

$$\begin{aligned} \delta m_h^2|_t &= -iN_c\, y_t^2 \mu^{4-d} \int \frac{d^d k}{(2\pi)^d} \,\mathrm{Tr}\left[\frac{1}{\not{k} - m_t + i0}\frac{1}{\not{k} - m_t + i0}\right] \\ &= \frac{3N_c\, y_t^2}{4\pi^2}\, m_t^2 \left[\frac{1}{\epsilon} - \gamma_E + \ln 4\pi + \ln\frac{\mu^2}{m_t^2} + \frac{1}{3} + \mathcal{O}(\epsilon)\right] , \end{aligned} \tag{1.11}$$

where we have expanded the final result for $\epsilon \ll 1$. The UV divergence is contained in the pole $1/\epsilon$. After *modified minimal subtraction* ($\overline{\text{MS}}$) the finite correction is given by $\delta m_h^2|_t = 3N_c\, y_t^2\, m_t^2/(4\pi^2)(\ln \mu^2/m_t^2 + 1/3)$ and we observe only a logarithmic dependence on the dimensionful scale μ^2, that is introduced by the dimensional regularization procedure. The fine-tuning problem seems to be just an artifact of a poorly chosen regulator. However, the regulator-independent point is that the Higgs mass is still renormalized additively. Consequently, if the underlying UV theory introduces new particles with a mass scale M that couple to the Higgs boson, directly or indirectly, radiative corrections would lead in general (without additional symmetries) to corrections that are quadratically sensitive on M. In this sense, the fine-tuning problem reappears for large masses M near the Planck scale.

Another interesting observation, since the discovery of a Higgs-like resonance at $m_h = (125.09 \pm 0.24)\,\text{GeV}$ [70], is the multiple near-criticality of the Higgs sector, which deals with the question of electroweak vacuum stability and symmetry breaking in the SM. The main assumption of the following analysis is that the SM is considered to be valid up to the Planck scale. Then, for large field values one can approximately work with the effective SM potential $V_{\text{eff}}(h) \approx \frac{1}{4}\lambda_{\text{eff}}(h)\, h^4$ where $\lambda_{\text{eff}}(\mu)$ is the effective quartic running coupling at the energy scale μ. It turns out that the effective coupling $\lambda_{\text{eff}}(\mu)$ is numerically close to $\lambda(\mu)$ which is obtained from solving the RG equations, see [71]. At one-loop and neglecting the contribution from the gauge-couplings the running of the quartic coupling in the $\overline{\text{MS}}$ sheme is given by [62]

$$\frac{d\lambda(\mu)}{d\ln\mu^2} = \frac{1}{(4\pi)^2}\left[-3y_t^4 + 6y_t^2\lambda + 12\lambda^2 + \dots\right] , \tag{1.12}$$

[16] Note that in the limit where the Higgs-mass term is sent to zero the SM Lagrangian (1.3) would be classically conformal. Still, our statement remains valid since we implicitly assume that the cutoff Λ is associated with some explicit particle-mass scale M of the underlying UV theory, which then breaks the conformal symmetry.

[17] We use $\ln x$ to denote the natural logarithm of x to the base e (Euler's number), in the literature one also often finds the notation $\log x$.

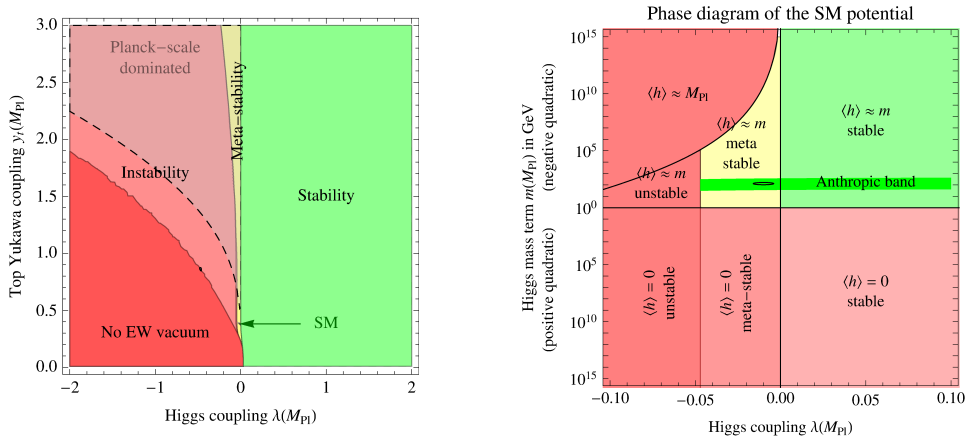

Figure 1.3: Left (right) is shown the SM phase diagram in terms of the quartic Higgs coupling λ and the top-Yukawa coupling y_t (mass parameter m), both renormalized at the Planck scale. Note that in the text we denote the parameter of the quadratic Higgs mass term by μ, see (1.6), instead of m as used in the plots. The SM input parameters lead to a meta-stable vacuum close to the phases of absolute stability, instability and the phase where EWSB does not occur below the Planck scale. Both plots are taken from [62].

where it is understood that the couplings on the right-hand side are the running couplings at the scale μ. At the electroweak scale the couplings $y_t(m_t) \approx 0.93558$ [62] and $\lambda(m_t) \approx 0.12711$ [62] imply that the first term in (1.12) dominates and drives the quartic coupling towards negative values with increasing energy scale, see Figure 1.1. Absolute stability of the SM vacuum up to the Planck scale would require that $\lambda(M_{\rm Pl}) > 0$. The left plot in Figure 1.3 shows the phase diagram in dependence of the renormalized top-Yukawa coupling $y_t(M_{\rm Pl})$ and Higgs quartic coupling $\lambda(M_{\rm Pl})$ at the Planck scale. The remarkable feature is that the SM input parameters[18] lead to the Yukawa coupling $y_t(M_{\rm Pl}) \approx 0.3813$ [62] and the Higgs quartic coupling $\lambda(M_{\rm Pl}) \approx -0.0113$ [62] which roughly correspond to the minimum values (at fixed gauge couplings) that allow for the existence of a sufficiently long-lived (meta-stable) electroweak vacuum.[19] Slightly smaller values for $\lambda(M_{\rm Pl})$ or $y_t(M_{\rm Pl})$ would lead to an unstable vacuum (lifetime shorter than the age of the universe) or would not allow for EWSB below the Planck scale.

Furthermore, it is convenient to plot the phase diagram in terms of the Higgs quartic coupling $\lambda(M_{\rm Pl})$ and the mass parameter $\mu(M_{\rm Pl})$ of the quadratic Higgs-mass term, which is shown by the right plot in Figure 1.3. Note that the quadratic Higgs-mass parameter is denoted by $m(M_{\rm Pl})$ in the plot instead of $\mu(M_{\rm Pl})$, which is only a notational difference. Thus, both parameters of the Higgs potential take values close to the boundaries between different phases of the SM. The notation is such that $\langle h\rangle = 0$ implies no EWSB, while $\langle h\rangle = \mu$ means that EWSB occurs at the energy scale μ. The upper bound on μ^2 can be deduced by considering the minimization condition of the potential [62] and the green band follows from anthropic considerations [72].[20] The coefficient μ^2 is the order parameter that describes the transition between the symmetric

[18] The analysis [62] uses the pole masses m_W, m_Z, m_h, m_t, the Fermi constant G_F extracted from muon decay and the $\overline{\rm MS}$ gauge $SU(3)_c$ coupling $\alpha_3(m_Z)$.

[19] Meta-stability means that the probability of quantum tunnelling out of the electroweak vacuum is small enough such that the lifetime of the SM vacuum is longer than the age of the universe.

[20] Roughly stated, the anthropic principle says that the parameters of the universe that we observe are governed by the requirement that they must be able to support intelligent life, as otherwise we would not exist to observe our universe.

phase (positive quadratic Higgs-mass term) and the broken phase (negative quadratic Higgs-mass term) [73]. While in principle μ^2 can take any value in the range $-M_{\rm Pl}^2$ to $+M_{\rm Pl}^2$, the gauge-hierarchy problem can be interpreted as the observation that the value of $\mu^2(M_{\rm Pl}) \approx (140.3\,\text{GeV})^2$ [62] is close to the critical value $\mu^2 = 0$ (with respect to the Planck scale) representing the boundary between the symmetric and broken electroweak phase.

In summary, it is an interesting observation that both $\mu(M_{\rm Pl})$ and $\lambda(M_{\rm Pl})$ (the two parameters of the Higgs potential), on the assumption that the SM is valid up to the Planck scale, happen to lie very close to boundaries between different phases of the SM. There are several possible explanations for the near-critical behavior of the high-energy SM couplings:

- The occurrence of near-criticality could be a consequence of a slightly broken symmetry. For instance, the realization of *supersymmetry* (SUSY) implies that $\mu^2 = 0$ and if marginally broken μ^2 would remain near zero. Another possibility is that the Higgs is a *pseudo Nambu-Goldstone boson* (PNGB) of a strongly-coupled sector, where both μ^2 and λ vanish at tree-level. Loop-suppressed radiative corrections might induce a potential and generate a small and negative value of λ at the Planck scale. Both ideas will be discussed in Section 1.3.

- In the limit where the Higgs-mass term is set to zero the SM Lagrangian only contains dimensionless couplings and respects *conformal symmetry* at the classical level. The idea is that radiative corrections lead to a Higgs potential that triggers EWSB and that the approximate conformal symmetry stabilizes the Higgs-mass at the electroweak scale [74]. However, this concept faces the problem how the (classically) conformally invariant SM can emerge from gravity, which is not conformally invariant due to the presence of the dimensionful Planck scale.

- Another possibility is to accept the fine-tuning of parameters in the SM. In this context, arguments based on the *anthropic principle* can be used to explain the "unnatural" sizes of the cosmological constant [75] and the weak scale [72]. The underlying statistical ensemble might be provided by the hypothetical idea of a multitude of parallel universes.

While the last option cannot be disregarded, it has the major disadvantage that it currently lacks the possibility of being tested experimentally. The major benefit of addressing the gauge-hierarchy problem via new symmetries and particles at the TeV scale is that it will allow for experimental discoveries of new-physics phenomena at accessible energy scales.

1.2.2 The flavor puzzle

Apart from the Higgs sector, the structure of the Yukawa interactions lacks a satisfactory explanation. Entries of the Yukawa matrices are dimensionless couplings of marginal operators and we expect complex values with $\mathcal{O}(1)$ magnitudes and arbitrary phases. Instead they admit a hierarchical pattern which accounts for the hierarchies of the fermion masses and mixing-angle disparities in the quark sector. The mass ratios of the charged fermions are given roughly by [76]

$$m_{u,d} : m_s : m_{b,c} : m_t \approx 1 : 50 : 1000 : 100000\,, \quad m_e : m_\mu : m_\tau \approx 1 : 200 : 3500\,, \quad (1.13)$$

while the mass hierarchy of the neutrinos is not yet resolved, see [77] for a recent review.[21] Assuming there are three neutrino generations with Dirac masses the so-called *Pontecorvo-Maki-Nakagawa-Sakata* (PMNS) matrix [78–80] connects the three neutrino flavor eigenstates ν_e, ν_μ, ν_τ with the three mass eigenstates ν_1, ν_2, ν_3. It can be described by three mixing angles and one CP-violating phase. While the PMNS matrix involves large mixing angles[22] and does not possess a simple hierarchical structure the CKM matrix in the quark sector admits small mixing angles and shows a hierarchical pattern. The Wolfenstein parametrization [81] illustrates the pattern of the CKM matrix

$$\boldsymbol{V}_{\text{CKM}} = \begin{pmatrix} 1-\lambda^2/2 & \lambda & A\lambda^3(\bar{\rho}-i\bar{\eta}) \\ -\lambda & 1-\lambda^2/2 & A\lambda^2 \\ A\lambda^3(1-\bar{\rho}-i\bar{\eta}) & -A\lambda^2 & 1 \end{pmatrix}, \tag{1.14}$$

where the parameters are defined by ($V_{ij} \equiv (\boldsymbol{V}_{\text{CKM}})_{ij}$)

$$\lambda = \frac{|V_{us}|}{\sqrt{|V_{ud}|^2+|V_{us}|^2}}, \qquad A = \frac{1}{\lambda}\left|\frac{V_{cb}}{V_{us}}\right|, \qquad \bar{\rho}-i\bar{\eta} = -\frac{V_{ud}^* V_{ub}}{V_{cd}^* V_{cb}}. \tag{1.15}$$

The parameter $\lambda \approx 0.23$ sets the typical size of each entry, since A, $\bar{\rho}$ and $\bar{\eta}$ are numbers of order one. To zeroth order in λ, the CKM matrix is a diagonal matrix while the mixing of different flavors is suppressed by powers of λ.

As already mentioned earlier, the flavor structure of the SM forbids FCNCs at tree-level. Besides being loop suppressed, they are further suppressed in the quark sector by the *Glashow-Iliopoulos-Maiani* (GIM) mechanism [82], which states that in case of equal quark masses the unitarity of the CKM matrix forbids FCNC processes to all orders in perturbation theory. The size of breaking is mainly given by the disparity of the quark masses, which is more distinctive in the up-quark sector. Both ingredients in the SM can successfully explain the suppression of rare meson decays and neutral meson mixing. Consequently, higher dimensional operators in the effective SM Lagrangian (1.2) that contribute to FCNCs at tree-level must be sufficiently suppressed by powers of Λ, which sets the energy scale for new physics. For instance, the model-independent analysis of $\Delta F = 2$ processes[23], which takes into account the contribution of dimension-six operators with general $\mathcal{O}(1)$ Wilson coefficients, imposes a lower bound $\Lambda \gtrsim (10^4 - 10^5)\,\text{TeV}$ [83]. Any extension of the SM near the TeV scale that is consistent with experimental data on flavor observables must explain why the Wilson coefficients of the higher dimensional operators in (1.2) are sufficiently small.

1.3 Extensions of the Standard Model in 4D space-time

In the following, we will briefly discuss two common extensions of the SM, supersymmetry and theories with a composite Higgs boson. Both ideas primarily address the gauge-hierarchy problem.

[21] Assuming that the neutrino flavor eigenstates are superpositions of the mass eigenstates ν_1, ν_2, ν_3 the squared mass differences are given by $\Delta m_{21}^2 = (7.53 \pm 0.18)\,10^{-5}\text{eV}^2$ [76] and $|\Delta m_{32}^2| = (2.42 \pm 0.06)\,10^{-3}\text{eV}^2$ [76], where $\Delta m_{ij}^2 = m_i^2 - m_j^2$. The scenario, in which ν_3 is heavier (lighter), is referred to as the normal (inverted) mass hierarchy.

[22] The mixing angles of the PMNS matrix are given by $\sin^2\theta_{12} = 0.304 \pm 0.014$ [76], $\sin^2\theta_{23} = 0.514^{+0.055}_{-0.056}$ [76] and $\sin^2\theta_{13} = 0.0219 \pm 0.0012$ [76].

[23] In a $\Delta F = 2$ process the quark-flavor quantum number changes by two units, e.g. neutral Kaon mixing (K^0-$\bar{K}^0$) is a $\Delta S = 2$ process where strangeness changes by two units.

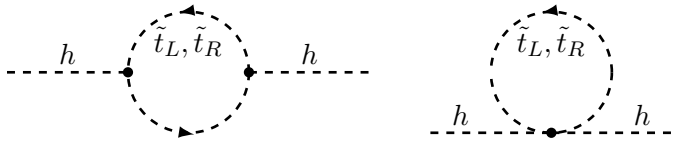

Figure 1.4: One-loop diagrams exchanging scalar stops $\tilde{t}_L$ and $\tilde{t}_R$, that contribute to the squared Higgs-boson mass in SUSY.

1.3.1 Supersymmetry

Arguably the most popular idea to address the gauge-hierarchy problem is to introduce *supersymmetry* (SUSY) that relates bosonic and fermionic particles, see [84] for a readable introduction. In 1974 Haag, Lopuszanski and Sohnius (HLS) published a proof [85] that weakened the assumptions of the Coleman-Mandula "no-go" theorem [86], which states that the symmetry group of a consistent[24] four-dimensional quantum field theory is the direct product of the internal symmetry group and the Poincaré group. HLS pointed out that the theorem implicitly assumes that the symmetry generators commute, and that there exists a non-trivial extension of the Poincaré algebra by allowing for anti-commuting symmetry generators. For instance, $N = 1$ SUSY inlcudes one single set of fermionic generators Q_α and the conjugate generator $\bar{Q}_{\dot{\alpha}} = (Q_\alpha)^\dagger$ with spinor index $\alpha = 1, 2$. The corresponding SUSY algebra reads[25]

$$\{Q_\alpha, Q_\beta\} = \{\bar{Q}_{\dot{\alpha}}, \bar{Q}_{\dot{\beta}}\} = 0\,, \quad \{Q_\alpha, \bar{Q}_{\dot{\beta}}\} = 2\sigma^\mu_{\alpha\dot{\beta}}\, P_\mu\,, \tag{1.16}$$
$$[Q_\alpha, P_\mu] = [\bar{Q}_\alpha, P_\mu] = 0\,, \quad [Q_\alpha, M_{\mu\nu}] = (\sigma_{\mu\nu})_\alpha{}^\beta\, Q_\beta\,, \quad [\bar{Q}^{\dot{\alpha}}, M_{\mu\nu}] = (\bar{\sigma}_{\mu\nu})^{\dot{\alpha}}{}_{\dot{\beta}}\, \bar{Q}^{\dot{\beta}}\,,$$

with the four-momentum and generalized momentum generators P_μ and $M_{\mu\nu}$. The non-vanishing commutators of the fermionic generators with $M_{\mu\nu}$ indicate that supersymmetry connects states of different spin and statistics. In a SUSY model, the fields are grouped into so-called *supermultiplets*, which are irreducible representations of the SUSY algebra. A minimal extension of the SM to a supersymmetric theory is the minimal supersymmetric SM (MSSM) [87], which for each SM degree of freedom includes one SUSY partner with a spin that differs by a half-integer. In the Higgs sector the particle spectrum has to be further enlarged since in the MSSM a second Higgs doublet is required to obtain gauge invariant Yukawa terms and to keep the theory free of anomalies. Two Higgs doublets have eight real degrees of freedom, where three are unphysical and represent the longitudinal degrees of freedom of the gauge bosons. The remaining five physical degrees of freedom distribute among a charged scalar $H^\pm$, a neutral CP-odd scalar A and two neutral CP-even scalars h and H, where the lighter one (usually denoted by h) could be identified with the SM-like Higgs boson detected at the LHC.

One of the main motivations for SUSY models is that radiative corrections to the Higgs-mass δm_h^2 are not quadratically sensitive to the cutoff, when regularizing the UV divergence in loop diagrams with a sharp cutoff. For instance, the top quark contribution from the left diagram in Figure 1.2 receives in the MSSM an additional contribution

[24] The underlying general assumptions include the analyticity and non-triviality of the S-matrix and the presence of a mass gap.

[25] Commutating and anti-commuting brackets of two operators are denoted by $[A, B] = AB - BA$ and $\{A, B\} = AB + BA$, respectively. The indices $\alpha, \dot{\alpha}$ can be raised or lowered with the Levi-Civita symbol in two dimensions $\epsilon_{\alpha\beta}$. We further used the notation $\sigma^\mu = (1, \vec{\sigma})$ and $\sigma_{\mu\nu} = \frac{i}{2}[\gamma_\mu, \gamma_\nu]$.

from diagrams exhanging stops[26] $\tilde{t}_L$ and $\tilde{t}_R$, which are the scalar superpartners of the top quark. The radiative corrections from the one-loop diagrams in Figure 1.4 are given by

$$\delta m_h^2\big|_{\tilde{t}} = \frac{3N_c\, y_{\tilde{t}}}{4\pi^2}\left[-\frac{\Lambda^2}{3} + m_{\tilde{t}}^2 \ln\frac{\Lambda^2}{m_{\tilde{t}}^2}\right] - \frac{N_c\, y_{\tilde{t}}^2\, v^2}{4\pi^2}\left[-1 + \ln\frac{\Lambda^2}{m_{\tilde{t}}^2}\right], \tag{1.17}$$

where $m_{\tilde{t}}$ is the stop mass. Supersymmetry imposes the condition $y_t^2 = -y_{\tilde{t}}$ which implies that the quadratically divergent terms in (1.10) and (1.17) cancel each other, when added together. Moreover, the logarithmic divergences would cancel in the limit of exact supersymmetry, where $m_{\tilde{t}} = m_t$ and the Higgs vev is sent to zero. In fact, exact supersymmetry implies that all masses are not renormalized at any order in perturbation theory [88]. Another aspect in favor of SUSY is that it allows in the MSSM for the unification of the three gauge couplings $g_1 = \sqrt{5/3}g'$, $g_2 = g$ and $g_3 = g_s$ at a scale $\Lambda_{\mathrm{GUT}} \sim 10^{16}\,\mathrm{GeV}$. This feature might hint at a more fundamental theory where the three gauge interactions at low energies emerge from a single gauge group at Λ_{GUT}. Furthermore, SUSY together with *R-parity*[27] [89] implies that superpartners can only be pair produced at colliders and that there exists a stable lightest supersymmetric particle (LSP), which can provide a viable dark-matter candidate.[28] It is worth mentioning that the MSSM constrains the Higgs-mass at tree-level to $m_h \leq m_Z|\cos 2\beta|$ [92, 93] with $\tan\beta = v_u/v_d$, and where v_u, v_d are the vevs belonging to the Higgs doublets giving masses to up- and down-type quarks. However, radiative corrections can lift the upper bound to $m_h \lesssim 135\,\mathrm{GeV}$ [94–97], which is compatible with the observed Higgs mass $m_h = (125.09 \pm 0.24)\,\mathrm{GeV}$ [70].

The conceptual downside of supersymmetric models is that SUSY cannot be exactly realized, as otherwise it would imply a degenerate mass spectrum of the SM particles and its superpartners, which is in conflict with experimental searches. Therefore, SUSY must be broken above the electroweak scale. In order to obtain a phenomenologically viable non-supersymmetric mass pattern it is not sufficient to incorporate SUSY breaking at tree level (via renormalizable interactions to a SUSY-breaking field) and with only the MSSM field content [84]. One assumes a *hidden sector* of particles that have no (or very small) direct coupling to the *visible sector*, that includes the chiral multiplets of the MSSM. In the EFT approach, we can ignore how the breaking is communicated from the hidden to the visible sector and write down all gauge and Lorentz invariant *soft*[29] SUSY-breaking terms in the Lagrangian for a general theory. This leads to 105 additional physical masses, phases and mixing angles in the MSSM that have no counterpart in the ordinary SM [98]. Furthermore, one must assume some organizing principle (e.g. flavor-diagonal squark and slepton mass matrices) for the additional parameters, since general values of order one would yield large contributions to FCNC processes. There are mainly two proposals how the SUSY breaking is modeled. In the so-called *gravity-mediated*

[26] The top quark is a Dirac fermion and has two complex (on-shell) degrees of freedom which distribute among the two complex scalars $\tilde{t}_L$ and $\tilde{t}_R$, where L, R are just labels referring to the two chiral components of the top quark spinor.

[27] R-parity is a discrete Z_2-symmetry and can be imposed to forbid baryon (B) and lepton (L) violating processes at tree-level in the MSSM. Each particle is assigned the number $P_R = (-1)^{3B+L+2s}$, where s denotes the spin of the particle, such that SM fields take the value $P_R = +1$ and their superpartners have $P_R = -1$.

[28] For instance, in the phenomenological MSSM the LSP is the lightest neutralino [90, 91], which is a massive, weakly interacting and electrically neutral Majorana fermion.

[29] Soft terms are renormalizable operators with couplings of positive mass dimension. The condition ensures that the relationship between dimensionless couplings (of marginal operators) that hold in an unbroken supersymmetric theory are maintained, e.g. that $y_t^2 = -y_{\tilde{t}}$.

scenario [99–104] SUSY gets broken in the hidden sector by the vev $\langle F \rangle$ of the SUSY-breaking field F and induces soft masses $m_{\text{soft}} \sim \langle F \rangle / M_{\text{Pl}}$. In the second possibility, *gauge-mediated* SUSY breaking [105–111], gauge interactions break SUSY at loop level, with the advantage of having flavor-diagonal soft masses.

General SUSY searches look for jets and missing energy, e.g. the decay process of two squarks $\tilde{q}\tilde{q} \to q\tilde{\chi}_1^0 q\tilde{\chi}_1^0$ where the decaying quarks lead to two jets and the missing energy stems from the neutralinos (LSPs) that escape the detector. Another typical final-state signature for many supersymmetric models consists of jets plus isolated leptons plus missing energy, e.g. the decay chain $\tilde{q}\tilde{q} \to \bar{q}\bar{q}\tilde{\chi}_1^\pm \tilde{\chi}_1^\pm \to \bar{q}\bar{q} l^\pm \nu \tilde{\chi}_1^0 l^\pm \nu \tilde{\chi}_1^0$ where two leptons with the same charge are produced. However, after the first run of the LHC no statistically significant sign for the existence of supersymmetric particles has been found, see [112] for a review.

1.3.2 Composite pseudo Nambu-Goldstone Higgs

Another idea to address the gauge-hierarchy problem is to suppose that the Higgs boson is an extended object with a finite geometric size of order 1/TeV, instead of being a point-like particle as in the SM. One assumes that there exists an underlying UV theory which contains a strongly-interacting sector, the so-called *composite sector*. In order to address the gauge-hierarchy problem the Lagrangian of the composite sector must not contain operators with a scaling dimension considerably below four, which means that unprotected energy scales are absent in the UV theory. In the language of the RG flow, this statement means that strongly relevant deformations are absent which makes the RG flow from the UV scale Λ towards the IR scale a slow process, i.e. a logarithmic running of the dimensionless strong coupling g_* of the composite sector. In analogy to QCD, one assumes that the RG running of g_* leads to the formation of bound states at the energy $m_* \sim \Lambda\, e^{-16\pi^2/g_*^2(\Lambda)}$, which sets the mass scale of the new heavy resonances of the composite sector. This mechanism by which the mass scale m_* is generated through the RG running without dimensionful couplings in the UV theory is referred to as *dimensional transmutation*.[30] Thus, the essential ingredient of the composite-Higgs idea is the strongly-coupled nature of an underlying UV theory, by which the Higgs mass is stabilized through dimensional transmutation.

Modern models with a composite Higgs implement the Higgs boson as a *pseudo Nambu-Goldstone boson* (PNGB) [113–117] of an enlarged global symmetry of the composite sector, which explains why the Higgs boson can be lighter than other (unobserved) composite resonances, see e.g. the recent review [118]. A minimal model that incorporates this idea and also includes a custodial symmetry is given by the so-called *minimal composite Higgs model* (MCHM) [119, 120]. The Lagrangian of the MCHM splits into three parts $\mathcal{L} = \mathcal{L}_{\text{cp}} + \mathcal{L}_{\text{el}} + \mathcal{L}_{\text{mix}}$. The first term $\mathcal{L}_{\text{cp}}$ describes the composite sector and is assumed to be invariant under the global symmetry group $\mathcal{G} = SU(3)_c \times SO(5) \times U(1)_{B-L}$. However, the vacuum state of the composite sector is only invariant under the subgroup $\mathcal{H} = SU(3)_c \times SO(4) \times U(1)_{B-L}$, and spontaneously breaks $\mathcal{G} \to \mathcal{H}$ which gives rise to $\dim \mathcal{G}/\mathcal{H} = 4$ NGBs that can be identified with the four degrees of freedom of the Higgs doublet. The dynamical breaking occurs at the energy scale f, which sets the mass scale for heavy resonances $m_* \sim g_* f$ in the TeV range, where $g_* \in (1, 4\pi)$ is

[30] The term is usually used in the context of QCD. While massless QCD is classically scale invariant, this is not true quantum mechanically. The RG running of the dimensionless QCD gauge coupling $\alpha_s(\mu) = g_s^2(\mu)/4\pi$ is determined at one-loop by the differential equation $(4\pi)^2 d\alpha_s(\mu)/d\ln\mu = -2\beta_0 \alpha_s^2(\mu)$ with $\beta_0 = 11/3N_c - N_f$, where $N_c = 3$ is the number of colors and N_f the number of active fermions. The solution of the differential equation introduces the squared QCD scale $\Lambda_{\text{QCD}}^2 = \mu^2 \exp(-4\pi/(\beta_0 \alpha_s(\mu)))$, which sets the mass scale for bound states in QCD.

the coupling strength of the composite sector. The second term $\mathcal{L}_{\rm el}$ contains the SM fermions and gauge bosons, i.e. the SM Lagrangian excluding the terms that involve the Higgs doublet. In this elementary sector the subgroup $SU(3)_c \times SU(2)_L \times U(1)_Y \subset \mathcal{H}$ is gauged where the $U(1)_Y$ hypercharge is given by $Q_Y = T_R^3 + Q_{B-L}/2$. The Higgs field transforms as a **4** of $SO(5)$ and is protected by the Goldstone symmetry, which forbids a Higgs potential at any order in perturbation theory. In order to explicitly break the global symmetry $SO(5)$ one includes interaction terms in $\mathcal{L}_{\rm mix}$, that couple SM fields to the composite sector. The gauging of the subgroup $SU(3)_c \times SU(2)_L \times U(1)_Y \subset \mathcal{G}$ explicitly violates the global symmetry $\mathcal{G}$ and gives rise to a non-vanishing potential at the one-loop level for the PNGB Higgs. Loops of the SM gauge bosons and fermions generate a Higgs potential that triggers EWSB with the vev $v = \sqrt{\xi}\, f$, where $0 \leq \xi \leq 1$ is obtained by minimizing the PNGB potential. In general the potential tends to maximally break EWSB, i.e. $\xi \sim 1$. Therefore, some amount of tuning of the Higgs potential is necessary in order to obtain an experimentally preferred value $\xi \ll 1$, that allows for a large enough mass gap between the Higgs and SM gauge bosons on the one side and the heavy resonances of the composite sector on the other side.[31]

The most important constraint on ξ is imposed by electroweak precision measurements. Tree- and loop-level corrections to the Peskin-Takeuchi parameters S and T require that $\xi = v^2/f^2 \lesssim 0.1$ [121], which can be achieved by some $\mathcal{O}(10\%)$ amount of tuning of the contributions to the Higgs potential. Another interesting prediction of the MCHM is that the Higgs couplings to gauge bosons and fermions are modified with respect to the SM couplings to [122]

$$\frac{g_{hVV}}{(g_{hVV})_{\rm SM}} = \sqrt{1-\xi}\,, \quad \frac{g_{hhVV}}{(g_{hhVV})_{\rm SM}} = 1-2\xi\,, \quad \frac{g_{hff}}{(g_{hff})_{\rm SM}} = \frac{1-(1+n)\xi}{\sqrt{1-\xi}}\,, \tag{1.18}$$

where $n = 0, 1$ depends on how fermions are implemented in the model. By comparing the predictions with experimental fits of couplings one can derive upper bounds on ξ [123], but which are currently less stringent than the one obtained from electroweak precision tests. It is noteworthy that one adjustable parameter ξ controls all the departures from the SM Higgs couplings and determines the compatibility with electroweak precision physics. This mechanism is referred to as *vacuum misalignment* [113, 114, 117]. Another key ingredient of modern PNGB models is the concept of *partial compositeness* [124] which means that the SM fermions are linear combinations of elementary and composite fields, where light fermions are almost elementary while the third generation is strongly or entirely composite. This leads to a structural suppression of all effects that involve the first two generations which helps to suppress FCNCs.

1.4 Basics of models in a warped 5D space-time

This section discusses the main concepts of embedding the SM into a *five-dimensional anti-de Sitter space* (AdS_5), which will form the foundation for the construction of phenomenological models in Chapter 2. The original idea of solving the gauge-hierarchy problem with one *warped extra dimension* (WED) was developed by L. Randall and R. Sundrum in 1999 [125]. Models that incorporate one WED are therefore referred to as *Randall-Sundrum* (RS) models. The extra dimension is chosen to be an S^1/Z_2 orbifold with the parametrization $\phi \in [-\pi, \pi]$. This is a circle of (compactification)

[31] While the contributions from the gauge-boson loops to the Higgs potential tend to align the electroweak vacuum in the $SU(2)_L \times U(1)_Y$ preserving direction [113–117], the fermion (dominantly the top quark) loops lead to misaligned contributions that are necessary in order to trigger EWSB [119].

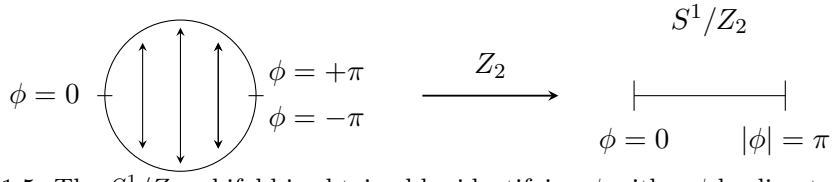

Figure 1.5: The S^1/Z_2 orbifold is obtained by identifying ϕ with $-\phi$ leading to two fixed points at $\phi = 0$ and $|\phi| = \pi$.

radius r where the points are related to each other by a Z_2 symmetry transformation $(x^\mu, \phi) \leftrightarrow (x^\mu, -\phi)$, see Figure 1.5 for an illustration. For a general 5D field $\Phi(x, \phi)$ the orbifold construction requires that two successive Z_2 transformations leave the field invariant. This implies the transformation behavior

$$\Phi(x, \phi) \xrightarrow{Z_2} \pm\, \Phi(x, -\phi)\,, \tag{1.19}$$

where the function with the eigenvalue $+1\,(-1)$ is referred to as being Z_2-even (-odd). In addition, the S^1 symmetry leads to the periodic boundary condition

$$\Phi(x, -\pi) = \Phi(x, \pi)\,. \tag{1.20}$$

Both relations (1.19) and (1.20) imply that Z_2-odd functions must vanish at the orbifold fixed points $\phi = 0, \pm\pi$. This orbifold construction will be important in order to arrive at a chiral low-energy spectrum for the fermions, as will be discussed in Section 1.4.2. The fixed points provide support for two 3-branes which are sub-manifolds with one time and three spatial dimensions. The 3-brane attached at $\phi = 0$ is called the *ultra-violet (UV) brane* and the one at $\phi = \pm\pi$ is denoted as the *infra-red (IR) brane*.[32] The region in between the two branes is referred to as the *bulk* of the extra dimension. The local geometry of the 5D space-time is given by the metric [125]

$$ds^2 = G_{MN}\, dx^M dx^N = e^{-2\sigma(\phi)}\, \eta_{\mu\nu}\, dx^\mu dx^\nu - r^2 d\phi^2\,, \tag{1.21}$$

where Latin (Greek) indices $M, N = 0, 1, 2, 3, 5$ ($\mu, \nu = 0, 1, 2, 3$) denote the 5D (4D) space-time coordinates with $x^5 \equiv r\phi$. Here, $\eta_{\mu\nu}$ is the 4D Minkowski metric with signature $(+, -, -, -)$ and G_{MN} is the representation of the 5D metric

$$G_{MN} = \begin{pmatrix} \eta_{\mu\nu}\, e^{-2\sigma(\phi)} & 0 \\ 0 & -1 \end{pmatrix}. \tag{1.22}$$

The function $\sigma(\phi)$ contains information about how the geometry of the 4D space-time varies along the fifth dimension. For an arbitrary function $\sigma(\phi)$ the metric (1.21) represents a general ansatz that respects four-dimensional Poincaré invariance in the x^μ directions. The classical 5D action that describes the above set-up, with the addition of brane-localized vacuum-energy densities, is given by [125]

$$S = \int d^4x \int_{-\pi}^{\pi} d\phi\, r \sqrt{|G|} \left[2M_5^3 R_5 - \Lambda_5 - \frac{\delta(\phi)}{r} V_{\rm UV} - \frac{\delta(|\phi| - \pi)}{r} V_{\rm IR} + \mathcal{L}_{\rm Fields} \right], \tag{1.23}$$

where $|G| = e^{-8\sigma(\phi)}$ is the determinant of the metric (1.22), M_5 is the 5D Planck mass, R_5 is the 5D Ricci-scalar and Λ_5 is the 5D cosmological constant. The energy densities

[32] In the literature one also finds the term Planck (TeV) brane for the brane localized at $\phi = 0$ ($\phi = \pm\pi$).

$V_{\rm UV}$ and $V_{\rm IR}$ are localized via δ-functions on the UV and the IR branes. At the IR-fixed point we define the δ-function in terms of a limiting procedure

$$\delta(|\phi| - \pi) = \lim_{\eta \to 0^+} \frac{1}{2} \left[\delta(\phi - \pi + \eta) + \delta(\phi + \pi - \eta)\right] \,, \tag{1.24}$$

where it is understood that the limit $\eta \to 0^+$ is taken after the integration over ϕ is performed in (1.23). This procedure ensures that possible discontinuities of some of the 5D fields at the IR brane are moved into the bulk, such that the RS model is properly defined. We will discuss the implementation of the δ-function at the IR brane in more detail in Section 1.4.5. The Lagrangian $\mathcal{L}_{\rm Fields}$ contains the gauge- and matter fields (at least the SM fields) of the specific model under consideration. It is assumed that the back-reaction of those fields is negligible when calculating the metric [125]. The 5D Einstein equations, that follow from the variational principle of the action (1.23) with $\mathcal{L}_{\rm Fields}$ set to zero, can be solved by [125]

$$k = \sqrt{\frac{-\Lambda_5}{24 M_5^3}} \,, \qquad V_{\rm UV} = -V_{\rm IR} = 24 M_5^3 k \,, \qquad \sigma(\phi) = kr|\phi| \,. \tag{1.25}$$

The parameter k is referred to as the curvature since it is related to the 5D Ricci-scalar $R_5 = 24k^2$, which is positive and corresponds with our conventions to a 5D anti-de Sitter space-time. This is consistent with the requirement of a negative 5D cosmological constant required by the first relation in (1.25). The second equation in (1.25) relates the energy densities on both branes. It turns out that their contribution to the 4D cosmological constant exactly cancels the one coming from Λ_5, which is consistent with the 4D Poincaré invariant ansatz (1.21) in the x^μ directions.[33] Due to the non-vanishing 5D cosmological constant the extra dimension has a finite curvature, which can be seen by the non-constant solution for the function $\sigma(\phi)$ in (1.25). Therefore, RS models are referred to as *warped* extra-dimensional models and (1.21) with $\sigma(\phi) = kr|\phi|$ is denoted as the *RS metric*, see Figure 1.6 for an illustration of the setup. The important ingredient of the RS metric is the so-called *warp factor* [125]

$$e^{-kr|\phi|} \,, \tag{1.26}$$

which exponentially rescales length and energy units when moving along the extra dimension. This feature will allow for a solution to the gauge-hierarchy problem. At this point the theory contains three fundamental scales M_5, k and r. Considering massless fluctuations around the vacuum solutions one can derive the reduced effective 4D Planck mass and finds $M_{\rm Pl}^2 = (M_5^3/k)\left(1 - e^{-2kr\pi}\right)$ [125]. We will see that the solution to the gauge-hierarchy problem requires that the product $kr \approx 10$, which implies that $M_{\rm Pl}$ is very weakly dependent on the warp factor. Since we do not assume large hierarchies in the fundamental parameters, such that $M_5 \sim k$, the above-mentioned relation implies that M_5 is of Planck size.

Later in Chapter 2, we will see that the presence of 5D fields in $\mathcal{L}_{\rm Fields}$ leads to interaction couplings of negative mass dimension, which directly follows from a quantum field theory in more than four dimensions. As a consequence RS models must be treated as EFTs with a 5D cutoff of order the Planck scale, and which must be replaced by a

[33] However, the cosmological-constant problem of the SM is only reformulated in the RS model into the question why the contributions from the energy densities and the 5D cosmological constant cancel each other (to very high precision).

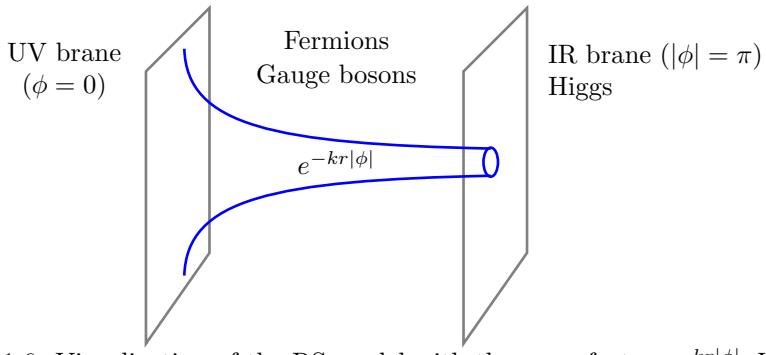

Figure 1.6: Visualization of the RS model with the warp factor $e^{-kr|\phi|}$. While the Higgs sector is confined on the IR brane, the fermions and gauge bosons are allowed to propagate into the bulk. The blue line indicates the effect of the warp factor.

more fundamental theory above this scale. This translates into an inherent, position-dependent UV cutoff given by the warped Planck mass $\Lambda_{\rm UV}(\phi) \sim M_{\rm Pl}\, e^{-kr|\phi|}$ [126–130], which accounts for the fact that RS models do not provide a description of quantum gravity. For the calculation of Feynman diagrams it implies that each vertex at a position ϕ_i is associated with a position-depending cutoff $\Lambda_{\rm UV}(\phi_i)$. We can think of it as modeling the effect of a form factor, which accounts for the impact of quantum gravity on energy scales above the effective Planck scale at that point. In general the coordinates ϕ_i are integrated along the complete extra-dimension $-\pi \leq \phi_i \leq \pi$, and hence the cutoff values vary between $M_{\rm Pl}\, e^{-kr\pi}$ and the fundamental Planck scale.

1.4.1 Solution to the gauge-hierarchy problem

Let us investigate how we can address the gauge-hierarchy problem assuming that all fundamental parameters of the RS model take values of order the Planck mass, i.e. $M_5 \sim k \sim r^{-1} \sim M_{\rm Pl}$. The main idea is to localize the Higgs doublet $\Phi(x)$ at the IR brane such that the action of the Higgs sector reads

$$S_{\rm Higgs} = \int d^4x \int_{-\pi}^{\pi} d\phi\, \sqrt{|G|}\, \delta(|\phi| - \pi) \left[G^{\mu\nu} (D_\mu \Phi)^\dagger D_\nu \Phi - \frac{\lambda_5}{2} \left(\Phi^\dagger \Phi - \frac{v_5^2}{2} \right)^2 \right] , \quad (1.27)$$

where λ_5 is the dimensionless 5D quartic coupling and v_5 denotes the 5D vev. Later in Section 1.4.5 we will come back to the issue of how to properly localize the Higgs sector at the IR brane, since this subject will be very important when performing loop calculations in the RS model. However, for the purpose of this section the δ-function can be defined according to equation (1.24). Without introducing large hierarchies we assume that $\lambda_5 = \mathcal{O}(1)$ and $v_5 = \mathcal{O}(M_{\rm Pl})$. Using the metric representation (1.22) with $\sigma(\phi) = kr|\phi|$ the Higgs action reads

$$S_{\rm Higgs} = \int d^4x \left[\eta^{\mu\nu} (D_\mu \Phi)^\dagger D_\nu \Phi - \frac{\lambda_5}{2} \left(\Phi^\dagger \Phi - e^{-2kr\pi} \frac{v_5^2}{2} \right)^2 \right] , \quad (1.28)$$

where we have redefined the Higgs field $\Phi(x) \to e^{kr\pi}\, \Phi(x)$ such that the kinetic term is canonically normalized. The crucial feature is that the position of the minimum of the classical potential is given by the effective 4D vev $v = e^{-kr\pi}\, v_5$, where $e^{-kr\pi}$ is the warp factor (1.26) evaluated at the IR brane $\phi = \pm\pi$. The dimensionless coefficient λ_5 is not rescaled. Consequently, the Higgs mass at tree-level is given by the 5D Higgs mass

reduced by the warp factor at the IR brane, such that

$$m_h = m_{h,5}\, e^{-kr\pi}\,, \tag{1.29}$$

with $m_{h,5} = \sqrt{2\lambda_5}\, v_5$. A small tuning of the product $kr \approx 12$ is sufficient to reproduce the physical Higgs mass if $m_{h,5}$ is of order the Planck mass. However, we have to choose a slightly smaller value $kr \approx 10$. The reason is that the physical cutoff evaluated at the IR brane is given by

$$\Lambda_{\rm TeV} = M_{\rm Pl}\, e^{-kr\pi} \sim 10\, M_{\rm KK}\,, \tag{1.30}$$

where $M_{\rm KK}$ sets the mass scale of new particles predicted in the RS model. The so-called *Kaluza-Klein (KK) scale* is defined via

$$M_{\rm KK} \equiv k\, e^{-kr\pi}\,. \tag{1.31}$$

For example, RS models generically predict the existence of a massive version of the SM gluon, the so-called first KK gluon resonance, with the mass $M_{g^{(1)}} = 2.45\, M_{\rm KK}$.[34] The non-observation of this particle implies a lower bound of $M_{\rm KK} \gtrsim 1\,\text{TeV}$, see Section 2.5 for more details. Thus, equation (1.30) ensures that the RS model contains new heavy particles with masses lying below the physical cutoff, in order to deserve the attribute "extra-dimensional".[35] Throughout this thesis we will therefore implement the following value[36]

$$L \equiv kr\pi \approx 33.5\,, \tag{1.32}$$

where L is referred to as the *volume* of the RS space. Such a value can be stabilized by the Goldberger-Wise mechanism [131]. In order to reproduce the Higgs mass in (1.29) we need to assume that the 5D mass $m_{h,5}$ is a factor of roughly 100 smaller than the Planck mass (*little hierarchy problem*).

Finally, we have to consider radiative corrections to the tree-level Higgs mass in RS models. As an example, we consider the one-loop Higgs self-energy diagram exchanging virtual fermions where both vertices are localized at the extra-dimensional coordinates ϕ_1 and ϕ_2. Due to the presence of a position-dependent 4D cutoff, the Euclidean loop momentum is bounded from above by $p_E \leq \min(\Lambda_{\rm UV}(\phi_1)), \Lambda_{\rm UV}(\phi_2) = \Lambda_{\rm TeV}$. Consequentially the Higgs mass will receive radiative corrections dependent on the scale $\Lambda_{\rm TeV}$ instead of $M_{\rm Pl}$. With the help of naive dimensional arguments (NDA) the one-loop correction to the squared Higgs mass can be estimated to $\delta m_h^2 \sim \Lambda_{\rm TeV}^4/(16\pi^2 M_{\rm KK}^2)$ [132]. The correction grows like the fourth power of the cutoff scale, not like the second power

[34] Later in this thesis, we will often quote bounds on the mass of the first KK gluon resonance, which can be directly translated into bounds on the KK scale.

[35] For instance, the first four KK resonances of the gluon have the masses $M_{g^{(1)}} = 2.45\, M_{\rm KK}$, $M_{g^{(2)}} = 5.57\, M_{\rm KK}$, $M_{g^{(3)}} = 8.70\, M_{\rm KK}$ and $M_{g^{(4)}} = 11.84\, M_{\rm KK}$, which shows the approximately equidistant mass spectrum. Equation (1.30) implies that the first three KK-gluon modes have masses below $\Lambda_{\rm TeV}$.

[36] Let us motivate this value for L. The starting point is that the RS model should solve the gauge-hierarchy problem, which implies that the "little" hierarchy between the electroweak and the KK scale should be as small as possible. Experimentally, $M_{\rm KK}$ cannot be smaller than 1 TeV. Furthermore, $M_{\rm KK}$ should not be larger than roughly 10 TeV, otherwise the "little" hierarchy problem becomes worse and the detection of KK resonances gets out of reach for current collider experiments. So, assuming the range $M_{\rm KK} \in [1, 10]\,\text{TeV}$, equation (1.30) leads to $\Lambda_{\rm TeV} \in [10, 100]\,\text{TeV}$. With $M_{\rm Pl} = 1.22 \times 10^{19}\,\text{GeV}$ this translates into $L \in [32.4, 34.7]$. Instead of varying L within this range we have decided to choose the specific value (1.32). We emphasize that all analytical results in this thesis are presented for arbitrary values of L, the specific value (1.32) only enters the numerical calculations in the phenomenological sections.

as it is the case in the SM. Again, we see that some amount of tuning is necessary in RS models with a Higgs sector localized at the IR brane since there is no mechanism that separates the cutoff scale $\Lambda_{\rm TeV}$ from the electroweak scale.[37] Still, the large hierarchy between the Planck mass and the multiple TeV scale can be successfully addressed by the RS models considered in this thesis.

1.4.2 Bulk fields in a warped space-time

Apart from the Higgs doublet all other fields are genuinely five-dimensional. In the following we will present the basic properties when dealing with bulk gauge bosons and bulk fermions in a warped space-time, the content is partly based on [135, 136]. Let us start with the 5D action S_5 for a general bulk field, which is denoted in this section by $\Phi(x,\phi)$, and apply the variational principle $\delta S_5 = 0$. In general, the variation of the action can be written in the form

$$\delta S_5 = \int d^4x \int_{-\pi}^{\pi} d\phi\, r\, \delta\Phi\, (\mathcal{D}\Phi) + \int d^4x\, \delta\Phi(\mathcal{B}\Phi)\big|_{\phi=0,\pm\pi}\,, \tag{1.33}$$

where $\mathcal{D}$ and $\mathcal{B}$ denote differential operators. Requiring that the first term in (1.33) vanishes leads to the so-called *equation of motion* (EOM) $\mathcal{D}\,\Phi(x,\phi) = 0$ of the bulk field Φ. The second term in (1.33) is evaluated at the orbifold fixed points at $\phi = 0, \pm\pi$ and vanishes if $\mathcal{B}\Phi(x,\phi)|_{\phi=0,\pm\pi} = 0$, which defines the *boundary conditions* (BCs) of Φ at the UV and IR branes. The bulk fields are assumed to vanish in the limit $x^\mu \to \pm\infty$. In order to solve the EOM one can make the ansatz (separation of variables)

$$\Phi(x,\phi) = \frac{1}{\sqrt{r}} \sum_{n=0}^{\infty} \Phi^{(n)}(x)\, \chi_n^{\Phi}(\phi)\,, \tag{1.34}$$

which is referred to as the *KK decomposition* of the bulk field Φ. The factor $1/\sqrt{r}$ is a conventional choice in order to arrive at the canonical mass dimension for the KK modes $\Phi^{(n)}$. In this thesis we only consider KK decompositions into mass eigenstates, where the corresponding mass spectrum is determined by the BCs of the bulk fields. The lightest KK mode that corresponds to a particle in the SM is referred to as the *zero mode* ($n = 0$). The remaining KK modes have masses that increase with their mode number n, starting with the lightest KK resonance ($n = 1$) that typically has a mass of order $M_{\rm KK}$. The functions χ_n^{Φ} in (1.34) depend on the position along the extra dimension and are referred to as the *profiles* of the KK modes. They form a complete set of functions and are subject to the orthonormality condition

$$\int_{-\pi}^{\pi} d\phi\, \chi_n^{\Phi}(\phi)\, \chi_m^{\Phi}(\phi) = \delta_{nm}\,. \tag{1.35}$$

As mentioned earlier each field Φ is assigned a Z_2-parity, see (1.19), that depends on the low-energy spectrum of the theory and which is reflected in the corresponding BCs. There

[37] There are also realizations of the RS idea where the Higgs boson corresponds to the fifth component of an additional bulk gauge boson. In this case the gauge symmetry forbids a scalar potential at tree-level and implies that the Higgs mass is smaller by a loop factor than the typical mass scale of the lightest KK resonances, see [119, 133]. In fact, based on the *AdS/CFT* correspondence conjectured by Maldacena [134] those 5D models are to be considered dual to 4D models where the Higgs is a composite PNGB, which we have discussed in Section 1.3.2. An introduction to this subject can be found, e.g. in [135].

are two basic types of BCs which are given by

$$\begin{aligned} \Phi(x,\phi)\big|_{\phi=0,\pm\pi} &= 0 \qquad \text{(Dirichlet BC)}\,, \\ \partial_\phi \Phi(x,\phi)\big|_{\phi=0,\pm\pi} &= 0 \qquad \text{(Neumann BC)}\,, \end{aligned} \tag{1.36}$$

with $\partial_\phi \equiv \partial/\partial\phi$. Requiring that the field Φ vanishes at the fixed point $\phi = 0, \pm\pi$ we speak of a *Dirichlet* (D) BC, which is automatically imposed for Z_2-odd fields. The important feature is that if the EOM allows for a constant solution of the zero-mode profile $\chi_0^\Phi(\phi) = \text{const}$, the assignment of Z_2-odd parity, or equivalently the Dirichlet BC, removes this solution from the spectrum. On the other hand, if one assigns a Z_2-even parity to the field, or equivalently the *Neumann* (N) BC, the constant solution is included in the spectrum. Now, upon inserting the KK decomposition (1.34) into the 5D action S_5 and performing the integration over ϕ, while making use of the EOMs and the BCs, we obtain an effective 4D action that contains the SM particles and massive KK modes. We refer to this as the *KK-decomposed theory*. Next, we will present more details on gauge bosons, fermions and interactions in the bulk of the extra dimension.

Bulk gauge bosons

Any phenomenological RS model is based (at least) on the SM gauge group which is extended to a bulk gauge group acting on 5D fields. As an example we can discuss the bulk photon, which is the gauge boson of the $U(1)$ bulk gauge group. The corresponding 5D action is given by

$$S_5 = -\int d^4x \int_{-\pi}^{\pi} d\phi\, r\, \sqrt{|G|}\, \frac{1}{4}\, F_{MN}\, F^{MN}\,, \tag{1.37}$$

with the field strength tensor $F_{MN} = \partial_M A_N - \partial_N A_M$. We see that the 5D gauge field has a canonical mass dimension of $[A_M] = 3/2$ instead of 1 as in the SM.[38] An explicit bulk mass term is forbidden by gauge invariance. Applying the variational principle to (1.37) yields a mixed boundary term such that the BCs for A_μ and A_5 are correlated. The phenomenologically interesting choice is

$$\partial_\phi A_\mu(x,\phi)\big|_{0,\pm\pi} = 0\,, \qquad\qquad A_5(x,\phi)\big|_{0,\pm\pi} = 0\,, \tag{1.38}$$

where A_μ is Z_2-even and A_5 is Z_2-odd. The first condition implies the existence of a massless solution with a constant (normalized) profile $\chi_0^A(\phi) = 1/\sqrt{2\pi}$, and the corresponding zero mode $A_\mu^{(0)}$ can be identified with the SM photon. Concerning the fifth component of the gauge field the Dirichlet BC implies the absence of a (scalar) zero mode. In fact, the remaining KK modes of A_5 are unphysical since they provide the necessary degrees of freedom for the vector-fields $A_\mu^{(n\geq 1)}$ in order to become massive. The mass spectrum of the KK photons is given by

$$m_{A_1} = 2.45\, M_{\rm KK}\,, \qquad\qquad m_{A_{n\geq 2}} \approx \left(n - \frac{1}{4}\right)\pi M_{\rm KK} \quad [135]\,, \tag{1.39}$$

which is the same for KK gluons. We observe that the KK masses increase with the mode number n in approximately equidistant steps of $\pi M_{\rm KK}$.

[38] This explains why we pulled out the factor $1/\sqrt{r}$ in the KK decomposition (1.34).

Bulk fermions

We continue with the treatment of bulk fermions. At first, we need a generalization of the gamma matrices in five space-time dimensions. The Clifford algebra is given by $\{\Gamma^a, \Gamma^b\} = 2\,\eta^{ab}$ with $a, b \in \{0, 1, 2, 3, 5\}$, where the metric η^{ab} is flat and has the signature $(+, -, -, -, -)$. This condition can be fulfilled by a set of five 4×4 Dirac matrices $\Gamma^a = \{\gamma^\mu, -i\gamma_5\}$ with $\mu \in \{0, 1, 2, 3\}$, where γ^μ are the usual Dirac matrices in four dimensions and $\gamma_5 \equiv i\gamma_0\gamma_1\gamma_2\gamma_3$. Secondly, in a curved space-time we have to generalize the Dirac operator $i\Gamma^M\partial_M$ of flat space-time. Since spinors transform under the Lorentz group and are not subject to the diffeomorphism group of General Relativity, one has to introduce a tangent frame that is spanned by the so-called vielbeins. For our purpose we need the inverse vielbeins in five dimensions, which are defined via the relation $G^{MN} = E_a^M E_b^N \eta^{ab}$. In addition, the curved space-time requires to use the covariant derivative $D_M\Psi = (\partial_M - \frac{i}{4}\omega_M^{ab}\sigma_{ab})\Psi$ with the spin connection ω_M^{ab} and $\sigma_{ab} \equiv \frac{i}{2}[\gamma_a, \gamma_b]$. Finally, the kinetic 5D action for a Dirac fermion Ψ in the bulk reads

$$S_5 = \int d^4x \int_{-\pi}^{\pi} d\phi\, r\, \sqrt{|G|}\, \left(E_a^M\, \bar{\Psi}\, i\gamma^a D_M \Psi\right)\,, \tag{1.40}$$

which is invariant under general coordinate transformations of General Relativity as well as Lorentz transformations. Making (1.40) manifest hermitian leads to [137]

$$S_5 = \int d^4x \int_{-\pi}^{\pi} d\phi\, r\, \sqrt{|G|} \Bigg[E_a^M \left(\frac{i}{2}\bar{\Psi}\,\gamma^a \left(\partial_M - \overleftarrow{\partial_M} \right) \Psi + \frac{\omega_{bcM}}{8} \bar{\Psi}\{\gamma^a, \sigma^{bc}\}\Psi \right) - \mathrm{sgn}(\phi)\, m_\Psi \bar{\Psi}\Psi \Bigg]\,, \tag{1.41}$$

where we have added a bulk mass for the fermion field in the last line. The sign function $\mathrm{sgn}(\phi)$ of the bulk-mass term is required such that the term is Z_2-even and does not vanish under the integration over the extra-dimensional coordinate ϕ. The vielbeins are given by $E_a^M = \mathrm{diag}(e^{\sigma(\phi)}, e^{\sigma(\phi)}, e^{\sigma(\phi)}, e^{\sigma(\phi)}, 1)$ with $\sigma(\phi) = kr|\phi|$. Since the RS metric is diagonal the term with the spin connection in (1.41) actually vanishes [137]. The third important issue concerning fermions in five dimensions is the question of obtaining a chiral spectrum. In a 4D theory the matrix γ_5 can be used to distinguish between left- and right-chiral solutions of the Dirac equation by means of the projectors $P_{L,R} = (1 \mp \gamma_5)/2$. The Dirac-spinor representation in four dimensions is reducible and allows for left- and right-chiral (2-component) Weyl spinors. But in theories with an odd number of dimensions the Dirac-spinor representation is irreducible and does not allow for two independent solutions. In our case γ_5 is part of the 5D gamma matrices and cannot be used to construct a chiral projection operator. However, the orbifold construction will allow for a chiral projection via BCs. The idea is that a 5D fermion can be decomposed into two Weyl spinors in four dimensions, Ψ_L and Ψ_R with $\Psi_{L,R} \equiv P_{L,R}\Psi$, which can be distinguished by having different BCs. In fact, applying the variational principle to (1.41) with respect to Ψ automatically leads to a correlation between their BCs. For example, let us assume a Dirichlet BC for Ψ_R then the BC for Ψ_L is automatically fixed by the fermionic EOM to

$$\Psi_R(x, \phi)\big|_{0,\pm\pi} = 0 \quad \rightarrow \quad \frac{1}{r}\partial_\phi \Psi_L(x, \phi)\big|_{0,\pm\pi} = \left(\frac{k}{2} - m_\Psi\right) \Psi_L(x, \phi)\big|_{0,\pm\pi}\,, \tag{1.42}$$

where we see that the BC for Ψ_L is of a mixed type. Combined with a positive parity for Ψ_L and a negative parity for Ψ_R, equation (1.42) implies the existence of a left-chiral

but not of a right-chiral zero mode. Only the low-energy spectrum is affected. At the level of KK modes there are both left- and right-chiral modes present. Thus, the BCs can be used in order to obtain the low-energy spectrum of the SM in case of the $SU(2)_L$ quark doublet $Q(x,\phi)$. While at the zero-mode level one degree of freedom (the right-chiral zero mode) has been removed, the number of degrees of freedom is doubled at the level of massive KK modes. In a similar way we can proceed in case of a $SU(2)_L$ quark singlet $q(x,\phi)$, where we impose negative Z_2-parity and Dirichlet BCs on q_L. A further important consequence of the chiral projection via boundary conditions is that the RS model allows for explicit bulk-mass terms for the $SU(2)_L$ doublets and singlets, see (1.41), without breaking the gauge symmetry.

Interactions in the bulk

The strength of interactions is determined by the 5D coupling constant and the so-called *overlap integrals*. For instance, a vertex that couples one gauge boson and two fermions has a (4D) Feynman rule that is proportional to

$$\int_{-\pi}^{\pi} d\phi\, \chi_n^A(\phi)\, \chi_m^\Psi(\phi)\, \chi_k^\Psi(\phi)\,, \tag{1.43}$$

where n, m, k are the corresponding mode numbers. The integral becomes trivial for the special case of a SM photon or gluon ($n = 0$). Their constant profiles allow to use the orthonormality relation (1.35) for fermions, such that the integral is trivial for $m = k$ and vanishes for $m \neq k$. Consequently, in case of the SM photon and gluon the gauge interactions are universal which means that their couplings to fermions are independent of the localization of the fermion profiles.

1.4.3 Switching to the *t*-notation

Before discussing the solution to the flavor puzzle, we introduce the so-called *t-notation* that will allow for a simplification of the calculations in the subsequent chapters. Therefore, we define the dimensional variable

$$t \equiv \epsilon\, e^{kr|\phi|}\,; \qquad \epsilon = e^{-kr\pi}\,, \tag{1.44}$$

where ϵ denotes the warp factor at the IR brane and t can take values in the region $[\epsilon, 1]$. The UV and IR branes are localized at $t = \epsilon$ and $t = 1$, respectively. When we integrate over the extra-dimensional coordinate we can substitute ϕ with t and replace

$$\int_{-\pi}^{\pi} d\phi \ldots \;\longrightarrow\; \frac{2\pi}{L} \int_{\epsilon}^{1} \frac{dt}{t} \ldots\,, \tag{1.45}$$

where the integration on the right side extends from the UV to the IR brane. In terms of the new extra-dimensional coordinate the RS metric now reads

$$ds^2 = \frac{\epsilon^2}{t^2} \left(\eta_{\mu\nu}\, dx^\mu dx^\nu - \frac{1}{M_{\rm KK}^2}\, dt^2 \right) . \tag{1.46}$$

Note that the dimensionless variable t is related to the conformal coordinate z frequently used in the literature by the simple rescaling $z = t/M_{\rm KK} \equiv R'\, t$.

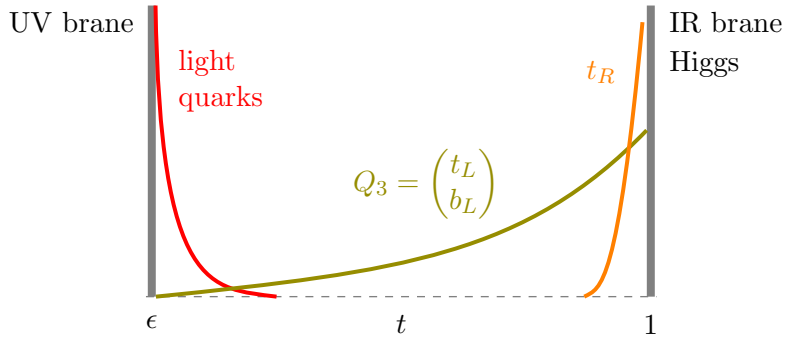

Figure 1.7: Qualitative description of the fermion localization along the fifth dimension. Light fermions must have a small overlap with the IR brane, where the Higgs is localized, and are therefore localized close to the UV brane. Heavy fermions like the third generation of the quarks are more localized towards the IR brane in order to generate larger masses.

1.4.4 Solution to the flavor puzzle and the RS-GIM mechanism

Now, we are in a position to discuss the second motivation for RS models which concerns the flavor sector. We begin with the explanation how the hierarchical pattern of the quark sector, discussed in Section 1.2.2, can be generated without introducing large hierarchies in the fundamental 5D parameters.[39] For this purpose we only need approximate solutions for the fermion profiles, which will be calculated in full detail in Chapter 2. The Z_2-even profiles of the left- and right-chiral zero modes are given to good approximation by

$$\chi_{0,A}^{\Psi}(t) \approx \sqrt{\frac{L}{\pi}}\, F(c_A)\, t^{c_A+\frac{1}{2}}\,; \qquad\qquad A = L, R\,, \tag{1.47}$$

where we made use of the t-notation defined in (1.44).[40] The dimensionless coefficients c_L and c_R are the bulk masses of the left- and right-chiral fermions rescaled by the Planck mass. They are called *bulk-mass parameters* and we expect them to be of $\mathcal{O}(1)$ without introducing new hierarchies. Importantly, their values determine the overlap of the profiles (1.47) with the IR brane at $t = 1$ via the function

$$F(c) \equiv \mathrm{sgn}(\cos \pi c) \sqrt{\frac{1+2c}{1-e^{-(1+2c)L}}}\,, \tag{1.48}$$

which is referred to as the *zero-mode profile*. This function can be approximated for two different ranges of the bulk-mass parameters by

$$F(c) \approx \mathrm{sgn}(\cos \pi c)\, \sqrt{|1+2c|} \times \begin{cases} e^{-\left|\frac{1}{2}+c\right| L}\,, & c < -1/2\,, \\ 1\,, & c > -1/2\,. \end{cases} \tag{1.49}$$

We observe that the size of $F(c)$ is exponentially sensitive on small $\mathcal{O}(1)$ variations of the bulk-mass parameters for $c < -1/2$. Keeping in mind that $e^{-L} \approx 10^{-15}$ for $L \approx 33.5$ the zero-mode profile can generate large hierarchies. For instance, the quark masses are

[39] In this thesis we focus on the quark sector, while it is also possible to include leptons in RS models. The main difference is that the neutrino mixing angles are non-hierarchical, which requires an additional 5D flavor structure, see e.g. [138].

[40] The exact fermion profiles for three family generations are given by (2.28).

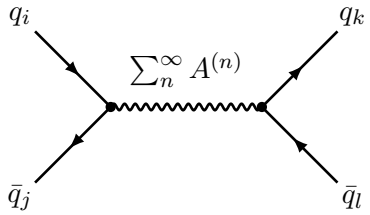

Figure 1.8: Tree-level diagram of four external fermions with flavor indices i, j, k, l that exchange a bulk photon, which can be decomposed into the SM photon and a tower of massive KK modes. The zero mode ($n = 0$), which is identified with the SM photon, has a flat profile such that FCNC processes are forbidden. Massive KK modes ($n \geq 1$) have non-flat profiles and allow for FCNC transitions at each of the two vertices.

given approximately by ($q = u, d$)

$$m_{q_i} \approx \frac{v}{\sqrt{2}} |Y_q| \, |F(c_{Q_i})| \, |F(c_{q_i})| \,, \tag{1.50}$$

where Y_q denotes a typical entry of the 5D Yukawa matrix $\boldsymbol{Y}_q$.[41] We can assume anarchic 5D Yukawa matrices where each entry has a magnitude of $\mathcal{O}(1)$ with an arbitrary complex phase, since the presence of the zero-mode profiles in (1.50) are sufficient to generate the required hierarchies observed in the quark-mass spectrum. The bulk-mass parameters for the $SU(2)_L$ doublets are denoted by c_{Q_i} and for the $SU(2)_L$ singlets by c_{q_i}. In order to correctly reproduce the quark masses (1.50) we have to properly adjust them. It will turn out to be sufficient to choose values in the range $-1 < c_{Q_i,q_i} < 1$ in order to generate the hierarchies. Figure 1.7 shows qualitatively the geometrical localization of the quark profiles along the extra-dimension. Light quarks are assigned values in the range $c_{Q_i,q_i} < -1/2$ which localize the corresponding profiles near the UV brane. The profiles of heavier quarks must have a larger overlap with the IR brane. The (right-chiral) singlet profile of the top quark is localized most closely to the IR brane.

Let us summarize the above findings. In the RS model all fundamental parameters in the fermion sector, the entries of the 5D Yukawa matrices and the bulk-mass parameters, can be chosen to have (absolute) values of order one. Small variations in the bulk-mass parameters determine the geometric localization of the fermion profiles along the extra-dimensions, and thus the overlap with the IR brane. And this overlap determines the size of the effective 4D Yukawa coupling which is responsible for the generation of the quark masses.

The fermion localization has important consequences on couplings between one gauge boson and two fermions. Especially interesting are FCNC processes which are severely constrained by experimental studies. Contrary to the SM, FCNC processes in the RS model are already possible at tree-level, see for instance the diagram in Figure 1.8 exchanging a bulk photon. Let us consider four external $SU(2)_L$ singlet quarks with flavor indices i, j, k, l. Neglecting the external quark spinors the corresponding amplitude is proportional to (in Feynman 't Hooft gauge)

$$\mathcal{A}_{ijkl} \sim \frac{e_5^2}{2\pi r} \int_\epsilon^1 \frac{dt}{t} \int_\epsilon^1 \frac{dt'}{t'} \, \chi^\Psi_{i,R}(t) \, \chi^\Psi_{j,R}(t) \sum_{n=0}^{\infty} \frac{\chi^A_n(t) \, \chi^A_n(t')}{m^2_{A_n} - p^2} \, \chi^\Psi_{k,R}(t') \, \chi^\Psi_{l,R}(t') \,, \tag{1.51}$$

where e_5 is the 5D electromagnetic gauge coupling. The infinite sum in (1.51) is part of the 5D photon propagator, which will be calculated among other 5D propagators in

[41] The exact dependence of the quark masses on the entries of the Yukawa matrices is given by (2.32).

Chapter 3. At low energies we can expand this expression for $|p^2| \ll M_{\rm KK}^2$ and obtain

$$\sum_{n=0}^{\infty} \frac{\chi_n^A(t)\,\chi_n^A(t')}{m_{A_n}^2 - p^2} = -\frac{1}{2\pi p^2} + \frac{1}{4\pi M_{\rm KK}^2}\left[L t_<^2 - t^2\left(\frac{1}{2} - \ln t\right) - t'^2\left(\frac{1}{2} - \ln t'\right) + \frac{1}{2L} + \mathcal{O}\left(\frac{p^2}{M_{\rm KK}^2}\right)\right], \tag{1.52}$$

which has been first derived by using a recursive approach [132]. The result can also be obtained by expanding the exact expression (3.23) for small momenta. The first term on the right side of (1.52) stems from the exchange of the photon zero mode and is independent of the t, t' coordinates, since the zero-mode profile is flat. Inserting this term into the amplitude (1.51) we can apply twice the orthonormality condition (1.35) of fermions for t and t', which implies that only the combination $i = j$ and $k = l$ yields a non-zero contribution. In other words, FCNC transitions are forbidden for the photon zero mode due to its flat profile. The remaining terms in (1.52) stem from the exchange of massive KK modes. Terms that depend only on t or t' can lead to a flavor change at one of the two vertices, while the other vertex remains flavor diagonal. Such processes are referred to as $\Delta F = 1$ transitions. Flavor changes at both vertices can be induced by the term proportional to $t_<^2 \equiv \min(t^2, t'^2)$ and are called $\Delta F = 2$ transitions. The next step is to determine the size of the FCNC couplings. As an example, we consider the term proportional to t^2 in (1.52) which is integrated together with the fermion profiles in (1.51). Using (1.47) for the profiles the corresponding overlap integral reads

$$\frac{\pi}{L}\int_\epsilon^1 \frac{dt}{t}\, t^2\, \chi_{i,R}^\Psi(t)\,\chi_{j,R}^\Psi(t) \sim F(c_{q_i})\,F(c_{q_j})\,, \tag{1.53}$$

where the right-hand side sets the size of the integral provided that $c_{q_i} + c_{q_j} > -3$. The latter condition is fulfilled for all RS points, since $c_{Q_i,q_i} > -1$. Thus, the size of the overlap integral depends on the localization of the fermions along the extra dimension. One can derive analogous relations like (1.53) for the overlap integrals including the remaining t, t'-dependent terms, see [132, 139, 140]. The fact that overlap integrals with light fermions are automatically suppressed by their localization near the UV brane is referred to as the *RS-GIM mechanism*, see Figure 1.9 for a qualitative description. One important reason why this works is that the bracket in (1.52) includes only non-negative powers of t and t', which implies that the tower of massive KK modes is either delocalized (the constant term) or localized near the IR brane.

It turns out that the RS-GIM mechanism is very successful in suppressing corrections to FCNC processes in the RS model such that many observables are in agreement with experimental measurements for KK scales of a few TeV, or equivalently the first KK-gluon mass in the multiple TeV range [132, 140, 142–146].[42] Still, there are some exceptions. For instance, corrections to the $Zb_L\bar{b}_L$ coupling can be large since the left-chiral bottom quark profile is localized close to the IR brane, which implies that the zero-mode profile $F(c_{b_L})$ is in general not suppressed. One can suppress the $Zb_L\bar{b}_L$ coupling by embedding the SM quarks into a $SU(2)_L \times SU(2)_R$ model, where the left-chiral bottom quark is symmetric under the exchange of $SU(2)_L$ and $SU(2)_R$ [147, 148]. Such a model will be discussed in more detail in Section 2.4. Another important observable in the RS model is ϵ_K that measures CP violation in the neutral kaon sector (K^0-$\bar{K}^0$

[42] In general, RS corrections to the observables in the flavor sector depend on the 5D parameters in the fermion sector, i.e. on the distribution of the bulk-mass parameters and the structure of the Yukawa matrices. Therefore, one cannot formulate stringent bounds on the KK scale.

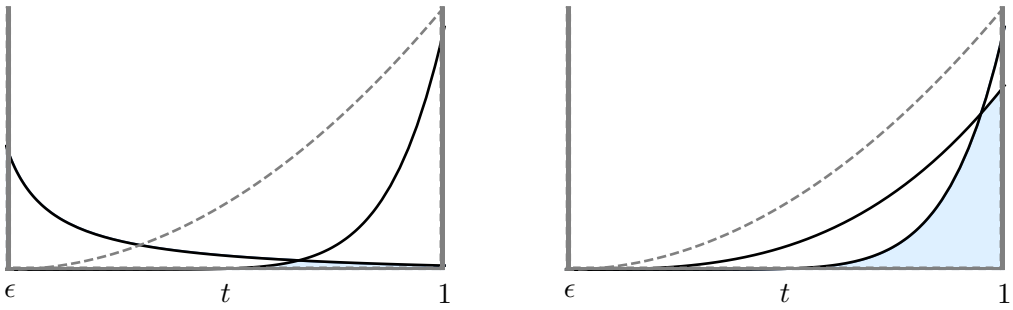

Figure 1.9: Qualitative illustration of the RS-GIM mechanism based on the description in [141]. In both plots the dashed line represents the t^2-term in (1.52) which indicates that the massive KK modes are localized near the IR brane. The left plot shows two fermion profiles, one localized near the UV brane and the other close to the IR brane. The size of the overlap integral (1.53) is indicated by the area shaded in light blue. The overlap region is much larger when both fermions are close to the IR brane as shown in the right plot.

mixing) [132, 144, 145, 149, 150]. Large RS corrections to the SM prediction can be induced due to a strong chiral enhancement of the Wilson coefficient of the four-quark operator $Q_4 = (\bar{d}_R s_L)(\bar{d}_L s_R)$, after performing the RG running from the KK scale down to the meson mass. Accepting a moderate fine-tuning KK-gluon masses in the range of $(10 - 20)$ TeV are required to mitigate the tension [140, 144]. In order to relax the constraints arising from the ϵ_K parameter one possibility is to extend the strong-interaction gauge group in the bulk by an additional $SU(3)$, and then break the enlarged symmetry to QCD via appropriate boundary conditions. Such a scenario was investigated in my diploma thesis [151] and published in [141, 152], with the result that the lower bound to the first KK-gluon mass could be reduced to roughly 5 TeV. Other approaches to mitigate the tension make use either of horizontal symmetries [153, 154], flavor alignment [155] or by moving the Higgs sector into the bulk [156]. Another constraint arises from the RS corrections to the *neutron electric dipole moment* (EDM), which have been estimated in [142, 143] leading to a first KK-gluon mass in the range of 10 TeV. Moreover, since the RS model is an effective field theory one can write down (non-renormalizable) four fermion operators mediating proton decay. However, when implementing discrete symmetries, for instance lepton number conservation to forbid operators of the type $q_1 q_2 q_3 l$, proton decay can be sufficienty suppressed [157, 158].

1.4.5 The Higgs-sector localization

In this thesis the primary focus lies on RS models with a Higgs sector localized on and very near the IR brane. There are two implementations of the Higgs sector which are referred to as the so-called brane-localized and the narrow bulk-Higgs scenarios. The reason for this distinction was first understood after calculating the one-loop triangle diagram for Higgs production via gluon fusion in the RS model, which is one of the main results of this thesis. Chapter 4 contains a comprehensive discussion of this point. Later it was realized that treating the Higgs boson as a general 5D field propagating in the extended bulk of the extra dimension [119, 133, 159–162] does not spoil the solution to the gauge-hierarchy problem. While the latter implementation of the Higgs sector seems to be more natural in the sense that all fields are now treated as genuinely five-dimensional the brane-localized and narrow bulk-Higgs scenarios can be treated as important benchmark models which should be considered first. In addition, the localization of the Higgs

on and near the IR brane allows to obtain closed analytic expressions for the results in Higgs production and decay and also for certain contributions in $b \to s\gamma$ transitions, both topics will be extensively covered in Chapters 4 and 5. A comprehensive study of the processes presented in the general set-up of a bulk-Higgs model is beyond the scope of this thesis.[43]

The brane-localized Higgs scenario can be defined in a general way which allows for a non-zero width of the Higgs profile, as long as it cannot be resolved by the modes of the RS model and hence does not affect any observables. We recall that RS models are EFTs with an inherent, position-dependent UV cutoff given by the warped Planck scale [126–130]

$$\Lambda_{\rm UV}(t) \sim M_{\rm Pl}\, e^{-\sigma(\phi)} = M_{\rm Pl}\,\frac{\epsilon}{t} \equiv \frac{\Lambda_{\rm TeV}}{t}\,. \tag{1.54}$$

This accounts for the fact that they do not provide a description of quantum gravity. The variation of the UV cutoff along the extra dimension is a crucial feature in order for RS models to provide a solution to the gauge-hierarchy problem, see Section 1.4.1. If the sector of electroweak symmetry breaking lives on or near the IR brane at $t = 1$, then the effective UV cutoff regularizing quantum corrections to the scalar sector is of order $\Lambda_{\rm TeV} \sim 10\, M_{\rm KK}$. As mentioned earlier the little hierarchy problem is not addressed by RS models, because the theory must contain several KK modes below the cutoff (and hence the value of $\Lambda_{\rm TeV}$ must be in the multi-TeV range). The scale $\Lambda_{\rm TeV}$ also provides the effective UV cutoff in loop graphs involving Higgs bosons. The condition that the modes in the effective theory cannot resolve the width of the Higgs-boson profile can be stated as

$$\eta \ll \frac{v|Y_q|}{\Lambda_{\rm TeV}} \quad \text{(brane-localized Higgs)}\,, \tag{1.55}$$

where $|Y_q|$ sets the scale for the dimensionless 5D Yukawa couplings of the model. The parameter η is understood as the width of the Higgs profile along the extra dimension that extends from the IR brane into the bulk. Only if condition (1.55) is satisfied, the Higgs field can be regarded as being localized on the IR brane in the sense that any possible extension into the bulk does not give rise to observable effects. This scenario is referred to as the *brane-localized Higgs* scenario. Relation (1.55) should be considered as a condition on the regulator η at fixed, physical UV cutoff $\Lambda_{\rm TeV}$. For a brane-localized Higgs field one should take the limit $\eta \to 0$ wherever possible, but the above condition states that keeping η finite but smaller than the bound on the right-hand side would not change the physics.

If the Higgs (zero mode) profile largely extends into the bulk such that the width fulfills the inequality $\eta > v|Y_q|/\Lambda_{\rm TeV}$, then we speak of bulk Higgs (zero mode). In this case we have to work with a five-dimensional Higgs field which decomposes into a Higgs zero mode and an infinite tower of Higgs KK modes.[44] In order to clarify the notation, for the remainder of this thesis we will always refer to the Higgs zero mode if not stated otherwise.[45] The Higgs profile can then be resolved by the high-momentum states in the effective theory. Moreover, the equivalent relation $\Lambda_{\rm TeV} > v|Y_q|/\eta$ shows that it is impossible in this case to take the limit $\eta \to 0$. This would send the cutoff to infinity, and thus the model would no longer provide a solution to the gauge-hierarchy problem. In the general case, results for amplitudes in the RS model with a bulk-Higgs

[43] Still, we will also discuss several aspects of the general bulk-Higgs model and will derive the profiles of the Higgs and gauge bosons, in Chapter 2, and the Higgs and $W^\pm$-boson 5D propagators in Chapter 3.

[44] We emphasize that Higgs KK modes are absent in the brane-localized Higgs scenario by construction, since their masses $m_{q_n} \sim M_{\rm KK}/\eta$ exceed the physical cutoff $\Lambda_{\rm TeV}$.

[45] For instance, when we speak of the Higgs profile we always mean the profile of the Higgs zero mode.

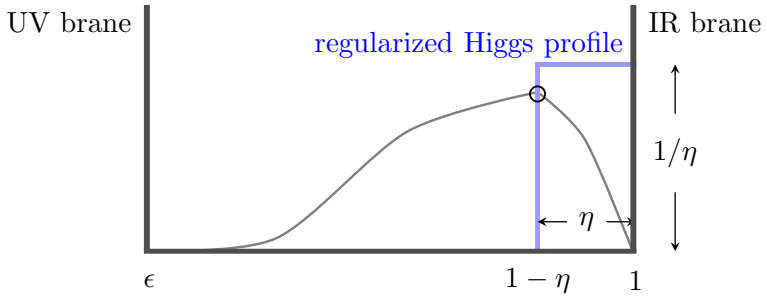

Figure 1.10: The presence of the rectangular regularization of the Higgs profile (1.58) splits the extra dimension into two regions $t \in [\epsilon, 1-\eta)$ and $t \in (1-\eta, 1]$. In each region one has to obtain solutions, e.g. for the fermion profiles and 5D propagators, which are supposed to match at $t = 1-\eta$. This is symbolically shown by the gray line and the black circle.

field depend in a complicated way on the shapes of the Higgs and fermion profiles along the extra dimension. However, for a narrow Higgs profile, defined by the relation

$$\frac{v|Y_q|}{\Lambda_{\rm TeV}} \ll \eta \ll \frac{v|Y_q|}{M_{\rm KK}} \quad \text{(narrow bulk Higgs)}, \tag{1.56}$$

model-independent expressions can be derived. Equation (1.56) defines the so-called *narrow bulk-Higgs* scenario. It will be shown in Chapters 4 and 5 that there can be different results obtained under the two assumptions (1.55) and (1.56), which are not connected to each other in a continuous way. Rather, one should consider the two scenarios as two different, distinguishable realizations of RS models. In this thesis, we take an agnostic point of view regarding the question which kind of RS model is theoretically most appealing. The overwhelming majority of the RS literature has been based on models in which the scalar sector is localized on the IR brane. These models should therefore be included as a benchmark in any phenomenological study.

Finally, we have to clarify how the regulator η is technically implemented when performing calculations. We point out that the brane-localized Higgs sector cannot be implemented in a well-defined way by a δ-function on the IR brane $\delta(t-1)$. For consistency reasons it is important that one can integrate by parts in the 5D action without encountering boundary terms. Otherwise the Lagrangian would not be hermitian. Usually this feature is ensured by the Z_2-parity assignments to the 5D fields, which imply that Z_2-odd profiles must vanish at the IR brane $t = 1$. However, the presence of the δ-function $\delta(t-1)$ would lead to discontinuities of some of the fermion profiles at $t = 1$, see the discussion below equation (2.21). One possibility to solve this ambiguity is to move the δ-function into the bulk such that

$$\delta(t-1) \to \delta(t-1+\eta)\,; \qquad\qquad \eta \ll 1\,. \tag{1.57}$$

The consequence is that the profiles now have discontinuities at $t = 1-\eta$. At the end of calculations the results are then obtained by taking the limit $\eta \to 0$. However, for the analysis in this thesis we will take a different approach and work with the regularized version of the δ-function denoted as $\delta^\eta(t-1)$. For the calculations we implement a square box of width η and height $1/\eta$, such that

$$\delta^\eta(t-1) \to \frac{1}{\eta}\,\theta(t-1+\eta)\,, \qquad \text{with} \qquad \eta \ll 1\,, \tag{1.58}$$

where $\theta(t)$ denotes the Heaviside step function. The regularized δ-function is normalized to 1 when integrated over the bulk of the extra dimension. Figure 1.10 shows a visualization of the function (1.58) which is marked as the regularized Higgs profile. The advantage of using (1.58) instead of (1.57) is that the regularization prescription can be connected to both brane-localized and narrow bulk-Higgs scenarios, as defined via the relations (1.55) and (1.56). We emphasize that the shape of the regularized profile is irrelevant for the physical results as long as $\eta \ll 1$.

2 Phenomenological models with one warped extra dimension

This chapter will introduce different versions of the RS model. We will limit the discussion to the basic ingredients and formulas which are necessary to perform the calculations and the phenomenological analyses in the subsequent chapters. In the first two sections we will discuss the *minimal RS model*, which is based on the SM gauge group $SU(3)_c \times SU(2)_L \times U(1)_Y$. It describes the simplest extension of the SM incorporating one warped extra dimension. While we will mainly focus on the Higgs sector localized on or near the IR brane, as explained in Section 1.4.5, we will also discuss some aspects of the minimal RS model for the case of a bulk-Higgs field. In general the 5D action of the RS model can be parametrized by

$$S = \int d^4x \, \left(\mathcal{L}_{\text{Ferm}} + \mathcal{L}_{\text{Gauge}} + \mathcal{L}_{\text{Higgs}} + \mathcal{L}_{\text{Yuk}} + \mathcal{L}_{\text{GF}} + \mathcal{L}_{\text{FPG}} \right) , \tag{2.1}$$

which includes kinetic terms for the fermions and gauge bosons, the Higgs and Yukawa sectors, and the gauge-fixing and Faddeev-Popov ghost terms. The discussion of the Lagrangian terms in Sections 2.1 and 2.2 is based on the content of [132], but we will use a more convenient notation. After that we will present the extension for a bulk-Higgs field in Section 2.3, which I have worked out, and which is based on our publications [2, 163]. One disadvantage of the minimal RS model is that it is in tension with some of the electroweak precision observables, especially with the Peskin-Takeuchi T parameter. As a consequence, we will consider in Section 2.4 the *custodial RS model* which is based on an enlarged gauge symmetry $SU(3)_c \times SU(2)_L \times SU(2)_R \times U(1)_X$, where the additional gauge group $SU(2)_R$ protects the T parameter from excessive corrections in this model. The details presented here are based on [149]. In the last section we will discuss the parameter space of the RS model and explain the generation of *RS points*, which will be important when we numerically compare the RS predictions with experimental measurements in Chapters 4 and 5. The procedure for generating RS points is based on a modified version of the algorithm that was first implemented in [132]. Finally, we will discuss tree-level corrections to the Peskin-Takeuchi parameters S, T, U in the minimal and custodial RS model. The analysis will allow us to derive universal bounds on the KK scale which are independent of the Yukawa matrices and the fermion bulk-mass parameters. This last part is based on an updated analysis of [164].

2.1 Higgs and gauge-boson sector

We begin with the minimal RS model where the Higgs sector is localized on or near the IR brane. Here, the SM gauge group $SU(3)_c \times SU(2)_L \times U(1)_Y$ lives in the bulk and gets broken to $SU(3)_c \times U(1)_{\text{EM}}$ on the IR brane, where the Higgs field develops

a vev. All gauge bosons are allowed to propagate in the bulk, i.e. in the 5D framework we deal with the 5D photon $A_M(x,t)$, the gluon $G_M(x,t)$, the $W^\pm$ boson $W_M^\pm(x,t)$ and the Z boson $Z_M(x,t)$. We can decompose the 5D fields into 4D mass eigenstates such that[1] ($B = A, G, Z, W^\pm$) [132]

$$B_\mu(x,t) = \frac{1}{\sqrt{r}} \sum_n B_\mu^{(n)}(x)\, \chi_n^B(t)\,, \quad B_5(x,t) = -\frac{1}{\sqrt{r}} \sum_n \frac{kt}{m_{B_n}} \varphi_B^{(n)}(x)\, \partial_t \chi_n^B(t)\,, \tag{2.2}$$

where $B_\mu^{(n)}$ is the n^{th} KK gauge boson with profile χ_n^B and mass m_{B_n}. We emphasize that each 5D field has the mass dimension $[B_M] = 3/2$ when the kinetic terms are canonically normalized, which is the reason for the factor $1/\sqrt{r}$ in (2.2). The scalar particles $\varphi_W^{\pm(n)}, \varphi_Z^{(n)}$ are "unphysical" in the sense that they provide the longitudinal degrees of freedom of the $W^\pm$, Z bosons ($n = 0$) and their KK modes ($n \geq 1$). Similarly the scalar particles $\varphi_A^{(n)}$ and $\varphi_G^{(n)}$ provide the longitudinal degrees of freedom for the photon and gluon KK modes.

We continue with the Higgs sector. The corresponding Lagrangian follows from (1.6) in the SM by localizing it via the regularized δ-function (1.58) at the IR brane, such that

$$\mathcal{L}_{\text{Higgs}} = \int_\epsilon^1 \frac{dt}{t} \sqrt{|G|}\, \delta^\eta(t-1) \left[G^{\mu\nu} (D_\mu \Phi)^\dagger (D_\nu \Phi) + \mu^2 \Phi^\dagger \Phi - \lambda \left(\Phi^\dagger \Phi \right)^2 \right], \tag{2.3}$$

where μ is the 5D Higgs-mass parameter and λ is the 5D quartic coupling. Furthermore, $\sqrt{|G|} = (\epsilon/t)^4$ is the square root of the determinant of the RS metric (1.46) in t-notation. After EWSB we can parametrize the Higgs doublet by

$$\Phi(x) = \frac{1}{\epsilon\sqrt{2}} \begin{pmatrix} -i\sqrt{2}\varphi^+(x) \\ v + h(x) + i\varphi^3(x) \end{pmatrix}, \tag{2.4}$$

where the factor $1/\epsilon$ is introduced in order to obtain canonically normalized kinetic terms. Here, $\varphi^\pm$ and φ^3 are the NGBs, h is the physical Higgs boson and $v = \epsilon\mu/\sqrt{\lambda}$ denotes the vev in the RS model. We determine the value of v from the shift to the Fermi constant G_F which can be derived in the RS model by considering (at tree level) the effect of the exchange of the infinite tower of KK $W^\pm$ bosons on the rate for muon decay. It differs from the SM value $(\sqrt{2}G_F)^{-1/2} \approx 246\,\text{GeV}$ by a small amount, see (2.94) for the precise relation. The scalar fields $\varphi^\pm$ and φ^3 in (2.4) are the NGBs which mix with the fifth components of the gauge fields $W_5^\pm$ and Z_5. This point can be seen by decomposing the NGBs into the mass eigenstates $\varphi_W^{\pm(n)}$ and $\varphi_Z^{(n)}$, such that [132]

$$\begin{aligned} \varphi^\pm(x) &= \sum_n \frac{\tilde{m}_W}{m_{W_n}} \sqrt{2\pi}\, \chi_n^W(1)\, \varphi_W^{\pm(n)}(x)\,; & \tilde{m}_W &\equiv \frac{g_5}{\sqrt{2\pi r}} \frac{v}{2}\,, \\ \varphi^3(x) &= \sum_n \frac{\tilde{m}_Z}{m_{Z_n}} \sqrt{2\pi}\, \chi_n^Z(1)\, \varphi_Z^{(n)}(x)\,; & \tilde{m}_Z &\equiv \sqrt{\frac{g_5^2 + g_5'^2}{2\pi r}} \frac{v}{2}\,, \end{aligned} \tag{2.5}$$

where g_5 and g_5' are the 5D gauge couplings of $SU(2)_L$ and $U(1)_Y$. We will see from (2.10) that $\tilde{m}_W$ and $\tilde{m}_Z$ are the leading contributions to the $W^\pm$- and Z-boson masses in an expansion in powers of v^2/M_{KK}^2. Furthermore, we will find that the profile of

[1] In case of the 5D $W^\pm$ boson we will denote the charged scalar particles as $\varphi_W^{\pm(n)}$ instead of $\varphi_{W^\pm}^{(n)}$ as suggested by equation (2.2). Furthermore, the profiles are denoted by χ_n^W without the $\pm$ superscript since the profiles coincide for positively and negatively charged W bosons.

the zero mode is flat up to corrections of order $v^2/M_{\rm KK}^2$, see (2.12). It then follows that $\sqrt{2\pi}\,\chi_n^{W,Z}(1)$ is close to one, and hence the fields $\varphi^\pm$, φ^3 coincide with $\varphi_W^{\pm(0)}$, $\varphi_Z^{(0)}$ to leading order. We mention that one can adjust the gauge-fixing Lagrangian so as to cancel any mixings between the vector and scalar fields. More details on the gauge-fixing procedure can be found in [132].

Now, let us turn to the 5D gauge couplings. We note that the covariant derivative in (2.3) is defined by

$$D_M = \partial_M - \frac{ig_5}{2\sqrt{2}}\left(\sigma^+ W_M^+ + \sigma^- W_M^-\right) - \frac{ig_5}{2\cos\theta_w} Z_M \left(\sigma^3 - 2Q\sin^2\theta_w\right) - ie_5 Q A_M\,, \tag{2.6}$$

where $\sigma^\pm \equiv \sigma^1 \pm i\sigma^2$, Q is the $U(1)_{\rm EM}$ charge, θ_w is the weak mixing angle and e_5 is the 5D electromagnetic gauge coupling. In the context of RS models the weak mixing angle can be expressed as $\sin^2\theta_w \equiv g_5'^2/(g_5^2 + g_5'^2)$, which can be studied experimentally via the Z-pole polarization asymmetries observed at the Large Electron-Positron (LEP) Collider. As in the SM the 5D electromagnetic and $SU(2)_L$ gauge couplings are related by $e_5 = g_5 \sin\theta_w$. We note that all 5D gauge couplings, including the QCD gauge coupling $g_{s,5}$, are dimensionful quantities with mass dimensions $[g_5] = [g_5'] = [e_5] = [g_{s,5}] = -1/2$. In case of the photon and the gluon we can obtain the corresponding 4D gauge couplings in the SM by $e \equiv e_5/\sqrt{2\pi r}$ and $g_s \equiv g_{s,5}/\sqrt{2\pi r}$ [165, 166], which follows from the flatness of the profiles of the photon and gluon zero modes. In case of the massive gauge bosons with non-flat profiles the corresponding gauge couplings to fermions receive corrections of order $v^2/M_{\rm KK}^2$, see (2.95). More details on the relation between the 5D gauge couplings with physical observables will be presented in Section 2.5.2.

Gauge-boson profiles and masses

When we insert the KK decomposition (2.2) into the 5D action for the gauge bosons we can derive the following EOM for the profiles ($B = A, G, Z, W$) [132]

$$\left(t\partial_t \frac{1}{t}\partial_t + x_{B_n}^2 \chi_n^B(t) - \delta^\eta(t-1)\,\frac{L\tilde{m}_B^2}{M_{\rm KK}^2}\right)\chi_n^B(t) = 0\,, \tag{2.7}$$

where $x_{B_n} \equiv m_{B_n}/M_{\rm KK}$. The δ-function is only present in case of the W- and Z-boson profiles and stems from the Higgs Lagrangian (2.3). Integrating the differential equation over a small interval around the coordinate $t = \epsilon$ we obtain the Neumann BC $\partial_t \chi_n^B(t)|_\epsilon = 0$ at the UV brane. We implement (1.58) for the regularized δ-function in (2.7). The presence of the regulator η splits the calculation into two regions $t < 1-\eta$ and $t > 1-\eta$. In the first region for $t < 1-\eta$ we can implement the UV BC and find $\chi_n^B(t) = N_n \sqrt{L/\pi}\, t\, (Y_0(x_n\epsilon)J_1(x_n t) - J_0(x_n\epsilon)Y_1(x_n t))$ with one coefficient N_n that remains to be determined. In the second region $t > 1-\eta$ we can take care of the BC $\partial_t \chi_n^B(t)|_1 = 0$ at the IR brane and obtain the solution $\chi_n^B(t) = \bar{N}_n \sqrt{L/\pi}\, t\, (K_0(\eta^{-1/2}S_n)I_1(\eta^{-1/2}S_n t) + I_0(\eta^{-1/2}S_n)K_1(\eta^{-1/2}S_n t))$ with the coefficient $\bar{N}_n$ and the abbreviation $S_n \equiv (L\,\tilde{m}_B^2/M_{\rm KK}^2 - \eta x_{B_n}^2)^{1/2}$. We can fix one of the remaining two coefficients by demanding continuity of both solutions at $t = 1-\eta$. The last coefficient can be numerically fixed by imposing the orthonormality condition [132, 165, 166]

$$\frac{2\pi}{L}\int_\epsilon^1 \frac{dt}{t}\,\chi_m^B(t)\,\chi_n^B(t) = \delta_{mn}\,, \tag{2.8}$$

which then provides a solution to the gauge-boson profiles for finite values of η.

In fact, we are more interested in the limit of very small values of $\eta \ll 1$, for which we can derive closed analytic solutions. Integrating the differential equation (2.7) along the interval $[1-\eta, 1]$ and sending then $\eta \to 0$ we can derive the *modified BC* at the IR brane [132]

$$\partial_t \chi_n^{W,Z}(t)\big|_{t=1^-} \equiv \lim_{\eta \to 0^+} \partial_t \chi_n^{W,Z}(t-\eta) = -\frac{L\tilde{m}_{W,Z}^2}{M_{\rm KK}^2} \chi_n^{W,Z}(1)\,, \tag{2.9}$$

which is considered as a limiting procedure. Since the derivative $\partial_t \chi_n^{W,Z}$ is a Z_2-odd function and must vanish exactly at $t = 1$ by symmetry arguments, the modified BC (2.9) implies that $\partial_t \chi_n^{W,Z}$ is discontinuous at the IR brane $t = 1$. In other words the profiles $\chi_n^{W,Z}$ have a kink at $t = 1$, which means that they are not continuously differentiable at that point. In case of the photon and gluon profiles the absence of brane-localized terms in the EOMs (2.7) implies that $\partial_t \chi_n^{A,G}(t)|_{t=1} = 0$ can be unambiguously imposed at the IR brane. As a consequence the profiles $\chi_n^{A,G}$ are continuously differentiable at $t = 1$. The IR BCs of the profiles can be used to determine the mass eigenvalues m_{B_n}. At leading order in $v^2/M_{\rm KK}^2$ we find the following physical W- and Z-boson masses [132]

$$m_{W,Z}^2 = \tilde{m}_{W,Z}^2 \left[1 - \frac{\tilde{m}_{W,Z}^2}{2M_{\rm KK}^2}\left(L - 1 + \frac{1}{2L}\right) + \mathcal{O}\left(\frac{v^4}{M_{\rm KK}^4}\right)\right], \tag{2.10}$$

where $\tilde{m}_{W,Z}$ is defined in (2.5). Since the masses of the KK modes are determined by zeros of Bessel functions they admit an approximate equidistant spacing, such that $m_{B_{n+1}} \approx m_{B_n} + \pi M_{\rm KK}$ for $n \geq 1$. As already stated in (1.39) the mass of the first photon and gluon KK mode is given by $m_{A_1} = M_{g^{(1)}} = 2.45\, M_{\rm KK}$, with small deviations from this value in case of the first KK W- and Z-boson modes. Finally, we present the exact results for the gauge-boson profiles ($B = A, G, Z, W$) [132]

$$\chi_n^B(t) = N_n \sqrt{\frac{L}{\pi}}\, t\, c_n^+(t)\,, \tag{2.11}$$

with the linear combinations $c_n^+(t) = Y_0(x_n\epsilon)J_1(x_n t) - J_0(x_n\epsilon)Y_1(x_n t)$ and $c_n^-(t) = Y_0(x_n\epsilon)J_0(x_n t) - J_0(x_n\epsilon)Y_0(x_n t)$. The normalization constant is fixed and takes the value $N_n^{-2} = [c_n^+(1)]^2 + [c_n^-(1^-)]^2 - \frac{2}{x_n} c_n^+(1)\, c_n^-(1^-) - \epsilon^2 [c_n^+(\epsilon)]^2$ [132]. In later chapters we will need the profiles of the zero modes expanded in orders of $v^2/M_{\rm KK}^2$. Expanding (2.11) for $n = 0$ we obtain [132]

$$\begin{aligned} \chi_0^{A,G}(t) &= \frac{1}{\sqrt{2\pi}}\,, \\ \chi_0^{W,Z}(t) &= \frac{1}{\sqrt{2\pi}}\left[1 - \frac{m_{W,Z}^2}{2M_{\rm KK}^2}\left(t^2\left(L - \frac{1}{2} + \ln t\right) - \frac{1}{2} + \frac{1}{2L}\right) + \mathcal{O}\left(\frac{v^4}{M_{\rm KK}^4}\right)\right], \end{aligned} \tag{2.12}$$

where the photon and gluon profiles are exact. We see that the W- and Z-boson profiles receive corrections of order $v^2/M_{\rm KK}^2$ which is a consequence of the IR brane-localized term in (2.7) which stems from the Higgs sector (2.3).

2.2 Quark sector

The 5D quark Lagrangian contains the $SU(2)_L$ doublet $Q(x,t)$ and the two $SU(2)_L$ singlets $u(x,t)$ and $d(x,t)$, each of which are three-component vectors in generation space. The 5D fermion states can be described by four-component Dirac spinors [137, 157]. We use a compact notation, where we collect the left- and right-chiral components of the up- and down-type states into six-component vectors $\mathcal{U}_A = (U_A, u_A)^T$ and $\mathcal{D}_A = (D_A, d_A)^T$ with $A = L, R$, which are collectively referred to as $\mathcal{Q}_{L,R}$. Using this notation the quark Lagrangian can be expressed by

$$\mathcal{L}_{\text{Ferm}} = \int_\epsilon^1 \frac{dt}{t}\sqrt{|G|}\sum_{\mathcal{Q}=\mathcal{U},\mathcal{D}} \bar{\mathcal{Q}}(x,t)\left[i\partial\!\!\!/ - M_{\text{KK}}\gamma_5\partial_t - \frac{M_{\text{KK}}}{t}\begin{pmatrix}\boldsymbol{c}_Q & 0\\ 0 & -\boldsymbol{c}_q\end{pmatrix}\right]\mathcal{Q}(x,t)\,, \quad (2.13)$$

where $\mathcal{Q} = \mathcal{Q}_L + \mathcal{Q}_R$. Equation (2.13) contains the (dimensionless) bulk-mass parameters $\boldsymbol{c}_Q$ and $\boldsymbol{c}_q$ which are 3×3 matrices in generation space. It is always possible to choose a basis where these matrices are real and diagonal [132], which we will assume in the following. In this basis the Yukawa interactions read

$$\begin{aligned}\mathcal{L}_{\text{Yuk}} = -\int_\epsilon^1 \frac{dt}{t}\,\frac{M_{\text{KK}}}{2}\,\delta^\eta(t-1)\Big[&\bar{Q}_L(x,t)\,\Phi(x)\,\boldsymbol{Y}_d^{\text{5D}}\,d_R(x,t)\\ &+\bar{Q}_R(x,t)\,\Phi(x)\,\boldsymbol{Y}_d^{\text{5D}}\,d_L(x,t) + \epsilon_{ab}\,\bar{Q}_{a,L}(x,t)\,\Phi_b^\dagger(x)\,\boldsymbol{Y}_u^{\text{5D}}\,u_R(x,t)\\ &+\epsilon_{ab}\,\bar{Q}_{a,R}(x,t)\,\Phi_b^\dagger(x)\,\boldsymbol{Y}_u^{\text{5D}}\,u_L(x,t) + \text{h.c.}\Big]\,,\end{aligned} \quad (2.14)$$

where $\epsilon = i\sigma^2$ is two-dimensional Levi-Civita symbol with $\epsilon_{12} = 1$. Note that the entries of the Yukawa matrix $\boldsymbol{Y}_q^{\text{5D}}$ have negative mass dimension, $[(\boldsymbol{Y}_q^{\text{5D}})_{ij}] = -1$. Inserting the parametrization of the Higgs doublet (2.4) into (2.14), and neglecting the NGBs, we obtain

$$\mathcal{L}_{\text{Yuk}} = -\sum_{q=u,d}\int_\epsilon^1 dt\,\frac{v+h(x)}{\sqrt{2}}\,\delta^\eta(t-1)\,\bar{\mathcal{Q}}_L(x,t)\,\frac{k}{2}\begin{pmatrix}0 & \boldsymbol{Y}_q^{\text{5D}}\\ \boldsymbol{Y}_q^{\text{5D}\dagger} & 0\end{pmatrix}\mathcal{Q}_R(x,t) + \text{h.c.}\,. \quad (2.15)$$

Based on this equation it is convenient to define dimensionless Yukawa matrices ($q = u, d$) [137, 157]

$$\boldsymbol{Y}_q \equiv \frac{k}{2}\,\boldsymbol{Y}_q^{\text{5D}}\,, \quad (2.16)$$

where k is the curvature defined in (1.25). In this thesis we will assume that the Yukawa matrices, as defined in (2.16), exhibit an anarchical structure with $|(\boldsymbol{Y}_q)_{ij}| = \mathcal{O}(1)$. Note that we can generalize (2.14) and (2.15) by introducing two different Yukawa matrices $\boldsymbol{Y}_q^{\text{5D},C}$ and $\boldsymbol{Y}_q^{\text{5D},S}$ that couple to Z_2-even and Z_2-odd fields, respectively. In the literature the interaction terms with $\boldsymbol{Y}_q^{\text{5D},C}$ are often referred to as the *correct-chirality Higgs couplings*, since they are also present in the SM. The remaining interactions that involve $\boldsymbol{Y}_q^{\text{5D},S}$ couple right-chiral $SU(2)_L$ doublets with left-chiral $SU(2)_L$ singlets. Those terms are called the *wrong-chirality Higgs couplings* since they are absent in the SM. The distinction between $\boldsymbol{Y}_q^{\text{5D},C}$ and $\boldsymbol{Y}_q^{\text{5D},S}$ is only allowed in brane-localized Higgs scenarios, and would be forbidden by 5D Lorentz invariance for a generic bulk Higgs. However, since we can consider the brane-localized Higgs scenario as a special limit of the more general bulk-Higgs model we can motivate to set both Yukawa matrices equals to each

other.[2] Therefore, we will assume in the following that $\boldsymbol{Y}_q^{5\mathrm{D}} \equiv \boldsymbol{Y}_q^{5\mathrm{D},C} = \boldsymbol{Y}_q^{5\mathrm{D},S}$.

We continue with the decomposition of the 5D quark fields into KK mass eigenstates and profiles

$$\mathcal{Q}_A(x,t) = \sum_n \; \mathcal{Q}_A^{(n)}(t)\, q_A^{(n)}(x)\,; \qquad\qquad A = L, R\,, \tag{2.17}$$

where $\mathcal{Q}, q = (\mathcal{U}, u), (\mathcal{D}, d)$. The superscript n labels the different mass eigenstates $q_A^{(n)}$ in the effective 4D theory, such that $n = 1, 2, 3$ refer to the SM quarks, while $n = 4, \ldots, 9$ label the six fermion modes of the first KK level, and so on. The functions $\mathcal{Q}_{L,R}^{(n)}$ denote the profiles of the left- and right-chiral components of the n^{th} KK-mass eigenstate. The upper (lower) components of $\mathcal{Q}_A^{(n)}$ include the profiles of the $SU(2)_L$ doublet (singlet) quark fields. They can be parametrized by

$$\mathcal{Q}_L^{(n)}(t) = \sqrt{\frac{2\pi}{L\epsilon}} \begin{pmatrix} \boldsymbol{C}_n^Q(t)\, a_n^Q \\ \boldsymbol{S}_n^q(t)\, a_n^q \end{pmatrix}, \qquad \mathcal{Q}_R^{(n)}(t) = \sqrt{\frac{2\pi}{L\epsilon}} \begin{pmatrix} \boldsymbol{S}_n^Q(t)\, a_n^Q \\ \boldsymbol{C}_n^q(t)\, a_n^q \end{pmatrix}, \tag{2.18}$$

for $(\mathcal{Q}, Q, q) = (\mathcal{U}, U, u), (\mathcal{D}, D, d)$. Here, the Z_2-even profiles are denoted by $\boldsymbol{C}_n^{Q,q}(t)$ while $\boldsymbol{S}_n^{Q,q}(t)$ are Z_2-odd functions. They are diagonal 3×3 matrices in generation space with real-valued entries and they depend on the bulk-mass parameters $\boldsymbol{c}_Q$ and $\boldsymbol{c}_q$. The $SU(2)_L$ gauge symmetry implies that the $SU(2)_L$ doublet quark fields have the same profile functions $\boldsymbol{C}_n^Q \equiv \boldsymbol{C}_n^U = \boldsymbol{C}_n^D$ and $\boldsymbol{S}_n^Q \equiv \boldsymbol{S}_n^U = \boldsymbol{S}_n^D$. The 3-component complex-valued vectors $a_n^{U,u}$ and $a_n^{D,d}$ in (2.18) describe the flavor mixing of the 5D interaction states into 4D mass eigenstates which are generated by the Yukawa interaction. Switching off the Yukawa interactions, e.g. by taking the limit $v \to 0$, the vectors $a_n^{Q,q}$ become unit vectors and no flavor mixing occurs [132].

Quark profiles and masses

After inserting the KK decomposition (2.17) into the fermion action (2.13) we can derive the fermion EOMs for the left- and right-chiral profiles [132]

$$[\partial_t - \mathcal{M}_q(t)]\, \mathcal{Q}_L^{(n)}(t) = -x_{q_n}\, \mathcal{Q}_R^{(n)}(t)\,, \qquad [\partial_t + \mathcal{M}_q(t)]\, \mathcal{Q}_R^{(n)}(t) = x_{q_n}\, \mathcal{Q}_L^{(n)}(t)\,, \tag{2.19}$$

which are coupled first-order differential equations. The normalized masses are denoted by $x_{q_n} \equiv m_{q_n}/M_{\text{KK}}$. Equation (2.19) contains the *generalized mass matrix* ($q = u, d$)

$$\mathcal{M}_q(t) = \frac{1}{t} \begin{pmatrix} \boldsymbol{c}_Q & 0 \\ 0 & -\boldsymbol{c}_q \end{pmatrix} + \varrho\, \delta^\eta(t-1) \begin{pmatrix} 0 & \boldsymbol{Y}_q \\ \boldsymbol{Y}_q^\dagger & 0 \end{pmatrix}; \qquad \varrho \equiv \frac{v}{\sqrt{2} M_{\text{KK}}}\,, \tag{2.20}$$

which is a t-dependent 6×6 matrix. We emphasize that the regularized δ-function in (2.20) is necessary. A naive treatment of the δ-function would be mathematically not well-defined as was first pointed out in [167]. We can see this from the upper component of the second differential equation in (2.19) which explicitly reads

$$\left(\partial_t + \frac{1}{t}\boldsymbol{c}_Q\right) \boldsymbol{S}_n^Q(t)\, a_n^Q = x_{q_n} \boldsymbol{C}_n^Q(t)\, a_n^Q - \varrho\, \delta^\eta(t-1)\, \boldsymbol{Y}_q\, \boldsymbol{C}_n^q(t)\, a_n^q\,. \tag{2.21}$$

[2] In Chapter 4 we will also comment on the possibility of two different Yukawa matrices $\boldsymbol{Y}_q^{5\mathrm{D},C}$ and $\boldsymbol{Y}_q^{5\mathrm{D},S}$ in the brane-localized Higgs scenario. We will find find that the leading effects of the results for the loop-induced processes $gg \to h$ and $h \to \gamma\gamma$ depend only on the Yukawa matrices of the correct-chirality Higgs couplings.

Integrating (2.21) along infinitesimal intervals around the IR brane at $t = 1$ the presence of the naive δ-function on the right side would lead to a non-zero value for the fermion profile $\boldsymbol{S}_n^Q(t)$ at the IR brane. But this is in conflict with the BC $\boldsymbol{S}_n^Q(1) = 0$, which follows from the Z_2-odd parity of the profile. We mention that one can also treat the Yukawa interactions as perturbations and solve the free EOMs [137, 157, 158, 168–170]. Still, when rotating into the mass basis the Yukawa interactions are included and a regularization procedure has to be applied. In order to solve the ambiguity, one possibility is to move the δ-function into the bulk using the prescription (1.57), which implies that the Z_2-odd profiles are discontinuous at $t = 1 - \eta$ [171]. However, we focus on the other prescription where the δ-function is regularized by a box-shaped function, see (1.58). In the following we derive solutions with an exact dependence on the Yukawa matrices [132, 149, 157, 167, 172]. The presence of the regulator splits the fifth dimension into two regions $t \in [\epsilon, 1-\eta)$ and $t \in (1-\eta, 1]$. Instead of deriving the full solution in both regions we will focus on the latter region in order to correctly determine the (modified) IR BCs for the profiles. Then, we will use the IR BCs to determine the quark profiles in the brane-localized Higgs scenario with η sent to zero.

We begin with the region $t > 1 - \eta$ where we can replace $\delta^\eta(t-1)$ by $1/\eta$ in the generalized mass matrix (2.20). We assume that η is small enough such that the Yukawa term dominates over the bulk-mass term, which imposes the condition $\eta \ll v|Y_q|/M_{\text{KK}}$. Note that this upper bound on η is part of the definition of the narrow bulk-Higgs scenario (1.56) in Section 1.4.5. Then, based on the EOMs (2.19) we can derive the second-order differential equations ($t > 1 - \eta$)

$$\left[\partial_t^2 - \frac{1}{\eta^2}\begin{pmatrix} \boldsymbol{X}_q^2 - \eta^2 x_{q_n}^2 & 0 \\ 0 & \bar{\boldsymbol{X}}_q^2 - \eta^2 x_{q_n}^2 \end{pmatrix}\right] \mathcal{Q}_A^{(n)}(t) = 0\,; \qquad A = L, R\,, \tag{2.22}$$

where we introduced positive, hermitian 3×3 matrices ($q = u, d$)

$$\boldsymbol{X}_q \equiv \varrho\sqrt{\boldsymbol{Y}_q \boldsymbol{Y}_q^\dagger}\,, \qquad\qquad \bar{\boldsymbol{X}}_q \equiv \varrho\sqrt{\boldsymbol{Y}_q^\dagger \boldsymbol{Y}_q}\,. \tag{2.23}$$

The square root is understood in terms of its series representation. General solutions to (2.22) are given by the trigonometric functions

$$\mathcal{S}(t) \equiv \sinh\left(\boldsymbol{S}_{q_n}\frac{1-t}{\eta}\right)\,, \quad \mathcal{C}(t) \equiv \cosh\left(\boldsymbol{S}_{q_n}\frac{1-t}{\eta}\right)\,; \quad \boldsymbol{S}_{q_n} \equiv \sqrt{\boldsymbol{X}_q^2 - \eta^2 x_{q_n}^2}\,. \tag{2.24}$$

Moreover, we need the functions $\bar{\mathcal{S}}(t)$ and $\bar{\mathcal{C}}(t)$ which are defined like $\mathcal{S}(t)$ and $\mathcal{C}(t)$ with $\bar{\boldsymbol{X}}_q$ instead of $\boldsymbol{X}_q$. With the help of the Neumann (Dirichlet) BCs of the Z_2-even (-odd) profiles at the IR brane we can obtain the solutions

$$\mathcal{Q}_L^{(n)}(t) = \begin{pmatrix} \frac{\mathcal{C}(t)}{\mathcal{C}(1_\eta)} & 0 \\ 0 & \frac{\bar{\mathcal{S}}(t)}{\mathcal{S}(1_\eta)} \end{pmatrix} \mathcal{Q}_L^{(n)}(1_\eta)\,, \qquad \mathcal{Q}_R^{(n)}(t) = \begin{pmatrix} \frac{\mathcal{S}(t)}{\mathcal{S}(1_\eta)} & 0 \\ 0 & \frac{\bar{\mathcal{C}}(t)}{\mathcal{C}(1_\eta)} \end{pmatrix} \mathcal{Q}_R^{(n)}(1_\eta)\,, \tag{2.25}$$

where $1_\eta \equiv 1 - \eta$. They depend on two coefficients $\mathcal{Q}_L^{(n)}(1_\eta)$ and $\mathcal{Q}_R^{(n)}(1_\eta)$, which need to be determined from the continuity condition at $t = 1 - \eta$. At this point we make another assumptions that $\eta \ll v|Y_q|/m_{q_n}$, which implies that we can neglect the mass-dependent terms such that $\boldsymbol{S}_{q_n} \to \boldsymbol{X}_q$. Thus, inserting the solutions (2.25) into the first-order differential equations we obtain the modified BCs at the IR brane

$$\begin{pmatrix} \varrho\tilde{\boldsymbol{Y}}_q^\dagger & 1 \end{pmatrix} \mathcal{Q}_L^{(n)}(1^-) = 0\,, \qquad\qquad \begin{pmatrix} 1 & -\varrho\tilde{\boldsymbol{Y}}_q \end{pmatrix} \mathcal{Q}_R^{(n)}(1^-) = 0\,, \tag{2.26}$$

which are understood as a limiting procedure for $\eta \to 0$. The limiting procedure is important since the Z_2-odd profiles in the lower (upper) components of $\mathcal{Q}_L^{(n)}$ ($\mathcal{Q}_R^{(n)}$) are discontinuous at $t = 1$. In (2.26) we introduced the *modified Yukawa matrix*

$$\tilde{\boldsymbol{Y}}_q \equiv \frac{\tanh \boldsymbol{X}_q}{\boldsymbol{X}_q} \boldsymbol{Y}_q \,, \tag{2.27}$$

that differs from the original Yukawa matrix $\boldsymbol{Y}_q$ by corrections of order $v^2/M_{\rm KK}^2$. In the limit $\eta \to 0$, the EOMs (2.19) together with the UV and the modified IR BCs (2.26) are solved exactly by [132]

$$\begin{aligned} \mathcal{Q}_L^{(n)}(t) &= \sqrt{2t} \begin{pmatrix} N_n(\boldsymbol{c}_Q)\, f_n^+(t,\boldsymbol{c}_Q)\, a_n^Q \\ -N_n(\boldsymbol{c}_q)\, f_n^-(t,\boldsymbol{c}_q)\, a_n^q \end{pmatrix} , \\ \mathcal{Q}_R^{(n)}(t) &= \sqrt{2t} \begin{pmatrix} N_n(\boldsymbol{c}_Q)\, f_n^-(t,\boldsymbol{c}_Q)\, a_n^Q \\ N_n(\boldsymbol{c}_q)\, f_n^+(t,\boldsymbol{c}_q)\, a_n^q \end{pmatrix} , \end{aligned} \tag{2.28}$$

for $\mathcal{Q}, Q, q = (\mathcal{U}, U, u), (\mathcal{D}, D, d)$ and with the linear combination of Bessel functions $f_n^\pm(t,c) = J_{-1/2-c}(x_n\epsilon)\, J_{\mp 1/2+c}(x_n t) \pm J_{1/2+c}(x_n\epsilon)\, J_{\pm 1/2-c}(x_n t)$. For the special case of $(c + 1/2) \in \mathbb{N}$, the correct solutions have to be obtained by a limiting procedure. The orthonormality condition of the fermion profiles [132]

$$\int_\epsilon^1 dt\, \mathcal{Q}_A^{(n)\dagger}(t)\, \mathcal{Q}_A^{(n')}(t) = \delta_{nn'} \,; \qquad\qquad A = L, R \,, \tag{2.29}$$

can be used to determine the normalization coefficient N_n in (2.28). One finds the result $N_n^{-2}(c) = [f_n^+(1,c)]^2 + [f_n^-(1,c)]^2 - 2c\, x_n^{-1} f_n^+(1,c) f_n^-(1,c) - \epsilon^2 [f_n^+(\epsilon,c)]^2$ [132]. The three-vectors $a_n^{Q,q}$ and the physical masses m_{q_n} can be determined from the modified IR BCs in (2.26).

We can derive approximate formulas for the SM quarks, since their masses are much smaller with respect to the KK scale, i.e. $m_{q_n} \ll M_{\rm KK}$ for $n = 1, 2, 3$. Expanding the profiles (2.28) in the limit $x_{q_n} \ll 1$ and working at zeroth order in $v^2/M_{\rm KK}^2$, we obtain ($n = 1, 2, 3$)

$$\begin{aligned} \mathcal{Q}_L^{(n)}(t) &\approx \begin{pmatrix} F(\boldsymbol{c}_Q)\, t^{\boldsymbol{c}_Q}\, \hat{a}_n^Q \\ -x_{q_n,0}\, F(\boldsymbol{c}_q)\, \frac{t^{1+\boldsymbol{c}_q} - \epsilon^{1+2\boldsymbol{c}_q} t^{-\boldsymbol{c}_q}}{1+2\boldsymbol{c}_q}\, \hat{a}_n^q \end{pmatrix} , \\ \mathcal{Q}_R^{(n)}(t) &\approx \begin{pmatrix} x_{q_n,0}\, F(\boldsymbol{c}_Q)\, \frac{t^{1+\boldsymbol{c}_Q} - \epsilon^{1+2\boldsymbol{c}_Q} t^{-\boldsymbol{c}_Q}}{1+2\boldsymbol{c}_Q}\, \hat{a}_n^Q \\ F(\boldsymbol{c}_q)\, t^{\boldsymbol{c}_q}\, \hat{a}_n^q \end{pmatrix} , \end{aligned} \tag{2.30}$$

where $x_{q_n,0} = m_{q_n,0}/M_{\rm KK}$. We refer to (2.30) as the quark profiles in the *zero-mode approximation* (ZMA). The function $F(c)$ has already been defined in (1.48) and is called the zero-mode profile. As discussed in Section 1.4.4 the size of the function is exponentially sensitive on small $\mathcal{O}(1)$ variations of the bulk-mass parameters, which allows to generate large hierarchies in the fermion sector. The zeroth-order masses $m_{q_n,0}$ and three-vectors $\hat{a}_n^{Q,q}$ in (2.30) can be inferred from the modified IR BCs. Inserting the profiles (2.30) into (2.26) we can derive the two equations [132]

$$\left(m_{q_n,0}^2 \mathbf{1} - \frac{v^2}{2} \boldsymbol{Y}_q^{\rm eff} \left(\boldsymbol{Y}_q^{\rm eff} \right)^\dagger \right) \hat{a}_n^Q = 0 \,, \quad \left(m_{q_n,0}^2 \mathbf{1} - \frac{v^2}{2} \left(\boldsymbol{Y}_q^{\rm eff} \right)^\dagger \boldsymbol{Y}_q^{\rm eff} \right) \hat{a}_n^q = 0 \,, \tag{2.31}$$

with the *effective Yukawa matrix* $\boldsymbol{Y}_q^{\rm eff} \equiv F(\boldsymbol{c}_Q)\, \tilde{\boldsymbol{Y}}_q\, F(\boldsymbol{c}_q)$ [132]. The masses $m_{q_n,0}$ are the (real) eigenvalues and the vectors $\hat{a}_n^{Q,q}$ are the eigenvectors of the equations in (2.31). We

can find analytical results for the SM masses [132]

$$\begin{aligned} m_u &= \frac{v}{\sqrt{2}} \frac{|\det(\boldsymbol{Y}_u)|}{(M_u)_{11}} |F(c_{Q_1})F(c_{u_1})|\,, & m_d &= \frac{v}{\sqrt{2}} \frac{|\det(\boldsymbol{Y}_d)|}{(M_d)_{11}} |F(c_{Q_1})F(c_{d_1})|\,, \\ m_c &= \frac{v}{\sqrt{2}} \frac{(M_u)_{11}}{(\boldsymbol{Y}_u)_{33}} |F(c_{Q_2})F(c_{u_2})|\,, & m_s &= \frac{v}{\sqrt{2}} \frac{(M_d)_{11}}{(\boldsymbol{Y}_d)_{33}} |F(c_{Q_2})F(c_{d_2})|\,, \\ m_t &= \frac{v}{\sqrt{2}} |(\boldsymbol{Y}_u)_{33}| |F(c_{Q_3})F(c_{u_3})|\,, & m_b &= \frac{v}{\sqrt{2}} |(\boldsymbol{Y}_d)_{33}| |F(c_{Q_3})F(c_{d_3})|\,, \end{aligned} \tag{2.32}$$

where $(M_q)_{ij}$ denotes the minor of $\boldsymbol{Y}_q$, i.e. the determinant of the square matrix formed by removing the i^{th} row and the j^{th} column from $\boldsymbol{Y}_q$. The formulas (2.32) justify the approximative equation (1.50). As already stated in Section 1.4.4 we find that the experimental mass hierarchies in the up- and down-type quark sector can be realized through the localization of the quark profiles in the bulk. This allows for a geometrical explanation of the mass splittings without relying on a hierarchical pattern in the 5D Yukawa matrices.

2.3 Extension to the RS model with a bulk-Higgs field

This section extends the previously discussed minimal RS model to a model in which the Higgs field and its vev have profiles along the extra dimension. The motivation is to relate the scenario of a strongly peaked Higgs and vev profile near the IR brane to the RS model with a brane-localized Higgs sector. The discussion follows the expositions given in [162, 173], but we will generalize these results in some aspects and use our own notation. The presented material is based on our publication [2].

Let us begin with the discussion of the bulk-Higgs sector. In contrast to (2.3) the Lagrangian for a bulk Higgs reads

$$\begin{aligned} \mathcal{L}_{\text{Higgs}} = \frac{2\pi r}{L} \int_\epsilon^1 \frac{dt}{t} \sqrt{|G|} \Big[& G^{MN} D_M \Phi^\dagger(x,t) D_N \Phi(x,t) - \mu^2 |\Phi(x,t)|^2 \\ & - \frac{M_{\text{KK}}}{2} V_{\text{UV}}(\Phi)\, \delta(t-\epsilon) - \frac{k}{2} V_{\text{IR}}(\Phi)\, \delta(t-1) \Big]\,, \end{aligned} \tag{2.33}$$

where μ provides a bulk mass for the scalar field. The scalar doublet $\Phi(x,t)$ is a 5D field with mass dimension $[\Phi] = 3/2$. The potentials localized on the UV and IR branes determine the BCs of the scalar fields and induce EWSB. They are chosen to be $V_{\text{UV}}(\Phi) = M_{\text{UV}} |\Phi|^2$ and $V_{\text{IR}}(\Phi) = -M_{\text{IR}} |\Phi|^2 + \lambda_{\text{IR}} |\Phi|^4$ with mass dimensions $[M_{\text{UV}}] = [M_{\text{IR}}] = 1$ and $[\lambda_{\text{IR}}] = -2$. The dimensionful parameters in the 5D action naturally scale with appropriate powers of M_{Pl}, and we find it useful to introduce dimensionless $\mathcal{O}(1)$ parameters by the rescalings $m_{\text{UV}} \equiv M_{\text{UV}}/(2k)$, $m_{\text{IR}} \equiv M_{\text{IR}}/(2k)$ and $\lambda \equiv \lambda_{\text{IR}}\, k/(4r)$. In analogy to (2.4) we parametrize the scalar doublet $\Phi(x,t)$ in the form

$$\Phi(x,t) = \frac{t}{\epsilon\sqrt{2r}} \begin{pmatrix} -i\sqrt{2}\varphi^+(x,t) \\ v(t) + h(x,t) + i\varphi_3(x,t) \end{pmatrix}, \tag{2.34}$$

where $v(t)$ denotes the profile of the Higgs vev along the extra dimension, $h(x,t)$ is the 5D physical Higgs scalar after electroweak symmetry breaking, and $\varphi^\pm(x,t)$, $\varphi_3(x,t)$ are 5D NGBs. For the following analysis we do not consider the NGBs any further. Integrating

by parts, the Lagrangian (2.33) can be rewritten in the form

$$\begin{aligned}\mathcal{L}_{\rm Higgs} = \frac{2\pi}{L}\int_\epsilon^1 \frac{dt}{t}\Bigg\{ &\frac{1}{2}\,\partial_\mu h(x,t)\,\partial^\mu h(x,t) + \frac{M_{\rm KK}^2}{2}\Bigg[\frac{v(t)+2h(x,t)}{t}\left(t^2\partial_t^2 + t\partial_t - \beta^2\right)\frac{v(t)}{t} \\ &+ \frac{h(x,t)}{t}\left(t^2\partial_t^2 + t\partial_t - \beta^2\right)\frac{h(x,t)}{t}\Bigg]\Bigg\} - \frac{\pi M_{\rm KK}^2}{L}\Bigg\{\frac{m_{\rm UV}}{\epsilon^2}\left[v(\epsilon)+h(x,\epsilon)\right]^2 \\ &+ \left[\frac{v(t)+2h(x,t)}{t^2}\,\partial_t\left[t\,v(t)\right] + \frac{h(x,t)}{t^2}\,\partial_t\left[t\,h(x,t)\right]\right]_{t=\epsilon^+}^{1^-} \\ &- m_{\rm IR}\left[v(1)+h(x,1)\right]^2 + \frac{\lambda}{M_{\rm KK}^2}\left[v(1)+h(x,1)\right]^4\Bigg\}, \end{aligned} \tag{2.35}$$

where

$$\beta \equiv \sqrt{4+\frac{\mu^2}{k^2}}\,. \tag{2.36}$$

The parameter β will turn out to be very important since it defines the localization of the vev and Higgs profiles. Requiring that the terms linear or quadratic in $h(x,t)$ cancel on the UV and IR branes yields the BCs

$$\begin{aligned} &\partial_t\left[t\,h(x,t)\right]_{t=\epsilon^+} = m_{\rm UV}\,h(x,\epsilon)\,, \quad \partial_t\left[t\,h(x,t)\right]_{t=1^-} = m_{\rm IR}\,h(x,1) - \frac{6\lambda}{M_{\rm KK}^2}\,v^2(1)\,h(x,1)\,, \\ &\partial_t\left[t\,v(t)\right]_{t=\epsilon^+} = m_{\rm UV}\,v(\epsilon)\,, \qquad\qquad \partial_t\left[t\,v(t)\right]_{t=1^-} = m_{\rm IR}\,v(1) - \frac{2\lambda}{M_{\rm KK}^2}\,v^3(1)\,. \end{aligned} \tag{2.37}$$

The notation ϵ^+ and 1^- indicates that the orbifold fixed points must be approached from the appropriate sides. We note that these conditions can also be derived by integrating the field equations over infinitesimal intervals about the branes.

Profile of the Higgs vev

By means of the variational principle with respect to $v(t)$ one obtains the differential equation

$$\left(t^2\partial_t^2 + t\partial_t - \beta^2\right)\frac{v(t)}{t} = 0\,, \tag{2.38}$$

which ensures that the tadpole terms in the Lagrangian (2.35) cancel out. We then obtain

$$\begin{aligned}\mathcal{L}_{\rm Higgs} = \frac{2\pi}{L}\int_\epsilon^1 \frac{dt}{t}\Bigg[&\frac{1}{2}\,\partial_\mu h(x,t)\,\partial^\mu h(x,t) + \frac{M_{\rm KK}^2}{2}\,\frac{h(x,t)}{t}\left(t^2\partial_t^2 + t\partial_t - \beta^2\right)\frac{h(x,t)}{t}\Bigg] \\ &- \frac{\pi}{L}\,\lambda\Big[-v^4(1) + 4v(1)\,h^3(x,1) + h^4(x,1)\Big]\,. \end{aligned} \tag{2.39}$$

The general solution to the differential equation (2.38) subject to the BCs (2.37) is given by

$$v(t) = N_v\left(t^{1+\beta} - r_v\,t^{1-\beta}\right)\,; \qquad\qquad r_v = \epsilon^{2\beta}\,\frac{2+\beta-m_{\rm UV}}{2-\beta-m_{\rm UV}}\,, \tag{2.40}$$

with

$$N_v^2 = \frac{M_{\rm KK}^2}{2\lambda}\,\frac{(m_{\rm IR}-2-\beta) - r_v\,(m_{\rm IR}-2+\beta)}{(1-r_v)^3}\,. \tag{2.41}$$

Before proceeding, let us first discuss which values the parameter β can take. Motivated by the observation that the energy-momentum flux in a pure anti-de Sitter space without an IR brane (which corresponds to taking the limit $r \to \infty$) vanishes at the boundary only if the 5D scalar field obeys the Breitenlohner-Friedman bound $\mu^2 > -4k^2$ [174], one usually assumes that β must be a real positive number, even though not necessarily larger than 2. Unless β is very close to zero, it follows that the coefficient $r_v \propto \epsilon^{2\beta}$ in (2.40) is extremely small and can be set to zero for all practical purposes. The only exception would be the region where $t \sim \epsilon$ is very near the UV brane, which however is irrelevant for our analysis here. It follows that

$$v(t) = v(1)\, t^{1+\beta}\,; \qquad\qquad v(1) = M_{\rm KK}\, \sqrt{\frac{m_{\rm IR} - 2 - \beta}{2\lambda}}\,. \tag{2.42}$$

The requirement that the Higgs vev be a real number imposes an upper bound on the parameter β, since $\lambda > 0$ is required by vacuum stability. We thus obtain the allowed range $0 < \beta < m_{\rm IR} - 2$.

We proceed to relate the parameter $v(1)$ to the physical value $v_{\rm SM}$ of the Higgs vev in the SM. After electroweak symmetry breaking, the mass terms for the W and Z bosons are generated by the 5D Lagrangian

$$\mathcal{L}_{\rm Higgs} \ni \frac{2\pi}{L} \int_\epsilon^1 \frac{dt}{t}\, \frac{v^2(t)}{4} \left[g_5^2\, W_\mu^+(x,t)\, W^{-\mu}(x,t) + \frac{g_5^2 + g_5'^2}{2}\, Z_\mu(x,t)\, Z^\mu(x,t) \right], \tag{2.43}$$

with the 5D gauge couplings g_5 and g_5'. Inserting the KK decompositions as given in (2.2) we can use that the zero-mode profiles are flat, $\chi_n^{W,Z}(t) = 1/\sqrt{2\pi}$ up to higher-order terms in $v^2/M_{\rm KK}^2$ [165], and we can identify

$$v_4^2 \equiv \frac{2\pi}{L} \int_\epsilon^1 \frac{dt}{t}\, v^2(t) = \frac{\pi}{L}\, \frac{v^2(1)}{1+\beta}\,, \tag{2.44}$$

where once again we neglect terms suppressed by powers of ϵ. It follows to leading order that

$$v(t) = v_4\, \sqrt{\frac{L}{\pi}\,(1+\beta)}\; t^{1+\beta}\,. \tag{2.45}$$

The parameter v_4 coincides with the parameter v used elsewhere in this thesis. At lowest order in an expansion in powers of $v^2/M_{\rm KK}^2$, it coincides with the SM value $(\sqrt{2}G_F)^{-1/2}$ as defined via the value of the Fermi constant G_F.

Profiles of the SM gauge bosons

Next, we will derive solutions for the gauge-boson profiles. The photon and gluon profiles are given by $\chi_0^{A,G}(t) = 1/\sqrt{2\pi}$. In case of the W and Z boson the corresponding EOM reads ($B = W, Z$)

$$\left(t\partial_t \frac{1}{t} \partial_t - \delta_B\, t^{2+2\beta} + x_B^2 \right) \chi_0^B(t) = 0\,; \quad \delta_W = \frac{g_5^2\, v^2(1)}{4r M_{\rm KK}^2}\,,\; \delta_Z = \frac{(g_5^2 + g_5'^2) v^2(1)}{4r M_{\rm KK}^2}\,, \tag{2.46}$$

with the normalized mass $x_B \equiv m_B/M_{\rm KK}$. The differential equation (2.46) cannot be solved in closed form to all orders in $v^2/M_{\rm KK}^2$. But we can derive a perturbative solution by making the ansatz of a product series for the profile $\chi_0^B(t) = \sum_{n=0}^\infty (\delta_B)^n\, f_n(t)$ and for the normalized mass $x_B^2 = \sum_{n=1}^\infty (\delta_B)^n\, c_n$, where we expand in the small parameter δ_B. Inserting the ansatz into (2.46) and collecting the different orders in powers of δ_B

the first three differential equations for the functions $f_n(t)$ are given by

$$-t\partial_t \frac{1}{t}\partial_t f_0(t) = 0\,, \qquad -t\partial_t \frac{1}{t}\partial_t f_1(t) = -t^{2+2\beta} f_0(t) + c_1 f_1(t)\,,$$
$$-t\partial_t \frac{1}{t}\partial_t f_2(t) = -t^{2+2\beta} f_1(t) + c_1 f_1(t) + c_2 f_0(t)\,. \tag{2.47}$$

Applying Neumann BCs for the functions f_n we obtain the solutions $f_0 = 1/\sqrt{2\pi}$ and

$$f_1(t) = \frac{1}{\sqrt{2\pi}} \frac{1}{4(1+\beta)} \left[\frac{(1+\beta)(3+\beta)}{2L(2+\beta)^2} - \frac{1}{2L^2} + t^2 \left(\frac{t^{2(1+\beta)}}{2+\beta} - 1 + \frac{1-2\ln t}{2L} \right) \right], \tag{2.48}$$

with the coefficient $c_1 = 1/(2L(1+\beta))$. Finally, the profiles of the massive gauge bosons are given to leading order in $v^2/M_{\rm KK}^2$ by

$$\chi_0^{W,Z}(t) = \frac{1}{\sqrt{2\pi}} \left[1 + \frac{\tilde{m}_{W,Z}^2}{2M_{\rm KK}^2} \left(\frac{L t^{4+2\beta}}{2+\beta} - t^2 \left(L - \frac{1}{2} + \ln t \right) + \frac{(1+\beta)(3+\beta)}{2(2+\beta)^2} - \frac{1}{2L} \right) \right] \tag{2.49}$$

with $\tilde{m}_W \equiv v_4 g_5/(2\sqrt{2\pi r})$ and $\tilde{m}_Z \equiv v_4 \sqrt{g_5^2 + g_5'^2}/(2\sqrt{2\pi r})$. The corresponding results in the brane-localized Higgs scenario (2.12) can be recovered by taking the limit $\beta \to \infty$.

Profiles for the Higgs boson and its KK excitations

We now proceed to study the eigenvalue problem for the physical Higgs boson and its KK excitations. We write the KK decomposition of the 5D Higgs field as

$$h(x,t) = \sum_{n=0}^{\infty} h_n(x)\, \chi_n^h(t)\,, \tag{2.50}$$

where the zero mode $h(x) \equiv h_0(x)$ corresponds to the SM Higgs boson. The profile functions obey the orthonormality condition

$$\frac{2\pi}{L} \int_\epsilon^1 \frac{dt}{t}\, \chi_m^h(t)\, \chi_n^h(t) = \delta_{mn}\,, \tag{2.51}$$

which ensures that the kinetic terms in the effective 4D Lagrangian are canonically normalized. In order to obtain canonical mass terms from the Lagrangian (2.39), we must impose the EOM

$$\left(t^2\partial_t^2 + t\partial_t + t^2 x_{h_n}^2 - \beta^2 \right) \frac{\chi_n^h(t)}{t} = 0\,, \tag{2.52}$$

where $x_{h_n} \equiv m_{h_n}/M_{\rm KK}$ denotes the mass of the $n^{\rm th}$ KK-scalar boson in units of $M_{\rm KK}$. The general solution to this equation is a linear combination of Bessel functions, $\chi_n^h(t) = N_n\, t \left[J_\beta(x_{h_n} t) - r_n Y_\beta(x_{h_n} t) \right]$, where the BC on the UV brane in (2.37) once again implies that $r_n \propto \epsilon^{2\beta}$ is extremely small and can be set to zero for all practical purposes, since we are not interested in the region where $t \sim \epsilon$. We then obtain

$$\chi_n^h(t) = \sqrt{\frac{L}{\pi}}\, \frac{t\, J_\beta(x_{h_n} t)}{\sqrt{J_\beta^2(x_{h_n}) - J_{\beta+1}(x_{h_n})\, J_{\beta-1}(x_{h_n})}}\,. \tag{2.53}$$

The BC on the IR brane gives rise to the eigenvalue equation, which determines the masses of the scalar modes. We find

$$x_{h_n}\,\frac{J_{\beta+1}(x_{h_n})}{J_\beta(x_{h_n})} = 2(m_{\rm IR}-2-\beta) \equiv 2\delta\,. \tag{2.54}$$

It follows from this equation that even the zero mode (the SM Higgs boson) has a mass that is naturally of order the KK scale which empirically cannot be less than a few TeV. This is the little hierarchy problem which as mentioned in Section 1.4.1 is not addressed in RS scenarios. In order to obtain a realistic Higgs mass $m_h \ll M_{\rm KK}$, we must assume that $\delta = m_{\rm IR} - 2 - \beta \ll 1$. Once this is done, it is straightforward to obtain a formula for the zero-mode mass in a power series in δ. We find

$$x_h^2 \equiv \frac{m_h^2}{M_{\rm KK}^2} = 4(1+\beta)\,\delta\left[1 - \frac{\delta}{2+\beta} + \frac{2\delta^2}{(2+\beta)^2\,(3+\beta)} + \ldots\right]. \tag{2.55}$$

Assuming $M_{\rm KK} = 2\,\text{TeV}$, for example, implies that $(1+\beta)\,\delta \approx 10^{-3}$, which corresponds to a fine-tuning of 1 in 1000. For the zero-mode profile, it is now straightforward to obtain an expansion in powers of x_h^2. The leading terms are given by

$$\chi_0^h(t) = \sqrt{\frac{L}{\pi}\,(1+\beta)}\;t^{1+\beta}\left[1 - \frac{x_h^2}{4}\left(\frac{t^2}{1+\beta} - \frac{1}{2+\beta}\right) + \ldots\right]. \tag{2.56}$$

Dropping the irrelevant constant proportional to $v^4(1)$, the Higgs Lagrangian (2.39) can now be written as

$$\begin{aligned}\mathcal{L}_h = &\sum_n \left[\frac{1}{2}\,\partial_\mu h_n(x)\,\partial^\mu h_n(x) - \frac{m_{h_n}^2}{2}\,h_n^2(x)\right] \\ &- v_4\,\frac{4L}{\pi}\,(1+\beta)^2\,\lambda \sum_{l,m,n} \xi_l\;\xi_m\,\xi_n\,h_l(x)\,h_m(x)\,h_n(x) \\ &- \frac{L}{\pi}\,(1+\beta)^2\,\lambda \sum_{k,l,m,n} \xi_k\,\xi_l\;\xi_m\,\xi_n\,h_k(x)\,h_l(x)\,h_m(x)\,h_n(x)\,,\end{aligned} \tag{2.57}$$

where $\xi_n \equiv \chi_n^h(1)/\sqrt{(L/\pi)(1+\beta)}$. From (2.56) we find $\xi_0 \approx 1$ for the zero mode, while (2.53) and (2.54) imply that $\xi_n \approx \pm 1/\sqrt{1+\beta}$ for the KK excitations. We proceed to relate the parameter λ to the physical value λ_4 of the Higgs self coupling. The relevant terms in the SM Lagrangian are

$$\mathcal{L}_{\rm SM} \ni -\frac{m_h^2}{2}\,h^2 - v_{\rm SM}\,\lambda_{\rm SM}\,h^3 - \frac{\lambda_{\rm SM}}{4}\,h^4\,, \tag{2.58}$$

where $m_h^2 = 2\lambda_{\rm SM}\,v_{\rm SM}^2$. Matching either one of these terms with the corresponding term in (2.57), we obtain at leading order

$$\lambda_{\rm SM} = \lambda_4 = \frac{4L}{\pi}\,(1+\beta)^2\,\lambda = \lambda_{\rm IR}\,k^2\,(1+\beta)^2\,. \tag{2.59}$$

The relation between $\lambda_{\rm SM}$ and λ_4 receives higher-order corrections in $v^2/M_{\rm KK}^2$, which are calculable in the model and depend on which of the three couplings in (2.58) is used to perform the matching.

Yukawa interactions

We finally consider the Yukawa couplings of the neutral scalar field to the quarks. First, it is useful to consider the brane-localized Higgs scenario with the Lagrangian (2.14). Without considering the NGBs we obtain[3]

$$\mathcal{L}_{\rm Yuk} = -\sum_{q=u,d} \int_\epsilon^1 dt \frac{v\,\delta_v^{1/\beta}(t-1) + h(x)\,\delta_h^{1/\beta}(t-1)}{\sqrt{2}} \bar{\mathcal{Q}}_L(x,t) \frac{k}{2} \begin{pmatrix} 0 & \boldsymbol{Y}_q^{5\rm D} \\ \boldsymbol{Y}_q^{5\rm D\dagger} & 0 \end{pmatrix} \mathcal{Q}_R(x,t) + \text{h.c.}\,, \tag{2.60}$$

where $\delta_v^{1/\beta}(t-1)$ and $\delta_h^{1/\beta}(t-1)$ represent regularized δ-functions for the localization of the vev and Higgs boson. In order to find an explicit form of those distributions we now consider the model with a bulk-Higgs field. We find

$$\mathcal{L}_{\rm Yuk} = -\sum_{q=u,d} \int_\epsilon^1 dt \frac{v(t) + \sum_n h_n(x)\,\chi_n^h(t)}{\sqrt{2}} \bar{\mathcal{Q}}_L(x,t) \frac{1}{\sqrt{r}} \begin{pmatrix} 0 & \boldsymbol{Y}_{q,\rm bulk}^{5\rm D} \\ \boldsymbol{Y}_{q,\rm bulk}^{5\rm D\dagger} & 0 \end{pmatrix} \mathcal{Q}_R(x,t) + \text{h.c.}\,, \tag{2.61}$$

where the 5D Yukawa matrices $\boldsymbol{Y}_{q,\rm bulk}^{5\rm D}$ now have mass dimension $-1/2$. In order to match the two expressions (2.60) and (2.61) onto each other, we must rewrite the functions $v(t)$ from (2.45) and $\chi_0^h(t)$ from (2.56) in terms of functions with unit area, which can be mapped onto the normalized distributions $\delta_v^{1/\beta}(t-1)$ and $\delta_h^{1/\beta}(t-1)$. We obtain

$$\begin{aligned} v(t) &= v_4 \sqrt{\frac{L}{\pi}} \frac{\sqrt{1+\beta}}{2+\beta}\,\delta_v^{1/\beta}(t-1)\,, \\ \chi_0^h(t) &= \sqrt{\frac{L}{\pi}} \frac{\sqrt{1+\beta}}{2+\beta} \left[1 + \frac{\beta\,x_h^2}{4(1+\beta)(2+\beta)(4+\beta)} + \ldots\right] \delta_h^{1/\beta}(t-1)\,, \end{aligned} \tag{2.62}$$

with

$$\begin{aligned} \delta_v^{1/\beta}(t-1) &= (2+\beta)\,t^{1+\beta}\,, \\ \delta_h^{1/\beta}(t-1) &= (2+\beta)\,t^{1+\beta} \left[1 - \frac{x_h^2}{4(1+\beta)} \left(t^2 - \frac{2+\beta}{4+\beta}\right) + \ldots\right]. \end{aligned} \tag{2.63}$$

We emphasize that the distributions (2.63) can be considered as representations of the regularized δ-function in the limit of large β. In this limit the parameter $1/\beta$ plays the role of η in (1.58). Using the quark bilinear terms as a reference, the corresponding matching relations between the two Yukawa matrices reads

$$\boldsymbol{Y}_q \equiv \frac{k}{2}\,\boldsymbol{Y}_q^{5\rm D} = \frac{\sqrt{k\,(1+\beta)}}{2+\beta}\,\boldsymbol{Y}_{q,\rm bulk}^{5\rm D}\,. \tag{2.64}$$

The quantities on the left-hand side of the equation are the dimensionless Yukawa matrices introduced in (2.16), whose elements are assumed to be random numbers. If one used the $hq\bar{q}$ couplings instead, the above relation would receive corrections of $\mathcal{O}(x_h^2)$.

Limit of a narrow bulk-Higgs field

We are now in a position to study the limit $\beta \gg 1$, in which the profile functions in (2.63) become strongly localized near the IR brane. We can then identify $1/\beta$ with the width of the Higgs profile, which plays the role of the regulator η in our brane-Higgs scenario. The Yukawa matrices of the bulk-Higgs model must then be identified with

[3] Note that (2.60) is consistent with the expression (2.15) in which we have used the same regularized δ-function for both the profiles of the Higgs boson and its vev.

$\boldsymbol{Y}_q \leftrightarrow \sqrt{k/\beta}\,\boldsymbol{Y}^{5D}_{q,\text{bulk}} = (k/\sqrt{\mu})\,\boldsymbol{Y}^{5D}_{q,\text{bulk}}$. Finally, since t is pushed near 1, we conclude from (2.63) that

$$\frac{\delta_h^{1/\beta}(t-1)}{\delta_v^{1/\beta}(t-1)} = 1 + \mathcal{O}\left(\frac{m_h^2}{\beta^2 M_{\text{KK}}^2}\right), \tag{2.65}$$

showing that the two profiles coincide. Taking the limit of very large β is not particularly natural, since $\beta = \sqrt{4+\mu^2/k^2}$ is naturally of $\mathcal{O}(1)$. For large β, we have the double hierarchy

$$\frac{1}{r} \ll k \ll \mu \approx \frac{M_{\text{IR}}}{2}, \qquad \text{or} \quad \frac{10}{r} \sim k \sim \frac{\mu}{\beta}. \tag{2.66}$$

Large β can be achieved by taking k significantly smaller than the Planck scale (and $1/r$ yet smaller by an order of magnitude), or by assuming that μ and M_{IR} are significantly larger than M_{Pl}. The first possibility appears more plausible. Note that for large β relation (2.59) implies that $\lambda_4 \approx \lambda_{\text{IR}}\,\mu^2$, indicating that increasing β by lowering the curvature parameter k does not affect the relation between λ_4 and λ_{IR} in a significant way.

2.4 Extension to the RS model with custodial symmetry

We will now present the RS model with custodial protection, which has been proposed to mitigate large corrections to electroweak precision observables, so that the lightest KK particles are in reach for the direct detection at the LHC [120, 147, 175, 176]. The difference to the minimal RS model is the enlarged gauge symmetry in the bulk

$$SU(3)_c \times SU(2)_L \times SU(2)_R \times U(1)_X \times P_{LR}, \tag{2.67}$$

whose $SU(2)$ subgroups are broken on the IR brane via the symmetry-breaking pattern $SU(2)_L \times SU(2)_R \to SU(2)_V$. The resulting $SU(2)_V$ supplies the custodial symmetry and protects the T parameter, as will be discussed in Section 2.5.2. The discrete left-right symmetry P_{LR}, which exchanges $SU(2)_L$ and $SU(2)_R$, prevents the left-chiral $Zb\bar{b}$ coupling [148] and its flavor-changing counterparts [145] from receiving too large corrections. On the UV brane, the symmetry breaking $SU(2)_R \times U(1)_X \to U(1)_Y$ generates the SM gauge group. This is achieved by an interplay between UV and IR BCs. Thorough discussions of this model containing many technical details can be found in [149, 150], and we will adopt the notations of the first reference throughout this analysis.

Higgs and gauge-boson sector

The $SU(2)_L$, $SU(2)_R$ and $U(1)_X$ 5D gauge-boson fields are denoted by L_M^i, R_M^i ($i = 1,2,3$) and X_M. The corresponding 4-components of the gauge fields are chosen to be even under the Z_2 parity, while the fifth components are chosen to be Z_2-odd, in order to derive at a low-energy spectrum that is compatible with observation. The Higgs transforms as a bi-doublet $(\mathbf{2},\mathbf{2})_0$ under $SU(2)_L \times SU(2)_R$ and is neutral with respect to $U(1)_X$ [149],

$$\Phi(x) = \frac{1}{\epsilon\sqrt{2}} \begin{pmatrix} v + h(x) - i\varphi^3(x) & -i\sqrt{2}\varphi^+(x) \\ -i\sqrt{2}\varphi^-(x) & v + h(x) + i\varphi^3(x) \end{pmatrix}, \tag{2.68}$$

where φ^i are real scalar fields, $\varphi^\pm = (\varphi^1 \mp i\varphi^2)/\sqrt{2}$, and v denotes the Higgs vev in the custodial RS model. The Higgs Lagrangian is given by

$$\mathcal{L}_{\text{Higgs}} = \int_\epsilon^1 \frac{dt}{t}\sqrt{|G|}\,\delta^\eta(t-1)\left[\frac{1}{2}\text{Tr}\left[(D^\mu\Phi)^\dagger D_\mu\Phi\right] + \mu^2\,\text{Tr}\left[\Phi^\dagger\Phi\right] - \lambda\,\text{Tr}\left[\Phi^\dagger\Phi\right]^2\right]. \quad (2.69)$$

In order to show how the symmetry breaking $SU(2)_L \times SU(2)_R \to SU(2)_V$ is accomplished, we use the covariant derivative $D_\mu\Phi = \partial_\mu\Phi - ig_{L,5}L^i_\mu T^i_L\,\Phi + ig_{R,5}\Phi R^i_\mu T^i_R$ where $g_{L,5}$ and $g_{R,5}$ are the 5D gauge couplings associated with $SU(2)_{L,R}$, and $T^i_{L,R} = \sigma^i/2$ are the corresponding generators. In order to evaluate the kinetic term for the scalar bi-doublet, it is convenient to rotate the gauge bosons L^i_μ and R^i_μ into a new basis of fields $\tilde{A}^i_\mu$ and V^i_μ, such that [177]

$$\begin{pmatrix}\tilde{A}^i_M\\ V^i_M\end{pmatrix} = \begin{pmatrix}\cos\vartheta_W & -\sin\vartheta_W\\ \sin\vartheta_W & \cos\vartheta_W\end{pmatrix}\begin{pmatrix}L^i_M\\ R^i_M\end{pmatrix} \equiv \boldsymbol{R}_{\vartheta_W}\begin{pmatrix}L^i_M\\ R^i_M\end{pmatrix};\;\; \sin\vartheta_W \equiv \frac{g_{R,5}}{\sqrt{g^2_{L,5}+g^2_{R,5}}}. \quad (2.70)$$

The P_{LR} symmetry, which is imposed to protect the left-chiral $Z\bar{b}b$ couplings from receiving large corrections [148], enforces that $g_{L,5} = g_{R,5}$, and hence $\cos\vartheta_W = \sin\vartheta_W = 1/\sqrt{2}$. In our discussion in this section we will however keep the value of ϑ_W as a free parameter. The Higgs vev $\langle\Phi\rangle$ then generates a mass term $M^2_{\tilde{A}} = v^2(g^2_{L,5}+g^2_{R,5})/4$ for the fields $\tilde{A}^i_\mu$, while the fields V^i_μ remain massless. We can also read off the coupling to the Higgs boson, once we replace v^2 by $(v+h)^2$. Note that only the fields $\tilde{A}^i_\mu$ couple to the Higgs boson h. Appropriate BCs break the extended electroweak gauge group down to the SM gauge group on the UV boundary $SU(2)_R \times U(1)_X \to U(1)_Y$. This is accomplished by introducing the new fields [149]

$$\begin{pmatrix}Z'_M\\ B_M\end{pmatrix} = \frac{1}{\sqrt{g^2_{R,5}+g^2_{X,5}}}\begin{pmatrix}g_{R,5} & -g_{X,5}\\ g_{X,5} & g_{R,5}\end{pmatrix}\begin{pmatrix}R^3_M\\ X_M\end{pmatrix}, \quad (2.71)$$

and by giving Dirichlet BCs to Z'_μ and $R^{1,2}_\mu$ on the UV brane. Here $g_{X,5}$ denotes the 5D gauge coupling of the $U(1)_X$ symmetry group. The field B_μ can be identified with the $U(1)_Y$ gauge field. The SM-like neutral electroweak gauge bosons can be defined as in the SM by [149]

$$\begin{pmatrix}Z_M\\ A_M\end{pmatrix} = \frac{1}{\sqrt{g^2_{L,5}+g^2_{Y,5}}}\begin{pmatrix}g_{L,5} & -g_{Y,5}\\ g_{Y,5} & g_{L,5}\end{pmatrix}\begin{pmatrix}L^3_M\\ B_M\end{pmatrix};\qquad g_{Y,5} \equiv \frac{g_{X,5}\,g_{R,5}}{\sqrt{g^2_{R,5}+g^2_{X,5}}}. \quad (2.72)$$

The weak-mixing angle and the 5D electromagnetic gauge coupling are given by $\sin\theta_w = g_{Y,5}/(g^2_{L,5}+g^2_{Y,5})^{1/2}$ and $e_5 = g_{L,5}\sin\theta_w$ which agrees with the definition in the minimal RS model when replacing $g_{L,5} \to g_5$ and $g_{Y,5} \to g'_5$. The fields $L^\pm_\mu = L^1_M \pm L^2_M$, $R^\pm_M = R^1_M \pm R^2_M$, A_M, Z_M and Z'_M collectively define the so-called *UV basis* with Neumann BCs for $L^\pm_\mu$, Z_μ, A_μ and Dirichlet BCs for $R^\pm_\mu$, Z'_μ, $L^\pm_5$, $R^\pm_5$, Z_5, Z'_5, A_5 at the UV brane. While the photon field A_M has Neumann BCs for the vector components A_μ and Dirichlet BCs for the fifth component A_5 at the IR brane the other fields in the UV basis have in general complicated BCs at the IR brane. Therefore, it is convenient to define the so-called *IR basis* which includes the fields $A^\pm_M$, $V^\pm_M$, $\tilde{Z}_M$, Z^H_M with (modified) Neumann BCs for $A^\pm_\mu$, $V^\pm_\mu$, $\tilde{Z}_\mu$, Z^H_μ and Dirichlet BCs for $A^\pm_5$, $V^\pm_5$, $\tilde{Z}_5$, Z^H_5 at the IR brane. The fields $\tilde{Z}_M$ and Z^H_M are related to the UV-basis fields Z_M and Z'_M via the

relation [149]

$$\begin{pmatrix} \tilde{Z}_M \\ Z_M^H \end{pmatrix} = \begin{pmatrix} \cos\vartheta_Z & -\sin\vartheta_Z \\ \sin\vartheta_Z & \cos\vartheta_Z \end{pmatrix} \begin{pmatrix} Z_M \\ Z'_M \end{pmatrix} \equiv \boldsymbol{R}_{\vartheta_Z} \begin{pmatrix} Z_M \\ Z'_M \end{pmatrix} , \tag{2.73}$$

with the angle $\sin\vartheta_Z \equiv g_{R,5}^2/((g_{L,5}^2+g_{R,5}^2)(g_{R,5}^2+g_{X,5}^2))^{1/2}$. Now, we are in a position to switch between the UV and IR basis by using the matrices $\boldsymbol{R}_{\vartheta_W}$ and $\boldsymbol{R}_{\vartheta_Z}$ defined in (2.70) and (2.73). This will be frequently used in the following analysis.

We continue with the KK decomposition of the 5D gauge-boson fields. Concerning the W- and Z-boson fields it is useful to define the vectors [149]

$$\vec{W}_M^{\pm} \equiv \begin{pmatrix} \tilde{A}_M^{\pm} \\ V_M^{\pm} \end{pmatrix} = \boldsymbol{R}_{\vartheta_W} \begin{pmatrix} L_M^{\pm} \\ R_M^{\pm} \end{pmatrix} , \qquad \vec{Z}_M \equiv \begin{pmatrix} \tilde{Z}_M \\ Z_M^H \end{pmatrix} = \boldsymbol{R}_{\vartheta_Z} \begin{pmatrix} Z_M \\ Z'_M \end{pmatrix} . \tag{2.74}$$

Those vectors can be decomposed via [149]

$$\begin{aligned} \vec{W}_\mu^{\pm}(x,t) &= \frac{\boldsymbol{R}_{\vartheta_W}}{\sqrt{r}} \sum_{n=0}^{\infty} \vec{\chi}_n^W(t)\, W_\mu^{\pm(n)}(x), \quad \vec{W}_5^{\pm}(x,t) = \frac{\boldsymbol{R}_{\vartheta_W}}{\sqrt{r}} \sum_{n=0}^{\infty} \frac{-kt}{m_{W_n}} \varphi_W^{\pm(n)}(x)\, \partial_t \vec{\chi}_n^W(t), \\ \vec{Z}_\mu(x,t) &= \frac{\boldsymbol{R}_{\vartheta_Z}}{\sqrt{r}} \sum_{n=0}^{\infty} \vec{\chi}_n^Z(t)\, Z_\mu^{(n)}(x), \qquad \vec{Z}_5(x,t) = \frac{\boldsymbol{R}_{\vartheta_Z}}{\sqrt{r}} \sum_{n=0}^{\infty} \frac{-kt}{m_{Z_n}} \varphi_Z^{(n)}(x)\, \partial_t \vec{\chi}_n^Z(t), \end{aligned} \tag{2.75}$$

with the Z_2-even profiles $\vec{\chi}_n^{W,Z}(t)$. Their upper (lower) components are "untwisted" ("twisted") functions. Untwisted even functions obey Neumann BCs on the UV brane, allowing for light zero modes. Twisted even functions obey Dirichlet BCs on the UV brane and are thus not smooth at this orbifold fixed point. The KK decompositions of the photon and gluon are analogous to the case in the minimal RS model (2.2). In analogy to (2.5) we can expand the 4D NGBs in the basis of mass eigenstates and find [149]

$$\begin{aligned} \vec{\varphi}_W^{\pm}(x) &= \sum_n \frac{\tilde{m}_W}{m_{W_n}} \sqrt{2\pi}\, \boldsymbol{P}_+ \boldsymbol{R}_{\vartheta_W} \vec{\chi}_n^W(1)\, \varphi_W^{\pm(n)} ; \qquad \tilde{m}_W = \frac{g_{L,5}}{\sqrt{2\pi r}} \frac{v}{2} , \\ \vec{\varphi}_Z(x) &= \sum_n \frac{\tilde{m}_Z}{m_{Z_n}} \sqrt{2\pi}\, \boldsymbol{P}_+ \boldsymbol{R}_{\vartheta_Z} \vec{\chi}_n^Z(1)\, \varphi_Z^{(n)} ; \qquad \tilde{m}_Z = \sqrt{\frac{g_{L,5}^2+g_{Y,5}^2}{2\pi r}} \frac{v}{2} , \end{aligned} \tag{2.76}$$

where $\boldsymbol{P}_+ \equiv \mathrm{diag}(1,0)$ is a projector on the upper component. As in the minimal RS model, the parameter $\tilde{m}_{W,Z}$ is the leading contribution to the W,Z-boson mass in an expansion in powers of v^2/M_{KK}^2, see (2.79) below. Inserting the KK decompositions (2.75) and (2.76) into the 5D action on can derive the differential equation $\left(t\partial_t t^{-1}\partial_t + x_{B_n}^2\right)\vec{\chi}_n^B(t) = 0$ [149] for $B = W, Z$ with the BCs

$$(\boldsymbol{P}_+\partial_t + \boldsymbol{P}_-)\, \vec{\chi}_n^B(t)\big|_{t=\epsilon^+} = 0 , \qquad \left(\mathbf{1} + \frac{L\tilde{m}_W^2}{c_{\vartheta_W}^2 M_{\mathrm{KK}}^2} \boldsymbol{P}_+\right) \boldsymbol{R}_{\vartheta_B}\, \partial_t \vec{\chi}_n^B(t)\big|_{t=1^-} = 0 . \tag{2.77}$$

Above we used $\boldsymbol{P}_- \equiv \mathrm{diag}(0,1)$ and $c_{\vartheta_W} \equiv \cos\vartheta_W$. The photon and gluon profiles $\chi_n^{A,G}$ obey the same EOMs as in the minimal RS model (2.7). Exact solutions for the profiles can be found in [149]. For the analysis in this thesis, it is sufficient to know the zero-mode

profiles of the W and Z boson to leading order in $v^2/M_{\rm KK}^2$ [149]

$$\begin{aligned}\vec{\chi}_0^W(t) &= \frac{1}{\sqrt{2\pi}}\begin{pmatrix} 1-\frac{m_W^2}{2M_{\rm KK}^2}\left[t^2\left(L-\frac{1}{2}+\ln t\right)-\frac{1}{2}+\frac{1}{2L}\right] \\ \frac{\sin\vartheta_W}{\cos\vartheta_W}\frac{Lm_W^2}{2M_{\rm KK}^2}\,t^2 \end{pmatrix}, \\ \vec{\chi}_0^Z(t) &= \frac{1}{\sqrt{2\pi}}\begin{pmatrix} 1-\frac{m_Z^2}{2M_{\rm KK}^2}\left[t^2\left(L-\frac{1}{2}+\ln t\right)-\frac{1}{2}+\frac{1}{2L}\right] \\ \frac{\sin\vartheta_Z\cos\vartheta_Z}{\cos^2\vartheta_W}\frac{Lm_W^2}{2M_{\rm KK}^2}\,t^2 \end{pmatrix},\end{aligned} \tag{2.78}$$

where we see that the untwisted (upper) components are the same profiles as in the minimal model, see (2.12). The twisted (lower) components are suppressed by $v^2/M_{\rm KK}^2$. The physical W,Z-boson masses can be determined from the IR BC (2.77) and are given to leading order by [149]

$$\begin{aligned} m_W^2 &= \tilde{m}_W^2\left[1-\frac{\tilde{m}_W^2}{2M_{\rm KK}^2}\left(\frac{L}{c_{\vartheta_W}^2}-1+\frac{1}{2L}\right)+\mathcal{O}\left(\frac{v^4}{M_{\rm KK}^4}\right)\right], \\ m_Z^2 &= \tilde{m}_Z^2\left[1-\frac{\tilde{m}_W^2}{2M_{\rm KK}^2}\left(\frac{L}{c_{\vartheta_W}^2}-1+\frac{1}{2L}\right)+\frac{\tilde{m}_Z^2}{2M_{\rm KK}^2}\left(1-\frac{1}{2L}\right)+\mathcal{O}\left(\frac{v^4}{M_{\rm KK}^4}\right)\right], \end{aligned} \tag{2.79}$$

with $\tilde{m}_W$ and $\tilde{m}_Z$ defined in (2.76). We see that the (numerically) leading correction to the Z-boson mass is proportional to $L\tilde{m}_W^2/M_{\rm KK}^2$, which is a consequence of the enlarged bulk gauge symmetry.

Quark sector

Since the bulk gauge group is larger than in the minimal model the quark representations include bi-doublets, triplets and singlets under the two $SU(2)$ gauge groups. We choose the quark representations such that they can be embedded into complete $SO(5)$ multiplets used in the context of models with gauge-Higgs unification [120, 176, 178]. As a consequence of the discrete P_{LR} symmetry, which is instrumental in protecting the left-chiral $Zb\bar{b}$ coupling [148] and its flavor-changing counterparts [145], the left-chiral bottom quark has to be embedded in a $SU(2)_L\times SU(2)_R$ bi-doublet with isospin quantum numbers $T_L^3=-T_R^3=-1/2$. This fixes the quantum numbers of the other fields uniquely. In particular, the right-chiral down-type quarks have to be embedded in a $SU(2)_R$ triplet in order to obtain an $U(1)_X$-invariant Yukawa coupling. One arrives at the following multiplet structure for the quark fields with even Z_2 parity

$$\begin{aligned} Q_L &= \begin{pmatrix} u_L^{(+)}{}_{\frac{2}{3}} & \lambda_L^{(-)}{}_{\frac{5}{3}} \\ d_L^{(+)}{}_{-\frac{1}{3}} & u_L'^{(-)}{}_{\frac{2}{3}} \end{pmatrix}_{\frac{2}{3}}, \qquad u_R^c = \left(u_R^{c\,(+)}{}_{\frac{2}{3}}\right)_{\frac{2}{3}}, \\ \mathcal{T}_R &= \mathcal{T}_{1R}\oplus\mathcal{T}_{2R} = \begin{pmatrix} \Lambda_R'^{(-)}{}_{\frac{5}{3}} \\ U_R'^{(-)}{}_{\frac{2}{3}} \\ D_R'^{(-)}{}_{-\frac{1}{3}} \end{pmatrix}_{\frac{2}{3}} \oplus \left(D_R^{(+)}{}_{-\frac{1}{3}} \quad U_R^{(-)}{}_{\frac{2}{3}} \quad \Lambda_R^{(-)}{}_{\frac{5}{3}}\right)_{\frac{2}{3}}, \end{aligned} \tag{2.80}$$

where Q_L is a bi-doublet under $SU(2)_L\times SU(2)_R$, while $\mathcal{T}_R$ transforms as $(\mathbf{3},\mathbf{1})\oplus(\mathbf{1},\mathbf{3})$. The fields with odd Z_2 parity have the opposite chirality. Their profiles are related to those of the Z_2-even fields by the field equations. The inner and outer subscripts on the various fields denote their $U(1)_{\rm EM}$ and $U(1)_X$ charges, respectively, which are connected through the relations $Y=-T_R^3+Q_X$ and $Q=T_L^3+Y$. The superscripts on the fields

specify the type of BCs they obey on the UV boundary. Fields with superscript (+) obey the usual mixed BCs allowing for a light zero mode, meaning that we impose the Dirichlet condition on the profile functions of the corresponding Z_2-odd fields. These zero modes correspond to the SM quarks.[4] Fields with superscripts (−) correspond to heavy, exotic fermions with no counterparts in the SM. For these states, the Dirichlet BC is imposed on the Z_2-even fields in order to avoid the presence of a zero mode. The remaining UV BCs are of mixed type and follow from the field equations. Note that we have chosen the same $SU(2)_L \times SU(2)_R$ representations for all three quark generations, which is necessary if one wants to consistently incorporate quark mixing in the fully anarchic approach to flavor in warped extra dimensions. The chosen representations also play a crucial role in the suppression of flavor-changing, left-chiral Z-boson couplings [145, 149]. Altogether, there are fifteen different quark states in the up sector and nine in the down sector. The BCs give rise to three light modes in each sector, which are identified with the SM quarks. These are accompanied by KK towers consisting of groups of fifteen and nine modes of similar masses in the up and down sectors, respectively. In addition, there is a KK tower of exotic fermion states with electric charge 5/3, which exhibits nine excitations in each KK level.

In order to simplify the notation as much as possible, it is convenient to introduce the vectors

$$\vec{U} = \begin{pmatrix} u \\ u' \end{pmatrix}, \quad \vec{u} = \begin{pmatrix} u^c \\ U' \\ U \end{pmatrix}, \quad \vec{D} = d\,, \quad \vec{d} = \begin{pmatrix} D \\ D' \end{pmatrix}, \quad \vec{\Lambda} = \lambda\,, \quad \vec{\lambda} = \begin{pmatrix} \Lambda' \\ \Lambda \end{pmatrix}, \tag{2.81}$$

which collect the fields with same electric charges (2/3, −1/3, and 5/3). Upper-case (lower-case) symbols denote fields whose left-chiral (right-chiral) components are Z_2 even. We now collect all left- and right-chiral fields in the up, down, and exotic sectors into the 15-component vectors $(\vec{U}_A, \vec{u}_A)^T$ and the 9-component vectors $(\vec{D}_A, \vec{d}_A)^T$ and $(\vec{\Lambda}_A, \vec{\lambda}_A)^T$ (with $A = L, R$), to which we will collectively refer as $\mathcal{Q}_{L,R}$ with $\mathcal{Q} = \mathcal{U}$, $\mathcal{D}$, Λ. Similar to (2.13) the Lagrangian, including terms bilinear in the quark fields, is given by

$$\mathcal{L}_{\rm Ferm} = \int_\epsilon^1 \frac{dt}{t} \sqrt{|G|} \sum_{\mathcal{Q}=\mathcal{U},\mathcal{D},\Lambda} \bar{\mathcal{Q}}(x,t) \left[i\not{\partial} - M_{\rm KK}\gamma_5 \partial_t - \frac{M_{\rm KK}}{t} \begin{pmatrix} \vec{\boldsymbol{c}}_Q & 0 \\ 0 & -\vec{\boldsymbol{c}}_q \end{pmatrix} \right] \mathcal{Q}(x,t)\,, \tag{2.82}$$

with the bulk-mass parameters

$$\begin{aligned} &\boldsymbol{c}_{\vec{U}} = \mathrm{diag}\big(\boldsymbol{c}_Q, \boldsymbol{c}_Q\big)\,, && \boldsymbol{c}_{\vec{D}} = \boldsymbol{c}_Q\,, && \boldsymbol{c}_{\vec{\Lambda}} = \boldsymbol{c}_Q\,, \\ &\boldsymbol{c}_{\vec{u}} = \mathrm{diag}\big(\boldsymbol{c}_{u^c}, \boldsymbol{c}_{\tau_1}, \boldsymbol{c}_{\tau_2}\big)\,, && \boldsymbol{c}_{\vec{d}} = \mathrm{diag}\big(\boldsymbol{c}_{\tau_2}, \boldsymbol{c}_{\tau_1}\big)\,, && \boldsymbol{c}_{\vec{\lambda}} = \mathrm{diag}\big(\boldsymbol{c}_{\tau_1}, \boldsymbol{c}_{\tau_2}\big)\,. \end{aligned} \tag{2.83}$$

Each entry is a 3×3 diagonal matrix in generation space. The fields $\vec{U}$, $\vec{D}$, and $\vec{\Lambda}$ are governed by the same bulk-mass matrix $\boldsymbol{c}_Q$ as in the minimal model, while $\vec{u}$, $\vec{d}$, and $\vec{\lambda}$ are associated with three different mass matrices $\boldsymbol{c}_{u^c}$, $\boldsymbol{c}_{\tau_2}$, and $\boldsymbol{c}_{\tau_1}$. The first two of them, $\boldsymbol{c}_{u^c} \equiv \boldsymbol{c}_u$ and $\boldsymbol{c}_{\tau_2} \equiv \boldsymbol{c}_d$, can be identified with the mass matrices appearing in the minimal RS model. The three new parameters contained in the matrix $\boldsymbol{c}_{\tau_1}$ can be related to the other ones by extending the P_{LR} symmetry to the part of the quark sector that mixes with the left-chiral down-type zero modes, by requiring that the action be invariant under the exchange of the fields D' and D [149]. This extended version of the P_{LR} symmetry implies that $\boldsymbol{c}_{\tau_1} = \boldsymbol{c}_{\tau_2}$ and hence the number of independent bulk-mass

[4] Note that the notation u_L, d_L, u_R^c, D_R for these fields adopted here differs from the notation U_L, D_L, u_R, d_R we used for the minimal RS model.

parameters is reduced to the same number as in the minimal RS model. In the remainder of this thesis we will implement the extended version of the P_{LR} symmetry. Without considering the NGBs in (2.68) the Yukawa couplings are given by

$$\mathcal{L}_{\text{Yuk}} = -\sum_{\vec{q}=\vec{u},\vec{d},\vec{\lambda}} \int_\epsilon^1 dt\, \frac{v+h(x)}{\sqrt{2}}\, \delta^\eta(t-1)\, \bar{\mathcal{Q}}_L(x,t) \begin{pmatrix} 0 & \boldsymbol{Y}_{\vec{q}} \\ \boldsymbol{Y}_{\vec{q}}^\dagger & 0 \end{pmatrix} \mathcal{Q}_R(x,t) + \text{h.c.}\,, \quad (2.84)$$

with the dimensionless Yukawa matrices

$$\boldsymbol{Y}_{\vec{u}} = \begin{pmatrix} \boldsymbol{Y}_u & \frac{1}{\sqrt{2}}\boldsymbol{Y}_d & \frac{1}{\sqrt{2}}\boldsymbol{Y}_d \\ \boldsymbol{Y}_u & -\frac{1}{\sqrt{2}}\boldsymbol{Y}_d & -\frac{1}{\sqrt{2}}\boldsymbol{Y}_d \end{pmatrix}, \qquad \boldsymbol{Y}_{\vec{d}} = \boldsymbol{Y}_{\vec{\lambda}} = \begin{pmatrix} \boldsymbol{Y}_d & \boldsymbol{Y}_d \end{pmatrix}. \quad (2.85)$$

The 3×3 block matrices $\boldsymbol{Y}_q$ appearing in these expressions are the same as in the minimal RS model. Even though the extended RS model with custodial symmetry has a much richer structure than the minimal model, it thus features the same number of parameters in the fermion sector, once the extended P_{LR} symmetry is imposed.

With $\mathcal{Q}_{L,R}$ as defined here the corresponding KK decomposition is given by the same equation as in the minimal model (2.17). In the up-quark sector the superscript n labels the different mass eigenstates such that $n = 1, 2, 3$ refer to the SM quarks, while $n = 4, ..., 18$ label the fifteen quark modes of the first level and so on. In the down- and λ-type sector there are nine modes in each KK level. In analogy to (2.18) we can parametrize the profiles

$$\mathcal{Q}_L^{(n)}(t) = \sqrt{\frac{2\pi}{L\epsilon}} \begin{pmatrix} \boldsymbol{C}_n^Q(t)\, \vec{a}_n^{\,Q} \\ \boldsymbol{S}_n^q(t)\, \vec{a}_n^{\,q} \end{pmatrix}, \qquad \mathcal{Q}_R^{(n)}(t) = \sqrt{\frac{2\pi}{L\epsilon}} \begin{pmatrix} \boldsymbol{S}_n^Q(t)\, \vec{a}_n^{\,Q} \\ \boldsymbol{C}_n^q(t)\, \vec{a}_n^{\,q} \end{pmatrix}, \quad (2.86)$$

with $(\mathcal{Q}, Q, q) = (\mathcal{U}, U, u)$, $(\mathcal{D}, D, d)$, $(\Lambda, \Lambda, \lambda)$. The functions $\boldsymbol{C}_n^A$ and $\boldsymbol{S}_n^A$ denote the Z_2-even and -odd fermion profiles and exact solutions are given in [149]. Analogous to the minimal RS model the flavor structure is encoded in the vectors $\vec{a}_n^{\,Q,q}$.

2.5 The Randall-Sundrum parameter space

This section discusses the parameter space of the RS model. Compared to the SM there are additional fundamental parameters. In the minimal model the hermitian 3×3 bulk-mass matrices $\boldsymbol{c}_{Q,u,d}$ introduce 27 parameters, 18 moduli and 9 complex phases.[5] They are supplemented with 36 parameters from the up- and down-type Yukawa matrices $\boldsymbol{Y}_u$ and $\boldsymbol{Y}_d$. Focusing on the quark sector the global symmetry group $U(3)_Q \times U(3)_u \times U(3)_d$ with 27 generators gets broken by the Yukawa interactions to the abelian subgroup $U(1)_B$. We end up with 27 moduli and ten phases [143]. This can be compared to the SM with nine moduli, the six quark masses and three angles of the CKM matrix, and one CP-violating phase. In Section 2.5.1 we will show that the experimental values for the quark masses and the Wolfenstein parameters can be used to fix 10 of the parameters in the RS model. We note that the number of parameters in the RS model with custodial symmetry is the same as in the minimal RS model.[6]

An obvious RS prediction is the existence of additional heavy resonances at the TeV scale that can be searched for experimentally. Figure 2.1 shows exclusion limits on the lightest KK gluon via the search of resonances in the invariant mass spectrum of $t\bar{t}$

[5] A general $N \times N$ hermitian matrix has $N(N+1)/2$ real parameters and $N(N-1)/2$ complex phases.

[6] This statement is true when we impose the extended P_{LR} symmetry, which we will assume throughout this thesis.

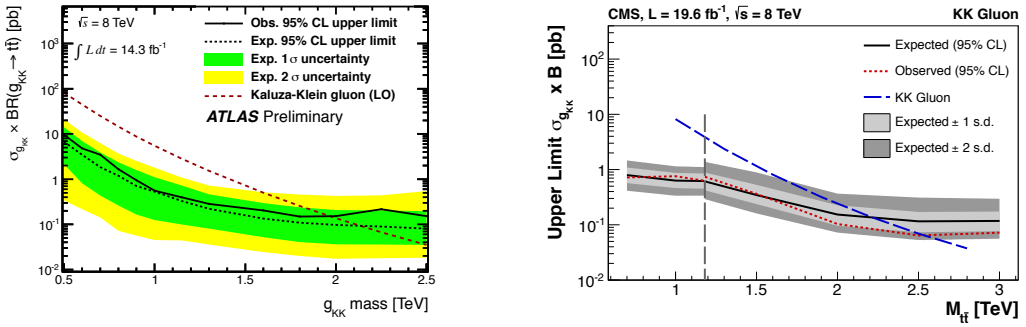

Figure 2.1: Exclusion plots for the mass of the lightest KK gluon obtained from an analyses of the invariant mass spectrum of $t\bar{t}$ production by the ATLAS [179] (left) and CMS [180] (right) collaborations.

production by the ATLAS (left) and CMS (right) collaborations. The current exclusion limits read[7]

$$M_{g^{(1)}}\big|_{\text{ATLAS}} > 2.0\,\text{TeV}\ [179] \qquad \text{and} \qquad M_{g^{(1)}}\big|_{\text{CMS}} > 2.54\,\text{TeV}\ [180]\,, \tag{2.87}$$

both at 95% confidence level (CL).[8] Besides KK gluons the RS model predicts the existence of heavy excitations of the graviton. The 5D graviton can be decomposed into a tower of KK excitations, where the lightest KK graviton $h^{(1)}_{\mu\nu}$ has the mass $m_{h^{(1)}} \approx 3.83\,M_{\text{KK}}$. In order to search for this particle one can look out for high-mass diphoton resonances at the LHC. The signal rate $(\sigma \cdot \text{Br})(pp \to h^{(1)} \to \gamma\gamma)$ depends essentially on two parameters, the KK graviton mass $m_{h^{(1)}}$ and the ratio $k/\bar{M}_{\text{Pl}}$, where $\bar{M}_{\text{Pl}} = M_{\text{Pl}}/\sqrt{8\pi}$ is the reduced Planck mass. Here, the factor $k/\bar{M}_{\text{Pl}} = \sqrt{8\pi}\frac{M_{\text{KK}}}{\Lambda_{\text{TeV}}}$ sets the interaction strength of the KK graviton coupling to two gluons (photons).[9] Current searches by the ATLAS and CMS collaborations can put a lower limit on the KK graviton mass $M_{g^{(1)}} > 2.66\,\text{TeV}\,(1.41\,\text{TeV})$ [183] and $M_{g^{(1)}} > 2.78\,\text{TeV}\,(1.45\,\text{TeV})$ [184], both at 95% CL and for $k/\bar{M}_{\text{Pl}} = 0.1\,(0.01)$.[10]

It is not surprising that KK modes have not been directly detected since indirect searches already impose stronger bounds. However, a comprehensive study of tree-level weak interaction processes for the minimal and custodial RS model is not the scope of this thesis and can be found in [132, 140, 142–146]. The only exception are the Peskin-Takeuchi parameters S, T, U, which receive corrections in the RS model at tree-level. In Section 2.5.2 we will derive bounds on the KK scale, which are independent of the

[7] We remark that in the RS model the first KK gluon coupling to quarks are roughly given by $c_{q\bar{q}G^{(1)}} \approx (1/\sqrt{L})\,g_s$ for light quarks ($q = u, d$), $c_{t_L\bar{t}_L G^{(1)}} \approx -g_s$ and $c_{t_R\bar{t}_R G^{(1)}} \approx -\sqrt{L}\,g_s$, where g_s is the QCD gauge coupling. However, the precise values of the couplings depend on the RS point under consideration, and have to be calculated from the overlap integrals of the first KK gluon profile with the corresponding quark profiles. Consequently, one has to keep in mind that the analyses, leading to the exclusion limits in (2.87), are based on a specific choice of the couplings, see [179, 180].

[8] It is reported in [181] that the future exclusion limit on the first KK gluon mass at 95% CL will be 4.3 TeV (6.7 TeV) for the LHC at $\sqrt{s} = 14\,\text{TeV}$ with an integrated luminosity of $300\,\text{fb}^{-1}$ ($3000\,\text{fb}^{-1}$).

[9] For instance, the coupling of the first KK graviton to two gluons is given by the interaction $\mathcal{L}(x) \ni 0.054 \times \frac{k}{M_{\text{Pl}}}\frac{1}{m_{h^{(1)}}} h^{(1)}_{\mu\nu}(x)\,T^{\mu\nu}_{\text{gluon}}(x)$ [182], where $T^{\mu\nu}_{\text{gluon}}$ is the 4D energy-momentum tensor of the gluon.

[10] One can also search for KK excitations of the Z, $W^{\pm}$ bosons and fermions. However, their production and decay processes depend on the concrete implementation of the flavor sector (bulk-mass parameters and 5D Yukawa matrices). Prospects for discovering these particles with future LHC collision data can be found in [185].

structure of the quark sector, i.e. at tree-level the bounds are independent of the bulk-mass parameters and the 5D Yukawa matrices. Therefore, those bounds will be used as reference values when we discuss the phenomenological implications of the RS model for processes in Higgs physics and for the $b \to s\gamma$ transition in Chapters 4 and 5.

2.5.1 Generating RS points

The procedure of generating RS parameter sets, referred to as *RS points*, is based on a modified version of the algorithms used first in [132, 140]. The numerical code is implemented using *Mathematica* [186]. The first step is to generate anarchic 5D Yukawa matrices where the real and imaginary parts of each entry are randomized with a flat distribution. In order to investigate the sensitivity of observables on the generic size of the Yukawa matrix elements we impose the constraint ($q = u, d$)

$$|(\boldsymbol{Y}_q)_{ij}| \leq y_* \,, \tag{2.88}$$

for different values of y_*. There exists an upper limit $y_* \leq y_{\max}$ when requiring that the Yukawa sector remains in the perturbative regime. It is conventional to choose the value $y_{\max} \approx 3$ [144]. In our analysis we will consider sets of RS points with different values of y_* in the range between 0.5 and 3. If we work at leading (zeroth) order in $v^2/M_{\rm KK}^2$ for the zero-mode profiles and masses (ZMA) we can directly calculate the Wolfenstein parameters $\bar\rho$ and $\bar\eta$ solely from the 5D Yukawa matrices [132]

$$\bar\rho - i\bar\eta = \frac{(\boldsymbol{Y}_d)_{33}(M_u)_{31} - (\boldsymbol{Y}_d)_{23}(M_u)_{21} + (\boldsymbol{Y}_d)_{13}(M_u)_{11}}{(\boldsymbol{Y}_d)_{33}(M_u)_{11}\left[\frac{(\boldsymbol{Y}_d)_{23}}{(\boldsymbol{Y}_d)_{33}} - \frac{(\boldsymbol{Y}_u)_{23}}{(\boldsymbol{Y}_u)_{33}}\right]\left[\frac{(M_d)_{21}}{(M_d)_{11}} - \frac{(M_u)_{21}}{(M_u)_{11}}\right]} \,,$$

where $(M_q)_{ij}$ is the ij-minor of $\boldsymbol{Y}_q$. Next, we choose a random value for the zero-mode function $F(c_{u_3}) \in [0, \sqrt{3}]$, which implies that $c_{u_3} \in [-\frac{1}{2}, 1]$. The lower bound is motivated since the (right-chiral) top quark should have an $\mathcal{O}(1)$ overlap with the IR brane. The upper bound on the other hand is motivated by the fact that the 5D bulk mass should not exceed the curvature scale k. The remaining eight zero-mode functions $F(c_{Q_{1,2,3}})$, $F(c_{u_{1,2}})$ and $F(c_{d_{1,2,3}})$ can be calculated in the ZMA directly from the experimental values for the six quark masses and the two Wolfenstein parameters A and λ. The required analytical relations in the ZMA are given by [132, 141]

$$\begin{aligned}
|F(c_{Q_1})| &= \frac{\sqrt{2}\,m_t}{v}\left(|(Y_u)_{33}|\left|\frac{(\boldsymbol{Y}_d)_{23}}{(\boldsymbol{Y}_d)_{33}} - \frac{(\boldsymbol{Y}_u)_{23}}{(\boldsymbol{Y}_u)_{33}}\right|\left|\frac{(M_d)_{21}}{(M_d)_{11}} - \frac{(M_u)_{21}}{(M_u)_{11}}\right|\right)^{-1}\frac{\lambda^3\,A}{|F(c_{u_3})|} \,, \\
|F(c_{Q_2})| &= \frac{\sqrt{2}\,m_t}{v}\left(|(\boldsymbol{Y}_u)_{33}|\left|\frac{(\boldsymbol{Y}_d)_{23}}{(\boldsymbol{Y}_d)_{33}} - \frac{(\boldsymbol{Y}_u)_{23}}{(\boldsymbol{Y}_u)_{33}}\right|\right)^{-1}\frac{\lambda^2\,A}{|F(c_{u_3})|} \,, \\
|F(c_{Q_3})| &= \frac{\sqrt{2}\,m_t}{v}\frac{1}{|(\boldsymbol{Y}_u)_{33}|}\frac{1}{|F(c_{u_3})|} \,, \\
|F(c_{u_1})| &= \frac{m_u}{m_t}\frac{|(\boldsymbol{Y}_u)_{33}||(M_u)_{11}|}{\det \boldsymbol{Y}_u}\left|\frac{(\boldsymbol{Y}_d)_{23}}{(\boldsymbol{Y}_d)_{33}} - \frac{(\boldsymbol{Y}_u)_{23}}{(\boldsymbol{Y}_u)_{33}}\right|\left|\frac{(M_d)_{21}}{(M_d)_{11}} - \frac{(M_u)_{21}}{(M_u)_{11}}\right|\frac{|F(c_{u_3})|}{\lambda^3\,A} \,, \\
|F(c_{u_2})| &= \frac{m_c}{m_t}\frac{|(\boldsymbol{Y}_u)_{33}|^2}{|(M_u)_{11}|}\left|\frac{(\boldsymbol{Y}_d)_{23}}{(\boldsymbol{Y}_d)_{33}} - \frac{(\boldsymbol{Y}_u)_{23}}{(\boldsymbol{Y}_u)_{33}}\right|\frac{|F(c_{u_3})|}{\lambda^2\,A} \,, \\
|F(c_{d_1})| &= \frac{m_d}{m_t}\frac{|(\boldsymbol{Y}_u)_{33}||(M_d)_{11}|}{\det \boldsymbol{Y}_d}\left|\frac{(\boldsymbol{Y}_d)_{23}}{(\boldsymbol{Y}_d)_{33}} - \frac{(\boldsymbol{Y}_u)_{23}}{(\boldsymbol{Y}_u)_{33}}\right|\left|\frac{(M_d)_{21}}{(M_d)_{11}} - \frac{(M_u)_{21}}{(M_u)_{11}}\right|\frac{|F(c_{u_3})|}{\lambda^3\,A} \,, \\
|F(c_{d_2})| &= \frac{m_s}{m_t}\frac{|(\boldsymbol{Y}_u)_{33}||(\boldsymbol{Y}_d)_{33}|}{|(M_d)_{11}|}\left|\frac{(\boldsymbol{Y}_d)_{23}}{(\boldsymbol{Y}_d)_{33}} - \frac{(\boldsymbol{Y}_u)_{23}}{(\boldsymbol{Y}_u)_{33}}\right|\frac{|F(c_{u_3})|}{\lambda^2\,A} \,,
\end{aligned}$$

$$|F(c_{d_3})| = \frac{m_b}{m_t}\frac{(\boldsymbol{Y}_u)_{33}}{(\boldsymbol{Y}_d)_{33}}|F(c_{u_3})|\,. \tag{2.89}$$

As reference values for the quark masses we take the $\overline{\text{MS}}$ quark masses at the scale $\mu = 1\,\text{TeV}$ given by

$$\begin{aligned} m_u &= (1.0 \pm 0.7)\,\text{MeV}\,, \quad m_c = (500 \pm 25)\,\text{MeV}\,, \quad m_t = (141 \pm 5)\,\text{GeV}\,, \\ m_d &= (2.2 \pm 0.5)\,\text{MeV}\,, \quad m_s = (43 \pm 5)\,\text{MeV}\,, \qquad m_b = (2.31 \pm 0.03)\,\text{GeV}\,, \end{aligned} \tag{2.90}$$

which have been obtained from the low-energy values given in [76]. The central values and errors for the Wolfenstein parameters are taken from [187] and read

$$\lambda = 0.22548^{+0.00068}_{-0.00034}\,, \quad A = 0.810^{+0.018}_{-0.024}\,, \quad \bar{\rho} = 0.145^{+0.013}_{-0.007}\,, \quad \bar{\eta} = 0.343^{+0.011}_{-0.012}\,. \tag{2.91}$$

Next, we calculate the the full set of observables $x = \{m_u, m_d, m_s, m_c, m_b, m_t, A, \lambda, \bar{\rho}, \bar{\eta}\}$ in the RS model using the exact formulas for the quark masses and Wolfenstein parameters, that are valid to all orders in v^2/M_{KK}^2. In a first step we remove all points that show a deviation of more than 3σ in at least one observable. Secondly, we calculate the function

$$\chi^2(x) = \sum_n \left(\frac{x_{\text{exp}}(n) - x_{\text{theo}}(n)}{\sigma_{\text{exp}}(n)}\right)^2\,, \tag{2.92}$$

where $x_{\text{exp}}(n)$ and $x_{\text{theo}}(n)$ denote the experimental and theoretical values and $\sigma_{\text{exp}}(n)$ is the standard deviation of the corresponding measurements. Points with $\chi^2(x)/\text{dof} > 11.5/10$ corresponding to 68% CL are rejected. In order to check that we cover the parameter space in an unbiased way we have analyzed the final distributions of the parameters. In the complex plane each entry of the Yukawa matrices is nearly flatly distributed. Only the $(\boldsymbol{Y}_u)_{33}$ element shows an excluded region in the range $(\boldsymbol{Y}_u)_{33} \lesssim \frac{1}{2}$, which can be explained by the fact that this entry contributes to the top quark mass, see (2.32). The shapes of the distributions of the quark masses and Wolfenstein parameters are approximately Gaussian with a width of at most twice the corresponding experimental uncertainty. It is instructive to show the distributions of the bulk-mass parameters in Figure 2.2. The *probability density distributions* of the nine bulk-mass parameters are shown, which were generated from a total set of 5000 RS parameter points with $y_* = 3$. We observe that c_{u_3} is flatly distributed over the allowed range $c_{u_3} \in [-\frac{1}{2}, 1]$ while the remaining bulk-mass parameters admit peaked distributions.

2.5.2 Compatibility with the Peskin-Takeuchi parameters

In order to calculate predictions for the Peskin-Takeuchi parameters we first need to establish the connection between the parameters of the 5D Lagrangian with physical observables [164]. We comment that new-physics effects in RS models cannot be uniquely described in terms of oblique corrections due to the heavy KK modes and the non-universality of the fermion and gauge-boson profiles. However, we can approximately fit to a selected subset of the most precisely measured observables and parametrize electroweak corrections in terms of S, T and U.

In a first step we determine the parameters v, g_5, g_5' in terms of the observables G_F, m_Z (m_W) and s_w^2. We begin with the relation between the vev v and the Fermi constant G_F, which can be derived by constructing the effective four-fermion interaction mediating muon decay. Corrections in RS models originate from modifications of the W-boson coupling to fermions and due to the presence of heavy KK resonances. Both effects

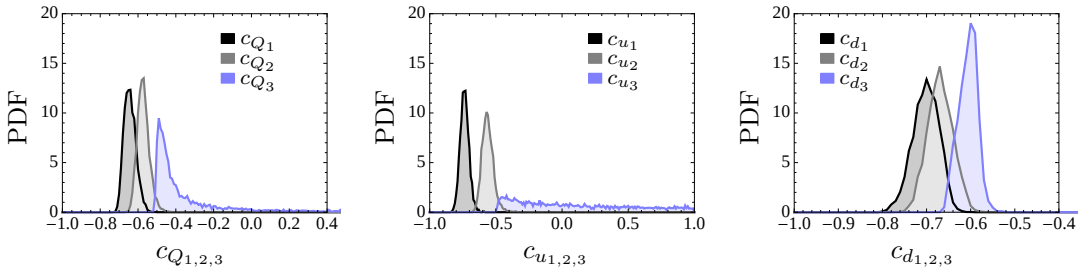

Figure 2.2: Shown are the probability density distributions (PDF) for the bulk mass parameters $c_{Q_i}, c_{u_i}, c_{d_i}$ generated from a set of 5000 RS parameter points with $y_* = 3$. While we choose for c_{u_3} a random value in the allowed range $c_{u_3} \in [-\frac{1}{2}, 1]$ the remaining bulk-mass parameters are determined from the quark masses and the Wolfenstein parameters, see the text for more details.

are encoded in the 5D W-boson propagator, which will be comprehensively discussed in the next chapter. Here, it is sufficient to consider the 5D propagator evaluated at zero four-momentum transfer. Working at leading order in $v^2/M_{\rm KK}^2$ we find that the contribution from the W-boson and its KK excitations is given by the sum

$$\sum_{n=0}^{\infty} \frac{\chi_n^W(t)\chi_n^W(t')}{m_W^2} = \frac{1}{2\pi\tilde{m}_W^2}\left[1 + \frac{Lm_W^2}{2M_{\rm KK}^2}\left(1 - t_>^2\right) + \mathcal{O}\left(\frac{v^4}{M_{\rm KK}^4}\right)\right], \tag{2.93}$$

where $t_> = \max(t, t')$. When calculating the amplitude for muon decay, this sum is convoluted with the profiles of the external SM leptons. It turns out that the t- and t'-dependent terms yield exponentially suppressed contributions. Thus, the dominant correction stems from the t, t'-independent contribution in (2.93). We can extract the vev

$$v = (\sqrt{2}\, G_F)^{-1/2}\left[1 + \frac{Lm_W^2}{4M_{\rm KK}^2} + \mathcal{O}\left(\frac{v^4}{M_{\rm KK}^4}\right)\right], \tag{2.94}$$

with the SM value $v_{\rm SM} \equiv (\sqrt{2}G_F)^{-1/2} \approx 246.2\,\text{GeV}$. Next, we consider the 5D gauge couplings. Since the SM photon and the gluon have flat profiles we can simply obtain the 4D gauge-boson couplings by $e = e_5/\sqrt{2\pi r}$ and $g_s = g_{s,5}/\sqrt{2\pi r}$ [165, 166]. The 5D electroweak gauge couplings g_5 and g_5' can be related to the parameters $\tilde{m}_W$ and $\tilde{m}_Z$ in (2.5) and we obtain

$$\frac{g_5^2}{2\pi r} = 4\sqrt{2}\, G_F\, c_w^2 m_Z^2\left[1 + \frac{m_Z^2}{2M_{\rm KK}^2}\left(s_w^2 L - 1 + \frac{1}{2L}\right)\right], \qquad g_5'^2 = g_5^2 \tan^2\theta_w\,, \tag{2.95}$$

which are valid to leading order in $v^2/M_{\rm KK}^2$. As already mentioned in Section 2.1 the weak mixing angle θ_w is defined via $s_w^2 \equiv g_5'^2/(g_5^2 + g_5'^2)$. At last, we note that if we take G_F, m_Z and s_w^2 as input parameters the W-boson mass is a derived quantity. We find

$$m_W^2(m_Z, s_w^2) = m_Z^2 c_w^2\left[1 + \frac{m_Z^2 s_w^2}{2M_{\rm KK}^2}\left(L - 1 + \frac{1}{2L}\right) + \mathcal{O}\left(\frac{v^4}{M_{\rm KK}^4}\right)\right], \tag{2.96}$$

to leading order in $v^2/M_{\rm KK}^2$.

Now, we will discuss the Peskin-Takeuchi parameters S, T and U [46]. These weak-interaction parameters can be defined in terms of self-energy functions of the W-, Z-boson and photon propagators, see equation (3.12) in [46]. Furthermore, they are defined in such a way that they describe shifts relative to the SM values, hence in the SM $S = T = U = 0$. The Peskin-Takeuchi parameters are useful if we assume that physics beyond the SM appears dominantly through vacuum polarizations (oblique corrections) and that vertex corrections can be neglected. This assumption is approximately valid in RS models, where corrections to gauge-boson couplings of light fermions are chirally suppressed. Rather than using a definition in terms of self-energy functions we choose to define the Peskin-Takeuchi parameters in terms of a set of physical observables. The S, T, U parameters can be solved for by using the three equations [46]

$$\begin{aligned} c_W^2 - c_0^2 &= \frac{\alpha c_w^2}{c_w^2 - s_w^2}\left[-\frac{1}{2}S + c_w^2 T + \frac{c_w^2 - s_w^2}{4 s_w^2}U\right], \\ s_*^2 - s_0^2 &= \frac{\alpha}{c_w^2 - s_w^2}\left[\frac{1}{4}S - s_w^2 c_w^2 T\right], \\ \rho_* - 1 &= \alpha T\,, \end{aligned} \tag{2.97}$$

which depend on s_*^2, s_w^2, s_W^2, s_0^2, ρ_* and α. Let us begin with the different definitions of the weak mixing angle. The first definition employs the structure $\frac{1}{2}\sigma_3 - s_*^2 Q$ in the weak neutral current, as has been measured from the Z-pole polarization asymmetries at LEP, with $s_*^2 \equiv g_5'^2/(g_5^2 + g_5'^2)$. This definition in terms of 5D gauge couplings coincides with our definition of s_w^2. Secondly, we can define the weak mixing angle in terms of the ratio of electroweak gauge-boson masses, namely

$$s_W^2 = 1 - \frac{m_W^2}{m_Z^2} = \frac{g_5'^2}{g_5^2 + g_5'^2}\left[1 - \frac{m_W^2}{2M_{\rm KK}^2}\left(L - 1 + \frac{1}{2L}\right) + \mathcal{O}\left(\frac{v^4}{M_{\rm KK}^4}\right)\right]. \tag{2.98}$$

The third definition uses the precisely measured parameters G_F, α and m_Z. Defining $s_0^2 c_0^2 = \pi\alpha/(\sqrt{2} G_F m_Z^2)$ we can find

$$s_0^2 = \frac{g_5'^2}{g_5^2 + g_5'^2}\left[1 + \frac{m_W^2}{2M_{\rm KK}^2}\frac{1}{c_W^2 - s_W^2}\left(s_W^2 L - 1 + \frac{1}{2L}\right) + \mathcal{O}\left(\frac{v^4}{M_{\rm KK}^4}\right)\right]. \tag{2.99}$$

As a final electroweak observable we consider the parameter ρ_* which can be defined via the low-energy four-fermion Lagrangian $\mathcal{L}_{\rm eff} = -4\frac{G_F}{\sqrt{2}}[J_\mu^+ J^{-\mu} + \rho_*(J_3^\mu - s_*^2 J_Q^\mu)^2]$. It denotes the low-energy ratio of charged- to neutral-current amplitudes. Integrating out the W, Z bosons and their heavy KK resonances we find that

$$\rho_* = 1 + \frac{L(m_Z^2 - m_W^2)}{2M_{\rm KK}^2} + \mathcal{O}\left(\frac{v^4}{M_{\rm KK}^4}\right). \tag{2.100}$$

Using the fact that the photon has a flat profile along the extra dimension the electromagnetic coupling can be expressed via $4\pi\alpha = \frac{1}{2\pi r}\, g_5'^2 g_5^2/(g_5^2 + g_5'^2)$. Now, we can solve (2.97) for the parameters S, T, U and find in the minimal RS model

$$S = \frac{2\pi v^2}{M_{\rm KK}^2}\left(1 - \frac{1}{L}\right), \qquad T = \frac{L\,\pi v^2}{2 c_w^2 M_{\rm KK}^2}, \qquad U = 0\,, \tag{2.101}$$

to leading order in $v^2/M_{\rm KK}^2$. The results agree with the corresponding expressions derived in the literature [132, 188–192] up to very small $\mathcal{O}(1/L)$ corrections, which depend on

how one precisely deals with non-oblique effects in the definition of S, T and U. Equation 2.101 shows that the S parameter is not enhanced by the RS volume L, which is a result from placing the fermion fields in the bulk.[11] The left plot in Figure 2.3 shows the regions of 68%, 95% and 99% probability in the S-T plane. The brown-shaded regions are obtained from a three-parameter fit performed by the Gfitter group [193] yielding the best fit values

$$S_{\text{exp}} = 0.05 \pm 0.11\,, \qquad T_{\text{exp}} = 0.09 \pm 0.13\,, \qquad U_{\text{exp}} = 0.01 \pm 0.11\,, \tag{2.102}$$

with correlation coefficients of $+0.9$ between S and T, -0.59 (-0.83) between S and U (T and U). For this unconstrained fit we obtain a lower bound on the mass of the first KK-gluon resonance of

$$M_{g^{(1)}} \geq 11.3\,\text{TeV}\,, \qquad (95\%\,\text{CL}) \tag{2.103}$$

which corresponds to $M_{\text{KK}} \geq 4.6\,\text{TeV}$ at 95% CL. To obtain this bound we have used the SM vev $v_{\text{SM}} = 246.2\,\text{GeV}$ obtained from the measured Fermi constant $G_F = 1.1663787(6) \times 10^{-5}\,\text{GeV}^{-2}$ [76] via muon decay and $s_w^2 = 0.23176 \pm 0.0006$ [76] obtained from a study of the Z-pole polarization asymmetries observed at LEP. If we fix $U = 0$ the best fit values from the Gfitter group are $S_{\text{exp}} = 0.06 \pm 0.09$ and $T_{\text{exp}} = 0.10 \pm 0.07$ with a correlation coefficient of $+0.91$ [193]. The corresponding contours of the 68%, 95% and 99% CL regions are shown by the gray ellipses in Figure 2.3. For the constrained fit the lower bound on the mass of the first KK gluon resonance is given by $M_{g^{(1)}} \geq 13.5\,\text{TeV}$ or equivalently by $M_{\text{KK}} \geq 5.5\,\text{TeV}$, both at 95% CL. This bound is more restrictive since the 1σ error margins for the best fit value of the T parameter is smaller than in case of the unconstrained fit. Since we only consider tree-level corrections the condition $U = 0$ might be violated at loop level, therefore the unconstrained fit might be more appropriate to use in order to derive the lower bounds. Therefore, when we speak of the bounds imposed by electroweak precision observables we refer to the bounds obtained from the unconstrained fits, (2.103) for the minimal RS model and (2.107) for the custodial RS model.

The strong bound on $M_{g^{(1)}}$ in (2.103) results from large corrections to the T parameter. One possibility to mitigate those corrections is to allow the Higgs boson to propagate into the bulk of the extra dimension in which case the lower bound can be reduced (for the unconstrained fit) to $M_{g^{(1)}} \geq 6.1\,\text{TeV}$ for $\beta = 0$ [164]. Increasing β to larger values the lower bound tends towards the brane-localized Higgs limits. Another possibility to mitigate the T parameter in (2.101) would be to reduce the volume L of the extra dimension [194]. The drawback is that one gives up the solution to the full gauge hierarchy problem since for the so-called *little RS models* the cutoff at the UV brane is reduced to $\Lambda_{\text{UV}} \sim e^L M_{\text{KK}} < M_{\text{Pl}}$. In addition those models suffer from large corrections to the CP-violating observable ϵ_K [139]. The last cure for an excessive T parameter is to implement a custodial $SU(2)_R$ symmetry, which will be discussed in the following.

Extension to the custodial RS model

Now, we turn to the RS model with custodial protection which was discussed in Section 2.4. When we calculate the amplitude for muon decay, analogously to the case in

[11] In RS models with bulk gauge fields and brane-localized fermions one would obtain instead $S,\, T \sim -L\pi v^2/M_{\text{KK}}^2$, which are both large and negative [190].

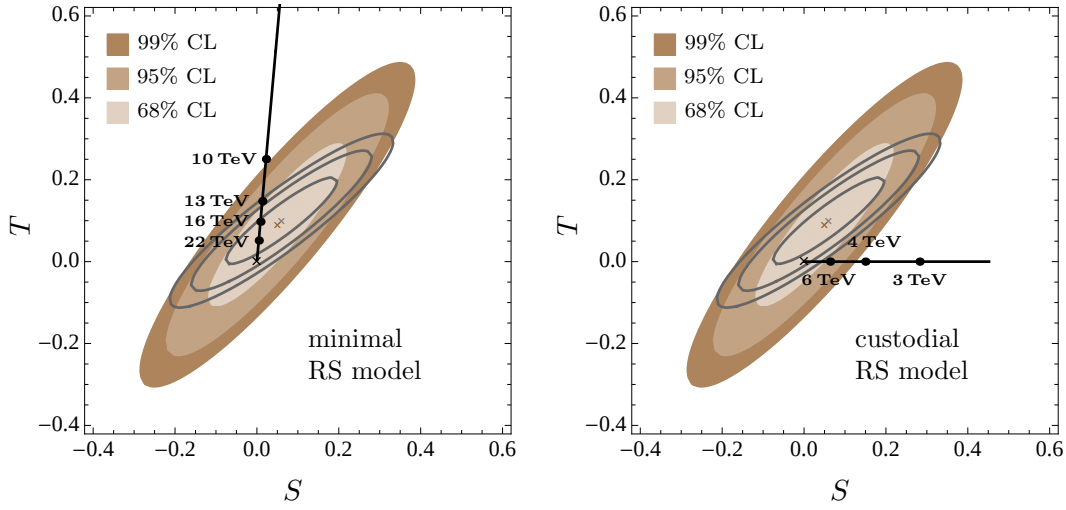

Figure 2.3: In the left (right) plot the black line shows the predicted values for the S and T parameters in the minimal (custodial) RS model depending on the value of the first KK-gluon resonance. The confidence-level contours in the S-T plane are derived from a fit to electroweak precision data using $m_h = 125\,\text{GeV}$ and $m_t = 173\,\text{GeV}$ [193]. The brown ellipses show the 68%, 95% and 99% CL regions of a three-parameter fit to S, T and U while the gray lines are obtained from a constrained fit where U is set to zero. The brown (gray) and black crosses denote the central values of the constrained (unconstrained) fit and the SM prediction.

the minimal RS model, we can extract the vev

$$v = (\sqrt{2}G_F)^{-1/2}\left[1 + \frac{Lm_W^2}{4c_{\vartheta_W}^2 M_{\text{KK}}^2} + \mathcal{O}\left(\frac{v^4}{M_{\text{KK}}^4}\right)\right], \tag{2.104}$$

where the parameter $c_{\vartheta_W} \equiv \cos\vartheta_W$ is defined in (2.70) and can take on a non-trivial value. If we impose the P_{LR} symmetry the parameter is fixed to $c_{\vartheta_W} = 1/\sqrt{2}$, and we observe that the leading corrections to the vev are larger by a factor of 2 compared with the minimal model.

In order to calculate the Peskin-Takeuchi parameters we first need to determine the different weak mixing angles s_*^2, s_W^2 and s_0^2. Proceeding analogously as in the minimal RS model, we find

$$\begin{aligned} s_*^2 &\equiv \frac{g_{Y,5}^2}{g_{L,5}^2 + g_{Y,5}^2} = s_w^2\,, \qquad s_W^2 \equiv \frac{g_{Y,5}^2}{g_{L,5}^2 + g_{Y,5}^2}\left[1 + \frac{1}{s_w^2}\frac{\tilde{m}_W^2}{2M_{\text{KK}}^2}\left(1 - \frac{1}{2L}\right) + \mathcal{O}\left(\frac{v^4}{M_{\text{KK}}^4}\right)\right], \\ s_0^2 &\equiv \frac{g_{Y,5}^2}{g_{L,5}^2 + g_{Y,5}^2}\left[1 - \frac{1}{c_w^2 - s_w^2}\frac{m_W^2}{2M_{\text{KK}}^2}\left(1 - \frac{1}{2L}\right) + \mathcal{O}\left(\frac{v^4}{M_{\text{KK}}^4}\right)\right], \end{aligned} \tag{2.105}$$

where the 5D hypercharge gauge coupling $g_{Y,5}$ is defined in (2.72). The low-energy ratio of charged- to neutral-current amplitudes is given by $\rho_* = 1$, which is a direct consequence of the custodial protection. Furthermore, the electromagnetic coupling can be expressed by $4\pi\alpha = \frac{1}{2\pi r}\, g_{Y,5}^2\, g_{L,5}^2/(g_{L,5}^2 + g_{Y,5}^2)$. Then we can solve for S, T and U in (2.97) and find

for the custodial RS model

$$S = \frac{2\pi v^2}{M_{\mathrm{KK}}^2}\left(1 - \frac{1}{L}\right), \qquad T = 0\,, \qquad U = 0\,. \tag{2.106}$$

This result agrees with the corresponding expressions in the literature up to very small $\mathcal{O}(1/L)$ corrections [132, 191, 192]. Comparing (2.106) with the results in the minimal RS model (2.101) we observe that the S parameter remains unaffected while the L-enhanced term of the T parameter is absent. The black line in the right plot of Figure 2.3 presents the corrections in the S-T plane for the RS model with custodial protection, showing that the corrections are driven by the S parameter. For the unconstrained fit we obtain the lower bound

$$M_{g^{(1)}} \geq 4.9\,\mathrm{TeV}\,, \qquad (95\%\,\mathrm{CL}) \tag{2.107}$$

which corresponds to $M_{\mathrm{KK}} \geq 2.0\,\mathrm{TeV}$ at 95% CL. This bound is sufficiently low such that the direct detection of KK gluons via the search for $t\bar{t}$ resonances can be tested experimentally. For instance, the high-luminosity LHC with $3000\,\mathrm{fb}^{-1}$ at $\sqrt{s} = 14\,\mathrm{TeV}$ is expected to be able to set a 95% confidence limit on KK-gluon masses up to 6.7 TeV [195]. On the other hand in case of the constrained fit with fixed $U = 0$ the lower bound is $M_{g^{(1)}} \geq 11.5\,\mathrm{TeV}$ ($M_{\mathrm{KK}} \geq 4.7\,\mathrm{TeV}$) at 95% which is even stronger than the bound in the minimal model for an unconstrained fit. The reason for such a strong bound lies in the reduced errors for S, T and in the enhanced correlation coefficient. Interestingly, in the constrained fit scenario the protection of the T parameter would not be sufficient. However, since the U parameter might receive corrections at loop level we will refer to the bound (2.107) when speaking about constraints from electroweak precision measurements in the custodial RS model.

3 Warped five-dimensional propagators

In this chapter we will derive and analyze boson and fermion 5D propagators in models with a warped extra dimension. The results will be necessary in order to calculate loop-induced processes in Higgs physics and for the $b \to s\gamma$ transition later in this thesis. Technically, it will be convenient to work in the mixed momentum-position representation of the 5D propagators, in which the extra-dimensional coordinates are kept in position space [126, 189, 196–198], i.e. 5D propagators are functions of the form $D(t, t'; p)$ depending on the coordinates t, t' and the four-momentum p. In this case, there exists a simple KK representation

$$D(t, t'; p) \sim \sum_{n=0}^{\infty} \frac{\chi_n(t)\, \chi_n(t')}{p^2 - m_n^2}\,, \tag{3.1}$$

where the 5D propagator is essentially the infinite sum of the propagators of the zero and KK modes including the corresponding profile functions. The immediate advantage of the 5D propagator is that it contains the contributions of all KK modes and therefore encodes the full 5D theory. In Chapters 4 and 5 we will perform calculations and derive results that probe the full structure of the 5D propagators and that could not have been explained by summing up the first few KK modes in the KK-decomposed theory. A further advantage will be that the 5D propagator allows to find analytically closed results for the amplitudes of loop-induced processes in Higgs physics and in case of the $b \to s\gamma$ transition. Moreover, we will be able to derive results for the 5D propagators that are valid to all orders in an expansion of $v^2/M_{\rm KK}^2$.

In the first section of this chapter we will discuss the Higgs 5D propagator in the minimal RS model, where we will derive a solution that can also be applied for a general 5D scalar with arbitrary boundary conditions. Section 3.2 deals with the solutions for the vector and scalar components of the gauge-boson 5D propagator in the minimal RS model with a brane-localized Higgs sector. In case of the W-boson 5D propagator, we will extend the results for the custodial RS model and for a bulk-Higgs sector. Section 3.3 is dedicated to the fermion 5D propagator in both the minimal and custodial version of the RS model, where we will derive results for the brane-localized and narrow bulk-Higgs scenarios. In the last section we will analyze the ultra-violet behavior of the gauge-boson and fermion 5D propagators in the minimal RS model.

The content of this chapter represents my own work, which has been partly published in our papers [2, 163, 199].

3.1 Higgs 5D propagator

We start with the calculation of the Higgs propagator in the minimal RS model with a bulk-Higgs sector as described in Section 2.3. Based on the Higgs Lagrangian (2.35) the corresponding 5D action is given by

$$S_{\text{Higgs}} = \frac{1}{2}\int d^4x\,\frac{2\pi}{L}\int_\epsilon^1 \frac{dt}{t}\,\frac{h(x,t)}{t}\left[-t^2\,\partial_\mu\partial^\mu + M_{\text{KK}}^2 t^3\partial_t\frac{1}{t^3}\partial_t\,t^2 - \mu^2\right]\frac{h(x,t)}{t}\,, \quad (3.2)$$

including only terms bilinear in the 5D Higgs field $h(x,t)$. We emphasize that (3.2) is the general action for a (real) 5D scalar field with a bulk mass μ when keeping track of the factor $t/(\epsilon\sqrt{r})$ that was pulled out of $h(x,t)$ in the definition of the Higgs doublet (2.34). Now, when we insert the KK decomposition of the 5D Higgs field (2.50) into (3.2) we can define the Higgs 5D propagator via the following KK representation

$$D_h(t,t';p) = \sum_{n=0}^{\infty}\frac{\chi_n^h(t)\,\chi_n^h(t')}{p^2 - m_{h_n}^2}\,, \quad (3.3)$$

where χ_n^h and m_{h_n} is the profile and mass of the n^{th} Higgs KK mode. Based on the 5D Higgs action (3.2) and the KK representation (3.3) we can derive the second-order differential equation

$$\left[t^2\hat{p}^2 + t^2\partial_t^2 + t\partial_t - \left(4 + \frac{\mu^2}{k^2}\right)\right]\frac{D_h(t,t';p)}{t} = -\frac{L\,t'^2}{2\pi M_{\text{KK}}^2}\delta(t-t')\,, \quad (3.4)$$

where $\hat{p}^2 \equiv p^2/M_{\text{KK}}^2$ is the normalized momentum squared. With $\beta \equiv \sqrt{4+\mu^2/k^2}$, as defined first in (2.36), and for time-like four-momenta $p^2 > 0$ the general solutions to (3.4) are given by linear combinations of the Bessel functions $J_\beta(\hat{p}t)$ and $Y_\beta(\hat{p}t)$.[1] The presence of the δ-function on the right side of (3.4) requires an ansatz that distinguishes between the two regions for $t > t'$ and $t < t'$. Consequently, there are in total four unknown coefficients that need to be determined. One of the coefficients can be determined by requiring that the propagator is continuous at $t = t'$, i.e.

$$D_h(t,t';p)\big|_{t=t'-0}^{t=t'+0} = 0\,. \quad (3.5)$$

Integrating (3.4) over an infinitesimal interval around $t = t'$ yields the jump condition

$$\partial_t\,D_h(t,t';p)\big|_{t=t'+0}^{t=t'-0} = -\frac{Lt'}{2\pi M_{\text{KK}}}\,, \quad (3.6)$$

which fixes another coefficient. Imposing the conditions (3.5) and (3.6) the general ansatz for time-like momenta reads

$$D_h(t,t';p) = \frac{L\,tt'}{4M_{\text{KK}}^2}\frac{[C_1^> J_\beta(\hat{p}t_>) + C_2^> Y_\beta(\hat{p}t_>)]\,[C_1^< J_\beta(\hat{p}t_<) + C_2^< Y_\beta(\hat{p}t_<)]}{C_1^> C_2^< - C_1^< C_2^>}\,, \quad (3.7)$$

where $t_> \equiv \max(t,t')$ and $t_< \equiv \min(t,t')$. The coefficients $C_{1,2}^>$ and $C_{1,2}^<$ are functions of the normalized momentum $\hat{p}$. We emphasize that they are not independent of each other, such that the two BCs of the 5D Higgs propagator will be sufficient to determine

[1] In case of space-like momenta $p^2 < 0$ the basic solutions are given by the modified Bessel functions $I_\beta(\hat{p}t)$ and $K_\beta(\hat{p}t)$ with $\hat{p} \equiv \sqrt{-p^2/M_{\text{KK}}^2}$. Note that once we have the final results of the 5D propagators for time-like momenta we can easily obtain the corresponding expressions for space-like momenta.

the complete solution. In general, we can consider the conditions

$$\left(\partial_t - \frac{b_\epsilon}{\epsilon}\right) D_h(t,t';p)\big|_{t=\epsilon^+} = 0\,, \qquad (\partial_t - b_1)\, D_h(t,t';p)\big|_{t=1^-} = 0\,, \tag{3.8}$$

where b_ϵ and b_1 parametrize the contributions of possible brane-localized terms in the 5D action. Keeping the derivation as general as possible, we apply the BCs (3.8) to the ansatz (3.7) and obtain the coefficients

$$\begin{aligned}
C_1^>(\hat{p}) &= -\hat{p}\, Y_{\beta-1}(\hat{p}) + (b_1 + \beta - 1)\, Y_\beta(\hat{p})\,,\\
C_1^<(\hat{p}) &= -\hat{p}\epsilon\, Y_{\beta-1}(\hat{p}\epsilon) + (b_\epsilon + \beta - 1)\, Y_\beta(\hat{p}\epsilon)\,,\\
C_2^>(\hat{p}) &= \hat{p}\, J_{\beta-1}(\hat{p}) - (b_1 + \beta - 1)\, J_\beta(\hat{p})\,,\\
C_2^<(\hat{p}) &= \hat{p}\epsilon\, J_{\beta-1}(\hat{p}\epsilon) - (b_\epsilon + \beta - 1)\, J_\beta(\hat{p}\epsilon)\,.
\end{aligned} \tag{3.9}$$

Thus, we have obtained an analytic solution for the Higgs 5D propagator with general BCs.

In case of the specific bulk-Higgs sector, as discussed in Section 2.3, the brane-localized terms in the Higgs Lagrangian (2.33) induce the BCs (2.37) for the 5D Higgs field. They translate to the values

$$\begin{aligned}
b_\epsilon &= m_{\rm UV} - 1 = \frac{M_{\rm UV}}{2k} - 1\,,\\
b_1 &= m_{\rm IR} - \frac{6\lambda}{M_{\rm KK}^2} v^2(1) - 1 = 5 + 3\beta - 2m_{\rm IR} = 1 + \beta - 2\delta\,.
\end{aligned} \tag{3.10}$$

As explained in the text below equation (2.54), the parameter $\delta = m_{\rm IR} - 2 - \beta$ has to be small in order to allow for a realistic Higgs mass $m_h \ll M_{\rm KK}$, which implies that $b_1 \approx 1 + \beta$.

3.2 Gauge-boson 5D propagator

Next, we will derive the vector and scalar components of the gauge-boson 5D propagator in various RS models. In the minimal RS model with a brane-localized Higgs sector we will derive solutions for the massless and massive gauge-boson propagators. For the remaining versions of the RS model we will focus on the W-boson 5D propagator which will be required for the analysis of processes in Higgs physics in Chapter 4. This section is mainly based on our publication [163].

Minimal RS model with a brane-localized Higgs sector

We begin with the minimal version of the RS model where the Higgs sector is localized at the IR brane, according to the scenario defined in (1.55). The action of a 5D gauge boson $B_M(x,t)$ that contains only terms bilinear in the field is given in general R_ξ gauge by [126]

$$S_{\rm Gauge} = \frac{1}{2}\int d^4x\, \frac{2\pi r}{L} \int_\epsilon^1 \frac{dt}{t}\, B_M(x,t)\, K_{B,\xi}^{MN}\, B_N(x,t)\,, \tag{3.11}$$

with the differential operators

$$\begin{aligned} K^{\mu\nu}_{B,\xi} &= \left(\partial_\alpha\partial^\alpha - M^2_{\mathrm{KK}} t\partial_t \frac{1}{t}\partial_t\right)\eta^{\mu\nu} - \left(1-\frac{1}{\epsilon}\right)\partial^\mu\partial^\nu\,, \\ K^{55}_{B,\xi} &= -\partial_\alpha\partial^\alpha \frac{1}{t^2} + \xi M^2_{\mathrm{KK}} t\partial_t t\partial_t \frac{1}{t^2}\,. \end{aligned} \tag{3.12}$$

The gauge-fixing procedure leads to vanishing off-diagonal entries $K^{\mu 5}_{B,\xi} = 0$ and $K^{5\nu}_{B,\xi} = 0$, which implies that the vector and scalar components of the gauge-boson 5D propagator decouple. Details on the gauge-fixing procedure can be found in [126, 132]. In order to identify the 5D propagator as an infinite sum of zero- and KK-mode propagators we rescale the 5D field $B_M \to B_M/\sqrt{r}$, such that the mass dimensions are consistent. Note that B_M has the canonical mass dimension $[B_M] = 3/2$. Then, the differential equations for the vector and scalar components are given by

$$\begin{aligned} \left[\left(\hat{p}^2 + t\partial_t\frac{1}{t}\partial_t\right)\eta^{\mu\nu} - \left(1-\frac{1}{\epsilon}\right)\hat{p}^\mu\hat{p}^\nu\right] D^\xi_{B,\nu\rho}(t,t';p) &= -\frac{Lt'}{2\pi M^2_{\mathrm{KK}}}\,\delta^\mu_\rho\,\delta(t-t')\,, \\ \left[\hat{p}^2 + \xi\, t\partial_t t\partial_t\frac{1}{t^2}\right] D^\xi_{B,55}(t,t';p) &= \frac{Lt'^3}{2\pi\epsilon^2 M^2_{\mathrm{KK}}}\,\delta(t-t')\,, \end{aligned} \tag{3.13}$$

where δ^μ_ρ denotes the Kronecker delta. Beginning with the vector component of the 5D propagator we can use Lorentz covariance to make the general ansatz

$$D^\xi_{B,\nu\rho}(t,t';p) = A^\xi_B(t,t';-p^2)\frac{p_\nu p_\rho}{p^2} + B_B(t,t';-p^2)\left(\eta_{\nu\rho} - \frac{p_\nu p_\rho}{p^2}\right)\,, \tag{3.14}$$

with two scalar functions $A^\xi_B(t,t';-p^2)$ and $B_B(t,t';-p^2)$. Inserting (3.14) into the first equation of (3.13) we obtain two partial differential equations

$$\begin{aligned} \left(\frac{\hat{p}^2}{\xi} + t\partial_t\frac{1}{t}\partial_t\right) A^\xi_B(t,t';-p^2) &= \left(\hat{p}^2 + t\partial_t\frac{1}{t}\partial_t\right) B_B(t,t';-p^2)\,, \\ \left(\hat{p}^2 + t\partial_t\frac{1}{t}\partial_t\right) B_B(t,t';-p^2) &= -\frac{Lt'}{2\pi M^2_{\mathrm{KK}}}\,\delta(t-t')\,. \end{aligned} \tag{3.15}$$

The first equation relates both scalar functions by $A^\xi_B(t,t';-p^2) = B_B(t,t';-p^2/\xi)$, such that it is sufficient to determine $B_B(t,t';-p^2)$ via the second equation in (3.15). If we insert the KK decomposition of the 5D field $B_M(x,t)$ into the action (3.11) we can deduce the KK representation of the propagator function

$$B_B(t,t';-p^2) = \sum_{n=0}^{\infty}\frac{\chi^B_n(t)\,\chi^B_n(t')}{m^2_{B_n} - p^2}\,. \tag{3.16}$$

We can relate this propagator function to the scalar component of the 5D propagator. For that purpose, it is useful to introduce the parametrization $D^\xi_{B,55}(t,t';p) = -\frac{1}{\xi}B_{B,55}(t,t';-p^2/\xi)$ with the scalar propagator function $B_{B,55}$. The KK representation is given by

$$B_{B,55}(t,t';-p^2) = \sum_{n=0}^{\infty}\frac{k^2 tt'}{m^2_{B_n}}\frac{\partial_t\chi^B_n(t)\,\partial_{t'}\chi^B_n(t')}{m^2_{B_n} - p^2}\,, \tag{3.17}$$

where k is the curvature scale. The propagator function (3.17) can be related to (3.16) by

$$B_{B,55}(t,t';-p^2) = \frac{k^2 tt'}{p^2}\partial_t\partial_{t'}\left[B_B(t,t';0) - B_B(t,t';-p^2)\right] , \tag{3.18}$$

which implies that the scalar component of the gauge-boson 5D propagator can be determined, once a solution for the vector component is known. Therefore, we now consider the second partial differential equation in (3.15) which can be reformulated to

$$\left(t^2\hat{p}^2 + t^2\partial_t^2 + t\partial_t - 1\right)\frac{B_B(t,t';-p^2)}{t} = -\frac{L\,t'^2}{2\pi M_{\rm KK}^2}\delta(t-t') . \tag{3.19}$$

This equation is very similar to the Bessel differential equation for the Higgs 5D propagator in (3.4). Following the derivational steps outlined in Section 3.1 we obtain the general result

$$B_B(t,t';-p^2) = \frac{L\,tt'}{4M_{\rm KK}^2}\frac{\left[C_1^> J_1(\hat{p}t_>) + C_2^> Y_1(\hat{p}t_>)\right]\left[C_1^< J_1(\hat{p}t_<) + C_2^< Y_1(\hat{p}t_<)\right]}{C_1^> C_2^< - C_1^< C_2^>} , \tag{3.20}$$

with

$$\begin{aligned} C_1^>(\hat{p}) &= -\hat{p}\,Y_0(\hat{p}) + b_1\,Y_1(\hat{p}) , & C_2^>(\hat{p}) &= \hat{p}\,J_0(\hat{p}) - b_1\,J_1(\hat{p}) , \\ C_1^<(\hat{p}) &= -\hat{p}\epsilon\,Y_0(\hat{p}\epsilon) + b_\epsilon\,Y_1(\hat{p}\epsilon) , & C_2^<(\hat{p}) &= \hat{p}\epsilon\,J_0(\hat{p}\epsilon) - b_\epsilon\,J_1(\hat{p}\epsilon) . \end{aligned} \tag{3.21}$$

The coefficients depend on the values b_ϵ, b_1 which parametrize the BCs

$$\left(\partial_t - \frac{b_\epsilon}{\epsilon}\right)B_B(t,t';-p^2)\big|_{t=\epsilon^+} = 0 , \qquad (\partial_t - b_1)\,B_B(t,t';-p^2)\big|_{t=1^-} = 0 , \tag{3.22}$$

at the UV and IR branes. The general expression (3.20) can be used to determine solutions for the photon, gluon, W- and Z-boson propagators, which have first been derived in [126, 190, 200]. In all these cases the BC at the UV brane is given by the first equation in (3.22) with the value $b_\epsilon = 0$. Implementing this condition, the solution (3.20) in the region of time-like momenta ($p^2 > 0$) takes the compact form

$$B_B(t,t';-p^2) = \frac{Ltt'}{4M_{\rm KK}^2}\frac{\left[\hat{p}D_{10}(t_>,1) - b_1 D_{11}(t_>,1)\right]D_{10}(t_<,\epsilon)}{\hat{p}D_{00}(1,\epsilon) - b_1 D_{10}(1,\epsilon)} , \tag{3.23}$$

with

$$D_{ij}(t,t') = J_i(\hat{p}t)\,Y_j(\hat{p}t') - Y_i(\hat{p}t)\,J_j(\hat{p}t') . \tag{3.24}$$

Later in this thesis when we calculate physical processes it will be convenient to perform a Wick rotation to the Euclidean momentum space with $p_E^2 \equiv -p^2 > 0$ and $\hat{p}_E^2 \equiv p_E^2/M_{\rm KK}^2$. In this case we obtain the solution

$$B_B(t,t';p_E^2) = \frac{Ltt'}{2\pi M_{\rm KK}^2}\frac{\left[\hat{p}_E D_{10}(t_>,1) + b_1 D_{11}(t_>,1)\right]D_{10}(t_<,\epsilon)}{\hat{p}_E D_{00}(1,\epsilon) - b_1 D_{10}(1,\epsilon)} , \tag{3.25}$$

with $D_{ij}(t,t') \equiv I_i(\hat{p}_E t)\,K_j(\hat{p}_E t') - (-1)^{i+j}K_i(\hat{p}_E t)\,I_j(\hat{p}_E t')$, where I_i and K_i are the modified Bessel functions of the first and second kind. The photon and gluon propagator functions B_A and B_G can be obtained by setting the boundary value $b_1 = 0$ in (3.23) and (3.25). For the W- and Z-boson propagator functions, B_W and B_Z, the corresponding

values are given by

$$b_1\big|_{W\text{ boson}} = -\frac{L\tilde{m}_W^2}{M_{\rm KK}^2}\,, \qquad\qquad b_1\big|_{Z\text{ boson}} = -\frac{L\tilde{m}_Z^2}{M_{\rm KK}^2}\,, \tag{3.26}$$

where the leading-order masses $\tilde{m}_W^2$ and $\tilde{m}_Z^2$ are defined in (2.5). Finally, we have derived exact results for the gauge-boson 5D propagator.

For the later analysis in Chapter 4 we will need to expand the W-boson propagator in powers of $v^2/M_{\rm KK}^2$, while keeping p^2 and m_W^2 fixed and of order v^2. For time-like momenta we find

$$B_W(t,t';-p^2) = \frac{1}{2\pi}\,\frac{-1}{(p^2-\tilde{m}_W^2)\,[1+\Pi(t,t';p^2)]+\Sigma(p^2)+i0}\,, \tag{3.27}$$

where

$$\begin{aligned}\Sigma(p^2) &= \frac{\tilde{m}_W^4}{2M_{\rm KK}^2}\left(L-\frac{p^2}{\tilde{m}_W^2}+\frac{1}{2L}\,\frac{p^4}{\tilde{m}_W^4}\right)\,,\\ \Pi(t,t';p^2) &= \frac{\tilde{m}_W^2}{2M_{\rm KK}^2}\left\{Lt_>^2+\frac{p^2}{\tilde{m}_W^2}\left[Lt_<^2-t^2\left(\frac{1}{2}-\ln t\right)-t'^2\left(\frac{1}{2}-\ln t'\right)\right]\right\}\,.\end{aligned} \tag{3.28}$$

Both equations are valid up to terms of order $v^4/M_{\rm KK}^4$. The zero of the denominator of the propagator in (5.5) defines the physical mass m_W of the ground state, such that $m_W^2 = \tilde{m}_W^2 - \Sigma(m_W^2)$. Using the first equation in (3.28) we can reproduce the result (2.10) obtained earlier in Section 2.1. The residue of the pole in (5.5) determines the product of the W-boson profiles $2\pi\,\chi_0^W(t)\,\chi_0^W(t') = 1-\Pi(t,t';m_W^2)-\partial\Sigma(p^2)/\partial p^2\big|_{p^2=m_W^2}$. Using (3.28) we can extract the zero-mode profile $\chi_0^W(t)$ to leading order in $v^2/M_{\rm KK}^2$, and reproduce the expression (2.12). Finally, the W-boson propagator function is given for time-like momenta $p^2 \lesssim v^2$ and to leading order in an expansion of $v^2/M_{\rm KK}^2$ by

$$B_W(t,t';-p^2) = \frac{1}{2\pi}\left[\frac{c_1(t,t')}{m_W^2-p^2}+\frac{c_2(t,t')}{2M_{\rm KK}^2}\right]+\mathcal{O}\left(\frac{v^2}{M_{\rm KK}^4}\right) \tag{3.29}$$

with

$$\begin{aligned}c_1(t,t') &= 2\pi\,\chi_0^W(t)\,\chi_0^W(t')\,,\\ c_2(t,t') &= L\,t_<^2+\frac{1}{2L}+t^2\left(\ln t-\frac{1}{2}\right)+t'^2\left(\ln t'-\frac{1}{2}\right)\,.\end{aligned} \tag{3.30}$$

In contrast to the exact result the expanded expression (3.29) is a simple function where the $v^2/M_{\rm KK}^2$ corrections from the zero mode and from the massive KK modes are clearly separated.

Minimal RS model with a bulk-Higgs sector

We continue with the minimal version of the RS model where the Higgs sector is extended into the bulk as described in Section 2.3. In the following we will focus on the W-boson 5D propagator which will be required for the analysis in Chapter 4. The action for the 5D gauge boson is given by (3.11) supplemented by an additional bulk mass for the 5D field. One can proceed in analogy to the brane-localized Higgs scenario, as described in the beginning of the previous subsection, and derive a second-order differential equation

for the propagator function

$$\left(t^2\hat{p}^2 + t^2\partial_t^2 + t\partial_t - c_W^2(t) - 1\right)\frac{B_W(t,t';-p^2)}{t} = -\frac{L\,t'^2}{2\pi M_{\rm KK}^2}\,\delta(t-t')\,. \tag{3.31}$$

In contrast to (3.19) it includes the normalized t-dependent bulk-mass coefficient

$$c_W^2(t) = \frac{2\pi\tilde{m}_W^2}{M_{\rm KK}^2}\frac{t^2v^2(t)}{v^2} = \frac{L\tilde{m}_W^2}{M_{\rm KK}^2}(1+\beta)t^{4+2\beta}\,, \tag{3.32}$$

where $v \equiv v_4$, see (2.44), and $\tilde{m}_W = vg_5/(2\sqrt{2\pi r})$. The propagator function is subject to the usual continuity and jump conditions and to Neumann BCs on both branes. In the special case of vanishing momentum $p^2 = 0$ we are able to derive the exact result

$$B_W(t,t';0) = -\frac{L\alpha\,tt'}{4M_{\rm KK}^2\sin(\pi\alpha)}\frac{D_1(t_>,1)D_1(t_<,\epsilon)}{D_2(1,\epsilon)}\,, \tag{3.33}$$

where $\alpha \equiv 1/(2+\beta)$. The t,t'-dependent functions are defined by

$$\begin{aligned} D_1(t,t') &= \tilde{I}_\alpha(t)\,\tilde{I}_{1-\alpha}(t') - \tilde{I}_{-\alpha}(t)\,\tilde{I}_{\alpha-1}(t')\,,\\ D_2(t,t') &= \tilde{I}_{\alpha-1}(t)\,\tilde{I}_{1-\alpha}(t') - \tilde{I}_{1-\alpha}(t)\,\tilde{I}_{\alpha-1}(t')\,, \end{aligned} \tag{3.34}$$

with

$$\tilde{I}_\alpha(t) \equiv I_\alpha\left(\frac{2L\tilde{m}_W^2}{M_{\rm KK}^2}\frac{1+\beta}{2+\beta}\,t^{2+\beta}\right)\,. \tag{3.35}$$

In order to better understand the W-boson 5D propagator we can expand the result (3.33) to leading order in $v^2/M_{\rm KK}^2$ and obtain

$$B_W(t,t';0) = \frac{1}{2\pi\tilde{m}_W^2} + \frac{L}{4\pi M_{\rm KK}^2}\left[\frac{2(1+\beta)^2}{(2+\beta)(3+\beta)} + \frac{t^{4+2\beta}+t'^{4+2\beta}}{2+\beta} - t_>^2\right]\,. \tag{3.36}$$

When we take the limit $\beta \to \infty$ ($\alpha \to 0$) we recover the corresponding result in the brane-localized Higgs scenario, see (3.29) for $p^2 = 0$.

Next, we continue with the case for non-zero momenta. In fact, for time-like momenta with $p^2 \lesssim v^2$ we can derive a solution to leading order in $v^2/M_{\rm KK}^2$. For this purpose we make the ansatz

$$B_W(t,t';-p^2) = B_0(t,t';-p^2) + \hat{\epsilon}\,B_1(t,t';-p^2) + \hat{\epsilon}^2\,B_2(t,t';-p^2) + \mathcal{O}(\hat{\epsilon}^3)\,, \tag{3.37}$$

where $\hat{\epsilon}$ is a small parameter and counts the orders of $v^2/M_{\rm KK}^2$. Plugging this ansatz into (3.31) and collecting all terms of the same order in $v^2/M_{\rm KK}^2$ we obtain three differential equations

$$\begin{aligned} t\partial_t\frac{1}{t}\partial_t B_0(t,t';-p^2) &= 0\,,\\ t\partial_t\frac{1}{t}\partial_t B_1(t,t';-p^2) + \left(\hat{p}^2 - \frac{c_W^2(t)}{t^2}\right)B_0(t,t';-p^2) &= -\frac{Lt'}{2\pi M_{\rm KK}^2}\delta(t-t')\,,\\ t\partial_t\frac{1}{t}\partial_t B_2(t,t';-p^2) + \left(\hat{p}^2 - \frac{c_W^2(t)}{t^2}\right)B_1(t,t';-p^2) &= 0\,. \end{aligned} \tag{3.38}$$

Each of the functions B_0, B_1 and B_2 is subject to the continuity condition and Neumann BCs at both branes. The jump condition is only relevant for B_1 while the derivatives of B_0 and B_2 are continuous at $t = t'$. The first equation in (3.38) implies that $B_0(t, t', -p^2) = C(t')$ is a function only of the t'-coordinate. The BCs together with the continuity condition at $t = t'$ imply that $C(t') = C$ is a constant. In order to determine the value for C we need to take the second equation of (3.38) into account including the continuity and jump conditions as well as the BCs at both branes. Analogously, the function B_1 can only be determined by using the last equation in (3.38). Finally, we find that the propagator function $B_W(t, t'; -p^2)$ is given to leading order in $v^2/M_{\rm KK}^2$ and for $|p^2| \lesssim v^2$ by the solution (3.29) with the modified (β-dependent) function

$$\begin{aligned} c_1(t,t') = 1 + \frac{m_W^2}{2M_{\rm KK}^2}\bigg[& \frac{L(t^{4+2\beta} + t'^{4+2\beta})}{2+\beta} + \frac{(1+\beta)(3+\beta)}{(2+\beta)^2} - \frac{1}{L} \\ & - t^2\left(L - \frac{1}{2} + \ln t\right) - t'^2\left(L - \frac{1}{2} + \ln t'\right)\bigg], \end{aligned} \tag{3.39}$$

while $c_2(t, t')$ is given by the same expression as in (3.30). We emphasize that in the limit $\beta \to \infty$ the function $c_1(t, t')$ reduces to the expression in the first line of (3.30) and we recover the W-boson 5D propagator in the brane-localized Higgs scenario.

Custodial RS model with a brane-localized Higgs sector

Next, we will focus on the RS model with custodial symmetry and a Higgs sector localized at the IR brane, see Section 2.4 for a description of this model. This subsection is based on our publication [163], where we have derived an exact expression of the W-boson 5D propagator in the custodial RS model for the first time. The differential equation for the propagator function in the UV basis, denoted by $\boldsymbol{B}_W^{\rm UV}$, is the same as in the minimal RS model (3.4). However, the BCs are modified to

$$\begin{aligned} (\boldsymbol{P}_+ \,\partial_t + \boldsymbol{P}_-)\, \boldsymbol{B}_W^{\rm UV}(t,t';-p^2)\big|_{t=\epsilon} &= 0\,, \\ \big(\partial_t - b_1\, \boldsymbol{R}_{\vartheta_W}^T \boldsymbol{P}_+ \boldsymbol{R}_{\vartheta_W}\big)\, \boldsymbol{B}_W^{\rm UV}(t,t';-p^2)\big|_{t=1^-} &= 0\,; \qquad b_1 = -\frac{L\tilde{m}_W^2}{c_{\vartheta_W}^2 M_{\rm KK}^2}\,, \end{aligned} \tag{3.40}$$

where $\boldsymbol{P}_+ = \mathrm{diag}(1,0)$ and $\boldsymbol{P}_- = \mathrm{diag}(0,1)$. The first equation follows from the BCs for the UV fields $L_M^\pm$ and $R_M^\pm$. The second equation is a direct consequence of (2.77). We find that, in the region of time-like momenta $p^2 > 0$, the general solution for the propagator function reads

$$\begin{aligned} \boldsymbol{B}_W^{\rm UV}(t,t';-p^2) = {} & \frac{Ltt'}{4M_{\rm KK}^2}\, \frac{1}{\big[\hat{p} D_{00}(1,\epsilon) - b_1 D_{10}(1,\epsilon)\big] D_{01}(1,\epsilon) - b_1 \frac{4 s_{\vartheta_W}^2}{\pi^2 \hat{p}^2 \epsilon}} \\ & \times \Bigg\{ \left[\big[\hat{p} D_{10}(t_>,1) - b_1 D_{11}(t_>,1)\big] D_{01}(1,\epsilon) - b_1 \frac{2 s_{\vartheta_W}^2}{\pi \hat{p}}\, D_{11}(t_>,\epsilon)\right] D_{10}(t_<,\epsilon)\, \boldsymbol{P}_+ \\ & + \left[\big[\hat{p} D_{00}(1,\epsilon) - b_1 D_{10}(1,\epsilon)\big] D_{10}(t_>,1) + b_1 \frac{2 s_{\vartheta_W}^2}{\pi \hat{p}}\, D_{10}(t_>,\epsilon)\right] D_{11}(t_<,\epsilon)\, \boldsymbol{P}_- \\ & - b_1 \frac{2 s_{\vartheta_W} c_{\vartheta_W}}{\pi \hat{p}} \big[D_{10}(t,\epsilon)\, D_{11}(t',\epsilon)\, \boldsymbol{P}_{12} + D_{11}(t,\epsilon)\, D_{10}(t',\epsilon)\, \boldsymbol{P}_{21}\big]\Bigg\}, \end{aligned} \tag{3.41}$$

which is valid to all orders in $v^2/M_{\rm KK}^2$. The functions $D_{ij}(t, t')$ have been defined in (3.24), and we have introduced the 2×2 matrices $\boldsymbol{P}_{12}$ and $\boldsymbol{P}_{21}$, which have an entry 1 at

the corresponding position indicated by the subscripts and entries 0 otherwise. Note that up to irrelevant $\mathcal{O}(\epsilon^2)$ terms we can replace $\hat{p}\epsilon D_{n1}(t,\epsilon) = -\frac{2}{\pi}\, J_n(\hat{p}t)$ for $n = 0, 1$. This gives rise to a simpler expression, in which the spurious $1/\epsilon$ term in the denominator is removed. In the limit $s_{\vartheta_W} \to 0$, we can identify the coefficient of $\boldsymbol{P}_+$ in (3.41) with the result (3.23) obtained in the minimal RS model. When we expand (3.41) to leading order in $v^2/M_{\rm KK}^2$ and for time-like momenta $p^2 \lesssim v^2$ we obtain the expression

$$2\pi\, \boldsymbol{B}_W^{\rm UV}(t,t';-p^2) = \begin{pmatrix} \frac{c_1(t,t')}{m_W^2-p^2} + \frac{c_2(t,t')}{2M_{\rm KK}^2} & \frac{Lm_W^2\tan\vartheta_W}{2M_{\rm KK}^2(m_W^2-p^2)}t'^2 \\ \frac{Lm_W^2\tan\vartheta_W}{2M_{\rm KK}^2(m_W^2-p^2)}t^2 & \frac{Lt_<^2}{2M_{\rm KK}^2} \end{pmatrix} + \mathcal{O}\left(\frac{v^2}{M_{\rm KK}^4}\right), \qquad (3.42)$$

where the functions $c_1(t,t')$ and $c_2(t,t')$ are given by the same expressions (3.30) as in the minimal RS model. For the special case of $p^2 = 0$ our result reduces to equation (54) in [149], which had already been obtained earlier. However the general result (3.41) is valid for arbitrary momentum.

Custodial RS model with a bulk-Higgs sector

At last, we will derive the W-boson 5D propagator in the RS model with custodial symmetry and a bulk-Higgs sector. It is convenient to work in the IR basis, see the text below (2.72), where the corresponding partial differential equations for the propagator function decouple. In analogy to (3.31) we find

$$\left(t^2\hat{p}^2 + t^2\partial_t^2 + t\partial_t - \frac{c_W^2(t)}{c_{\vartheta_W}^2}\boldsymbol{P}_+ - 1\right)\frac{\boldsymbol{B}_W^{\rm IR}(t,t';-p^2)}{t} = -\frac{L\,t'^2}{2\pi M_{\rm KK}^2}\delta(t-t')\,, \qquad (3.43)$$

where $c_W^2(t)$ is defined in (3.32). After rotating the IR basis fields into the UV basis via $\boldsymbol{R}_{\vartheta_W}$ in (2.70) we can derive the BCs

$$[\boldsymbol{P}_+\partial_t + \boldsymbol{P}_-]\;\boldsymbol{R}_{\vartheta_W}^T\,\boldsymbol{B}_W^{\rm IR}(t,t';-p^2)\big|_{t=\epsilon} = 0\,, \qquad \partial_t\boldsymbol{B}_W^{\rm IR}(t,t';-p^2)\big|_{t=1} = 0\,. \qquad (3.44)$$

Imposing the continuity and jump conditions we can proceed analogously to the calculation in the minimal RS model. For the special case of $p^2 = 0$ we can derive the exact result

$$\boldsymbol{B}_W^{\rm IR}(t,t';0) = \frac{L}{4\pi M_{\rm KK}^2}\Bigg\{\frac{-\pi\alpha\,tt'}{\sin\pi\alpha}\frac{D_1(t,\epsilon)D_1(t',\epsilon)}{D_2(1,\epsilon)}\boldsymbol{P}_+ + \left[t_<^2 - \epsilon^2 - \frac{2\tan\vartheta_W}{c_W(1)\epsilon^\beta}\frac{D_1(\epsilon,1)}{D_2(\epsilon,1)}\right]\boldsymbol{P}_- \\ + \frac{2\tan\vartheta_W}{c_W(1)\epsilon^{1+\beta}}\left[\frac{tD_1(t,1)}{D_2(1,\epsilon)}\boldsymbol{P}_{12} + \frac{t'D_1(t',1)}{D_2(1,\epsilon)}\boldsymbol{P}_{21}\right]\Bigg\}, \qquad (3.45)$$

where $\alpha = 1/(2+\beta)$ and $c_W(1) = \frac{\tilde{m}_W}{M_{\rm KK}}\sqrt{2L(1+\beta)}$. The functions $D_{1,2}(t,t')$ are defined in (3.34). We observe that the (11)-component in (3.45) coincides with the result in the minimal RS model (3.33). Expanding (3.45) to leading order in $v^2/M_{\rm KK}^2$ and rotating the propagator function into the UV basis we find

$$\boldsymbol{B}_W^{\rm UV}(t,t';0) = \frac{\boldsymbol{P}_+}{2\pi\tilde{m}_W^2} + \frac{L}{4\pi M_{\rm KK}^2}\Bigg[\left(\frac{2(1+\beta)^2}{c_{\vartheta_W}^2(2+\beta)(3+2\beta)} + \frac{t^{4+2\beta}+t'^{4+2\beta}}{2+\beta} - t_>^2\right)\boldsymbol{P}_+ \\ + \tan\vartheta_W\left(t'^2\left(1-\frac{t'^{2+2\beta}}{2+\beta}\right)\boldsymbol{P}_{12} + t^2\left(1-\frac{t^{2+2\beta}}{2+\beta}\right)\boldsymbol{P}_{21}\right) + t_<^2\boldsymbol{P}_-\Bigg]. \qquad (3.46)$$

In the limit $\beta \to \infty$ we recover the corresponding result for a brane-localized Higgs sector in (3.42) for $p^2 = 0$.

3.3 Fermion 5D propagator

This section is dedicated to the derivation of the fermion 5D propagator in the minimal and custodial RS model. We will derive results in the brane-localized and narrow bulk-Higgs scenarios which are distinguished by the conditions (1.55) and (1.56) on the regulator η of the Higgs profile as discussed in Section 1.4.5. We will need the results presented in this section to calculate the loop-induced processes in Higgs physics and for the $b \to s\gamma$ transition in Chapters 4 and 5. Previous calculations of the fermion 5D propagator in a warped extra dimension can be found in [189, 196], where the authors derived results for one family generation. The authors of [198] considered three family generations but derived the 5D propagator without including the Yukawa interactions within the IR BCs, i.e. their solutions are only valid at zeroth order in $v^2/M_{\rm KK}^2$. The first calculation in the minimal RS model including the Yukawa interactions and three family generations was performed in [200], where solutions were obtained in the brane-localized Higgs scenario with the regulator η sent to zero. This section contains a comprehensive discussion of derivational steps and explicit solutions for the fermion 5D propagator in the minimal and custodial RS model, which includes solutions in the brane-localized Higgs scenario and also for coordinates in the region $t, t' \in [1-\eta, 1]$ for the narrow bulk-Higgs with finite (non-zero) η. The presented material is based on our publications [2, 199] but also contains unpublished work.

3.3.1 Differential equations and boundary conditions

In the following, we will derive the quark 5D propagator in the custodial RS model. Calculation steps and results can be obtained by simple replacements for the case of the minimal model. The starting point is the 5D action that contains terms bilinear in the quark fields

$$S_{\rm Ferm} = \sum_{\mathcal{Q}=\mathcal{U},\mathcal{D},\Lambda} \int d^4x \int_\epsilon^1 dt\, \bar{\mathcal{Q}}(x,t) \Big[i\not{\partial} - M_{\rm KK}\gamma_5\partial_t - M_{\rm KK}\,\mathcal{M}_{\vec{q}}(t) \Big] \mathcal{Q}(x,t)\,, \tag{3.47}$$

where the six-component spinor fields $\mathcal{U}, \mathcal{D}, \Lambda$ are defined in the text below (2.81). The generalized mass matrix is defined in the custodial RS model by

$$\mathcal{M}_{\vec{q}}(t) = \frac{1}{t} \begin{pmatrix} \boldsymbol{c}_{\vec{Q}} & 0 \\ 0 & -\boldsymbol{c}_{\vec{q}} \end{pmatrix} + \varrho\, \delta^\eta(t-1) \begin{pmatrix} 0 & \boldsymbol{Y}_{\vec{q}} \\ \boldsymbol{Y}_{\vec{q}}^\dagger & 0 \end{pmatrix}; \qquad \varrho \equiv \frac{v}{\sqrt{2} M_{\rm KK}}\,, \tag{3.48}$$

for $(\vec{Q}, \vec{q}) = (\vec{U}, \vec{u}), (\vec{D}, \vec{d}), (\vec{\Lambda}, \vec{\lambda})$. The bulk-mass parameters $\boldsymbol{c}_{\vec{Q}}$ and $\boldsymbol{c}_{\vec{q}}$ and the Yukawa matrices are given by (2.83) and (2.85). The regularized δ-function is defined by equation (1.58). From (3.47) we can read off the partial differential equation ($\vec{q} = \vec{u}, \vec{d}, \vec{\lambda}$)

$$\Big[\not{p} - M_{\rm KK}\,\gamma_5\,\partial_t - M_{\rm KK}\,\mathcal{M}_{\vec{q}}(t) \Big]\, \boldsymbol{S}^{\vec{q}}(t,t';p) = \delta(t-t')\,, \tag{3.49}$$

where $\boldsymbol{S}^{\vec{q}}(t,t';p)$ is the 15×15 (for up-type quarks) or 9×9 (for down- and λ-type quarks) fermion propagator in the mixed momentum-position representation. The 5D

propagator is defined via

$$\begin{aligned} i\boldsymbol{S}^{\vec{q}}(t,t';p) &= \int d^4x\, e^{ip\cdot x}\, \langle 0|\, T(\mathcal{Q}_L(x,t)+\mathcal{Q}_R(x,t))(\bar{\mathcal{Q}}_L(x,t)+\bar{\mathcal{Q}}_R(x,t))\,|0\rangle \\ &= \left[\boldsymbol{\Delta}^{\vec{q}}_{LL}(t,t';-p^2)\,\not{p} + \boldsymbol{\Delta}^{\vec{q}}_{RL}(t,t';-p^2)\right] P_R + (L\leftrightarrow R)\,, \end{aligned} \tag{3.50}$$

where we have introduced a parametrization in the second line in terms of the propagator functions $\boldsymbol{\Delta}^{\vec{q}}_{AB}$ with $A,B\in\{L,R\}$. When we insert the KK decomposition of the 5D fermions (2.17) with (2.86) into the first line of (3.50) we can derive the KK representation of the propagator functions

$$\begin{aligned} \boldsymbol{\Delta}^{\vec{q}}_{LL}(t,t';-p^2) &= \sum_n \frac{1}{p^2-m^2_{q_n}}\,\mathcal{Q}^{(n)}_L(t)\,\mathcal{Q}^{(n)\dagger}_L(t')\,, \\ \boldsymbol{\Delta}^{\vec{q}}_{RL}(t,t';-p^2) &= \sum_n \frac{m_{q_n}}{p^2-m^2_{q_n}}\,\mathcal{Q}^{(n)}_R(t)\mathcal{Q}^{(n)\dagger}_L(t')\,, \end{aligned} \tag{3.51}$$

where analogous relations hold for $\boldsymbol{\Delta}^{\vec{q}}_{RR}$ and $\boldsymbol{\Delta}^{\vec{q}}_{LR}$. With the help of (2.81) and (2.86) we directly see how to interpret the various components of the propagator functions. As an example we consider the (15)-component of the 5×5 (without considering the generation multiplicity) matrix $\boldsymbol{\Delta}^{\vec{u}}_{RL}$. The subscripts denote the chirality of the incoming and outgoing fields while the components give information about the charges under the bulk gauge group. In the case at hand the outgoing field u_R is a right-chiral and Z_2-odd field with a Dirichlet BC on the UV brane and which is part of the $SU(2)_L\times SU(2)_R$ bi-doublet. The incoming field U_L, on the other hand, is a left-chiral, Z_2-even field with a Dirichlet BC at the UV brane and which is part of the $SU(2)_L\times SU(2)_R$ triplet representation. Using the KK representation of the propagator functions (3.51), the EOMs and the completeness condition for the fermion profiles we can check that equation (3.49) is consistent in the KK decomposed theory. Now, we can insert (3.50) into (3.49) and obtain the coupled first-order differential equations

$$\begin{aligned} p^2\,\boldsymbol{\Delta}^{\vec{q}}_{LL}(t,t';-p^2) - M_{\rm KK}\,\mathcal{D}^{\vec{q}}_+\,\boldsymbol{\Delta}^{\vec{q}}_{RL}(t,t';-p^2) &= \delta(t-t')\,, \\ \boldsymbol{\Delta}^{\vec{q}}_{RL}(t,t';-p^2) - M_{\rm KK}\,\mathcal{D}^{\vec{q}}_-\,\boldsymbol{\Delta}^{\vec{q}}_{LL}(t,t';-p^2) &= 0\,, \\ p^2\,\boldsymbol{\Delta}^{\vec{q}}_{RR}(t,t';-p^2) - M_{\rm KK}\,\mathcal{D}^{\vec{q}}_-\,\boldsymbol{\Delta}^{\vec{q}}_{LR}(t,t';-p^2) &= \delta(t-t')\,, \\ \boldsymbol{\Delta}^{\vec{q}}_{LR}(t,t';-p^2) - M_{\rm KK}\,\mathcal{D}^{\vec{q}}_+\,\boldsymbol{\Delta}^{\vec{q}}_{RR}(t,t';-p^2) &= 0\,, \end{aligned} \tag{3.52}$$

where we used the shorthand notation $\mathcal{D}^{\vec{q}}_\pm \equiv \pm\partial_t + \mathcal{M}_{\vec{q}}(t)$. The equations in (3.52) can be decoupled at the price of turning first-order into second-order differential equations

$$\begin{aligned} \left(\hat{p}^2 - \mathcal{D}^{\vec{q}}_+\,\mathcal{D}^{\vec{q}}_-\right)\boldsymbol{\Delta}^{\vec{q}}_{LL}(t,t';-p^2) &= M^{-2}_{\rm KK}\,\delta(t-t')\,, \\ \left(\hat{p}^2 - \mathcal{D}^{\vec{q}}_-\,\mathcal{D}^{\vec{q}}_+\right)\boldsymbol{\Delta}^{\vec{q}}_{RR}(t,t';-p^2) &= M^{-2}_{\rm KK}\,\delta(t-t')\,, \\ \left(\hat{p}^2 - \mathcal{D}^{\vec{q}}_-\,\mathcal{D}^{\vec{q}}_+\right)\boldsymbol{\Delta}^{\vec{q}}_{RL}(t,t';-p^2) &= M^{-1}_{\rm KK}\,\mathcal{D}_-\,\delta(t-t')\,, \\ \left(\hat{p}^2 - \mathcal{D}^{\vec{q}}_+\,\mathcal{D}^{\vec{q}}_-\right)\boldsymbol{\Delta}^{\vec{q}}_{LR}(t,t';-p^2) &= M^{-1}_{\rm KK}\,\mathcal{D}_+\,\delta(t-t')\,, \end{aligned} \tag{3.53}$$

with the normalized momentum squared $\hat{p}^2 \equiv p^2/M_{\rm KK}^2$. Integrating (3.53) over an infinitesimal interval $t \in [t'-0, t'+0]$ at fixed t' one obtains the conditions

$$\begin{aligned}
&\boldsymbol{\Delta}^{\vec{q}}_{AA}(t'+0,t';-p^2) - \boldsymbol{\Delta}^{\vec{q}}_{AA}(t'-0,t';-p^2) = 0\,; \qquad A = L,R\,,\\
&\boldsymbol{\Delta}^{\vec{q}}_{RL}(t'+0,t';-p^2) - \boldsymbol{\Delta}^{\vec{q}}_{RL}(t'-0,t';-p^2) = -M_{\rm KK}^{-1}\,,\\
&\boldsymbol{\Delta}^{\vec{q}}_{LR}(t'+0,t';-p^2) - \boldsymbol{\Delta}^{\vec{q}}_{LR}(t'-0,t';-p^2) = M_{\rm KK}^{-1}\,.
\end{aligned} \tag{3.54}$$

The first equation shows the continuity of the propagator functions $\boldsymbol{\Delta}^{\vec{q}}_{LL}$ and $\boldsymbol{\Delta}^{\vec{q}}_{RR}$ at $t = t'$, while the last two equations show the discontinuity of $\boldsymbol{\Delta}^{\vec{q}}_{RL}$ and $\boldsymbol{\Delta}^{\vec{q}}_{LR}$. Further conditions on the propagator functions are imposed on the boundaries of the extra dimension, which follow from the implementation of the quark sector discussed in Section 2.4. The BCs at the UV brane are given by ($A = L, R$)

$$\begin{aligned}
\mathrm{diag}(0,1,1,0,0)\,\boldsymbol{\Delta}^{\vec{u}}_{LA}(\epsilon,t';-p^2) = 0 = \mathrm{diag}(1,0,0,1,1)\,\boldsymbol{\Delta}^{\vec{u}}_{RA}(\epsilon,t';-p^2)\,,\\
\mathrm{diag}(0,1,0)\,\boldsymbol{\Delta}^{\vec{d}}_{LA}(\epsilon,t';-p^2) = 0 = \mathrm{diag}(1,0,1)\,\boldsymbol{\Delta}^{\vec{d}}_{RA}(\epsilon,t';-p^2)\,,\\
\mathrm{diag}(1,0,0)\,\boldsymbol{\Delta}^{\vec{\lambda}}_{LA}(\epsilon,t';-p^2) = 0 = \mathrm{diag}(0,1,1)\,\boldsymbol{\Delta}^{\vec{\lambda}}_{RA}(\epsilon,t';-p^2)\,,
\end{aligned} \tag{3.55}$$

which differ for the corresponding quark types. The IR BCs take the simple form

$$\mathrm{diag}(0 \quad 1)\,\boldsymbol{\Delta}^{\vec{q}}_{LA}(1,t';-p^2) = 0 = \mathrm{diag}(1 \quad 0)\,\boldsymbol{\Delta}^{\vec{q}}_{RA}(1,t';-p^2)\,, \qquad A = L,R \tag{3.56}$$

where the entries 0 and 1 are zero and unit matrices of ranks according to the structure of the propagator functions in (3.51). Both UV and IR BCs follow from the BCs for the fields embedded in the 15- and 9-component vectors of (2.80).

3.3.2 Details on the derivation

Now, we can start with the calculation of the propagator functions. First, we will focus on the determination of $\boldsymbol{\Delta}^{\vec{q}}_{LL}$ and $\boldsymbol{\Delta}^{\vec{q}}_{RL}$. Later, we will explain how the results for the two remaining propagator functions with reversed chiralities can be obtained. As already mentioned, we will implement the regularized δ-function (1.58) with the regulator η. The presence of the regulator will split the calculation of the propagator functions into two regions where $t < 1-\eta$ and $t > 1-\eta$. For both regions we will derive basic solutions for $\boldsymbol{\Delta}^{\vec{q}}_{LL}$ and $\boldsymbol{\Delta}^{\vec{q}}_{RL}$, where we conveniently work in Euclidean momentum space. Furthermore, we will have to distinguish the different cases $t < t'$ and $t > t'$ for the extra-dimensional coordinates. Then, we will include the continuity, jump and BCs. Finally, we will match the solutions at $t = 1-\eta$.

Solution in the region $t < 1-\eta$

We begin with the region $t < 1-\eta$, where the regularized δ-function (1.58) has no support implying that the Yukawa matrices are absent in the generalized mass matrix (3.48). In this case, the differential operators in (3.53) are given by ($t < 1-\eta$)

$$\mathcal{D}^{\vec{q}}_{\pm}\mathcal{D}^{\vec{q}}_{\mp} = -\frac{\partial^2}{\partial t^2} + \mathcal{M}^2_{\vec{q}}(t) \pm \frac{d\mathcal{M}_{\vec{q}}(t)}{dt} = -\frac{\partial^2}{\partial t^2} + \frac{1}{t^2}\begin{pmatrix} \boldsymbol{c}_{\vec{Q}}(\boldsymbol{c}_{\vec{Q}} \mp \mathbf{1}) & 0 \\ 0 & \boldsymbol{c}_{\vec{q}}(\boldsymbol{c}_{\vec{q}} \pm \mathbf{1}) \end{pmatrix}. \tag{3.57}$$

Inserting (3.57) into (3.53) we observe that the basic solution to the differential equation of $\boldsymbol{\Delta}^{\vec{q}}_{LL}$ is given by linear combinations of the functions $\sqrt{t}\,I_\alpha(\hat{p}_E t)$ and $\sqrt{t}\,I_{-\alpha}(\hat{p}_E t)$, where α depends on the bulk-mass parameters. Here, $\hat{p}_E^2 = -p^2/M_{\rm KK}^2$ denotes the

square of the Euclidean momentum normalized to the KK scale. For the special case of integer values for α the solutions are given by a limiting procedure. In the region $t < 1 - \eta$ we can implicitly take into account the UV BCs (3.55) which leads to the ansatz $(t < 1 - \eta)$

$$\boldsymbol{\Delta}^{\vec{q}\,<}_{LL}(t,t';p_E^2) = \sqrt{t}\begin{pmatrix} \boldsymbol{D}_1^{\vec{Q}}(\hat{p}_E,t) & 0 \\ 0 & \boldsymbol{D}_2^{\vec{q}}(\hat{p}_E,t)\end{pmatrix}\begin{pmatrix} \boldsymbol{K}_1(t') & \boldsymbol{K}_2(t') \\ \boldsymbol{K}_3(t') & \boldsymbol{K}_4(t')\end{pmatrix}, \tag{3.58}$$

where the superscript of $\boldsymbol{\Delta}^{\vec{q}\,<}_{LL}$ indicates that the solution is valid for $t < t'$. The zeros and the four integration functions $\boldsymbol{K}_i(t')$ are matrices of corresponding rank. The matrix functions $\boldsymbol{D}_1^{\vec{A}}(\hat{p}_E,t)$ and $\boldsymbol{D}_2^{\vec{A}}(\hat{p}_E,t)$ depend on the specific choice of $\vec{A} = \vec{U},\vec{D},\vec{\Lambda},\vec{u},\vec{d},\vec{\lambda}$. They read

$$\begin{aligned}
\boldsymbol{D}^{\vec{U}}_{1,2}(\hat{p}_E,t) &= \mathrm{diag}\left(\boldsymbol{D}^{Q}_{1,2}(\hat{p}_E,t),\, \boldsymbol{D}^{Q}_{3,4}(\hat{p}_E,t)\right), \\
\boldsymbol{D}^{\vec{u}}_{1,2}(\hat{p}_E,t) &= \mathrm{diag}\left(\boldsymbol{D}^{u^c}_{1,2}(\hat{p}_E,t),\, \boldsymbol{D}^{\tau_1}_{3,4}(\hat{p}_E,t),\, \boldsymbol{D}^{\tau_2}_{3,4}(\hat{p}_E,t)\right), \\
\boldsymbol{D}^{\vec{D}}_{1,2}(\hat{p}_E,t) &= \boldsymbol{D}^{Q}_{1,2}(\hat{p}_E,t), \\
\boldsymbol{D}^{\vec{d}}_{1,2}(\hat{p}_E,t) &= \mathrm{diag}\left(\boldsymbol{D}^{\tau_2}_{1,2}(\hat{p}_E,t),\, \boldsymbol{D}^{\tau_1}_{3,4}(\hat{p}_E,t)\right), \\
\boldsymbol{D}^{\vec{\Lambda}}_{1,2}(\hat{p}_E,t) &= \boldsymbol{D}^{Q}_{3,4}(\hat{p}_E,t), \\
\boldsymbol{D}^{\vec{\lambda}}_{1,2}(\hat{p}_E,t) &= \mathrm{diag}\left(\boldsymbol{D}^{\tau_1}_{3,4}(\hat{p}_E,t),\, \boldsymbol{D}^{\tau_2}_{3,4}(\hat{p}_E,t)\right),
\end{aligned} \tag{3.59}$$

where we used a short-hand notation for $\boldsymbol{D}_i^A(\hat{p}_E,t) \equiv \boldsymbol{D}_i^A(\hat{p}_E,t,\epsilon)$. The latter functions are defined by $(A = Q,u^c,\tau_1,\tau_2)$

$$\begin{aligned}
\boldsymbol{D}^A_{1,2}(\hat{p}_E,t,t') &\equiv I_{-\boldsymbol{c}_A-\frac{1}{2}}(\hat{p}_E t')\, I_{\boldsymbol{c}_A\mp\frac{1}{2}}(\hat{p}_E t) - I_{\boldsymbol{c}_A+\frac{1}{2}}(\hat{p}_E t')\, I_{-\boldsymbol{c}_A\pm\frac{1}{2}}(\hat{p}_E t), \\
\boldsymbol{D}^A_{3,4}(\hat{p}_E,t,t') &\equiv I_{-\boldsymbol{c}_A+\frac{1}{2}}(\hat{p}_E t')\, I_{\boldsymbol{c}_A\mp\frac{1}{2}}(\hat{p}_E t) - I_{\boldsymbol{c}_A-\frac{1}{2}}(\hat{p}_E t')\, I_{-\boldsymbol{c}_A\pm\frac{1}{2}}(\hat{p}_E t),
\end{aligned} \tag{3.60}$$

which are (diagonal) 3×3 matrices in generation space. Antisymmetry in the last two arguments implies that $\boldsymbol{D}^A_{2,3}(\hat{p}_E,t,t) = 0$. With respect to the UV BCs we note that $\boldsymbol{D}^A_{2,3}(\hat{p}_E,t,\epsilon) = 0$. Concerning the chirality-flipping propagator function $\boldsymbol{\Delta}^{\vec{q}}_{RL}$ we plug (3.58) into the first equation of (3.52) and obtain $(t < 1 - \eta)$

$$\boldsymbol{\Delta}^{\vec{q}\,<}_{RL}(t,t';p_E^2) = -\hat{p}_E M_{\mathrm{KK}}\sqrt{t}\begin{pmatrix} \boldsymbol{D}_2^{\vec{Q}}(\hat{p}_E,t) & 0 \\ 0 & \boldsymbol{D}_1^{\vec{q}}(\hat{p}_E,t)\end{pmatrix}\begin{pmatrix} \boldsymbol{K}_1(t') & \boldsymbol{K}_2(t') \\ \boldsymbol{K}_3(t') & \boldsymbol{K}_4(t')\end{pmatrix}. \tag{3.61}$$

Equipped with the ansatz for the propagator functions for $t < t'$ we can determine the functions for $t > t'$ by using the jump conditions (3.54). We obtain $(t < 1 - \eta)$

$$\begin{aligned}
\boldsymbol{\Delta}^{\vec{q}\,>}_{LL}(t,t';p_E^2) &= \boldsymbol{\Delta}^{\vec{q}\,<}_{LL}(t,t';p_E^2) + \frac{\sqrt{tt'}}{p_E M_{\mathrm{KK}} 1_\eta}\begin{pmatrix} -\boldsymbol{L}_3^{\vec{Q}}(\hat{p}_E,t,t') & 0 \\ 0 & \boldsymbol{L}_2^{\vec{q}}(\hat{p}_E,t,t')\end{pmatrix}, \\
\boldsymbol{\Delta}^{\vec{q}\,>}_{RL}(t,t';p_E^2) &= \boldsymbol{\Delta}^{\vec{q}\,<}_{RL}(t,t';p_E^2) + \frac{\sqrt{tt'}}{M_{\mathrm{KK}} 1_\eta}\begin{pmatrix} \boldsymbol{L}_4^{\vec{Q}}(\hat{p}_E,t,t') & 0 \\ 0 & -\boldsymbol{L}_1^{\vec{q}}(\hat{p}_E,t,t')\end{pmatrix},
\end{aligned} \tag{3.62}$$

where we used the abbreviation $1_\eta \equiv 1-\eta$. We further defined the functions

$$\boldsymbol{L}_i^{\vec{A}}(\hat{p}_E,t,t') \equiv \frac{\pi\hat{p}_E 1_\eta}{2\cos\left(\pi \boldsymbol{c}_{\vec{A}}\right)}\,\boldsymbol{D}_i^{\vec{A}}(\hat{p}_E,t,t')\,; \qquad i=1,2,3,4\,, \tag{3.63}$$

for a compact writeup. We recapitulate that (3.58), (3.61) and (3.62) are solutions for the propagator functions $\boldsymbol{\Delta}_{LL}^{\vec{q}}$ and $\boldsymbol{\Delta}_{RL}^{\vec{q}}$ in the region $t<1-\eta$, which depend on four matrix functions $\boldsymbol{K}_{1-4}(t')$.

Solution in the region $t>1-\eta$

In the region $t>1-\eta$ the Yukawa matrices contribute to the generalized mass matrix (3.48). We have not been able to find solutions for general values of η. But for small values $\eta \ll 1$ the Yukawa contribution is enhanced by η^{-1} and dominates over the term that involves the bulk-mass parameters. Therefore, we can work with approximate expressions for the differential operators in (3.53) ($t>1-\eta$)

$$\mathcal{D}_\pm^{\vec{q}}\mathcal{D}_\mp^{\vec{q}} = -\frac{\partial^2}{\partial t^2} + \frac{\varrho^2}{\eta^2}\left[\begin{pmatrix} \boldsymbol{Y}_{\vec{q}}\boldsymbol{Y}_{\vec{q}}^\dagger & 0 \\ 0 & \boldsymbol{Y}_{\vec{q}}^\dagger\boldsymbol{Y}_{\vec{q}}\end{pmatrix} + \mathcal{O}\left(\frac{\eta M_{\rm KK}}{v|Y_q|}\right)\right], \tag{3.64}$$

where Y_q presents a typical value of an entry of the 5D Yukawa matrix. The neglected terms are suppressed for $\eta \ll v|Y_q|/M_{\rm KK}$ which presents an upper bound on η in order to trust the following calculations. This also represents the technical reason for the upper bound on η in the definition of the narrow-bulk Higgs scenario in (1.56). When we insert (3.64) into the first equation of (3.53) we obtain a differential equation whose basic solutions are given by trigonometric matrix functions

$$\mathcal{S}(t) \equiv \sinh\left(\boldsymbol{S}_{\vec{q}}\frac{1-t}{\eta}\right), \qquad \mathcal{C}(t) \equiv \cosh\left(\boldsymbol{S}_{\vec{q}}\frac{1-t}{\eta}\right), \tag{3.65}$$

and $\bar{\mathcal{S}}(t)$, $\bar{\mathcal{C}}(t)$ which are defined analogously with $\bar{\boldsymbol{S}}_{\vec{q}}$ instead of $\boldsymbol{S}_{\vec{q}}$. The hyperbolic functions are defined via their series representations. The 3×3 matrices are defined by

$$\boldsymbol{S}_{\vec{q}} \equiv \sqrt{\boldsymbol{X}_{\vec{q}}^2+\eta^2\hat{p}_E^2}\,, \qquad \bar{\boldsymbol{S}}_{\vec{q}} \equiv \sqrt{\bar{\boldsymbol{X}}_{\vec{q}}^2+\eta^2\hat{p}_E^2}\,, \tag{3.66}$$

with

$$\boldsymbol{X}_{\vec{q}} \equiv \varrho\sqrt{\boldsymbol{Y}_{\vec{q}}\boldsymbol{Y}_{\vec{q}}^\dagger}\,, \qquad \bar{\boldsymbol{X}}_{\vec{q}} \equiv \varrho\sqrt{\boldsymbol{Y}_{\vec{q}}^\dagger\boldsymbol{Y}_{\vec{q}}}\,. \tag{3.67}$$

Let us first focus on the propagator functions for $t>t'$, where we can implement the IR BC (3.56). Then, we obtain the ansatz ($t>1-\eta$)

$$\begin{aligned}
\boldsymbol{\Delta}_{LL}^{\vec{q}>}(t,t';p_E^2) &= \begin{pmatrix}\mathcal{C}^\dagger(t) & 0\\ 0 & \bar{\mathcal{S}}^\dagger(t)\end{pmatrix}\begin{pmatrix}\boldsymbol{C}_1(t') & \boldsymbol{C}_2(t')\\ \boldsymbol{C}_3(t') & \boldsymbol{C}_4(t')\end{pmatrix},\\
\boldsymbol{\Delta}_{RL}^{\vec{q}>}(t,t';p_E^2) &= \frac{M_{\rm KK}}{\eta}\begin{pmatrix}\boldsymbol{S}_{\vec{q}}^\dagger\mathcal{S}^\dagger(t) & \varrho\boldsymbol{Y}_{\vec{q}}\bar{\mathcal{S}}^\dagger(t)\\ \varrho\boldsymbol{Y}_{\vec{q}}^\dagger\mathcal{C}^\dagger(t) & \bar{\boldsymbol{S}}_{\vec{q}}^\dagger\bar{\mathcal{C}}^\dagger(t)\end{pmatrix}\begin{pmatrix}\boldsymbol{C}_1(t') & \boldsymbol{C}_2(t')\\ \boldsymbol{C}_3(t') & \boldsymbol{C}_4(t')\end{pmatrix},
\end{aligned} \tag{3.68}$$

where the second ansatz for $\boldsymbol{\Delta}_{RL}^{\vec{q}}$ was obtained from the first line by using the first equation in (3.52). Both solutions in (3.68) depend on four matrix coefficients $\boldsymbol{C}_{1-4}(t')$. The

corresponding propagator functions for $t < t'$ can be obtained by taking the jump conditions (3.54) into account, such that $(t > 1-\eta)$

$$\begin{aligned}
\boldsymbol{\Delta}^{\vec{q}<}_{LL}(t,t';p_E^2) &= \boldsymbol{\Delta}^{\vec{q}>}_{LL}(t,t';p_E^2) + \frac{\eta}{M_{\rm KK}^2}\begin{pmatrix} \frac{\mathcal{S}^\dagger(1-t'+t)}{\boldsymbol{S}^\dagger_{\vec{q}}} & 0 \\ 0 & \frac{\bar{\mathcal{S}}^\dagger(1-t'+t)}{\bar{\boldsymbol{S}}^\dagger_{\vec{q}}} \end{pmatrix}, \\
\boldsymbol{\Delta}^{\vec{q}<}_{RL}(t,t';p_E^2) &= \boldsymbol{\Delta}^{\vec{q}>}_{RL}(t,t';p_E^2) + \frac{1}{M_{\rm KK}}\begin{pmatrix} \mathcal{C}^\dagger(1-t'+t) & \varrho \boldsymbol{Y}_{\vec{q}}\frac{\bar{\mathcal{S}}^\dagger(1-t'+t)}{\bar{\boldsymbol{S}}^\dagger_{\vec{q}}} \\ \varrho \boldsymbol{Y}^\dagger_{\vec{q}}\frac{\mathcal{S}^\dagger(1-t'+t)}{\boldsymbol{S}^\dagger_{\vec{q}}} & \bar{\mathcal{C}}^\dagger(1-t'+t) \end{pmatrix}.
\end{aligned} \tag{3.69}$$

Up to now, we have determined basic solutions for the propagator functions $\boldsymbol{\Delta}^{\vec{q}}_{LL}$ and $\boldsymbol{\Delta}^{\vec{q}}_{RL}$ in both regions for $t < 1-\eta$ and $t > 1-\eta$ and which are compatible with the jump and BCs. In total there remain eight unspecified matrix coefficients $\boldsymbol{K}_{1-4}(t')$ and $\boldsymbol{C}_{1-4}(t')$.

Matching the propagator functions at $t = 1-\eta$

The remaining eight matrix coefficients can be determined by requiring that the basic solutions are continuous at $t = 1-\eta$. This procedure has to be performed in two steps whether $t' < 1-\eta$ or $t' > 1-\eta$. Requiring continuos solutions in case of $t' < 1-\eta$ leads to the condition $\boldsymbol{\Delta}^{\vec{q}>}_{AL}\left(1-\eta-0,t';p_E^2\right) = \boldsymbol{\Delta}^{\vec{q}>}_{AL}\left(1-\eta+0,t';p_E^2\right)$ for $A = L,R$. Inserting the solutions (3.62) and (3.68) for $A = L$ we obtain the equations $(t' < 1-\eta)$

$$\begin{aligned}
-\frac{\sqrt{t'/1_\eta}}{\hat{p}_E M_{\rm KK}^2}\boldsymbol{L}^{\vec{Q}}_3(\hat{p}_E,1_\eta,t') + \boldsymbol{D}^{\vec{Q}}_1(\hat{p}_E,1_\eta)\,\boldsymbol{K}_1(t') &= \mathcal{C}^\dagger(1_\eta)\,\boldsymbol{C}_1(t')\,, \\
\sqrt{1_\eta}\,\boldsymbol{D}^{\vec{Q}}_1(\hat{p}_E,1_\eta)\,\boldsymbol{K}_2(t') &= \mathcal{C}^\dagger(1_\eta)\,\boldsymbol{C}_2(t')\,, \\
\sqrt{1_\eta}\,\boldsymbol{D}^{\vec{q}}_2(\hat{p}_E,1_\eta)\,\boldsymbol{K}_3(t') &= \bar{\mathcal{S}}^\dagger(1_\eta)\,\boldsymbol{C}_3(t')\,, \\
\frac{\sqrt{t'/1_\eta}}{\hat{p}_E M_{\rm KK}^2}\boldsymbol{L}^{\vec{q}}_2(\hat{p}_E,1_\eta,t') + \sqrt{1_\eta}\,\boldsymbol{D}^{\vec{q}}_2(\hat{p}_E,1_\eta)\,\boldsymbol{K}_4(t') &= \bar{\mathcal{S}}^\dagger(1_\eta)\,\boldsymbol{C}_4(t')\,.
\end{aligned} \tag{3.70}$$

Together with the corresponding four equations for $A = R$ of the matching condition we have enough conditions to uniquely determine the eight matrix functions $\boldsymbol{K}_{1-4}(t')$ and $\boldsymbol{C}_{1-4}(t')$ for $t' < 1-\eta$. After some algebra we find[2] $(t' < 1-\eta)$

$$\begin{aligned}
\boldsymbol{K}_1(t') &= \frac{\sqrt{t'}}{\hat{p}_E M_{\rm KK}^2 \boldsymbol{D}^{\vec{Q}}_1(\hat{p}_E,1_\eta)}\Bigg[\boldsymbol{L}^{\vec{Q}}_3(\hat{p}_E,1_\eta,t') - \left(\boldsymbol{R}_{\vec{Q}}(\hat{p}_E) + \eta\hat{p}_E\frac{\coth\boldsymbol{S}_{\vec{q}}}{\boldsymbol{S}_{\vec{q}}}\,\boldsymbol{Z}^{\eta,1}_{\vec{q}}(p_E^2)\right) \\
&\qquad\qquad \times \frac{1}{\boldsymbol{N}^{\eta,1}_{\vec{q}}(p_E^2)}\frac{\boldsymbol{D}^{\vec{Q}}_1(\hat{p}_E,t')}{\boldsymbol{D}^{\vec{Q}}_1(\hat{p}_E,1_\eta)}\Bigg], \\
\boldsymbol{K}_2(t') &= \frac{\sqrt{t'}}{\hat{p}_E M_{\rm KK}^2 \boldsymbol{D}^{\vec{Q}}_2(\hat{p}_E,1_\eta)}\,\boldsymbol{R}_{\vec{Q}}(\hat{p}_E)\frac{1}{\boldsymbol{N}^{\eta,2}_{\vec{q}}(p_E^2)}\,\varrho\tilde{\boldsymbol{Y}}_{\vec{q}}\frac{\boldsymbol{D}^{\vec{q}}_2(\hat{p}_E,t')}{\boldsymbol{D}^{\vec{q}}_2(\hat{p}_E,1_\eta)}\,,
\end{aligned}$$

[2]Some convenient relations in order to arrive at (3.72) are given by

$$\begin{aligned}
\boldsymbol{R}^{-1}_{\vec{Q}}(\hat{p}_E 1_\eta)\boldsymbol{L}^{\vec{Q}}_3(\hat{p}_E,1_\eta,t') - \boldsymbol{L}^{\vec{Q}}_4(\hat{p}_E,1_\eta,t') &= \boldsymbol{D}^{\vec{Q}}_1(\hat{p}_E,t')/\boldsymbol{D}^{\vec{Q}}_1(\hat{p}_E,1_\eta)\,, \\
\boldsymbol{L}^{\vec{q}}_1(\hat{p}_E,1_\eta,t') - \boldsymbol{R}_{\vec{q}}(\hat{p}_E 1_\eta)\boldsymbol{L}^{\vec{q}}_2(\hat{p}_E,1_\eta,t') &= \boldsymbol{D}^{\vec{q}}_2(\hat{p}_E,t')/\boldsymbol{D}^{\vec{q}}_2(\hat{p}_E,1_\eta)\,.
\end{aligned} \tag{3.71}$$

$$
\begin{aligned}
\boldsymbol{K}_3(t') &= \frac{\sqrt{t'}}{\hat{p}_E M_{\mathrm{KK}}^2 \boldsymbol{D}_2^{\vec{q}}(\hat{p}_E,1_\eta)}\, \varrho \tilde{\boldsymbol{Y}}_{\vec{q}}^\dagger\, \boldsymbol{R}_{\vec{Q}}(\hat{p}_E)\, \frac{1}{\boldsymbol{N}_{\vec{q}}^{\eta,1}(p_E^2)} \frac{\boldsymbol{D}_1^{\vec{Q}}(\hat{p}_E,t')}{\boldsymbol{D}_1^{\vec{Q}}(\hat{p}_E,1_\eta)}\,, \\
\boldsymbol{K}_4(t') &= \frac{-\sqrt{t'}}{\hat{p}_E M_{\mathrm{KK}}^2 \boldsymbol{D}_2^{\vec{q}}(\hat{p}_E,1_\eta)} \Bigg[\boldsymbol{L}_2^{\vec{q}}(\hat{p}_E,1_\eta,t') + \varrho \tilde{\boldsymbol{Y}}_{\vec{q}}^\dagger \frac{\boldsymbol{S}_{\vec{q}}^2}{\boldsymbol{X}_{\vec{q}}^2} \left(\boldsymbol{R}_{\vec{Q}}(\hat{p}_E) + \eta \hat{p}_E \frac{\coth \boldsymbol{S}_{\vec{q}}}{\boldsymbol{S}_{\vec{q}}} \right) \\
&\qquad \times \frac{1}{\boldsymbol{N}_{\vec{q}}^{\eta,2}(p_E^2)} \varrho \tilde{\boldsymbol{Y}}_{\vec{q}} \frac{\boldsymbol{D}_2^{\vec{q}}(\hat{p}_E,t')}{\boldsymbol{D}_2^{\vec{q}}(\hat{p}_E,1_\eta)} \Bigg]\,,
\end{aligned}
\tag{3.72}
$$

where the coefficients $\boldsymbol{C}_{1-4}(t')$ can be calculated from (3.70). In (3.72) we have used the modified Yukawa matrix

$$
\tilde{\boldsymbol{Y}}_{\vec{q}} \equiv \frac{\tanh \boldsymbol{S}_{\vec{q}}}{\boldsymbol{S}_{\vec{q}}}\, \boldsymbol{Y}_{\vec{q}}\,, \tag{3.73}
$$

and the following ratio of linear combinations of Bessel functions

$$
\boldsymbol{R}_{\vec{Q},\vec{q}}(\hat{p}_E) \equiv \frac{\boldsymbol{D}_1^{\vec{Q},\vec{q}}(\hat{p}_E,1_\eta)}{\boldsymbol{D}_2^{\vec{Q},\vec{q}}(\hat{p}_E,1_\eta)}\,. \tag{3.74}
$$

Furthermore we defined the matrix-valued functions

$$
\begin{aligned}
\boldsymbol{Z}_{\vec{q}}^{\eta,1}(p_E^2) &\equiv \varrho^2 \frac{\boldsymbol{S}_{\vec{q}}^2}{\boldsymbol{X}_{\vec{q}}^2}\, \tilde{\boldsymbol{Y}}_{\vec{q}}\, \boldsymbol{R}_{\vec{q}}(\hat{p}_E)\, \tilde{\boldsymbol{Y}}_{\vec{q}}^\dagger \boldsymbol{R}_{\vec{Q}}(\hat{p}_E)\,, \\
\boldsymbol{Z}_{\vec{q}}^{\eta,2}(p_E^2) &\equiv \varrho^2 \tilde{\boldsymbol{Y}}_{\vec{q}}\, \boldsymbol{R}_{\vec{q}}(\hat{p}_E)\, \tilde{\boldsymbol{Y}}_{\vec{q}}^\dagger \frac{\boldsymbol{S}_{\vec{q}}^2}{\boldsymbol{X}_{\vec{q}}^2}\, \boldsymbol{R}_{\vec{Q}}(\hat{p}_E)\,,
\end{aligned}
\tag{3.75}
$$

and

$$
\begin{aligned}
\boldsymbol{N}_{\vec{q}}^{\eta,1}(p_E^2) &\equiv 1 + \boldsymbol{Z}_{\vec{q}}^{\eta,1}(p_E^2) + \eta \hat{p}_E \left[\frac{1}{\boldsymbol{R}_{\vec{Q}}(\hat{p}_E)} \frac{\coth \boldsymbol{S}_{\vec{q}}}{\boldsymbol{S}_{\vec{q}}} \boldsymbol{Z}_{\vec{q}}^{\eta,1}(p_E^2) + \frac{\tanh \bar{\boldsymbol{S}}_{\vec{q}}}{\bar{\boldsymbol{S}}_{\vec{q}}} \boldsymbol{R}_{\vec{Q}}(\hat{p}_E) \right]\,, \\
\boldsymbol{N}_{\vec{q}}^{\eta,2}(p_E^2) &\equiv 1 + \boldsymbol{Z}_{\vec{q}}^{\eta,2}(p_E^2) + \eta \hat{p}_E \left[\boldsymbol{Z}_{\vec{q}}^{\eta,2}(p_E^2) \frac{1}{\boldsymbol{R}_{\vec{Q}}(\hat{p}_E)} \frac{\coth \boldsymbol{S}_{\vec{q}}}{\boldsymbol{S}_{\vec{q}}} + \frac{\tanh \boldsymbol{S}_{\vec{q}}}{\boldsymbol{S}_{\vec{q}}} \boldsymbol{R}_{\vec{Q}}(\hat{p}_E) \right]\,.
\end{aligned}
\tag{3.76}
$$

So far, we have have derived the matrix coefficients in the region $t' < 1-\eta$. For the other case $t' > 1-\eta$ the matching condition is given by $\boldsymbol{\Delta}_{AL}^{\vec{q}<}\left(1-\eta-0,t';p_E^2\right) = \boldsymbol{\Delta}_{AL}^{\vec{q}<}\left(1-\eta+0,t';p_E^2\right)$ for $A = L,R$. When inserting the solutions (3.58), (3.61) and (3.69), the case $A = L$ leads to the equations ($t' > 1-\eta$)

$$
\begin{aligned}
\sqrt{1_\eta}\, \boldsymbol{D}_1^{\vec{Q}}(\hat{p}_E,1_\eta)\, \boldsymbol{K}_1(t') &= \mathcal{C}(1_\eta)\, \boldsymbol{C}_1(t') - \eta M_{\mathrm{KK}}^{-2}\, \mathcal{S}(t'+\eta)\, \boldsymbol{S}_{\vec{q}}^{-1}\,, \\
\sqrt{1_\eta}\, \boldsymbol{D}_1^{\vec{Q}}(\hat{p}_E,1_\eta)\, \boldsymbol{K}_2(t') &= \mathcal{C}(1_\eta)\, \boldsymbol{C}_2(t')\,, \\
\sqrt{1_\eta}\, \boldsymbol{D}_2^{\vec{q}}(\hat{p}_E,1_\eta)\, \boldsymbol{K}_3(t') &= \bar{\mathcal{S}}(1_\eta)\, \boldsymbol{C}_3(t')\,, \\
\sqrt{1_\eta}\, \boldsymbol{D}_2^{\vec{q}}(\hat{p}_E,1_\eta)\, \boldsymbol{K}_4(t') &= \bar{\mathcal{S}}(1_\eta)\, \boldsymbol{C}_4(t') - \eta M_{\mathrm{KK}}^{-2}\, \bar{\mathcal{S}}(t'+\eta)\, \bar{\boldsymbol{S}}_{\vec{q}}^{-1}\,.
\end{aligned}
\tag{3.77}
$$

Four more equations are given by the matching condition for $A = R$ and we can uniquely determine the eight matrix coefficients for $t' > 1-\eta$. We find ($t' > 1-\eta$)

$$
\boldsymbol{K}_1(t') = \frac{-1}{\hat{p}_E M_{\mathrm{KK}}^2} \frac{1}{\boldsymbol{D}_1^{\vec{Q}}(\hat{p}_E,1_\eta)} \left[\boldsymbol{R}_{\vec{Q}}(\hat{p}_E) + \eta \hat{p}_E \frac{\coth \boldsymbol{S}_{\vec{q}}}{\boldsymbol{S}_{\vec{q}}}\, \boldsymbol{Z}_{\vec{q}}^{\eta,1}(p_E^2) \right] \frac{1}{\boldsymbol{N}_{\vec{q}}^{\eta,1}(p_E^2)} \frac{\mathcal{C}(t')}{\mathcal{C}(1_\eta)}\,,
$$

$$
\begin{aligned}
\boldsymbol{K}_2(t') &= \frac{1}{\hat{p}_E M_{\rm KK}^2}\,\frac{1}{\boldsymbol{D}_2^{\vec{Q}}(\hat{p}_E,1_\eta)}\,\boldsymbol{R}_{\vec{Q}}(\hat{p}_E)\frac{1}{\boldsymbol{N}_{\vec{q}}^{\eta,2}(p_E^2)}\,\frac{\mathcal{S}(t')}{\mathcal{S}(1_\eta)}\,\varrho\tilde{\boldsymbol{Y}}_{\vec{q}}\,,\\
\boldsymbol{K}_3(t') &= \frac{1}{\hat{p}_E M_{\rm KK}^2}\,\frac{1}{\boldsymbol{D}_2^{\vec{q}}(\hat{p}_E,1_\eta)}\,\varrho\tilde{\boldsymbol{Y}}_{\vec{q}}^\dagger\boldsymbol{R}_{\vec{Q}}(\hat{p}_E)\frac{1}{\boldsymbol{N}_{\vec{q}}^{\eta,1}(p_E^2)}\,\frac{\bar{\mathcal{C}}^\dagger(t')}{\bar{\mathcal{C}}^\dagger(1_\eta)}\,,\\
\boldsymbol{K}_4(t') &= \frac{-1}{\hat{p}_E M_{\rm KK}^2}\,\frac{1}{\boldsymbol{D}_2^{\vec{q}}(\hat{p}_E,1_\eta)}\,\varrho\tilde{\boldsymbol{Y}}_{\vec{q}}^\dagger\,\frac{\boldsymbol{S}_{\vec{q}}^2}{\boldsymbol{X}_{\vec{q}}^2}\left[\boldsymbol{R}_{\vec{Q}}(\hat{p}_E)+\eta\hat{p}_E\frac{\coth\boldsymbol{S}_{\vec{q}}}{\boldsymbol{S}_{\vec{q}}}\right]\frac{1}{\boldsymbol{N}_{\vec{q}}^{\eta,2}(p_E^2)}\,\frac{\bar{\mathcal{S}}(t')}{\bar{\mathcal{S}}(1_\eta)}\,\varrho\tilde{\boldsymbol{Y}}_{\vec{q}}\,,
\end{aligned}
\tag{3.78}
$$

where the remaining coefficients $\boldsymbol{C}_{1-4}(t')$ can be deduced from (3.77). We can show that all coefficients $\boldsymbol{K}_{1-4}(t')$ and $\boldsymbol{C}_{1-4}(t')$ are continuous at $t'=1-\eta$. Finally, we have uniquely determined all eight coefficients $\boldsymbol{K}_{1-4}(t')$ and $\boldsymbol{C}_{1-4}(t')$ for the full range $t'\in[\epsilon,1]$ and have obtained final results of the propagator functions $\boldsymbol{\Delta}_{LL}^{\vec{q}}$ and $\boldsymbol{\Delta}_{RL}^{\vec{q}}$.

Extending the results to $\boldsymbol{\Delta}_{RR}^{\vec{q}}$ and $\boldsymbol{\Delta}_{LR}^{\vec{q}}$

We can repeat all previous steps in case of the propagator functions $\boldsymbol{\Delta}_{RR}^{\vec{q}}$ and $\boldsymbol{\Delta}_{LR}^{\vec{q}}$. We find that the corresponding solutions can be obtained by applying the following replacements to the final results for $\boldsymbol{\Delta}_{LL}^{\vec{q}}$ and $\boldsymbol{\Delta}_{RL}^{\vec{q}}$

$$
\begin{aligned}
&\boldsymbol{D}_{1,2}^{\vec{A}}(\hat{p}_E,t)\to\boldsymbol{D}_{2,1}^{\vec{A}}(\hat{p}_E,t)\,, && \mathcal{S}(t)\to\mathcal{C}(t)\,, && \mathcal{S}(t+\eta)\to\mathcal{S}(t+\eta)\,,\\
&\boldsymbol{L}_{2,3}^{\vec{A}}(\hat{p}_E,1_\eta,t)\to-\boldsymbol{L}_{3,2}^{\vec{A}}(\hat{p}_E,1_\eta,t)\,, && \mathcal{C}(t)\to\mathcal{S}(t)\,, && \mathcal{C}(t+\eta)\to\mathcal{C}(t+\eta)\,,\\
&\boldsymbol{L}_{1,4}^{\vec{A}}(\hat{p}_E,1_\eta,t)\to-\boldsymbol{L}_{4,1}^{\vec{A}}(\hat{p}_E,1_\eta,t)\,, && \boldsymbol{Y}_{\vec{q}}\to-\boldsymbol{Y}_{\vec{q}}\,,
\end{aligned}
\tag{3.79}
$$

for $\vec{A}=\vec{U},\vec{D},\vec{\Lambda},\vec{u},\vec{d},\vec{\lambda}$ and $\vec{q}=\vec{u},\vec{d},\vec{\lambda}$. Furthermore, we encounter an additional global minus sign for $\boldsymbol{\Delta}_{LR}^{\vec{q}}$. The replacements imply that the functions $\boldsymbol{Z}_{\vec{q}}^{\eta,i}(p_E^2)$ and $\boldsymbol{N}_{\vec{q}}^{\eta,i}(p_E^2)$ transform via

$$
\begin{aligned}
\boldsymbol{Z}_{\vec{q}}^{\eta,i}(p_E^2)&\to\boldsymbol{R}_{\vec{Q}}(\hat{p}_E)\,\frac{1}{\boldsymbol{Z}_{\vec{q}}^{\eta,i}(p_E^2)}\,\frac{1}{\boldsymbol{R}_{\vec{Q}}(\hat{p}_E)}\,,\\
\frac{1}{\boldsymbol{N}_{\vec{q}}^{\eta,1}(p_E^2)}&\to\boldsymbol{R}_{\vec{Q}}(\hat{p}_E)\,\boldsymbol{Z}_{\vec{q}}^{\eta,1}(p_E^2)\,\frac{1}{\boldsymbol{N}_{\vec{q}}^{\eta,1}(p_E^2)}\,\frac{1}{\boldsymbol{R}_{\vec{Q}}(\hat{p}_E)}\,,\\
\frac{1}{\boldsymbol{N}_{\vec{q}}^{\eta,2}(p_E^2)}&\to\boldsymbol{R}_{\vec{Q}}(\hat{p}_E)\,\frac{1}{\boldsymbol{N}_{\vec{q}}^{\eta,2}(p_E^2)}\,\boldsymbol{Z}_{\vec{q}}^{\eta,2}(p_E^2)\,\frac{1}{\boldsymbol{R}_{\vec{Q}}(\hat{p}_E)}\,.
\end{aligned}
\tag{3.80}
$$

In the last two subsections we will explicitly present the final results of the propagator functions for two different implementations of the Higgs sector. Those solutions will be crucial for the analysis in Chapters 4 and 5.

3.3.3 Final results in the brane-localized Higgs scenario

In this subsection we will focus on the final result of the quark 5D propagator with extra-dimensional coordinates in the range $t,t'\in[\epsilon,1-\eta]$ and after eliminating the regulator by sending $\eta\to0$. The corresponding propagator functions are necessary for the calculation of Feynman diagrams with delocalized vertices in RS models with a brane-localized Higgs sector, where the regulator $\eta\ll v|Y_q|/\Lambda_{\rm TeV}$ can be effectively set to zero. The results will be especially important for the 5D calculation of the $b\to s\gamma$ transition in Chapter 5. In order to obtain the final propagator solutions we insert the matrix coefficients $\boldsymbol{K}_i(t')$ and $\boldsymbol{C}_i(t')$ into (3.58), (3.61), (3.62), (3.68) and (3.69). Then,

we take the limit $\eta \to 0$ which implies that

$$1_\eta \to 1\,, \qquad \boldsymbol{S}_{\vec{q}} \to \boldsymbol{X}_{\vec{q}}\,, \qquad \bar{\boldsymbol{S}}_{\vec{q}} \to \bar{\boldsymbol{X}}_{\vec{q}} \qquad \boldsymbol{Z}^{\eta,i}_{\vec{q}} \to \boldsymbol{Z}_{\vec{q}}\,, \qquad \boldsymbol{N}^{\eta,i}_{\vec{q}} \to 1 + \boldsymbol{Z}_{\vec{q}}\,, \tag{3.81}$$

where $\boldsymbol{X}_{\vec{q}}$, $\bar{\boldsymbol{X}}_{\vec{q}}$ are defined in (3.67) and

$$\boldsymbol{Z}_{\vec{q}}(p_E^2) \equiv \varrho^2\, \tilde{\boldsymbol{Y}}_{\vec{q}}\, \boldsymbol{R}_{\vec{q}}(\hat{p}_E)\, \tilde{\boldsymbol{Y}}^\dagger_{\vec{q}}\, \boldsymbol{R}_{\vec{Q}}(\hat{p}_E)\,. \tag{3.82}$$

The components of the propagator functions are given by the compact expressions $(\vec{q},\vec{Q}) = (\vec{u},\vec{U}), (\vec{d},\vec{D}), (\vec{\lambda},\vec{\Lambda})$

$$\begin{aligned}
\boldsymbol{\Delta}^{\vec{q},11}_{LL} &= \frac{-\sqrt{tt'}}{p_E M_{\rm KK}} \left[\frac{\boldsymbol{D}^{\vec{Q}}_1(\hat{p}_E,t)}{\boldsymbol{D}^{\vec{Q}}_1(\hat{p}_E,1)} \boldsymbol{R}_{\vec{Q}} \frac{1}{1+\boldsymbol{Z}_{\vec{q}}} \frac{\boldsymbol{D}^{\vec{Q}}_1(\hat{p}_E,t')}{\boldsymbol{D}^{\vec{Q}}_1(\hat{p}_E,1)} - \frac{\boldsymbol{D}^{\vec{Q}}_1(\hat{p}_E,t_<)}{\boldsymbol{D}^{\vec{Q}}_1(\hat{p}_E,1)} \boldsymbol{L}^{\vec{Q}}_3(\hat{p}_E,1,t_>) \right], \\
\boldsymbol{\Delta}^{\vec{q},12}_{LL} &= \frac{\sqrt{tt'}}{p_E M_{\rm KK}} \frac{\boldsymbol{D}^{\vec{Q}}_1(\hat{p}_E,t)}{\boldsymbol{D}^{\vec{Q}}_1(\hat{p}_E,1)} \boldsymbol{R}_{\vec{Q}} \frac{1}{1+\boldsymbol{Z}_{\vec{q}}} \varrho \tilde{\boldsymbol{Y}}_{\vec{q}} \frac{\boldsymbol{D}^{\vec{q}}_2(\hat{p}_E,t')}{\boldsymbol{D}^{\vec{q}}_2(\hat{p}_E,1)}\,, \\
\boldsymbol{\Delta}^{\vec{q},21}_{LL} &= \frac{\sqrt{tt'}}{p_E M_{\rm KK}} \frac{\boldsymbol{D}^{\vec{q}}_2(\hat{p}_E,t)}{\boldsymbol{D}^{\vec{q}}_2(\hat{p}_E,1)} \varrho \tilde{\boldsymbol{Y}}^\dagger_{\vec{q}} \boldsymbol{R}_{\vec{Q}} \frac{1}{1+\boldsymbol{Z}_{\vec{q}}} \frac{\boldsymbol{D}^{\vec{Q}}_1(\hat{p}_E,t')}{\boldsymbol{D}^{\vec{Q}}_1(\hat{p}_E,1)}\,, \\
\boldsymbol{\Delta}^{\vec{q},22}_{LL} &= \frac{-\sqrt{tt'}}{p_E M_{\rm KK}} \left[\frac{\boldsymbol{D}^{\vec{q}}_2(\hat{p}_E,t)}{\boldsymbol{D}^{\vec{q}}_2(\hat{p}_E,1)} \varrho \tilde{\boldsymbol{Y}}^\dagger_{\vec{q}} \boldsymbol{R}_{\vec{Q}} \frac{1}{1+\boldsymbol{Z}_{\vec{q}}} \varrho \tilde{\boldsymbol{Y}}_{\vec{q}} \frac{\boldsymbol{D}^{\vec{q}}_2(\hat{p}_E,t')}{\boldsymbol{D}^{\vec{q}}_2(\hat{p}_E,1)} + \frac{\boldsymbol{D}^{\vec{q}}_2(\hat{p}_E,t_<)}{\boldsymbol{D}^{\vec{q}}_2(\hat{p}_E,1)} \boldsymbol{L}^{\vec{q}}_2(\hat{p}_E,1,t_>) \right],
\end{aligned} \tag{3.83}$$

$$\begin{aligned}
\boldsymbol{\Delta}^{\vec{q},11}_{RL} &= \frac{-\sqrt{tt'}}{M_{\rm KK}} \begin{cases} \frac{\boldsymbol{D}^{\vec{Q}}_2(\hat{p}_E,t)}{\boldsymbol{D}^{\vec{Q}}_2(\hat{p}_E,1)} \frac{\boldsymbol{Z}_{\vec{q}}}{1+\boldsymbol{Z}_{\vec{q}}} \frac{\boldsymbol{D}^{\vec{Q}}_1(\hat{p}_E,t')}{\boldsymbol{D}^{\vec{Q}}_1(\hat{p}_E,1)} + \frac{\boldsymbol{D}^{\vec{Q}}_2(\hat{p}_E,t)}{\boldsymbol{D}^{\vec{Q}}_2(\hat{p}_E,1)} \boldsymbol{L}^{\vec{Q}}_4(\hat{p}_E,t',\epsilon) & ,t<t' \\ \frac{\boldsymbol{D}^{\vec{Q}}_2(\hat{p}_E,t)}{\boldsymbol{D}^{\vec{Q}}_2(\hat{p}_E,1)} \frac{\boldsymbol{Z}_{\vec{q}}}{1+\boldsymbol{Z}_{\vec{q}}} \frac{\boldsymbol{D}^{\vec{Q}}_1(\hat{p}_E,t')}{\boldsymbol{D}^{\vec{Q}}_1(\hat{p}_E,1)} + \frac{\boldsymbol{D}^{\vec{Q}}_1(\hat{p}_E,t')}{\boldsymbol{D}^{\vec{Q}}_1(\hat{p}_E,1)} \boldsymbol{R}_{\vec{Q}} \boldsymbol{L}^{\vec{Q}}_2(\hat{p}_E,1,t) & ,t>t' \end{cases}, \\
\boldsymbol{\Delta}^{\vec{q},12}_{RL} &= -\frac{\sqrt{tt'}}{M_{\rm KK}} \frac{\boldsymbol{D}^{\vec{Q}}_2(\hat{p}_E,t)}{\boldsymbol{D}^{\vec{Q}}_2(\hat{p}_E,1)} \frac{1}{1+\boldsymbol{Z}_{\vec{q}}} \varrho \tilde{\boldsymbol{Y}}_{\vec{q}} \frac{\boldsymbol{D}^{\vec{q}}_2(\hat{p}_E,t')}{\boldsymbol{D}^{\vec{q}}_2(\hat{p}_E,1)}\,, \\
\boldsymbol{\Delta}^{\vec{q},21}_{RL} &= -\frac{\sqrt{tt'}}{M_{\rm KK}} \frac{\boldsymbol{D}^{\vec{q}}_1(\hat{p}_E,t)}{\boldsymbol{D}^{\vec{q}}_1(\hat{p}_E,1)} \frac{1}{\varrho \tilde{\boldsymbol{Y}}_{\vec{q}}} \frac{\boldsymbol{Z}_{\vec{q}}}{1+\boldsymbol{Z}_{\vec{q}}} \frac{\boldsymbol{D}^{\vec{Q}}_1(\hat{p}_E,t')}{\boldsymbol{D}^{\vec{Q}}_1(\hat{p}_E,1)}\,, \\
\boldsymbol{\Delta}^{\vec{q},22}_{RL} &= \frac{\sqrt{tt'}}{M_{\rm KK}} \begin{cases} \frac{\boldsymbol{D}^{\vec{q}}_1(\hat{p}_E,t)}{\boldsymbol{D}^{\vec{q}}_1(\hat{p}_E,1)} \frac{1}{\tilde{\boldsymbol{Y}}_{\vec{q}}} \frac{\boldsymbol{Z}_{\vec{q}}}{1+\boldsymbol{Z}_{\vec{q}}} \tilde{\boldsymbol{Y}}_{\vec{q}} \frac{\boldsymbol{D}^{\vec{q}}_2(\hat{p}_E,t')}{\boldsymbol{D}^{\vec{q}}_2(\hat{p}_E,1)} + \frac{\boldsymbol{D}^{\vec{q}}_1(\hat{p}_E,t)}{\boldsymbol{D}^{\vec{q}}_1(\hat{p}_E,1)} \boldsymbol{R}_{\vec{q}} \boldsymbol{L}^{\vec{q}}_2(\hat{p}_E,1,t') & ,t<t' \\ \frac{\boldsymbol{D}^{\vec{q}}_1(\hat{p}_E,t)}{\boldsymbol{D}^{\vec{q}}_1(\hat{p}_E,1)} \frac{1}{\tilde{\boldsymbol{Y}}_{\vec{q}}} \frac{\boldsymbol{Z}_{\vec{q}}}{1+\boldsymbol{Z}_{\vec{q}}} \tilde{\boldsymbol{Y}}_{\vec{q}} \frac{\boldsymbol{D}^{\vec{q}}_2(\hat{p}_E,t')}{\boldsymbol{D}^{\vec{q}}_2(\hat{p}_E,1)} + \frac{\boldsymbol{D}^{\vec{q}}_2(\hat{p}_E,t')}{\boldsymbol{D}^{\vec{q}}_2(\hat{p}_E,1)} \boldsymbol{L}^{\vec{q}}_4(\hat{p}_E,1,t) & ,t>t' \end{cases},
\end{aligned} \tag{3.84}$$

$$\begin{aligned}
\boldsymbol{\Delta}^{\vec{q},11}_{LR} &= \frac{\sqrt{tt'}}{M_{\rm KK}} \begin{cases} \frac{\boldsymbol{D}^{\vec{Q}}_1(\hat{p}_E,t)}{\boldsymbol{D}^{\vec{Q}}_1(\hat{p}_E,1)} \boldsymbol{R}_{\vec{Q}} \frac{1}{1+\boldsymbol{Z}_{\vec{q}}} \frac{1}{\boldsymbol{R}_{\vec{Q}}} \frac{\boldsymbol{D}^{\vec{Q}}_2(\hat{p}_E,t')}{\boldsymbol{D}^{\vec{Q}}_2(\hat{p}_E,1)} - \frac{\boldsymbol{D}^{\vec{Q}}_1(\hat{p}_E,t)}{\boldsymbol{D}^{\vec{Q}}_1(\hat{p}_E,1)} \boldsymbol{L}^{\vec{Q}}_1(\hat{p}_E,1,t') & ,t<t' \\ \frac{\boldsymbol{D}^{\vec{Q}}_1(\hat{p}_E,t)}{\boldsymbol{D}^{\vec{Q}}_1(\hat{p}_E,1)} \boldsymbol{R}_{\vec{Q}} \frac{1}{1+\boldsymbol{Z}_{\vec{q}}} \frac{1}{\boldsymbol{R}_{\vec{Q}}} \frac{\boldsymbol{D}^{\vec{Q}}_2(\hat{p}_E,t')}{\boldsymbol{D}^{\vec{Q}}_2(\hat{p}_E,1)} - \frac{\boldsymbol{D}^{\vec{Q}}_2(\hat{p}_E,t')}{\boldsymbol{D}^{\vec{Q}}_2(\hat{p}_E,1)} \frac{1}{\boldsymbol{R}_{\vec{Q}}} \boldsymbol{L}^{\vec{Q}}_3(\hat{p}_E,1,t) & ,t>t' \end{cases}, \\
\boldsymbol{\Delta}^{\vec{q},12}_{LR} &= \frac{-\sqrt{tt'}}{M_{\rm KK}} \frac{\boldsymbol{D}^{\vec{Q}}_1(\hat{p}_E,t)}{\boldsymbol{D}^{\vec{Q}}_1(\hat{p}_E,1)} \boldsymbol{R}_{\vec{Q}} \frac{\boldsymbol{Z}_{\vec{q}}}{1+\boldsymbol{Z}_{\vec{q}}} \frac{1}{\boldsymbol{R}_{\vec{Q}}} \frac{1}{\varrho \tilde{\boldsymbol{Y}}^\dagger_{\vec{q}}} \frac{\boldsymbol{D}^{\vec{q}}_1(\hat{p}_E,t')}{\boldsymbol{D}^{\vec{q}}_1(\hat{p}_E,1)}\,, \\
\boldsymbol{\Delta}^{\vec{q},21}_{LR} &= \frac{-\sqrt{tt'}}{M_{\rm KK}} \frac{\boldsymbol{D}^{\vec{q}}_2(\hat{p}_E,t)}{\boldsymbol{D}^{\vec{q}}_2(\hat{p}_E,1)} \varrho \tilde{\boldsymbol{Y}}^\dagger_{\vec{q}} \boldsymbol{R}_{\vec{Q}} \frac{1}{1+\boldsymbol{Z}_{\vec{q}}} \frac{1}{\boldsymbol{R}_{\vec{Q}}} \frac{\boldsymbol{D}^{\vec{Q}}_2(\hat{p}_E,t')}{\boldsymbol{D}^{\vec{Q}}_2(\hat{p}_E)}\,,
\end{aligned} \tag{3.85}$$

$$\boldsymbol{\Delta}^{\vec{q},22}_{LR} = \frac{-\sqrt{tt'}}{M_{\rm KK}} \begin{cases} \frac{\boldsymbol{D}^{\vec{q}}_2(\hat{p}_E,t)}{\boldsymbol{D}^{\vec{q}}_2(\hat{p}_E,1)} \tilde{\boldsymbol{Y}}^\dagger_{\vec{q}} \boldsymbol{R}_{\vec{Q}} \frac{1}{1+\boldsymbol{Z}_{\vec{q}}} \frac{1}{\boldsymbol{R}_{\vec{Q}}} \frac{1}{\tilde{\boldsymbol{Y}}^\dagger_{\vec{q}}} \frac{\boldsymbol{D}^{\vec{q}}_1(\hat{p}_E,t')}{\boldsymbol{D}^{\vec{q}}_1(\hat{p}_E,1)} - \frac{\boldsymbol{D}^{\vec{q}}_2(\hat{p}_E,t)}{\boldsymbol{D}^{\vec{q}}_2(\hat{p}_E,1)} \frac{1}{\boldsymbol{R}_{\vec{q}}} \boldsymbol{L}^{\vec{q}}_3(\hat{p}_E,1,t') \,, t<t' \\ \frac{\boldsymbol{D}^{\vec{q}}_2(\hat{p}_E t)}{\boldsymbol{D}^{\vec{q}}_2(\hat{p}_E,1)} \tilde{\boldsymbol{Y}}^\dagger_{\vec{q}} \boldsymbol{R}_{\vec{Q}} \frac{1}{1+\boldsymbol{Z}_{\vec{q}}} \frac{1}{\boldsymbol{R}_{\vec{Q}}} \frac{1}{\tilde{\boldsymbol{Y}}^\dagger_{\vec{q}}} \frac{\boldsymbol{D}^{\vec{q}}_1(\hat{p}_E,t')}{\boldsymbol{D}^{\vec{q}}_1(\hat{p}_E,1)} - \frac{\boldsymbol{D}^{\vec{q}}_1(\hat{p}_E,t')}{\boldsymbol{D}^{\vec{q}}_1(\hat{p}_E,1)} \boldsymbol{L}^{\vec{q}}_1(\hat{p}_E,1,t) \quad , t>t' \end{cases},$$

$$\begin{aligned}
\boldsymbol{\Delta}^{\vec{q},11}_{RR} &= \frac{-\sqrt{tt'}}{p_E M_{\rm KK}} \left[\frac{\boldsymbol{D}^{\vec{Q}}_2(\hat{p}_E,t)}{\boldsymbol{D}^{\vec{Q}}_2(\hat{p}_E,1)} \frac{\boldsymbol{Z}_{\vec{q}}}{1+\boldsymbol{Z}_{\vec{q}}} \frac{1}{\boldsymbol{R}_{\vec{Q}}} \frac{\boldsymbol{D}^{\vec{Q}}_2(\hat{p}_E,t')}{\boldsymbol{D}^{\vec{Q}}_2(\hat{p}_E,1)} + \frac{\boldsymbol{D}^{\vec{Q}}_2(\hat{p}_E,t_<)}{\boldsymbol{D}^{\vec{Q}}_2(\hat{p}_E,1)} \boldsymbol{L}^{\vec{Q}}_2(\hat{p}_E,1,t_>) \right], \\
\boldsymbol{\Delta}^{\vec{q},12}_{RR} &= \frac{-\sqrt{tt'}}{p_E M_{\rm KK}} \frac{\boldsymbol{D}^{\vec{Q}}_2(\hat{p}_E,t)}{\boldsymbol{D}^{\vec{Q}}_2(\hat{p}_E,1)} \frac{\boldsymbol{Z}_{\vec{q}}}{1+\boldsymbol{Z}_{\vec{q}}} \frac{1}{\boldsymbol{R}_{\vec{Q}}} \frac{1}{\varrho \tilde{\boldsymbol{Y}}^\dagger_{\vec{q}}} \frac{\boldsymbol{D}^{\vec{q}}_1(\hat{p}_E,t')}{\boldsymbol{D}^{\vec{q}}_1(\hat{p}_E,1)}, \\
\boldsymbol{\Delta}^{\vec{q},21}_{RR} &= \frac{-\sqrt{tt'}}{p_E M_{\rm KK}} \frac{\boldsymbol{D}^{\vec{q}}_1(\hat{p}_E,t)}{\boldsymbol{D}^{\vec{q}}_1(\hat{p}_E,1)} \frac{1}{\varrho \tilde{\boldsymbol{Y}}_{\vec{q}}} \frac{\boldsymbol{Z}_{\vec{q}}}{1+\boldsymbol{Z}_{\vec{q}}} \frac{1}{\boldsymbol{R}_{\vec{Q}}} \frac{\boldsymbol{D}^{\vec{Q}}_2(\hat{p}_E,t')}{\boldsymbol{D}^{\vec{Q}}_2(\hat{p}_E,1)}, \\
\boldsymbol{\Delta}^{\vec{q},22}_{RR} &= \frac{-\sqrt{tt'}}{p_E M_{\rm KK}} \left[\frac{\boldsymbol{D}^{\vec{q}}_1(\hat{p}_E,t)}{\boldsymbol{D}^{\vec{q}}_1(\hat{p}_E,1)} \frac{1}{\varrho \tilde{\boldsymbol{Y}}_{\vec{q}}} \frac{\boldsymbol{Z}_{\vec{q}}}{1+\boldsymbol{Z}_{\vec{q}}} \frac{1}{\boldsymbol{R}_{\vec{Q}}} \frac{1}{\varrho \tilde{\boldsymbol{Y}}^\dagger_{\vec{q}}} \frac{\boldsymbol{D}^{\vec{q}}_1(\hat{p}_E,t')}{\boldsymbol{D}^{\vec{q}}_1(\hat{p}_E,1)} - \frac{\boldsymbol{D}^{\vec{q}}_1(\hat{p}_E,t_<)}{\boldsymbol{D}^{\vec{q}}_1(\hat{p}_E,1)} \boldsymbol{L}^{\vec{q}}_3(\hat{p}_E,1,t_>) \right].
\end{aligned} \tag{3.86}$$

For the sake of readability we have suppressed the arguments of the propagator functions $\boldsymbol{\Delta}^{\vec{q}}_{AB}(t,t';p^2_E)$ for $A,B = L,R$ on the left side, and of $\boldsymbol{Z}_{\vec{q}}(p^2_E)$ and $\boldsymbol{R}_{\vec{Q},\vec{q}}(\hat{p}_E)$. We note that $\boldsymbol{\Delta}^{\vec{q}}_{LR}$ is related to $\boldsymbol{\Delta}^{\vec{q}}_{RL}$ by complex conjugation and by interchanging the extra-dimensional coordinates $t \leftrightarrow t'$. We have checked that the propagator functions satisfy the continuity and jump conditions in (3.54). Furthermore, we can easily verify that the corresponding UV BCs (3.55) are fulfilled by noting that $\boldsymbol{D}^{\vec{Q},\vec{q}}_2(\hat{p}_E,\epsilon) = 0$. After a short calculation the IR BCs (3.56) are satisfied as well. In view of the KK representation of $\boldsymbol{\Delta}^{\vec{q}}_{AA}$ for $A = L,R$, see (3.51), we can check that the hermitian conjugate of $\boldsymbol{\Delta}^{\vec{q}}_{AA}$ coincides with $\boldsymbol{\Delta}^{\vec{q}}_{AA}$ after interchanging the extra-dimensional coordinates $t \leftrightarrow t'$. Note, that we can obtain the corresponding results in the minimal RS model by making the formal replacements $\vec{Q} \to Q$ and $\vec{q} \to q$ in (3.83) - (3.86) which implies that we only keep the (11)-components (3×3 matrix) in the higher-dimensional representation space.

Alternative derivation of the results

There exists another method to determine the propagator functions without using the notation of a regulator η of the regularized δ-function (1.58). We can also compute the propagator functions $\boldsymbol{\Delta}^{\vec{q}}_{AB}$ by solving the coupled system of differential equations (3.52) without including the term that includes the Yukawa matrices in the generalized mass matrix $\mathcal{M}_{\vec{q}}(t)$ in (3.48). Instead of the IR BCs (3.56) we can impose the modified conditions

$$\left(\varrho \tilde{\boldsymbol{Y}}^\dagger_{\vec{q}} \quad 1 \right) \boldsymbol{\Delta}^{\vec{q}}_{LL}(1^-,t';-p^2) = \left(1 \quad -\varrho \tilde{\boldsymbol{Y}}_{\vec{q}} \right) \boldsymbol{\Delta}^{\vec{q}}_{RL}(1^-,t';-p^2) = 0 \,. \tag{3.87}$$

The BCs on the UV brane (3.55), the continuity and the jump conditions (3.54) remain unchanged. It is a straightforward exercise to derive the propagator functions from these equations. This method provides an independent derivation of the propagator functions (3.83) - (3.86) for RS models with a brane-localized Higgs sector, in which the notion of a regulator η never appears.

Generalization of the results to different Yukawa matrices

We can generalize the results of the propagator functions in case of two different Yukawa matrices. This possibility was mentioned in the text below (2.16) in the context of correct- and wrong-chirality Higgs couplings. In the following we will focus on the minimal version of the RS model. In this scenario the first two equations in (3.52) are generalized to ($q = u, d$)

$$\begin{aligned} p^2\,\boldsymbol{\Delta}^q_{LL}(t,t';-p^2) - M_{\rm KK}\,\mathcal{D}^q_+\,\boldsymbol{\Delta}^q_{RL}(t,t';-p^2) &= \delta(t-t')\,, \\ \boldsymbol{\Delta}^q_{RL}(t,t';-p^2) - M_{\rm KK}\,\mathcal{D}^{q\dagger}_-\,\boldsymbol{\Delta}^q_{LL}(t,t';-p^2) &= 0\,, \end{aligned} \tag{3.88}$$

with $\mathcal{D}^q_+ = \partial_t + \mathcal{M}_q(t)$ and $\mathcal{D}^{q\dagger}_- = -\partial_t + \mathcal{M}^\dagger_q(t)$. The generalized mass matrix is now given by

$$\mathcal{M}_q(t) = \frac{1}{t}\begin{pmatrix} \boldsymbol{c}_Q & 0 \\ 0 & -\boldsymbol{c}_q \end{pmatrix} + \varrho\,\delta^\eta(t-1)\begin{pmatrix} 0 & \boldsymbol{Y}^C_q \\ \boldsymbol{Y}^{S\,\dagger}_q & 0 \end{pmatrix}; \qquad \varrho \equiv \frac{v}{\sqrt{2}M_{\rm KK}}\,, \tag{3.89}$$

which includes the two different Yukawa matrices $\boldsymbol{Y}^C_q$ and $\boldsymbol{Y}^S_q$. We begin with the propagator function $\boldsymbol{\Delta}^{q,<}_{LL}$. The coupled set of first-order differential equations in (3.88) can be combined to yield the second-order differential equation

$$\left[\hat{p}^2 + \partial_t^2 - \mathcal{M}_q(t)\mathcal{M}^\dagger_q(t) - \frac{d\mathcal{M}^\dagger_q(t)}{dt} + \Big\{\mathcal{M}_q(t) - \mathcal{M}^\dagger_q(t)\Big\}\partial_t\right]\boldsymbol{\Delta}^q_{LL}(t,t';-p^2) = \frac{\delta(t-t')}{M^2_{\rm KK}}\,. \tag{3.90}$$

In the region $t < 1-\eta$ the regularized δ-function (1.58) has no support. The generalized mass matrix (3.89) is hermitian and the differential equation (3.90) reduces to the original equation given by the first line of (3.53) with (3.57). Thus, the ansatz for the propagator functions $\boldsymbol{\Delta}^{q,<}_{LL}$ and $\boldsymbol{\Delta}^{q,<}_{RL}$ are given by (3.58) and (3.61) as obtained earlier. However, the differential equations becomes much more complicated in the region $t > 1-\eta$. We have not succeeded to derive a general solution for that region. But, in case of infinitesimal values $\eta \ll 1$ (at fixed p^2) it is consistent to only keep the terms in (3.88) that are enhanced by $1/\eta$ for $1-\eta < t < 1$. In this limit and for $t' < 1-\eta$ the resulting differential equations are given by

$$\begin{aligned} \left[\frac{\partial^2}{\partial t^2} - \frac{\varrho^2}{\eta^2}\begin{pmatrix} \boldsymbol{Y}^C_q\boldsymbol{Y}^{S\dagger}_q & 0 \\ 0 & \boldsymbol{Y}^{S\,\dagger}_q\boldsymbol{Y}^C_q \end{pmatrix}\right]\boldsymbol{\Delta}^q_{RL}(t,t';-p^2) &= 0 + \dots\,, \\ \left[\frac{\partial^2}{\partial t^2} - \frac{\varrho^2}{\eta^2}\begin{pmatrix} \boldsymbol{Y}^S_q\boldsymbol{Y}^{C\dagger}_q & 0 \\ 0 & \boldsymbol{Y}^{C\,\dagger}_q\boldsymbol{Y}^S_q \end{pmatrix}\right]\boldsymbol{\Delta}^q_{LL}(t,t';-p^2) &= 0 + \dots\,, \end{aligned} \tag{3.91}$$

where the dots denote subleading terms. The solutions to these equations involve the hyperbolic trigonometric functions (3.65), whose arguments contain the matrices

$$\boldsymbol{X}_q \equiv \varrho\sqrt{\boldsymbol{Y}^C_q\boldsymbol{Y}^{S\,\dagger}_q}\,, \qquad\qquad \bar{\boldsymbol{X}}_q \equiv \varrho\sqrt{\boldsymbol{Y}^{S\,\dagger}_q\boldsymbol{Y}^C_q}\,, \tag{3.92}$$

and their hermitian conjugates. It is then not difficult to show that, in the limit $\eta \to 0$, the BCs given in (3.87) still hold, provided we use $\boldsymbol{X}_q$ and $\bar{\boldsymbol{X}}_q$ as defined here instead of the original definition (2.23). Furthermore, the modified Yukawa matrix $\tilde{\boldsymbol{Y}}_q$ is defined

here by

$$\tilde{\boldsymbol{Y}}_q \equiv \frac{\tanh \boldsymbol{X}_q}{\boldsymbol{X}_q} \boldsymbol{Y}_q^C \,, \tag{3.93}$$

instead of (2.27). Solving the differential equations for the propagator functions with these BCs, we recover our previous solutions (3.83)-(3.86) for the minimal RS model with the substitutions just described. We further note that the function $\boldsymbol{Z}_q(p_E^2)$ is now given by

$$\boldsymbol{Z}_q(p_E^2) = \frac{v^2}{2M_{\rm KK}^2} \frac{\tanh \boldsymbol{X}_q}{\boldsymbol{X}_q} \boldsymbol{Y}_q^C \boldsymbol{R}_q(\hat{p}_E) \boldsymbol{Y}_q^{C\dagger} \frac{\tanh \boldsymbol{X}_q^\dagger}{\boldsymbol{X}_q^\dagger} \boldsymbol{R}_Q(\hat{p}_E) \,. \tag{3.94}$$

The results for the propagator functions with two different Yukawa matrices will be used in the discussion of the loop-induced processes in Higgs physics and for the $b \to s\gamma$ transition.

3.3.4 Final results in the narrow bulk-Higgs scenario

At last, we present the results of the propagator functions with extra-dimensional coordinates in the range $t, t' \in [1-\eta, 1]$ while keeping the full dependence on the regulator η. As mentioned in the text below (3.64) we have to impose the upper bound $\eta \ll v|Y_q|/M_{\rm KK}$ in order to trust the calculations. The solutions will be important when calculating Feynman diagrams with vertices that are localized on or near the IR brane, which is the case for vertices that couple to the scalar particles of the Higgs sector. For instance the solutions will be used in case of the one-loop triangle diagram that contributes to Higgs production via gluon fusion as discussed in Chapter 4. We obtain the following results with $t, t' \in [1-\eta, 1]$ and $(\vec{q}, \vec{Q}) = (\vec{u}, \vec{U}), (\vec{d}, \vec{D}), (\vec{\lambda}, \vec{\Lambda})$

$$\begin{aligned}
\boldsymbol{\Delta}_{LL}^{\vec{q},11} &= \frac{-1}{p_E M_{\rm KK}} \left[\frac{\mathcal{C}(t)}{\mathcal{C}(1_\eta)} \Big(\eta \hat{p}_E \frac{\coth \boldsymbol{S}_{\vec{q}}}{\boldsymbol{S}_{\vec{q}}} \boldsymbol{Z}_{\vec{q}}^{\eta,1} + \boldsymbol{R}_{\vec{Q}} \Big) \frac{1}{\boldsymbol{N}_{\vec{q}}^{\eta,1}} \frac{\mathcal{C}(t')}{\mathcal{C}(1_\eta)} - \eta \hat{p}_E \frac{\mathcal{C}(t_>)}{\mathcal{C}(1_\eta)} \frac{\mathcal{S}(t_< + \eta)}{\boldsymbol{S}_{\vec{q}}} \right] , \\
\boldsymbol{\Delta}_{LL}^{\vec{q},12} &= \frac{1}{p_E M_{\rm KK}} \frac{\mathcal{C}(t)}{\mathcal{C}(1_\eta)} \boldsymbol{R}_{\vec{Q}} \frac{1}{\boldsymbol{N}_{\vec{q}}^{\eta,2}} \frac{\mathcal{S}(t')}{\mathcal{S}(1_\eta)} \varrho \tilde{\boldsymbol{Y}}_{\vec{q}} \,, \\
\boldsymbol{\Delta}_{LL}^{\vec{q},21} &= \frac{1}{p_E M_{\rm KK}} \varrho \tilde{\boldsymbol{Y}}_{\vec{q}}^\dagger \frac{\mathcal{S}(t)}{\mathcal{S}(1_\eta)} \boldsymbol{R}_{\vec{Q}}(\hat{p}_E) \frac{1}{\boldsymbol{N}_{\vec{q}}^{\eta,1}} \frac{\mathcal{C}(t')}{\mathcal{C}(1_\eta)} \,, \\
\boldsymbol{\Delta}_{LL}^{\vec{q},22} &= \frac{-1}{p_E M_{\rm KK}} \varrho \tilde{\boldsymbol{Y}}_{\vec{q}}^\dagger \frac{\boldsymbol{S}_{\vec{q}}^2}{\boldsymbol{X}_{\vec{q}}^2} \left[\frac{\mathcal{S}(t)}{\mathcal{S}(1_\eta)} \Big(\eta \hat{p}_E \frac{\coth \boldsymbol{S}_{\vec{q}}}{\boldsymbol{S}_{\vec{q}}} + \boldsymbol{R}_{\vec{Q}} \Big) \frac{1}{\boldsymbol{N}_{\vec{q}}^{\eta,2}} \frac{\mathcal{S}(t')}{\mathcal{S}(1_\eta)} \right. \\
&\qquad \left. - \eta \hat{p}_E \frac{\mathcal{S}(t_>)}{\mathcal{S}(1_\eta)} \frac{\mathcal{S}(t_< + \eta)}{\boldsymbol{S}_{\vec{q}} \tanh^2 \boldsymbol{S}_{\vec{q}}} \right] \varrho \tilde{\boldsymbol{Y}}_{\vec{q}} \,,
\end{aligned} \tag{3.95}$$

$$\begin{aligned}
\boldsymbol{\Delta}_{RL}^{\vec{q},11} &= \frac{-1}{M_{\rm KK}} \left[\frac{\mathcal{S}(t)}{\mathcal{S}(1_\eta)} \Big(\boldsymbol{Z}_{\vec{q}}^{\eta,1} + \eta \hat{p}_E \frac{\tanh \boldsymbol{S}_{\vec{q}}}{\boldsymbol{S}_{\vec{q}}} \boldsymbol{R}_{\vec{Q}} \Big) \frac{1}{\boldsymbol{N}_{\vec{q}}^{\eta,1}} \frac{\mathcal{C}(t')}{\mathcal{C}(1_\eta)} - \frac{\mathcal{C}(t+\eta)\mathcal{C}(t')}{\mathcal{C}(1_\eta)} \right. \\
&\qquad \left. + \theta(t-t') \mathcal{C}(1+t-t') \right] ,
\end{aligned}$$

$$
\begin{aligned}
\boldsymbol{\Delta}^{\vec{q},12}_{RL} &= \frac{-1}{M_{\rm KK}}\left[\frac{\mathcal{S}(t)}{\mathcal{S}(1_\eta)}\frac{1-\boldsymbol{N}^{\eta,2}_{\vec{q}}}{\boldsymbol{N}^{\eta,2}_{\vec{q}}}\varrho\tilde{\boldsymbol{Y}}_{\vec{q}}\frac{\bar{\mathcal{S}}(t')}{\bar{\mathcal{S}}(1_\eta)}+\frac{\mathcal{S}(t_>)\mathcal{C}(t_<+\eta)}{\mathcal{S}(1_\eta)}\varrho\tilde{\boldsymbol{Y}}_{\vec{q}}\right],\\
\boldsymbol{\Delta}^{\vec{q},21}_{RL} &= \frac{-1}{M_{\rm KK}}\left[\frac{\bar{\mathcal{C}}(t)}{\bar{\mathcal{C}}(1_\eta)}\frac{1}{\varrho\tilde{\boldsymbol{Y}}_{\vec{q}}}\frac{\boldsymbol{X}^2_{\vec{q}}}{\boldsymbol{S}^2_{\vec{q}}}\boldsymbol{Z}^{\eta,1}_{\vec{q}}\frac{1}{\boldsymbol{N}^{\eta,1}_{\vec{q}}}\frac{\mathcal{C}(t')}{\mathcal{C}(1_\eta)}-\frac{1}{\varrho\tilde{\boldsymbol{Y}}_{\vec{q}}}\frac{\boldsymbol{X}^2_{\vec{q}}}{\boldsymbol{S}^2_{\vec{q}}}\frac{\mathcal{C}(t_>)\mathcal{S}(t_<+\eta)}{\mathcal{C}(1_\eta)\coth\boldsymbol{S}_{\vec{q}}}\right],\\
\boldsymbol{\Delta}^{\vec{q},22}_{RL} &= \frac{-1}{M_{\rm KK}}\left[\frac{\bar{\mathcal{C}}(t)}{\bar{\mathcal{C}}(1_\eta)}\frac{1}{\tilde{\boldsymbol{Y}}_{\vec{q}}}\Big[1-\boldsymbol{N}^{\eta,2}_{\vec{q}}+\eta\hat{p}_E\frac{\tanh\boldsymbol{S}_{\vec{q}}}{\boldsymbol{S}_{\vec{q}}}\boldsymbol{R}_{\vec{Q}}\Big]\frac{1}{\boldsymbol{N}^{\eta,2}_{\vec{q}}}\tilde{\boldsymbol{Y}}_{\vec{q}}\frac{\bar{\mathcal{S}}(t')}{\bar{\mathcal{S}}(1_\eta)}+\frac{\bar{\mathcal{S}}(t+\eta)\bar{\mathcal{S}}(t')}{\bar{\mathcal{C}}(1_\eta)}\right.\\
&\qquad\left.+\,\theta(t-t')\mathcal{C}(1+t-t')\right],
\end{aligned}
\tag{3.96}
$$

$$
\begin{aligned}
\boldsymbol{\Delta}^{\vec{q},11}_{RR} &= \frac{-1}{p_E M_{\rm KK}}\left[\frac{\mathcal{S}(t)}{\mathcal{S}(1_\eta)}\Big(\boldsymbol{Z}^{\eta,1}_{\vec{q}}+\eta\hat{p}_E\frac{\tanh\boldsymbol{S}_{\vec{q}}}{\boldsymbol{S}_{\vec{q}}}\boldsymbol{R}_{\vec{Q}}\Big)\frac{1}{\boldsymbol{N}^{\eta,1}_{\vec{q}}}\frac{1}{\boldsymbol{R}_{\vec{Q}}}\frac{\mathcal{S}(t')}{\mathcal{S}(1_\eta)}\right.\\
&\qquad\left.-\,\eta\hat{p}_E\frac{\mathcal{S}(t_>)\mathcal{S}(t_<+\eta)}{\mathcal{S}(1_\eta)\boldsymbol{S}_{\vec{q}}}\right],\\
\boldsymbol{\Delta}^{\vec{q},12}_{RR} &= \frac{-1}{p_E M_{\rm KK}}\frac{\mathcal{S}(t)}{\mathcal{S}(1_\eta)}\frac{1}{\boldsymbol{N}^{\eta,2}_{\vec{q}}}\boldsymbol{Z}^{\eta,2}_{\vec{q}}\frac{1}{\boldsymbol{R}_{\vec{Q}}}\frac{\mathcal{C}(t')}{\mathcal{C}(1_\eta)}\frac{\boldsymbol{X}^2_{\vec{q}}}{\boldsymbol{S}^2_{\vec{q}}}\frac{1}{\tilde{\boldsymbol{Y}}^\dagger_{\vec{q}}},\\
\boldsymbol{\Delta}^{\vec{q},21}_{RR} &= \frac{-1}{p_E M_{\rm KK}}\frac{1}{\tilde{\boldsymbol{Y}}_{\vec{q}}}\frac{\boldsymbol{X}^2_{\vec{q}}}{\boldsymbol{S}^2_{\vec{q}}}\frac{\mathcal{C}(t)}{\mathcal{C}(1_\eta)}\boldsymbol{Z}^{\eta,1}_{\vec{q}}\frac{1}{\boldsymbol{N}^{\eta,1}_{\vec{q}}}\frac{1}{\boldsymbol{R}_{\vec{Q}}}\frac{\mathcal{S}(t')}{\mathcal{S}(1_\eta)},\\
\boldsymbol{\Delta}^{\vec{q},22}_{RR} &= \frac{-1}{p_E M_{\rm KK}}\frac{1}{\varrho\tilde{\boldsymbol{Y}}_{\vec{q}}}\left[\frac{\mathcal{C}(t)}{\mathcal{C}(1_\eta)}\Big(1+\eta\hat{p}_E\frac{\tanh\boldsymbol{S}_{\vec{q}}}{\boldsymbol{S}_{\vec{q}}}\boldsymbol{R}_{\vec{Q}}\Big)\frac{1}{\boldsymbol{N}^{\eta,2}_{\vec{q}}}\boldsymbol{Z}^{\eta,2}_{\vec{q}}\frac{1}{\boldsymbol{R}_{\vec{Q}}}\frac{\mathcal{C}(t')}{\mathcal{C}(1_\eta)}\right.\\
&\qquad\left.-\,\eta\hat{p}_E\frac{\mathcal{C}(t_>)\mathcal{S}(t_<+\eta)}{\mathcal{C}(1_\eta)\boldsymbol{S}_{\vec{q}}\coth^2\boldsymbol{S}_{\vec{q}}}\right].
\end{aligned}
\tag{3.97}
$$

Again, for the sake of readability we have suppressed arguments of some of the functions. The solution for the propagator function $\boldsymbol{\Delta}^{\vec{q}}_{LR}$ can be obtained from $\boldsymbol{\Delta}^{\vec{q}}_{RL}$ in (3.96) by complex conjugation and by interchanging the coordinates $t \leftrightarrow t'$. The corresponding solutions in the minimal RS model can be obtained by replacing $\vec{Q} \to Q$ and $\vec{q} \to q$ in (3.95) - (3.97).

3.4 Ultra-violet behavior of 5D propagators

This final section discusses the behavior of the gauge-boson and fermion 5D propagators in the minimal RS model with a brane-localized Higgs sector and for large Euclidean momentum $p_E \gg M_{\rm KK}/t$, exceeding the effective Planck scale at each point in the extra dimension. The results will be used to show the finiteness of the penguin diagrams contributing to the $b \to s\gamma$ transition and to calculate boundary terms for large Euclidean momenta in Chapter 5. Most of the material presented here is based on our publication [199].

Gauge-boson propagator functions

We begin with the vector and scalar components of the gauge-boson 5D propagator. The corresponding propagator functions are defined via their KK representations in (3.16) and (3.17). Expanding the solutions (3.25) and (3.18) for large Euclidean momenta we

find to leading order ($\hat{p}_E \gg 1/t, 1/t'$)

$$\begin{aligned} B_B(t,t';p_E^2) &= \frac{L\sqrt{tt'}}{2\pi}\frac{e^{-\hat{p}_E(t_>-t_<)}}{2p_E M_{\rm KK}}\Big[1+e^{2\hat{p}_E(t_>-1)}\Big]\Big[1+e^{2\hat{p}_E(\epsilon-t_<)}\Big]+\dots\,, \\ B_{B,55}(t,t';p_E^2) &= \frac{L(tt')^{\frac{3}{2}}}{2\pi\epsilon^2}\frac{e^{-\hat{p}_E(t_>-t_<)}}{2p_E M_{\rm KK}}\left[1-e^{2\hat{p}_E(t_>-1)}+\frac{L\tilde{m}_B^2\big(1+e^{2\hat{p}_E(t_>-1)}\big)}{p_E M_{\rm KK}}\right] \\ &\quad\times\Big[1-e^{2\hat{p}_E(\epsilon-t_<)}\Big]+\dots\,, \end{aligned} \tag{3.98}$$

for (subscript) $B = A, G, W, Z$. In case of $B = W, Z$ the scalar propagator function includes the contributions from the fifth component of the 5D W, Z boson and from the corresponding NGBs in the Higgs sector. The latter contribution gives rise to the term proportional to $L\tilde{m}_B^2/(p_E M_{\rm KK})$. Such a term would be absent in case of the photon or gluon scalar propagator function ($B = A, G$). Integrating (3.98) with a (well-behaved) function $f(t,t')$ along both extra dimensional coordinates we can show the relations

$$\begin{aligned} \int_\epsilon^1 dtdt'\, B_B(t,t';p_E^2)\, f(t,t') &\approx \frac{L}{4\pi p_E^2}\int_\epsilon^1 dt\, f(t,t)\,, \\ \int_\epsilon^1 dtdt'\, B_{B,55}(t,t';p_E^2)\, f(t,t') &\approx \frac{L}{8\pi\epsilon^2 p_E^2}\int_\epsilon^1 dt\, f(t,t)\,. \end{aligned} \qquad (\hat{p}_E \gg 1/\epsilon) \tag{3.99}$$

We cannot prove (3.99) in general but we checked analytically that the relations are valid for the functions relevant in the calculations of this thesis. The relations (3.99) imply that for large Euclidean momenta the propagator functions can be effectively replaced by the δ-function $\delta(t-t')$ apart from a constant factor.

Fermion propagator functions

The results for the quark propagator functions in the brane-localized Higgs scenario are listed in (3.83) - (3.86). The solutions contain several functions that have a simple form when expanded for large Euclidean momenta. To leading order we find the approximate expressions $\boldsymbol{R}_{Q,q}(\hat{p}_E) \approx 1$, $\boldsymbol{Z}_q(p_E^2) \approx \varrho^2 \tilde{\boldsymbol{Y}}_q \tilde{\boldsymbol{Y}}_q^\dagger$ and ($\hat{p}_E \gg 1/t$)

$$\begin{aligned} &\frac{\boldsymbol{D}^A_{1,4}(\hat{p}_E,t)}{\boldsymbol{D}^A_{1,4}(\hat{p}_E,1)} \approx \frac{e^{\hat{p}_E(t-1)}}{\sqrt{t}}\Big[1+e^{2\hat{p}_E(\epsilon-t)}\Big]\,, \qquad \frac{\boldsymbol{D}^A_{2,3}(\hat{p}_E,t)}{\boldsymbol{D}^A_{2,3}(\hat{p}_E,1)} \approx \frac{e^{\hat{p}_E(t-1)}}{\sqrt{t}}\Big[1-e^{2\hat{p}_E(\epsilon-t)}\Big]\,, \\ &\boldsymbol{L}^A_{1,2}(\hat{p}_E,1,t) = -\boldsymbol{L}^A_{4,3}(\hat{p}_E,1,t) \approx \frac{e^{\hat{p}_E(1-t)}}{2\sqrt{t}}\Big[1\pm e^{2\hat{p}_E(t-1)}\Big]\,, \end{aligned} \tag{3.100}$$

for $A = Q, q$ and $q = u, d$. Note that the expansions are independent of the bulk-mass parameters. Using the above expressions in case of the propagator function $\boldsymbol{\Delta}^q_{LL}(t,t';p_E^2)$ we find ($\hat{p}_E \gg 1/t,\ 1/t'$)

$$\begin{aligned} \boldsymbol{\Delta}^{q,11}_{LL}(t,t';p_E^2) &\approx -\frac{e^{-\hat{p}_E(t_>-t_<)}}{2p_E M_{\rm KK}}\Big[1+e^{2\hat{p}_E(\epsilon-t_<)}\Big]\left[1+\frac{1-\varrho^2\tilde{\boldsymbol{Y}}_q\tilde{\boldsymbol{Y}}_q^\dagger}{1+\varrho^2\tilde{\boldsymbol{Y}}_q\tilde{\boldsymbol{Y}}_q^\dagger}e^{2\hat{p}_E(t_>-1)}\right]\,, \\ \boldsymbol{\Delta}^{q,12}_{LL}(t,t';p_E^2) &\approx \frac{e^{-\hat{p}_E(2-t-t')}}{p_E M_{\rm KK}}\frac{1}{1+\varrho^2\tilde{\boldsymbol{Y}}_q\tilde{\boldsymbol{Y}}_q^\dagger}\varrho\tilde{\boldsymbol{Y}}_q\Big[1+e^{2\hat{p}_E(\epsilon-t)}\Big]\Big[1-e^{2\hat{p}_E(\epsilon-t')}\Big]\,, \\ \boldsymbol{\Delta}^{q,21}_{LL}(t,t';p_E^2) &\approx \frac{e^{-\hat{p}_E(2-t-t')}}{p_E M_{\rm KK}}\varrho\tilde{\boldsymbol{Y}}_q^\dagger\frac{1}{1+\varrho^2\tilde{\boldsymbol{Y}}_q\tilde{\boldsymbol{Y}}_q^\dagger}\Big[1-e^{2\hat{p}_E(\epsilon-t)}\Big]\Big[1+e^{2\hat{p}_E(\epsilon-t')}\Big]\,, \end{aligned}$$

$$\boldsymbol{\Delta}^{q,22}_{LL}(t,t';p_E^2) \approx -\frac{e^{-\hat{p}_E(t_>-t_<)}}{2p_E M_{\rm KK}}\left[1-e^{2\hat{p}_E(\epsilon-t_<)}\right]\left[1-\frac{1-\varrho^2\tilde{\boldsymbol{Y}}_q^\dagger\tilde{\boldsymbol{Y}}_q}{1+\varrho^2\tilde{\boldsymbol{Y}}_q^\dagger\tilde{\boldsymbol{Y}}_q}e^{2\hat{p}_E(t_>-1)}\right]. \quad (3.101)$$

For a (well-behaved) function $f(t,t')$ we can show that

$$\int_\epsilon^1 dtdt'\,\boldsymbol{\Delta}^q_{LL}(t,t';p_E^2)\,f(t,t') \approx -\frac{1}{p_E^2}\int_\epsilon^1 dt\,f(t,t)\,, \qquad (\hat{p}_E \gg 1/\epsilon) \quad (3.102)$$

implying that the propagator function behaves like the δ-function $\delta(t-t')$ for large Euclidean momentum. For functions that are localized near the IR brane the equation is already a good approximation for $\hat{p}_E \gg 1$. Equation (3.102) is also valid in case of the propagator function $\boldsymbol{\Delta}^q_{RR}$.

We continue with the chirality-changing propagator functions. Making use of the second differential equation in (3.52), after complex conjugation and replacing $t \leftrightarrow t'$, we can show for a (well-behaved) function $f(t,t')$ that

$$\begin{aligned}\int_\epsilon^1 dtdt'\,\frac{\boldsymbol{\Delta}^q_{LR}(t,t';p_E^2)}{M_{\rm KK}}f(t,t') =& \int_\epsilon^1 dt\left[-\boldsymbol{\Delta}^q_{LL}(t,1;p_E^2)f(t,1)+\boldsymbol{\Delta}^q_{LL}(t,\epsilon;p_E^2)f(t,\epsilon)\right]\\ &+\int_\epsilon^1 dtdt'\boldsymbol{\Delta}^q_{LL}(t,t';p_E^2)\left[\partial_{t'}+\mathcal{M}_q(t')\right]f(t,t')\,, \quad (3.103)\end{aligned}$$

where we have performed a partial integration in t'. In the large Euclidean momentum region we can show that $(\hat{p}_E \gg 1/\epsilon)$

$$\begin{aligned}\int_\epsilon^1 dt\,\boldsymbol{\Delta}^q_{LL}(t,1;p_E^2)\,f(t,1) \approx& \frac{-1}{p_E^2}\left[\frac{\boldsymbol{P}_+}{1+\varrho^2\tilde{\boldsymbol{Y}}_q\tilde{\boldsymbol{Y}}_q^\dagger}+\frac{\boldsymbol{P}_-\,\varrho^2\tilde{\boldsymbol{Y}}_q^\dagger\tilde{\boldsymbol{Y}}_q}{1+\varrho^2\tilde{\boldsymbol{Y}}_q^\dagger\tilde{\boldsymbol{Y}}_q}-\frac{\boldsymbol{P}_{12}}{1+\varrho^2\tilde{\boldsymbol{Y}}_q\tilde{\boldsymbol{Y}}_q^\dagger}\varrho\tilde{\boldsymbol{Y}}_q\right.\\ &\left.-\varrho\tilde{\boldsymbol{Y}}_q^\dagger\frac{\boldsymbol{P}_{21}}{1+\varrho^2\tilde{\boldsymbol{Y}}_q\tilde{\boldsymbol{Y}}_q^\dagger}\right]f(1,1)\,,\\ \int_\epsilon^1 dt\,\boldsymbol{\Delta}^q_{LL}(t,\epsilon;p_E^2)\,f(t,\epsilon) \approx& -\frac{1}{p_E^2}\,\boldsymbol{P}_+\,f(\epsilon,\epsilon)\,, \quad (3.104)\end{aligned}$$

where higher order terms are suppressed at least by p_E^{-3}. The first relation is approximately valid already for $\hat{p}_E \gg 1$ if $f(t,1)$ has most of its support near the IR brane. Using (3.104) in (3.103) we finally find for a (well-behaved) function $f(t,t')$ and for large Euclidean momentum $(\hat{p}_E \gg 1/\epsilon)$

$$\begin{aligned}\int_\epsilon^1 dtdt'\boldsymbol{\Delta}^q_{LR}(t,t';p_E^2)f(t,t') \approx& \frac{M_{\rm KK}}{p_E^2}\left[\left(\frac{\boldsymbol{P}_+}{1+\varrho^2\tilde{\boldsymbol{Y}}_q\tilde{\boldsymbol{Y}}_q^\dagger}+\frac{\boldsymbol{P}_-\,\varrho^2\tilde{\boldsymbol{Y}}_q^\dagger\tilde{\boldsymbol{Y}}_q}{1+\varrho^2\tilde{\boldsymbol{Y}}_q^\dagger\tilde{\boldsymbol{Y}}_q}-\frac{\boldsymbol{P}_{12}}{1+\varrho^2\tilde{\boldsymbol{Y}}_q\tilde{\boldsymbol{Y}}_q^\dagger}\varrho\tilde{\boldsymbol{Y}}_q\right.\right.\\ &\left.-\varrho\tilde{\boldsymbol{Y}}_q^\dagger\frac{\boldsymbol{P}_{21}}{1+\varrho^2\tilde{\boldsymbol{Y}}_q\tilde{\boldsymbol{Y}}_q^\dagger}\right)f(1,1)-\boldsymbol{P}_+\,f(\epsilon,\epsilon)\\ &\left.-\int_\epsilon^1 dt\left(\frac{f'(t,t^+)+f'(t,t^-)}{2}+\mathcal{M}_q(t)f(t,t)\right)\right], \quad (3.105)\end{aligned}$$

where $f'(t,t^\pm) \equiv \lim_{s\to t\pm 0}\partial_s\,f(t,s)$ is understood as a limiting procedure. An analogous equation can be derived for the propagator function $\boldsymbol{\Delta}^q_{RL}$.

4 Higgs physics in a warped 5D space-time

The direct detection of massive KK resonances would be a clear indication for models with one warped extra dimension. Unfortunately, none of these predicted particles have been observed yet, and a tree-level analysis of the Peskin-Takeuchi parameters indicates that their masses could be too large for direct detection at the LHC. A comprehensive discussion of these points has been given in Section 2.5. Thus, indirect searches like precision measurements of the Higgs-boson couplings to SM particles have become an attractive alternative.

Therefore, this chapter is dedicated to the detailed analysis of Higgs-boson production cross sections and various decay rates in models with one warped extra dimension. The first two sections will cover the loop-induced processes $gg \to h$ and $h \to \gamma\gamma$ in the minimal and custodial RS model. We will perform the calculations of the corresponding amplitudes in a novel way, as 5D loop calculations, i.e. we will work with the fermion and boson 5D propagators derived in Chapter 3. This technique will allow us to show that the fermion triangle diagram is sensitive on the precise localization of the Higgs sector on or near the IR brane. The content of Section 4.1 is based on our publication [2], where I have worked out the ideas of M. Neubert and performed all the calculations contained in the paper. Section 4.2 contains material of our publication [163], where I have done all calculations except for the R_ξ gauge invariance of the $h \to \gamma\gamma$ decay amplitude in the RS model, which has been first shown by J. Hahn. The subsequent Section 4.3 will complete the previous analysis by discussing the tree-level Higgs production and decay processes via W and Z bosons. Here, the main source is my work which has been published in our paper [201]. The last section includes the phenomenological implications. Current studies by the ATLAS and CMS collaborations indicate that the couplings of the Higgs-like boson to SM particles appear to be close to those predicted for an elementary scalar with couplings as given by the SM. The experimental one-sigma uncertainties are given roughly at the level of 10-50%, which allows new-physics effects to hide in the data. Still, even at this level of experimental accuracy we will see that RS corrections to the (effective) Higgs couplings $c_W, c_Z, c_t, c_b, c_\tau, c_g^{\text{eff}}, c_\gamma^{\text{eff}}$ and signal rates of the processes $pp \to h \to \gamma\gamma, ZZ^*, WW^*, \tau^+\tau^-, b\bar{b}$ can significantly constrain the RS parameter space. Section 4.4 is based on my extended and updated phenomenological analysis of our publication [201].

4.1 Loop-induced Higgs production via gluon fusion

This section discusses the important Higgs production process of gluon fusion for different versions of the RS model. In order to put our work into perspective we first summarize earlier works on the process $gg \to h$. In [202], the authors investigated the

effects on the $gg \to h$ amplitude caused by the heavy b' state, the $SU(2)_R$ partner of the top quark predicted in RS models with custodial symmetry. Models in which the Higgs scalar is a pseudo NGB, such as warped gauge-Higgs unification scenarios, were studied in [203, 204]. One finds that the result for the $gg \to h$ amplitude only depends on the fundamental parameter v/f of these models, but that it is insensitive to the details about the spectrum of the KK quarks. The authors of [205, 206] studied the effect of KK resonances on the loop-induced hgg and $h\gamma\gamma$ couplings by working out the corrections to the top- and bottom-quark Yukawa couplings induced by their mixing with KK states. In these papers no significant contributions from the heavy KK-quark states propagating in the loop were observed because the Yukawa interactions coupling the Higgs to two Z_2-odd fermions (the second term in the last line of (4.3) below) were implicitly assumed to be zero.[1] The possibly large effect on the Higgs-boson couplings induced by the shift of the Higgs vev relative to its SM value, which can arise in RS models with custodial symmetry, was emphasized in [206]. The first complete calculation of the hgg and $h\gamma\gamma$ couplings, in which both types of Yukawa interactions in (4.3) were included, was performed in [149]. In this paper both the production of Higgs bosons in the gluon fusion process as well as the main decay channels were studied in an extended RS model with custodial symmetry. It was observed that the dominant corrections to the hgg and $h\gamma\gamma$ couplings arise from the towers of KK-quark states propagating in the loop, and that these effects are to a very good approximation independent of the masses of the corresponding SM quarks. The production rate was found to be suppressed in most regions of parameter space, while the branching fraction for the diphoton channel $h \to \gamma\gamma$ tends to be enhanced with respect to the SM. At about the same time, an independent analysis of the Higgs couplings to gluons and photons appeared [209], which reached the opposite conclusions. In a recent paper [207], it was shown that the discrepancy between the two sets of results can be traced back to a subtlety in the calculation of the loop-induced Higgs couplings to gluons and photons. In order to compute the relevant overlap integrals of fermion wave functions with the brane-localized Higgs field, it is necessary to regularize the Higgs profile in an intermediate step and give it an infinitesimal width η [210]. When the calculation of the gluon-fusion amplitude is performed in a naive way, the limits of sending the regulator to zero ($\eta \to 0$) and including an infinite number of KK modes ($N \to \infty$) in the sum over virtual states do not commute. This ambiguity disappears once the loop calculation is performed in the presence of a consistent UV regulator, such as dimensional regularization with $d < 4$ space-time dimensions. For the case of a brane-localized Higgs sector, one then obtains the results of [149] no matter in which order the limits are taken. The same conclusion can be reached by using a hard UV momentum cutoff on the four-dimensional loop integral. The physical significance of the results found in [209] was not fully elucidated in [207], but the discussion in that paper suggests that they might refer to a certain limit of a model featuring a Higgs boson living in the bulk of the extra dimension. It was demonstrated that the gluon-fusion amplitude receives an unsuppressed "resonance contribution" from high-mass KK states, which can resolve the wave function of the Higgs boson (see also [211]). This effect is absent for a brane-localized scalar sector.

In this work, we shed new light on these issues by performing the calculation of the $gg \to h$ amplitude in a novel way, as a 5D loop calculation. In this way the very notion of KK states is avoided, and the only relevant limit to be considered is that of sending the

[1] The fact that there are two towers of KK-quark states for every massive SM quark, which is deeply connected to the finiteness of the 5D loop amplitude [207], was overlooked in [208]. In order to obtain a finite sum for the infinite KK tower, the authors made the approximation $m_{q_n} = \lambda_{q_n} v/\sqrt{2}$ with $\lambda_{q_n} \approx 1$ for the masses of the KK quarks, see eqs. (8) and (10) of their paper, which is incorrect.

regulator η of the Higgs profile to zero. In the context of dimensional regularization, we find that this limit can be taken either before or after performing the loop integration. In both cases we confirm the results obtained in [149, 207]. If the width of the Higgs profile is kept finite, in a way that is specified more precisely below, we recover the findings of [209]. They correspond to a model with a narrow bulk-Higgs field, whose shape along the extra dimension can be resolved by the high-momentum modes of the RS model.

In Section 4.1.1, we derive an exact representation of the dimensionally-regularized gluon-fusion amplitude in terms of an integral over the mixed-chirality components of the 5D quark propagator in the mixed momentum-position representation, including the contributions of the SM quarks and the full dependence on the Higgs-boson mass. To the best of our knowledge, such a result has not been presented before. Our expression holds for an arbitrary Higgs profile. The calculation of the fermion 5D propagator for the case of a very narrow Higgs profile localized near the IR brane has been performed in Chapter 3. We use these results to evaluate the $gg \to h$ amplitude and show explicitly that taking the limit $\eta \to 0$ commutes with the integration over the 4D loop momentum. We prove a conjecture made in [207] for the analytic form of the contribution of the infinite tower of heavy KK quark states. We also present an alternative derivation of the same result by implementing the brane-localized Yukawa terms via appropriate BCs in the field equations for the fermion mass eigenstates. In this approach, the notion of an infinitesimal regulator η does not appear. We also consider a generalization of the model in which two different Yukawa matrices enter in the 5D Yukawa interactions. We then discuss the changes that occur when the width of the Higgs profile is kept small but non-zero, corresponding to the case of a narrow bulk-Higgs field. In Section 4.1.2 we discuss the impact of higher-dimensional operators on our results. Then in Section 4.1.3, we derive an upper bound on the size of the 5D Yukawa couplings by requiring that the Yukawa interactions remain perturbative. While most of our discussion refers to the minimal RS model with the SM gauge group in the bulk, we generalize our results in Section 4.1.4 to the RS model with custodial symmetry. Finally, we summarize the conceptual results of our analysis and make a classification of RS models in Section 4.1.5.

4.1.1 5D analysis of $gg \to h$

We start with the calculation of the gluon-fusion amplitude in the minimal RS model. We can summarize the results in terms of two Wilson coefficients C_{1g} and C_{5g} defined by the decomposition

$$\mathcal{A}(gg \to h) = C_{1g}\,\frac{\alpha_s}{12\pi v}\,\langle\,0\,|G^a_{\mu\nu}\,G^{\mu\nu,a}|gg\rangle - C_{5g}\,\frac{\alpha_s}{8\pi v}\,\langle\,0\,|G^a_{\mu\nu}\,\widetilde{G}^{\mu\nu,a}|gg\rangle\,, \tag{4.1}$$

where $\widetilde{G}^{\mu\nu,a} = -\frac{1}{2}\epsilon^{\mu\nu\alpha\beta}\,G^a_{\alpha\beta}$ (with $\epsilon^{0123} = -1$) denotes the dual field-strength tensor. Note that the Wilson coefficients C_{1g} and C_{5g} also include the contributions of the SM quarks. The one-loop graph giving rise to the gluon-fusion amplitude is shown in Figure 4.1, where at each vertex an integral over the fifth coordinate t is implied, which varies between $\epsilon \approx 10^{-15}$ on the UV brane and $t = 1$ on the IR brane. The Yukawa interactions of the Higgs boson with up- and down-type quarks can be deduced from (2.15) and are given by

$$\begin{aligned}\mathcal{L}_{hqq}(x) &= -\sum_{q=u,d}\int_\epsilon^1 dt\,\delta_h^\eta(t-1)\,h(x)\,\bar{\mathcal{Q}}_L(x,t)\,\frac{1}{\sqrt{2}}\begin{pmatrix}0 & \boldsymbol{Y}_q\\ \boldsymbol{Y}_q^\dagger & 0\end{pmatrix}\mathcal{Q}_R(x,t) + \text{h.c.}\\ &= -\sum_{q=u,d}\sum_{m,n} g^q_{mn}\,h(x)\,\bar{q}_L^{(m)}(x)\,q_R^{(n)}(x) + \text{h.c.}\,,\end{aligned} \tag{4.2}$$

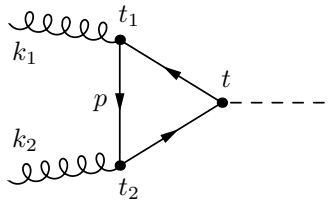

Figure 4.1: Effective hgg couplings induced by the exchange of 5D quark states. The positions of the vertices along the extra dimension are denoted by $t_{1,2}$ and t.

where the zeros in the diagonal blocks of the 6×6 matrix are required by gauge invariance. The function $\delta_h^\eta(t-1)$ denotes the normalized Higgs profile along the extra dimension. In the second line of (4.2) we have decomposed the 5D quark spinors into 4D KK modes according to (2.17). The Yukawa couplings g^q_{mn} are given in terms of the overlap integrals [149]

$$\begin{aligned} g^u_{mn} &= \frac{1}{\sqrt{2}} \int_\epsilon^1 dt\, \delta_h^\eta(t-1)\, \mathcal{U}_L^{\dagger(m)}(t) \begin{pmatrix} 0 & \boldsymbol{Y}_u \\ \boldsymbol{Y}_u^\dagger & 0 \end{pmatrix} \mathcal{U}_R^{(n)}(t) \\ &= \frac{\sqrt{2}\pi}{L\epsilon} \int_\epsilon^1 dt\, \delta_h^\eta(t-1) \Big[a_m^{U\dagger}\, \boldsymbol{C}_m^Q(t)\, \boldsymbol{Y}_u\, \boldsymbol{C}_n^u(t)\, a_n^u + a_m^{u\dagger}\, \boldsymbol{S}_m^u(t)\, \boldsymbol{Y}_u^\dagger\, \boldsymbol{S}_n^Q(t)\, a_n^U \Big] , \end{aligned} \tag{4.3}$$

and likewise in the down-type quark sector. In the last step we have rewritten the answer in terms of the Z_2-even and Z_2-odd fermion profiles $\boldsymbol{C}_n^A(t)$ and $\boldsymbol{S}_n^A(t)$ which have been introduced in the text below (2.18).

In order to perform the calculation of the gluon-fusion amplitude at one-loop order consistently, it is necessary to introduce two different kinds of regulators. For a brane-localized scalar sector, the fermion profile functions are discontinuous on the IR brane, and hence their overlap integrals with a δ-function type Higgs profile are ill defined. We have discussed this point in the text below equation (2.21). Therefore, it is important to regularize the Higgs profile by giving it a small but finite width $\eta \ll 1$ [210]. We therefore use the notation $\delta_h^\eta(t-1)$ in (4.2) and (4.3) where the regularized profile has unit area and support on the interval $1-\eta \le t \le 1$, see the definition (1.58). Many of our results will be independent of the shape of the Higgs profile and would remain valid for the case of a general bulk-Higgs field. Only at the end of our analysis we will specialize to the case of a very narrow Higgs profile, with η satisfying one of the conditions (1.55) or (1.56).

Secondly, as has been emphasized in [207], it is important to introduce a consistent UV regulator in the calculation, even though the final answer for the gluon-fusion amplitude is UV finite. This should not come as a surprise, as it is well known that even in the 4D case the introduction of a UV regulator is required in order to obtain a gauge-invariant answer. To see this, consider the loop diagram for a single KK mode, which naively is linearly divergent. Using invariance under $p \to -p$, a superficial logarithmic divergence remains. In dimensional regularization, one encounters the integral

$$\int \frac{d^dp}{(2\pi)^d} \left[\frac{4-d}{d} \frac{p^2}{(p^2-\Delta)^3} + \frac{\Delta}{(p^2-\Delta)^3} \right] \varepsilon(k_1) \cdot \varepsilon(k_2) , \tag{4.4}$$

which identically vanishes for $d \neq 4$. Here, $\Delta = m_{q_n}^2 - xy(1-y)m_h^2$ arises after combining the denominator using Feynman parameters. Note that if the calculation was performed

naively in four dimensions, then only the second term would be present, and it would correspond to a gauge-dependent operator $G^a_\mu\, G^{\mu,a}$. In the 5D model, the UV regulator has the additional effect of regularizing the infinite sum over KK modes, which once again is superficially logarithmically divergent [207]. The relevant sum is of the form (recall that $n = 4$ labels the lightest KK excitation)

$$\lim_{N\to\infty,\ \eta\to 0} \sum_{q=u,d} \sum_{n=4}^{3+6N} \frac{v g^q_{nn}}{m_{q_n}} \left(\frac{\mu}{m_{q_n}}\right)^{4-d}, \tag{4.5}$$

where m_{q_n} are the masses of the KK quarks and g^q_{nn} denote their effective 4D Yukawa couplings as defined in (4.3). For $d = 4$, one obtains different results depending on which of the two limits is evaluated first. However, in the presence of the dimensional regulator $d < 4$ the order of limits becomes irrelevant, and one obtains a unique answer for the sum, which in the limit $d \to 4$ (taken at the end of the calculation) coincides with the result found in [149]. Note that regularizing only the ordinary (4D) components of momentum space with a dimensional regulator is justified, since the warp factor and the presence of the branes break 5D Lorentz invariance, and because the integral over the compact interval $t \in [\epsilon, 1]$ does not give rise to additional singularities. Introducing a UV cutoff in a way that respects the AdS_5 geometry leads to a warped 4D cutoff, as shown in (1.54). Likewise, the scale μ of dimensional regularization should be replaced by μ_{TeV} in the present case.

With the regulators in place, the gluon-fusion amplitude (4.1) can be written in the form

$$\begin{aligned}\mathcal{A}(gg \to h) = {} & i g_s^2\, \delta^{ab} \sum_{q=u,d} \int \frac{d^d p}{(2\pi)^d} \int_\epsilon^1 dt_1 \int_\epsilon^1 dt_2 \int_\epsilon^1 dt\, \delta_h^\eta(t-1) \\ & \times \mathrm{Tr}\left[\frac{1}{\sqrt{2}} \begin{pmatrix} 0 & \boldsymbol{Y}_q \\ \boldsymbol{Y}_q^\dagger & 0 \end{pmatrix} \boldsymbol{S}^q(t, t_2; p - k_2)\, \not{\varepsilon}(k_2)\, \boldsymbol{S}^q(t_2, t_1; p)\, \not{\varepsilon}(k_1)\, \boldsymbol{S}^q(t_1, t; p + k_1)\right],\end{aligned} \tag{4.6}$$

where k_i denote the incoming four-momenta of the external gluons, a and b their color indices, and $\varepsilon(k_i)$ their polarization vectors. We may now insert the decomposition of the 5D propagator given in (3.50) and try to simplify the result. This task is made complicated by the fact that the propagator functions $\boldsymbol{\Delta}^q_{AB}$ are complicated functions of the four-momentum p and the coordinates t, t'. In order to simplify the calculation, it is convenient to use in intermediate steps their representations as sums over KK modes (3.51). With the dimensional regulator in place, the 4D loop integral as well as the infinite sums over KK modes converge. The integrals over the coordinates t_1 and t_2 of the two external gluons can then be performed using the orthonormality relations (2.29). After this is done, the 5D loop amplitude $\mathcal{A}$ in (4.6) is expressed as a single sum over KK modes, and we find that it can be reduced to integrals of the regularized Higgs profile with traces of the mixed-chirality components of the 5D propagator evaluated at $t = t'$. We define

$$\begin{aligned} T_+(p_E^2) &= -\sum_{q=u,d} \frac{v}{\sqrt{2}} \int_\epsilon^1 dt\, \delta_h^\eta(t-1)\, \mathrm{Tr}\left[\begin{pmatrix} 0 & \boldsymbol{Y}_q \\ \boldsymbol{Y}_q^\dagger & 0 \end{pmatrix} \frac{\boldsymbol{\Delta}^q_{RL}(t,t;p_E^2) + \boldsymbol{\Delta}^q_{LR}(t,t;p_E^2)}{2}\right], \\ T_-(p_E^2) &= -\sum_{q=u,d} \frac{v}{\sqrt{2}} \int_\epsilon^1 dt\, \delta_h^\eta(t-1)\, \mathrm{Tr}\left[\begin{pmatrix} 0 & \boldsymbol{Y}_q \\ \boldsymbol{Y}_q^\dagger & 0 \end{pmatrix} \frac{\boldsymbol{\Delta}^q_{RL}(t,t;p_E^2) - \boldsymbol{\Delta}^q_{LR}(t,t;p_E^2)}{2i}\right], \end{aligned} \tag{4.7}$$

where $p_E^2 \equiv -p^2$ denotes the square of the Euclidean loop momentum after the Wick

rotation. Matching the resulting expression for the amplitude $\mathcal{A}$ with the two-gluon matrix elements in (4.1), we obtain

$$\begin{aligned} C_{1g} &= \frac{3}{2}\int_0^1 dx \int_0^1 dy \left(1-4xy\bar{y}\right) I_+(xy\bar{y}\, m_h^2) = \frac{3}{2}\int_0^1 dz\,(1-z)\, f(z)\, I_+\Big(z\,\frac{m_h^2}{4}\Big)\,, \\ C_{5g} &= \int_0^1 dx \int_0^1 dy\; I_-(xy\bar{y}\, m_h^2) = \int_0^1 dz\, f(z)\, I_-\Big(z\,\frac{m_h^2}{4}\Big)\,, \end{aligned} \tag{4.8}$$

where m_h is the Higgs-boson mass, x and y are Feynman parameters, and we abbreviate $\bar{y} \equiv 1-y$ and $f(z) = \text{arctanh}\sqrt{1-z}$. The quantities

$$\begin{aligned} I_\pm(m^2) &= \frac{e^{\hat{\epsilon}\gamma_E}\mu^{2\hat{\epsilon}}}{\Gamma(2-\hat{\epsilon})}\int_0^\infty dp_E^2\, p_E^{2(1-\hat{\epsilon})}\left(\frac{\partial}{\partial p_E^2}\right)^2 T_\pm\big(p_E^2-m^2-i0\big) \\ &= -\frac{e^{\hat{\epsilon}\gamma_E}\mu^{2\hat{\epsilon}}}{\Gamma(1-\hat{\epsilon})}\int_0^\infty dp_E\, p_E^{-2\hat{\epsilon}}\frac{\partial}{\partial p_E}\, T_\pm\big(p_E^2-m^2-i0\big) \end{aligned} \tag{4.9}$$

are the dimensionally regularized loop-momentum integrals (after Wick rotation) over the functions $T_\pm(p_E^2)$ in (4.7), shifted by an amount m^2. We work in the $\overline{\text{MS}}$ scheme with $d = 4-2\hat{\epsilon}$ space-time dimensions. In the last step we have integrated by parts, which is justified as long as the quantity $p_E\,\partial T_\pm/\partial p_E$ vanishes at $p_E = 0$ and at $p_E \to \infty$. Our analysis in the following section confirms that these conditions are satisfied.

We can also implement a more intuitive regularization scheme based on using a hard UV momentum cutoff on the loop integral. This can be readily implemented once we have the answers in the form given above. Setting $\hat{\epsilon} = 0$ and restricting the loop momentum to the range $0 \le p_E \le \Lambda$, we obtain

$$I_\pm(m^2) = T_\pm(-m^2-i0) - T_\pm(\Lambda^2-m^2) + \Lambda^2\,\frac{\partial}{\partial\Lambda^2}\, T_\pm(\Lambda^2-m^2)\,, \tag{4.10}$$

where Λ should be identified with the physical UV cutoff Λ_{TeV} of the RS model.

The relations (4.8) are one of our main results. They provide exact expressions for the Wilson coefficients corresponding to the 5D loop integral. The trick of using the KK representation in intermediate steps is legitimate and not different from similar techniques routinely used in 4D loop calculations. Note that in our analysis we have not taken the limit $m_h \to 0$, which is often adopted in discussions of the gluon-fusion amplitude and provides a good approximation if the mass of the particle in the loop satisfies the inequality $m_{q_n}^2 \gg m_h^2/4$. There would be no problem in using this approximation for the KK excitations, but for the light SM quarks (and to some extent even for the top quark) the Higgs mass must be kept in order to obtain a reliable result. The strategy adopted in [149, 202–209, 212] was to first evaluate the gluon-fusion amplitude in the limit $m_h \to 0$, then to subtract the contributions of the zero modes by hand, and finally to add back the contributions of the top and bottom quarks using the proper loop functions calculated with the physical value of the Higgs mass. Since in a 5D framework there is no distinction between zero modes and KK excitations, we are forced to keep the Higgs mass finite in order to include the SM contributions in the correct way.

Our results (4.7) and (4.8) are valid for an arbitrary Higgs-boson profile along the extra dimension. As long as one succeeds in computing the mixed-chirality components of the 5D propagator in a generic bulk-Higgs model, one can use (4.8) to compute the corresponding effective hgg couplings. The limit of a brane-localized scalar sector corresponds to taking the limit $\eta \to 0$ in (4.7). It suffices to focus on one of the mixed-chirality components, since for space-like momenta the two components are related by

$\boldsymbol{\Delta}^q_{LR}(t,t';p_E^2) = [\boldsymbol{\Delta}^q_{RL}(t',t;p_E^2)]^\dagger$. The calculation of the propagator function $\boldsymbol{\Delta}^q_{RL}$ was presented in detail in Section 3.3 with the results given in (3.84) and (3.96).

Analysis of the functions $T_\pm(p_E^2)$

We now show how to calculate the loop integrals $I_\pm(m^2)$ in (4.9) for the cases of a brane-localized Higgs boson and a narrow bulk-Higgs field, as defined in (1.55) and (1.56). We perform the calculation in dimensional regularization, but we first motivate the results in the context of the more intuitive scheme in which a hard UV cutoff is used. We begin collecting some general properties of the functions $T_\pm(p_E^2)$.

A first we need to derive explicit expressions for the quantities $T_\pm(p_E^2)$ defined in (4.7). Required are solutions for the mixed-chirality components $\boldsymbol{\Delta}^q_{RL}(t,t';p_E^2)$ of the 5D quark propagator in the region $t,t' > 1-\eta$, which are given in (3.96). Then, we obtain the result

$$\begin{aligned} T_+(p_E^2) = \sum_{q=u,d} \int_\epsilon^1 dt\, \delta_h^\eta(t-1)\, \mathrm{Tr}\Bigg\{ & \frac{\boldsymbol{X}_q^2}{\boldsymbol{S}_q \sinh 2\boldsymbol{S}_q} \\ & \times \left[\sinh^2 \boldsymbol{S}_q + \mathcal{C}^2(t)\, \boldsymbol{Z}_q^{\eta,1}(p_E^2)\, \frac{1}{\boldsymbol{N}_q^{\eta,1}(p_E^2)} - \mathcal{S}^2(t)\, \frac{\boldsymbol{N}_q^{\eta,2}(p_E^2) - 1}{\boldsymbol{N}_q^{\eta,2}(p_E^2)} + \text{h.c.} \right] \Bigg\}, \end{aligned} \tag{4.11}$$

and analogously for $T_-(p_E^2)$. The matrix-valued functions in (4.11) are defined in (2.23), (3.65), (3.66), (3.75) and (3.76). The dependence on the Euclidean momentum enters our results via the quantities $\boldsymbol{S}_q$, $\bar{\boldsymbol{S}}_q$ and $\boldsymbol{R}_A$ for $A = Q, q$ introduced in (3.66) and (3.74). The functions $\boldsymbol{R}_A$ are diagonal matrices in generation space. A significant complication originates from the fact that they do not commute with the matrices $\boldsymbol{S}_q$ and $\bar{\boldsymbol{S}}_q$, giving rise to non-trivial matrix products. It will be important for our discussion to exploit the asymptotic behavior of the ratio $\boldsymbol{R}_A$ for large and small values of $\hat{p}_E$. Using the well-known properties of the modified Bessel functions $I_\alpha(z)$, we find that for $\mathrm{Re}\,\hat{p}_E \gg 1$

$$\boldsymbol{R}_A(\hat{p}_E) = 1 + \frac{\boldsymbol{c}_A}{\hat{p}_E} + \frac{\boldsymbol{c}_A\,(1+\boldsymbol{c}_A)}{2\hat{p}_E^2} + \mathcal{O}(\hat{p}_E^{-3})\,, \tag{4.12}$$

up to exponentially small $\mathcal{O}(e^{-2\hat{p}_E})$ terms. The asymptotic behavior for small values of $\hat{p}_E$ is

$$\boldsymbol{R}_A(\hat{p}_E) = \frac{F^2(\boldsymbol{c}_A)}{\hat{p}_E} + \frac{\hat{p}_E}{1-2\boldsymbol{c}_A}\left[1 - F^2(\boldsymbol{c}_A) + \frac{F^4(\boldsymbol{c}_A)}{3+2\boldsymbol{c}_A}\right] + \mathcal{O}(\hat{p}_E^3)\,, \tag{4.13}$$

where $F(c)$ denotes the value of the profile of a chiral component of a SM fermion on the IR brane, defined in (1.48).

Now, it is convenient to discuss the properties of (4.11) in different regions of the Euclidean momenta. In the region of small momenta ($|p_E| \ll M_{\rm KK}$), the functions $T_\pm(p_E^2)$ vary rapidly and in a way that is strongly dependent on the values of the bulk-mass parameters c_i. This is expected because in this momentum range their behavior is dominated by the contributions of the SM quarks. Remarkably, we find that at the special value $p_E = 0$ the results are given by the very simple expressions

$$T_+(0) = \sum_{q=u,d} \mathrm{Tr}\left[\boldsymbol{X}_q \coth \boldsymbol{X}_q\right] \equiv t_0\,, \qquad\qquad T_-(0) = 0\,, \tag{4.14}$$

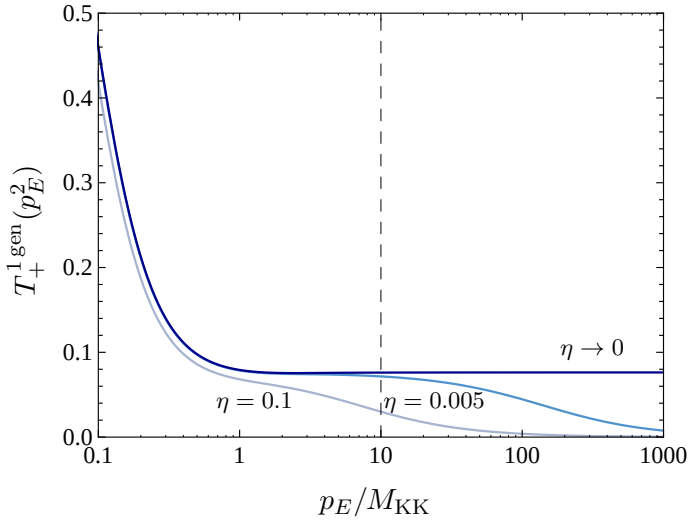

Figure 4.2: Momentum dependence of the propagator function $T_+(p_E^2)$ for the case of one fermion generation and parameters corresponding to the top quark. The three curves refer to different values of the regulator η, as indicated. The vertical dashed line indicates the value of the UV cutoff of the RS model (for $\Lambda_{\mathrm{TeV}} = 10\, M_{\mathrm{KK}}$).

which only depend on the 5D Yukawa couplings, via the quantity $\boldsymbol{X}_q$ defined in (2.23). In the neighborhood of this point the behavior is complicated and not described by a simple formula. For larger values of the Euclidean momentum, such that $p_E \gg M_{\mathrm{KK}}$, the function $T_+(p_E^2)$ converges towards a universal limiting value

$$\begin{aligned} T_+(p_E^2) &= \sum_{q=u,d} \mathrm{Tr}\left\{ \boldsymbol{X}_q \tanh 2\boldsymbol{X}_q + \frac{1}{2\hat{p}_E}\left[\frac{\boldsymbol{c}_Q\, \boldsymbol{X}_q \tanh 2\boldsymbol{X}_q}{\cosh 2\boldsymbol{X}_q} + \frac{\boldsymbol{c}_q\, \bar{\boldsymbol{X}}_q \tanh 2\bar{\boldsymbol{X}}_q}{\cosh 2\bar{\boldsymbol{X}}_q} \right] + \mathcal{O}(\hat{p}_E^{-2}) \right\} \\ &\equiv t_1 + \frac{t_2}{\hat{p}_E} + \dots\,, \qquad (M_{\mathrm{KK}} \ll p_E \ll v|Y_q|/\eta) \end{aligned} \tag{4.15}$$

while $T_-(p_E^2) = \mathcal{O}(\hat{p}_E^{-2})$ falls off more rapidly. To derive this result, we have taken the limit $\eta\hat{p}_E \to 0$ and used the asymptotic expansion in (4.12). A dependence on the bulk-mass parameters enters only at subleading order. Interestingly, there exists a third region of extremely large Euclidean momentum, $p_E \gg v|Y_q|/\eta$, for which the behavior changes once again, and the function $T_+(p_E^2)$ tends to zero according to

$$T_+(p_E^2) = \frac{1}{\eta\hat{p}_E} \sum_{q=u,d} \mathrm{Tr}\, \boldsymbol{X}_q^2 + \mathcal{O}(\hat{p}_E^{-2}) \equiv \frac{t_3}{\eta\hat{p}_E} + \dots\,, \qquad (p_E \gg v|Y_q|/\eta) \tag{4.16}$$

while still $T_-(p_E^2) = \mathcal{O}(\hat{p}_E^{-2})$. Note that in this region the loop momentum p_E exceeds the value of the intrinsic UV cutoff of a consistent RS model with a brane-localized Higgs sector because condition (1.55) implies $\Lambda_{\mathrm{TeV}} \ll v|Y_q|/\eta$. It can therefore only contribute if we consider a bulk-Higgs field as defined in (1.56).

It follows from this discussion that the functions $T_\pm(p_E^2)$ have all the properties required for the integration by parts in (4.9). The exact momentum dependence of these functions is rather complicated, and we refrain from giving explicit expressions for the general case. We will instead discuss the simpler case of a single fermion generation, which exhibits all the relevant features mentioned above. In this case we have obtained

the analytic expression

$$T_+^{1\,\mathrm{gen}}(p_E^2) = \sum_{q=u,d} \frac{X_q^2}{S_q} \frac{k_1(\hat{p}_E)\, S_q \sinh 2S_q + k_2(\hat{p}_E)\, \eta\hat{p}_E \left(\cosh 2S_q - \frac{\sinh 2S_q}{2S_q}\right)}{k_1(\hat{p}_E)\, S_q\, (\cosh 2S_q - 1) + k_2(\hat{p}_E)\, \eta\hat{p}_E \sinh 2S_q + 2S_q}\,, \quad (4.17)$$

where S_q has been defined in (3.66). We further abbreviated $k_1(\hat{p}_E) = 1 + R_q(\hat{p}_E)\, R_Q(\hat{p}_E)$ and $k_2(\hat{p}_E) = R_q(\hat{p}_E) + R_Q(\hat{p}_E)$. The function $T_-^{1\,\mathrm{gen}}(p_E^2) = 0$ vanishes trivially. It is a simple exercise to derive from (4.17) the various limiting behaviors shown in (4.14)–(4.16), simplified to the one-generation case. Figure 4.2 shows the behavior of the result (4.17) for the parameter choices $c_Q = -0.45$, $c_q = 0.395$, and $|Y_q| = 2.3$, which correspond to the physical mass $m_q = 172.6\,\mathrm{GeV}$ of the top quark. We set the KK scale to $M_{\mathrm{KK}} = 2\,\mathrm{TeV}$, such that $X_q \approx 0.2$. The three curves correspond to different values of the regulator η. The three regions of Euclidean momenta mentioned above ($p_E/M_{\mathrm{KK}} \sim 1$, $p_E/M_{\mathrm{KK}} \gg 1$, and $p_E/M_{\mathrm{KK}} \gg X_q/\eta$) are clearly visible from the plot. The dark and light blue curves correspond to models for which $\Lambda_{\mathrm{TeV}}/M_{\mathrm{KK}} \ll X_q/\eta$, and hence condition (1.55) defining a brane-localized Higgs field holds. The gray curve corresponds to the case of a narrow bulk Higgs, as defined in (1.56).

Analysis of the loop integrals $I_\pm(m^2)$

Our final goal is to calculate the loop integrals $I_\pm(m^2)$ defined in (4.9) in the dimensional regularization scheme. For simplicity, however, we first consider the integral $I_+(0)$ at the special point $m^2 = 0$ and work with a hard momentum cutoff $\Lambda = \Lambda_{\mathrm{TeV}}$. For the case of a brane-localized Higgs sector, defined according to condition (1.56), we obtain from (4.10)

$$I_+(0)\big|_{\text{brane Higgs}} = t_0 - t_1 - \frac{3t_2}{2}\frac{M_{\mathrm{KK}}}{\Lambda_{\mathrm{TeV}}} + \dots\,, \quad (4.18)$$

with t_0 and $t_{1,2}$ as defined in (4.14) and (4.15), respectively. The last term is a small threshold correction (suppressed by the UV cutoff, which we assume to be much larger than the KK mass scale), which is present in a hard-cutoff scheme but will not be visible in the dimensional regularization scheme discussed below. Such power-suppressed terms can be included via higher-dimensional operators in the effective Lagrangian of the RS model.

The difference $(t_0 - t_1)$ coincides with the expression for the quantity $\Sigma_q^{(\mathrm{CGHNP})}$ (summed over $q = u, d$) derived in [207] for the case of a brane-localized Higgs sector. It corresponds to the numerical result first derived in [149]. The same result would be obtained if one would take the limit $\eta \to 0$ before performing the integral over the loop momentum. For the opposite case of a narrow bulk-Higgs field, defined according to condition (1.56), the UV cutoff is such that the quantity $T_+(\Lambda^2)$ in (4.10) must be evaluated using (4.16), so that we obtain

$$I_+(0)\big|_{\text{narrow bulk Higgs}} = t_0 - \frac{3t_3}{2}\frac{M_{\mathrm{KK}}}{\eta\Lambda_{\mathrm{TeV}}} + \dots \quad (4.19)$$

instead of (4.18). The two answers differ by an amount t_1 given by the first term on the right-hand side in (4.15). The term t_0 coincides with the expression for the quantity $\Sigma_q^{(\mathrm{ATZ})}$ (summed over $q = u, d$) derived in [207], which corresponds to the result first obtained in [209]. We emphasize that the threshold corrections are enhanced by a factor $1/\eta$ in this case.

It is instructive to reproduce the above results in the less intuitive, but more consistent (from a mathematical point of view) dimensional regularization scheme. We will argue that also in this case the limit of a brane-localized Higgs sector can be taken without encountering any ambiguities. In order to demonstrate this, we should perform the integrals over p_E in (4.9) and then take the limit $\eta \to 0$, and show that this yields the same answer as first setting $\eta \to 0$ and then integrating over the loop momentum. However, our explicit result in (4.17) and its generalization to three generations are so complicated that the dimensionally regularized integral cannot be evaluated in closed form. We will instead consider a toy model, which captures all important features of the exact result. To this end, we study the function

$$T_+^{\rm model}(p_E^2) = \frac{t_0 - t_1 - t_2}{1 + \hat{p}_E^2} + \frac{t_2}{\sqrt{1 + \hat{p}_E^2}} + \frac{t_3}{\sqrt{(t_3/t_1)^2 + (\eta \hat{p}_E)^2}}\,, \tag{4.20}$$

which exhibits the same asymptotic behavior in the three regions as the exact result. Evaluating the integrals in (4.9) for this function, we obtain

$$I_+^{\rm model}(0) = (t_0 - t_1 - t_2)\left(\frac{\mu}{M_{\rm KK}}\right)^{2\hat{\epsilon}} + t_2\left(\frac{\mu}{2M_{\rm KK}}\right)^{2\hat{\epsilon}} + t_1\left(\frac{t_1}{2t_3}\right)^{2\hat{\epsilon}}\left(\frac{\mu\eta}{M_{\rm KK}}\right)^{2\hat{\epsilon}} + \mathcal{O}(\hat{\epsilon}^2)\,, \tag{4.21}$$

where $t_1/(2t_3) = 1 + \mathcal{O}(v^2/M_{\rm KK}^2)$. While the first two contributions are associated with the scale $M_{\rm KK}$, i.e. with low-lying KK modes, the third contribution is associated with the super-heavy scale $M_{\rm KK}/\eta$, which for a brane-localized Higgs sector is larger than the physical UV cutoff of the RS model. Note that in the limit $\eta \to 0$ this contribution tends to zero, leaving $I_+^{\rm model}(0) = (t_0 - t_1)$ as the final result for the integral after the UV regulator $\hat{\epsilon}$ has been removed, in accordance with (4.18). The same result is obtained if the limit $\eta \to 0$ is taken in (4.20) before the integral is evaluated. The last term in (4.20) then reduces to a constant, which does not contribute to (4.9). In the dimensional regularization scheme, the case of a narrow bulk Higgs, for which the loop momenta can resolve the shape of the Higgs profile, is obtained by removing the UV regulator $\hat{\epsilon}$ at small but finite value of η. In this case one finds $I_+^{\rm model}(0) = t_0$, in accordance with (4.19).

Final expressions for the loop integrals

The above discussion shows that in the presence of the UV regulator, and for a brane-localized Higgs boson, it is possible to take the limit $\eta \to 0$ at the level of the functions $T_\pm(p_E^2)$, before the loop integral is performed. We can extend the form (4.17) valid for one fermion generation to the general case of three fermion generations. For $\eta \to 0$, we find

$$\begin{aligned} T_+(p_E^2) &= \sum_{q=u,d} \mathrm{Tr}\left\{\frac{2\boldsymbol{X}_q}{\sinh 2\boldsymbol{X}_q}\left[\sinh^2\boldsymbol{X}_q + \frac{1}{2}\left(\frac{\boldsymbol{Z}_q(p_E^2)}{1+\boldsymbol{Z}_q(p_E^2)} + \frac{\boldsymbol{Z}_q^\dagger(p_E^2)}{1+\boldsymbol{Z}_q^\dagger(p_E^2)}\right)\right]\right\}, \\ T_-(p_E^2) &= \sum_{q=u,d} \mathrm{Tr}\left\{\frac{2\boldsymbol{X}_q}{\sinh 2\boldsymbol{X}_q}\left[\frac{1}{2i}\left(\frac{\boldsymbol{Z}_q(p_E^2)}{1+\boldsymbol{Z}_q(p_E^2)} - \frac{\boldsymbol{Z}_q^\dagger(p_E^2)}{1+\boldsymbol{Z}_q^\dagger(p_E^2)}\right)\right]\right\}. \end{aligned} \tag{4.22}$$

The quantity $\boldsymbol{Z}_q$ involves a non-trivial product of matrix-valued functions and is defined in (3.82). Note that we have removed any reference to the matrices $\bar{\boldsymbol{X}}_q$ in the final expressions by using the identities $\boldsymbol{Y}_q\, f(\bar{\boldsymbol{X}}_q) = f(\boldsymbol{X}_q)\,\boldsymbol{Y}_q$ and $f(\bar{\boldsymbol{X}}_q)\,\boldsymbol{Y}_q^\dagger = \boldsymbol{Y}_q^\dagger\, f(\boldsymbol{X}_q)$,

which hold for an arbitrary function $f(\boldsymbol{X}_q)$ that has a non-singular expansion in powers of $\boldsymbol{X}_q^2$.

We are now ready to derive the final expressions for the loop integrals in (4.9). The quantities $T_\pm(-m^2 - i0)$ computed using (4.22) replace the quantity t_0 in (4.18), (4.19), and (4.21), while t_1 has already been given in (4.14). Removing the UV regulator after the integral over the loop momentum has been performed, we obtain

$$\begin{aligned} I_+(m^2) &= \sum_{q=u,d} \left\{ \mathrm{Tr}\, g(\boldsymbol{X}_q) + \frac{1}{2}\,\mathrm{Tr}\left[\frac{2\boldsymbol{X}_q}{\sinh 2\boldsymbol{X}_q} \left(\frac{\boldsymbol{Z}_q(-m^2)}{1+\boldsymbol{Z}_q(-m^2)} + \frac{\boldsymbol{Z}_q^\dagger(-m^2)}{1+\boldsymbol{Z}_q^\dagger(-m^2)} \right) \right] \right\}, \\ I_-(m^2) &= \sum_{q=u,d} \frac{1}{2i}\,\mathrm{Tr}\left[\frac{2\boldsymbol{X}_q}{\sinh 2\boldsymbol{X}_q} \left(\frac{\boldsymbol{Z}_q(-m^2)}{1+\boldsymbol{Z}_q(-m^2)} - \frac{\boldsymbol{Z}_q^\dagger(-m^2)}{1+\boldsymbol{Z}_q^\dagger(-m^2)} \right) \right], \end{aligned} \tag{4.23}$$

where $m^2 \equiv m^2 + i0$, and the function

$$g(\boldsymbol{X}_q)\big|_{\text{brane Higgs}} = \boldsymbol{X}_q \tanh \boldsymbol{X}_q - \boldsymbol{X}_q \tanh 2\boldsymbol{X}_q = -\frac{\boldsymbol{X}_q \tanh \boldsymbol{X}_q}{\cosh 2\boldsymbol{X}_q} \tag{4.24}$$

obeys a non-singular series expansions in powers of $\boldsymbol{X}_q^2$. Note that due to the presence of strong-interaction phases arising from the analytic continuation from a Euclidean momentum p_E^2 to $-m^2 - i0$, the functions $I_\pm(m^2)$ cannot simply be written in terms of the real and imaginary parts of a trace over matrices. If instead of the brane-localized Higgs boson we consider a narrow bulk-Higgs state, then the subtraction term t_1 is absent, see (4.18) and (4.19). The expressions in (4.23) remain valid also in this case, provided we use

$$g(\boldsymbol{X}_q)\big|_{\text{narrow bulk Higgs}} = \boldsymbol{X}_q \tanh \boldsymbol{X}_q\,. \tag{4.25}$$

The above equations are the main result. Up to some small corrections to be determined below, the first term on the right-hand side of the equation for $I_+(m^2)$ corresponds to the contribution of the infinite tower of KK quarks to the $gg \to h$ amplitude. The remaining terms describe the contributions of the SM quarks. For the case of a brane-localized Higgs sector, the function $g(\boldsymbol{X}_q)$ coincides with an expression first obtained in [207] by means of a conjecture. In the present work we have derived this form. For the case of a narrow bulk-Higgs field, the expansion of $g(\boldsymbol{X}_q)$ to $\mathcal{O}(\boldsymbol{X}_q^2)$ reproduces the result derived in [209]. This demonstrates that the "brane-Higgs limit" considered in that paper really corresponds to the case of a narrow bulk scalar, as defined in (1.56).

Alternative derivation of the result for a brane Higgs

For the case of a brane-localized scalar sector, it has been shown in [207] that the fermion bulk profiles and the Yukawa couplings g_{mn}^q to the fermion mass eigenstates defined in (4.3) can also be derived in a different way, by solving the field equations for the fermion modes in the bulk and incorporating the effects of the Yukawa interactions by imposing appropriate BCs on the IR brane. The Yukawa couplings are then derived by evaluating the fermion profiles in the limit $t \to 1^-$ (approached from the left), which defines their values on the IR brane by continuous extension.

This method, which in [207] was established for individual fermion states, can also be applied to the infinite tower of KK modes, by imposing similar BCs on the 5D propagator functions. Indeed, we find that with a brane-localized Higgs field the functions $T_\pm(p_E^2)$

defined in (4.7) can also be computed as

$$T_+(p_E^2)\big|_{\substack{\text{brane}\\ \text{Higgs}}} = -\sum_{q=u,d} \frac{v}{\sqrt{2}}\,\text{Tr}\left[\begin{pmatrix} 0 & \boldsymbol{Y}_q \\ \boldsymbol{Y}_q^\dagger & 0 \end{pmatrix} \frac{\boldsymbol{\Delta}^q_{RL}(1^-,1^-;p_E^2)+\boldsymbol{\Delta}^q_{LR}(1^-,1^-;p_E^2)}{2}\right], \quad (4.26)$$

and similarly for $T_-(p_E^2)$. The propagator functions $\boldsymbol{\Delta}^q_{AB}$ are now computed by solving the coupled system of differential equations (3.52) without including the Yukawa term in the generalized mass matrix (3.48). Instead, one modifies the BCs on the IR brane, see (3.87) and the text below. We have confirmed that inserting these results into (4.26) one reproduces the expressions given in (4.23). This method provides an independent derivation of the result for the brane-localized Higgs boson, in which the notion of a regulator η never appears.

Analysis of the zero-mode contributions

We will now analyze the terms involving the matrices $\boldsymbol{Z}_q$ used in (4.23) and defined in (3.82), which include the contributions of the SM quarks, in more detail. The first step is to expand $\boldsymbol{Z}_q$ to leading order in v^2/M_{KK}^2. Working in the ZMA, see the text below (2.30) for an explanation, we obtain

$$\boldsymbol{Z}_q(p_E^2) = F^{-1}(\boldsymbol{c}_Q)\,\boldsymbol{U}_q \left[\frac{\boldsymbol{m}_{q,0}^2}{p_E^2} + \Big(\boldsymbol{\delta}_Q + \boldsymbol{m}_{q,0}\,\boldsymbol{\delta}_q\,\boldsymbol{m}_{q,0}^{-1}\Big) + \dots\right] \boldsymbol{U}_q^\dagger\, F(\boldsymbol{c}_Q)\,, \quad (4.27)$$

where

$$\begin{aligned} \boldsymbol{\delta}_Q &= \frac{\boldsymbol{m}_{q,0}}{M_{\text{KK}}^2}\,\boldsymbol{W}_q^\dagger \left[\frac{1}{1-2\boldsymbol{c}_q}\left(\frac{1}{F^2(\boldsymbol{c}_q)} - 1 + \frac{F^2(\boldsymbol{c}_q)}{3+2\boldsymbol{c}_q}\right)\right] \boldsymbol{W}_q\,\boldsymbol{m}_{q,0}\,,\\ \boldsymbol{\delta}_q &= \frac{\boldsymbol{m}_{q,0}}{M_{\text{KK}}^2}\,\boldsymbol{U}_q^\dagger \left[\frac{1}{1-2\boldsymbol{c}_Q}\left(\frac{1}{F^2(\boldsymbol{c}_Q)} - 1 + \frac{F^2(\boldsymbol{c}_Q)}{3+2\boldsymbol{c}_Q}\right)\right] \boldsymbol{U}_q\,\boldsymbol{m}_{q,0}\,. \end{aligned} \quad (4.28)$$

Here, the matrices $\boldsymbol{U}_q$, $\boldsymbol{W}_q$ and $\boldsymbol{m}_{q,0}$ are defined from a singular value decomposition of the effective Yukawa matrix $\boldsymbol{Y}_q^{\text{eff}} \equiv F(\boldsymbol{c}_Q)\tilde{\boldsymbol{Y}}_q F(\boldsymbol{c}_q) = \frac{\sqrt{2}}{v}\,\boldsymbol{U}_q\,\boldsymbol{m}_{q,0}\,\boldsymbol{W}_q$. The entries $m_{q_i,0}$ denote the zeroth-order values of the masses of the SM quarks. The quantities (4.28) give rise to some small corrections of order v^2/M_{KK}^2, which except for the two entries proportional to $m_{u_3}^2 = m_t^2$ carry an additional strong chiral suppression [132]. Interestingly, the matrix $\boldsymbol{Z}_q$ can be used to express the eigenvalue equation which determines the KK masses, such that $\det\big[1+\boldsymbol{Z}_q(-m_n^2)\big] = 0$. This equation directly follows from the modified BCs at the IR brane (2.26) when the exact solutions for the quark profiles (2.28) are inserted. Introducing the abbreviation $\boldsymbol{\varepsilon}_q = \boldsymbol{\delta}_Q + \boldsymbol{m}_{q,0}\,\boldsymbol{\delta}_q\,\boldsymbol{m}_{q,0}^{-1}$, and working to first order in v^2/M_{KK}^2, we can rewrite the eigenvalue equation in the form $\det\big[m_n^2 - \boldsymbol{m}_{q,0}^2\,(1-\boldsymbol{\varepsilon}_q) + \dots\big] = 0$. Using the quantity $\boldsymbol{\epsilon}_q$ we obtain the expansion

$$\frac{\boldsymbol{Z}_q(p_E^2)}{1+\boldsymbol{Z}_q(p_E^2)} = F^{-1}(\boldsymbol{c}_Q)\,\boldsymbol{U}_q \left[\boldsymbol{\varepsilon}_q + \frac{(1-\boldsymbol{\varepsilon}_q)\,\boldsymbol{m}_{q,0}^2\,(1-\boldsymbol{\varepsilon}_q)}{p_E^2 + \boldsymbol{m}_{q,0}^2\,(1-\boldsymbol{\varepsilon}_q)} + \dots\right] \boldsymbol{U}_q^\dagger\, F(\boldsymbol{c}_Q)\,. \quad (4.29)$$

Only the diagonal elements of the matrices $\boldsymbol{\varepsilon}_q$ contribute when the mass eigenvalue equation and traces of (4.29) are evaluated to first order in v^2/M_{KK}^2. It is then not difficult to show that the masses of the SM quarks are given by $m_{q_i}^2 = m_{q_i,0}^2\,(1-\varepsilon_{q_i}+\dots)$ with $\varepsilon_{q_i} \equiv (\boldsymbol{\varepsilon}_q)_{ii} = (\boldsymbol{\delta}_Q)_{ii} + (\boldsymbol{\delta}_q)_{ii}$, where the dots represent terms of order v^4/M_{KK}^4 and

higher. Moreover, we find

$$\sum_{q=u,d} \mathrm{Tr}\left[\frac{2\boldsymbol{X}_q}{\sinh 2\boldsymbol{X}_q}\,\frac{\boldsymbol{Z}_q(p_E^2)}{1+\boldsymbol{Z}_q(p_E^2)}\right] = \sum_i \left[\kappa_{q_i}\,\frac{m_{q_i}^2}{m_{q_i}^2+p_E^2} + \varepsilon_{q_i}\right] + \dots\,, \tag{4.30}$$

where

$$\kappa_{q_i} = 1 - \varepsilon_{q_i} - \frac{2}{3}\left[\boldsymbol{U}_q^\dagger\, F(\boldsymbol{c}_Q)\,\boldsymbol{X}_q^2\, F^{-1}(\boldsymbol{c}_Q)\,\boldsymbol{U}_q\right]_{ii}. \tag{4.31}$$

Note that while the parameters κ_{q_i} are in general complex, the quantities ε_{q_i} are real. The sum in (4.30) extends over all six SM quarks. However, in practice the contributions of the light quarks can safely be neglected. For the third-generation quarks, we find that

$$\kappa_t = 1 - \varepsilon_t - \frac{v^2}{3M_{\rm KK}^2}\,\frac{\left(\boldsymbol{Y}_u\boldsymbol{Y}_u^\dagger\boldsymbol{Y}_u\right)_{33}}{(\boldsymbol{Y}_u)_{33}}\,, \tag{4.32}$$

up to chirality-suppressed terms, and a corresponding formula holds for κ_b. This expression coincides with the result derived in [207]. It is now a simple exercise to evaluate the Wilson coefficients using (4.8). We obtain

$$\begin{aligned} C_{1g} &= \sum_{q=u,d} \mathrm{Tr}\left[g(\boldsymbol{X}_q) + \boldsymbol{\varepsilon}_q\right] + \sum_i \mathrm{Re}(\kappa_{q_i})\,A_q(\tau_i) + \dots \\ &\approx \left[1 - \frac{v^2}{3M_{\rm KK}^2}\,\mathrm{Re}\,\frac{\left(\boldsymbol{Y}_u\boldsymbol{Y}_u^\dagger\boldsymbol{Y}_u\right)_{33}}{(\boldsymbol{Y}_u)_{33}}\right] A_q(\tau_t) + A_q(\tau_b) + \mathrm{Tr}\,g(\boldsymbol{X}_u) + \mathrm{Tr}\,g(\boldsymbol{X}_d)\,, \\ C_{5g} &= \sum_i \mathrm{Im}(\kappa_{q_i})\,B_q(\tau_i) + \dots \approx -\frac{v^2}{3M_{\rm KK}^2}\,\mathrm{Im}\left[\frac{\left(\boldsymbol{Y}_u\boldsymbol{Y}_u^\dagger\boldsymbol{Y}_u\right)_{33}}{(\boldsymbol{Y}_u)_{33}}\right] B_q(\tau_t)\,, \end{aligned} \tag{4.33}$$

where $\tau_i = 4m_{q_i}^2/m_h^2 - i0$, and the parameter integrals evaluate to [213, 214]

$$A_q(\tau) = \frac{3\tau}{2}\left[1 + (1-\tau)\arctan^2\frac{1}{\sqrt{\tau-1}}\right], \qquad B_q(\tau) = \tau\arctan^2\frac{1}{\sqrt{\tau-1}}\,. \tag{4.34}$$

For the light SM quarks, these functions must be analytically continued to $\tau < 1$. In (4.33), we first present expressions that are exact up to small corrections of order $v^4/M_{\rm KK}^4$, represented by the dots, which are numerically insignificant. The leading effects, which involve traces over functions of Yukawa matrices and thus increase with the number of fermion generations, are exact to all orders in $v^2/M_{\rm KK}^2$. The infinite sum over KK quark states contributes the trace term in the expression for C_{1g}. The second term contains the sum over the contributions of the SM quarks, whose Yukawa interactions are modified with respect to the SM by factors κ_{q_i}.

In the final, approximate expressions we have used the fact that all ε_{q_i} parameters other than ε_t can be neglected to a very good approximation, and that for the term proportional to ε_t we can neglect the small deviation of the function $A_q(\tau_t) \approx 1.03$ from 1. Also, for the small b-quark contribution, it is safe to neglect the small deviation of κ_b from 1. In this approximation, which is accurate to better than 1% for $M_{\rm KK} \gtrsim 2\,\mathrm{TeV}$, we observe that the Wilson coefficients C_{1g} and C_{5g} become independent of the bulk-mass parameters c_i. They are entirely given in terms of the 5D Yukawa matrices of the RS model. In the SM, we have $C_{1g}^{\rm SM} = A_q(\tau_t) + A_q(\tau_b)$ and $C_{5g}^{\rm SM} = 0$.

Brane-localized Higgs sector with different Yukawa matrices

Now, we turn to the generalization of the RS model with a brane-localized Higgs sector in which one allows for different Yukawa matrices $\boldsymbol{Y}_q^C$ and $\boldsymbol{Y}_q^{S\dagger}$ in the two terms in the last line of (4.3). We refer to this model as *type-II brane-Higgs* scenario. Details on the derivation of the 5D quark propagator in this scenario can be found in the last paragraph of Section 3.3.3. We find that the expressions can be obtained from the ones derived so far by means of some simple manipulations. Instead of the matrices $\boldsymbol{X}_q$, $\tilde{\boldsymbol{Y}}_q$, $\boldsymbol{Z}_q$ defined in (2.23), (2.27), (3.82) we must use the expressions (3.92), (3.93), (3.94). Also, the master formulae (4.23) must be generalized to

$$\begin{aligned}
I_+(m^2) &= \sum_{q=u,d}\left\{\mathrm{Re}\,\mathrm{Tr}\,g(\boldsymbol{X}_q,\tilde{\boldsymbol{Y}}_q) + \frac{1}{2}\mathrm{Tr}\left[\frac{2\boldsymbol{X}_q}{\sinh 2\boldsymbol{X}_q}\frac{\boldsymbol{Z}_q(-m^2)}{1+\boldsymbol{Z}_q(-m^2)} + \frac{2\boldsymbol{X}_q^\dagger}{\sinh 2\boldsymbol{X}_q^\dagger}\frac{\boldsymbol{Z}_q^\dagger(-m^2)}{1+\boldsymbol{Z}_q^\dagger(-m^2)}\right]\right\},\\
I_-(m^2) &= \sum_{q=u,d}\left\{\mathrm{Im}\,\mathrm{Tr}\,g(\boldsymbol{X}_q,\tilde{\boldsymbol{Y}}_q) + \frac{1}{2i}\mathrm{Tr}\left[\frac{2\boldsymbol{X}_q}{\sinh 2\boldsymbol{X}_q}\frac{\boldsymbol{Z}_q(-m^2)}{1+\boldsymbol{Z}_q(-m^2)} - \frac{2\boldsymbol{X}_q^\dagger}{\sinh 2\boldsymbol{X}_q^\dagger}\frac{\boldsymbol{Z}_q^\dagger(-m^2)}{1+\boldsymbol{Z}_q^\dagger(-m^2)}\right]\right\},
\end{aligned} \tag{4.35}$$

where

$$g(\boldsymbol{X}_q,\tilde{\boldsymbol{Y}}_q)\big|^{\text{type-II}}_{\text{brane Higgs}} = -\frac{2\boldsymbol{X}_q}{\sinh 2\boldsymbol{X}_q}\,\frac{\frac{v^2}{2M_{\rm KK}^2}\,\tilde{\boldsymbol{Y}}_q\tilde{\boldsymbol{Y}}_q^\dagger}{1+\frac{v^2}{2M_{\rm KK}^2}\,\tilde{\boldsymbol{Y}}_q\tilde{\boldsymbol{Y}}_q^\dagger} = -\frac{v^2}{2M_{\rm KK}^2}\,\boldsymbol{Y}_q^C\boldsymbol{Y}_q^{C\dagger} + \ldots\,. \tag{4.36}$$

In the formulae for κ_t in (4.32) one must replace the combination $\big(\boldsymbol{Y}_u\boldsymbol{Y}_u^\dagger\boldsymbol{Y}_u\big)_{33}/\big(\boldsymbol{Y}_u\big)_{33}$ by $\big(\boldsymbol{Y}_u^C\boldsymbol{Y}_u^{S\dagger}\boldsymbol{Y}_u^C\big)_{33}/\big(\boldsymbol{Y}_u^C\big)_{33}$. Note that because $\boldsymbol{X}_q$ is no longer a positive hermitian matrix, traces of $\boldsymbol{X}_q^n$ can now have arbitrary phases. However, at leading order in the expansion in $v^2/M_{\rm KK}^2$ the trace of the function $g(\boldsymbol{X}_q,\tilde{\boldsymbol{Y}}_q)$ is a negative real number. Indeed, at this order there is no difference between the result (4.36) and the original result in (4.24) valid for the brane-Higgs scenario with $\boldsymbol{Y}_q^C = \boldsymbol{Y}_q^S$.

An interesting special case is that where $\boldsymbol{Y}_q^S = 0$ meaning that the Yukawa couplings involving a product of two Z_2-odd fields, given by the second term in the last line of (4.3), is put to zero. This choice was frequently adopted in the literature. It corresponds to taking the limit $\boldsymbol{X}_q \to 0$ in our results, in which case $\tilde{\boldsymbol{Y}}_q \to \boldsymbol{Y}_q^C$, and the quantities κ_{q_i} in (4.31) reduce to $\kappa_{q_i} = 1-\varepsilon_{q_i}$. It follows that in this particular model one obtains

$$\begin{aligned}
C_{1g} &= \sum_{q=u,d}\mathrm{Tr}\left[g(0,\boldsymbol{Y}_q^C) + \boldsymbol{\varepsilon}_q\right] + \sum_i (1-\varepsilon_{q_i})\,A_q(\tau_i) + \ldots\\
&\approx C_{1g}^{\rm SM} + [1-A_q(\tau_t)]\,\varepsilon_t + \varepsilon_b - \frac{v^2}{2M_{\rm KK}^2}\,\mathrm{Tr}\left[\boldsymbol{Y}_u^C\boldsymbol{Y}_u^{C\dagger} + \boldsymbol{Y}_d^C\boldsymbol{Y}_d^{C\dagger}\right],
\end{aligned} \tag{4.37}$$

whereas $C_{5g} = 0$. The first term in the first line is the result of the summation over the KK tower of quark states, while the second term gives the contributions of the SM quarks, whose Yukawa couplings are modified with respect to their values in the SM by factors $(1-\varepsilon_{q_i})$. It suffices for all practical purposes to keep only the terms shown in the second line. Apart from the last term, they agree with a corresponding result presented in [206]. The first two corrections to the SM result are numerically very small because $1-A_q(\tau_t) \approx -0.03$ and the quantity ε_b is chirally suppressed. The third correction, which arises from the infinite sum over KK states, gives the dominant contribution by far. This effect was not found in [209] because in this paper the brane-Higgs case was derived by taking a limit of a bulk-Higgs result. If one formally introduces two different

Yukawa matrices in the narrow bulk-Higgs scenario, one indeed finds that $g(\boldsymbol{X}_q)$ defined in (4.25) vanishes in the limit where $\boldsymbol{Y}_q^S \to 0$. However, in the context of a bulk-Higgs model taking $\boldsymbol{Y}_q^S$ different from $\boldsymbol{Y}_q^C$ violates 5D Lorentz invariance, and moreover the brane-Higgs case cannot be derived by taking a limit of the bulk-Higgs results.

4.1.2 Power corrections and higher-dimensional operators

As we have mentioned earlier RS models must be considered as EFTs valid below a (position-dependent) UV cutoff which is given by the warped Planck scale. The UV completion of these models is unknown. It may be strongly coupled, for instance due to effects of quantum gravity. Short-distance contributions from physics above the cutoff scale give rise to higher-dimensional operators. In the following we will comment on their impact on our results.

Power corrections

Generic power corrections can be described in terms of higher-dimensional operators added to the Lagrangian of the RS model (with unknown coefficients). For example, we can ask what one should expect for the magnitude of the leading power corrections to the Yukawa interactions (4.2) coupling the Higgs boson to bulk fermions. In general, higher-dimensional operators can be constructed by inserting one or more (covariant) derivatives acting on the fields.[2] These operators are suppressed by the fundamental, physical UV cutoff of RS models, which is of order the Planck scale. The leading such operators involving a fermion bilinear contain a single derivative, possibly accompanied by a factor $\mathrm{sgn}(\phi)$. We are thus led to study the object

$$\frac{1}{M_{\rm Pl}}\, E_a^M\, iD_M\Gamma^a = \frac{1}{M_{\rm Pl}}\left(e^{\sigma(\phi)}\, i\partial\!\!\!/ + \frac{1}{r}\,\gamma_5\,\partial_\phi\right) + \text{terms containing gauge fields}, \quad (4.38)$$

where $\Gamma^a = \{\gamma^\mu, -i\gamma_5\}$ are the 5D Dirac matrices and E_a^M denotes the inverse vielbein, as discussed in Section 1.4.2. From now on we focus on the derivative terms only. Changing variables from ϕ to t, and using the definition of the warped UV cutoff in (1.54), we obtain

$$\frac{1}{M_{\rm Pl}}\, E_a^M\, iD_M\Gamma^a = \frac{1}{\Lambda_{\rm UV}(t)}\,(i\partial\!\!\!/ + \gamma_5\, M_{\rm KK}\,\partial_t) + \dots\,. \quad (4.39)$$

Operators containing more than one derivative contain similar structures. For example, the 5D d'Alembertian can be written as[3]

$$\frac{1}{M_{\rm Pl}^2}\,\Box_5 = \frac{e^{2\sigma(\phi)}}{M_{\rm Pl}^2}\left(\Box_4 - \frac{e^{-2\sigma(\phi)}}{r^2}\,\partial_\phi^2\right) = \frac{1}{\Lambda_{\rm UV}^2(t)}\left(\Box_4 - M_{\rm KK}^2\,\frac{1}{t}\,\partial_t\, t\,\partial_t\right). \quad (4.40)$$

Several comments are in order. First, we note that higher-derivative operators in the effective Lagrangian are indeed suppressed by the position-dependent UV cutoff $\Lambda_{\rm UV}(t)$. If we consider power corrections to couplings involving the Higgs boson (no matter whether the Higgs field is localized on or near the IR brane), the corresponding cutoff scale is $\Lambda_{\rm TeV}$. The 4D derivatives contained in (4.39) and (4.40) will produce powers of external momenta or masses of the various fermion modes. The corresponding terms

[2] Note that the 5D Lagrangian does not contain any small mass parameters, which could be used to construct non-derivative operators of higher dimension.

[3] The 5D d'Alembert operator is defined by $\Box_5 \equiv G^{MN}\partial_M\partial_N$ with the RS-metric representation given in (1.22).

scale like $(M_{\rm KK}/\Lambda_{\rm TeV})^n$. For models in which the Higgs field is a generic bulk scalar (with width $\eta \sim 1$) or a brane-localized field, derivatives ∂_t acting on the fields near $t = 1$ produce $\mathcal{O}(1)$ factors, since the wave functions are naturally expressed in terms of the t variable, typically involving Bessel functions of argument $x_n t$ with $x_n = m_n/M_{\rm KK}$, or powers of t in the case of the SM fermions. (For a brane-localized Higgs field, these derivatives must be evaluated at $t = 1^-$, i.e., by approaching the IR brane from the left.) Hence, the ∂_t terms in the derivative operators shown above also give rise to $(M_{\rm KK}/\Lambda_{\rm TeV})^n$ corrections. The situation changes if we consider a limit of a bulk-Higgs model in which the width η of the Higgs profile becomes parametrically suppressed. Then the Higgs profile itself, as well as the profiles of particles coupling to the Higgs field, change rapidly over a small interval of width η near the IR brane. In such a scenario, a derivative ∂_t acting on the Higgs field or any field coupling to the Higgs boson picks up a factor $1/\eta$, and hence the corresponding power corrections scale like $(M_{\rm KK}/\eta\Lambda_{\rm TeV})^n$.

Impact of $|\Phi|^2\, \mathcal{G}^a_{MN}\mathcal{G}^{MN,a}$ and $|\Phi|^2\, \mathcal{G}^a_{MN}\widetilde{\mathcal{G}}^{MN,a}$ operators

Two particularly interesting higher-dimensional operators relevant for Higgs production are $\Phi^\dagger\Phi\, \mathcal{G}^a_{MN}\mathcal{G}^{MN,a}$ and $\Phi^\dagger\Phi\, \mathcal{G}^a_{MN}\widetilde{\mathcal{G}}^{MN,a}$, which mediate effective hgg couplings at tree level. Here, $\mathcal{G}^a_{MN}$ is the 5D gluon field-strength tensor. We will now address the question how important the contributions of these operators are in the low-energy effective theory, focussing on the first operator for concreteness. In the RS model with the scalar sector localized on the IR brane, the relevant effective action is

$$S_{\rm eff} = \int d^4x \int_{-r\pi}^{r\pi} dx_5\, c_{\rm eff}\, \delta(|x_5| - r\pi)\, \frac{\Phi^\dagger\Phi}{\Lambda^2_{\rm TeV}}\, \frac{g^2_{s,5}}{4}\, \mathcal{G}^a_{\mu\nu}\, \mathcal{G}^{\mu\nu,a} + \dots\,, \tag{4.41}$$

where we do not bother to write down terms involving $\mathcal{G}^a_{\mu 5}$. Here, $g_{s,5}$ is the five-dimensional strong coupling, which is related to the coupling g_s of the SM by $g_{s,5} = \sqrt{2\pi r}\, g_s$ [165]. The natural UV cutoff governing the suppression of the brane-localized higher-dimensional operator is $\Lambda_{\rm TeV}$. NDA suggests that the dimensionless coupling $c_{\rm eff}$ could be as large as $\mathcal{O}(1)$ if the UV completion above the cutoff of the RS model is strongly coupled. In the absence of a complete model, it is impossible to say how $c_{\rm eff}$ might depend on other parameters, such as the Yukawa couplings or the number of fermion generations. Even in a strongly coupled theory, it is possible that $c_{\rm eff}$ could be significantly smaller than 1,[4] for instance because the effective degrees of freedom coupling the Higgs boson to two gluons can only be pair produced, or because they have suppressed couplings to the operators $\Phi^\dagger\Phi$ or $\mathcal{G}^a_{\mu\nu}\, \mathcal{G}^{\mu\nu,a}$. Following common practice, we shall assume that taking $c_{\rm eff} = \mathcal{O}(1)$ provides a conservative upper bound for the effect of the brane-localized operators on the gluon-fusion amplitude. Using the KK decomposition of the gluon field (strength tensor),

$$\mathcal{G}^a_{\mu\nu}(x,\phi) = \frac{1}{\sqrt{r}} \sum_n G^{(n)\,a}_{\mu\nu}(x)\, \chi^G_n(\phi) = \frac{1}{\sqrt{2\pi r}}\, G^a_{\mu\nu}(x) + \text{KK modes}\,, \tag{4.42}$$

where the zero mode (the SM gluon $G^a_{\mu\nu} \equiv G^{(0)\,a}_{\mu\nu}$) has a flat profile along the extra dimension, and writing the scalar doublet in the standard form (equation (2.4) without the factor ϵ) we find that the relevant terms in the action (4.41) gives rise to the effective

[4] An example is provided by the $\pi^0 \to \gamma\gamma$ decay amplitude, which is loop suppressed in the SM despite the fact that QCD is strongly coupled in the low-energy regime.

Lagrangian

$$\mathcal{L}_{\text{eff}} = \frac{c_{\text{eff}}}{\Lambda_{\text{TeV}}^2}\,\mathcal{O}_{\text{eff}}\,, \tag{4.43}$$

where

$$\mathcal{O}_{\text{eff}} = \Phi^\dagger\Phi\,\frac{g_s^2}{4}\,G^a_{\mu\nu}\,G^{\mu\nu,a} \ni \frac{g_s^2 v^2}{8}\left(1+\frac{h(x)}{v}\right)^2 G^a_{\mu\nu}\,G^{\mu\nu,a}\,. \tag{4.44}$$

We now repeat this analysis for an RS model in which the Higgs field lives in the bulk of the extra dimension. A detailed discussion of the properties of a bulk-Higgs field and its vev was presented in Section 2.3. In this case, the higher-dimensional operator can be localized on both the IR and UV branes, or it can live in the bulk. We thus consider the action

$$S_{\text{eff}} = \int d^4x \int_{-r\pi}^{r\pi} dx_5 \left[c_1 + c_2\,\delta(|x_5|-r\pi) + c_3\,\delta(x_5)\right] \frac{\Phi^\dagger\Phi}{M_{\text{Pl}}^2}\,\frac{g_{s,5}^2}{4}\,\mathcal{G}^a_{\mu\nu}\,\mathcal{G}^{\mu\nu,a} + \dots\,, \tag{4.45}$$

where the coupling c_1 is dimensionless, while $c_{2,3} \sim 1/M_{\text{Pl}}$. Since all fields live in the bulk, the natural cutoff suppressing the operator is set by the Planck scale. Also, the scalar field now takes the form shown in relation (2.34). Using the KK decomposition of the Higgs field given in (2.50), we find that

$$\begin{aligned} S_{\text{eff}} = \int d^4x\,\frac{g_s^2}{4}\,G^a_{\mu\nu}(x)\,G^{\mu\nu,a}(x)\,\frac{2\pi}{L}\int_\epsilon^1 \frac{dt}{t}\,\frac{v^2(t)}{2\Lambda_{\text{UV}}^2(t)}\left(1+h(x)\,\frac{\chi_0^h(t)}{v(t)}\right)^2 \\ \times\left\{c_1 + \frac{k}{2}\left[c_2\,\delta(t-1) + \epsilon\,c_3\,\delta(t-\epsilon)\right]\right\} + \dots\,, \end{aligned} \tag{4.46}$$

where $\Lambda_{\text{UV}}(t) = M_{\text{Pl}}\,\epsilon/t$ is the warped Planck scale as introduced in (1.54), and $v(t)$ and $\chi_0^h(t)$ are the profiles of the Higgs vev and the physical SM Higgs boson along the extra dimension. We now use the explicit form of the profile of the Higgs vev given in (2.45), as well as the fact that according to (2.56) we have $\chi_0^h(t)/v(t) = 1/v$ up to corrections of order m_h^2/M_{KK}^2, which we neglect here. Here, $v \approx 246\,\text{GeV}$ denotes the SM value of the Higgs vev. It is then straightforward to perform the integration over t in the above result. Matching the answer onto the effective Lagrangian given in (4.43), we obtain

$$c_{\text{eff}} = \frac{1+\beta}{2+\beta}\,c_1 + (1+\beta)\,kc_2 \quad\overset{\beta\gg1}{\longrightarrow}\quad c_1 + |\mu|c_2\,, \tag{4.47}$$

where the parameter $\beta \sim 1/\eta$, defined in (2.36), is related to the width of the profile of the scalar field. NDA suggests that c_1 and kc_2 can be as large as $\mathcal{O}(1)$ if the UV completion of the RS model is strongly coupled. The contribution of the operator localized on the UV brane is of $\mathcal{O}(\epsilon^{4+2\beta})\,c_3$ and thus entirely negligible. This suppression results from a factor $1/M_{\text{Pl}}^2$ times $v^2(\epsilon) \sim \epsilon^{2+2\beta}$ reflecting the smallness of the Higgs vev profile on the UV brane. Note that in the limit of a very narrow bulk-Higgs field, corresponding to $\beta \gg 1$ (or $\eta \ll 1$), the largest mass scale in the model is the Higgs mass parameter $|\mu| \approx \beta k = \mathcal{O}(M_{\text{Pl}})$ in (2.33) and (2.38), and hence it is more appropriate to assume that $c_2 \sim 1/|\mu| \sim 1/M_{\text{Pl}}$. Once again, this leads to $c_{\text{eff}} = \mathcal{O}(1)$. The structure of the result (4.47) is completely analogous to the corresponding expression in (4.43) valid for a brane-localized Higgs boson. In both cases the results for c_{eff}, and hence the magnitude of the contributions of higher-dimensional operators, are expected to be of the same order.

The effective Lagrangian (4.43) yields a contribution to the Wilson coefficient C_{1g} in (4.1) given by

$$\Delta C_{1g} = \frac{3c_{\rm eff}}{4}\left(\frac{4\pi v}{\Lambda_{\rm TeV}}\right)^2 \approx c_{\rm eff}\left(\frac{2.7\,\text{TeV}}{\Lambda_{\rm TeV}}\right)^2 . \tag{4.48}$$

In order for this contribution to be much smaller than the SM value $C_{1g} = 1$, we need to assume that either the cutoff scale is much larger than about 3 TeV or that $|c_{\rm eff}| \ll 1$ for some reason. With $\Lambda_{\rm TeV} \sim 10\, M_{\rm KK} \sim 20-50\,\text{TeV}$, the first criterion is satisfied in realistic RS models even if $c_{\rm eff} = \mathcal{O}(1)$. The expected contribution to the Wilson coefficient C_{1g} is then in the percent range, which is negligible in view of the current experimental uncertainty in the measurements of the Higgs-boson couplings. Another interesting question is under which assumptions the contribution (4.48) is much smaller than the corrections to the SM result $C_{1g} = 1$ which we have obtained from loop effects in the RS model, which are approximately given by

$$|C_{1g} - 1| \approx \frac{v^2}{2M_{\rm KK}^2}\sum_{q=u,d}\text{Tr}\left(\boldsymbol{Y}_q\boldsymbol{Y}_q^\dagger\right) \approx \frac{v^2}{2M_{\rm KK}^2}\,2N_g^2\,|Y_q|^2\,, \tag{4.49}$$

where $N_g = 3$ is the number of fermion generations, and $|Y_q|$ is the typical size of an element of the anarchic 5D Yukawa matrices, defined by

$$|Y_q|^2 \equiv \langle|(\boldsymbol{Y}_q)_{ij}|^2\rangle = \frac{y_*^2}{2}\,. \tag{4.50}$$

As explained in Section 2.5.1 we work with anarchic 5D Yukawa matrices and assume that the entries $(\boldsymbol{Y}_q)_{ij}$ are random complex numbers, which with equal probability can take any value in the complex plane inside a circle of radius $y_* \sim \mathcal{O}(1)$. It follows that the power-suppressed contribution (4.48) can be neglected as long as

$$c_{\rm eff}\left(\frac{M_{\rm KK}}{\Lambda_{\rm TeV}}\right)^2 \ll \frac{N_g^2\,y_*^2}{24\pi^2}\,, \tag{4.51}$$

which for $\Lambda_{\rm TeV} \approx 10 M_{\rm KK}$ can be rewritten as $c_{\rm eff} \ll 3.8\,y_*^2$. In the custodial RS model, which will be studied in Section 4.1.4, the expression on the right-hand side of this relation is multiplied by 4, yielding the weaker condition $c_{\rm eff} \ll 15.2\,y_*^2$. In our phenomenological analysis in Section 4.4 we will consider values of y_* between 0.5 and 3. In order to neglect the power-suppressed contributions for $y_* = 0.5$ in the minimal RS model, we would need to rely on the assumption that $|c_{\rm eff}| \ll 1$.

Relation (4.51) makes it clear that, in comparing the contributions from higher-dimensional operators with the contribution from virtual KK states, we are comparing a power-suppressed effect with a loop effect. Since we treat the dimensionless Yukawa couplings as $\mathcal{O}(1)$ random complex parameters, it would follow that in the formal limit $\Lambda_{\rm TeV} \to \infty$ the higher-dimensional operator contribution tends to zero, while the loop contribution remains as the dominant effect.[5] However, since by construction the RS model is free of large hierarchies, the ratio $M_{\rm KK}/\Lambda_{\rm TeV}$ cannot be made arbitrarily small. We therefore do not expect a strong hierarchy between the contribution from virtual KK states and those from higher-dimensional operators. In practice, which of the effect wins is more of a numerical question than a parametric one.

For our loop calculation to be trustable, we should impose an upper bound on the size of y_* by requiring that the Yukawa interactions remain perturbative up to the cutoff

[5] Since for too large values of the cutoff the Yukawa sector becomes strongly coupled (see below), our result in such an academic limit could at best be taken as a rough estimate of the KK loop contributions.

of the RS model under consideration. Following common practice, we will assume that $y_* \leq y_{\max} \approx 3$. A detailed discussion of different estimates of the perturbativity bound $y_{\max}$ is presented in the next section.

4.1.3 Perturbativity bounds on the Yukawa couplings

One can impose an upper bound on the size of the 5D Yukawa couplings by requiring that the Yukawa interactions remain perturbative up to the cutoff of the RS model under consideration (see e.g. [144, 173]). In 5D language, NDA estimates of the one-loop corrections to the Yukawa interactions in a model with brane-localized Higgs sector hint at a quadratic divergence. One thus obtains a condition of the form [136]

$$c_g \left(\frac{|Y_q^{5\mathrm{D}}|}{\sqrt{2}}\right)^2 \frac{l_4}{l_5^2}\, M_{\mathrm{Pl}}^2 = \frac{c_g |Y_q|^2}{18\pi^4} \left(\frac{\Lambda_{\mathrm{TeV}}}{M_{\mathrm{KK}}}\right)^2 \stackrel{!}{<} 1\,, \tag{4.52}$$

where $|Y_q^{5\mathrm{D}}| = 2|Y_q|/k$ sets the scale of the dimensionful 5D Yukawa couplings, $l_4 = 16\pi^2$ and $l_5 = 24\pi^3$ are appropriate 4D and 5D phase-space factors, M_{Pl} is the physical UV cutoff of the RS model, and in the last step we have used that $\Lambda_{\mathrm{TeV}} = M_{\mathrm{Pl}}\epsilon$ and $M_{\mathrm{KK}} = k\epsilon$. The coefficient c_g accounts for the multiplicity of fermion generations and is chosen such that $c_g = 1$ for the case of one generation. In general, for N_g fermion generations, its value $c_g = 2N_g - 1$ is determined by the relation

$$\left\langle \left(\boldsymbol{Y}_q \boldsymbol{Y}_q^\dagger \boldsymbol{Y}_q\right)_{ij} \right\rangle = (2N_g - 1)\, |Y_q|^2\, (\boldsymbol{Y}_q)_{ij}\,, \tag{4.53}$$

which holds in the sense of an expectation value for a large sample of anarchic, complex random matrices. It is instructive to reproduce condition (4.52) by employing a 4D picture in terms of KK modes, where the quadratic behavior on the cutoff arises from a double sum over the N_{KK} levels of states with masses below the cutoff Λ_{TeV} [144]. This leads to the condition

$$c_g \left(\frac{|Y_q|}{\sqrt{2}}\right)^2 \frac{1}{l_4}\, N_{\mathrm{KK}}^2 \approx \frac{c_g |Y_q|^2}{32\pi^4} \left(\frac{\Lambda_{\mathrm{TeV}}}{M_{\mathrm{KK}}}\right)^2 \stackrel{!}{<} 1\,, \tag{4.54}$$

where we have used that the masses of the KK modes are determined by the zeroes of some Bessel functions, such that the states in the N^{th} KK level have masses approximately given by $N\pi M_{\mathrm{KK}}$ (valid for large N), and hence $N_{\mathrm{KK}} \approx \Lambda_{\mathrm{TeV}}/(\pi M_{\mathrm{KK}})$. The two estimates in (4.52) and (4.54) differ by a harmless $\mathcal{O}(1)$ factor but are parametrically equivalent (including factors of π) as NDA estimates. Employing (4.50) and solving for y_*, we find the condition $y_* \leq y_{\max}$, with the upper bounds $y_{\max} = (6\pi^2/\sqrt{c_g})\, M_{\mathrm{KK}}/\Lambda_{\mathrm{TeV}}$ derived from (4.52) and $y_{\max} = (8\pi^2/\sqrt{c_g})\, M_{\mathrm{KK}}/\Lambda_{\mathrm{TeV}}$ derived from (4.54). Assuming as before that $\Lambda_{\mathrm{TeV}} \sim 10 M_{\mathrm{KK}}$, one obtains $y_{\max} \approx 2.6$ in the first case and $y_{\max} \approx 3.5$ in the second. These estimates are somewhat more refined than those presented elsewhere in the literature (because we include the dependence on N_g), but they are compatible with the conventional choice $y_{\max} = 3$ adopted in most phenomenological analyses of RS models. Using the more stringent upper bound derived from (4.52), and assuming that the Yukawa couplings are not much smaller than the values given by the perturbativity bound, we can rewrite condition (4.51) in the form

$$c_{\mathrm{eff}} \ll \frac{3\pi^2}{2}\, \frac{N_g^2}{2N_g - 1} \approx 27\,, \tag{4.55}$$

which is now independent of the value of the ratio $M_{\rm KK}/\Lambda_{\rm TeV}$. This argument shows that, even if the UV completion of the RS model is strongly coupled and $c_{\rm eff} = \mathcal{O}(1)$, the contributions from higher-dimensional operators are expected to be numerically much smaller than the KK loop effects, provided that the Yukawa couplings are not much smaller than the perturbativity bounds.

Repeating the same argument for the case of an RS model in which the Higgs sector lives in the bulk, we obtain from relation (2.64) the condition

$$c_g \left(\frac{|Y_q^{\rm 5D}|}{\sqrt{2}}\right)^2 \frac{1}{l_5}\, M_{\rm Pl} = \frac{c_g |Y_q|^2}{48\pi^3}\, \frac{(2+\beta)^2}{1+\beta}\, \frac{\Lambda_{\rm TeV}}{M_{\rm KK}} \stackrel{!}{<} 1\,, \tag{4.56}$$

which translates into $y_* \leq y_{\rm max}$ with $y_{\rm max} = \sqrt{96\pi^3/c_g}\, \frac{\sqrt{1+\beta}}{2+\beta}\, \sqrt{M_{\rm KK}/\Lambda_{\rm TeV}}$. Here, $\beta \sim 1/\eta$ is related to the width of the Higgs profile. Note that in the bulk-Higgs case the suppression in the ratio $M_{\rm KK}/\Lambda_{\rm TeV}$ is parametrically weaker than in the case of a brane-localized Higgs field. In practice, with $\Lambda_{\rm TeV} \sim 10 M_{\rm KK}$, this effect is not too important, however. Even for a very broad bulk Higgs with $\beta \to 0$, we obtain $y_{\rm max} \approx 3.9$, which is of the same order as the bound in the brane-Higgs case. In the present work we are only interested in a narrow bulk-Higgs scenario, for which $\eta = 1/\beta \ll 1$ is a small parameter. We can then simplify $y_{\rm max} = \sqrt{96\pi^3/c_g}\, \sqrt{\eta M_{\rm KK}/\Lambda_{\rm TeV}} \approx 7.7\sqrt{\eta}$. This formula can only be trusted as long as $\eta \gtrsim M_{\rm KK}/\Lambda_{\rm TeV} \approx 0.1$. For smaller η, the relevant bound is that found in the brane-Higgs case, $y_{\rm max} \approx 2.6$. From a practical point of view, there is no significant difference between the two bounds.

4.1.4 Extension to the RS model with custodial symmetry

We will now present the generalization of the above results to an extended version of the RS model, in which large corrections to electroweak precision observables are avoided by means of an enlarged gauge symmetry in the bulk of the extra dimension. This custodial RS model has been discussed in Section 2.4. The Yukawa interaction of the Higgs boson (4.2) is generalized to

$$\mathcal{L}_{hqq}(x) = -\sum_{q=u,d,\lambda} \int_\epsilon^1 dt\, \delta_h^\eta(t-1)\, h(x)\, \bar{\mathcal{Q}}_L(x,t)\, \frac{1}{\sqrt{2}} \begin{pmatrix} 0 & \boldsymbol{Y}_{\vec{q}} \\ \boldsymbol{Y}_{\vec{q}}^\dagger & 0 \end{pmatrix} \mathcal{Q}_R(x,t) + \text{h.c.}\,, \tag{4.57}$$

where the Yukawa matrices are defined in (2.85). Here, the 5D quark spinors $\mathcal{Q}_{L,R}$ collect all left- and right-chiral fields in the up, down, and exotic sectors, according to the text below (2.81). Since the Yukawa interactions (4.57) have the same structure as in (4.2), and since the BCs on the IR brane are the same as in the minimal model, the only difference concerns the UV BCs imposed on the propagator functions. The BCs for fields with superscripts $(+)$ and $(-)$ give rise to particular combinations of Bessel functions, such that $\boldsymbol{R}_A^{(+)}(\hat{p}_E) \equiv \boldsymbol{D}_1^A(\hat{p}_E,1)/\boldsymbol{D}_2^A(\hat{p}_E,1)$ and $\boldsymbol{R}_A^{(-)}(\hat{p}_E) \equiv \boldsymbol{D}_3^A(\hat{p}_E,1)/\boldsymbol{D}_4^A(\hat{p}_E,1)$. The functions $\boldsymbol{D}_i^A$ for $A = Q, u^c, \tau_1, \tau_2$ are defined in (3.60). Apart from this effect, we find that the central results (4.23) remain valid if we extend the sum over flavors appropriately, i.e.

$$I_+(m^2) = \sum_{q=u,d,\lambda} \left\{ \text{Tr}\, g(\boldsymbol{X}_{\vec{q}}) + \frac{1}{2}\,\text{Tr}\left[\frac{2\boldsymbol{X}_{\vec{q}}}{\sinh 2\boldsymbol{X}_{\vec{q}}} \left(\frac{\boldsymbol{Z}_{\vec{q}}(-m^2)}{1+\boldsymbol{Z}_{\vec{q}}(-m^2)} + \frac{\boldsymbol{Z}_{\vec{q}}^\dagger(-m^2)}{1+\boldsymbol{Z}_{\vec{q}}^\dagger(-m^2)} \right) \right] \right\}, \tag{4.58}$$

and similarly for $I_-(m^2)$. The matrices $\boldsymbol{Z}_{\vec{q}}(p_E^2)$ are defined in (3.82) for $\eta \to 0$. The relevant squared Yukawa matrices entering the quantities $\boldsymbol{X}_{\vec{q}}$, which are defined in (3.67), are given by the 6×6 matrix

$$\boldsymbol{Y}_{\vec{u}}\boldsymbol{Y}_{\vec{u}}^\dagger = \boldsymbol{V}\begin{pmatrix} 2\boldsymbol{Y}_d\boldsymbol{Y}_d^\dagger & 0 \\ 0 & 2\boldsymbol{Y}_u\boldsymbol{Y}_u^\dagger \end{pmatrix}\boldsymbol{V}^\dagger; \qquad \boldsymbol{V} = \boldsymbol{V}^\dagger = \frac{1}{\sqrt{2}}\begin{pmatrix} -1 & 1 \\ 1 & 1 \end{pmatrix}, \tag{4.59}$$

and the 3×3 matrices $\boldsymbol{Y}_{\vec{d}}\boldsymbol{Y}_{\vec{d}}^\dagger = \boldsymbol{Y}_{\vec{\lambda}}\boldsymbol{Y}_{\vec{\lambda}}^\dagger = 2\boldsymbol{Y}_d\boldsymbol{Y}_d^\dagger$. It follows that

$$\sum_{q=u,d,\lambda} \mathrm{Tr}\, g(\boldsymbol{X}_{\vec{q}}) = \mathrm{Tr}\, g\big(\sqrt{2}\boldsymbol{X}_u\big) + 3\,\mathrm{Tr}\, g\big(\sqrt{2}\boldsymbol{X}_d\big)\,, \tag{4.60}$$

where the final answer is now expressed in terms of traces over the same 3×3 matrices $\boldsymbol{X}_q$ as in the minimal RS model. Our next task is to reduce also the second term in (4.58) to traces over 3×3 matrices. It is straightforward to derive that

$$\begin{aligned}
\boldsymbol{Z}_{\vec{u}}(p_E^2) &= \frac{v^2}{2M_{\rm KK}^2}\,\boldsymbol{V}\begin{pmatrix} \tilde{\boldsymbol{Y}}_d\left[\boldsymbol{R}_{\tau_1}^{(-)} + \boldsymbol{R}_{\tau_2}^{(-)}\right]\tilde{\boldsymbol{Y}}_d^\dagger & 0 \\ 0 & 2\tilde{\boldsymbol{Y}}_u\,\boldsymbol{R}_{u^c}^{(+)}\,\tilde{\boldsymbol{Y}}_u^\dagger \end{pmatrix}\boldsymbol{V}^\dagger\begin{pmatrix} \boldsymbol{R}_Q^{(+)} & 0 \\ 0 & \boldsymbol{R}_Q^{(-)} \end{pmatrix}, \\
\boldsymbol{Z}_{\vec{d}}(p_E^2) &= \frac{v^2}{2M_{\rm KK}^2}\,\tilde{\boldsymbol{Y}}_d\left[\boldsymbol{R}_{\tau_2}^{(+)} + \boldsymbol{R}_{\tau_1}^{(-)}\right]\tilde{\boldsymbol{Y}}_d^\dagger\,\boldsymbol{R}_Q^{(+)}\,, \\
\boldsymbol{Z}_{\vec{\lambda}}(p_E^2) &= \frac{v^2}{2M_{\rm KK}^2}\,\tilde{\boldsymbol{Y}}_d\left[\boldsymbol{R}_{\tau_1}^{(-)} + \boldsymbol{R}_{\tau_2}^{(-)}\right]\tilde{\boldsymbol{Y}}_d^\dagger\,\boldsymbol{R}_Q^{(-)}\,,
\end{aligned} \tag{4.61}$$

where we have omitted the argument $\hat{p}_E$ of the $\boldsymbol{R}_A^{(\pm)}$ matrices on the right-hand side of the equations. In the custodial model, the modified Yukawa matrices are defined as $\tilde{\boldsymbol{Y}}_q = \big[\tanh(\sqrt{2}\boldsymbol{X}_q)/(\sqrt{2}\boldsymbol{X}_q)\big]\,\boldsymbol{Y}_q$ [149], with an extra factor of $\sqrt{2}$ inserted compared with the minimal model (2.27).[6]

In (4.8), we need to evaluate the result (4.58) for values $|p_E^2| \ll M_{\rm KK}^2$. Using the expansion in (4.13), we obtain (again with $\boldsymbol{x}_q = \boldsymbol{m}_{q,0}/M_{\rm KK}$)

$$\begin{aligned}
\boldsymbol{V}^\dagger\boldsymbol{Z}_{\vec{u}}(p_E^2)\boldsymbol{V} &= F^{-1}(\boldsymbol{c}_Q)\,\boldsymbol{U}_u\left\{\left[\frac{\boldsymbol{m}_{u,0}^2}{p_E^2} + \Big(\boldsymbol{\Phi}_U + \boldsymbol{m}_{u,0}\,\boldsymbol{\Phi}_u\,\boldsymbol{m}_{u,0}^{-1}\Big) + \ldots\right]\begin{pmatrix} 0 & 0 \\ -1 & 1 \end{pmatrix}\right. \\
&\quad + \boldsymbol{V}_{\rm CKM}\,\boldsymbol{x}_d\,\boldsymbol{W}_d^\dagger\,\frac{1}{2F^2(\boldsymbol{c}_{\tau_2})}\left[\frac{1}{F^2(-\boldsymbol{c}_{\tau_1})} + \frac{1}{F^2(-\boldsymbol{c}_{\tau_2})}\right]\boldsymbol{W}_d\,\boldsymbol{x}_d\,\boldsymbol{V}_{\rm CKM}^\dagger\begin{pmatrix} 1 & -1 \\ 1 & -1 \end{pmatrix} \\
&\quad \left. + \boldsymbol{x}_u^2\,\boldsymbol{U}_u^\dagger\,\frac{2}{F^2(\boldsymbol{c}_Q)\,F^2(-\boldsymbol{c}_Q)}\,\boldsymbol{U}_u\begin{pmatrix} 0 & 0 \\ 1 & 0 \end{pmatrix} + \ldots\right\}\boldsymbol{U}_u^\dagger\,F(\boldsymbol{c}_Q)\,, \\
\boldsymbol{Z}_{\vec{d}}(p_E^2) &= F^{-1}(\boldsymbol{c}_Q)\,\boldsymbol{U}_d\left[\frac{\boldsymbol{m}_{d,0}^2}{p_E^2} + \Big(\boldsymbol{\Phi}_D + \boldsymbol{m}_{d,0}\,\boldsymbol{\Phi}_d\,\boldsymbol{m}_{d,0}^{-1}\Big) + \ldots\right]\boldsymbol{U}_d^\dagger\,F(\boldsymbol{c}_Q)\,,
\end{aligned} \tag{4.62}$$

where $\boldsymbol{V}_{\rm CKM} = \boldsymbol{U}_u^\dagger\boldsymbol{U}_d$ is the CKM mixing matrix. The terms shown explicitly above are of leading and subleading order in $v^2/M_{\rm KK}^2$. To this order, the quantity $\boldsymbol{Z}_{\vec{\lambda}}(p_E^2)$ vanishes. The quantities $\boldsymbol{\Phi}_A$ are generalizations of the matrices $\boldsymbol{\delta}_A$ given in (4.28). They

[6] Note, that this should not be confused with the modified Yukawa matrix $\tilde{\boldsymbol{Y}}_{\vec{q}} \neq \tilde{\boldsymbol{Y}}_q$ which is defined in (3.73).

are defined as [149]

$$\begin{aligned}
\boldsymbol{\Phi}_U &= \boldsymbol{x}_u\,\boldsymbol{W}_u^\dagger\left[\frac{1}{1-2\boldsymbol{c}_u}\left(\frac{1}{F^2(\boldsymbol{c}_u)}-1+\frac{F^2(\boldsymbol{c}_u)}{3+2\boldsymbol{c}_u}\right)\right]\boldsymbol{W}_u\,\boldsymbol{x}_u \\
&\quad+\boldsymbol{V}_{\rm CKM}\,\boldsymbol{x}_d\,\boldsymbol{W}_d^\dagger\,\frac{1}{2F^2(\boldsymbol{c}_{\tau_2})}\left[\frac{1}{F^2(-\boldsymbol{c}_{\tau_1})}+\frac{1}{F^2(-\boldsymbol{c}_{\tau_2})}\right]\boldsymbol{W}_d\,\boldsymbol{x}_d\,\boldsymbol{V}_{\rm CKM}^\dagger\,, \\
\boldsymbol{\Phi}_u &= \boldsymbol{x}_u\,\boldsymbol{U}_u^\dagger\left[\frac{1}{1-2\boldsymbol{c}_Q}\left(\frac{1}{F^2(\boldsymbol{c}_Q)}\left[1+\frac{1-2\boldsymbol{c}_Q}{F^2(-\boldsymbol{c}_Q)}\right]-1+\frac{F^2(\boldsymbol{c}_Q)}{3+2\boldsymbol{c}_Q}\right)\right]\boldsymbol{U}_u\,\boldsymbol{x}_u\,, \\
\boldsymbol{\Phi}_D &= \boldsymbol{x}_d\,\boldsymbol{W}_d^\dagger\left[\frac{1}{1-2\boldsymbol{c}_{\tau_2}}\left(\frac{1}{F^2(\boldsymbol{c}_{\tau_2})}\left[1+\frac{1-2\boldsymbol{c}_{\tau_2}}{F^2(-\boldsymbol{c}_{\tau_1})}\right]-1+\frac{F^2(\boldsymbol{c}_{\tau_2})}{3+2\boldsymbol{c}_{\tau_2}}\right)\right]\boldsymbol{W}_d\,\boldsymbol{x}_d\,, \\
\boldsymbol{\Phi}_d &= \boldsymbol{x}_d\,\boldsymbol{U}_d^\dagger\left[\frac{1}{1-2\boldsymbol{c}_Q}\left(\frac{1}{F^2(\boldsymbol{c}_Q)}-1+\frac{F^2(\boldsymbol{c}_Q)}{3+2\boldsymbol{c}_Q}\right)\right]\boldsymbol{U}_d\,\boldsymbol{x}_d\,.
\end{aligned} \tag{4.63}$$

After a lengthy calculation, we find that in analogy with (4.30)

$$\sum_{q=u,d,\lambda}\mathrm{Tr}\left[\frac{2\boldsymbol{X}_{\vec{q}}}{\sinh 2\boldsymbol{X}_{\vec{q}}}\,\frac{\boldsymbol{Z}_{\vec{q}}(p_E^2)}{1+\boldsymbol{Z}_{\vec{q}}(p_E^2)}\right]=\sum_i\left[\kappa_{q_i}\,\frac{m_{q_i}^2}{m_{q_i}^2+p_E^2}+\varepsilon_{q_i}\right]+\dots\,, \tag{4.64}$$

where

$$\kappa_{q_i}=1-\varepsilon_{q_i}-\frac{2}{3}\left[\boldsymbol{U}_q^\dagger\,F(\boldsymbol{c}_Q)\,2\boldsymbol{X}_q^2\,F^{-1}(\boldsymbol{c}_Q)\,\boldsymbol{U}_q\right]_{ii} \tag{4.65}$$

now contains an extra factor of 2 in the last term compared with the result (4.31) for the minimal model, while $\varepsilon_{q_i}=(\boldsymbol{\Phi}_Q)_{ii}+(\boldsymbol{\Phi}_q)_{ii}$. We are now ready to present our final expressions for the Wilson coefficients C_{1g} and C_{5g} in the RS model with custodial symmetry. To an excellent approximation, we obtain instead of (4.33)

$$\begin{aligned}
C_{1g} &\approx \left[1-\frac{2v^2}{3M_{\rm KK}^2}\,\mathrm{Re}\,\frac{\left(\boldsymbol{Y}_u\boldsymbol{Y}_u^\dagger\boldsymbol{Y}_u\right)_{33}}{(\boldsymbol{Y}_u)_{33}}\right]A_q(\tau_t)+A_q(\tau_b)+\mathrm{Tr}\,g\big(\sqrt{2}\boldsymbol{X}_u\big)+3\,\mathrm{Tr}\,g\big(\sqrt{2}\boldsymbol{X}_d\big)\,, \\
C_{5g} &\approx -\frac{2v^2}{3M_{\rm KK}^2}\,\mathrm{Im}\left[\frac{\left(\boldsymbol{Y}_u\boldsymbol{Y}_u^\dagger\boldsymbol{Y}_u\right)_{33}}{(\boldsymbol{Y}_u)_{33}}\right]B_q(\tau_t)\,,
\end{aligned} \tag{4.66}$$

which once again is independent of the bulk-mass parameters c_i. We find that this approximation is accurate to better than 2% for $M_{\rm KK}\gtrsim 2\,\mathrm{TeV}$. Whereas the small corrections parameterized by κ_{q_i} and ε_{q_i} have only a minor impact, the main difference between the minimal and the custodial RS models consists in the different multiplicity factors in the trace terms in (4.33) and (4.66). Since the functions $g(\boldsymbol{X}_q)$ start with a quadratic term, we must compare $\boldsymbol{X}_u^2+\boldsymbol{X}_d^2$ in the minimal model with the combination $2\boldsymbol{X}_u^2+6\boldsymbol{X}_d^2$ in the custodial model. Since we assume that the 5D Yukawa matrices in the up- and down-type quark sectors are random matrices of similar magnitude, it follows that the effect of the KK modes in the custodial model is approximately four times as large as in the minimal model.[7]

4.1.5 Classification of RS models

Let us recapitulate the main conceptual conclusion of the analysis on the process of gluon fusion. We have seen that the results obtained in the brane-localized and narrow

[7] Based on a naive counting of degrees of freedom, this factor was estimated as 11/4 (instead of 4) in [212].

Model	bulk Higgs	narrow bulk Higgs	transition region	brane Higgs
Higgs width	$\eta = \mathcal{O}(1)$	$\frac{v\lvert Y_q\rvert}{\Lambda_{\rm TeV}} \ll \eta \ll \frac{v\lvert Y_q\rvert}{M_{\rm KK}}$	$\eta \sim \frac{v\lvert Y_q\rvert}{\Lambda_{\rm TeV}}$	$\eta \ll \frac{v\lvert Y_q\rvert}{\Lambda_{\rm TeV}}$
Power corrections	$\left(\frac{M_{\rm KK}}{\Lambda_{\rm TeV}}\right)^n$	$\left(\frac{M_{\rm KK}}{\eta\Lambda_{\rm TeV}}\right)^n$ $\frac{M_{\rm KK}}{\Lambda_{\rm TeV}}\frac{M_{\rm KK}}{v\lvert Y_q\rvert} \ll \frac{M_{\rm KK}}{\eta\Lambda_{\rm TeV}} \ll \frac{M_{\rm KK}}{v\lvert Y_q\rvert}$	$\left(\frac{M_{\rm KK}}{v\lvert Y_q\rvert}\right)^n$	$\left(\frac{M_{\rm KK}}{\Lambda_{\rm TeV}}\right)^n$
Higgs profile	resolved by all modes	resolved by high-momentum modes	partially resolved by high-mom. modes	not resolved
$\mathcal{A}(gg \to h)$	enhanced	enhanced	not calculable	suppressed
Result	model-dep.	model-independent	unreliable	model-indep.

Table 4.1: Comparison of the main features of various versions of the Higgs sector in RS models (see text for further explanation). The label "model-independent result" means that the corrections to the SM prediction for the Higgs production cross section can be calculated (to excellent approximation) without any reference to the Higgs and fermion bulk profiles.

bulk-Higgs scenarios, which are defined by (1.55) and (1.56), are rather different, both qualitatively and quantitatively. Indeed, one should consider the two scenarios as two different, distinguishable realizations of RS models. This fact has also been realized in [215]. The situation resembles that encountered when one compares the original RS model, in which only gravity was allowed to propagate in the extra dimension while all SM fields were confined to the IR brane [125], with the more popular models in which all matter and gauge fields live in the bulk [168]. While the original model only addressed the gauge-hierarchy problem the latter models are qualitatively different in that they also provide successful theories of flavor, as we have explained in Sections 1.4.1 and 1.4.4.

While the width of the Higgs profile is a physical parameter, which in principle can be adjusted to take any desired value, the transition from the narrow bulk-Higgs scenario (1.56) to the brane-Higgs scenario (1.55) cannot be described in a controlled analytical way. This fact can be understood by investigating the structures of the corresponding effective theories in more detail. Table 4.1 summarizes the main features of the various models as defined by the size of the width parameter η. The second row in the table shows the scaling of power corrections, as represented by higher-dimensional operators in the effective Lagrangian of the RS model. Both in a generic bulk-Higgs model (with $\eta = \mathcal{O}(1)$) and in models where the scalar sector is localized on the IR brane, effects of higher-dimensional operators in Higgs physics are suppressed by powers of the ratio $M_{\rm KK}/\Lambda_{\rm TeV}$, since as explained earlier the warped Planck scale $\Lambda_{\rm TeV}$ is the natural UV cutoff of these theories. The situation changes if one considers bulk-Higgs models, in which the width parameter η is parametrically suppressed. Then the effective theory knows about an extra small parameter, and derivatives ∂_t acting on the bulk scalar field can produce powers of $1/\eta$. As a result, there is a class of enhanced power corrections scaling like $(M_{\rm KK}/\eta\Lambda_{\rm TeV})^n$. In the transition region between the narrow bulk-Higgs and brane-localized Higgs scenarios, these enhanced power corrections become of $\mathcal{O}(1)$ or larger, and hence the effective field-theory approach breaks down. In other words, because of the uncontrolled behavior of power-suppressed terms in the transition region, we lack the analytical control over the theory, which would be required to see how the results interpolate from the bulk-Higgs case to the brane-Higgs scenario as one reduces the value of η. In [209], the authors computed the $gg \to h$ amplitude in the context of a bulk-Higgs model and took the limit $\eta \to 0$ at the end of their calculation, stating that

the answer corresponds to the case of a brane-localized Higgs. As we have just argued, such an approach gives the correct result in the model (1.56), and we thus find it more appropriate to refer to it as a narrow bulk-Higgs scenario.

The above remarks referred to an idealized case, in which the electroweak scale $v|Y_q|$ and the KK mass $M_{\rm KK}$ are of comparable magnitude. In practice, due to the lack of KK modes below the TeV scale, there appears to be a little hierarchy between these scales, such that $v|Y_q|/M_{\rm KK} \lesssim 0.3$ or less. Then the power corrections in the transition region are even larger than $\mathcal{O}(1)$, and also in the narrow bulk-Higgs case the lower bound on $M_{\rm KK}/(\eta\Lambda_{\rm TeV})$ cannot be much smaller than 1. In view of this fact, one must consider the results derived for the narrow bulk-Higgs case with some caution. A more reliable calculation should stay in a regime where $\eta = \mathcal{O}(1)$. But this has the disadvantage that the results will depend in a complicated way on the shapes of the Higgs and fermion profiles.

4.2 Loop-induced Higgs decay into two photons

In this section we focus on the Higgs decay into two photons. Analogously to the process of gluon fusion we work in the 5D framework, where the calculation is performed using 5D propagators. Earlier discussions of the Higgs decay into two photons can be found in [149, 205, 206, 208, 209]. The first analysis of the effects of the KK tower of the W boson on the $h \to \gamma\gamma$ amplitude was performed in [206]. The first complete calculation of the $h \to \gamma\gamma$ decay rate, in which both the Yukawa couplings to the Z_2-even and Z_2-odd fermions were included, was performed in [149]. It was found in this paper that the Higgs decay rate into two photons is enhanced relative to the SM due to the effect of the KK fermions, which turned out to give the dominating correction. At about the same time, an independent analysis of the $h \to \gamma\gamma$ decay rate came to the opposite conclusion [209].

We show that the different results obtained in [149] and [209] belong to two different scenarios of the RS model, the brane-localized and narrow bulk-Higgs scenario. This is analogous to the quark KK-tower contribution to the Higgs production process $gg \to h$. Up to different factors for the color multiplicity and electric charges, an analogous discussion holds for the quark and lepton KK-tower contributions to $h \to \gamma\gamma$. In addition, we provide a detailed analysis of the bosonic loop contributions to the $h \to \gamma\gamma$ amplitude, which in unitary gauge stem from the W bosons and their KK excitations. It is also straightforward to extend our formulas to the case where the Higgs boson lives in the bulk of the extra dimension. Our approach also allows us to carefully study the effects of the fifth components of the gauge fields, whose profiles are discontinuous on the IR brane, similar to the Z_2-odd fermion profiles which indeed require a careful treatment. As we show, however, the bosonic contributions to the $h \to \gamma\gamma$ amplitude are insensitive to the precise localization of the scalar sector and approach an unambiguous result in the limit where $\eta \ll 1$.

Section 4.2.1 discusses the general structure of the $h \to \gamma\gamma$ amplitude and summarizes the results for the fermionic contributions from charged quarks and leptons propagating in the loop. We then focus on the bosonic loop contributions, calculate them in the KK-decomposed theory and show that the result for the contributions of each individual KK mode is gauge invariant. In the next step we resum the KK towers and derive an exact formula for the $h \to \gamma\gamma$ amplitude in terms of an overlap integral over the Higgs-boson profile and the transverse part of the gauge-boson 5D propagator, including the exact dependence on the Higgs-boson mass. To the best of our knowledge, such a formula has not been obtained before. By expanding our results in powers of $v^2/M_{\rm KK}^2$, we can identify the contributions from the W bosons (with modified couplings to the Higgs boson) and

their KK towers, confirming the results of [206]. In Section 4.2.2 we generalize our findings to the custodial RS model. Again, we obtain an exact formula for the $h \to \gamma\gamma$ amplitude. When expanded to order $v^2/M_{\rm KK}^2$, our findings for the contributions of the W boson and its KK excitations are consistent with the findings of [149].

4.2.1 5D analysis of $h \to \gamma\gamma$

Our goal is to calculate the $h \to \gamma\gamma$ decay amplitude entirely in terms of the 5D propagators for both gauge bosons and fermions. While the contributions from quarks and charged leptons can be easily deduced from the corresponding results for the $gg \to h$ amplitude in Section 4.1, a detailed consideration of the gauge-boson contribution has not yet been performed in 5D language. In a first step, we calculate the bosonic contributions to the $h \to \gamma\gamma$ amplitude in the KK-decomposed, 4D effective theory and show that at each KK level the sum of all diagrams is gauge-invariant. The only contributing diagrams in unitary gauge are those with vector bosons propagating in the loop. We can then rewrite the amplitude, summed over KK states, as an expression involving the gauge-boson 5D propagator in the mixed momentum-position representation which has been derived in Section 3.2.

We begin with the calculation in the minimal RS model, which has been discussed in Chapter 2. Appendix A includes a summary of the relevant Feynman rules needed for our analysis. The one-loop Feynman diagrams contributing to the $h \to \gamma\gamma$ decay amplitude are shown in Figure 4.3 for a general R_ξ gauge. In the subsequent section we demonstrate that the full amplitude is gauge invariant. In the unitary gauge only the diagrams $(a)-(c)$ contribute. In order to present our results, we find it convenient to parametrize the $h \to \gamma\gamma$ amplitude, including the contributions from SM particles, by means of two Wilson coefficients $C_{1\gamma}$ and $C_{5\gamma}$ defined via

$$\mathcal{A}(h \to \gamma\gamma) = C_{1\gamma}\,\frac{\alpha}{6\pi v}\,\langle\gamma\gamma|F_{\mu\nu}F^{\mu\nu}|0\rangle - C_{5\gamma}\,\frac{\alpha}{4\pi v}\,\langle\gamma\gamma|F_{\mu\nu}\tilde{F}^{\mu\nu}|0\rangle\,, \tag{4.67}$$

where $\tilde{F}^{\mu\nu} = -\frac{1}{2}\epsilon^{\mu\nu\alpha\beta}F_{\alpha\beta}$ with $\epsilon^{0123} = -1$. Each Wilson coefficient can be written as a sum of three terms,

$$C_i = C_i^W + C_i^q + C_i^l\,, \tag{4.68}$$

where in a general gauge C_i^W includes the bosonic contributions from gauge bosons, scalar bosons, and ghosts. The calculation of these bosonic contributions is the main subject of this work.

In our analysis we also discuss the narrow bulk-Higgs scenario where the Higgs profile $\delta^\eta(t-1)$ has a characteristic width η subject to the condition $M_{\rm KK} \ll v|Y_q|/\eta \ll \Lambda_{\rm TeV}$, see Section 1.4.5 for more details. In principle, such a scenario gives rise to a tower of *physical* scalar particles $\phi_W^{\pm(n)}$, which in some sense are the KK excitations of the charged components of the Higgs doublet. As discussed in detail in [164], these fields are defined in terms of a gauge-invariant superposition of $W_\phi^\pm$ and $\varphi^\pm$. It has been shown in the same reference that the effect of these heavy scalar particles on the $h \to \gamma\gamma$ amplitude is

$$C_{1\gamma}^\phi = \frac{1}{8}\sum_{n=1}^{\infty}\frac{v g_{h\phi\phi}^{(n,n)}}{\left(m_n^\phi\right)^2}\,A_\phi(\tau_n^\phi)\,, \qquad C_{5\gamma}^\phi = 0\,, \tag{4.69}$$

where $\tau_n^\phi = 4(m_n^\phi)^2/m_h^2$, and the function

$$A_\phi(\tau) = 3\tau\left[\tau f(\tau) - 1\right], \quad \text{with} \quad f(\tau) = \arctan^2\frac{1}{\sqrt{\tau-1}}\,, \tag{4.70}$$

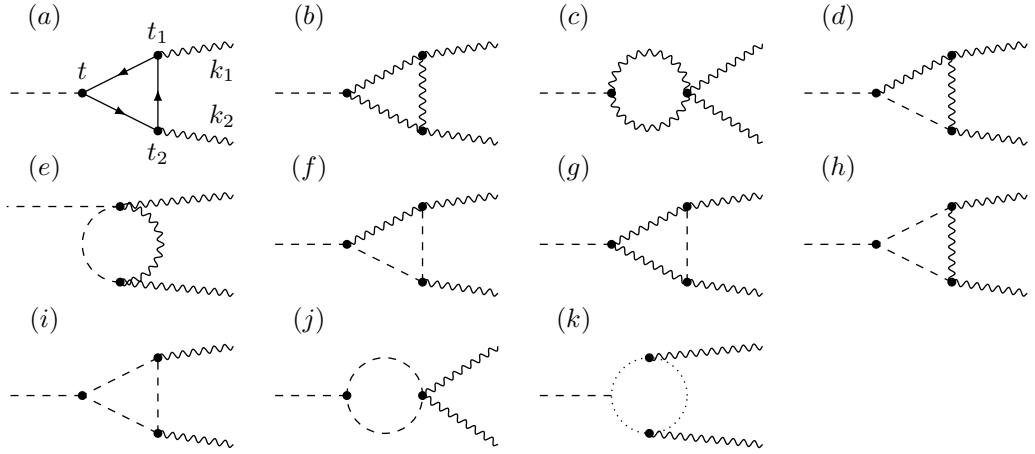

Figure 4.3: One-loop Feynman diagrams for the process $h \to \gamma\gamma$. Diagram (a) contains the fermion loops, while diagrams $(b)-(k)$ show the contributions from the gauge sector in a general R_ξ gauge. Solid lines represent fermion mass eigenstates, wavy lines vector-boson mass eigenstates $W_\mu^{\pm(n)}$, dashed lines scalar mass eigenstates $\varphi_W^{\pm(n)}$, and dotted lines ghost mass eigenstates $c_W^{\pm(n)}$. The ghost masses and profiles are the same as for the W bosons and their KK excitations.

approaches 1 for $\tau \to \infty$. In the limit of a very narrow Higgs profile the couplings $g_{h\phi\phi}^{(n,n)}$ scale like $1/\eta$, while the masses of the heavy scalar particles scale like $M_{\rm KK}/\eta$. It follows that $C_{1\gamma}^{\phi} = \mathcal{O}(\eta)$, and hence this contribution decouples in the limit $\eta \to 0$, as expected. We will therefore not consider the corresponding Feynman diagrams in our analysis.

Fermionic contributions to the Wilson coefficients

The one-loop contributions to the $h \to \gamma\gamma$ amplitude due to the exchange of virtual quarks and leptons can be derived in a straightforward way from analogous results for the quark contributions to the $gg \to h$ amplitude, see (4.8), (4.9) and (4.10). All that is necessary is to include appropriate factor of color and electric charges. The exact result can be written in the form

$$\begin{aligned} C_{1\gamma}^q &= 3N_c \sum_{f=u,d} Q_q^2 \int_0^1 dx \int_0^{1-x} dy\, (1-4xy) \left[T_+^q(-xym_h^2) - T_+^q(\Lambda_{\rm TeV}^2) \right], \\ C_{5\gamma}^q &= 2N_c \sum_{f=u,d} Q_q^2 \int_0^1 dx \int_0^{1-x} dy \left[T_-^q(-xym_h^2) - T_-^q(\Lambda_{\rm TeV}^2) \right], \end{aligned} \tag{4.71}$$

where $Q_u = 2/3$ and $Q_d = -1/3$ are the electric charges of the quarks, and $N_c = 3$ is the number of colors. The functions $T_\pm^q(-p^2)$ are defined in terms of linear combinations of overlap integrals of the Higgs-boson profile with the chirality-odd components of the fermion 5D propagator, see (4.7) for more details. An analogous expression, with N_c replaced by 1 and Q_q replaced by $Q_e = -1$ holds for the charged-lepton contribution. These exact results can be simplified by neglecting some terms of order $v^4/M_{\rm KK}^4$ and chirally-suppressed $\mathcal{O}(v^2/M_{\rm KK}^2)$ terms, which is an excellent approximation numerically. This leads to the explicit expressions

$$C_{1\gamma}^q \approx \left[1 - \frac{v^2}{3M_{\rm KK}^2} {\rm Re} \frac{(\boldsymbol{Y}_u \boldsymbol{Y}_u^\dagger \boldsymbol{Y}_u)_{33}}{(\boldsymbol{Y}_u)_{33}} \right] N_c\, Q_u^2\, A_q(\tau_t) + N_c\, Q_d^2\, A_q(\tau_b) + \sum_{q=u,d} N_c\, Q_q^2\, {\rm Re\,Tr}\, g(\boldsymbol{X}_q)\,,$$

$$C_{5\gamma}^q \approx -\frac{v^2}{3M_{\rm KK}^2}\,{\rm Im}\left[\frac{(\boldsymbol{Y}_u\boldsymbol{Y}_u^\dagger\boldsymbol{Y}_u)_{33}}{(\boldsymbol{Y}_u)_{33}}\right] N_c\,Q_u^2\,B_q(\tau_t) + \sum_{q=u,d} N_c\,Q_q^2\,{\rm Im\,Tr}\,g(\boldsymbol{X}_q)\,, \tag{4.72}$$

and

$$C_{1\gamma}^l + iC_{5\gamma}^l \approx Q_e^2\;{\rm Tr}\,g(\boldsymbol{X}_e)\,, \tag{4.73}$$

where the contributions from the SM fermions and the KK excitations can now readily be identified. The loop functions A_q and B_q are defined in (4.34) with $\tau_i = 4m_i^2/m_h^2$. They both approach 1 for $\tau \to \infty$. For values $\tau < 1$ the function $f(\tau)$ in (4.70) must be analytically continued, with $\tau \to \tau - i0$. The quantities

$$\boldsymbol{X}_f = \varrho\,\sqrt{\boldsymbol{Y}_f\boldsymbol{Y}_f^\dagger}\,; \quad f = u,d,e \tag{4.74}$$

are defined in terms of the dimensionless 5D Yukawa matrices of the RS model. Note that with the hermitian matrices $\boldsymbol{X}_f$ the traces over matrix-valued functions $g(\boldsymbol{X}_f)$ are real, so that $C_{5\gamma}^l = 0$ and the only contribution to the coefficient $C_{5\gamma}^q$ arises from the top-quark contribution given by the first term on the right-hand side of (4.72). The precise form of the function $g(\boldsymbol{X}_f)$ depends on the details of the localization of the scalar sector on or near the IR brane. For the two scenarios with a brane-localized Higgs and a narrow bulk Higgs, as defined in Section 1.4.5, one finds to leading order in $v^2/M_{\rm KK}^2$ the functions $g(\boldsymbol{X}_f) \approx -\boldsymbol{X}_f^2$ and $g(\boldsymbol{X}_f) \approx +\boldsymbol{X}_f^2$. The exact expressions are given by (4.24) and (4.25). The effect of the KK tower is approximately equal but of opposite sign in the two cases. As we have explained for the gluon fusion process, the difference is due to a "resonance effect" in the narrow bulk-Higgs scenario, where very heavy KK modes with masses of order the inverse Higgs width $\Delta_h = v/\eta$ give an unsuppressed contribution to the loop amplitude. At a technical level, the difference arises from the subtraction term at large Euclidean momentum in (4.71), which is relevant for the function $T_+^f(-p^2)$ only. For a brane-localized Higgs, this function approaches a plateau at large momenta, such that $T_+^f(\Lambda_{\rm TeV}^2) = {\rm Tr}[\boldsymbol{X}_f \tanh 2\boldsymbol{X}_f]$. For a narrow bulk Higgs, on the other hand, the function $T_+^f(p_E^2)$ vanishes like $1/p_E$ in the region of large Euclidean momenta $p_E^2 = -p^2 \gg (v/\eta)^2$, and hence $T_+^f(\Lambda_{\rm TeV}^2)$ can be set to zero. We can also consider a variant of the brane-Higgs scenario with two different Yukawa matrices $\boldsymbol{Y}_f^C$ and $\boldsymbol{Y}_f^S$ for the Z_2-even and Z_2-odd fermion fields. In this type-II brane-Higgs model the matrices $\boldsymbol{X}_f$ are no longer hermitian, but to leading order $g(\boldsymbol{Y}_f^C, \boldsymbol{Y}_f^S) \approx -\varrho^2\boldsymbol{Y}_f^C\boldsymbol{Y}_f^{C\dagger}$ is still a hermitian matrix. The exact function is given by (4.36). The type-II brane-Higgs scenario is thus rather similar to the original brane-Higgs model with identical Yukawa matrices $\boldsymbol{Y}_f^C = \boldsymbol{Y}_f^S = \boldsymbol{Y}_f$. Numerically, we find that the main difference is a slightly larger spread of the distribution of scatter points when one scans over the parameter space of the model. In our phenomenological analysis in Section 4.4, we will therefore restrict ourselves to a study of the brane-localized and narrow bulk-Higgs scenarios.

Gauge invariance of the amplitude

In the SM, a recent paper [216] has thoroughly discussed the ξ independence of the $h \to \gamma\gamma$ amplitude in dimensional regularization and has shown that the calculation can be performed consistently in the unitary gauge $\xi \to \infty$. In the case of the RS model, it is convenient to first work in the KK-decomposed theory, where 4D Feynman propagators have the same structure as in the SM. The Feynman rules required to evaluate the one-loop diagrams shown in Figure 4.3 are summarized in Appendix A. From these rules, it follows that:

- All vertices involving one or two external photons but no Higgs boson are diagonal in KK number after one integrates over the extra-dimensional coordinate of the vertex with measure $\int_{-\pi}^{\pi} d\phi = (2\pi/L)\int_{\epsilon}^{1} dt/t$. The Feynman rules for these vertices have the same form as in the SM after one identifies the 4D electromagnetic coupling as $e = e_5/\sqrt{2\pi r}$. For the mass-dependent vertex connecting a photon to $W_\mu^{\pm(n)}\varphi_W^{\mp(n)}$, one must replace $m_W \to m_{W_n}$.

- As a result, all one-loop diagrams contributing to the $h \to \gamma\gamma$ amplitude involve a single KK particle in the loop. Hence, only KK-diagonal Higgs couplings are required in the calculation.

- All KK-diagonal Higgs couplings have the same structure as in the SM but come with an overall prefactor

$$\frac{v}{2}\,\frac{g_5^2}{2\pi r}\,2\pi\left[\chi_n^W(1)\right]^2 = \frac{2\tilde{m}_W^2}{v}\,2\pi\left[\chi_n^W(1)\right]^2, \tag{4.75}$$

  which replaces the corresponding factor $g m_W = 2m_W^2/v_{\rm SM}$ in the SM. Note that $v_{\rm SM}$ is the vev in the SM which we define via the Fermi constant $v_{\rm SM} \equiv (\sqrt{2}G_F)^{-1/2}$, see the discussion in Section 2.5.2 for more details. In addition, for each scalar boson $\varphi_W^{\pm(n)}$ a factor $1/m_{W_n}$ appears, which replaces $1/m_W$ in the corresponding SM Feynman rule for vertices involving the NGBs $\varphi^\pm$.

It follows from these observations that, diagram by diagram and in a general R_ξ gauge, the bosonic loop contributions obtained in the RS model resemble those of the SM up to trivial substitutions, such that

$$\mathcal{A}_{\rm RS}^W(h\to\gamma\gamma) = \frac{\tilde{m}_W^2}{v}\sum_{n=0}^{\infty} 2\pi\left[\chi_n^W(1)\right]^2\left[\frac{v_{\rm SM}}{m_W^2}\,\mathcal{A}_{\rm SM}^W(h\to\gamma\gamma)\right]_{m_W\to m_{W_n}}. \tag{4.76}$$

The statement made in the first bullet point above requires some comments. For vertices involving a photon and a pair of vector bosons, fermions or ghosts, the statement that the vertex is diagonal in KK number is a direct consequence of the flatness of the photon profile, enforced by $U(1)_{\rm EM}$ gauge invariance, and the orthogonality of the relevant vector-boson and fermion profiles. However, the situation is different for vertices involving the scalar bosons $\varphi_W^{\pm(n)}$, which receive contributions from the 5D fields $W_5^\pm$ and $\varphi^\pm$, see (2.2) and (2.5). In this case, the vertex becomes diagonal only after one adds up these two contributions. Consider, as an example, the vertex

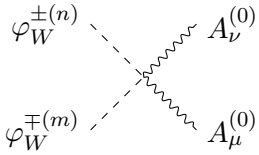

needed for diagram (j) in Figure 4.3. After integrating over the coordinate of this vertex, we obtain the Feynman rule

$$2ie^2\eta_{\mu\nu}\left[\frac{M_{\rm KK}^2}{m_{W_m}\,m_{W_n}}\,\frac{2\pi}{L}\int_\epsilon^1\frac{dt}{t}\left[\partial_t\chi_m^W(t)\right]\left[\partial_t\chi_n^W(t)\right] + \frac{2\pi\,\tilde{m}_W^2}{m_{W_m}\,m_{W_n}}\,\chi_m^W(1)\,\chi_n^W(1)\right], \tag{4.77}$$

where the first contribution originates from the $W_5W_5A_\mu A^\mu$ term contained in the Yang-Mills action for the W-boson fields using the KK decomposition (2.2), while the second

contribution arises from the $\varphi^+\varphi^- A_\mu A^\mu$ term contained in the kinetic term for the Higgs doublet using the KK decomposition (2.5). We now integrate by parts in the first term and use the equations of motion (2.7). In this way, we obtain the Feynman rule

$$2ie^2\eta_{\mu\nu}\left[\frac{m_{W_n}}{m_{W_m}}\,\frac{2\pi}{L}\int_\epsilon^1\frac{dt}{t}\,\chi_m^W(t)\,\chi_n^W(t)\right], \tag{4.78}$$

where the boundary term cancels the contribution arising from the $\varphi^+\varphi^- A_\mu A^\mu$ term. Using finally the orthonormality relation (2.8) for the gauge-boson profiles, we obtain the SM expression $2ie^2\eta_{\mu\nu}\,\delta_{mn}$ for the vertex.

Let us now return to the general result (4.76) and explore its consequences. Obviously, this relation implies that for each single KK mode the $h\to\gamma\gamma$ amplitude in the RS model is gauge invariant provided the amplitude is gauge invariant in the SM. Since, as we will demonstrate below, the sum over KK modes is convergent, it follows that gauge invariance is maintained also in the 5D theory. We recall that to show gauge invariance in the SM one divides the W-boson propagator in R_ξ gauge into two parts,

$$\frac{i}{p^2-m_W^2}\left[\frac{(1-\xi)\,p^\mu p^\nu}{p^2-\xi m_W^2}-\eta^{\mu\nu}\right]=\frac{i}{p^2-m_W^2}\left(\frac{p^\mu p^\nu}{m_W^2}-\eta^{\mu\nu}\right)-\frac{i}{p^2-\xi m_W^2}\,\frac{p^\mu p^\nu}{m_W^2}\,, \tag{4.79}$$

where the first part coincides with the propagator in unitary gauge and the second part has the same structure as the scalar-boson and ghost propagators. It has been shown in [216] that, after adding up all diagrams, many intricate cancellations occur, and at the end only the diagrams (b) and (c) in Figure 4.3 with the W-boson propagators in unitary gauge, as well as the fermion loop contributions shown in diagram (a), remain. We have repeated this analysis and checked these cancellations by explicit calculation, thereby confirming that it is justified to use the unitary gauge also in the RS model.

Calculation of the bosonic loop contributions to $h\to\gamma\gamma$

We now perform the calculation of the bosonic loop contributions to the $h\to\gamma\gamma$ amplitude using the 5D approach. We adopt the unitary gauge and consider only the contributions of diagrams (b) and (c) in Figure 4.3. We employ the mixed momentum-position representation of the gauge-boson 5D propagator $D^\xi_{W,\mu\nu}(t,t';p)$. It is well known that even in the SM the loop-momentum integral must be regularized dimensionally in order to preserve gauge invariance. We will thus introduce a dimensional regulator $d=4-2\hat\epsilon$ on the loop integral in intermediate steps. This regulator can be removed at the end of the calculation. We also regularize the Higgs profile by using the function $\delta^\eta(t-1)$ in (1.58) with the regulator $\eta\ll 1$. However, we will find that in the calculation of the bosonic loop contributions the limit $\eta\to 0$ can be taken without encountering any ambiguities. Diagrams (b) and (c) give rise to the amplitude

$$\begin{aligned}i\mathcal{A}(h\to\gamma\gamma)=&-\frac{2\tilde m_W^2}{v}\,2\pi e^2\,\epsilon_\mu^*(k_1)\,\epsilon_\nu^*(k_2)\,\eta^{\alpha\beta}\int\frac{d^dp}{(2\pi)^d}\int_\epsilon^1 dt\,\delta^\eta(t-1)\,\frac{2\pi}{L}\int_\epsilon^1\frac{dt_1}{t_1}\\
&\times\left[\frac{2\pi}{L}\int_\epsilon^1\frac{dt_2}{t_2}\,2V^{\gamma\mu\lambda\rho\nu\delta}\,D^{\xi\to\infty}_{W,\alpha\gamma}(t,t_1,p+k_1)\,D^{\xi\to\infty}_{W,\lambda\rho}(t_1,t_2,p)\,D^{\xi\to\infty}_{W,\delta\beta}(t_2,t,p-k_2)\right.\\
&\left.+\left(2\eta^{\gamma\delta}\eta^{\mu\nu}-\eta^{\delta\nu}\eta^{\gamma\mu}-\eta^{\nu\gamma}\eta^{\mu\delta}\right)D^{\xi\to\infty}_{W,\alpha\gamma}(t,t_1,p+k_1)\,D^{\xi\to\infty}_{W,\beta\delta}(t_1,t,p-k_2)\right],\end{aligned} \tag{4.80}$$

where $V^{\gamma\mu\lambda\rho\nu\delta}=V^{\gamma\mu\lambda}(p+k_1,-k_1,-p)\,V^{\rho\nu\delta}(p,-k_2,-p+k_2)$ arises from the product of two triple gauge-boson vertices, with $V^{\mu\nu\rho}(k,p,q)=\eta^{\mu\nu}(k-p)^\rho+\eta^{\nu\rho}(p-q)^\mu+\eta^{\rho\mu}(q-k)^\nu$.

Our goal is to rewrite this result as a Feynman parameter integral over a *single* gauge-boson 5D propagator, which should be possible since in the KK-decomposed theory only a single KK mode propagates in the loops. In order to simplify the answer, we decompose the 5D propagator according to (3.14) and use the KK decomposition (3.16) in an intermediate step. The use of the KK representation is merely a mathematical trick, similar to the use of Feynman parameters in conventional loop calculations. It is justified because all expressions are finite and the KK sum converges. At the end of the calculation we obtain an expression without any reference to KK modes.

Due to the mode-diagonality of the vertices involving a photon, we can perform the integration over t_1 and t_2 using the orthonormality relation (2.8) for the gauge-boson profiles. Working out the Dirac algebra and making use of Passarino-Veltman reductions, we can reduce the answer to a simple Feynman parameter integral. After the contributions from the various diagrams have been combined, the dimensional regulator $\hat{\epsilon}$ can be set to 0. We find

$$C_{1\gamma}^W = -3\pi\,\tilde{m}_W^2 \int_\epsilon^1 dt\,\delta^\eta(t-1) \sum_{n=0}^\infty \left[\chi_n^W(t)\right]^2 \left[\frac{1}{m_{W_n}^2} + 6\int_0^1 dx \int_0^{1-x} dy\,\frac{1-2xy}{m_{W_n}^2 - xym_h^2 - i0}\right], \tag{4.81}$$

and $C_{5\gamma}^W = 0$. It is now a simple exercise to recast the answer in terms of the 5D propagator function $B_W(t,t';-p^2)$ defined in (3.16). We obtain

$$C_{1\gamma}^W = -3\pi\tilde{m}_W^2 \left[T_W(0) + 6\int_0^1 dx \int_0^{1-x} dy\,(1-2xy)\,T_W(-xym_h^2)\right], \tag{4.82}$$

where $T_W(-p^2)$ denotes the overlap integral of the Higgs profile with the transverse part of the W-boson 5D propagator evaluated at $t = t'$,

$$T_W(-p^2) = \int_\epsilon^1 dt\,\delta^\eta(t-1)\,B_W(t,t;-p^2-i0) = B_W(1,1;-p^2-i0) + \mathcal{O}(\eta)\,. \tag{4.83}$$

Relation (4.82) is one of the main results of this work. It shows the exact result for the Wilson coefficient $C_{1\gamma}$ in dependence of overlap integrals of the Higgs profile and the gauge-boson 5D propagator. With the help of the findings in [164], it can be shown that this relation also holds for an arbitrary bulk-Higgs profile $\chi_h(t)$, provided one uses the corresponding gauge-boson 5D propagator in the bulk-Higgs model. Then the regularized δ-function in (4.83) must be replaced by

$$\delta^\eta(t-1) \to \frac{2\pi}{Lt}\,\frac{v(t)}{v}\,\chi_h(t) = 2(1+\beta)\,t^{1+2\beta} + \dots\,, \tag{4.84}$$

where $v(t)$ is the profile of the Higgs vev. Details on the bulk-Higgs model have been given in Section 2.3. Note, however, that in this case it is necessary to also include the contribution (4.69) due to the physical scalar excitations of the bulk Higgs field. In the region where $\beta \gg 1$, the function on the right-hand side indeed approaches a regularized δ-distribution, with a characteristic width given by $\eta = 1/(2\beta)$.

Note that relation (4.81) results after integrating a Feynman loop integrand of the type $(p_E^2 + m_{W_n}^2 - xym_h^2)^{-3}$ over d^4p_E (after the Wick rotation), which corresponds to the integral over the second derivative $\partial_{p_E^2}^2 T_W(p_E^2 - xym_h^2)$. In order for this integral to exist, we need to require that both functions $T_W(p_E^2)$ and $p_E\,\partial_{p_E} T_W(p_E^2)$ vanish for very large Euclidean momenta. Now, we will show that this is indeed the case. The calculation of the propagator function B_W in the RS model with a brane-localized Higgs

field has been performed in Section 3.2. For our result (4.83) we need the propagator in the time-like region, evaluated at $t = t' = 1$. Using the general solution in (3.25), we obtain (with $\hat{p} \equiv p/M_{\rm KK} + i0$)

$$T_W(-p^2) = \frac{1}{2\pi\tilde{m}_W^2}\left[1 + \frac{\hat{p}M_{\rm KK}^2}{L\tilde{m}_W^2}\frac{J_0(\hat{p})\,Y_0(\hat{p}\epsilon) - Y_0(\hat{p})\,J_0(\hat{p}\epsilon)}{J_1(\hat{p})\,Y_0(\hat{p}\epsilon) - Y_1(\hat{p})\,J_0(\hat{p}\epsilon)}\right]^{-1} \equiv \frac{1}{2\pi\tilde{m}_W^2}\,\hat{T}_W(-p^2)\,, \tag{4.85}$$

which is exact to all orders in $v^2/M_{\rm KK}^2$.[8] It follows from this expression that $\hat{T}_W(0) = 1$. We have thus succeeded in deriving a closed analytic expression for the Wilson coefficient $C_{1\gamma}^W$ in (4.82), valid for the minimal RS model with a Higgs sector localized on the IR brane. Note that we have kept the quantity $\tilde{m}_W$, which is the leading-order contribution to the mass of the physical W boson, in the prefactor above, since it will cancel against a corresponding factor in the definition of the Wilson coefficient (4.82). Indeed, our final result for this coefficient takes the form

$$C_{1\gamma}^W = -\frac{3}{2}\left[1 + 6\int_0^1 dx \int_0^{1-x} dy\,(1-2xy)\,\hat{T}_W(-xym_h^2)\right]. \tag{4.86}$$

Before proceeding, we briefly study the behavior of the propagator function in the region of large space-like momenta. For large Euclidean momenta $p_E \gg M_{\rm KK}$, this function approaches an inverse power-law behavior given by

$$T_W(p_E^2) = \frac{L}{2\pi M_{\rm KK}}\,\frac{1}{p_E} + \mathcal{O}(p_E^{-2})\,. \tag{4.87}$$

It follows that both $T_W(p_E^2)$ and $p_E\,\partial_{p_E} T_W(p_E^2)$ vanish for large Euclidean momenta $p_E^2 = -p^2 \to \infty$, and hence the conditions required for the validity of our relation (4.82) are indeed satisfied.

Bosonic contributions to the Wilson coefficients

Our exact expression for the overlap integral $T_W(-p^2)$ in (4.85) contains the contribution of the zero mode – the standard W boson with its modified coupling to the Higgs field – as well as the infinite tower of KK excitations. It is instructive to isolate the contribution from the zero mode and the KK tower explicitly. To this end, we expand the exact formula in powers of $v^2/M_{\rm KK}^2$, using that we need this function for values $|p^2| = \mathcal{O}(m_h^2)$ much smaller than the KK scale $M_{\rm KK}^2$. We find to leading order in $v^2/M_{\rm KK}^2$ that

$$\hat{T}_W(-p^2) = \frac{m_W^2}{m_W^2 - p^2 - i0}\left[1 - \frac{m_W^2}{2M_{\rm KK}^2}\left(\frac{L}{c_{\vartheta_W}^2} - 1 + \frac{1}{2L}\right)\right] + \frac{m_W^2}{2M_{\rm KK}^2}\left(\frac{L}{c_{\vartheta_W}^2} - 1 + \frac{1}{2L}\right), \tag{4.88}$$

where $c_{\vartheta_W} = 1$ in the minimal RS model. In Section 4.2.2 we will show that the same result holds in the custodial RS model, where however the parameter c_{ϑ_W} takes a different value. In the above result we have replaced the parameter $\tilde{m}_W$ by the physical W-boson mass m_W using relation (2.10). Based on the formulas above, we can perform the integration over the Feynman parameters in (4.82) and find the Wilson coefficient

$$C_{1\gamma}^W = -\frac{21}{4}\left[\kappa_W A_W(\tau_W) + \nu_W\right] + \mathcal{O}\left(\frac{v^4}{M_{\rm KK}^4}\right), \qquad C_{5\gamma}^W = 0\,, \tag{4.89}$$

[8] The result can be simplified using that $J_0(\hat{p}\epsilon) = 1 + \mathcal{O}(\epsilon^2)$ and $Y_0(\hat{p}\epsilon) = (2/\pi)(\gamma_E + \ln(\hat{p}/2) - L) + \mathcal{O}(\epsilon^2)$.

where $\tau_W = 4m_W^2/m_h^2$, and the function

$$A_W(\tau) = \frac{1}{7}\left[2 + 3\tau + 3\tau(2-\tau)\, f(\tau)\right] \tag{4.90}$$

with $f(\tau)$ from (4.70) approaches 1 for $\tau \to \infty$. The first contribution to $C_{1\gamma}^W$ arises from the standard W boson, whose coupling to the Higgs boson is modified, compared with the SM, by a factor κ_W times $v_{\rm SM}/v$. The last factor is accounted for by using the Higgs vev in the RS model in the definition of the effective operators in (4.67). The term ν_W in (4.89) is due to the W-boson KK excitations. Explicitly, we obtain

$$\kappa_W = 1 - \frac{m_W^2}{2M_{\rm KK}^2}\left(\frac{L}{c_{\vartheta_W}^2} - 1 + \frac{1}{2L}\right), \qquad \nu_W = \frac{m_W^2}{2M_{\rm KK}^2}\left(\frac{L}{c_{\vartheta_W}^2} - 1 + \frac{1}{2L}\right). \tag{4.91}$$

Note that at this order $\nu_W = (1-\kappa_W)$, such that the RS corrections to $C_{1\gamma}$ in (4.89) would cancel in the limit $\tau_W \to \infty$. This simple relation is however not preserved in higher orders. Our result for $C_{1\gamma}^W$ agrees with a corresponding expression derived in [206]. Notice also that the value of κ_W is consistent with relation (4.75), which gives $\kappa_W = \frac{\tilde m_W^2}{m_W^2}\, 2\pi[\chi_0^W(1)]^2$.

We close this section by returning briefly to the case of a narrow bulk-Higgs model, in which the scalar sector is localized not on but near the IR brane. As discussed earlier, relation (4.83) still holds in this model provided one makes the replacement (4.84) and calculates the gauge-boson propagator in the background of a bulk-Higgs field. The propagator function B_W in the bulk-Higgs scenario was derived in Section 3.2. Using these results in the limit where $\eta = 1/(2\beta) \ll 1$ we obtain the Wilson coefficients (4.89) with

$$\kappa_W\big|_{\substack{\rm bulk\\ \rm Higgs}} = \kappa_W + \frac{3Lm_W^2}{2M_{\rm KK}^2}\,\eta + \mathcal{O}(\eta^2)\,, \qquad \nu_W\big|_{\substack{\rm bulk\\ \rm Higgs}} = \nu_W - \frac{Lm_W^2}{M_{\rm KK}^2}\,\eta + \mathcal{O}(\eta^2)\,, \tag{4.92}$$

instead of (4.91). This demonstrates that the result for the bosonic loop contributions to the $h \to \gamma\gamma$ amplitude interpolates smoothly from the narrow bulk-Higgs scenario into a scenario with a brane-localized scalar sector.

4.2.2 Extension to the RS model with custodial symmetry

We will now present the generalization of the above results to the RS model with custodial protection. Details on this model have been discussed in Section 2.4.

Quark contributions to the Wilson coefficients

The fermionic loop contributions to the $h \to \gamma\gamma$ amplitude in the custodial RS model can be parameterized in terms of the same 3×3 Yukawa matrices appearing in the minimal model, however with different coefficients that reflect the embeddings of the various fermion species under the enlarged bulk gauge group. The generalizations of relations (4.72) for the quark contributions have been worked out in Section 4.1.1. They

are

$$\begin{aligned} C_{1\gamma}^q &\approx \left[1 - \frac{2v^2}{3M_{\rm KK}^2}\,{\rm Re}\,\frac{(\boldsymbol{Y}_u\boldsymbol{Y}_u^\dagger\boldsymbol{Y}_u)_{33}}{(\boldsymbol{Y}_u)_{33}}\right] N_c\,Q_u^2\,A_q(\tau_t) + N_c\,Q_d^2\,A_q(\tau_b) \\ &\quad + N_c\,Q_u^2\;{\rm Re\,Tr}\,g(\sqrt{2}\boldsymbol{X}_u) + N_c\left(Q_u^2+Q_d^2+Q_\lambda^2\right){\rm Re\,Tr}\,g(\sqrt{2}\boldsymbol{X}_d)\,, \\ C_{5\gamma}^q &\approx -\frac{2v^2}{3M_{\rm KK}^2}\,{\rm Im}\left[\frac{(\boldsymbol{Y}_u\boldsymbol{Y}_u^\dagger\boldsymbol{Y}_u)_{33}}{(\boldsymbol{Y}_u)_{33}}\right] N_c\,Q_u^2\,B_q(\tau_t) \\ &\quad + N_c\,Q_u^2\;{\rm Im\,Tr}\,g(\sqrt{2}\boldsymbol{X}_u) + N_c\left(Q_u^2+Q_d^2+Q_\lambda^2\right){\rm Im\,Tr}\,g(\sqrt{2}\boldsymbol{X}_d)\,. \end{aligned} \tag{4.93}$$

For various RS models with a brane-localized scalar sector or a narrow bulk-Higgs sector, the explicit forms of the function $g(\boldsymbol{X}_f)$ have been given in (4.24) and (4.25). Recall that the Taylor expansion of these functions starts with $\boldsymbol{X}_f^2$, and thus the factors of $\sqrt{2}$ arising in the quark contributions in the custodial model approximately double the contribution arising in the minimal model. Combined with the large electric charge of the λ-type quarks, one finds that due to the higher multiplicity of KK quark states the contribution in the custodial RS model is much larger than in the minimal model, by approximately a factor 68/5.

Charged-lepton contributions to the Wilson coefficients

The result for the loop contributions to the $h \to \gamma\gamma$ amplitude involving charged leptons depends on the way in which the lepton fields are embedded into the extended gauge symmetry of the custodial RS model. As a first possibility, we consider a model in which the lepton multiplets are chosen in analogy to the quark multiplets in (2.80). In component notation, the corresponding fields are

$$\begin{aligned} \xi_{1L} &= \begin{pmatrix} \nu_L^{(+)}{}_0 & \psi_L^{(-)}{}_1 \\ e_L^{(+)}{}_{-1} & \nu_L'^{(-)}{}_0 \end{pmatrix}_0\,, \qquad \xi_{2R} = \left(\nu_R^{c\,(+)}{}_0\right)_0\,, \\ \xi_{3R} &= \mathcal{T}_{3R}\oplus\mathcal{T}_{4R} = \begin{pmatrix} \Psi_R'^{(-)}{}_1 \\ N_R'^{(-)}{}_0 \\ E_R'^{(-)}{}_{-1} \end{pmatrix}_0 \oplus \left(E_R^{(+)}{}_{-1} \quad N_R^{(-)}{}_0 \quad \Psi_R^{(-)}{}_1\right)_0\,. \end{aligned} \tag{4.94}$$

There are fifteen different lepton states in the neutrino sector and nine in the charged-lepton sector. The BCs give rise to three light modes in each sector, which are identified with the SM neutrinos and charged leptons. These are accompanied by KK towers consisting of groups of fifteen and nine modes in the two sectors, respectively. In addition, there is a KK tower of exotic lepton states with electric charge $Q_\psi = +1$, which exhibits nine excitations in each KK level. The gauge-invariant Yukawa interactions for these fields are constructed in complete analogy with the quark Yukawa interactions. They can be expressed in terms of two dimensionless 3×3 Yukawa matrices $\boldsymbol{Y}_\nu$ and $\boldsymbol{Y}_e$, which we assume to have an anarchic structure. When dressed with the fermion profiles on the IR brane, these matrices give masses to the SM leptons. The resulting contributions to the Wilson coefficients have the same structure as in (4.93), except that there are no zero-mode contributions (they are proportional to m_l^2/m_h^2 and thus can be neglected) and that we must replace $\boldsymbol{Y}_u \to \boldsymbol{Y}_\nu$, $\boldsymbol{Y}_d \to \boldsymbol{Y}_e$, $N_c \to 1$, and $Q_u \to Q_\nu = 0$, $Q_d \to Q_e = -1$, $Q_\lambda \to Q_\psi = +1$. We thus obtain

$$C_{1\gamma}^l + iC_{5\gamma}^l \approx \left(Q_e^2+Q_\psi^2\right){\rm Tr}\,g(\sqrt{2}\boldsymbol{X}_e)\,, \tag{4.95}$$

with $\boldsymbol{X}_e$ as defined in (4.74). It follows that the leptonic contribution in the custodial RS model is approximately 4 times larger than in the minimal model.

As a second possibility, we consider a model with a more minimal embedding of the leptons into the extended gauge group. The simplest assignment is to put the left-chiral neutrino and electron into an $SU(2)_L$ doublet (as in the SM) and the right-chiral electron along with a new, exotic neutral particle N_R into an $SU(2)_R$ doublet. The lepton fields with even Z_2 parity are then chosen as

$$L_L = \begin{pmatrix} \nu_L^{(+)} & 0 \\ e_L^{(+)} & -1 \end{pmatrix}_{-\frac{1}{2}}, \qquad L_R^c = \begin{pmatrix} e_R^{c(+)} & -1 \\ N_R^{(-)} & 0 \end{pmatrix}_{-\frac{1}{2}}, \tag{4.96}$$

and they transform as $(\mathbf{2},\mathbf{1})$ and $(\mathbf{1},\mathbf{2})$, respectively. The choice of the BCs is such that the zero modes correspond to the light leptons of the SM, without a right-chiral neutrino. The gauge-invariant Yukawa interaction that can be built using these fields is

$$\mathcal{L}_{\text{Yuk}} = -\int_\epsilon^1 \frac{dt}{t}\,\frac{M_{\text{KK}}}{2}\,\delta^\eta(t-1)\,\frac{2}{k}\,\big(Y_e\big)_{ij}\big(\bar{L}_L^i \Phi\,\varepsilon L_R^{c\,j} + \bar{L}_R^i \Phi\,\varepsilon L_L^{c\,j}\big) + \text{h.c.}\,, \tag{4.97}$$

where $\varepsilon = i\sigma^2$. Upon EWSB this generates a mass term for the zero modes of the charged leptons. The SM neutrinos remain massless at this order. Their masses can be explained by means of higher-dimensional operators. The only additional lepton field is the right-chiral neutrino, which is charged under $SU(2)_R$ but electrically neutral, so that it does not affect the $h \to \gamma\gamma$ decay amplitude. The lepton contribution is therefore the same as in the minimal version of the RS model, namely $C_{1\gamma}^l + iC_{5\gamma}^l \approx Q_e^2\,\text{Tr}\,g(\boldsymbol{X}_e)$ as in (4.73).

Bosonic contributions to the Wilson coefficients

It is straightforward to deduce the Feynman rules in the custodial model from the ones in the minimal model compiled in Appendix A. Using the orthonormality condition for the gauge-boson profiles, we can convince ourselves that the $W_M^\pm$ couplings to the photon are not changed at all. This statement is independent of the basis, since the rotation matrix $\boldsymbol{R}_{\vartheta_W}$ drops out in the orthonormalization condition. In contrast, as mentioned in Section 2.4, the Higgs only couples to the IR basis fields $\tilde{A}_\mu^\pm$ with a strength proportional to $(g_{L,5}^2 + g_{R,5}^2)$. This can be taken into account with the help of the projection operator $\boldsymbol{P}_+$ rotated into the IR basis and accompanied by a factor $1/c_{\vartheta_W}^2$. It follows that, compared with the SM, all KK-diagonal Higgs couplings in the custodial RS model come with a prefactor

$$\frac{2\tilde{m}_W^2}{c_{\vartheta_W}^2\,v}\,2\pi\,\vec{\chi}_n^W(1)^T\,\boldsymbol{R}_{\vartheta_W}^T\,\boldsymbol{P}_+\,\boldsymbol{R}_{\vartheta_W}\,\vec{\chi}_n^W(1) \equiv \frac{2\tilde{m}_W^2}{c_{\vartheta_W}^2\,v}\,2\pi\,\vec{\chi}_n^W(1)^T\,\boldsymbol{D}_{\vartheta_W}\,\vec{\chi}_n^W(1)\,, \tag{4.98}$$

which replaces the corresponding factor (4.75) in the minimal model. Here, $\boldsymbol{D}_{\vartheta_W}$ is defined by $\boldsymbol{D}_{\vartheta_W} = \boldsymbol{R}_{\vartheta_W}^T\,\boldsymbol{P}_+\,\boldsymbol{R}_{\vartheta_W}$. In analogy with expression (4.76) valid in the minimal RS model, we find that the $h \to \gamma\gamma$ amplitude in the custodial RS model can be written as

$$\mathcal{A}_{\text{RS}}^W(h\to\gamma\gamma)\big|_{\text{cust}} = \frac{\tilde{m}_W^2}{c_{\vartheta_W}^2\,v}\sum_{n=0}^{\infty} 2\pi\,\vec{\chi}_n^W(1)^T\boldsymbol{D}_{\vartheta_W}\,\vec{\chi}_n^W(1)\left[\frac{v_{\text{SM}}}{m_W^2}\,\mathcal{A}_{\text{SM}}^W(h\to\gamma\gamma)\right]_{m_W\to m_{W_n}}. \tag{4.99}$$

It follows that expression (4.82) for the Wilson coefficient $C_{1\gamma}^W$ remains valid, provided we replace the quantity $T_W(-p^2)$ defined in (4.83) with

$$T_W(-p^2) = \mathrm{Tr}\left[\frac{\boldsymbol{D}_{\vartheta_W}}{c_{\vartheta_W}^2}\,\boldsymbol{B}_W^{\mathrm{UV}}(1,1;-p^2-i0)\right]. \tag{4.100}$$

The solution of the propagator function $\boldsymbol{B}_W^{\mathrm{UV}}$ in the UV basis is given in (3.41). It is now straightforward to calculate the quantity $T_W(-p^2)$ in (4.100), which we need for the calculation of the Wilson coefficient $C_{1\gamma}$ in (4.82). Expanding this answer in powers of v^2/M_{KK}^2 and for $|p^2| = \mathcal{O}(m_h^2)$, we recover expression (4.88). With respect to the minimal RS model, the only modification concerns the coefficient of the leading L-enhanced correction terms, which is enhanced by $1/c_{\vartheta_W}^2$. This affects both the contributions from the W boson and the KK tower. In the custodial RS model with P_{LR} symmetry, this enhancement factor is equal to 2. Note that with $c_{\vartheta_W}^2 = 1/2$ the expressions in (4.91) are compatible with corresponding results obtained in [149]. In this reference the Wilson coefficient $C_{1\gamma}$ belonged to the operator $vhF_{\mu\nu}F^{\mu\nu}$ instead of the one in (4.67), and hence $\kappa_W|_{\text{Ref. [149]}} = \kappa_W \frac{v_{\mathrm{SM}}^2}{v^2}$.

4.3 Tree-level Higgs production and decay via massive vector bosons

In this section we discuss in detail the structure of new-physics effects in the couplings of the Higgs boson to a pair of massive electroweak gauge bosons. These couplings are probed in the off-shell Higgs decays $h \to WW^*$ and $h \to ZZ^*$ with subsequent decays into four fermions, as well as in the production of the Higgs boson in vector-boson fusion or in the Higgs-strahlung process, see Figure 4.4. These tree-level processes have in common that they involve the exchange of virtual vector bosons, which implies that in addition to the SM W and Z bosons we must consider the effect of the infinite towers of KK resonances. It is often assumed in the literature that the main effect of new physics on these processes arises from a rescaling of the on-shell hVV couplings. We show that there are also several other effects that need to be accounted for, namely a possible rescaling of the Higgs vev, a modification of the couplings of the W and Z bosons to light fermions, and the exchange of new heavy particles in the off-shell propagators. In RS models all of these effects are indeed present, and accounting for them correctly will be important for a general definition of the signal strength in terms of the Higgs couplings to fermions and vector bosons in Section 4.4.3. To good approximation, however, we show that the main effects can be accounted for by a multiplicative rescaling of the SM decay rates and production cross sections.

The Higgs decay into massive vector bosons in the minimal RS model is presented in Section 4.3.1. Subsequent sections then discuss the corrections to the Higgs production in vector-boson fusion and the Higgs-strahlung process. The final Section 4.3.4 extends our analysis to the RS scenario with custodial symmetry.

4.3.1 Higgs decay into W and Z bosons

We begin by studying the decay of the Higgs boson to a pair of electroweak gauge bosons, taking $h \to WW^*$ as a concrete example. Since $m_h < 2m_W$, this decay is only allowed if at least one of the W bosons is produced off-shell. We thus consider the process

(a) $h \to WW^*, ZZ^*$ decays (b) Higgs-strahlung (c) Vector-boson fusion

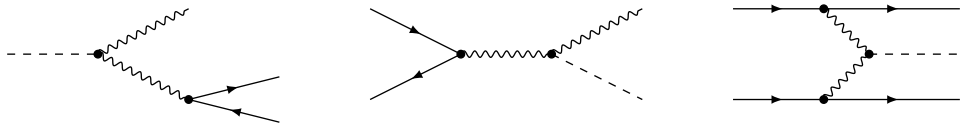

Figure 4.4: Tree-level Feynman diagrams for the off-shell Higgs decays to pairs of W and Z bosons, and Higgs production in the Higgs-strahlung and vector-boson fusion processes.

$h \to W^- W^{+*} \to W^- f_i \bar{f}'_j$, where the off-shell boson decays into a pair of light fermions f_i and $\bar{f}'_j$ with generation indices i, j.

Calculation in the Standard Model

In the SM, the corresponding differential decay rate is given by [217]

$$\frac{d\Gamma}{ds} = \frac{\Gamma(W^+ \to f_i \bar{f}'_j)}{16\pi^2 m_h^3 \, m_W} \frac{m_W^2}{v_{\rm SM}^2} \frac{\lambda^{\frac{1}{2}}(m_h^2, m_W^2, s)}{\left(m_W^2 - s\right)^2} \Big[\left(m_h^2 - m_W^2\right)^2 + 2s(5m_W^2 - m_h^2) + s^2\Big], \quad (4.101)$$

where s is the invariant mass squared of the fermion pair, and $\lambda(x,y,z) = (x-y-z)^2 - 4yz$. We have expressed the result in terms of the on-shell decay rate for the process $W^+ \to f_i \bar{f}'_j$,

$$\Gamma(W^+ \to f_i \bar{f}'_j) = N_c^f m_W \frac{g^2}{24\pi} |g_{ij,L}|^2 \,, \quad (4.102)$$

where g denotes the $SU(2)_L$ gauge coupling, the color factor $N_c^f = 1$ for leptons and 3 for quarks, and $g_{ij,L} = \delta_{ij}/\sqrt{2}$ for leptons and $(V_{\rm CKM})_{ij}/\sqrt{2}$ for quarks. Performing the remaining integration over s in the interval $0 \le s \le (m_h - m_W)^2$ and neglecting fermion-mass effects, one obtains

$$\Gamma(h \to W^- W^{+*} \to W^- f_i \bar{f}'_j) = \frac{m_h^3}{32\pi v_{\rm SM}^2} \frac{\Gamma(W^+ \to f_i \bar{f}'_j)}{\pi m_W} \, g\left(\frac{m_W^2}{m_h^2}\right), \quad (4.103)$$

where the first factor is one half of the (would-be) on-shell $h \to WW$ width in the limit $m_h \gg m_W$, the second factor accounts for the suppression due to the fact that one of the W bosons in the decay $h \to WW^*$ is produced off-shell, and the phase-space function is given by

$$\begin{aligned} g(x) = {} & \frac{6x(1 - 8x + 20x^2)}{\sqrt{4x-1}} \arccos\left(\frac{3x-1}{2x^{3/2}}\right) \\ & - 3x(1 - 6x + 4x^2) \ln x - (1-x)(2 - 13x + 47x^2) \,. \end{aligned} \quad (4.104)$$

The off-shell decay considered here arises if $x > 1/4$. In the literature, it is common practice to define the off-shell $h \to WW^*$ decay rate as

$$\Gamma(h \to WW^*) \equiv 2 \sum_{f_i, f'_j} \Gamma(h \to W^+ f_i \bar{f}'_j) \,, \quad (4.105)$$

where the sum includes all fermion pairs with total mass lighter than m_W. The factor 2 accounts for the charge-conjugated decays $h \to W^- \bar{f}_i f'_j$. In the SM the expression for $\Gamma(h \to WW^*)$ has the same form as in (4.103), but with the partial decay rate

$\Gamma(W^+ \to f_i \bar{f}'_j)$ replaced by twice the total decay width Γ_W of the W boson. Analogous formulas hold for the decays based on $h \to ZZ^*$, where we must replace $W \to Z$ everywhere and use the corresponding expression

$$\Gamma(Z \to f\bar{f}) = N_c^f m_Z \frac{g^2}{24\pi c_w^2} \left(g_{f,L}^2 + g_{f,R}^2\right), \tag{4.106}$$

for the partial decay rates of the Z boson in the SM, where $g_{f,L} = T_3^f - s_w^2 Q_f$ and $g_{f,R} = -s_w^2 Q_f$ are the left-chiral and right-chiral couplings of the various fermion species, and $s_w \equiv \sin\theta_w$ and $c_w \equiv \cos\theta_w$ are the sine and cosine of the weak mixing angle. In this case the total off-shell decay rate is defined as

$$\Gamma(h \to ZZ^*) \equiv \sum_f \Gamma(h \to Zf\bar{f}), \tag{4.107}$$

where the sum includes all fermions lighter than $m_Z/2$. It follows from this definition that we obtain

$$\Gamma(h \to ZZ^* \to l^+l^-l^+l^-) = \Gamma(h \to ZZ^*) \left[\mathrm{Br}(Z \to l^+l^-)\right]^2, \tag{4.108}$$

for the golden channel.

Modifications in the minimal RS model

We now discuss in detail how the above results must be modified in the context of the minimal RS model. For the purpose of this discussion it is convenient to define the weak mixing angle s_w^2 via the structure of the neutral current. Alternative definitions are related to this one through the electroweak precision variables S, T and U, see Section 2.5.2 for a detailed discussion of this point. In the context of RS models one has $s_w^2 = g_5'^2/(g_5^2 + g_5'^2)$ in terms of the 5D gauge couplings. If this ratio is extracted from experiment there are no new-physics corrections to the branching ratios $\mathrm{Br}(W \to f_i\bar{f}'_j)$ and $\mathrm{Br}(Z \to f\bar{f})$. Modifications arise for the Higgs couplings to vector bosons, the electroweak gauge couplings entering the partial decay rates (4.102) and (4.106), and due to the contributions of heavy KK resonances, which change the momentum-dependent gauge-boson propagator. Let us for concreteness consider the decay $h \to W^-W^{+*}$ to study the impact of these corrections. In the Feynman diagram in Figure 4.4(a) the off-shell gauge-boson propagator now contains the SM gauge boson and its infinite tower of KK excitations. The Feynman rule for the $W_\mu^{+(0)} W_\nu^{-(n)} h$ vertex is (with $n = 0$ for the zero mode and $n > 0$ for the KK excitations)

$$\frac{2i\tilde{m}_W^2}{v}\, \eta_{\mu\nu}\, 2\pi\, \chi_0^W(1)\, \chi_n^W(1), \tag{4.109}$$

which follows from (4.75). The vev v is defined in (2.94) and the quantity $\tilde{m}_W$ is given in (2.5). For the W-boson zero mode given in (2.12), we encounter the correction factor

$$c_W = \frac{v_{\rm SM}}{v} \frac{\tilde{m}_W^2}{m_W^2}\, 2\pi \left[\chi_0^W(1)\right]^2 = 1 - \frac{m_W^2}{2M_{\rm KK}^2} \left(\frac{3L}{2} - 1 + \frac{1}{2L}\right) + \ldots \tag{4.110}$$

relative to the SM. Here and below the ellipses denote terms of order $v^4/M_{\rm KK}^4$ and higher. Note that c_W is related to κ_W in (4.91) by $c_W = \frac{v_{\rm SM}}{v}\kappa_W$. The Feynman rule for the $W_\mu^{+(n)} \bar{u}_A^{(i)} d_A^{(j)}$ vertex, where $A = L, R$ is a chirality label and i, j labels the flavors

of the SM quarks, is to an excellent approximation given by [132]

$$\frac{i}{\sqrt{2}}\,\frac{g_5}{\sqrt{2\pi r}}\,\sqrt{2\pi}\,\chi_n^W(\epsilon)\,V_{ij}^{\rm CKM}\,\gamma^\mu P_L\,, \tag{4.111}$$

where $P_L = \frac{1}{2}(1-\gamma_5)$ is a chiral projection operator. Corrections to this result, including the couplings to right-chiral fermions, are strongly chirality suppressed. Note, in particular, that for the zero mode one encounters a correction factor

$$c_{\Gamma_W}^{1/2} \equiv \frac{g_5}{\sqrt{2\pi r g}}\,\sqrt{2\pi}\,\chi_0^W(\epsilon) = 1 - \frac{m_W^2}{2M_{\rm KK}^2}\,\frac{1}{4L} + \dots \tag{4.112}$$

relative to the SM, which will affect all decay amplitudes of the W boson into light fermions. It follows that, relative to the SM, we must make the following replacements in the SM decay amplitude for $h \to W^- W^{+*} \to W^- u_i \bar{d}_j$:

$$\frac{1}{m_W^2 - s} \to \frac{v_{\rm SM}}{v}\,\frac{\tilde{m}_W^2}{m_W^2}\,\sqrt{2\pi}\,\chi_0^W(1)\,\frac{g_5}{\sqrt{2\pi r g}}\,2\pi\,B_W(1,\epsilon;-s)\,, \tag{4.113}$$

where the propagator function B_W expanded to leading order in $v^2/M_{\rm KK}^2$ is given by (3.29). Details on the caluclation of the gauge-boson 5D propagator can be found in Section 3.2. At subleading order, we can now rewrite the right-hand side of (4.113) in the form

$$\frac{1}{m_W^2 - s} \to c_{\Gamma_W}^{1/2}\,c_W\left[\frac{1}{m_W^2 - s} - \frac{1}{4M_{\rm KK}^2}\left(1 - \frac{1}{L}\right) + \dots\right]. \tag{4.114}$$

This result has an intuitive form. The factor $c_{\Gamma_W}^{1/2}$ rescales the W-boson decay amplitudes of the SM in a uniform way, the factor c_W rescales the Higgs-boson coupling to a W^+W^- pair, and the last term in brackets is the contribution of heavy KK resonances. Substituting the above expression for the gauge-boson propagator into (4.101) and performing the integration over s, we obtain

$$\Gamma(h \to WW^*) = \frac{m_h^3}{16\pi v_{\rm SM}^2}\,\frac{c_{\Gamma_W}\Gamma_W^{\rm SM}}{\pi m_W}\,c_W^2\left[g\left(\frac{m_W^2}{m_h^2}\right) - \frac{m_h^2}{2M_{\rm KK}^2}\left(1 - \frac{1}{L}\right)h\left(\frac{m_W^2}{m_h^2}\right) + \dots\right], \tag{4.115}$$

where $\Gamma_W^{\rm SM}$ is the total decay width of the W boson in the SM. The new phase-space function is given by

$$\begin{aligned} h(x) = &-(1 - 4x + 12x^2)\,\sqrt{4x-1}\,\arccos\left(\frac{3x-1}{2x^{3/2}}\right) \\ &- \frac{1}{2}(1 - 6x + 36x^2)\ln x + \frac{1}{6}\,(1-x)(11 - 61x + 38x^2)\,. \end{aligned} \tag{4.116}$$

The analysis of new-physics effects on the $h \to ZZ^*$ decay rate proceeds analogously. Instead of c_W in (4.110) one finds the correction factor

$$c_Z = \frac{v_{\rm SM}}{v}\,\frac{\tilde{m}_Z^2}{m_Z^2}\,2\pi\left[\chi_0^Z(1)\right]^2 = 1 - \frac{m_Z^2}{2M_{\rm KK}^2}\left(L - 1 + \frac{1}{2L}\right) - \frac{L m_W^2}{4M_{\rm KK}^2} + \dots \tag{4.117}$$

for the hZZ coupling. Moreover, in the RS model the $Zf\bar{f}$ couplings entering the partial rates in (4.106) get replaced by

$$\frac{g}{c_w}\,g_{f,A}(s_w^2) \to \frac{g_5}{\sqrt{2\pi r}\,c_w}\,\sqrt{2\pi}\,\chi_0^Z(\epsilon)\,g_{f,A}(s_w^2)\,. \tag{4.118}$$

If the weak mixing angle is defined via the structure of the couplings $g_{f,A}(s_w^2)$, then the only difference with regard to the SM is a factor

$$c_{\Gamma_Z}^{1/2} \equiv \frac{g_5}{\sqrt{2\pi r g}}\sqrt{2\pi}\,\chi_0^Z(\epsilon) = c_{\Gamma_W}^{1/2}\left[1+\frac{m_Z^2-m_W^2}{4M_{\rm KK}^2}\left(1-\frac{1}{L}\right)+\dots\right]. \tag{4.119}$$

Note that, if m_Z and s_w^2 are taken as inputs, then the W-boson mass is a derived quantity and the corresponding expression can be found in (2.96). As long as we choose $M_{\rm KK}$ consistent with the bounds from electroweak precision tests, this value will be consistent within errors with the measured W mass.

The fact that the L-enhanced terms in the effective couplings c_W in (4.110) and c_Z in (4.117) are different is problematic from a phenomenological point of view, as this amounts to a breaking of custodial symmetry in the effective couplings of the Higgs to electroweak gauge bosons. Indeed, the difference $(c_W - c_Z)$ is related to the T parameter, which receives dangerously large corrections in the minimal RS model, see Section 2.5.2.

4.3.2 Higgs-strahlung

We now move on to study the cross section for the Higgs-strahlung process, in which the Higgs boson is produced in pp collisions in association with a W or Z boson, see Figure 4.4(b). Since the Feynman diagram for Higgs-strahlung is identical to that for the Higgs-boson decay into a pair of electroweak gauge bosons, it follows that the amplitude at the quark level receives exactly the same corrections as the Higgs decay amplitude discussed in the previous section. If we denote the invariant mass squared of the hV pair in the final state by s, we immediately obtain from (4.114) (for $V = W, Z$)

$$\frac{d\sigma(pp\to hV)}{ds} = c_{\Gamma_V}\,c_V^2\left[1+\frac{s-m_V^2}{2M_{\rm KK}^2}\left(1-\frac{1}{L}\right)+\dots\right]\frac{d\sigma(pp\to hV)_{\rm SM}}{ds}\,. \tag{4.120}$$

Because the s dependence of the SM cross section is sensitive to the shapes of the parton distribution functions, it is not possible to derive a simple analytic formula for the corrections to the total Higgs-strahlung cross sections. However, the leading correction terms enhanced by L are universal and independent of s. When only these terms are kept, one obtains $\sigma(pp\to hV) \approx c_V^2\,\sigma(pp\to hV)_{\rm SM}$. This approximation has been frequently used in the literature. In RS models it is accurate up to small corrections not enhanced by L.

4.3.3 Higgs production in vector-boson fusion

We finally consider the vector-boson fusion process shown in Figure 4.4(c). It involves two gauge-boson propagators, whose momenta we denote by $p_{1,2}$. In analogy with the discussion in the previous sections, we find that in order to account for new-physics effects one must replace

$$\begin{aligned}\frac{1}{(m_V^2-p_1^2)(m_V^2-p_2^2)} &\to \frac{v_{\rm SM}}{v}\frac{\tilde m_V^2}{m_V^2}\left(\frac{g_5}{\sqrt{2\pi r g}}\right)^2(2\pi)^2\,B_V(1,\epsilon;-p_1^2)\,B_V(1,\epsilon;-p_2^2)\\ &= \frac{c_{\Gamma_V}\,c_V}{(m_V^2-p_1^2)(m_V^2-p_2^2)}\left[1-\frac{2m_V^2-p_1^2-p_2^2}{4M_{\rm KK}^2}\left(1-\frac{1}{L}\right)+\dots\right]\end{aligned} \tag{4.121}$$

in the expression for the scattering amplitude. Once again the integrations over the virtual momenta flowing through the propagators cannot be performed in closed form

because they involve convolutions with parton distribution functions. However, the leading correction terms enhanced by L are universal. When only these terms are kept, one obtains $\sigma(pp \to hqq') \approx c_V^2\, \sigma(pp \to hqq')_{\rm SM}$.

4.3.4 Extension to the RS model with custodial symmetry

Details on the custodial RS model can be found in Section 2.4. We start with the relevant Feynman rules needed for the discussion of the decays $h \to VV^*$ in Section 4.3.1. Instead of (4.109) in the minimal model, the Feynman rules for the $W_\mu^{+(0)} W_\nu^{-(n)} h$ and $Z_\mu^{(0)} Z_\nu^{(n)} h$ vertices read

$$\begin{aligned} W \text{ boson:} \quad & \frac{2i\tilde{m}_W^2}{c_{\vartheta_W}^2 v}\, \eta_{\mu\nu}\, 2\pi\, \vec{\chi}_0^W(1)^T \boldsymbol{D}_{\vartheta_W}\, \vec{\chi}_n^W(1)\,, \\ Z \text{ boson:} \quad & \frac{i\tilde{m}_W^2}{c_{\vartheta_W}^2 v}\, \eta_{\mu\nu}\, 2\pi\, \vec{\chi}_0^Z(1)^T \boldsymbol{D}_{\vartheta_Z}\, \vec{\chi}_n^Z(1)\,, \end{aligned} \tag{4.122}$$

where we have introduced the matrices $\boldsymbol{D}_{\vartheta_V} \equiv \boldsymbol{R}_{\vartheta_V}^T \boldsymbol{P}_+ \boldsymbol{R}_{\vartheta_V}$ for $V = W, Z$. Furthermore, we have used $c_{\vartheta_W} \equiv \cos\vartheta_W$ with ϑ_W defined in (2.70). Note that demanding the P_{LR} symmetry fixes $\cos\vartheta_W = 1/\sqrt{2}$. The angle ϑ_Z depends on the 5D gauge couplings in a more complicated way, but under the assumption of the P_{LR} symmetry one finds $\tan^2\vartheta_Z = 1 - 2s_w^2$. As in the minimal RS model, the parameter $\tilde{m}_W$ is the leading contribution to the W-boson mass in an expansion in powers of $v^2/M_{\rm KK}^2$, see (2.79). Due to the custodial symmetry in the bulk, this parameter appears in the Higgs coupling to both W and Z bosons. The zero-mode profiles are explicitly given in (2.78). It follows that the correction factors become

$$\begin{aligned} c_W|_{\rm cust} &= \frac{v_{\rm SM}}{v}\frac{\tilde{m}_W^2}{m_W^2 c_{\vartheta_W}^2} 2\pi\, \vec{\chi}_0^W(1)^T \boldsymbol{D}_{\vartheta_W} \vec{\chi}_0^W(1) = 1 - \frac{m_W^2}{2M_{\rm KK}^2}\left(3L - 1 + \frac{1}{2L}\right) + \ldots\,, \\ c_Z|_{\rm cust} &= \frac{v_{\rm SM}}{v}\frac{\tilde{m}_W^2}{m_Z^2 c_{\vartheta_W}^2} 2\pi\, \vec{\chi}_0^Z(1)^T \boldsymbol{D}_{\vartheta_Z} \vec{\chi}_0^Z(1) = 1 - \frac{m_W^2}{2M_{\rm KK}^2}\left(3L + 1 - \frac{1}{2L}\right) + \ldots\,, \end{aligned} \tag{4.123}$$

instead of (4.110) and (4.117), where we have imposed the P_{LR} symmetry in the final expressions. The custodial protection mechanism ensures that the leading, L-enhanced terms are now the same for both couplings, whereas the subleading terms are different. The Feynman rules for the couplings of the W and Z bosons and their KK excitations to SM quarks, the $W_\mu^{+(n)} \bar{u}_A^{(i)} d_A^{(j)}$ and the $Z_\mu^{(n)} \bar{q}_A^{(i)} q_A^{(i)}$ vertices (with $A = L, R$), are given by

$$\begin{aligned} W \text{ boson:} \quad & \frac{i}{\sqrt{2}}\frac{g_{L,5}}{\sqrt{2\pi r}} \int_\epsilon^1 dt\, \sqrt{2\pi}\, \mathcal{U}_A^{\dagger(i)}(t) \begin{pmatrix} \Omega_W & \frac{g_{R,5}}{g_{L,5}}\,\Omega_2 \end{pmatrix} \vec{\chi}_n^W(t)\, \gamma^\mu\, \mathcal{D}_A^{(j)}(t) P_A\,, \\ Z \text{ boson:} \quad & \frac{i}{\sqrt{2}}\frac{g_{L,5}}{\sqrt{2\pi r c_w}} \int_\epsilon^1 dt\, \sqrt{2\pi}\, \mathcal{Q}_A^{\dagger(i)}(t) \begin{pmatrix} Q_Z & \frac{g_{Z',5}}{g_{Z,5}}\, Q_{Z'} \end{pmatrix} \vec{\chi}_n^Z(t)\, \gamma^\mu\, \mathcal{Q}_A^{(i)}(t) P_A\,, \end{aligned} \tag{4.124}$$

with the chiral projectors $P_{R,L} = \frac{1}{2}(1 \pm \gamma_5)$. The Ω_W and Ω_2 matrices appearing in (4.124) are 5×3 matrices and given by

$$\Omega_W = \begin{pmatrix} 1 & 0 & 0 \\ 0 & 0 & 0 \\ 0 & 0 & 0 \\ 0 & 0 & 1 \\ 0 & 0 & 0 \end{pmatrix}, \qquad \Omega_2 = \begin{pmatrix} 0 & 0 & 0 \\ 1 & 0 & 0 \\ 0 & 0 & 0 \\ 0 & 0 & 0 \\ 0 & 1 & 0 \end{pmatrix}. \tag{4.125}$$

Note that for the W-boson the leading contribution to the CKM matrix arises from the (11)-component of Ω_W. For vertices involving the light SM fermions, corrections coming from the t-dependent term in the gauge-boson profile as well as from the admixture of the U' and D' states are chirally suppressed and can be neglected. This feature extends to the case of the KK excitations of the W boson. Effectively this means that we only need to keep the constant contributions of the W profiles, which survive near the UV brane and are given by $\vec{\chi}_n^W(\epsilon)$. In case of the Z-boson vertices in the second Feynman rule in (4.124), we have defined the couplings

$$\frac{g_{Z',5}^2}{g_{Z,5}^2} = \frac{c_w^2 \tan^4\vartheta_W}{\tan^2\vartheta_W - \tan^2\theta_w}, \quad Q_Z = T_L^{q3} - s_w^2 Q, \quad Q_{Z'} = -T_R^{q3} - \frac{\tan^2\theta_w}{\tan^2\vartheta_W} Y, \tag{4.126}$$

where $T_{L,R}^{q3}$ denote the eigenvalues under the third generator of $SU(2)_{L,R}$, Y is the weak hypercharge, and Q denotes the electric charge of the fermion. Once again we only need to keep the t-independent contributions in the gauge-boson profile functions. Thus, as in the minimal RS model we can approximate the Feynman rules in (4.124) by

$$\begin{aligned} W \text{ boson}: &\quad \frac{i}{\sqrt{2}} \frac{g_{5,L}}{\sqrt{2\pi r}} \sqrt{2\pi} \begin{pmatrix} 1 & 0 \end{pmatrix} \vec{\chi}_n^W(\epsilon)\, V_{ij}^{\rm CKM} \gamma^\mu P_L\,, \\ Z \text{ boson}: &\quad \frac{i}{\sqrt{2}} \frac{g_{5,L}}{\sqrt{2\pi r} c_w} \sqrt{2\pi} \begin{pmatrix} 1 & 0 \end{pmatrix} \vec{\chi}_n^Z(\epsilon)\, \gamma^\mu \left[g_{q,L}(s_w^2)\, P_L + g_{q,R}(s_w^2)\, P_R \right]. \end{aligned} \tag{4.127}$$

For the SM W and Z bosons ($n = 0$), the Feynman rules coincide with the corresponding rules (4.111) and (4.118) found in the minimal RS model, since the first components of the profiles in the custodial RS model (2.78) are the same as the profiles in the minimal RS model (2.12). Combining all pieces, we find that instead of (4.113) we must perform the following replacement in the SM amplitude (with $V = W, Z$)

$$\frac{1}{m_V^2 - s} \to \frac{v_{\rm SM}}{v} \frac{\tilde{m}_W^2}{m_V^2 c_{\vartheta_W}^2} \sqrt{2\pi}\, \chi_0^V(1)^T \frac{g_{L,5}}{\sqrt{2\pi r} g} 2\pi\, \boldsymbol{B}_V^{\rm UV}(1, \epsilon; -s) \begin{pmatrix} 1 \\ 0 \end{pmatrix}. \tag{4.128}$$

The exact solution of the propagator function $\boldsymbol{B}_W^{\rm UV}$ is given in (3.41), while (3.42) presents an expansion of $\boldsymbol{B}_W^{\rm UV}$ to first non-trivial order in $v^2/M_{\rm KK}^2$. In case of the Z-boson propagator, the function $\boldsymbol{B}_Z^{\rm UV}$ can be obtained from (3.42) by replacing $m_W \to m_Z$ and $\vartheta_W \to \vartheta_Z$, and with $c_1(t,t') = 2\pi\, \chi_0^Z(t)\chi_0^Z(t')$, while $c_2(t,t')$ coincides with the expression given in (3.30). Inserting the expanded versions of the propagator functions into (4.128), we arrive at (4.114) with c_W and c_Z given by (4.123), while

$$\begin{aligned} c_{\Gamma_W}^{1/2}\big|_{\rm cust} &\equiv \frac{g_{L,5}}{\sqrt{2\pi r} g} \sqrt{2\pi} \begin{pmatrix} 1 & 0 \end{pmatrix} \vec{\chi}_0^W(\epsilon) = 1 - \frac{m_W^2}{2M_{\rm KK}^2} \frac{1}{4L} + \dots\,, \\ c_{\Gamma_Z}^{1/2}\big|_{\rm cust} &\equiv \frac{g_{L,5}}{\sqrt{2\pi r} g} \sqrt{2\pi} \begin{pmatrix} 1 & 0 \end{pmatrix} \vec{\chi}_0^Z(\epsilon) \;= c_{\Gamma_W}^{1/2} \left[1 + \frac{m_Z^2 - m_W^2}{4M_{\rm KK}^2} \left(1 - \frac{1}{L} \right) + \dots \right], \end{aligned} \tag{4.129}$$

remain the same as in the minimal model, see (4.112) and (4.119). Thus, the correction factors $c_{\Gamma_{W,Z}}$ to the $W \to f\bar{f}'$ and $Z \to f\bar{f}$ decay rates remain unchanged. The vector-boson fusion process analyzed in Section 4.3.3 can be studied analogously. In this case,

we need to replace the first line of (4.121) by

$$\begin{aligned}\frac{1}{(m_V^2-p_1^2)\,(m_V^2-p_2^2)} \to \frac{v_{\rm SM}}{v}\,\frac{\tilde m_W^2}{m_V^2 c_{\vartheta_W}^2}\left(\frac{g_{L,5}}{\sqrt{2\pi r}g}\right)^2 (2\pi)^2 \\ \times \begin{pmatrix}1 & 0\end{pmatrix} \boldsymbol{B}_V^{\rm UV}(\epsilon,1;-p_1^2)\,\boldsymbol{D}_{\vartheta_V}\,\boldsymbol{B}_V^{\rm UV}(1,\epsilon;-p_2^2)\begin{pmatrix}1\\0\end{pmatrix}.\end{aligned} \tag{4.130}$$

Using the expansions for the propagator functions and evaluating the rescaling factors, we confirm the second line of (4.121) with c_V and $c_{\Gamma_V}^{1/2}$ given above.

4.4 Phenomenological implications

In the context of Higgs physics, new-physics deviations from the SM can be searched for by measuring the signal rates[9]

$$R_X \equiv \frac{(\sigma\cdot{\rm BR})(pp\to h\to X)_{\rm NP}}{(\sigma\cdot{\rm BR})(pp\to h\to X)_{\rm SM}} = \frac{\sigma(pp\to h)_{\rm NP}}{\sigma(pp\to h)_{\rm SM}}\,\frac{\Gamma(h\to X)_{\rm NP}}{\Gamma(h\to X)_{\rm SM}}\,\frac{\Gamma_h^{\rm SM}}{\Gamma_h^{\rm NP}} \tag{4.131}$$

for the production of the Higgs boson in pp collisions at the LHC and its subsequent inclusive decay into an arbitrary final state X. Our work includes a detailed discussion of the signal rates R_X for the most relevant decays into $X = b\bar b$, $\tau^+\tau^-$, WW^*, ZZ^*, and $\gamma\gamma$ in different incarnations of RS models. From (4.131) we can read off that new physics can show up in three different ways. Firstly, it can lead to deviations in the Higgs production cross section $\sigma(pp\to h)$, which can be decomposed into the cross sections for Higgs production via gluon fusion, vector-boson fusion, Higgs-strahlung, and the associated production with a $t\bar t$ pair.[10] The relative contributions read (for $m_h = 125\,{\rm GeV}$) [218]

$$\sigma(pp\to h) = 0.872\,\sigma_{ggh} + 0.070\,\sigma_{VVh} + 0.033\,\sigma_{Wh} + 0.020\,\sigma_{Zh} + 0.005\,\sigma_{t\bar t h}\,. \tag{4.132}$$

Secondly, new-physics effects can change the Higgs decay rates $\Gamma(h\to X)$, and thirdly they can modify the total Higgs width Γ_h. Via the latter quantity the rates are sensitive to non-standard or invisible Higgs decays. In our analysis we take into account all three possibilities.

In addition to the signal rates we can search for new-physics effects in terms of the Higgs couplings. Recently, the ATLAS and CMS collaborations have published a combined analysis of the full Run 1 collision data sets at the LHC [219] with seven independent coupling modifiers. This allows us to compare the predictions for the tree-level $c_W, c_Z, c_t, c_b, c_\tau$ and loop-induced (effective) Higgs couplings $c_g^{\rm eff}, c_\gamma^{\rm eff}$ in RS models with current data from the LHC. In order to explore the future sensitivity on the Higgs couplings we consider two more scenarios. It has been reported in [220] that the LHC at $\sqrt{s} = 14\,{\rm TeV}$ and with an integrated luminosity of $300\,{\rm fb}^{-1}$ has the potential to probe, in a model-independent way, deviations of the Higgs couplings to fermions in the range of $\sim 30\%$ and to gauge bosons in the range of $\sim 16\%$, both at 95% confidence level (CL). At future lepton colliders like the International Linear Collider (ILC) [221–224], the sensitivity to deviations can be improved by almost one order of magnitude (assuming

[9] Here, the Higgs-boson width, which is predicted in the SM to be approximately 4 MeV, is assumed to be small such that the narrow-width approximation is valid and that Higgs production and decay can be decomposed.

[10] Other less important Higgs production processes in the SM that are not directly searched for are $q\bar q, gg \to b\bar b h$ and the Higgs production in association with a single top quark.

$\sqrt{s} = 1\,\text{TeV}$ and an integrated luminosity of $1000\,\text{fb}^{-1}$). We illustrate which regions of parameter space could be probed at these facilities.

In Section 4.4.1 we give a summary of the main Higgs couplings to fermions and gauge bosons as well as the Higgs self-couplings in various RS models. We present expressions that are exact at first order in $v^2/M_{\rm KK}^2$. A numerical study of both the CP-even and CP-odd Higgs couplings in the minimal and custodial RS model is performed in Section 4.4.2. We compare the predictions for $c_W, c_Z, c_t, c_b, c_\tau, c_g^{\rm eff}, c_\gamma^{\rm eff}$ in the minimal and custodial RS model with current data from the LHC. Then, we comment on the future sensitivity to detect deviations from the SM values of the Higgs couplings at the LHC and ILC. Finally, in Section 4.4.3 we compare the RS predictions for the signal rates of $pp \to h \to b\bar{b}$, $\tau^+\tau^-$, WW^*, ZZ^*, $\gamma\gamma$ with LHC data, which can be used to deduce bounds on the relevant model parameters.

4.4.1 Summary of Higgs couplings in RS models

In order to parameterize the RS contributions to the various Higgs couplings, we match them onto an effective Lagrangian defined at the electroweak scale $\mu \approx v$. For simplicity we neglect the effects of renormalization-group running from the new-physics scale $\mu \approx M_{\rm KK}$ down to the electroweak scale, as their numerical impact is of minor importance. The phenomenologically most relevant Higgs couplings can be described using the following Lagrangian in the broken electroweak phase

$$\begin{aligned}\mathcal{L}_{\rm eff} = {} & c_W \frac{2m_W^2}{v_{\rm SM}}\, h W_\mu^+ W^{-\mu} + c_Z \frac{m_Z^2}{v_{\rm SM}}\, h Z_\mu Z^\mu - \sum_{f=t,b,\tau} \frac{m_f}{v_{\rm SM}}\, h \bar{f}\,(c_f + c_{f5}\, i\gamma_5)\, f \\ & - c_{3h} \frac{m_h^2}{2v_{\rm SM}}\, h^3 - c_{4h} \frac{m_h^2}{8v_{\rm SM}^2}\, h^4 + c_g \frac{\alpha_s}{12\pi v_{\rm SM}}\, h G^a_{\mu\nu} G^{a,\mu\nu} - c_{g5} \frac{\alpha_s}{8\pi v_{\rm SM}}\, h G^a_{\mu\nu} \tilde{G}^{a,\mu\nu} \\ & + c_\gamma \frac{\alpha}{6\pi v_{\rm SM}}\, h F_{\mu\nu} F^{\mu\nu} - c_{\gamma 5} \frac{\alpha}{4\pi v_{\rm SM}}\, h F_{\mu\nu} \tilde{F}^{\mu\nu} + \dots\,, \end{aligned} \tag{4.133}$$

where the SM vev is given by $v_{\rm SM} \equiv (\sqrt{2} G_F)^{-1/2}$. We emphasize that it is not a complete list of operators. For instance, we have not included the operators $h Z_\mu \bar{f} \gamma^\mu f$ and $h Z_\mu \bar{f} \gamma^\mu \gamma_5 f$ contributing to the $h \to ZZ^* \to Z\bar{f}f$ decay amplitude (and corresponding operators for $h \to WW^*$), since as shown in Section 4.3.1 their contribution is subdominant. Furthermore, we do not consider the Higgs decay $h \to Z\gamma$ or any flavor-violating couplings in this work. Both the CP-even couplings c_i and the CP-odd coefficients c_{i5} are real-valued. In the SM $c_W = c_Z = c_f = c_{3h} = c_{4h} = 1$ and $c_{f5} = c_g = c_{g5} = c_\gamma = c_{\gamma 5} = 0$.

Higgs couplings to electroweak gauge bosons and fermions

In the SM, the Higgs boson couples to electroweak gauge bosons and fermions at tree level, with coupling strengths proportional to the masses of these particles. The non-universality of these couplings is the most distinguished feature of the Higgs mechanism. In RS models, modifications of the couplings arise from two effects: genuine corrections to the hVV (with $V = W, Z$) and $h\bar{f}f$ vertices, and an overall rescaling of all couplings due to the shift of the Higgs vev, which appears because we use the SM vev $v_{\rm SM}$ in the effective Lagrangian (4.133). As we have explained in Section 2.5.2 we determine v from the shift to the Fermi constant derived in the RS model by considering (at tree level) the effect of the exchange of the infinite tower of KK gauge bosons on the rate for muon decay. We now present explicit expressions for the various c_i parameters, working consistently to first order in $v^2/M_{\rm KK}^2$. Wherever possible, we will parameterize the differences between the minimal and the custodial RS model by means of a parameter

ξ, which equals 1 in the minimal model and 2 in the custodial model (with imposed P_{LR} symmetry).

The Higgs couplings to W and Z bosons in RS models have been derived in Section 4.3 and are collectively given to leading order in $v^2/M_{\rm KK}^2$ by

$$\begin{aligned} c_W\big|_{\rm min} &= 1 - \frac{m_W^2}{2M_{\rm KK}^2}\left(\frac{3L}{2} - 1 + \frac{1}{2L}\right), & c_W\big|_{\rm cust} &= 1 - \frac{m_W^2}{2M_{\rm KK}^2}\left(3L - 1 + \frac{1}{2L}\right), \\ c_Z\big|_{\rm min} &= 1 - \frac{m_Z^2}{2M_{\rm KK}^2}\left(L - 1 + \frac{1}{2L}\right) - \frac{Lm_W^2}{4M_{\rm KK}^2}, & c_Z\big|_{\rm cust} &= 1 - \frac{m_W^2}{2M_{\rm KK}^2}\left(3L + 1 - \frac{1}{2L}\right), \end{aligned} \tag{4.134}$$

which follow from (4.110), (4.117), and (4.123). With $L \approx 33.5$, the L-enhanced contributions in these expressions are by far numerically dominant. Future precise measurements of c_W and c_Z would thus provide a direct tool to determine the ratio $M_{\rm KK}/\sqrt{L}$ in the RS model.

The couplings of the Higgs boson to the third-generation fermions have been studied in Section 4.1.1, where it was found that flavor-changing couplings are strongly suppressed. The CP-even and CP-odd flavor-diagonal couplings, c_f and c_{f5}, are related to the κ_f couplings defined in (4.31) by the equation $c_f + ic_{f5} = \kappa_f \frac{v_{\rm SM}}{v}$. It then follows that (with $f = t, b, \tau$ on the left-hand side and $f = u, d, e$ on the right-hand side)

$$c_f + ic_{f5} = 1 - \varepsilon_f - \frac{\xi L m_W^2}{4M_{\rm KK}^2} - \frac{\xi v^2}{3M_{\rm KK}^2}\,\frac{\big(\boldsymbol{Y}_f \boldsymbol{Y}_f^\dagger \boldsymbol{Y}_f\big)_{33}}{\big(\boldsymbol{Y}_f\big)_{33}} + \dots\,, \tag{4.135}$$

where $\boldsymbol{Y}_{u,d,e}$ denote the dimensionless, anarchic 5D Yukawa matrices in the up, down and lepton sectors. Note that the CP-odd couplings in (4.135) are given solely due to the "three-Yukawa terms". The real-valued quantities ε_f arise from overlap integrals of the "wrong-chirality" fermion profiles. They are given by $\varepsilon_f = \big(\boldsymbol{\delta}_F\big)_{33} + \big(\boldsymbol{\delta}_f\big)_{33}$ in the minimal RS model and by $\varepsilon_f = \big(\boldsymbol{\Phi}_F\big)_{33} + \big(\boldsymbol{\Phi}_f\big)_{33}$ in the custodial RS model. Explicit expressions for the matrices $\boldsymbol{\delta}_{U,D,E}$ and $\boldsymbol{\delta}_{u,d,e}$ can be found in (4.28), while those for the matrices $\boldsymbol{\Phi}_{U,D,E}$ and $\boldsymbol{\Phi}_{u,d,e}$ are given in (4.63). They depend in a complicated way on the bulk-mass parameters of the various 5D fermion fields. All of the quantities ε_f are of $\mathcal{O}(v^2/M_{\rm KK}^2)$, but in addition some of them are strongly chirality suppressed. For all practical purposes, one can retain $\varepsilon_u = (\boldsymbol{\delta}_U)_{33} + (\boldsymbol{\delta}_u)_{33}$ but approximate $\varepsilon_d \approx (\boldsymbol{\delta}_D)_{33}$, $\varepsilon_e \approx 0$, and similarly in the custodial model. Numerically, the ε_f parameters turn out to play a numerically subleading role compared with the "three-Yukawa terms" in (4.135).

The Higgs couplings to fermions do not only depend on the KK mass scale, but also on the dimensionless 5D Yukawa matrices. When scanning over the parameter space of an RS model, see Section 2.5.1, the various entries of the Yukawa matrices are taken to be complex random numbers subject to the condition $|(\boldsymbol{Y}_f)_{ij}| \le y_\star$, where the upper bound $y_\star = \mathcal{O}(1)$ is a free parameter. For an ensemble of sufficiently many random matrices constructed in this manner, one can show that on average

$$\left\langle \frac{\big(\boldsymbol{Y}_f \boldsymbol{Y}_f^\dagger \boldsymbol{Y}_f\big)_{33}}{\big(\boldsymbol{Y}_f\big)_{33}} \right\rangle = (2N_g - 1)\,\frac{y_\star^2}{2}\,, \tag{4.136}$$

where $N_g = 3$ is the number of generations. It follows that the Higgs couplings to fermions are rather insensitive to the individual entries of the Yukawa matrices, but they do scale with $y_\star^2$. Hence, we encounter a similar situation as in the gauge-boson case, where the relevant parameter is now given by $M_{\rm KK}/y_\star$. We should add at this

point that in practice relation (4.136) is subject to some flavor-dependent corrections, which arise when the scan over random Yukawa matrices is performed subject to the constraint that one obtains acceptable values for the quark and lepton masses and for the CKM matrix in the quark sector.[11] When this is done, one finds numerically that the expectation value (4.136) is slightly enhanced for the top quark and somewhat reduced for the bottom quark.[12]

Higgs self-couplings

One of the predictions of the SM is that the trilinear and quartic Higgs couplings can be expressed in terms of the Higgs-boson mass and the vev of the Higgs field, such that $c_{3h} = c_{4h} = 1$ in (4.133). In RS models these coefficients receive calculable corrections, which for the minimal and the custodial RS models are described by the same formula in terms of the correction to the Higgs vev. As long as the Higgs sector is localized on or near the IR brane, one obtains

$$c_{3h} = \frac{v_{\rm SM}}{v} = 1 - \frac{\xi L m_W^2}{4M_{\rm KK}^2} + \dots\,, \qquad c_{4h} = \frac{v_{\rm SM}^2}{v^2} = 1 - \frac{\xi L m_W^2}{2M_{\rm KK}^2} + \dots\,. \tag{4.137}$$

For a KK mass scale of $M_{\rm KK} = 1.5\,\text{TeV}$, one finds a 2.4% (4.8%) reduction of the trilinear coupling and a 4.8% (9.6%) reduction of the quartic coupling in the minimal (custodial) RS model. We mention that moving the Higgs field into the bulk would attenuate these deviations and move the couplings closer to their SM values. Such small deviations will not be measurable by the LHC, and even for a future linear collider like the ILC this is probably out of reach. Therefore, we refrain from presenting a detailed numerical analysis of the Higgs self-couplings.

Loop-induced Higgs couplings to two gluons

In the SM, the Higgs boson couples to massless gluons and photons only via loop diagrams containing heavy SM particles. Direct couplings, such as the ones contained in the effective Lagrangian (4.133), are absent in the SM. In the context of RS models such direct couplings are induced at one-loop order via the exchange of heavy KK resonances.

We begin with the loop-induced Higgs couplings to gluons, which are relevant for the calculation of the gluon-fusion cross section $\sigma(gg \to h)$, which is the main Higgs production channel at high-energy hadron colliders such as the LHC. A detailed discussion can be found in Section 4.1. In the limit where we neglect $\mathcal{O}(v^2/M_{\rm KK}^2)$ corrections which in addition are strongly chirality suppressed, the expressions for the induced Higgs couplings to two gluons read

$$c_g + i c_{g5} = \begin{cases} \operatorname{Tr} g(\boldsymbol{X}_u) + \operatorname{Tr} g(\boldsymbol{X}_d) + \varepsilon_u + \varepsilon_d\,; & \text{minimal RS model,} \\ \operatorname{Tr} g(\sqrt{2}\boldsymbol{X}_u) + 3\operatorname{Tr} g(\sqrt{2}\boldsymbol{X}_d) + \varepsilon_u + \varepsilon_d\,; & \text{custodial RS model.} \end{cases} \tag{4.138}$$

[11] For $y_\star = 1$, we find numerically that the expectation value (4.136) is equal to 2.5 (as expected) for anarchic matrices, while it is 2.7 in the up-quark sector and 2.2 in the down-quark sector. We do not consider neutrino masses or the PMNS matrix in our analysis, since this would require the specification of the neutrino sector, which is both model dependent and of little relevance to Higgs physics.

[12] We comment on the type-II brane-Higgs models, in which one uses two different Yukawa matrices $\boldsymbol{Y}_f^C$ and $\boldsymbol{Y}_f^S$ in the Higgs couplings to the Z_2-even and Z_2-odd fermion fields. In these scenarios, the Yukawa-dependent term $\big(\boldsymbol{Y}_f \boldsymbol{Y}_f^\dagger \boldsymbol{Y}_f\big)_{33}/\big(\boldsymbol{Y}_f\big)_{33}$ in (4.135) must be replaced by $\big(\boldsymbol{Y}_f^C \boldsymbol{Y}_f^{S\dagger} \boldsymbol{Y}_f^C\big)_{33}/\big(\boldsymbol{Y}_f^C\big)_{33}$. For the special case $\boldsymbol{Y}_f^S = 0$, which was sometimes adopted in the literature, this term vanishes. There is then no contribution to the CP-odd couplings c_{f5}.

The quantities $\boldsymbol{X}_f$, defined in (4.74), are entirely given by the dimensionless 5D Yukawa matrices of the RS model. For the two scenarios with a brane-localized and a narrow bulk-Higgs sector, one finds $g(\boldsymbol{X}_f) = \mp \boldsymbol{X}_f^2 + \ldots$ (see (4.24) and (4.25)), so that the effect from the KK tower is approximately equal but of opposite sign in the two scenarios. For a large ensemble of random matrices, one obtains on average

$$\left\langle \operatorname{Tr} \boldsymbol{Y}_f \boldsymbol{Y}_f^\dagger \right\rangle = N_g^2 \, \frac{y_\star^2}{2} \,. \tag{4.139}$$

Due to the additional factors $\sqrt{2}$ and 3 in the second case in (4.138), the quark KK tower contribution in the custodial RS model is roughly four times larger than in the minimal RS model. Note that with the hermitian matrices $\boldsymbol{X}_f$ the traces over the matrix-valued functions $g(\boldsymbol{X}_f)$ are real, so that $c_{g5} = 0$ irrespective of the Higgs localization or the type of RS model (minimal or custodial).[13]

When the top-quark is integrated out from the effective Lagrangian (4.133), additional contributions to the effective hgg couplings are induced at one-loop order. They can be accounted for by introducing the effective coefficients

$$c_g^{\text{eff}} = \frac{c_g + A_q(\tau_t)\, c_t}{A_q(\tau_t)} \,, \qquad\qquad c_{g5}^{\text{eff}} = \frac{c_{g5} + B_q(\tau_t)\, c_{t5}}{A_q(\tau_t)} \,, \tag{4.140}$$

which we have normalized such that $c_g^{\text{eff}} = 1$ in the SM. Explicit expressions for the top-quark loop functions $A_q(\tau_t) \approx 1.03$ and $B_q(\tau_t) \approx 1.05$ (with $\tau_t = 4m_t^2/m_h^2$) are given in (4.34). Both approach 1 for $\tau_t \to \infty$, and it is an excellent approximation to use the asymptotic values for the small new-physics corrections to the Wilson coefficients. It then follows that the terms proportional to ε_u, which in c_g^{eff} combine to $\varepsilon_u\big[1 - A_q(\tau_t)\big]$, can be safely neglected. Note also that to a very good approximation $c_{g5}^{\text{eff}} \approx c_{t5}$.

Loop-induced Higgs couplings to two photons

We finally turn our attention to the couplings of the Higgs boson to two photons, which play a crucial role for the $h \to \gamma\gamma$ decay channel, in which the Higgs boson has been discovered in 2012. Neglecting as before $\mathcal{O}(v^2/M_{\text{KK}}^2)$ corrections, which in addition are strongly chirality suppressed, the expressions for the induced Higgs couplings to two photons in the minimal RS model read

$$\begin{aligned} c_\gamma + i c_{\gamma 5}\big|_{\text{min}} &= N_c Q_u^2 \left[\operatorname{Tr} g(\boldsymbol{X}_u) + \varepsilon_u\right] + N_c Q_d^2 \left[\operatorname{Tr} g(\boldsymbol{X}_d) + \varepsilon_d\right] + Q_e^2 \operatorname{Tr} g(\boldsymbol{X}_e) - \frac{21}{4}\,\nu_W \,, \\ c_\gamma + i c_{\gamma 5}\big|_{\text{cust}} &= N_c Q_u^2 \operatorname{Tr} g(\sqrt{2}\boldsymbol{X}_u) + N_c\big(Q_u^2 + Q_d^2 + Q_\lambda^2\big) \operatorname{Tr} g(\sqrt{2}\boldsymbol{X}_d) + Q_e^2 \operatorname{Tr} g(\boldsymbol{X}_e) \\ &\quad + N_c Q_u^2\, \varepsilon_u + N_c Q_d^2\, \varepsilon_d - \frac{21}{4}\,\nu_W \,. \end{aligned} \tag{4.141}$$

They receive KK contributions from the quark and lepton loops as well as from loops of W bosons and charged NGBs. Here, $Q_{u,d,e}$ denote the electric charges of the SM fermions, and $Q_\lambda = \frac{5}{3}$ is the charge of a new exotic, heavy fermion species encountered in the custodial RS model. The precise embeddings of the SM quark fields into the extended gauge symmetry has been discussed in detail in Section 2.4. For the lepton

[13] For the type-II brane-Higgs model, the function $g(\boldsymbol{X}_f)$ must be replaced by $-\varrho^2 \boldsymbol{Y}_f^C \boldsymbol{Y}_f^{C\dagger} + \ldots$, and hence to leading order there is no difference with the result shown above. In this model the CP-odd coupling c_{g5} receives contributions starting at $\mathcal{O}(v^4/M_{\text{KK}}^4)$, which are however too small to be of any phenomenological significance. In the subsequent sections we will therefore not discuss the type-II brane-Higgs model any further.

	LHC: 7 & 8 TeV, 5 & 20 fb^{-1}	LHC: 14 TeV, 300 fb^{-1}	ILC: 1 TeV, 1000 fb^{-1}
c_W	$0.90^{+0.09}_{-0.09}$	$1_{-0.069}$	$1_{-0.004}$
c_Z	$1.00_{-0.08}$	$1_{-0.077}$	$1_{-0.006}$
$c_g^{\rm eff}$	$0.81^{+0.13}_{-0.10}$	$1^{+0.10}_{-0.078}$	$1^{+0.014}_{-0.014}$
$c_\gamma^{\rm eff}$	$0.90^{+0.10}_{-0.09}$	$1^{+0.059}_{-0.096}$	$1^{+0.035}_{-0.032}$
c_t	$1.42^{+0.23}_{-0.22}$	$1^{+0.147}_{-0.154}$	$1^{+0.035}_{-0.044}$
c_b	$0.57^{+0.16}_{-0.16}$	$1^{+0.041}_{-0.231}$	$1^{+0.011}_{-0.003}$
c_τ	$0.87^{+0.12}_{-0.11}$	$1^{+0.132}_{-0.093}$	$1^{+0.017}_{-0.013}$

Table 4.2: The first column shows the fit results with 1σ uncertainties for the Higgs couplings obtained from a combined ATLAS and CMS analysis of the LHC pp collision data at $\sqrt{s} = 7\,\text{TeV}$ and $\sqrt{s} = 8\,\text{TeV}$ [219]. The last two columns show SM-like Higgs couplings for the high-luminosity LHC at $\sqrt{s} = 14\,\text{TeV}$ and for the ILC at $\sqrt{s} = 1\,\text{TeV}$, where the 1σ confidence intervals emerged from a fit performed in [220].

fields two types of embeddings have been studied in Section 4.2.2. Here we adopt the simplest assignment, in which the left-chiral neutrino and electron are put into an $SU(2)_L$ doublet (as in the SM) and the right-chiral electron along with a new, exotic neutral particle N_R into an $SU(2)_R$ doublet. The infinite tower of the KK excitations of the W bosons (including the charged NGBs) contributes

$$\nu_W = \frac{m_W^2}{2M_{\rm KK}^2}\left(\xi L - 1 + \frac{1}{2L}\right) + \dots\,, \tag{4.142}$$

which follows from (4.91). Like in the case of the gluon-fusion channel $gg \to h$, we define effective coefficients obtained after the heavy particles t, W and Z of the SM have been integrated out. They are related to the above coefficients by

$$c_\gamma^{\rm eff} = \frac{c_\gamma + N_c Q_u^2\, A_q(\tau_t)\, c_t - \frac{21}{4}\, A_W(\tau_W)\, c_W}{N_c Q_u^2\, A_q(\tau_t) - \frac{21}{4}\, A_W(\tau_W)}\,, \qquad c_{\gamma 5}^{\rm eff} = \frac{c_{\gamma 5} + N_c Q_u^2\, B_q(\tau_t)\, c_{t5}}{N_c Q_u^2\, A_q(\tau_t) - \frac{21}{4}\, A_W(\tau_W)}\,, \tag{4.143}$$

where again we have chosen the normalization such that $c_\gamma^{\rm eff} = 1$ in the SM. The explicit form of the W-boson loop function $A_W(\tau_W) \approx 1.19$ (with $\tau_W = 4m_W^2/m_h^2$), which approaches 1 for $\tau_W \to \infty$, is given by (4.90). From the fact that the coefficient $c_{\gamma 5}$ in (4.141) vanishes, it follows that to a very good approximation $c_{\gamma 5}^{\rm eff} \approx -0.28\, c_{t5}$.

4.4.2 Numerical analysis of Higgs couplings

We now study the structure of new-physics effects to both tree-level and loop-induced Higgs couplings to fermions and gauge bosons in the context of the minimal and custodial RS model. In our analysis we take $m_h = 125.09 \pm 0.24\,\text{GeV}$ [70] for the Higgs mass and $m_{t,\rm pole} = 174.6 \pm 1.9\,\text{GeV}$ [76] for the pole mass of the top quark. The parameter L defined in (1.32) is chosen to be $L = 33.5$. We generate three sets of 5000 RS points for different values of maximal Yukawa couplings $y_\star = 0.5$, 1.5, and 3, according to the procedure described in Section 2.5.1. We will analyze the RS predictions with respect to the first KK gluon mass $M_{g^{(1)}}$ and the maximal Yukawa value $y_\star$.

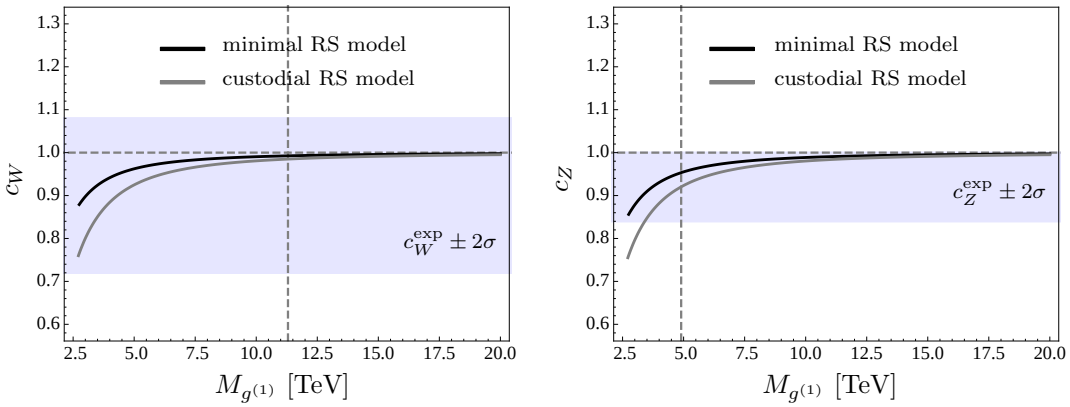

Figure 4.5: Left (right) are shown the predictions for the Higgs couplings to the W (Z) boson as a function of the first KK gluon mass $M_{g^{(1)}}$ in the minimal (custodial) RS models. The blue bands show the 2σ error regions of c_W and c_Z obtained from a fit of the Higgs couplings by the ATLAS and CMS collaborations [219], see Table 4.2. The vertical dashed lines represent the lower bounds on $M_{g^{(1)}}$, see (2.103) and (2.107), which have been deduced from a tree-level analysis of the Peskin-Takeuchi parameters.

In order to compare the Higgs couplings in the RS model with respect to the SM, we will rely on a model-independent[14] fit of the ATLAS and CMS collaborations [219]. Their analysis is based on the data of the first run of the LHC, corresponding to integrated luminosities per experiment of about $5\,\text{fb}^{-1}$ at a centre-of-mass energy of $\sqrt{s} = 7\,\text{TeV}$ and $20\,\text{fb}^{-1}$ at $\sqrt{s} = 8\,\text{TeV}$ by the ATLAS and CMS detectors. Basic assumptions of the analysis are that the SM-like Higgs-boson state is a CP-even scalar with the tensor structure of the SM interactions. Furthermore, the total Higgs-boson width is assumed to be small enough ($\Gamma_h^{\rm SM} = 4.10\,\text{MeV}$ for $m_h = 125.09\,\text{GeV}$) in order to apply the narrow-width approximation and that Higgs production and decay can be decomposed. These assumptions are supported by the experimental measurements of the spin and CP properties of the Higgs-like boson [225, 226] and by direct [227] and indirect [228, 229] studies of the Higgs-boson width. In addition, the fit assumes that the tree-level Higgs couplings to the W and Z bosons are reduced with respect to the SM values, i.e. $c_V \leq 1$ for $V = W, Z$. Indeed, these conditions are fulfilled for the RS models under consideration, see (4.134) and Figure 4.5. The fit results for the tree-level $c_W, c_Z, c_t, c_b, c_\tau$ and loop-induced (effective) Higgs couplings $c_g^{\rm eff}, c_\gamma^{\rm eff}$ are listed in Table 4.2.

Tree-level Higgs couplings

Figure 4.5 shows the tree-level Higgs couplings to the W and Z bosons in the minimal and custodial RS model in dependence of the lightest KK gluon mass. We find it useful to convert the mass parameter $M_{\rm KK}$ to the physical mass $M_{g^{(1)}} \approx 2.45\, M_{\rm KK}$ of the lightest KK gluon (or KK photon) state, which is independent of the details of the localization of the scalar sector and of the choice of the electroweak gauge group in the bulk. The couplings, based on (4.134), can be parametrized by

$$c_V \approx 1 - a_V \left(5\,\text{TeV}/M_{g^{(1)}}\right)^2 ; \qquad V = W, Z\,, \tag{4.144}$$

[14] The term *model-independent fit* means that the ATLAS and CMS collaborations have used 7 independent coupling modifiers, one for each SM particle involved in the studied Higgs production and decay processes. The assumptions that enter the fit procedure are given in the text.

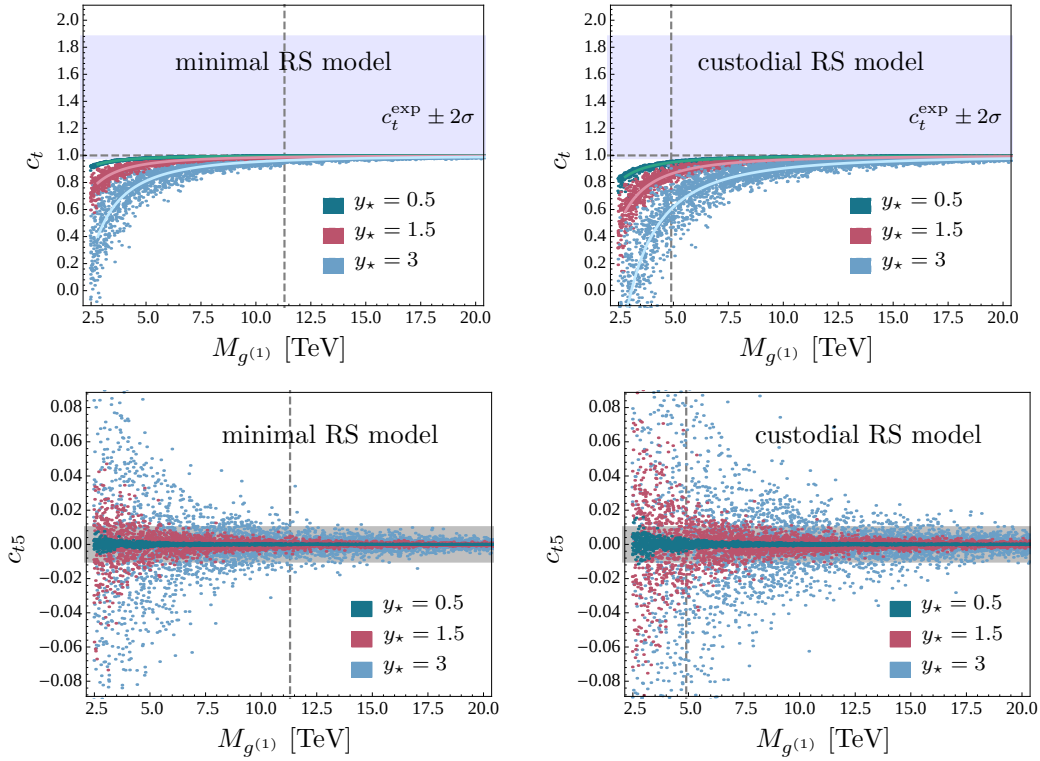

Figure 4.6: Predictions for the Higgs couplings to top quarks as a function of the KK gluon mass $M_{g^{(1)}}$ in the minimal (left) and custodial (right) RS model. The green, red, and blue scatter points correspond to model points obtained using $y_\star = 0.5$, 1.5, and 3. The overlaid lines in the plots of the upper row show fits to the various distributions as explained in the text. The blue band represents the 2σ fit region of c_t obtained from a combined ATLAS and CMS analysis, see Table 4.2. The gray band in the lower plots show the experimental bound on $|c_{t5}|$ derived from the electron EDM (at 90% CL). The vertical dashed lines denote the bounds from electroweak precision tests.

with $a_W \approx 0.038$ and $a_Z \approx 0.045$ in the minimal RS model. In the custodial RS model, the corrections to the tree-level Higgs couplings to W and Z bosons in (4.123) are identical up to very small corrections not enhanced by $L \approx 33.5$, and we obtain $a_W \approx a_Z \approx 0.076$. Realistically, with KK masses not in conflict with electroweak precision tests, we might thus expect corrections of a few up to a maximum of 10%.

Next we study the corrections to the CP-even and CP-odd Higgs couplings c_f and c_{f5} to the third-generation fermions, as obtained from (4.135). Figure 4.6 shows the Higgs couplings to top quarks as a function of the mass of the lightest KK gluon state. The green, red, and blue scatter points in the figure correspond to RS model points obtained using three different values of $y_\star = 0.5$, 1.5 and 3. In accordance with (4.135) and (4.136) we observe that c_t is reduced compared to the SM value 1 for almost all parameter points, where the depletion increases with larger values of $y_\star$. The corresponding plots for c_b and c_τ would look very similar, with the magnitude of the corrections somewhat reduced. The main difference is due to the different values of the ε_f parameters in the three cases, but their numerical impact is subleading. The solid lines in the upper plots in the figure show simple polynomial fits of the form

$$c_f \approx 1 - a_f \left(5\,\text{TeV}/M_{g^{(1)}}\right)^2 ; \qquad f = t, b, \tau\,, \tag{4.145}$$

minimal RS model

$y_\star$	0.5	1.5	3
a_t	0.021	0.064	0.19
a_b	0.017	0.042	0.12
a_τ	0.015	0.037	0.11
b_t	0.00067	0.0069	0.029
b_b	0.00060	0.0058	0.023
b_τ	0.00060	0.0058	0.023

custodial RS model

$y_\star$	0.5	1.5	3
a_t	0.050	0.13	0.38
a_b	0.033	0.085	0.24
a_τ	0.030	0.076	0.22
b_t	0.0013	0.014	0.059
b_b	0.0012	0.012	0.048
b_τ	0.0012	0.012	0.048

Table 4.3: Fit coefficients a_f and b_f of the functions (4.145) and (4.146) for different values of $y_\star$ in the minimal (left) and custodial (right) RS model.

to the scatter points, with coefficients $a_f = a_f(y_\star)$ given in Table 4.3. For example, with $y_\star = 3$ a modification of c_t by 19% (38%) is possible for KK excitations as heavy as 5 TeV in the minimal (custodial) RS model.[15]

The CP-odd couplings of the Higgs to two fermions c_{f5} in the RS model are given by the imaginary part of (4.135). For random complex Yukawa matrices with entries bounded by $|(\boldsymbol{Y}_f)_{ij}| \leq y_\star$, we find an approximately Gaussian distribution with zero mean and non-Gaussian tails, which can be reduced by imposing a lower bound on the magnitude of $\big|(\boldsymbol{Y}_f)_{33}\big|$. In the vicinity of the peak the distribution is approximately normal, with standard deviation

$$\sigma_{c_{f5}} \approx b_f \, (5\,\text{TeV}/M_{g^{(1)}})^2 \,; \qquad\qquad f = t, b, \tau \,, \tag{4.146}$$

where the fit parameter b_f is listed in Table 4.3 for different values of $y_\star$. Due to the constraint that we must obtain realistic values of the quark masses and CKM mixing angles the parameters b_f can have different values for $f = t, b, \tau$. It has been argued in [230] that present experimental bounds on electric dipole moments (EDMs) of the electron, neutron and mercury impose non-trivial bounds on the CP-odd Higgs couplings to the third-generation fermions. The strongest constraint exists for the magnitude on c_{t5} and comes from the EDM of the electron, which is sensitive to the $ht\bar{t}$ couplings via two-loop Barr-Zee diagrams. Using the present 90% CL upper limit $d_e < 8.7 \cdot 10^{-29} e\,\text{cm}$ [231] and assuming that the Higgs coupling to electrons is not changed with respect to its SM value, one obtains $|c_{t5}| < 0.01$ [230]. In the RS models considered in this work this assumption is valid to high accuracy, since corrections to the he^+e^- coupling are strongly chirality suppressed. This resulting bound is shown by the gray band in the lower plots in Figure 4.6. Interestingly, we find that for $y_\star \gtrsim 1$ there are many points in RS parameters space for which c_{t5} takes values of the same order of magnitude as the experimental bound. Hence, in the context of RS models it is conceivable that first hints of a non-zero electron EDM might be seen in the next round of experiments.

Loop-induced Higgs couplings

We move on to study the loop-induced hgg and $h\gamma\gamma$ couplings. They are of special interest, since they are very sensitive probes of the effects of virtual KK resonances. We

[15] We like to add a brief comment concerning the type-II brane Higgs model at this point, in which the three-Yukawa terms have a vanishing expectation value. While the remaining terms in (4.135) still give rise to small negative corrections, the corresponding scatter plots would show points scattered more or less around the central value $c_i = 1$, and which can become larger than 1 for not too small values for $y_\star$ due to the indefinite sign of the three-Yukawa terms.

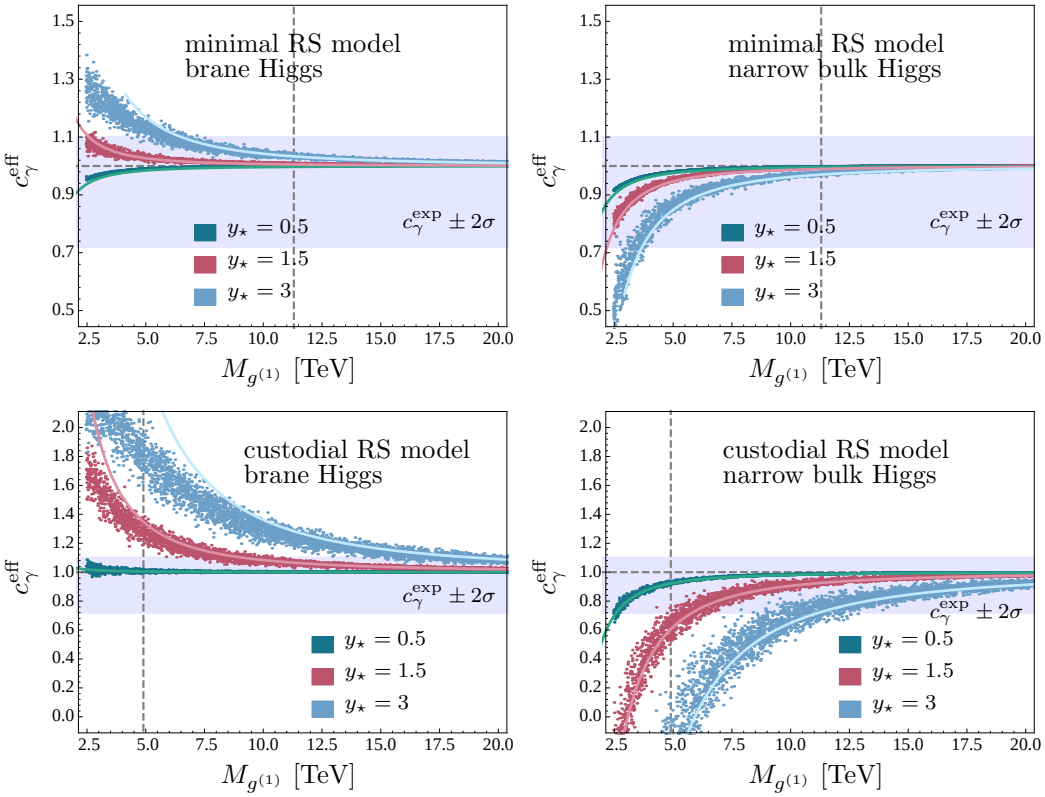

Figure 4.7: Predictions for the CP-even effective Higgs coupling to two photons as a function of the KK gluon mass $M_{g^{(1)}}$ in the minimal (top) and custodial (bottom) RS model, for the scenarios with a brane-localized scalar sector (left) and a narrow bulk-Higgs field (right). The green, red, and blue scatter points correspond to model points obtained using $y_\star = 0.5$, 1.5, and 3. The overlaid lines are obtained from the approximate results (4.147) and (4.148). The blue band represents the 2σ error margin of the fit result for $c_\gamma^{\rm eff}$ in the first column of Table 4.2. Vertical dashed lines show the bounds from a tree-level analysis of the Peskin-Takeuchi parameters.

concentrate on the CP-even couplings $c_g^{\rm eff}$ and $c_\gamma^{\rm eff}$, since current measurements are not sufficiently precise to probe the CP-odd couplings.[16] Using the explicit expressions for $c_g^{\rm eff}$ and $c_\gamma^{\rm eff}$ in (4.140) and (4.143), it is straightforward to derive approximate expressions for these coefficients which help to understand the interplay of the various contributions. To this end, we expand the fermion KK-tower contributions in (4.138) and (4.141) to first order in $v^2/M_{\rm KK}^2$ and employ (4.136) and (4.139). We also approximate the top-quark loop function $A_q(\tau_t)$ by its asymptotic value 1 and neglect subleading terms not enhanced by L in the bosonic contributions. This yields

$$c_g^{\rm eff}|_{\rm min} \approx 1 + \frac{v^2}{2M_{\rm KK}^2}\left[\left(\mp 9 - \frac{5}{3}\right) y_\star^2 - \frac{L m_W^2}{2v^2}\right] \approx 1 + \frac{v^2}{2M_{\rm KK}^2}\left[(\mp 9.0 - 1.7)\, y_\star^2 - 1.8\right] ,$$

$$c_\gamma^{\rm eff}|_{\rm min} \approx 1 + \frac{v^2}{2M_{\rm KK}^2}\left[\frac{1}{|C_\gamma^{\rm SM}|}\left(\pm 12 + \frac{20}{9}\right) y_\star^2 - \frac{21(A_W(\tau_W)-1)}{2|C_\gamma^{\rm SM}|}\,\frac{L m_W^2}{2v^2} - \frac{L m_W^2}{2v^2}\right]$$

[16] There exist proposals for how to probe $c_{\gamma 5}^{\rm eff}$ in $h \to \gamma\gamma$ decays in which both photons undergo nuclear conversion, by measuring certain kinematic distributions of the electron-positron pairs [232]. Unfortunately, however, the level of sensitivity one can achieve does not allow one to probe the very small effects $c_{\gamma 5}^{\rm eff} \approx -0.28\, c_{t5}$ predicted in RS models, where the CP-odd $ht\bar{t}$ coupling is the only source of the effect.

$$\approx 1 + \frac{v^2}{2M_{\rm KK}^2}\left[(\pm 2.5 + 0.5)\, y_\star^2 - 2.6\right] , \tag{4.147}$$

in the minimal and

$$\begin{aligned} c_g^{\rm eff}|_{\rm cust} &\approx 1 + \frac{v^2}{2M_{\rm KK}^2}\left[\left(\mp 36 - \frac{10}{3}\right) y_\star^2 - \frac{Lm_W^2}{v^2}\right] \approx 1 + \frac{v^2}{2M_{\rm KK}^2}\left[(\mp 36.0 - 3.3)\, y_\star^2 - 3.6\right] , \\ c_\gamma^{\rm eff}|_{\rm cust} &\approx 1 + \frac{v^2}{2M_{\rm KK}^2}\left[\frac{1}{|C_\gamma^{\rm SM}|}\left(\pm\frac{213}{2} + \frac{40}{9}\right) y_\star^2 - \frac{21(A_W(\tau_W)-1)}{2|C_\gamma^{\rm SM}|}\,\frac{Lm_W^2}{v^2} - \frac{Lm_W^2}{v^2}\right] \\ &\approx 1 + \frac{v^2}{2M_{\rm KK}^2}\left[(\pm 21.7 + 0.9)\, y_\star^2 - 5.1\right] , \end{aligned} \tag{4.148}$$

in the custodial RS model. Here the upper sign holds for the brane-Higgs case, while the lower one corresponds to the narrow bulk-Higgs scenario. We have kept the dependence on the one-loop SM amplitude $C_\gamma^{\rm SM} = \frac{4}{3} - \frac{21}{4}A_W(\tau_W) \approx -4.9$ explicit. In each square bracket, the first term is due to the effects of KK fermion resonances, while the second term accounts for the vev shift and the contribution of bosonic KK states (for $c_\gamma^{\rm eff}$). The fermionic contributions enter the two coefficients with opposite signs and are larger in magnitude in the case of $c_g^{\rm eff}$. Figure 4.7 shows our predictions for the coefficient $c_\gamma^{\rm eff}$ as a function of the mass of the lightest KK gluon resonance and for different values of $y_\star$. We recall that the results exhibit a large sensitivity to the precise nature of the localization of the scalar sector on or near the IR brane. On average, the distributions of scatter points follow the approximate formulas shown in (4.147) and (4.148); however, in the brane-Higgs case higher-order corrections become important for small $M_{g^{(1)}}$ values, and they are included in our phenomenological analysis below. The corresponding information on how $c_g^{\rm eff}$ depends on $M_{g^{(1)}}$ and $y_\star$ can be deduced from the correlation between the two loop-induced couplings, to which we turn now.

Correlations between Higgs couplings

We have explained earlier that, to good approximation, the average results for the various Higgs couplings in RS models can be expressed in terms of only two parameters $M_{\rm KK}$ and $y_\star$, with some relatively narrow distribution of model points about these average predictions. As a result, in these models there are strong correlations between various Higgs couplings. This important fact is illustrated in Figure 4.8, where we display our predictions in the $c_t - c_b$ and $c_\gamma^{\rm eff} - c_g^{\rm eff}$ planes for RS points with $M_{g^{(1)}} = 10\,\text{TeV}$. In the lower plots, scatter points below $c_g^{\rm eff} = 1$ (lower right plane) correspond to the brane-localized Higgs scenario, while points above $c_g^{\rm eff} = 1$ (upper left plane) refer to the narrow bulk-Higgs scenario. In the case of the fermionic couplings c_t and c_b we observe a clear correlation in the sense that both couplings are smaller than 1 by approximately equal amounts. On the other hand, we see a clear anti-correlation between $c_\gamma^{\rm eff}$ and $c_g^{\rm eff}$, which is due to the fermion KK contributions as explained above. This implies that there are no regions of parameter space where both couplings are smaller or larger than 1. Thus, a precise measurement of such values could rule out all RS scenarios considered in this work. The gray and blue bands in the lower plots denote the 2σ error margins of the fit values $c_g^{\rm eff} = 0.81^{+0.13}_{-0.10}$ and $c_\gamma^{\rm eff} = 0.90^{+0.10}_{-0.09}$ obtained from a combined analysis of the ATLAS and CMS measurements [219]. Those fit values have a slight tendency to values smaller than 1 for both couplings.

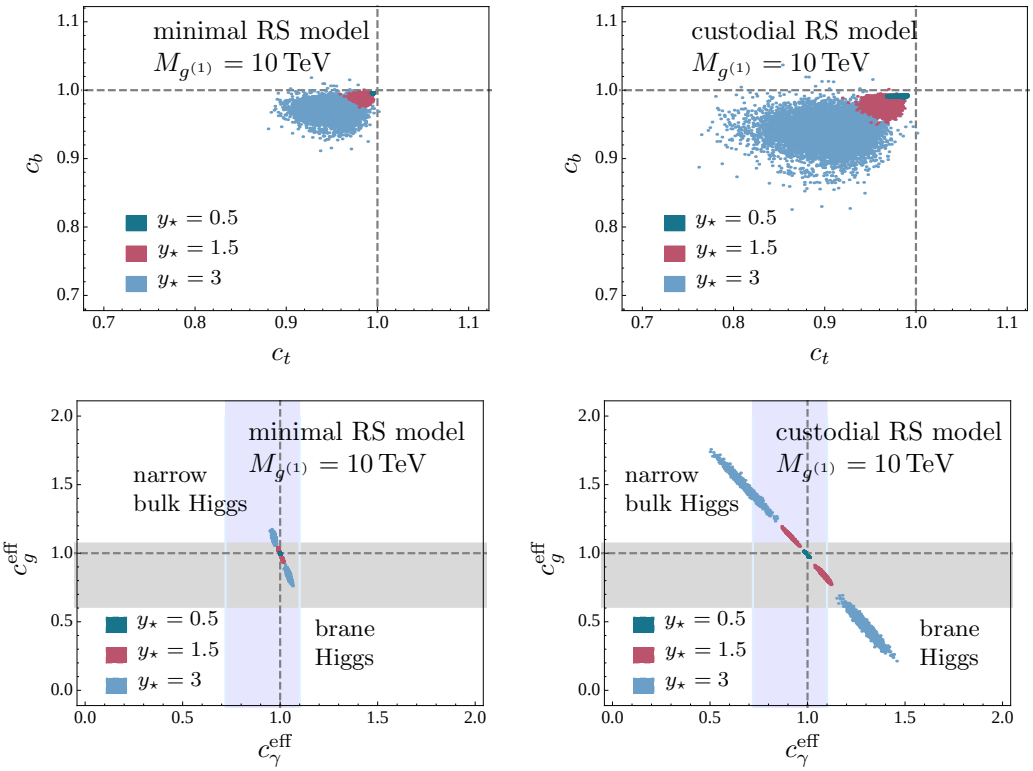

Figure 4.8: Correlation between the Higgs couplings c_t and c_b (upper row) and the effective Higgs couplings c_γ^{eff} and c_g^{eff} (lower row) in the minimal and custodial RS models for $M_{g^{(1)}} = 10\,\text{TeV}$ and different values of $y_\star$. In the lower plots, the blue and gray bands denote the fit results for the corresponding Higgs couplings within 2σ errors, see Table 4.2 for details. The crossing of the dashed lines denotes the SM prediction.

Total Higgs width

The correction to the total Higgs width relative to the SM total width $\Gamma_h^{\text{SM}} = 4.10\,\text{MeV}$ (for $m_h = 125.09\,\text{GeV}$) can be accounted for by the parameter [233]

$$\begin{aligned} c_h = \frac{\Gamma_h^{\text{RS}}}{\Gamma_h^{\text{SM}}} \approx 0.57(c_b^2 + c_{b5}^2) + 0.22 c_W^2 + 0.03 c_Z^2 + 0.09\big(|c_g^{\text{eff}}|^2 + |c_{g5}^{\text{eff}}|^2\big) \\ + 0.06(c_\tau^2 + c_{\tau 5}^2) + 0.03\,. \end{aligned} \tag{4.149}$$

The corrections to the decay modes $h \to c\bar{c}, Z\gamma, \ldots$ have a numerically insignificant effect and can therefore be neglected; the combined branching fraction of these modes is about 3% in the SM. Figure 4.9 shows the ratio $c_h = \Gamma_h^{\text{RS}}/\Gamma_h^{\text{SM}}$ in the minimal and custodial RS model. We see that in the brane-Higgs scenario the Higgs width can be reduced by about 15–30% (25–50%) for a KK gluon mass $M_{g^{(1)}} \approx 5\,\text{TeV}$ and maximal Yukawa value $y_\star = 3$ in the minimal (custodial) RS model. The dominant effects come from the decays $h \to b\bar{b}$ and $h \to gg$, both of which receive negative corrections. The situation is different in the case of the narrow bulk-Higgs scenario, where the $h \to gg$ decay rate receives a large positive correction, which enhances the Higgs width and counteracts the suppression of the $h \to b\bar{b}$ decay rate. In the custodial RS model this effect dominates for $y_\star \gtrsim 1.5$, leading to a Higgs width larger than in the SM.

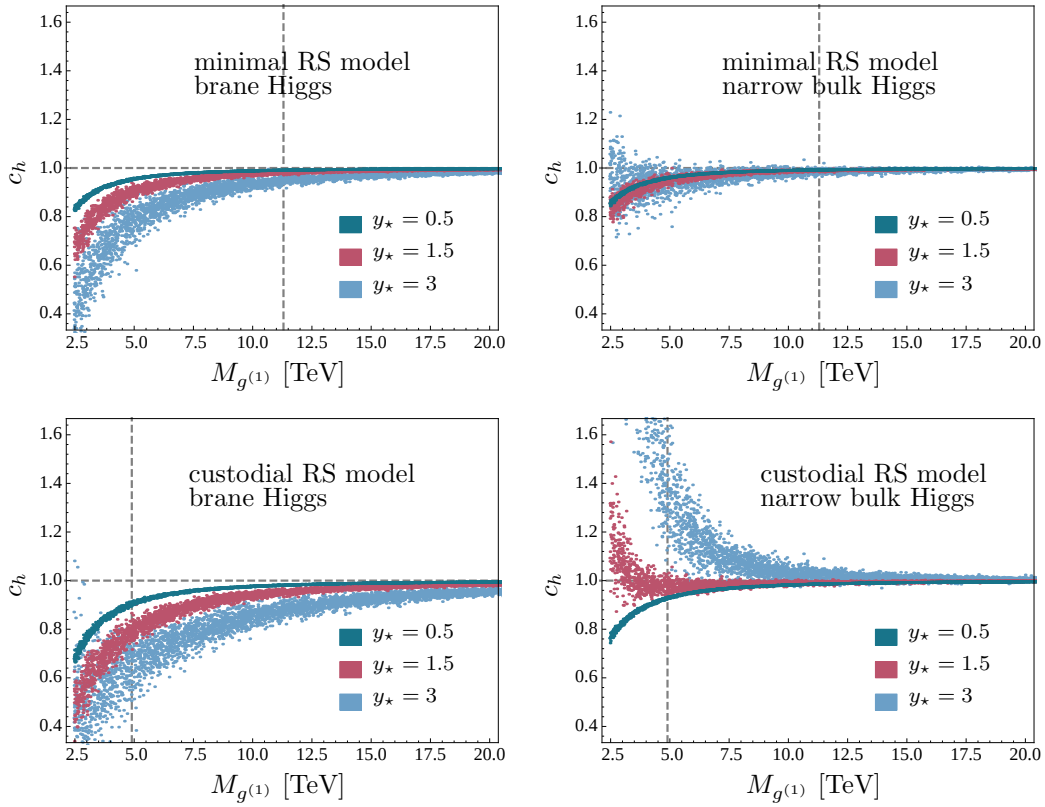

Figure 4.9: Predictions for $c_h = \Gamma_h^{\rm RS}/\Gamma_h^{\rm SM}$ as a function of $M_{g^{(1)}}$ in the minimal (top) and custodial (bottom) RS model, for the cases of a brane-localized (left) and a narrow bulk-Higgs field (right). Vertical dashed lines show the lower bounds from a tree-level analysis of the Peskin-Takeuchi parameters.

Summary of exclusion bounds for $M_{g^{(1)}}$

In the last part of this section, we constrain the parameter space of the various RS models by current and future analyses of Higgs couplings. Our goal is to derive exclusion bounds for the mass of the first KK gluon resonance from each of the Higgs couplings. To obtain these bounds, we plot each coupling c_i as in Figure 4.7, fit a Gaussian distribution to the model points for each pair of $y_\star$ and $M_{g^{(1)}}$, and determine the mean values c_i with the standard deviations $\sigma(c_i)$. The experimental Higgs couplings $c_i^{\rm exp}$ and their 1σ uncertainties $\sigma(c_i^{\rm exp})$ are taken from Table 4.2. We then consider the ratio $c_i/c_i^{\rm exp}$ and calculate the corresponding standard deviation by combining the theoretical and experimental errors in quadrature.[17] Finally, we test at which confidence level the coefficient $c_i/c_i^{\rm exp}$ is compatible with 1. The results are compiled in Figure 4.10 for $y_\star = 3$. The colored regions are the 95% CL excluded regions for the mass of the lightest KK gluon resonance. The only exception is the exclusion limit for c_t in the upper two plots which is given at 99% CL. To obtain exclusion bounds for arbitrary values of $y_\star$, one can make use of the fact that the exclusion limits depend linearly on $y_\star$ to good approximation (except for c_W and c_Z).

[17] The standard deviation for the ratio $c_i/c_i^{\rm exp}$ is calculated via

$$\sigma(c_i/c_i^{\rm exp}) = \frac{c_i}{c_i^{\rm exp}}\sqrt{\left(\frac{\sigma(c_i)}{c_i}\right)^2 + \left(\frac{\sigma(c_i^{\rm exp})}{c_i^{\rm exp}}\right)^2}\,. \tag{4.150}$$

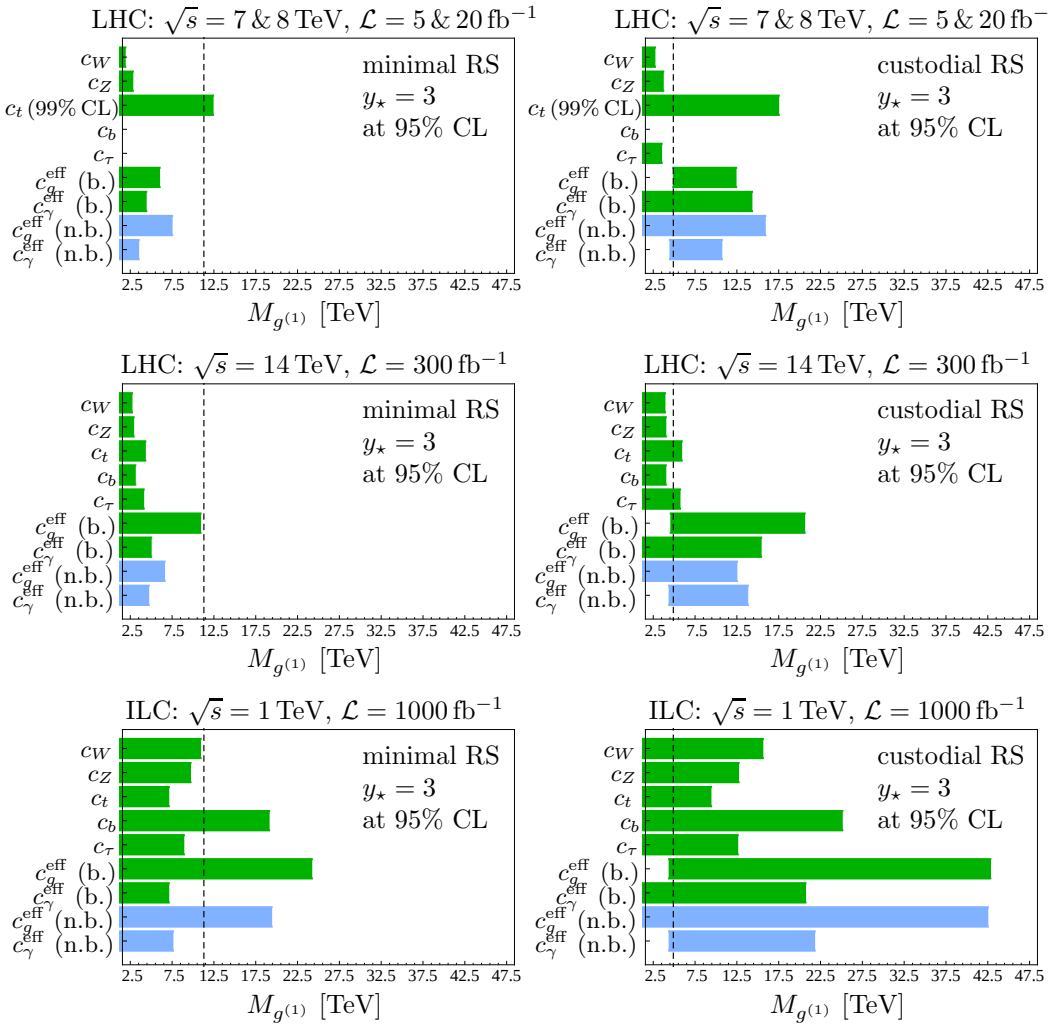

Figure 4.10: Summary of the exclusion limits at 95% CL on the mass of the first KK gluon resonance in the minimal (left) and custodial (right) RS model for the maximal Yukawa value $y_\star = 3$. The exclusion limits have been derived by comparing the RS predictions with fit results of the Higgs couplings at the LHC (top), high-luminosity LHC (middle) and the ILC (bottom), that can be found in Table 4.2. Note that the bounds obtained from c_t in the upper two plots are given at 99% CL. For the loop-induced couplings c_g^{eff} and c_γ^{eff}, we distinguish between the brane (green) and the narrow bulk-Higgs (blue) scenarios. The dashed vertical lines show the lower bounds on $M_{g^{(1)}}$ obtained from a tree-level analysis of the Peskin-Takeuchi parameters.

We observe that the measured Higgs coupling to top quarks from current LHC data $c_t = 1.42^{+0.23}_{-0.22}$ [219] imposes a strong constraint on the first KK gluon mass, since the RS predictions for c_t are always reduced with respect to the SM value $c_t^{\text{SM}} = 1$. As a consequence KK gluon masses in the range $M_{g^{(1)}} < 12\,\text{TeV} \times (y_\star/3)$ in the minimal and $M_{g^{(1)}} < 18\,\text{TeV} \times (y_\star/3)$ in the custodial RS model are excluded at 99% CL. For $y_* = 3$, the bounds are already stronger than those obtained from a tree-level analysis of the Peskin-Takeuchi parameters, even in the minimal RS model. Apart from c_t, in general the strongest bounds emerge from the loop-induced Higgs couplings, for which we distinguish between the brane-Higgs (b.) and narrow bulk-Higgs (n.b.) scenarios. The middle and bottom rows of Figure 4.10 show the exclusion bounds for the case of SM-like Higgs couplings at future experiments. Concerning the high-luminosity run at the

	R_{bb}	$R_{\tau\tau}$	R_{WW}	R_{ZZ}	$R_{\gamma\gamma}$
ATLAS	$0.52^{+0.40}_{-0.40}$ [234]	$1.43^{+0.43}_{-0.37}$ [235]	$1.16^{+0.24}_{-0.21}$ [236]	$1.44^{+0.40}_{-0.33}$ [237]	$1.17^{+0.27}_{-0.27}$ [238]
CMS	$1.03^{+0.44}_{-0.42}$ [239]	$0.78^{+0.27}_{-0.27}$ [240]	$0.72^{+0.20}_{-0.18}$ [241]	$0.93^{+0.29}_{-0.25}$ [242]	$1.14^{+0.26}_{-0.23}$ [243]
Average	$0.76^{+0.30}_{-0.29}$	$0.98^{+0.23}_{-0.22}$	$0.90^{+0.15}_{-0.14}$	$1.11^{+0.23}_{-0.20}$	$1.15^{+0.19}_{-0.18}$

Table 4.4: Experimental values for the individual signal rates measured by the ATLAS and CMS collaborations including the 1σ errors. The assumed Higgs masses are $m_h = 125\,\text{GeV}$ [239, 240, 243], $m_h = 125.36\,\text{GeV}$ in [234–237], $m_h = 125.4\,\text{GeV}$ [238] and $m_h = 125.6\,\text{GeV}$ [241, 242]. The last row contains the weighted averages of the signal rates with 1σ errors, which were obtained by combining the experimental errors in quadrature.

LHC one can probe or exclude KK gluon masses in the range $M_{g^{(1)}} < 11\,\text{TeV} \times (y_\star/3)$ ($M_{g^{(1)}} < 7\,\text{TeV} \times (y_\star/3)$) in the minimal RS model and $M_{g^{(1)}} < 21\,\text{TeV} \times (y_\star/3)$ ($M_{g^{(1)}} < 13\,\text{TeV} \times (y_\star/3)$) in the custodial RS model with a brane (narrow bulk) Higgs, both at 95% CL. For the ILC, one expects to probe or rule out KK gluon masses in the range $M_{g^{(1)}} < 24\,\text{TeV} \times (y_\star/3)$ ($M_{g^{(1)}} < 19\,\text{TeV} \times (y_\star/3)$) in the minimal and $M_{g^{(1)}} < 43\,\text{TeV} \times (y_\star/3)$ ($M_{g^{(1)}} < 42\,\text{TeV} \times (y_\star/3)$) in the custodial model for a brane (narrow bulk) Higgs. Independently of the realization of the Yukawa sector (and hence the parameter $y_\star$), the analysis of the Higgs couplings to W bosons at the ILC is expected to be sensitive to KK gluon masses of up to 11 TeV (16 TeV) in the minimal (custodial) RS model.

4.4.3 Numerical analysis of signal rates

We finally investigate the Higgs decay rates into pairs of electroweak gauge bosons and third-generation fermions. In order to directly compare our predictions with experimental measurements, we study the signal rates R_X defined in (4.131), which can be expressed in terms of the effective couplings c_i and c_{i5} derived in Section 4.4.1 via

$$R_X \equiv \frac{(\sigma \cdot \text{BR})(pp \to h \to X)_{\text{RS}}}{(\sigma \cdot \text{BR})(pp \to h \to X)_{\text{SM}}} = \frac{\left[\left(|c_g^{\text{eff}}|^2 + |c_{g5}^{\text{eff}}|^2\right) f_{\text{GF}} + c_V^2 f_{\text{VBF}}\right]\left[|c_X^{(\text{eff})}|^2 + |c_{X5}^{(\text{eff})}|^2\right]}{c_h}\,. \tag{4.151}$$

We take into account the probabilities to produce a Higgs boson via gluon fusion (GF), or via vector-boson fusion and associated hV production (collectively referred to as VBF). Concerning the latter production processes, we have implemented the findings of Section 4.3.3, showing that the leading corrections (proportional to L) to the corresponding cross sections are given by c_V^2, where in the custodial RS model there is no need to distinguish between c_W and c_Z as far as these terms are concerned, see (4.123). In case of the minimal RS model we will approximately use c_W which is sufficiently accurate for our purpose. Other production channels such as $pp \to ht\bar{t}$ can be neglected to very good approximation. For inclusive Higgs production at the LHC the appropriate fractions are $f_{\text{GF}} \approx 0.9$ and $f_{\text{VBF}} \approx 0.1$. For the case of the final state $X = b\bar{b}$, Higgs-strahlung is an experimentally more feasible Higgs-production channel at the LHC than gluon fusion, since the latter suffers from an overwhelming QCD background [244]. For the case of the signal rate R_{bb} we thus have to set $f_{\text{GF}} = 0$ and $f_{\text{VBF}} = 1$ in (4.151). A further comment concerns the Higgs decays into WW^* and ZZ^*, with subsequent decays of the off-shell vector boson into fermions. According to the discussion in Section 4.3.1, we use the expression for $\Gamma(h \to VV^*)/\Gamma(h \to VV^*)_{\text{SM}}$ derived from (4.115) instead of c_V^2 in this case.

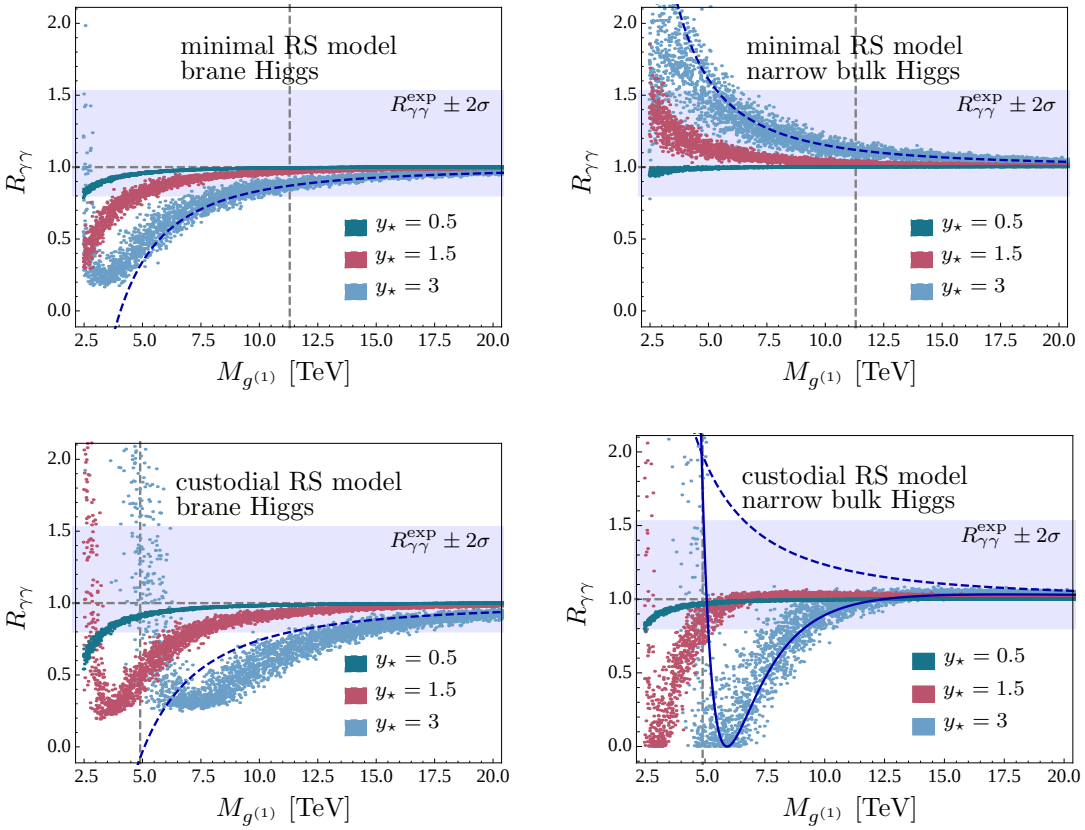

Figure 4.11: Predictions for the ratio $R_{\gamma\gamma}$ as a function of the lightest KK gluon mass $M_{g^{(1)}}$ and for three different values of the parameter $y_\star$ in the minimal (top) and custodial (bottom) RS model, for the cases of a brane-localized Higgs boson (left) and a narrow bulk-Higgs field (right). The dashed curves in blue show the approximations (4.152) and (4.153) for $y_\star = 3$. The blue band represents the 2σ experimental error for the averaged signal rate $R_{\gamma\gamma}$ in Table 4.4. Vertical dashed lines denote the lower bounds from a tree-level analysis of the Peskin-Takeuchi parameters.

Analysis of the signal rate $R_{\gamma\gamma}$

We start our analysis with a discussion of Higgs decays into two photons. Figure 4.11 shows our predictions for $R_{\gamma\gamma}$ obtained in the minimal and custodial RS model with a brane-localized Higgs sector and a narrow bulk-Higgs state, as a function of the mass of the lightest KK gluon state and for three different values for $y_\star$. The latest experimental values for $R_{\gamma\gamma}$ reported by the ATLAS and CMS collaborations, see Table 4.4, can be averaged to $R_{\gamma\gamma} = 1.15^{+0.19}_{-0.18}$. The 2σ-error band corresponding to this result is shown by the blue band in the four plots. Model points falling outside these bands are excluded at 95% CL.

Let us understand the shape of the various bands of scatter points shown in the plots, beginning with the minimal RS model. For not too small Yukawa couplings, the largest RS corrections are those arising from fermionic loop contributions. In the brane-localized Higgs (narrow bulk-Higgs) scenario, they suppress (enhance) the gluon-fusion cross section and enhance (suppress) the decay rate into photons. Since the dominant SM contribution to $h \to \gamma\gamma$ involves W-boson loops and acts in the opposite direction as the fermionic contributions, the RS corrections to the Higgs production cross section dominate over those to the decay rate. Hence, we find a suppression (an enhancement)

of $R_{\gamma\gamma}$ in the brane-Higgs (narrow bulk-Higgs) scenario. To see this more explicitly, it is instructive to expand the various expressions in (4.151) to first order in $v^2/M_{\rm KK}^2$ and to approximate $A_q(\tau_t) \approx 1$ and $A_q(\tau_b) \approx 0$. Keeping the dependence on $A_W(\tau_W) \approx 1.19$ explicit, we obtain

$$\begin{aligned} R_{\gamma\gamma}\big|_{\rm min} &\approx 1 + \frac{v^2}{2M_{\rm KK}^2}\left[\left(f_{\rm GF} - \frac{4}{3|C_\gamma^{\rm SM}|}\right)\left(\mp 18 - \frac{10}{3}\right) y_\star^2 \right. \\ &\quad - \left(f_{\rm VBF} + \frac{21\big[A_W(\tau_W)-1\big]}{4|C_\gamma^{\rm SM}|}\right)\frac{2m_W^2}{v^2}\left(L - 1 + \frac{1}{2L}\right) - \frac{Lm_W^2}{v^2} \\ &\quad \left. + 0.57\,\frac{10}{3}\,y_\star^2 + 0.22\,\frac{2m_W^2}{v^2}\left(L - 1 + \frac{1}{2L}\right) - 0.09\left(\mp 18 - \frac{10}{3}\right) y_\star^2\right] \\ &\approx 1 - \frac{v^2}{2M_{\rm KK}^2}\big[(\pm 9.7 - 0.1)\,y_\star^2 + 4.1\big]\,, \end{aligned} \tag{4.152}$$

where the first two lines contain the corrections to the production and decay rates, with corrections to the $h \to \gamma\gamma$ rate being accompanied by a factor of $1/|C_\gamma^{\rm SM}|$ with $C_\gamma^{\rm SM} \approx \frac{4}{3} - \frac{21}{4}A_W(\tau_W) \approx -4.9$. The third line shows the corrections to the total Higgs width, as parameterized by c_h in (4.149). The upper sign holds for the brane-localized Higgs scenario, while the lower sign corresponds to the narrow bulk-Higgs case. Above we have used equations (4.136) and (4.139) for a large set of random complex matrices on average. We explicitly see from the first term on the right-hand side of (4.152) that the fermionic contributions to the $gg \to h$ production process dominate over those to the $h \to \gamma\gamma$ decay rate and come with opposite sign. Altogether, we find the last line in (4.152) which is shown, for the case where $y_* = 3$, by the dashed (blue) lines in the figure. Note also that due to the contribution of the VBF production process the observable $R_{\gamma\gamma}$ is bounded from below in the brane-Higgs case. This explains the behavior for very small $M_{g^{(1)}}$ values seen in the upper left plot in Figure 4.11. For $y_* = 3$, the $gg \to h$ production cross section vanishes for $M_{g^{(1)}} \approx 3.5\,\text{TeV}$, because the new-physics contribution cancels the SM amplitude. However, due to the VBF production process a non-zero value of $R_{\gamma\gamma}$ remains.

The corresponding effects on the quantity $R_{\gamma\gamma}$ arising in the RS model with custodial symmetry, implementing the minimal lepton sector shown in (4.96), are studied in the lower two plots of Figure 4.11. In analogy with (4.152), we can expand the result in powers of $v^2/M_{\rm KK}^2$, exploiting the anarchy of the 5D Yukawa matrices and making the same approximations as above. For the model with the minimal lepton sector this yields

$$\begin{aligned} R_{\gamma\gamma}\big|_{\rm cust} &\approx 1 + \frac{v^2}{2M_{\rm KK}^2}\left[\mp\left(72 f_{\rm GF} - \frac{213}{|C_\gamma^{\rm SM}|}\right) y_\star^2 - \frac{20}{3}\left(f_{\rm GF} - \frac{4}{3|C_\gamma^{\rm SM}|}\right) y_\star^2 \right. \\ &\quad - \left(f_{\rm VBF} + \frac{21\big[A_W(\tau_W)-1\big]}{4|C_\gamma^{\rm SM}|}\right)\frac{2m_W^2}{v^2}\left(2L - 1 + \frac{1}{2L}\right) - \frac{2Lm_W^2}{v^2} \\ &\quad \left. + 0.57\,\frac{20}{3}\,y_\star^2 + 0.22\,\frac{2m_W^2}{v^2}\left(2L - 1 + \frac{1}{2L}\right) - 0.09\left(\mp 72 - \frac{20}{3}\right) y_\star^2\right] \\ &\approx 1 - \frac{v^2}{2M_{\rm KK}^2}\big[(\pm 15.0 - 0.2)\,y_\star^2 + 8.3\big]\,. \end{aligned} \tag{4.153}$$

If instead the extended lepton sector shown in (4.94) is employed, then the coefficient 213 inside the parenthesis in the first term must be replaced by 240. Note that the individual

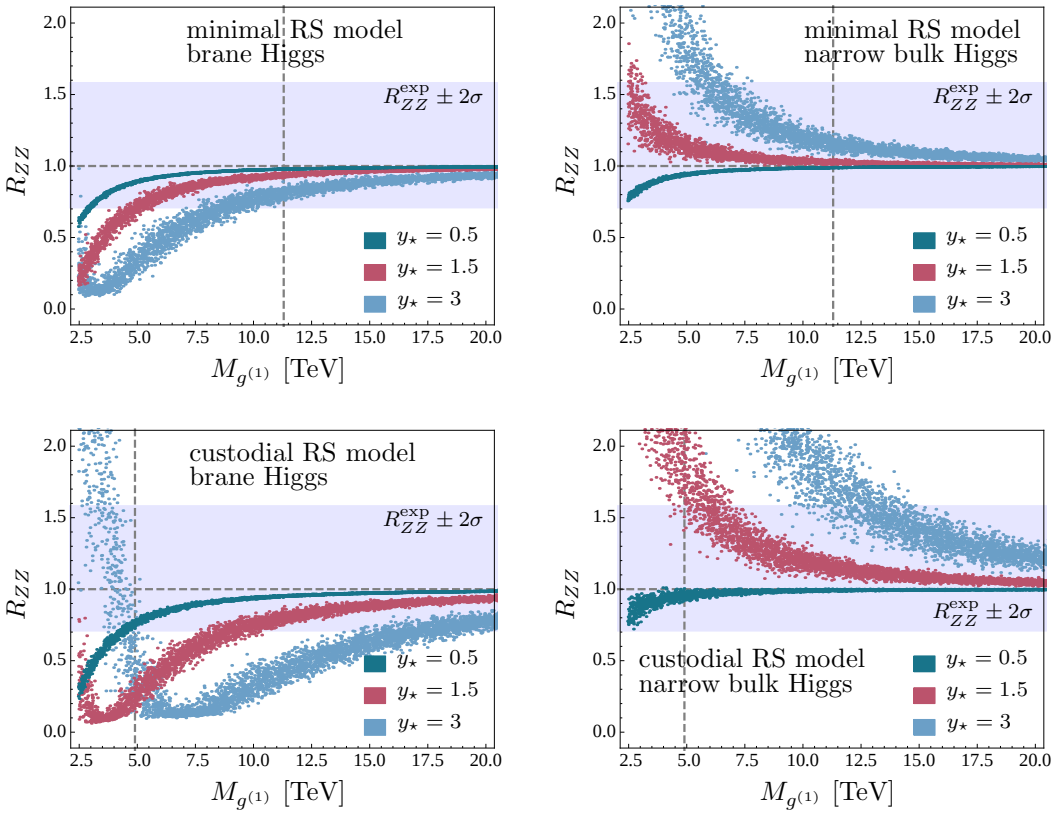

Figure 4.12: Predictions for the ratio R_{ZZ} as a function of the KK gluon mass $M_{g^{(1)}}$ in the minimal (top) and custodial (bottom) RS model, for the cases of a brane-localized Higgs boson (left) and a narrow bulk-Higgs field (right). The scatter points with different color correspond to different values of $y_\star$. The blue band represents the 2σ experimental error range for the observable R_{ZZ}, see Table 4.4.

corrections due to fermion loops are huge, however significant cancellations take place when one adds the corrections to the $gg \to h$ and $h \to \gamma\gamma$ rates. Altogether, we obtain for the model with the minimal lepton sector the last line in (4.153). In the model with the extended lepton sector the coefficient ± 15.0 in the first term must be replaced by ± 9.5. We observe that in linearized form the corrections are only moderately larger than in the minimal model. Once again, for $y_* = 3$ this result is shown by the dashed lines in the lower plots of Figure 4.11, where we show results for the custodial model with the minimal lepton sector. If instead the model with an extended lepton sector is considered, the distribution of scatter points looks very similar. For the brane-localized Higgs scenario, the scatter points show a similar behavior as in the minimal model, but the new-physics effects are slightly larger. For $y_* = 1.5$ and 3, the $gg \to h$ production cross section vanishes near $M_{g^{(1)}} \approx 3.5\,\text{TeV}$ and 7 TeV, respectively, and the VBF process remains as the only production mechanism. This explains the minimum values for $R_{\gamma\gamma}$ at these points. For even smaller masses the ratio $R_{\gamma\gamma}$ increases and can even exceed 1. In the narrow bulk-Higgs case, on the other hand, the linearized approximation (4.153) breaks down for large values y_*, as is evident from the discrepancy between the dashed curve and the blue band of scatter points. A reasonable approximation, shown by the solid line, is obtained by linearizing the expressions for the various c_i parameters but not further expanding expression (4.151). It turns out that the negative corrections to the $h \to \gamma\gamma$ decay rate are so significant in this model that they compensate the large

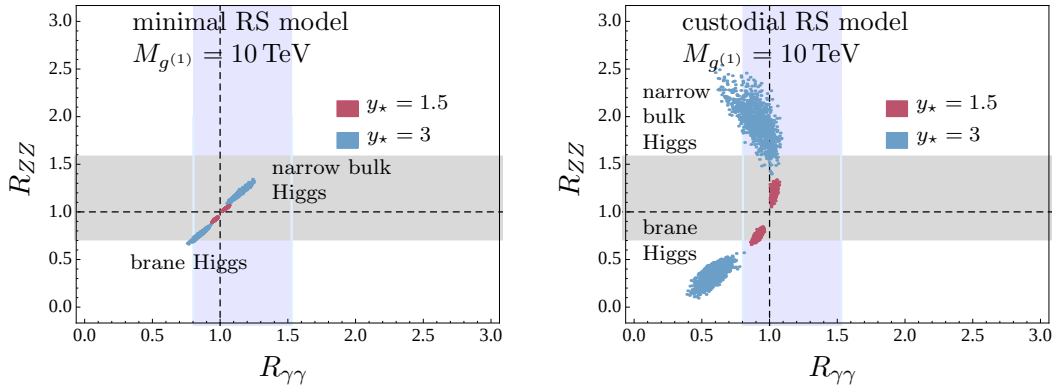

Figure 4.13: Correlation of the predictions for the signal rates R_{ZZ} and $R_{\gamma\gamma}$ in the minimal (left) and custodial (right) RS model for $M_{g^{(1)}} = 10\,\text{TeV}$ and different values of $y_\star$. The gray and blue bands denote the 2σ errors of the experimental signal rates given in Table 4.4.

positive corrections to the gluon-fusion rate in the region of large $M_{g^{(1)}}$. For smaller KK masses, these negative corrections become dominant and drive the ratio $R_{\gamma\gamma}$ toward values significantly less than 1. Eventually, for $M_{g^{(1)}} \approx 3\,\text{TeV}$ (for $y_* = 1.5$) and 5.5 TeV (for $y_* = 3$), the diphoton decay rate even vanishes. It is obvious that in regions of parameter space where such dramatic cancellations occur our predictions are highly model dependent.

Analysis of the signal rates R_{ZZ} and R_{WW}

Figure 4.12 shows the results for the ratio R_{ZZ}. In the custodial RS model the scatter points also represent to excellent approximation the results for the observable R_{WW}, since at the level of the L-enhanced terms the Higgs decays into ZZ^* and WW^* are expressed by the same modification factor $c_Z^2 \approx c_W^2$, see (4.115) and (4.123). In case of the minimal RS model the observable R_{WW} is slightly enhanced compared to R_{ZZ}, since to good approximation $R_{WW} \approx R_{ZZ} \times (c_W/c_Z)^2$ with $(c_W/c_Z)^2 \approx 1 + L(m_Z^2 - m_W^2)/M_{\text{KK}}^2$. Since the shape of the scatter points is only slightly affected we do not show plots for R_{WW}. The blue bands in Figure 4.12 represent the 2σ-error range corresponding to the latest experimental values for R_{ZZ} given in Table 4.4, where the naively averaged value has been used. Alternatively we could have used the average experimental value for the ratio R_{WW}, in which case the excluded set of model points is a different one. It is interesting to observe that for relatively large values for $y_\star$ the data already disfavor KK gluon masses in the low TeV range. The tension between the theoretical predictions for R_{ZZ} (R_{WW}) and the experimental data are stronger for the brane-Higgs (narrow bulk-Higgs) model due to the mild tendency of an enhanced (suppressed) cross section seen in the data, $R_{ZZ} = 1.11^{+0.23}_{-0.20}$ ($R_{WW} = 0.90^{+0.15}_{-0.14}$), which is in conflict with the suppression (enhancement) of the predicted cross section.

The shapes of the curves can be explained by the fact that, for not too small Yukawa couplings, the RS corrections to the gluon-fusion cross section by far dominate over the corrections to the Higgs decay rates. The dependence of this production channel on the details of the localization of the Higgs profile on or near the IR brane explains why the ratios R_{VV} are suppressed (enhanced) in the brane-localized (narrow bulk-Higgs) scenario. For small values of $M_{g^{(1)}}$ and $y_\star$, however, the loop-induced couplings become subdominant, and the negative corrections to the $h \to ZZ^*$ decay width give rise to a

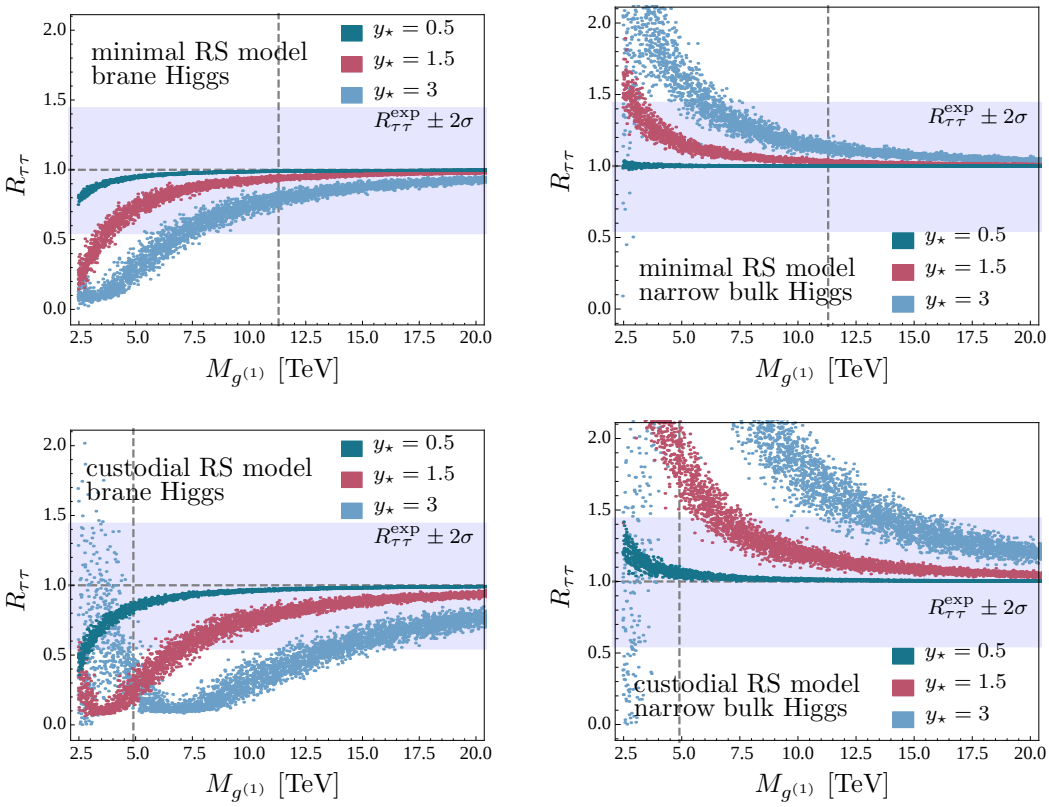

Figure 4.14: Predictions for the ratios $R_{\tau\tau}$ as a function of the KK gluon mass $M_{g^{(1)}}$ in the minimal (upper plots) and custodial (lower plots) RS model, for the cases of a brane-localized Higgs boson (left plots) and a narrow bulk-Higgs field (right plots). The blue band shows the 2σ-error margin of the averaged experimental value $R_{\tau\tau}$ in Table 4.4.

reduction of the signal rate even in the narrow bulk-Higgs scenario. The peculiar behavior seen for very small KK scales in the lower left plot in Figure 4.12 can be understood as follows. For $y_\star = 3$, the $gg \to h$ production cross section vanishes for $M_{g^{(1)}} \approx 7.0\,\text{TeV}$, because the new-physics contribution cancels the SM amplitude. However, due to the vector-boson fusion production process a non-zero value of R_{ZZ} remains. For even smaller values of $M_{g^{(1)}}$ the new-physics amplitude dominates over the SM one and the cross section rises again.

Correlation between $R_{\gamma\gamma}$ and R_{ZZ}

The new-physics effects on the signal rates R_{ZZ} and R_{WW} are stronger than those on $R_{\gamma\gamma}$, since in the latter case there is a partial compensation between the contributions of fermionic KK resonances to the Higgs production cross section via gluon fusion and to the $h \to \gamma\gamma$ decay rate (this effect is more pronounced in the custodial RS model). The strong correlation between R_{ZZ} and $R_{\gamma\gamma}$ resulting from these fermionic corrections is examined in Figure 4.13, for RS points with fixed value $M_{g^{(1)}} = 10\,\text{TeV}$. The SM predicts the values $R_{ZZ}^{\rm SM} = R_{\gamma\gamma}^{\rm SM} = 1$ denoted by the crossing position of the dashed lines. Scatter points below the horizontal dashed line belong to the brane-localized Higgs scenario, while the points above the line belong to the narrow bulk-Higgs scenario. We only show scatter points for $y_\star = 1.5$ and 3. For $y_\star = 0.5$, both R_{ZZ} and $R_{\gamma\gamma}$ are always reduced, see Figure 4.11 and Figure 4.12. Notice that the naively averaged current experimental data slightly favor the narrow bulk-Higgs over the brane-localized Higgs scenario.

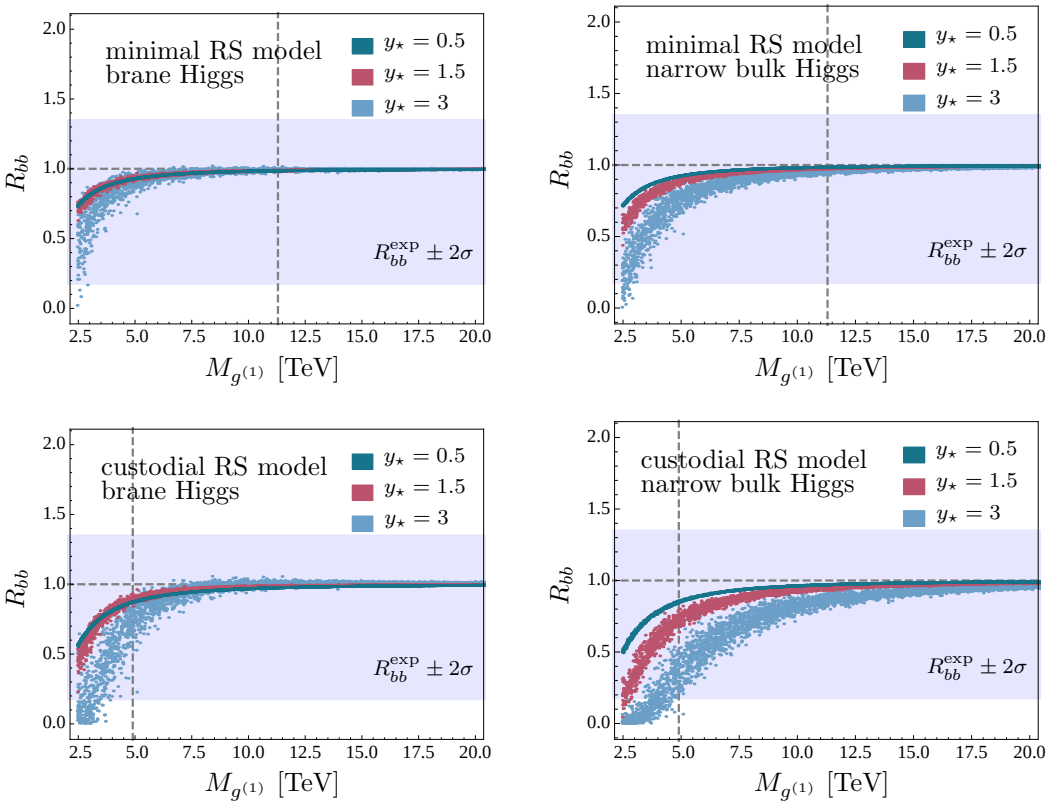

Figure 4.15: Predictions for the ratio R_{bb} as a function of the KK gluon mass $M_{g^{(1)}}$ in the minimal (upper plots) and custodial (lower plots) RS model, for the cases of a brane-localized Higgs boson (left plots) and a narrow bulk-Higgs field (right plots). Blue bands denote the 2σ error of the experimental signal rate R_{bb} given in Table 4.4.

Analysis of the signal rates $R_{\tau\tau}$ and R_{bb}

We now turn to the predictions for $R_{\tau\tau}$ and R_{bb} in the minimal and custodial RS model. The plots in Figure 4.14 show the observable $R_{\tau\tau}$ as a function of $M_{g^{(1)}}$. As in the previous cases, the shapes of the curves are largely due to the behavior of the Higgs-boson production cross section, which is dominated by the gluon-fusion process. Particularly for small KK scales, these effects are quite large and have the potential to compensate and even exceed the SM contribution. For very small KK scales ($M_{g^{(1)}} \lesssim 3\,\text{TeV}$), on the other hand, the negative corrections to the c_τ coupling can become so large that the $h \to \tau^+\tau^-$ decay rate almost vanishes (see Figure 4.6), and hence $R_{\tau\tau}$ can drop close to zero. The observable R_{bb}, shown in Figure 4.15, receives more moderate corrections, since in this case the only production channel included is Higgs-strahlung. Although there is no need to distinguish between the brane-localized and narrow bulk-Higgs scenario in the Higgs production cross section and the $h \to b\bar{b}$ decay rate, the plots on the left and right still differ due to the contribution of the $h \to gg$ decay rate to the total Higgs width. This partial rate is reduced in the brane-Higgs scenario and enhanced in bulk-Higgs models. The present data on R_{bb} only imply weak constraints on the RS parameter space, because the experimental accuracy is worse than for all other channels, see Table 4.4. Nevertheless, the Higgs coupling to bottom quarks c_b is an important quantity, since it gives rise to one of the most significant corrections to the total Higgs width (4.149), which enters all of the signal rates in (4.151).

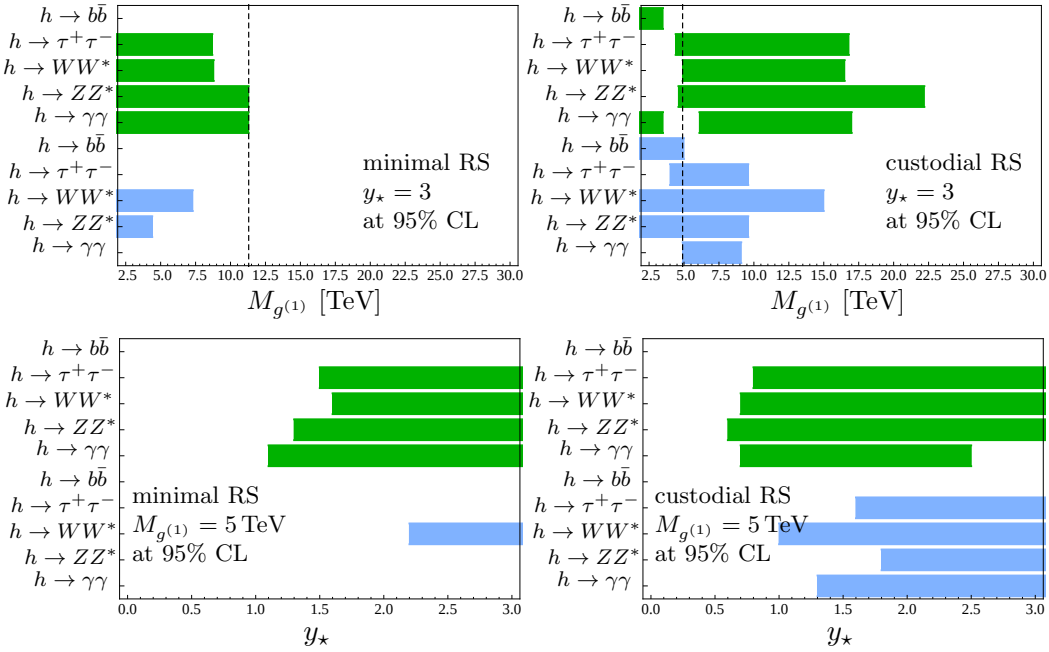

Figure 4.16: Summary of the exclusion bounds on the mass of the lightest KK gluon (top) and the parameter $y_\star$ (bottom) in the minimal (left) and custodial (right) RS model for the brane-localized (green) and narrow bulk-Higgs scenario (blue). The shaded regions are excluded at 95% CL for each corresponding decay channel. The vertical dashed lines in the upper plots show the lower bounds obtained from a tree-level analysis of the Peskin-Takeuchi parameters.

Summary of exclusion bounds for $M_{g^{(1)}}$ and $y_\star$

Even at the present level of precision, the existing measurements of the signal rates for the various Higgs-boson decays provide strong constraints on the parameter space of the RS models under consideration. In Figure 4.16 we show the exclusion limits obtained at 95% CL on the mass of the first KK gluon resonance and the maximum value $y_\star$ of the elements of the anarchic 5D Yukawa matrices in the minimal and custodial RS model, derived by an analysis of the various decay rates using the latest experimental results shown in Table 4.4. To obtain these limits, we have fitted a Gaussian distribution to the model points for each pair of $M_{g^{(1)}}$ and $y_\star$, and determined the mean values R_X and the standard deviations $\sigma(R_X)$ for these parameters, in analogy with our treatment of the (effective) Higgs couplings in Section 4.4.1. We have then calculated the ratios $R_X/R_X^{\rm exp}$, combined the theoretical and experimental errors in quadrature, and tested at which confidence levels these ratios are compatible with 1. The green (blue) bars in the figure refer to the brane-localized (narrow bulk-Higgs) RS scenario. The most stringent bounds emerge from the signal rates for $pp \to h \to ZZ^*\,(\gamma\gamma)$ in the brane-localized Higgs scenario and for $pp \to h \to WW^*$ in the narrow bulk-Higgs scenario. Taking the most stringent bounds from the upper plots in Figure 4.16, which have been obtained for $y_\star = 3$, we can derive lower bounds on the mass of the first KK gluon resonance (at 95% CL)

$$\begin{aligned} M_{g^{(1)}}\big|^{\text{minimal RS}}_{\text{brane Higgs}} &\geq 11.3\,\text{TeV}\,, & M_{g^{(1)}}\big|^{\text{minimal RS}}_{\text{narrow bulk Higgs}} &\geq 7.3\,\text{TeV}\,, \\ M_{g^{(1)}}\big|^{\text{custodial RS}}_{\text{brane Higgs}} &\geq 22.2\,\text{TeV}\,, & M_{g^{(1)}}\big|^{\text{custodial RS}}_{\text{narrow bulk Higgs}} &\geq 15.0\,\text{TeV}\,. \end{aligned} \tag{4.154}$$

We obtain much stronger bounds for a brane than for a narrow bulk Higgs. Furthermore, in the custodial RS model the bounds derived from Higgs physics are much stronger than those stemming from the Peskin-Takeuchi parameters. While the custodial symmetry can tame the large tree-level effects on the T parameter in RS models, we find very large contributions to loop-induced processes in the Higgs sector. Thus, from a phenomenological point of view there is not much gained by implementing the custodial protection mechanism. A possible way out would be to lower the value of $y_\star$. The lower plots in Figure 4.16 summarize the exclusion regions on $y_\star$ obtained for a lightest KK gluon mass of $M_{g^{(1)}} = 5\,\text{TeV}$. The analysis has been restricted to values for $y_\star$ below the perturbativity bound $y_\star \leq y_{\max} \approx 3$. The most stringent bounds for $M_{g^{(1)}} = 5\,\text{TeV}$ come from the processes $pp \to h \to ZZ^*, WW^*, \gamma\gamma$ and can be combined to give the constraints (at 95% CL)

$$\begin{aligned} y_\star\big|^{\text{minimal RS}}_{\text{brane Higgs}} &\leq 1.1\,, & y_\star\big|^{\text{minimal RS}}_{\text{narrow bulk Higgs}} &\leq 2.2\,, \\ y_\star\big|^{\text{custodial RS}}_{\text{brane Higgs}} &\leq 0.6\,, & y_\star\big|^{\text{custodial RS}}_{\text{narrow bulk Higgs}} &\leq 1.0\,. \end{aligned} \tag{4.155}$$

We see that in particular in the brane-Higgs scenario small values are preferred. However, too small Yukawa couplings would give rise to enhanced corrections to ϵ_K [144] and hence they would reintroduce the RS flavor problem. Also for $y_\star$ significantly smaller than 1 it becomes difficult to reproduce the physical value for the top-quark mass.

5 The $b \to s\gamma$ transition in a warped 5D space-time

In the last chapter we will investigate the flavor-changing neutral current $b \to s\gamma$ in the minimal Randall-Sundrum model with a brane-localized Higgs sector. This transition is interesting in order to search for new physics, since it is one-loop and GIM suppressed in the Standard Model.

The first discussions on $b \to s\gamma$ in the context of RS models can be found in [142, 143, 245]. In these works, the authors showed that the penguin diagrams with the exchange of charged Higgs scalars (NGBs of the $W^{\pm}$ boson) along with KK fermions give the dominant contribution to the dipole coefficients. Furthermore, the authors claimed that the dipole coefficients in the brane-localized Higgs scenario are logarithmically divergent and sensitive to the UV cutoff. Later, it was shown in [198] that the diagrams contributing to the leptonic decay $\mu \to e\gamma$ at one-loop are indeed finite. With the same technique the authors of [246] investigated the process $b \to s\gamma$, by working with 5D propagators and treating the Yukawa interactions as perturbations. In [247] the author discussed the $b \to s\gamma$ process in the minimal RS model with a brane-localized Higgs sector working in the KK-decomposed theory, where the dipole coefficients are expressed via infinite sums over the contributions from different levels of KK modes. In [248] the authors calculated the dipole coefficients in the custodial RS model with a brane-localized Higgs sector, focusing only on the diagrams with an exchange of the first level of KK fermions along with gluons and charged NGBs. The authors of [211, 249] calculated the RS contributions to the dipole operators in the KK-decomposed theory for a general bulk-Higgs field, where the localization parameter is taken to be $\beta \sim 1$ (β is defined in (2.36)). Numerically, they also discussed the quasi IR-localized limit by increasing β, i.e. by pushing the Higgs profile towards the IR brane. They found that heavy KK fermion modes with masses $m_{q_n} \sim \beta M_{\rm KK}$ yield unsuppressed contributions in the case where the Higgs inverse width is of order the UV cutoff, $\beta \sim \Lambda_{\rm TeV}/v$. In this case, there are still some high-momentum KK modes that can probe the "bulky nature" of the Higgs field. In addition, the authors of [249, 250] observed the non-decoupling of heavy KK excitations of the Higgs boson itself in the quasi IR-localized limit of large β. These findings showed that the results of Higgs-induced contributions to the dipole operators depend on the implementation of the Higgs sector. The authors of [250] discussed this point in the context of lepton flavor violation in RS models. They calculated the electromagnetic (leptonic) dipole operator in RS models with a brane-localized or nearly brane-localized Higgs and treated the Yukawa interactions as perturbations. Recently, the work [251] appeared, which contains an analysis of the decay $\bar{B} \to X_s\gamma$ in the minimal and custodial RS model with an IR-localized bulk Higgs, and where the scalar sector includes contributions from the Higgs zero mode and its KK excitations.

In our work, we will include the effects of the RS model on the transition $b \to s\gamma$ by using an effective Lagrangian, in which the heavy KK quarks and bosons are integrated

out. The most important operators are the electromagnetic dipole operators

$$Q_{7\gamma} = -\frac{e\, m_b}{4\pi^2}\, \bar{s}\, \sigma_{\mu\nu} F^{\mu\nu} P_R\, b\,, \qquad \tilde{Q}_{7\gamma} = -\frac{e\, m_b}{4\pi^2}\, \bar{s}\, \sigma_{\mu\nu} F^{\mu\nu} P_L\, b\,, \tag{5.1}$$

with $\sigma_{\mu\nu} = \frac{i}{2}\,[\gamma_\mu, \gamma_\nu]$ and the projection operators $P_{R,L} = \frac{1}{2}(1 \pm \gamma_5)$. Due to operator mixing we will also consider the chromomagnetic dipole operators

$$Q_{8g} = -\frac{g_s m_b}{4\pi^2}\, \bar{s}\, \sigma_{\mu\nu}\, G_a^{\mu\nu} t_a P_R\, b\,, \qquad \tilde{Q}_{8g} = -\frac{g_s m_b}{4\pi^2}\, \bar{s}\, \sigma_{\mu\nu}\, G_a^{\mu\nu} t_a P_L\, b\,, \tag{5.2}$$

where t_a are the generators of $SU(3)_c$. In Section 5.1, we will perform a complete calculation of the electro- and chromomagnetic (quark) penguin diagrams including all contributions at one-loop order in the minimal RS model with a brane Higgs. We will derive expressions for the dipole Wilson coefficients using 5D propagators by retaining the full dependence on the Yukawa interactions. The only two other works on the $b \to s\gamma$ transition that performed comprehensive calculations in the 5D framework are [246, 251]. In contrast to both works, we will obtain expressions that are formally valid to all orders in $v^2/M_{\rm KK}^2$. Furthermore, we will show analytically and numerically in Section 5.2 that the results coincide with the corresponding expressions in the KK-decomposed (4D) theory. After implementing the renormalization-group evolution from the KK scale down to the B-meson scale we will discuss the phenomenological implications in Section 5.3.

This chapter is based on our publication [199], which has been mainly worked out by myself. Concerning the calculation of the dipole Wilson coefficients in the KK-decomposed theory I have benefited from earlier calculations and analyses by C. Schmell that are contained in his doctoral thesis [247].

5.1 5D calculation of the dipole Wilson coefficients

Like in the SM, the leading-order contributions to the $b \to s\gamma$ and $b \to sg$ dipole coefficients in the RS model are loop suppressed because there are no flavor-changing gauge-boson couplings that can induce a chirality flip. However, in contrast to the SM there are more one-loop diagrams to be considered. Besides the additional exchange of KK $W^\pm$ bosons, new topologies appear due to the flavor-changing couplings of the Higgs boson, the Z boson and its KK modes, and the photon and gluon KK modes. Figure 5.1 shows all relevant Feynman diagrams contributing in a general R_ξ gauge.[1] Internal scalar lines of the diagrams (II), (III) and (IV) include the contributions from the scalar component of the 5D gauge bosons and from the corresponding NGBs in the Higgs sector. In this section, the Wilson coefficients $C_{7\gamma,8g}$ and $\tilde{C}_{7\gamma,8g}$ are defined via the general parametrization of the transition amplitude

$$\mathcal{A}_{7\gamma,8g} = i\frac{G_F}{\sqrt{2}}\, \lambda_t \left[C_{7\gamma,8g}\, \langle s\gamma | Q_{7\gamma,8g} | b\rangle + \tilde{C}_{7\gamma,8g}\, \langle s\gamma | \tilde{Q}_{7\gamma,8g} | b\rangle \right], \tag{5.3}$$

where G_F is the Fermi constant, and $\lambda_t \equiv V_{ts}^* V_{tb}$ is the relevant product of entries of the CKM matrix. The matrix elements read $\langle Q_{7\gamma}\rangle = (e m_b/2\pi^2)\, \epsilon^{*\mu}(q)\, \bar{u}(p_s)\, i\sigma_{\mu\nu}\, q^\nu P_R\, u(p_b)$ and $\langle Q_{8g}\rangle = (g_s m_b/2\pi^2)\, \epsilon^{*\mu}(q)\, \bar{u}(p_s)\, i\sigma_{\mu\nu}\, q^\nu P_R\, u(p_b)$, where the outgoing photon (gluon) momentum is $q = p_b - p_s$. The chirality-flipped matrix elements $\langle \tilde{Q}_{7\gamma,8g}\rangle$ are given by analogous expressions with $P_R \to P_L$. Working in Feynman-'t Hooft gauge ($\xi = 1$),

[1] Note that it is sufficient to consider diagrams where the photon/gluon is radiated by an internal line, since diagrams with a vector boson attached to an external quark leg do not contribute to the dipole operators.

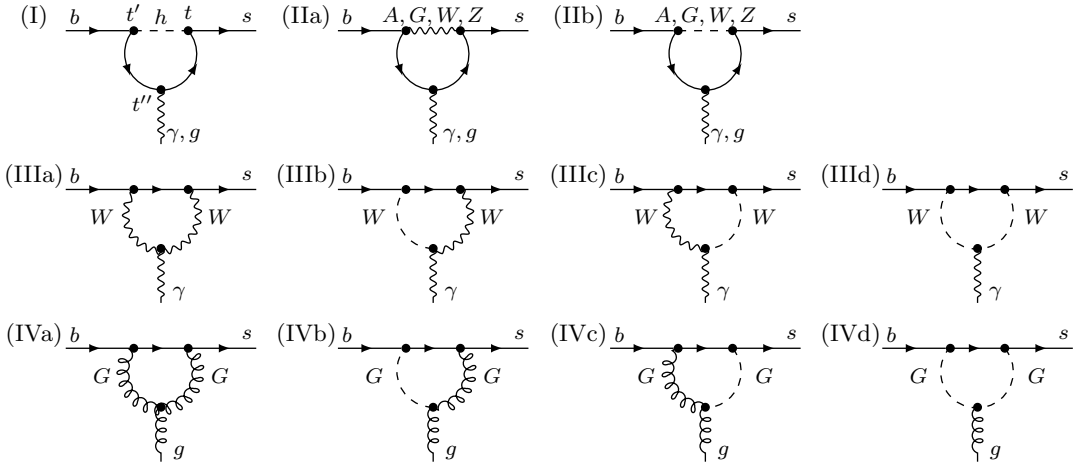

Figure 5.1: Diagrams contributing in the minimal RS model to the transitions $b \to s\gamma$ and $b \to sg$ at the one-loop level. Solid lines denote the exchange of up- or down-type quarks while wavy or curled lines denote the exchange of (vector) gauge-bosons. Apart from diagram (I) a scalar (dashed) line includes the contribution from the fifth component of the gauge boson and the corresponding contribution from the NGBs in the Higgs sector. The extra-dimensional coordinates of the vertices are labelled according to diagram (I).

we compute each amplitude in Figure 5.1 using the Feynman rules of the 5D theory collected in Appendix A.

As an example we consider the penguin diagram (IIa) in Figure 5.1, where one 5D $W^\pm$ boson and two 5D quarks are exchanged. The corresponding amplitude with an external photon is given by

$$\begin{aligned}\mathcal{A}_{7\gamma}^{W,\text{vector}} = {} & \frac{4\pi\, Q_u\, e_5\, g_5^2}{(2\pi r)^{3/2}} \int \frac{d^4k}{(2\pi)^4} \int_\epsilon^1 dt\, dt'\, dt''\, \epsilon_\mu^*(q)\, D_{W,\alpha\beta}^{\xi=1}(t',t;k)\, \bar{u}(p_s) \\ & \times \Big[\mathcal{D}_L^{(2)\dagger}(t) P_R + \mathcal{D}_R^{(2)\dagger}(t) P_L\Big]\, \boldsymbol{P}_W \gamma^\alpha\, \boldsymbol{S}^u(t,t'';p_s-k)\, \gamma^\mu \\ & \times \boldsymbol{S}^u(t'',t';p_b-k)\, \gamma^\beta\, \boldsymbol{P}_W \Big[\mathcal{D}_L^{(3)}(t') P_L + \mathcal{D}_R^{(3)}(t') P_R\Big] u(p_b)\,,\end{aligned} \tag{5.4}$$

where $Q_u = 2/3$. The functions $\mathcal{D}_{L,R}^{(2)}$ and $\mathcal{D}_{L,R}^{(3)}$ denote the profiles of the physical strange- and bottom-quark mass eigenstates, respectively, as defined in (2.17). The 2×2 matrix $\boldsymbol{P}_W \equiv \boldsymbol{P}_+ = \text{diag}(1,0)$ originates from the 5D Feynman rule for the $W_\mu^+ \bar{U}_A D_A$ vertices (with $A = L, R$) in (A.1) and projects out the profiles of the $SU(2)_L$ doublet quark fields. The $W^\pm$-boson 5D propagator in (5.4) has been calculated in closed form in Section 3.2. The quark 5D propagators in (5.4) can be decomposed into four propagator functions differing in chirality and Lorentz structure, $\boldsymbol{\Delta}_{AB}^q$ with $A, B \in \{L, R\}$, see (3.50). Next we outline some of the basic steps needed to extract the dipole coefficients from the diagrams in Figure 5.1:

- We perform a Taylor expansion of each 5D propagator in the external momenta p_s, p_b and keep the terms up to second order, since higher orders would contribute to higher-dimensional operators and yield suppressed contributions. For instance,

for the quark-propagator function we apply the expansion ($q = u, d$)

$$\begin{aligned}\mathbf{\Delta}^q_{AB}(t,t';-(p_i-k)^2) = \left[1 - 2(p_i\cdot k)\,\frac{\partial}{\partial k^2} + 2\,(p_i\cdot k)^2\left(\frac{\partial}{\partial k^2}\right)^2 \mp \dots\right] \\ \times\, \mathbf{\Delta}^q_{AB}(t,t';-k^2)\,,\end{aligned} \tag{5.5}$$

where $p_i = p_{s,b}$, k is the loop momentum, and $A, B \in \{L, R\}$. We need to expand up to second order in the external momenta in order to obtain the leading effects of the dipole Wilson coefficients, since the matrix elements of the dipole operators contain the bottom mass m_b and the momentum difference $q = p_b - p_s$. In fact, the term linear in p_i in (5.5) contributes only in the RS model, and not in the SM, to the dipole Wilson coefficients. Analogously we can expand the 5D vector-boson propagator function $B_B(t,t';-(p_i-k)^2)$ with subscript $B = A, G, W, Z$.

- The extra-dimensional integration of the vertex with the external photon or gluon can be performed analytically by using the flatness of their profiles and the orthonormality conditions for boson and fermion profiles in (2.8) and (2.29).

- The previous two bullets allow us to combine two 5D propagators of the same type when we expand them in the external momenta p_s, p_b and perform the extra-dimensional integration of the vertex that couples to the external photon or gluon. For instance we can apply ($q = u, d$)

$$\begin{aligned}&\int_\epsilon^1 dt''\,\mathbf{\Delta}^q_{RR}(t,t'';-(p_s-k)^2)\,\mathbf{\Delta}^q_{RL}(t'',t';-(p_b-k)^2) \\ &\quad= \Bigg\{-\frac{\partial}{\partial k^2} + k\cdot(p_s+p_b)\left(\frac{\partial}{\partial k^2}\right)^2 \\ &\qquad -\frac{2}{3}\Big[k\cdot p_s\, k\cdot p_b + (p_s\cdot k)^2 + (p_b\cdot k)^2\Big]\left(\frac{\partial}{\partial k^2}\right)^3 + \dots\Bigg\}\mathbf{\Delta}^q_{RL}(t,t';-k^2)\,,\end{aligned} \tag{5.6}$$

where we neglect terms of order $(k\cdot p_s)^n (k\cdot p_b)^{n'}$ with $n + n' \geq 3$. Analogous relations can be derived for products of different fermion and boson propagator functions. Equation (5.6) can be used to reduce each amplitude by one extra-dimensional integration and one 5D propagator.

- We perform a Wick rotation to Euclidean momenta with $k^0 = ik^0_E$ and $k_E = \sqrt{-k^2}$.

- For the matching procedure on the dipole operators we first use that the photon or gluon is on-shell, $q_\mu \epsilon^{\mu *}(q) = 0$, which allows us to rewrite $p^\mu_{s,b}\epsilon^*_\mu(q) = \frac{1}{2}(p_b + p_s)^\mu \epsilon^*_\mu(q)$. Then, we can use the Dirac equation $\not{p}_b u(p_b) = m_b\, u(p_b)$ and apply the Gordon identity

$$\begin{aligned}\bar u(p_s)\, i\sigma^{\mu\nu} q_\nu P_{L,R}\, u(p_b) = \bar u(p_s)\Big[&(p_s+p_b)^\mu P_{L,R} \\ &- \gamma^\mu\,(m_s P_{L,R} + m_b P_{R,L})\Big]u(p_b)\,,\end{aligned} \tag{5.7}$$

in order to extract the Wilson coefficients.

In the following three subsections we discuss the gauge-invariant subsets of the diagrams shown in Figure 5.1.

5.1.1 Higgs-boson contribution

We begin with the first diagram (I) in Figure 5.1, in which the Higgs boson and two down-type 5D quarks are exchanged. The Yukawa interactions of the Higgs boson with two down-type quarks are given by (4.2) with $q = d$. Concerning the regularized δ-function we implement the square box of width η and height $1/\eta$, see (1.58) for the definition. As explained in Section 1.4.5, the brane-localized Higgs scenario corresponds to values of $\eta \ll |Y_q| v/\Lambda_{\rm TeV}$, while the narrow bulk-Higgs scenario implies values in the range $|Y_q| v/\Lambda_{\rm TeV} \ll \eta \ll |Y_q| v/M_{\rm KK}$, where $|Y_q|$ sets the typical size for the dimensionless 5D Yukawa couplings. Note that the shape of the regularized profile is irrelevant as long as $\eta \ll 1$. With the Feynman rules in Appendix A and the basic steps outlined in the beginning of this section we can derive an expression for the Wilson coefficient and find

$$C^h_{7\gamma,8g} = \frac{\kappa_h^{7\gamma,8g}}{4G_F\lambda_t}\,\frac{1}{v}\int_0^\infty \frac{dk_E}{k_E^2+m_h^2}\left[\left(\frac{k_E^2}{8}\,\partial_{k_E} - \frac{k_E^3}{8}\,\partial^2_{k_E}\right)\frac{T^d_{RL}(k_E^2)}{m_b}\right.$$
$$\left. + \left(\frac{k_E^2}{32}\,\partial_{k_E} - \frac{k_E^3}{32}\,\partial^2_{k_E} - \frac{k_E^4}{96}\,\partial^3_{k_E}\right)\frac{T^d_{RR}(k_E^2)}{M_{\rm KK}}\right], \tag{5.8}$$

where m_h is the Higgs mass. Concerning the derivatives we use the notation $\partial_{k_E} \equiv \partial/\partial k_E$. Due to the parametrization of the amplitude in (5.3) we have to divide the dipole coefficient by λ_t and G_F. The couplings are given by $\kappa_h^{7\gamma} = Q_d$ and $\kappa_h^{8g} = 1$, where $Q_d = -1/3$. The dimensionless propagator functions in (5.8) are defined via

$$T^d_{RL}(k_E^2) = \frac{-v}{\sqrt{2}}\int_\epsilon^1 dt dt'\,\delta^\eta(t-1)\delta^\eta(t'-1)\mathcal{D}_L^{(2)\dagger}(t)\mathcal{M}_d^Y\,\mathbf{\Delta}^d_{RL}(t,t';k_E^2)\mathcal{M}_d^Y\mathcal{D}_R^{(3)}(t')\,, \tag{5.9}$$
$$T^d_{RR}(k_E^2) = \frac{-vM_{\rm KK}}{\sqrt{2}}\int_\epsilon^1 dt dt'\,\delta^\eta(t-1)\delta^\eta(t'-1)\mathcal{D}_L^{(2)\dagger}(t)\mathcal{M}_d^Y\,\mathbf{\Delta}^d_{RR}(t,t';k_E^2)\mathcal{M}_d^{Y\dagger}\mathcal{D}_L^{(3)}(t')\,,$$

with the regularized δ-function (1.58) and the matrix $\mathcal{M}_d^Y = \boldsymbol{P}_{12}\,\boldsymbol{Y}_d + \boldsymbol{P}_{21}\,\boldsymbol{Y}_d^\dagger$. The projector $\boldsymbol{P}_{ij}$ for $i,j = 1,2$ is a 2×2 matrix with zero entries except for the ij-component, which equals 1. In order to perform the integrations over t and t' we need solutions for the external quark profiles and the quark 5D propagators in the region $t,t' \in [1-\eta,1]$. The quark profiles are given by (2.25) with the trigonometric functions defined in (2.24). For the SM quarks, the mass-dependent terms in (2.24) are suppressed, since $\eta x_{q_n} \ll |Y_q|\varrho$, and we can make the replacement $\boldsymbol{S}_{q_n} \to \boldsymbol{X}_q$. Solutions for the quark 5D propagator are explicitly given in (3.95), (3.96) and (3.97).

It is instructive to discuss the calculation of the function $T^d_{RL}(k_E^2)$ in more detail, since it exhibits a sensitivity on the regulator η, which is similar to that observed in the calculation of the loop-induced Higgs coupling to two gluons in Section 4.1. Applying the δ-function regulator (1.58) and inserting the solutions for the external quark profiles (2.25) into (5.9), we obtain

$$T^d_{RL}(k_E^2) = \frac{-v}{\sqrt{2}}\,\mathcal{D}_L^{(2)\dagger}(1_\eta)\int_{1_\eta}^1\frac{dtdt'}{\eta^2}\left[\left(\frac{\mathcal{C}(t)}{\mathcal{C}(1_\eta)}\boldsymbol{Y}_d\,\mathbf{\Delta}^{d,21}_{RL}(t,t';k_E^2)\right.\right.$$
$$\left. - \frac{\boldsymbol{X}_d}{\varrho}\frac{\mathcal{S}(t)}{\mathcal{C}(1_\eta)}\mathbf{\Delta}^{d,11}_{RL}(t,t';k_E^2)\right)\frac{\mathcal{C}(t')}{\mathcal{C}(1_\eta)}\boldsymbol{Y}_d \tag{5.10}$$
$$\left. + \left(\frac{\mathcal{C}(t)}{\mathcal{C}(1_\eta)}\boldsymbol{Y}_d\,\mathbf{\Delta}^{d,22}_{RL}(t,t';k_E^2) - \frac{\boldsymbol{X}_d}{\varrho}\frac{\mathcal{S}(t)}{\mathcal{C}(1_\eta)}\mathbf{\Delta}^{d,12}_{RL}(t,t';k_E^2)\right)\frac{\bar{\boldsymbol{X}}_d}{\varrho}\frac{\bar{\mathcal{S}}(t')}{\bar{\mathcal{C}}(1_\eta)}\right]\boldsymbol{P}_{12}\mathcal{D}_R^{(3)}(1_\eta),$$

using $1_\eta \equiv 1-\eta$, and where $\mathcal{C}(t), \mathcal{S}(t)$ are defined in (2.24) with $q = d$. We are not interested in the full dependence of $T^d_{RL}(k_E^2)$ on η, since in the end of the calculation we will always remove the regulator ($\eta \to 0$). However, since $T^d_{RL}(k_E^2)$ depends on the product $\eta \hat{k}_E$, where $\hat{k}_E \equiv k_E/M_{\rm KK}$, via the quark propagator functions and we integrate the function in (5.8) from zero to infinite Euclidean momentum, we have to investigate whether the momentum integration commutes with the limit $\eta \to 0$. If we implement a four-momentum cutoff $k_E \leq \Lambda_{\rm cut}$ for the integral, the question can be reformulated as whether (5.8) yields the same results when imposing the constraints $\eta \gg |Y_q| v/\Lambda_{\rm cut}$ or $\eta \ll |Y_q| v/\Lambda_{\rm cut}$. Thus, we need to investigate the UV behavior of $T^d_{RL}(k_E^2)$ for large Euclidean momenta near the cutoff $k_E \sim \Lambda_{\rm cut}$.

Let us begin with the first scenario $\eta \gg |Y_q| v/\Lambda_{\rm cut}$, where η is bounded from below. In fact, we also have to impose an upper bound $\eta \ll |Y_q| v/M_{\rm KK}$, which is required in order to find reliable solutions for the 5D propagator functions in the region $t, t' \in [1_\eta, 1]$. When we consider large Euclidean momenta near the UV cutoff ($k_E \sim \Lambda_{\rm cut}$), the allowed range of η implies the hierarchy $\hat{k}_E \gg |Y_q| \varrho/\eta$. Consequently, the function $\boldsymbol{S}_d = (\boldsymbol{X}_d^2 + \eta^2 \hat{k}_E^2)^{1/2}$, which is contained in the 5D propagator solutions, becomes approximately independent of the Yukawa-dependent term, such that $\boldsymbol{S}_d \approx \eta \hat{k}_E$. In this limit, we find that ($\eta \hat{k}_E \gg |Y_q| \varrho$)

$$T^d_{RL}(k_E^2) \sim (\eta \hat{k}_E)^{-3} \tag{5.11}$$

falls off with the third inverse power of the product $\eta \hat{k}_E$. An analogous analysis for $T^d_{RR}(k_E^2)$ shows that it exhibits the same behavior as in (5.11). Since the imposed cutoff can be identified with the effective UV cutoff of the theory near the IR brane, $\Lambda_{\rm cut} \approx \Lambda_{\rm TeV}$, the behavior in (5.11) refers to the case of a narrow bulk-Higgs scenario.

We continue with the second scenario, where the δ-function regulator is bounded from above by $\eta \ll |Y_q| v/\Lambda_{\rm cut}$. This case represents the brane-localized Higgs scenario for $\Lambda_{\rm cut} \approx \Lambda_{\rm TeV}$. Consequently, the product $\eta \hat{k}_E$ is much smaller than $|Y_q| \varrho$ implying that $\boldsymbol{S}_d$ becomes approximately independent of the regulator, $\boldsymbol{S}_d \approx \boldsymbol{X}_d$. In this limit, we find ($\eta \hat{k}_E \ll |Y_q| \varrho$)

$$\begin{aligned} T^d_{RL}(k_E^2) = \mathcal{D}_L^{(2)\dagger}(1_\eta) \int_{1_\eta}^1 \frac{dt dt'}{\eta^2} \Bigg[\Bigg(& \frac{2\boldsymbol{X}_d}{\sinh 2\boldsymbol{X}_d} \frac{\boldsymbol{Z}_d(k_E^2)}{1+\boldsymbol{Z}_d(k_E^2)} \frac{\mathcal{C}(t')}{\mathcal{C}(1_\eta)} \\ & + \frac{\boldsymbol{X}_d}{\coth \boldsymbol{X}_d} \frac{\mathcal{C}(t')}{\mathcal{C}(1_\eta)} - \theta(t-t')\, \boldsymbol{X}_d \frac{\mathcal{S}(t')}{\mathcal{C}(1_\eta)} \Bigg) \frac{\mathcal{C}(t')}{\mathcal{C}(1_\eta)} \boldsymbol{Y}_d \\ - \Bigg(& \frac{2\boldsymbol{X}_d}{\sinh 2\boldsymbol{X}_d} \frac{\boldsymbol{Z}_d(k_E^2)}{1+\boldsymbol{Z}_d(k_E^2)} \frac{\mathcal{S}(t')}{\mathcal{C}(1_\eta)} \\ & + \frac{\boldsymbol{X}_d}{\coth \boldsymbol{X}_d} \frac{\mathcal{S}(t')}{\mathcal{C}(1_\eta)} - \theta(t-t')\, \boldsymbol{X}_d \frac{\mathcal{C}(t')}{\mathcal{C}(1_\eta)} \Bigg) \frac{\mathcal{S}(t')}{\mathcal{C}(1_\eta)} \boldsymbol{Y}_d \Bigg] \boldsymbol{P}_{12}\, \mathcal{D}_R^{(3)}(1_\eta)\,. \end{aligned} \tag{5.12}$$

where $\theta(t-t')$ denotes the Heaviside step function. The function $\boldsymbol{Z}_q(k_E^2)$ and the modified Yukawa matrix $\tilde{\boldsymbol{Y}}_q$ are defined in (3.82) and (2.27). In (5.12) we have not yet combined the terms inside the two round brackets. But when combining them we find that the t, t' dependence completely cancels and the t, t' integrations become trivial, an analogous observation was made for the Higgs production process via gluon fusion in Section 4.1. In addition the remaining η dependence completely cancels. Finally, in the brane-localized

Higgs scenario we find the results ($\eta \hat{k}_E \ll |Y_q| \varrho$)

$$T^d_{RL}(k_E^2) = \mathcal{D}^{(2)\dagger}_L(1^-) \left[\frac{2\boldsymbol{X}_d}{\sinh 2\boldsymbol{X}_d} \frac{\boldsymbol{Z}_d(k_E^2)}{1+\boldsymbol{Z}_d(k_E^2)} \frac{2\boldsymbol{X}_d}{\sinh 2\boldsymbol{X}_d} + \frac{\boldsymbol{X}_d^2}{\cosh^2 \boldsymbol{X}_d} \right] \tilde{\boldsymbol{Y}}_d \boldsymbol{P}_{12} \mathcal{D}^{(3)}_R(1^-) \,,$$
$$T^d_{RR}(k_E^2) = \mathcal{D}^{(2)\dagger}_L(1^-) \frac{1}{\hat{k}_E} \frac{2\boldsymbol{X}_d}{\sinh 2\boldsymbol{X}_d} \frac{\boldsymbol{Z}_d(k_E^2)}{1+\boldsymbol{Z}_d(k_E^2)} \frac{1}{\boldsymbol{R}_Q(\hat{k}_E)} \frac{2\boldsymbol{X}_d}{\sinh 2\boldsymbol{X}_d} \boldsymbol{P}_+ \mathcal{D}^{(3)}_L(1^-) \,, \quad (5.13)$$

where $\boldsymbol{R}_Q(\hat{k}_E)$ is defined in (3.74). The expressions are independent of the δ-function regulator. We have also included the final result for $T^d_{RR}(k_E^2)$, which can be obtained by an analogous calculation. For large Euclidean momenta $k_E \gg M_{\rm KK}$ the structure $\boldsymbol{Z}_d(k_E^2)$ can be expanded as $\boldsymbol{Z}_d(k_E^2) \approx \varrho^2 \tilde{\boldsymbol{Y}}_d \tilde{\boldsymbol{Y}}_d^\dagger + \mathcal{O}(\hat{k}_E^{-2})$. We observe that $T^d_{RL}(k_E^2)$ reaches a non-zero plateau in this limit, which is different to the case in the narrow bulk-Higgs scenario in (5.11). Consequently, the contribution of $T^d_{RL}(k_E^2)$ to the dipole coefficient (5.8) exhibits a dependence on the model under consideration. On the other hand, the function $T^d_{RR}(k_E^2)$ vanishes also in the brane-localized Higgs scenario and does not lead to a model-dependent contribution.

Interestingly we could have obtained the same results for $T^d_{RL}(k_E^2)$ and $T^d_{RR}(k_E^2)$ in (5.13) if we had naively evaluated the extra-dimensional coordinates at $t = t' = 1^-$ instead of using the regularized δ-function in (5.9). We have explicitly confirmed that ($\eta \hat{k}_E \ll |Y_q| \varrho$)

$$\begin{aligned} T^d_{RL}(k_E^2) &= -\frac{v}{\sqrt{2}} \mathcal{D}^{(2)\dagger}_L(1^-) \mathcal{M}_d^Y \boldsymbol{\Delta}^d_{RL}(1^-,1^-;k_E^2) \mathcal{M}_d^Y \mathcal{D}^{(3)}_R(1^-) \,, \\ T^d_{RR}(k_E^2) &= -\frac{v M_{\rm KK}}{\sqrt{2}} \mathcal{D}^{(2)\dagger}_L(1^-) \mathcal{M}_d^Y \boldsymbol{\Delta}^d_{RR}(1^-,1^-;k_E^2) \mathcal{M}_d^{Y\dagger} \mathcal{D}^{(3)}_L(1^-) \,, \end{aligned} \quad (5.14)$$

lead to the results (5.13). An analogous situation has been encountered for the calculation of the propagator functions $T_\pm(k_E^2)$ in the case of the Higgs production process via gluon fusion in Section 4.1.

Final result for the Wilson coefficient

The above analysis shows that the integrand of the dipole coefficient in (5.8) falls off with at least two inverse powers of Euclidean momenta in the UV, which implies the finiteness of the integral. Thus, we are allowed to perform partial momentum integrations in (5.8) and find

$$C^h_{7\gamma,8g} = \frac{\kappa_h^{7\gamma,8g}}{4 G_F \lambda_t} \frac{1}{v} \left[\lim_{k_E \to \infty} \frac{T^d_{RL}(k_E^2)}{4 m_b} - \int_0^\infty \frac{dk_E\, k_E m_h^4}{(k_E^2+m_h^2)^3} \left(\frac{T^d_{RL}(k_E^2)}{m_b} + \frac{k_E^2}{k_E^2+m_h^2} \frac{T^d_{RR}(k_E^2)}{2M_{\rm KK}} \right) \right] , \quad (5.15)$$

where all boundary terms at $k_E^2 = 0$ vanish. Based on the previous analysis only for large Euclidean momenta we can have a non-zero boundary term in case of the brane-localized Higgs scenario, where $T^d_{RL}(k_E^2)$ approaches a non-zero plateau. This is accounted for by the first term in the outer bracket of (5.15). We can insert our results (5.13) for $T^d_{RL}(k_E^2)$

and $T^d_{RR}(k_E^2)$ into (5.15) and find

$$C^h_{7\gamma,8g} = \frac{\kappa_h^{7\gamma,8g}}{4G_F\lambda_t}\frac{1}{v}\,\mathcal{D}_L^{(2)\dagger}(1^-)\left[\boldsymbol{P}_{12}\,\frac{g(\boldsymbol{X}_d,\tilde{\boldsymbol{Y}}_d)}{4m_b}\,\mathcal{D}_R^{(3)}(1^-)\right.$$
$$-\frac{2\boldsymbol{X}_d}{\sinh 2\boldsymbol{X}_d}\int_0^\infty \frac{dk_E\,k_E m_h^4}{(k_E^2+m_h^2)^3}\left(\frac{\boldsymbol{P}_{12}}{m_b}\frac{\boldsymbol{Z}_d(k_E^2)}{1+\boldsymbol{Z}_d(k_E^2)}\frac{2\boldsymbol{X}_d}{\sinh 2\boldsymbol{X}_d}\tilde{\boldsymbol{Y}}_d\,\mathcal{D}_R^{(3)}(1^-)\right. \tag{5.16}$$
$$\left.\left.+\frac{\boldsymbol{P}_+}{2}\frac{k_E}{k_E^2+m_h^2}\frac{\boldsymbol{Z}_d(k_E^2)}{1+\boldsymbol{Z}_d(k_E^2)}\frac{1}{\boldsymbol{R}_Q(\hat{k}_E)}\frac{2\boldsymbol{X}_d}{\sinh 2\boldsymbol{X}_d}\mathcal{D}_L^{(3)}(1^-)\right)\right],$$

with

$$g(\boldsymbol{X}_q,\tilde{\boldsymbol{Y}}_q)\Big|_{\substack{\text{brane}\\ \text{Higgs}}} = \frac{2\boldsymbol{X}_q}{\sinh 2\boldsymbol{X}_q}\,\frac{\varrho^2\tilde{\boldsymbol{Y}}_q\tilde{\boldsymbol{Y}}_q^\dagger}{1+\varrho^2\tilde{\boldsymbol{Y}}_q\tilde{\boldsymbol{Y}}_q^\dagger}\,\frac{2\boldsymbol{X}_q}{\sinh 2\boldsymbol{X}_q}\,\tilde{\boldsymbol{Y}}_q = \varrho^2\boldsymbol{Y}_q\boldsymbol{Y}_q^\dagger\boldsymbol{Y}_q + \mathcal{O}(\varrho^4)\,,$$
$$g(\boldsymbol{X}_q,\tilde{\boldsymbol{Y}}_q)\Big|_{\substack{\text{narrow}\\ \text{bulk Higgs}}} = -\frac{\boldsymbol{X}_q^2}{\cosh^2\boldsymbol{X}_q}\,\tilde{\boldsymbol{Y}}_q = -\varrho^2\boldsymbol{Y}_q\boldsymbol{Y}_q^\dagger\boldsymbol{Y}_q + \mathcal{O}(\varrho^4)\,. \tag{5.17}$$

The function $g(\boldsymbol{X}_q,\tilde{\boldsymbol{Y}}_q)$ is model dependent and emerges from the penguin diagrams exchanging KK quarks. To leading order in $v^2/M_{\rm KK}^2$ it only differs in the relative sign for a brane-localized and narrow bulk-Higgs. A similar observation was made for the KK tower contribution in case of Higgs production via gluon fusion, see (4.24) and (4.25). Note that we limit our analysis of the narrow bulk-Higgs model to the contributions involving the zero modes of the scalar doublet (see in particular Section 5.2.4). The contributions of scalar KK excitations have been studied in [249–251].

We can generalize the results obtained in the brane-localized Higgs sector by allowing for two different Yukawa matrices $\boldsymbol{Y}_q^C$ and $\boldsymbol{Y}_q^S$ associated with orbifold-even and -odd quark profiles, see the text below (2.16). In this "type-II brane-Higgs" scenario we find that our previous analysis still holds, provided that we use $\tilde{\boldsymbol{Y}}_q = (\tanh\boldsymbol{X}_q/\boldsymbol{X}_q)\boldsymbol{Y}_q^C$ for the modified Yukawa matrix and $\boldsymbol{X}_q = \varrho(\boldsymbol{Y}_q^C\boldsymbol{Y}_q^{S\dagger})^{1/2}$. We then obtain

$$g(\boldsymbol{X}_q,\tilde{\boldsymbol{Y}}_q)\Big|_{\substack{\text{type-II}\\ \text{brane Higgs}}} = \frac{2\boldsymbol{X}_d}{\sinh 2\boldsymbol{X}_d}\,\frac{\varrho^2\tilde{\boldsymbol{Y}}_q\tilde{\boldsymbol{Y}}_q^\dagger}{1+\varrho^2\boldsymbol{Y}_q\tilde{\boldsymbol{Y}}_q^\dagger}\,\frac{2\boldsymbol{X}_d}{\sinh 2\boldsymbol{X}_d}\,\tilde{\boldsymbol{Y}}_q = \varrho^2\boldsymbol{Y}_q^C\boldsymbol{Y}_q^{C\dagger}\boldsymbol{Y}_q^C + \mathcal{O}(\varrho^4)\,, \tag{5.18}$$

where to leading order in $v^2/M_{\rm KK}^2$ the KK contribution emerges from the correct-chirality Higgs coupling. At this order there is no difference between the original result (5.17) and (5.18). The wrong-chirality Higgs coupling only contributes at order $v^4/M_{\rm KK}^4$. Therefore, we will set $\boldsymbol{Y}_q^C = \boldsymbol{Y}_q^S \equiv \boldsymbol{Y}_q$ in the following analyses. Furthermore, from now on we will concentrate on the brane-localized Higgs scenario. The only exception is Section 5.2.4, where we discuss some results in the narrow bulk-Higgs scenario.

5.1.2 Gauge-boson contribution

We continue with the diagrams (IIa) and (IIb) in Figure 5.1, where two internal 5D quarks and one 5D gauge boson are exchanged. The Wilson coefficients for the vector

and scalar contributions are given by (with $B = A, G, W, Z$)

$$\begin{aligned}
C_{7\gamma,8g}^{B,\text{vector}} &= \frac{\kappa_B^{7\gamma,8g}}{4\sqrt{2}G_F\lambda_t}\,2\pi\int_0^\infty dk_E\int_\epsilon^1 dtdt'\,B_B(t',t;k_E^2)\,\mathcal{D}_L^{(2)\dagger}(t)\,\boldsymbol{P}_B \\
&\quad\times\left[\left(\frac{11k_E^2}{16}\partial_{k_E}+\frac{5k_E^3}{16}\,\partial_{k_E}^2+\frac{k_E^4}{48}\,\partial_{k_E}^3\right)\boldsymbol{\Delta}_{LL}^q(t,t';k_E^2)\,\boldsymbol{P}_B\,\mathcal{D}_L^{(3)}(t')\right. \\
&\qquad\left.+\left(-\frac{3k_E^2}{2}\,\partial_{k_E}-\frac{k_E^3}{2}\,\partial_{k_E}^2\right)\frac{\boldsymbol{\Delta}_{LR}^q(t,t';k_E^2)}{m_b}\,\boldsymbol{P}_B\,\mathcal{D}_R^{(3)}(t')\right], \\
C_{7\gamma,8g}^{B,\text{scalar}} &= \frac{\kappa_B^{7\gamma,8g}}{4\sqrt{2}G_F\lambda_t}\,2\pi\int_0^\infty dk_E\int_\epsilon^1 dtdt'\,B_{B,55}(t',t;k_E^2)\,\mathcal{D}_L^{(2)\dagger}(t)\,\tilde{\boldsymbol{V}}_{B_5^-}(t) \\
&\quad\times\left[\left(\frac{k_E^2}{32}\,\partial_{k_E}-\frac{k_E^3}{32}\,\partial_{k_E}^2-\frac{k_E^4}{96}\,\partial_{k_E}^3\right)\boldsymbol{\Delta}_{RR}^q(t,t';k_E^2)\,\boldsymbol{V}_{B_5^+}(t')\,\mathcal{D}_L^{(3)}(t')\right. \\
&\qquad\left.+\left(\frac{k_E^2}{8}\,\partial_{k_E}-\frac{k_E^3}{8}\,\partial_{k_E}^2\right)\frac{\boldsymbol{\Delta}_{RL}^q(t,t';k_E^2)}{m_b}\,\tilde{\boldsymbol{V}}_{B_5^+}(t')\,\mathcal{D}_R^{(3)}(t')\right], \qquad (5.19)
\end{aligned}$$

where we introduced the matrices $\boldsymbol{P}_A = \boldsymbol{P}_G \equiv \mathbf{1}_{2\times2}$ and $\boldsymbol{P}_Z \equiv (\boldsymbol{P}_+ + g_R^d/g_L^d\,\boldsymbol{P}_-)$, with $g_L^d \equiv T_d^3 - Q_d\,s_w^2$ and $g_R^d \equiv -Q_d\,s_w^2$. In case of the $W^\pm$-boson loop up-type quark-propagator functions ($q = u$) arise, otherwise we need to set $q = d$ in (5.19). We remark that in case of the photon and gluon contributions to the Wilson coefficients ($B = A, G$) only KK resonances can contribute, therefore we have to subtract the zero-mode 4D propagator $(2\pi k_E^2)^{-1}$ from $B_B(t',t;k_E^2)$ in (5.19). The structures[2] $\boldsymbol{V}_{B_5^\pm}$ and $\tilde{\boldsymbol{V}}_{B_5^\pm}$ can be found in Appendix A. The coefficients $\kappa_B^{7\gamma,8g}$ are given by

$$\begin{aligned}
&\kappa_A^{7\gamma} = 2Q_d^3\,e^2\,, \quad \kappa_G^{7\gamma} = 2Q_d\,C_F\,g_s^2\,, \quad \kappa_W^{7\gamma} = Q_u\,\frac{g_5^2}{2\pi r}\,, \quad \kappa_Z^{7\gamma} = 2Q_d\,(g_L^d)^2\,\frac{g_5^2/c_w^2}{2\pi r}\,, \\
&\kappa_A^{8g} = 2Q_d^2\,e^2\,, \quad \kappa_G^{8g} = -\frac{1}{N_c}\,g_s^2\,, \quad \kappa_W^{8g} = \frac{g_5^2}{2\pi r}\,, \quad \kappa_Z^{8g} = 2(g_L^d)^2\,\frac{g_5^2/c_w^2}{2\pi r}\,, \qquad (5.20)
\end{aligned}$$

where e and g_s are the 4D electromagnetic and QCD gauge couplings. The 5D gauge coupling g_5 of $SU(2)_L$ can be obtained from (2.95). Furthermore, $C_F = (N_c^2-1)/(2N_c) = 4/3$ with $N_c = 3$ being the color factor for quarks. The largest factors occur in case of the penguin diagrams exchanging KK gluons and $W^\pm$-boson modes.

The scalar Wilson coefficient in (5.19) contains the propagator function $B_{B,55}$, which is defined in (3.17). Its KK decomposition can be used to express it in terms of the vector-boson propagator (3.16) by means of the relation (3.18). We can use this equation to eliminate the brane-localized terms inside the structures $\boldsymbol{V}_{B_5^\pm}$ and $\tilde{\boldsymbol{V}}_{B_5^\pm}$ in case of the massive gauge bosons ($B = W, Z$). For example, the 5D Feynman rule for the $W_5^-\bar{D}_L U_R$ vertex given in (A.2) contains the term

$$\tilde{\boldsymbol{V}}_{W_5^-}(t) = -\frac{\epsilon}{t}\left[\boldsymbol{P}_W - \frac{\varrho M_{\text{KK}}^2}{L\tilde{m}_W^2}\,\delta(t-1)\,\mathcal{M}_{ud}^Y\right], \qquad (5.21)$$

where $\mathcal{M}_{ud}^Y = \boldsymbol{Y}_u\,\boldsymbol{P}_{12} - \boldsymbol{Y}_d^\dagger\,\boldsymbol{P}_{21}$. The first term originates from the fifth component of the gauge-boson coupling to quarks, while the second brane-localized term is due to the Yukawa coupling of the $W^\pm$ NGBs. We now insert (3.17) into (5.19) and perform partial

[2]The $\pm$ labels on the subscripts of $\boldsymbol{V}_{B_5^\pm}$ and $\tilde{\boldsymbol{V}}_{B_5^\pm}$ are only relevant for $B = W$ and can be ignored otherwise.

integrations for the t, t' coordinates, taking into account that all terms on the boundary are orbifold-odd and therefore vanish. The partial integrations lead to derivatives acting on fermion profiles and propagators. We can use the equation of motions for the fermion profiles and the differential equations satisfied by the 5D propagators to show that all brane-localized terms contained in $\boldsymbol{V}_{W_5^\pm}$ and $\tilde{\boldsymbol{V}}_{W_5^\pm}$ cancel. For example, the partial t integration of the scalar Wilson coefficient in (5.19) leads to the term (for $B = W$)

$$\begin{aligned}\partial_t \left[\mathcal{D}_L^{(2)\dagger}(t)\boldsymbol{P}_W \boldsymbol{\Delta}^u_{RR}(t,t';k_E^2)\right] &= \mathcal{D}_L^{(2)\dagger}(t)\,\boldsymbol{P}_W\,\frac{\boldsymbol{\Delta}^u_{LR}(t,t';k_E^2)}{M_{\rm KK}} \\ &\quad - \frac{m_s}{M_{\rm KK}}\,\mathcal{D}_R^{(2)\dagger}(t)\,\boldsymbol{P}_W\,\boldsymbol{\Delta}^u_{RR}(t,t';k_E^2) \\ &\quad - \varrho\,\delta(t-1)\,\mathcal{D}_L^{(2)\dagger}(t)\,\mathcal{M}^Y_{ud}\,\boldsymbol{\Delta}^u_{RR}(t,t';k_E^2)\,,\end{aligned} \tag{5.22}$$

where we have used that

$$\begin{aligned}\partial_t \mathcal{Q}_L^{(n)}(t) &= -\frac{m_{q_n}}{M_{\rm KK}}\,\mathcal{Q}_R^{(n)}(t) + \mathcal{M}_q(t)\mathcal{Q}_L^{(n)}(t)\,, \\ \partial_t \boldsymbol{\Delta}^q_{RR}(t,t';k_E^2) &= \frac{1}{M_{\rm KK}}\,\boldsymbol{\Delta}^q_{LR}(t,t';k_E^2) - \mathcal{M}_q(t)\,\boldsymbol{\Delta}^q_{RR}(t,t';k_E^2)\,.\end{aligned} \tag{5.23}$$

The last term in (5.22) cancels with the remaining contribution from the brane-localized term in (5.21). Furthermore, we will discard contributions that are suppressed by the strange-quark mass.

In the last step we perform partial integrations of the Euclidean momentum variable, since momentum derivatives acting on fermion propagators lead to complicated expressions that are very inefficient to be evaluated numerically. Finally we obtain ($B = A, G, W, Z$)

$$\begin{aligned}C^B_{7\gamma,8g} = \frac{\kappa_B^{7\gamma,8g}}{4\sqrt{2}G_F\lambda_t}\Bigg\{&\frac{5}{24}\,R^B_{LL} - \frac{1}{4}\,R^B_{LR} + 2\pi\int_0^\infty dk_E \int_\epsilon^1 dtdt'\,\mathcal{D}_L^{(2)\dagger}(t)\,\boldsymbol{P}_B \\ &\times\Bigg[\frac{\boldsymbol{\Delta}^q_{LR}(t,t';k_E^2)}{m_b}\,\boldsymbol{P}_B\,\mathcal{D}_R^{(3)}(t')\left(-\frac{9k_E^2}{8}\partial_{k_E} - \frac{3k_E^3}{8}\partial^2_{k_E}\right) \\ &+ \boldsymbol{\Delta}^q_{LL}(t,t';k_E^2)\,\boldsymbol{P}_B\,\mathcal{D}_L^{(3)}(t')\left(\frac{3k_E^2}{32}\partial_{k_E} - \frac{3k_E^3}{32}\partial^2_{k_E} - \frac{k_E^4}{32}\partial^3_{k_E}\right)\Bigg] B_B(t',t;k_E^2)\Bigg\}\,,\end{aligned} \tag{5.24}$$

where we have combined both the vector and scalar Wilson coefficients. Note that the Wilson coefficients for $B = A, G$ differ only in the factors $\kappa_A^{7\gamma,8g}$ and $\kappa_G^{7\gamma,8g}$, see (5.20). Due to the partial momentum integrations we encounter non-zero boundary terms for large Euclidean momenta in (5.24), they are defined by

$$\begin{aligned}R^B_{LL} &= -2\pi \lim_{k_E\to\infty} k_E^2 \int_\epsilon^1 dtdt'\,B_B(t',t;0)\,\mathcal{D}_L^{(2)\dagger}(t)\,\boldsymbol{P}_B\,\boldsymbol{\Delta}^q_{LL}(t,t';k_E^2)\,\boldsymbol{P}_B\,\mathcal{D}_L^{(3)}(t')\,, \\ R^B_{LR} &= -2\pi \lim_{k_E\to\infty} k_E^2 \int_\epsilon^1 dtdt'\,B_B(t',t;0)\,\mathcal{D}_L^{(2)\dagger}(t)\,\boldsymbol{P}_B\,\frac{\boldsymbol{\Delta}^q_{LR}(t,t';k_E^2)}{m_b}\,\boldsymbol{P}_B\,\mathcal{D}_R^{(3)}(t')\,,\end{aligned} \tag{5.25}$$

where $q = u$ for $B = W$ and $q = d$ for $B = A, G, Z$. In case of the penguin diagrams, in which photon (gluon) modes are exchanged, we have to subtract the zero-mode contribution from the full propagator function $B_A(t,t';0)$. The reason is that massless gauge bosons have constant profiles that lead to flavor-conserving interactions and therefore do not contribute to the Wilson coefficients.

Calculation of the boundary terms

In order to determine the boundary terms in (5.25) we need to know the UV behavior of the boson and fermion propagator functions, which is worked out in Section 3.4. Using the results shown in equation (3.99), we can calculate the first boundary term in (5.25) and obtain

$$R^B_{LL} = 2\pi \int_\epsilon^1 dt\, B_B(t,t;0)\, \mathcal{D}_L^{(2)\dagger}(t)\, \boldsymbol{P}_B^2\, \mathcal{D}_L^{(3)}(t)\,, \tag{5.26}$$

where we have to remember to subtract the zero-mode propagator in case of $B = A, G$. We can further simplify (5.26) by using the explicit expressions for the propagator functions

$$\begin{aligned} B_B(t,t;0) &= \frac{1}{2\pi\tilde{m}_B^2} + \frac{L(1-t^2)}{4\pi M_{\rm KK}^2}\,; \quad B = W, Z\,, \\ B'_B(t,t;0) &= \frac{1}{4\pi M_{\rm KK}^2}\left(Lt^2 - t^2(1-2\ln t) + \frac{1}{2L}\right)\,; \quad B = A, G\,, \end{aligned} \tag{5.27}$$

where $B'_B(t,t;0)$ in the second line includes only KK modes. Inserting (5.27) into (5.26) and applying the orthonormality condition of the fermion profiles (2.29), we obtain

$$\begin{aligned} R^A_{LL} &= \frac{L}{2M_{\rm KK}^2}\left[(\boldsymbol{\Delta}_D)_{23} - \frac{2}{L}(\boldsymbol{\Delta}'_D)_{23}\right], \\ R^W_{LL} &= -\frac{L}{2M_{\rm KK}^2}\left[(\boldsymbol{\Delta}_D)_{23} + (\boldsymbol{\delta}_D)_{23} - (\boldsymbol{\varepsilon}_D)_{23}\right] - \frac{(\boldsymbol{\delta}_D)_{23}}{\tilde{m}_W^2}\,, \\ R^Z_{LL} &= -\frac{L}{2M_{\rm KK}^2}\left[(\boldsymbol{\Delta}_D)_{23} + \left(1 - \frac{(g_R^d)^2}{(g_L^d)^2}\right)\Big((\boldsymbol{\delta}_D)_{23} - (\boldsymbol{\varepsilon}_D)_{23}\Big)\right] - \left(1 - \frac{(g_R^d)^2}{(g_L^d)^2}\right)\frac{(\boldsymbol{\delta}_D)_{23}}{\tilde{m}_Z^2}\,, \end{aligned} \tag{5.28}$$

where $R^G_{LL} = R^A_{LL}$. We recover the known overlap integrals

$$\begin{aligned} (\boldsymbol{\Delta}_D)_{nn'} &= \int_\epsilon^1 dt\, t^2\, \mathcal{D}_L^{(n)\dagger}(t)\, \mathcal{D}_L^{(n')}(t)\,, \quad (\boldsymbol{\Delta}'_D)_{nn'} = \int_\epsilon^1 dt\, t^2 \left(\frac{1}{2} - \ln t\right) \mathcal{D}_L^{(n)\dagger}(t)\, \mathcal{D}_L^{(n')}(t)\,, \\ (\boldsymbol{\delta}_D)_{nn'} &= \int_\epsilon^1 dt\, \mathcal{D}_L^{(n)\dagger}(t)\, \boldsymbol{P}_-\, \mathcal{D}_L^{(n')}(t)\,, \quad (\boldsymbol{\varepsilon}_D)_{nn'} = \int_\epsilon^1 dt\, t^2\, \mathcal{D}_L^{(n)\dagger}(t)\, \boldsymbol{P}_-\, \mathcal{D}_L^{(n')}(t)\,, \end{aligned} \tag{5.29}$$

originally defined in [132]. For the other boundary term in (5.25), we can use relation (3.105) and obtain

$$\begin{aligned} R^B_{LR} = -\frac{2\pi}{x_b}\Bigg[& B_B(1^-,1^-;0)\, \mathcal{D}_L^{(2)\dagger}(1^-)\, \boldsymbol{P}_B \left(\frac{\boldsymbol{P}_+}{1+\varrho^2\tilde{\boldsymbol{Y}}_q\tilde{\boldsymbol{Y}}_q^\dagger} + \frac{\boldsymbol{P}_-\,\varrho^2\tilde{\boldsymbol{Y}}_q^\dagger\tilde{\boldsymbol{Y}}_q}{1+\varrho^2\tilde{\boldsymbol{Y}}_q^\dagger\tilde{\boldsymbol{Y}}_q}\right. \\ & \left. - \frac{\boldsymbol{P}_{12}}{1+\varrho^2\tilde{\boldsymbol{Y}}_q\tilde{\boldsymbol{Y}}_q^\dagger}\,\varrho\tilde{\boldsymbol{Y}}_q - \varrho\tilde{\boldsymbol{Y}}_q^\dagger\,\frac{\boldsymbol{P}_{21}}{1+\varrho^2\tilde{\boldsymbol{Y}}_q\tilde{\boldsymbol{Y}}_q^\dagger}\right) \boldsymbol{P}_B\, \mathcal{D}_R^{(3)}(1^-) \\ & - \int_\epsilon^1 dt\, \mathcal{D}_L^{(2)\dagger}(t)\, \boldsymbol{P}_B^2 \left(\mathcal{D}_R^{(3)}(t)\,\frac{\partial_t}{2} + x_b\,\mathcal{D}_L^{(3)}(t)\right) B_B(t,t;0)\Bigg]\,. \end{aligned} \tag{5.30}$$

We have omitted the terms at $t = \epsilon$, since the upper component of $\mathcal{D}_R^{(n)}$ and the lower component of $\mathcal{D}_L^{(n)}$ obey Dirichlet BCs at the UV brane and therefore vanish. In order to obtain the last term we have used that the function $B_B(t,t';0)$ vanishes for $t' < t$ and

we have applied the equation of motion for the fermion profiles. We can further simplify (5.30) by performing a partial t integration of the term involving $\partial_t B_B(t,t;0)$ and by using the fermion equation of motions to show that

$$R^B_{LR} = \frac{1}{2}\,R^B_{LL} - \frac{2\pi}{x_b}\,B_B(1^-,1^-;0)\,\mathcal{D}^{(2)\dagger}_L(1^-)\,\boldsymbol{P}_B\left[\frac{\boldsymbol{P}_+}{2}\,\frac{1-\varrho^2\tilde{\boldsymbol{Y}}_q\tilde{\boldsymbol{Y}}_q^\dagger}{1+\varrho^2\tilde{\boldsymbol{Y}}_q\tilde{\boldsymbol{Y}}_q^\dagger} - \frac{\boldsymbol{P}_-}{2}\,\frac{1-\varrho^2\tilde{\boldsymbol{Y}}_q^\dagger\tilde{\boldsymbol{Y}}_q}{1+\varrho^2\tilde{\boldsymbol{Y}}_q^\dagger\tilde{\boldsymbol{Y}}_q}\right.$$
$$\left. - \frac{\boldsymbol{P}_{12}}{1+\varrho^2\tilde{\boldsymbol{Y}}_q\tilde{\boldsymbol{Y}}_q^\dagger}\,\varrho\tilde{\boldsymbol{Y}}_q - \varrho\tilde{\boldsymbol{Y}}_q^\dagger\,\frac{\boldsymbol{P}_{21}}{1+\varrho^2\tilde{\boldsymbol{Y}}_q\tilde{\boldsymbol{Y}}_q^\dagger}\right]\boldsymbol{P}_B\,\mathcal{D}^{(3)}_R(1^-)\,, \tag{5.31}$$

where we have neglected a term suppressed by m_s/m_b and where we have recovered the term R^B_{LL}. Applying the modified BCs of the quark profiles (2.26) we obtain

$$\begin{aligned}
R^A_{LR} &= \frac{1}{2}\,R^A_{LL}\,,\\
R^W_{LR} &= \frac{1}{2}\,R^W_{LL} - \frac{1}{2\tilde{m}_W^2}\frac{v}{\sqrt{2}m_b}\,\mathcal{D}^{(2)\dagger}_L(1^-)\,\boldsymbol{P}_{12}\,\frac{1-\varrho^2\tilde{\boldsymbol{Y}}_u\tilde{\boldsymbol{Y}}_u^\dagger}{1+\varrho^2\tilde{\boldsymbol{Y}}_u\tilde{\boldsymbol{Y}}_u^\dagger}\,\tilde{\boldsymbol{Y}}_d\,\mathcal{D}^{(3)}_R(1^-)\,,\\
R^Z_{LR} &= \frac{1}{2}R^Z_{LL} - \frac{1}{2\tilde{m}_Z^2}\frac{v}{\sqrt{2}m_b}\left(1-\frac{g^d_R}{g^d_L}\right)^2\mathcal{D}^{(2)\dagger}_L(1^-)\,\boldsymbol{P}_{12}\,\frac{1-\varrho^2\tilde{\boldsymbol{Y}}_d\tilde{\boldsymbol{Y}}_d^\dagger}{1+\varrho^2\tilde{\boldsymbol{Y}}_d\tilde{\boldsymbol{Y}}_d^\dagger}\,\tilde{\boldsymbol{Y}}_d\,\mathcal{D}^{(3)}_R(1^-)\,,
\end{aligned} \tag{5.32}$$

where $R^G_{LR} = R^A_{LR}$. Yukawa-dependent terms appear in case of the massive gauge bosons and originate from the NGB degrees of freedom, which are localized at the IR brane.

We have succeeded in obtaining expressions for the boundary terms (5.28) and (5.32), such that the complete Wilson coefficient $C^B_{7\gamma,8g}$ in (5.24) can be evaluated numerically. The chirality-flipped Wilson coefficients $\tilde{C}_{7\gamma,8g}$ can be obtained from (5.24) and (5.25) by interchanging the label $L \leftrightarrow R$. The boundary terms can be calculated in analogy with the above steps, and we can use the results (5.26) and (5.31), for which we find $R^B_{RR} = R^B_{LL}|_{L\to R}$ and $R^B_{RL} = R^B_{LR}|_{L\leftrightarrow R}$.

5.1.3 Triple gauge-boson vertex contribution

Finally we discuss the diagrams exchanging two internal gauge bosons ($B = W, G$) and one quark, see diagrams (IIIa)-(IIId) and (IVa)-(IVd) in Figure 5.1. There are four diagrams each, involving vector and scalar components of the gauge-boson propagators. We refrain from showing intermediate steps of the calculation but mention that we can proceed analogously as in the previous section and combine the vector- and scalar-boson contributions. After some algebra we obtain the Wilson coefficients

$$\begin{aligned}
C^{WW}_{7\gamma} = \frac{\kappa_{WW}}{4\sqrt{2}G_F\lambda_t}\Bigg\{&\frac{1}{6}\,R^W_{LL} - \frac{1}{4}\,R^W_{LR} + 2\pi\int_0^\infty dk_E\int_\epsilon^1 dt dt'\,\mathcal{D}^{(2)\dagger}_L(t)\,\boldsymbol{P}_+\\
&\times\left[\boldsymbol{\Delta}^u_{LL}(t,t';k_E^2)\,\boldsymbol{P}_+\,\mathcal{D}^{(3)}_L(t')\left(\frac{3k_E^2}{32}\,\partial_{k_E} - \frac{3k_E^3}{32}\,\partial^2_{k_E} + \frac{k_E^4}{32}\,\partial^3_{k_E}\right)\right.\\
&\left.+\frac{\boldsymbol{\Delta}^u_{LR}(t,t';k_E^2)}{m_b}\,\boldsymbol{P}_+\,\mathcal{D}^{(3)}_R(t')\left(-\frac{3k_E^2}{8}\,\partial_{k_E} + \frac{3k_E^3}{8}\,\partial^2_{k_E}\right)\right]B_W(t',t;k_E^2)\Bigg\}\,,
\end{aligned}$$

$$C_{8g}^{GG} = \frac{\kappa_{GG}}{4\sqrt{2}G_F\lambda_t}\left\{\frac{1}{6}\,R_{LL}^G - \frac{1}{4}\,R_{LR}^G + 2\pi\int_0^\infty dk_E\int_\epsilon^1 dtdt'\,\mathcal{D}_L^{(2)\dagger}(t)\right.$$
$$\times\left[\boldsymbol{\Delta}_{LL}^d(t,t';k_E^2)\,\mathcal{D}_L^{(3)}(t')\left(-\frac{5k_E^2}{32}\,\partial_{k_E} + \frac{5k_E^3}{32}\,\partial_{k_E}^2 - \frac{k_E^4}{96}\,\partial_{k_E}^3\right)\right.$$
$$\left.\left. + \frac{\boldsymbol{\Delta}_{LR}^d(t,t';k_E^2)}{m_b}\,\mathcal{D}_R^{(3)}(t')\left(\frac{3k_E^2}{8}\,\partial_{k_E} - \frac{3k_E^3}{8}\,\partial_{k_E}^2\right)\right]B_G'(t',t;k_E^2)\right\}, \quad (5.33)$$

where $\kappa_{WW} = g_5^2/(2\pi r)$ and $\kappa_{GG} = N_c\,g_s^2$. Note that the factor κ_{GG} for the triple gluon vertex diagram is larger by $N_c^2 = 9$ compared to κ_G^{8g} and comes with a relative sign. We recover the same boundary terms that have already been calculated in Section 5.1.2 apart from constant factors.

5.2 Analysis of the dipole Wilson coefficients

In order to show the finiteness of the dipole coefficients in (5.8), (5.24) and (5.33) the UV behavior of the boson and fermion 5D propagators must be analyzed. This has been discussed in Section 3.4. For instance, the general behavior of the (vector) gauge-boson 5D propagator for large Euclidean momenta is given by (subscript $B = A, G, W, Z$)

$$B_B(t,t';k_E^2) \sim \frac{\sqrt{tt'}}{k_E}\,e^{-\hat{k}_E\,|t-t'|}\,, \qquad (\hat{k}_E \gg 1/t, 1/t') \quad (5.34)$$

which is exponentially suppressed except for $|t-t'| \sim 1/\hat{k}_E$. Integrating (5.34) along the coordinates t and t' we find

$$\int_\epsilon^1 dtdt'\,B_B(t,t';k_E^2) \sim \frac{1}{k_E^2}\,, \qquad (\hat{k}_E \gg 1/\epsilon) \quad (5.35)$$

showing that the integral scales like k_E^{-2} for $\hat{k}_E \gg 1/\epsilon$. Based on this analysis, and extending it to the case of the fermion propagator functions, we can formulate a power counting for integrals, where each extra-dimensional coordinate is integrated over the full interval. Excluding brane-localized terms, the counting in terms of Euclidean momenta can be formulated as

$$\boldsymbol{\Delta}_{AB}^q \to (k_E)^{-1}, \qquad B_{W,Z,A,G} \to (k_E)^{-1}\,, \qquad \int_\epsilon^1 dt \to (k_E)^{-1}\,, \quad (5.36)$$

with the additional condition that the last t integration is not counted. This condition can be traced back to the conservation of the total five-momentum. We can apply the power-counting scheme (5.36) to the penguin loops (5.24) and (5.33), showing that after the t, t' integrations the integrands fall off like k_E^{-2} for large Euclidean momenta. Thus the remaining momentum integration can be performed and yields a finite result. This is in agreement with the findings of [198], where the authors have derived a power-counting scheme for the penguin diagrams treating the Yukawa interactions as small perturbations. Since the Higgs contribution contains two brane-localized vertices, our scheme (5.36) does not apply here. The analysis of Section 5.1.1 has shown that the relevant functions in the brane-localized Higgs scenario scale like $T_{RR}^d(k_E^2) \sim \hat{k}_E^{-1}$ and $T_{RL}^d(k_E^2) \sim \text{const} + \mathcal{O}(\hat{k}_E^{-1})$ for large Euclidean momenta. Since the Higgs-boson propagator scales like k_E^{-2} the Wilson coefficient is finite, which is in agreement with the results of [198].

5.2.1 Connection with the KK-decomposed (4D) theory

We can express the dipole coefficients, as defined via the amplitude (5.3), in terms of sums over zero-mode and KK-mode contributions. Starting from the expressions (5.8), (5.24) and (5.33) in the 5D framework we replace the 5D propagator functions by their corresponding KK representations. The appearing momentum integrals can be performed analytically and we obtain the loop functions $I_{3,4}(x)$ and $I_{6\text{-}11}(x)$, which are defined in Appendix B. We find the compact expressions

$$\begin{aligned}
C^B_{7\gamma,8g} &= \frac{\kappa_B^{7\gamma,8g}}{4\sqrt{2}G_F\lambda_t}\sum_{n,m}\frac{1}{m^2_{B_m}}\left[\frac{m_{q_n}}{m_b}\frac{I_6(x^{q_n}_{B_m})}{2}V^{B^-}_{2mn}\,\tilde{V}^{B^+}_{nm3}+\frac{I_7(x^{q_n}_{B_m})}{2}V^{B^-}_{2mn}\,V^{B^+}_{nm3}\right],\\
C^{WW}_{7\gamma} &= \frac{\kappa_{WW}}{4\sqrt{2}G_F\lambda_t}\sum_{n,m}\frac{1}{m^2_{B_m}}\left[\frac{m_{u_n}}{m_b}I_8(x^{B_m}_{u_n})\,V^{W^-}_{2mn}\,\tilde{V}^{W^+}_{nm3}+I_9(x^{B_m}_{u_n})\,V^{W^-}_{2mn}\,V^{W^+}_{nm3}\right],\\
C^{GG}_{8g} &= \frac{\kappa_{GG}}{4\sqrt{2}G_F\lambda_t}\sum_{n,m}\frac{1}{m^2_{B_m}}\left[\frac{m_{d_n}}{m_b}I_{10}(x^{B_m}_{d_n})\,V^{G}_{2mn}\,\tilde{V}^{G}_{nm3}+I_{11}(x^{B_m}_{d_n})\,V^{G}_{2mn}\,V^{G}_{nm3}\right],\\
C^{h}_{7\gamma,8g} &= \frac{-\kappa_h^{7\gamma,8g}}{4\sqrt{2}G_F\lambda_t}\sum_{n}\frac{1}{m^2_{h}}\left[\frac{m_{d_n}}{m_b}I_3(x^{d_n}_{h})\,(g^d_h)_{2n}\,(g^d_h)_{n3}+I_4(x^{d_n}_{h})\,(g^d_h)_{2n}\,(\tilde{g}^d_h)_{n3}\right],
\end{aligned} \tag{5.37}$$

where $x^a_b \equiv m^2_a/m^2_b$, and $q = u$ for $B = W$ and $q = d$ for $B = A, G, Z$ in the first line. The summation index m counts the contributions from the gauge-boson zero ($m = 0$ for the SM gauge-bosons) and KK modes ($m \geq 1$), while n counts the quark zero ($n = 1, 2, 3$ for the SM quarks) and KK modes ($n = 4, ..., 9$ for the first KK level and so on). We mention that there are no contributions from the massless zero modes (the SM photon and gluon), which implies that the summation starts with $m = 1$ in the first line for $B = A, G$ and in the third line of (5.37). The $\pm$ superscripts on the overlap integrals $V^{B^\pm}_{nmk}$ and $\tilde{V}^{B^\pm}_{nmk}$ are only relevant in the case of $B = W$ and can be ignored otherwise. The definitions of the overlap integrals can be found in Appendix A, while explicit expressions for the loop functions $I_{3,4}(x)$ and $I_{6\text{-}11}(x)$ are given in (B.2). We note that when we insert the integral representations of the loop functions (B.1) into (5.37) we can identify the boundary terms R^B_{LL} and R^B_{LR}, defined in the 5D approach by (5.25), with the expressions ($B = A, G, W, Z$)

$$R^B_{LL} = \sum_{m,n}\frac{1}{m^2_{B_m}}V^{B^-}_{2mn}\,V^{B^+}_{nm3}\,, \qquad R^B_{LR} = \sum_{m,n}\frac{1}{m^2_{B_m}}\frac{m_{q_n}}{m_b}V^{B^-}_{2mn}\,\tilde{V}^{B^+}_{nm3} \tag{5.38}$$

in the KK-decomposed theory. Those terms originate from penguin diagrams where scalar components of the 5D gauge bosons are exchanged. In fact, we have also checked equation (5.37) by using the 4D Feynman rules listed in Appendix A and following the basic steps to obtain the dipole coefficients. The chirality-flipped coefficients $\tilde{C}^B_{7\gamma,8g}$ can be obtained by replacing $V^B_{nmk} \leftrightarrow \tilde{V}^B_{nmk}$ and $(g^d_h)_{nk} \leftrightarrow (\tilde{g}^d_h)_{nk}$.

There are two terms in each square bracket for the Wilson coefficients in (5.37). In the SM only diagrams with a chirality flip on the external b-quark line contribute to $C_{7\gamma}$, since the $W^\pm$ boson couples only to left-chiral quarks. Since in the RS model we can have also couplings to right-chiral quarks, there are additional contributions originating from diagrams where the chirality flip is performed on the internal quark line, which generates the factor m_{q_n}/m_b in front of the first term in each of the brackets in (5.37). When exchanging KK quarks in the loop this factor is large and enhances the contributions.

Picture	Average time to calculate $C_{7\gamma,8g}$ for one RS point	Average time fractions for each contribution					
		$C^W_{7\gamma,8g}$	$C^{WW}_{7\gamma}$	$C^Z_{7\gamma,8g}$	$C^{A/G}_{7\gamma,8g}$	C^{GG}_{8g}	$C^h_{7\gamma,8g}$
5D	571 min	2%	4%	21%	32%	41%	$\leq 0.01\%$
4D	9 min	16%		46%	38%		$\leq 0.1\%$

Table 5.1: Time performance for calculating the Wilson coefficients $C_{7\gamma}$ and C_{8g} in the 5D and 4D (including 5 KK levels) pictures. The first column contains the average time needed in order to calculate the Wilson coefficients for one RS point on a 2.4 GHz Intel Core i5 processor, such that the results are compatible at the few per mille level in both approaches (see Figure 5.2 for more details). The additional columns show the relative fractions of time needed for the calculation of the six different contributions. Similar values are obtained in case of the chirality-flipped Wilson coefficients.

We have numerically checked that all corrections in the RS model decouple with $M_{\rm KK}^{-2}$, which is not directly obvious from the expressions (5.37). For instance, let us discuss the KK contributions to $C^W_{7\gamma,8g}$. At first we stress that the loop functions can only take values from the compact intervals $I_6(x) \in [-2, -\frac{1}{2}]$ and $I_7(x) \in [\frac{5}{12}, \frac{2}{3}]$, and are irrelevant for the discussion. We begin with the contribution of penguin diagrams that exchange SM quarks ($n = 1, 2, 3$) with KK W bosons ($m \geq 1$) in the first line of (5.37). Obviously the suppression by the squared KK W-boson mass implies that the contribution decouples with $M_{\rm KK}^{-2}$. Next, we discuss the contribution from exchanging the W boson ($m = 0$) with KK quarks ($n \geq 4$). The overlap integrals scale like $V^{W^-}_{20n} \sim V^{W^+}_{n03} \sim \tilde{V}^{W^+}_{n03} \sim M_{\rm KK}^{-1}$ for $n \geq 4$, which implies that the second term in the round bracket of the first line in (5.37) decouples with $M_{\rm KK}^{-2}$. The first term in the round bracket is more subtle, since it is enhanced by the KK-quark mass $m_{q_n} \sim M_{\rm KK}$. However, numerically we observe that the summation over complete KK levels ($n = 4, ..., 9$ for the first KK level and so on) leads to cancellations such that there appears an additional $M_{\rm KK}^{-1}$ suppression. Hence, also the first term in the round bracket, when summed over complete KK levels, decouples with $M_{\rm KK}^{-2}$. In a similar fashion we can proceed with the contributions from the penguin diagrams with KK W bosons and KK quarks. The discussion can also be extended for the remaining Wilson coefficients. In fact the decoupling behavior with $M_{\rm KK}^{-2}$ is apparent in the approximate expressions that will be given in Section 5.2.3.

Finally, we remark that the Wilson coefficients in the SM can be recovered from the second terms in $C^W_{7\gamma,8g}$ and $C^{WW}_{7\gamma}$ by summing only over the gauge-boson ($m = 0$) and quark zero modes ($n = 1, 2, 3$), and by replacing the overlap integrals with the CKM matrix elements $V^{W^-}_{20n} \to V^*_{u_n s}$ and $V^{W^+}_{n03} \to V_{u_n b}$ with $u_{1,2,3} = u, c, t$.

5.2.2 Numerical evaluation

The first step is to generate six sets of 5000 RS points with different values for $y_* =$ 0.5, 1, 1.5, 2, 2.5 and 3 according to the procedure described in Section 2.5. Here, $y_\star$ sets the upper bound for each entry of the Yukawa matrices, such that $|(\boldsymbol{Y}_q)_{ij}| \leq y_*$. We have implemented the integrals arising in the expressions for the dipole coefficients in (5.8), (5.24) and (5.33) using *Mathematica* [186]. Since we expect the RS corrections to the SM Wilson coefficients to lie in the few percent range, we need to calculate the integrals to an accuracy of a few per mille. We therefore set PrecisonGoal to 3 for the numerical integrations. Furthermore we use a UV momentum cutoff such that $k_E \leq \Lambda_{\rm cut} = 100\, M_{\rm KK}$, which improves the time performance without losing the required

precision. It turns out that the numerical integrations over t and t' can be made faster by making the substitution $t \to \phi/\pi = \ln(t/\epsilon)/\ln(1/\epsilon)$ and analogously for t', which maps the integration region on the unit square. The first row of Table 5.1 compares the time performance of calculating the Wilson coefficients $C_{7\gamma}$ and C_{8g} in the 5D and 4D pictures, averaged over many sets of RS parameter points. We need on average 571 minutes per RS point on a 2.4 GHz Intel Core i5 processor to calculate $C_{7\gamma}$ and C_{8g} in the 5D approach. In more detail, the calculation splits into six parts belonging to different amplitude topologies. The least amount of time is required for the calculation of the Higgs contribution, since the t and t' integrations can be performed analytically, leaving over one momentum integral to be evaluated, see (5.8). Most of the computational time is needed for the KK contributions of the neutral gauge bosons, since the corresponding integrands involve all components of the 5D fermion propagator functions, in contrast to the $W^\pm$-boson Wilson coefficients in (5.24) and (5.33).

We can compare our results from the 5D approach with the summation over zero and KK modes in the KK-decomposed theory, based on the results shown in (5.37). In order to achieve a consistency between both approaches at the few per mille level, we need to sum over five complete KK levels. The left plot in Figure 5.2 confirms that the results for $C_{7\gamma}$ calculated in the 5D and 4D approaches (indicated by the superscripts "5D" and "4D") are consistent at the few per mille level. The results for the RS corrections relative to the SM Wilson coefficient $C_{7\gamma}^{\rm SM}$ are compatible at the 10% level in both pictures, as shown in the right plot in Figure 5.2. This presents a non-trivial cross-check of the formulas derived in Section 5.1. In both plots of Figure 5.2 we have focused on $C_{7\gamma}$, but we have checked that the histograms look similar in case of C_{8g} and the corresponding chirality-flipped Wilson coefficients. We need on average 9 minutes to calculate the KK quark and gauge-boson masses as well as the overlap integrals in the 4D formulation, see Table 5.1. Effectively there are only four different amplitude topologies, since $C_{7\gamma,8g}^{W}$ and $C_{7\gamma}^{WW}$ both depend on the same masses and overlap integrals, and analogously for $C_{7\gamma,8g}^{G}$ and C_{8g}^{GG}. Therefore we present combined time fractions for those Wilson coefficients in Table 5.1. When we require a consistency of a few per mille for the calculation of the Wilson coefficients between the 4D and 5D approaches, we find that the summation over KK levels is faster by a factor of order 60. As a consequence, after we have verified that the results in the 5D and 4D approaches agree at the required level of precision, we will implement the equations in (5.37) for the numerical calculation of the Wilson coefficients for most of the RS points used in the phenomenological analysis in Section 5.3.

We emphasize that the integral expressions (5.8), (5.24) and (5.33) and the corresponding results in the KK-decomposed theory (5.37) are formally valid to all orders in $v^2/M_{\rm KK}^2$. All numerical results that will be presented are calculated from those equations according to the procedure described above.

5.2.3 Separating the zero- and KK-mode contributions

We parametrize the RS corrections relative to the SM Wilson coefficients by

$$\begin{aligned} C_{7\gamma}^{\rm RS,0}(\mu_W) &= C_{7\gamma}^{W,0}(\mu_W) + C_{7\gamma}^{WW,0}(\mu_W) + C_{7\gamma}^{Z,0}(\mu_W) + C_{7\gamma}^{h,0}(\mu_W) - C_{7\gamma}^{\rm SM}(\mu_W)\,, \\ C_{7\gamma}^{\rm RS,KK}(\mu_{\rm KK}) &= C_{7\gamma}^{W,\rm KK}(\mu_{\rm KK}) + C_{7\gamma}^{WW,\rm KK}(\mu_{\rm KK}) + C_{7\gamma}^{A,\rm KK}(\mu_{\rm KK}) + C_{7\gamma}^{G,\rm KK}(\mu_{\rm KK}) \\ &\quad + C_{7\gamma}^{Z,\rm KK}(\mu_{\rm KK}) + C_{7\gamma}^{h,\rm KK}(\mu_{\rm KK})\,, \end{aligned} \tag{5.39}$$

where we distinguish corrections that arise from exchanging only zero modes and of loops including at least one virtual KK particle. The individual zero-mode contributions $C_{7\gamma}^{B,0}(\mu_W)$ for $B = W, WW, Z, h$ are defined at the electroweak scale $\mu_W \sim m_W$ and are

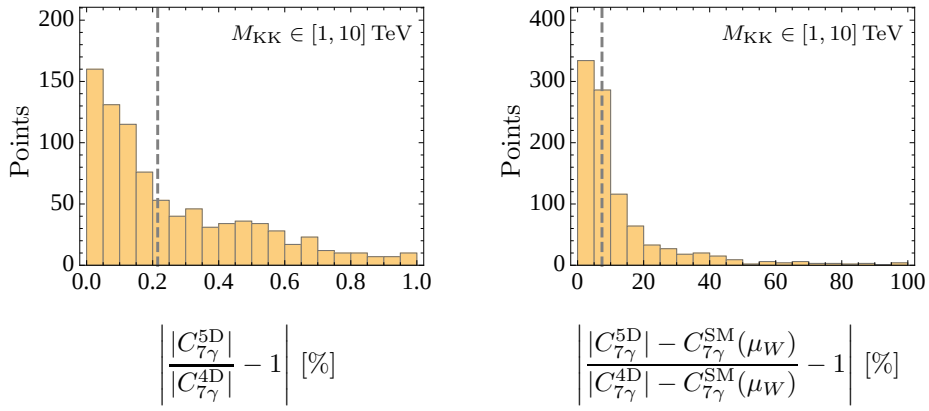

Figure 5.2: Compatibility of the results for the Wilson coefficient $C_{7\gamma}$ (left) and for the RS corrections relative to the SM Wilson coefficient $C_{7\gamma}^{\rm SM}(\mu_W) \approx -0.20$ (right) calculated in the 5D and 4D pictures. Both histograms contain RS parameter points with different values for y_* and $M_{\rm KK} \in [1, 10]$ TeV. The vertical dashed lines denote the median values of the corresponding distributions.

given simply by setting $m = 0$ and summing over $n = 1, 2, 3$ in (5.37). On the other hand the KK contributions $C_{7\gamma}^{B,\rm KK}(\mu_{\rm KK})$ are defined at the KK scale $\mu_{\rm KK} \sim M_{\rm KK}$. Analogous parametrizations hold for the chirality-flipped and chromomagnetic Wilson coefficients, where the triple gluon-vertex contribution must be included. In the SM the contribution to the Wilson coefficients at leading order is given by the penguin diagrams (II) and (III) in Figure 5.1, in which virtual $W^\pm$ bosons and up-type quarks are exchanged. The charm- and top-penguin diagrams yield comparable contributions,[3] since the product of the CKM matrix elements are of similar size,[4] $|\lambda_t| \approx |\lambda_c|$, where $\lambda_q \equiv V_{qs}^* V_{qb}$. Making use of the unitarity of the CKM matrix, which implies $\lambda_u + \lambda_c + \lambda_t = 0$, the SM Wilson coefficients at the electroweak scale are given by[5]

$$C_{7\gamma}^{\rm SM}(\mu_W) = Q_u \left(\frac{I_7(x_t)}{2} - \frac{1}{3}\right) + I_9(x_t^{-1}) - \frac{5}{12}\,, \qquad C_{8g}^{\rm SM}(\mu_W) = \frac{I_7(x_t)}{2} - \frac{1}{3}\,, \quad (5.40)$$

where $x_t \equiv m_t^2/m_W^2$. The loop functions $I_7(x)$ and $I_9(x)$ can be found in Appendix B. Using $m_{t,\rm pole} = 174.6 \pm 1.9\,\text{GeV}$ [76] and $m_W = 80.385^{+0.015}_{-0.015}\,\text{GeV}$ [76] we find $C_{7\gamma}^{\rm SM}(\mu_W) \approx -0.20$ and $C_{8g}^{\rm SM}(\mu_W) \approx -0.097$.

In a first step, we look at the relative size of the RS corrections, based on a set of RS points. To this end, we compare the median values of the distributions obtained from calculating $|C_{7\gamma,8g}^{B,0}(\mu_W)|$ and $|C_{7\gamma,8g}^{B,\rm KK}(\mu_{\rm KK})|$ and normalizing them to the total sum of each (absolute) correction $\sum_B |C_{7\gamma,8g}^{B,0}(\mu_W)|$ and $\sum_B |C_{7\gamma,8g}^{B,\rm KK}(\mu_{\rm KK})|$. Table 5.2 shows the results. The general pattern is that the penguin loop diagrams with $W^\pm$-boson exchange give the largest corrections. In case of the zero-mode contribution we find that the largest corrections are given by the deviations of the overlap integrals $V_{203}^{W^-}$ and $V_{303}^{W^+}$ in the RS model with respect to the CKM matrix elements V_{ts}^* and V_{tb} in the SM, and by

[3] In fact, the charm-quark contribution is slightly larger than the top-quark contribution due to the larger loop functions $I_7(x_c) \approx 0.66 > I_7(x_t) \approx 0.47$ and $I_9(x_c^{-1}) \approx 0.42 > I_9(x_t^{-1}) \approx 0.28$, where $x_{c,t} \equiv m_{c,t}^2/m_W^2$ and the loop functions are given in Appendix B.

[4] In more detail, λ_t and λ_c have a relative sign in common, $\lambda_t \approx -\lambda_c \approx -0.04$, such that the top- and charm-quark contributions interfere destructively.

[5] Since $x_{u,c} \ll 1$, we have taken the limit $x_{u,c} \to 0$ for the loop functions and used $I_7(x_{u,c}) \approx \frac{2}{3}$ and $I_9(x_{u,c}^{-1}) \approx \frac{5}{12}$ in (5.40).

Size of RS corrections	Median values of the distributions in [%]						
	W	WW	Z	A	G	GG	h
$\lvert C_{7\gamma}^{B,0}(\mu_W)\rvert / \sum_B \lvert C_{7\gamma}^{B,0}(\mu_W)\rvert$	32.6	65.8	1.6	-	-	-	0.04
$\lvert C_{8g}^{B,0}(\mu_W)\rvert / \sum_B \lvert C_{8g}^{B,0}(\mu_W)\rvert$	90.6	-	9.2	-	-	-	0.2
$\lvert C_{7\gamma}^{B,\mathrm{KK}}(\mu_{\mathrm{KK}})\rvert / \sum_B \lvert C_{7\gamma}^{B,\mathrm{KK}}(\mu_{\mathrm{KK}})\rvert$	33.7	51.4	7.7	0.0001	0.1	-	7.1
$\lvert C_{8g}^{B,\mathrm{KK}}(\mu_{\mathrm{KK}})\rvert / \sum_B \lvert C_{8g}^{B,\mathrm{KK}}(\mu_{\mathrm{KK}})\rvert$	52.8	-	24.1	0.0003	0.04	0.5	22.2

Table 5.2: Median values of the distributions in the left column based on RS points with $M_{\mathrm{KK}} \in [1, 10]\,\mathrm{TeV}$ and for different values of $y_\star$. The median values can be used to estimate the relative size of the RS corrections arising from the exchange of only zero modes $C_{7\gamma,8g}^{B,0}(\mu_W)$ and of loops including at least one virtual KK particle $C_{7\gamma,8g}^{B,\mathrm{KK}}(\mu_{\mathrm{KK}})$. Similar values are obtained in case of the chirality-flipped Wilson coefficients.

the coupling of the W boson to right-chiral quarks. Those corrections stem from the non-flatness of the W-boson profile and from deviations of the exact (Z_2-even) quark profiles from the ZMA expressions. The zero-mode contributions from the Z and Higgs bosons arise due to their flavor-changing couplings to quarks in the RS model, but they are suppressed by small down-type quark masses and can be neglected. Concerning the KK contributions we find, contrary to the observation made in [246], (independently of y_*) that the triple gluon vertex contribution is subdominant and does not enhance the chromomagnetic dipole coefficients. In general, we find that the penguin diagrams with the exchange of photon and gluon KK modes yield very small corrections. At last we can compare the relative magnitude between $C_{7\gamma,8g}^{\mathrm{RS},0}(\mu_W)$ and $C_{7\gamma,8g}^{\mathrm{RS,KK}}(\mu_{\mathrm{KK}})$. Numerically, we find that both contributions are similar in size for $y_* \approx 2$. For larger values of y_* the KK contributions dominate in size.[6]

In the next step, we will take a closer look at the main KK contributions to the Wilson coefficients and derive approximate expressions.

W- and Z-boson KK contributions

We begin with the KK contributions of the $W^\pm$- and Z-boson penguin diagrams to the dipole coefficients. These contributions are implicitly included in the first two expressions in (5.37). Numerically, the dominant contributions are coming from diagrams exchanging charged/neutral scalar zero modes (stemming from the fifth component of the 5D gauge-boson field and the NGBs in the Higgs sector) and KK quarks.[7] In this case we are allowed to take the limits $x_{B_m}^{q_n} \gg 1$ and $x_{q_n}^{B_m} \ll 1$ for the loop functions in (5.37), leading to $I_6(x) \approx -1/2$, $I_7(x) \approx 5/12$, $I_8(x) \approx -1$ and $I_9(x) \approx 5/12$. We find

$$C_{7\gamma,8g}^{W,\mathrm{KK}}(\mu_{\mathrm{KK}}) \approx \frac{\kappa_W^{7\gamma,8g}}{4\sqrt{2}G_F\lambda_t}\left[\frac{5}{24}\left(R_{LL}^W - \sum_{n=1}^{3}\frac{V_{20n}^{W^-}\,V_{n03}^{W^+}}{m_W^2}\right) - \frac{1}{4}\left(R_{LR}^W - \frac{m_t}{m_b}\,\frac{V_{203}^{W^-}\,\tilde{V}_{303}^{W^+}}{m_W^2}\right)\right],$$

[6] In case of the chirality-flipped Wilson coefficients, we find that $\tilde{C}_{7\gamma,8g}^{\mathrm{RS,KK}}(\mu_{\mathrm{KK}})$ is in general larger than $\tilde{C}_{7\gamma,8g}^{\mathrm{RS},0}(\mu_W)$ for $y_\star \gtrsim 1$.

[7] We like to stress that if we do not include the contributions from the NGBs, the diagrams with gauge-boson zero-modes and KK quarks would be suppressed to leading order by v^4/M_{KK}^4. In this case the contributions from KK gauge-bosons and KK quarks would be dominant, since they contribute already at order v^2/M_{KK}^2.

$$C_{7\gamma}^{WW,\mathrm{KK}}(\mu_{\mathrm{KK}}) \approx \frac{\kappa_{WW}^{7\gamma}}{4\sqrt{2}G_F\lambda_t}\left[\frac{1}{6}\left(R_{LL}^W - \sum_{n=1}^{3}\frac{V_{20n}^{W^-}V_{n03}^{W^+}}{m_W^2}\right) - \frac{1}{4}\left(R_{LR}^W - \frac{m_t}{m_b}\frac{V_{203}^{W^-}\tilde{V}_{303}^{W^+}}{m_W^2}\right)\right],$$
$$C_{7\gamma,8g}^{Z,\mathrm{KK}}(\mu_{\mathrm{KK}}) \approx \frac{\kappa_{Z}^{7\gamma,8g}}{4\sqrt{2}G_F\lambda_t}\left[\frac{5}{24}\left(R_{LL}^Z - \sum_{n=1}^{3}\frac{V_{20n}^{Z}V_{n03}^{Z}}{m_Z^2}\right) - \frac{1}{4}R_{LR}^Z\right], \tag{5.41}$$

where the boundary terms R_{LL}^B and R_{LR}^B are given in (5.28) and (5.32). Since the limits of the loop functions we have taken are not valid in case of SM quarks, we have to subtract the contributions from the quark zero modes in (5.41). We observe that the corrections of $C_{7\gamma}^{W,\mathrm{KK}}(\mu_{\mathrm{KK}})$ and $C_{7\gamma}^{WW,\mathrm{KK}}(\mu_{\mathrm{KK}})$ add up constructively, since $\kappa_W^{7\gamma} = Q_u\,\kappa_{WW}^{7\gamma}$. We can further simplify the boundary terms $R_{LL}^{W,Z}$ and $R_{LR}^{W,Z}$ in (5.41) by expanding them in v^2/M_{KK}^2 and neglecting terms that are suppressed by m_s/m_b. We obtain

$$\begin{aligned}
R_{LL}^W &\approx -\frac{L}{2M_{\mathrm{KK}}^2}\,(\boldsymbol{\Delta}_D)_{23} - \frac{(\boldsymbol{\delta}_D)_{23}}{\tilde{m}_W^2}\,,\\
R_{LR}^W &\approx -\frac{L}{4M_{\mathrm{KK}}^2}\,(\boldsymbol{\Delta}_D)_{23} + \frac{1}{2\tilde{m}_W^2}\,\frac{v}{\sqrt{2}m_b}\,\frac{v^2}{M_{\mathrm{KK}}^2}\mathcal{D}_L^{(2)\dagger}(1^-)\,\boldsymbol{P}_{12}\,\boldsymbol{Y}_u\,\boldsymbol{Y}_u^\dagger\,\boldsymbol{Y}_d\,\mathcal{D}_R^{(3)}(1^-)\,,\\
R_{LL}^Z &\approx -\frac{L}{2M_{\mathrm{KK}}^2}\,(\boldsymbol{\Delta}_D)_{23} - \left(1-\frac{(g_R^d)^2}{(g_L^d)^2}\right)\frac{(\boldsymbol{\delta}_D)_{23}}{\tilde{m}_Z^2}\,,\\
R_{LR}^Z &\approx -\frac{L}{4M_{\mathrm{KK}}^2}\,(\boldsymbol{\Delta}_D)_{23} - \frac{g_R^d}{g_L^d}\left(1-\frac{g_R^d}{g_L^d}\right)\frac{(\boldsymbol{\delta}_D)_{23}}{\tilde{m}_Z^2}\\
&\quad + \left(1-\frac{g_R^d}{g_L^d}\right)^2\frac{1}{2\tilde{m}_Z^2}\,\frac{v}{\sqrt{2}m_b}\,\frac{v^2}{M_{\mathrm{KK}}^2}\mathcal{D}_L^{(2)\dagger}(1^-)\,\boldsymbol{P}_{12}\,\boldsymbol{Y}_d\,\boldsymbol{Y}_d^\dagger\,\boldsymbol{Y}_d\,\mathcal{D}_R^{(3)}(1^-)\,,
\end{aligned} \tag{5.42}$$

where in the case of R_{LR}^W and R_{LR}^Z we have implemented the relation [149]

$$\frac{1}{\sqrt{2}}\,\mathcal{Q}_L^{(m)\dagger}(1^-)\,\boldsymbol{P}_{12}\,\tilde{\boldsymbol{Y}}_q\,\mathcal{Q}_R^{(n)}(1^-) = \delta_{mn}\,\frac{m_{q_n}}{v} - \frac{m_{q_m}}{v}\,(\boldsymbol{\delta}_q)_{mn} - \frac{m_{q_n}}{v}\,(\boldsymbol{\delta}_Q)_{mn}\,. \tag{5.43}$$

We checked numerically for different values of y_* that the approximate formulas (5.41) together with (5.42) are accurate at the 10% level compared with the exact expressions. We emphasize that the approximate expressions are independent of the masses and profiles of the KK quark and gauge-boson modes. In (5.42) we encounter terms including products of three Yukawa matrices $\boldsymbol{Y}_u\boldsymbol{Y}_u^\dagger\boldsymbol{Y}_d$ and $\boldsymbol{Y}_d\boldsymbol{Y}_d^\dagger\boldsymbol{Y}_d$ originating from the IR brane-localized terms in R_{LR}^W and R_{LR}^Z in (5.32). They originate from diagrams exchanging $W^\pm$ and Z NGBs with a chirality flip on the internal KK quark line as shown in Figure 5.3. Those terms yield the dominant KK corrections for not too small values of the Yukawa matrix entries, which is approximately fulfilled for RS points with $y_* \gtrsim 1$. In this case we can derive simpler expressions and find ($y_* \gtrsim 1$)

$$\begin{aligned}
C_{7\gamma}^{W,\mathrm{KK}}(\mu_{\mathrm{KK}}) &\approx \frac{Q_u}{\lambda_t}\left[-\frac{1}{8}\,\frac{v}{\sqrt{2}m_b}\,\frac{v^2}{M_{\mathrm{KK}}^2}\mathcal{D}_L^{(2)\dagger}(1^-)\,\boldsymbol{P}_{12}\,\boldsymbol{Y}_u\boldsymbol{Y}_u^\dagger\boldsymbol{Y}_d\,\mathcal{D}_R^{(3)}(1^-) + \frac{1}{4}\,\frac{m_t}{m_b}\,\frac{V_{203}^{W^-}\tilde{V}_{303}^{W^+}}{m_W^2}\right],\\
C_{7\gamma}^{Z,\mathrm{KK}}(\mu_{\mathrm{KK}}) &\approx \frac{Q_d}{\lambda_t}\left[-\frac{1}{16}\,\frac{v}{\sqrt{2}m_b}\,\frac{v^2}{M_{\mathrm{KK}}^2}\mathcal{D}_L^{(2)\dagger}(1^-)\,\boldsymbol{P}_{12}\,\boldsymbol{Y}_d\boldsymbol{Y}_d^\dagger\boldsymbol{Y}_d\,\mathcal{D}_R^{(3)}(1^-)\right],
\end{aligned} \tag{5.44}$$

where the chromomagnetic dipole Wilson coefficients $C_{8g}^{W,\mathrm{KK}}$ ($C_{8g}^{Z,\mathrm{KK}}$) can be obtained from the first (second) line in (5.44) by sending $Q_u \to 1$ ($Q_d \to 1$). Moreover, $C_{7\gamma}^{WW,\mathrm{KK}}$ is given analogously by the expression in the first line of (5.44) with Q_u set to 1. We

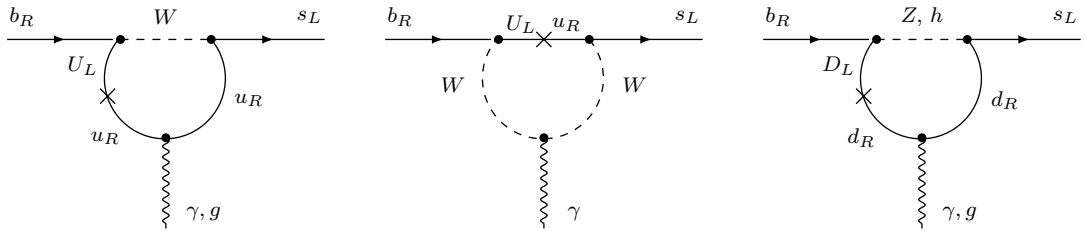

Figure 5.3: For $y_* \gtrsim 1$ those diagrams give the main KK corrections $C_{7\gamma,8g}^{\rm RS,KK}(\mu_{\rm KK})$ for the transitions $b \to s\gamma$ and $b \to sg$ at the one-loop level. Internal solid lines labelled by u_R denotes the exchange of singlet up-type KK quarks, while U_L, D_L imply the exchange of $SU(2)_L$ doublet KK quarks. Crosses denote a chirality flip on the internal KK quark lines. Here, dashed lines labelled with W or Z denote the contributions from the corresponding NGBs in the Higgs sector.

checked numerically that the approximate expressions are valid at the 10% level with respect to the exact expressions for RS points with $y_* \gtrsim 1$. Approximate formulas for the chirality flipped Wilson coefficients $\tilde{C}_{7\gamma,8g}^{B,\rm KK}(\mu_{\rm KK})$ can be obtained from (5.44) by making the replacements $L \leftrightarrow R$, $\boldsymbol{Y}_q \leftrightarrow \boldsymbol{Y}_q^\dagger$, $V_{203}^{W^-} \to \tilde{V}_{203}^{W^-}$ and $\tilde{V}_{303}^{W^+} \to V_{303}^{W^+}$.

Higgs KK contribution

The diagrams contributing to $C_{7\gamma,8g}^{h,\rm KK}(\mu_{\rm KK})$ involve the exchange of the Higgs boson with KK quark modes. For the exchange of KK quarks we can use that $x_h^{d_n} \gg 1$, allowing us to take the limits $I_3(x) = 1/(2x) + \mathcal{O}(x^{-2})$ and $I_4(x) = 1/(12x) + \mathcal{O}(x^{-2})$. The contribution associated with $I_3(x)$ dominates, since this loop function is less suppressed than $I_4(x)$ in the considered limit and the contribution is enhanced by m_{d_n}/m_b, which is a large factor for KK modes. If we only keep the corresponding contribution associated with $I_3(x)$, we obtain approximately

$$C_{7\gamma}^{h,\rm KK}(\mu_{\rm KK}) \approx \frac{Q_d}{\lambda_t}\left[\frac{1}{16}\frac{v}{\sqrt{2}m_b}\frac{v^2}{M_{\rm KK}^2}\,\mathcal{D}_L^{(2)\dagger}(1^-)\,\boldsymbol{P}_{12}\,\boldsymbol{Y}_d\boldsymbol{Y}_d^\dagger\boldsymbol{Y}_d\,\mathcal{D}_R^{(3)}(1^-) - \frac{1}{8}(\boldsymbol{\delta}_D)_{23}\right], \quad (5.45)$$

where we have expanded the expression to leading order in $v^2/M_{\rm KK}^2$ and neglected m_s/m_b suppressed terms. The corresponding expression for $C_{8g}^{h,\rm KK}$ is given by (5.45) with $Q_d \to 1$. Numerically we have checked that (5.45) is accurate at the 10% level with respect to the exact expressions. Note that the $\boldsymbol{Y}_d\boldsymbol{Y}_d^\dagger\boldsymbol{Y}_d$ structure in (5.45) originates from the leading order expansion in $v^2/M_{\rm KK}^2$ of the function $g(\boldsymbol{X}_d, \boldsymbol{Y}_d)$ defined in (5.17) and gives the dominant contribution for $y_* \gtrsim 1$. In fact, this term exactly cancels the expression $C_{7\gamma}^{Z,\rm KK}(\mu_{\rm KK})$ in (5.44). Consequently, for $y_* \gtrsim 1$ the KK corrections from the Z-Goldstone boson and Higgs diagrams cancel to very good approximation.

Dependence of the KK contributions on $M_{g^{(1)}}$ and y_*

Figure 5.4 shows histograms of the (absolute) KK corrections for a set of RS parameter points with $y_* = 3$ and $M_{g^{(1)}} = 10\,\text{TeV}$. We choose $y_* = 3$ to obtain maximal effects, while still staying in the perturbative regime for the Yukawa sector. The value $M_{g^{(1)}} = 10\,\text{TeV}$ is close to the lowest KK gluon mass that is consistent with the tree-level analysis of the Peskin-Takeuchi parameters, see Section 2.5.2. The distributions can be well described by the approximate formulas given in (5.44) and (5.45). For different values

of $M_{g^{(1)}}$ and y_*, the corresponding distributions can be obtained by the formula

$$C_{7\gamma,8g}^{\mathrm{RS,KK}}(\mu_{\mathrm{KK}}) \approx C_{7\gamma,8g}^{\mathrm{RS,KK}}(\mu_{\mathrm{KK}})\Big|_{M_{g^{(1)}}=10\,\mathrm{TeV},\, y_*=3} \times \left(\frac{10\,\mathrm{TeV}}{M_{g^{(1)}}}\right)^2 \times \left(\frac{y_*}{3}\right)^2, \tag{5.46}$$

which is a good approximation for $y_* \gtrsim 1$. For smaller values of y_* the KK contributions do not follow a simple scaling law with y_*. An analogous equation holds for the distributions of the chirality-flipped Wilson coefficients. In order to get a rough estimate for the typical size of the KK corrections, we can calculate the median values of the distributions of $|C_{7\gamma,8g}^{\mathrm{RS,KK}}(\mu_{\mathrm{KK}})|$ and find ($y_* \gtrsim 1$)

$$\mathrm{Median}\left(|C_{7\gamma,8g}^{\mathrm{RS,KK}}(\mu_{\mathrm{KK}})|\right) \approx a_{7\gamma,8g} \times \left(\frac{10\,\mathrm{TeV}}{M_{g^{(1)}}}\right)^2 \times \left(\frac{y_*}{3}\right)^2, \tag{5.47}$$

with $a_{7\gamma} = 0.012$ and $a_{8g} = 0.0072$. In case of the median values of $|\tilde{C}_{7\gamma,8g}^{\mathrm{RS,KK}}(\mu_{\mathrm{KK}})|$ the coefficients read $\tilde{a}_{7\gamma} = 0.021$ and $\tilde{a}_{8g} = 0.012$. These coefficients represent the median values of the distributions shown in Figure 5.4. We observe that the KK corrections to the chromomagnetic dipole coefficients are (approximately) smaller by the factor $\kappa_W^{8g}/(\kappa_W^{7\gamma} + \kappa_{WW}^{7\gamma}) = 3/5$ with respect to the electromagnetic dipole coefficients. Furthermore, we find the general pattern that the chirality-flipped Wilson coefficients are enhanced, which can be explained by the different localization of the left- and right-chiral bottom-quark profiles. The left-chiral bottom quark profile, which enters $\tilde{C}_{7\gamma,8g}^{\mathrm{RS,KK}}(\mu_{\mathrm{KK}})$ is more localized towards the IR brane ($c_{b_L} = c_{Q_3} > c_{b_R} = c_{d_3}$) and is thus more sensitive to flavor-violating effects. This hierarchy of the bulk mass parameters is due to the large mass difference of the top and the bottom quark, which requires that $F(c_{b_L}) > F(c_{b_R})$.

We can (approximately) relate our results with the numerical analysis of the Wilson coefficients performed in [246], where the case of $y_* = 3$ and $M_{g^{(1)}} = 2.5\,\mathrm{TeV}$ was discussed. When we consider $M_{g^{(1)}} = 2.5\,\mathrm{TeV}$ we find that the KK corrections $C_{7\gamma}^{\mathrm{RS,KK}}(\mu_{\mathrm{KK}})$ and $\tilde{C}_{7\gamma}^{\mathrm{RS,KK}}(\mu_{\mathrm{KK}})$ are larger by roughly one order of magnitude compared with the corresponding corrections given in [246]. We have been unable to trace the origin of these discrepancies. But, the fact that we have performed our analysis using both the 5D and 4D formulations of the RS model and found consistent results in both approaches provides a highly non-trivial cross-check of our calculations. Concerning the chromomagnetic dipole Wilson coefficients $C_{8g}^{\mathrm{RS,KK}}(\mu_{\mathrm{KK}})$ and $\tilde{C}_{8g}^{\mathrm{RS,KK}}(\mu_{\mathrm{KK}})$ we find that our corrections are similar in size compared to the ones in [246].

5.2.4 Comment on the narrow bulk-Higgs scenario

We have observed that the sum of the KK contributions $C_{7\gamma,8g}^{h,\mathrm{KK}}(\mu_{\mathrm{KK}})$ and $C_{7\gamma,8g}^{Z,\mathrm{KK}}(\mu_{\mathrm{KK}})$ cancels to a very good approximation for $y_* \gtrsim 1$. In this section we investigate whether this cancellation still holds in the narrow bulk-Higgs model.

The Higgs contribution was already calculated in Section 5.1.1, and the final result has been given in (5.16) and (5.17), including the case of a narrow bulk-Higgs. It follows that the first term (containing the $\boldsymbol{Y}_d\boldsymbol{Y}_d^\dagger\boldsymbol{Y}_d$ structure) in the approximative formula for $C_{7\gamma,8g}^{h,\mathrm{KK}}(\mu_{\mathrm{KK}})$ in (5.45) must be multiplied with a minus sign in case of a narrow bulk-Higgs. Concerning the Z-boson contribution we focus on the scalar diagram (IIb). For $y_* \gtrsim 1$ the dominant corrections are due to the exchange of the Z-Goldstone boson. The corresponding terms can be extracted from $C_{7\gamma,8g}^{Z,\mathrm{scalar}}$ in (5.19). We can proceed analogously to the calculation of the Higgs contribution discussed in Section 5.1.1. Therefore,

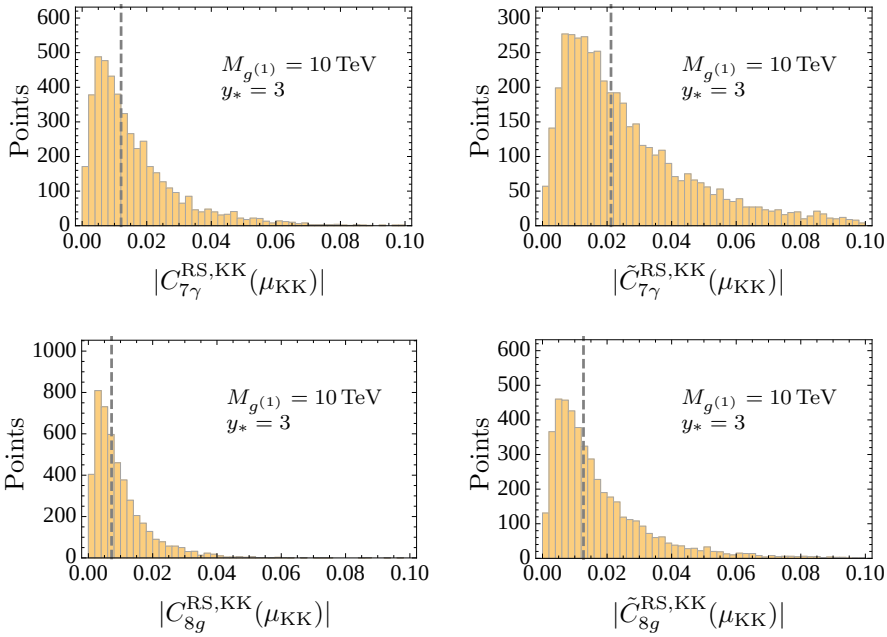

Figure 5.4: Absolute corrections from KK modes to the Wilson coefficients at the KK scale for a set of RS points with $y_* = 3$ and $M_{g^{(1)}} = 10\,\text{TeV}$. The vertical dashed lines denote the median values of the corresponding distributions. The size of the corrections are equally distributed among the real and imaginary parts of the Wilson coefficients.

we refrain from giving more details here and quote the final result ($y_* \gtrsim 1$)

$$
\begin{aligned}
C_{7\gamma,8g}^{Z,\text{scalar}} \approx \frac{\kappa_Z^{7\gamma,8g}}{4G_F\lambda_t}\,\frac{1}{(g_L^d)^2}\,\frac{1}{2v}\,\mathcal{D}_L^{(2)\dagger}(1^-)\Bigg\{ & \boldsymbol{P}_{12}\,\frac{h(\boldsymbol{X}_d,\tilde{\boldsymbol{Y}}_d)}{4m_b}\,\mathcal{D}_R^{(3)}(1^-) \\
& + 2\pi\int_0^\infty dk_E\,\frac{\boldsymbol{Z}_d(k_E^2)}{1+\boldsymbol{Z}_d(k_E^2)}\Bigg[\frac{1}{\varrho}\,\frac{\boldsymbol{P}_+}{\boldsymbol{R}_Q}\mathcal{D}_L^{(3)}(1^-)\left(\frac{5k_E}{32}\partial_{k_E}+\frac{3k_E^2}{32}\partial_{k_E}^2+\frac{k_E^3}{96}\partial_{k_E}^3\right) \\
& + \frac{\boldsymbol{P}_{12}}{m_b}\,\tilde{\boldsymbol{Y}}_d\,\mathcal{D}_R^{(3)}(1^-)\left(k_E+\frac{7k_E^2}{8}\partial_{k_E}+\frac{k_E^3}{8}\partial_{k_E}^2\right)\Bigg]\frac{\epsilon^2 M_{\text{KK}}^2}{L^2\tilde{m}_Z^2}\,B_{Z,55}(1^-,1^-;k_E^2)\Bigg\}\,.
\end{aligned}
\tag{5.48}
$$

The scalar Z-boson propagator behaves like $B_{Z,55}(1^-,1^-;k_E^2) = L^2\tilde{m}_Z^2/(2\pi\epsilon^2 k_E^2 M_{\text{KK}}^2) + \mathcal{O}(k_E^{-4})$ for large Euclidean momenta, rendering the integral finite. The function $h(\boldsymbol{X}_q,\tilde{\boldsymbol{Y}}_q)$ in the first line of (5.48) is given by

$$
\begin{aligned}
h(\boldsymbol{X}_q,\tilde{\boldsymbol{Y}}_q)\Big|_{\text{brane Higgs}} &= -\frac{\varrho^2\tilde{\boldsymbol{Y}}_q\tilde{\boldsymbol{Y}}_q^\dagger}{1+\varrho^2\boldsymbol{Y}_q\tilde{\boldsymbol{Y}}_q^\dagger}\,\tilde{\boldsymbol{Y}}_q = -\varrho^2\boldsymbol{Y}_q\boldsymbol{Y}_q^\dagger\boldsymbol{Y}_q + \mathcal{O}(\varrho^4)\,, \\
h(\boldsymbol{X}_q,\tilde{\boldsymbol{Y}}_q)\Big|_{\text{narrow bulk Higgs}} &= -\frac{1}{2}\left(\frac{\boldsymbol{X}_d\coth\boldsymbol{X}_d}{\cosh^2\boldsymbol{X}_d}-1\right)\tilde{\boldsymbol{Y}}_q = \frac{\varrho^2}{3}\boldsymbol{Y}_q\boldsymbol{Y}_q^\dagger\boldsymbol{Y}_q + \mathcal{O}(\varrho^4)\,,
\end{aligned}
\tag{5.49}
$$

where the difference between the brane-localized and narrow bulk-Higgs scenario is to leading order the relative factor $-1/3$. Thus, in the narrow bulk-Higgs scenario the approximate expression for $C_{7\gamma,8g}^{Z,\text{KK}}(\mu_{\text{KK}})$ in (5.44) must be multiplied with $-1/3$. Finally,

adding $C_{7\gamma,8g}^{h,\mathrm{KK}}(\mu_{\mathrm{KK}})$ and $C_{7\gamma,8g}^{Z,\mathrm{KK}}(\mu_{\mathrm{KK}})$ we obtain approximately (for $y_* \gtrsim 1$)

$$\begin{aligned} C_{7\gamma}^{h,\mathrm{KK}}(\mu_{\mathrm{KK}}) + C_{7\gamma}^{Z,\mathrm{KK}}(\mu_{\mathrm{KK}}) \approx \frac{Q_d}{2\lambda_t}\frac{v}{\sqrt{2}m_b}\frac{v^2}{M_{\mathrm{KK}}^2}\,\mathcal{D}_L^{(2)\dagger}(1^-)\,\boldsymbol{P}_{12}\,\boldsymbol{Y}_d\boldsymbol{Y}_d^\dagger\boldsymbol{Y}_d\,\mathcal{D}_R^{(3)}(1^-) \\ \times\begin{cases} 0\,; & \text{brane Higgs}\,, \\ -\frac{1}{12}\,; & \text{narrow bulk Higgs}\,. \end{cases} \end{aligned} \tag{5.50}$$

The corresponding expression for the coefficient of the chromomagnetic dipole operator is obtained by replacing $Q_d \to 1$. The structure $\boldsymbol{Y}_d\boldsymbol{Y}_d^\dagger\boldsymbol{Y}_d$ cancels in the brane-localized Higgs case, while there remains a non-zero contribution in case of the narrow bulk-Higgs scenario. This observation and the factors 0 and $-\frac{1}{12}$ in (5.50) were first encountered in [215, 252] for the case of lepton penguin loops. In fact, we can exactly reproduce the result (26) in [252] for the Higgs contribution in the lepton sector from equation (5.50) by replacing $Q_d \to Q_e = -1$ and by accounting for factors in the definition of the Wilson coefficient. We note that while the contributions from the neutral scalars cancel for $y_* \gtrsim 1$ in the brane-localized Higgs scenario, we still have left over the (dominant) contributions from the charged NGBs. The latter contribution is absent in case of the leptonic dipole coefficient for the transition $l_i \to l_j\gamma$ in the minimal RS model, which does not include right-chiral $SU(2)_L$ singlet neutrinos. However, a non-zero contribution from neutral scalars would be present in case of the RS model with custodial protection, which can be found in [250, 253].

Finally, we remark that in order to calculate the contribution of the charged $W^\pm$ NGBs in the narrow bulk-Higgs scenario, we would need to perform t, t' integrations over matrix-valued functions mixing $\boldsymbol{Y}_u$ with $\boldsymbol{Y}_d$. Since we could not handle those integrations in a semi-analytic way we will therefore confine our analysis to the brane-localized Higgs scenario in the remainder of this paper.

5.2.5 Renormalization-group running to the *B*-meson scale

In the previous section we have analyzed the corrections to the SM Wilson coefficients from the zero modes $C_{7\gamma,8g}^{\mathrm{RS},0}(\mu_W)$ defined at the electroweak scale $\mu_W \sim m_W$ and from the KK particles $C_{7\gamma,8g}^{\mathrm{RS,KK}}(\mu_{\mathrm{KK}})$ at the KK scale $\mu_{\mathrm{KK}} \sim M_{\mathrm{KK}}$. For the phenomenology we are interested in the Wilson coefficients $C_{7\gamma,8g}(\mu_b)$ at the B-meson scale $\mu_b \sim m_b$. When running down from higher scales down to μ_b, QCD effects generically lead to a mixing between dimension-6 operators. The general effective Lagrangian for a new-physics model at a high scale (μ_{KK} in our case) can be written in the form

$$\begin{aligned} \mathcal{L}_{\mathrm{eff}} = \frac{G_F}{\sqrt{2}}\,\lambda_t\Bigg[& C_{7\gamma}(\mu_{\mathrm{KK}})\,Q_{7\gamma} + C_{8g}(\mu_{\mathrm{KK}})\,Q_{8g} + \tilde{C}_{7\gamma}(\mu_{\mathrm{KK}})\,\tilde{Q}_{7\gamma} + \tilde{C}_{8g}(\mu_{\mathrm{KK}})\,\tilde{Q}_{8g} \\ & + \sum_{A,B=L,R}\;\sum_{q=u,c,t,d,s,b}\Big(C_1^q[A,B](\mu_{\mathrm{KK}})\,Q_1^q[A,B] + C_2^q[A,B](\mu_{\mathrm{KK}})\,Q_2^q[A,B]\Big) \\ & + \sum_{A,B=L,R}\Big(\hat{C}_1^d[A,B](\mu_{\mathrm{KK}})\,\hat{Q}_1^q[A,B] + \hat{C}_2^d[A,B](\mu_{\mathrm{KK}})\,\hat{Q}_2^q[A,B]\Big)\Bigg]\,, \end{aligned} \tag{5.51}$$

where we adopt the notation of [254]. The dipole operators $Q_{7\gamma,8g}$ and $\tilde{Q}_{7\gamma,8g}$ are defined in (5.1) and (5.2). Here, $Q^q_{1,2}[A,B]$ and $\hat{Q}^d_{1,2}[A,B]$ are neutral current-current operators,[8] which implicitly include the charged current-current, four-quark QCD and electroweak penguin operators of the SM.[9] In the RS model such operators are induced at tree-level by the exchange of the heavy KK modes of the Z boson, photon and gluon. For simplicity, however, they will be neglected in our analysis.[10] When running down from $\mu_{\rm KK} \sim M_{\rm KK}$ to $\mu_W \sim m_W$ we consider only the mixing between $Q_{7\gamma}$ and Q_{8g}.

Let us outline the basic steps how we evolve the Wilson coefficients down to the meson scale. We need the evolution matrix $U(\mu_1,\mu_2)$ which can be calculated from the anomalous-dimension matrix $\hat{\gamma}$ of our operator basis, which is contained in the more general basis considered in [254]. The running between scales is accomplished at leading order by

$$U(\mu_1,\mu_2) = \hat{V}\left(\left[\frac{\alpha_s(\mu_2)}{\alpha_s(\mu_1)}\right]^{\frac{\vec{\gamma}^{(0)}}{2\beta_0}}\right)_D \hat{V}^{-1}\,, \tag{5.53}$$

where $\vec{\gamma}^{(0)}$ includes the eigenvectors of the transposed anomalous-dimension matrix $\hat{\gamma}^{(0)^T}$. The matrices $\hat{V}$ diagonalize $\hat{\gamma}^{(0)^T}$, such that $\hat{V}^{-1}\hat{\gamma}^{(0)^T}\hat{V}$ is diagonal. Note that $\hat{\gamma}^{(0)}$ and $\beta_0 = (33-2n_f)/3$ depend on the number of active flavors n_f. Between the scales $\mu_{\rm KK}$ and μ_b we integrate out the top quark, such that the evolution matrix splits into two parts,

$$U(\mu_b,\mu_{\rm KK}) = U^{(n_f=5)}(\mu_b,\mu_W)\,U^{(n_f=6)}(\mu_W,\mu_{\rm KK})\,. \tag{5.54}$$

The RS corrections at the KK scale, coming from integrating out heavy KK resonances, are contained in the coefficient $\vec{C}^{\rm RS,KK}(\mu_{\rm KK})$. The evolution down to the electroweak scale is given by $\vec{C}^{\rm RS,KK}(\mu_W) = U(\mu_W,\mu_{\rm KK})\,\vec{C}^{\rm RS,KK}(\mu_{\rm KK})$. At the electroweak scale the W boson and the top quark are integrated out. Matching on this new effective Lagrangian we include the contributions from the boson and fermion zero modes, which are given by $\vec{C}^{(0)}(\mu_W) = \vec{C}^{\rm SM}(\mu_W) + \vec{C}^{\rm RS,0}(\mu_W)$, where $\vec{C}^{\rm RS,0}(\mu_W)$ contains the zero-mode corrections to the SM coefficient. Next we evolve this contribution down to the meson scale. The effective Wilson coefficient reads

$$\vec{C}(\mu_b) = \vec{C}^{\rm SM}(\mu_b) + U(\mu_b,\mu_{\rm KK})\,\vec{C}^{\rm RS,KK}(\mu_{\rm KK}) + U(\mu_b,\mu_W)\,\vec{C}^{\rm RS,0}(\mu_W)\,, \tag{5.55}$$

where the SM Wilson coefficients are given by $C^{\rm SM}_{7\gamma}(\mu_b) = -0.32$ [255] and $C^{\rm SM}_{8g}(\mu_b) = -0.15$ [255]. Performing all steps including the dipole and the charged current-current operators, the RS corrections to the electro- and chromomagnetic dipole operators at

[8] Explicitly, the neutral current-current operators are given by (α,β are the QCD color indices)

$$\begin{aligned} Q^q_1[A,B] &= 4(\bar{s}_\alpha\gamma_\mu P_A b_\beta)(\bar{q}_\beta\gamma^\mu P_B q_\alpha)\,, \quad & Q^q_2[A,B] &= 4(\bar{s}_\alpha\gamma_\mu P_A b_\alpha)(\bar{q}_\beta\gamma^\mu P_B q_\beta)\,, \\ \hat{Q}^d_1[A,B] &= 4(\bar{s}_\alpha\gamma_\mu P_A d_\beta)(\bar{d}_\beta\gamma^\mu P_B b_\alpha), \quad & \hat{Q}^d_2[A,B] &= 4(\bar{s}_\alpha\gamma_\mu P_A d_\alpha)(\bar{d}_\beta\gamma^\mu P_B b_\beta)\,. \end{aligned} \tag{5.52}$$

[9] For instance, the charged current-current operators of the SM, $Q_1 = 4(\bar{s}_\alpha\gamma_\mu P_L c_\beta)(\bar{c}_\beta\gamma^\mu P_L b_\alpha)$ and $Q_2 = 4(\bar{s}_\alpha\gamma_\mu P_L c_\alpha)(\bar{c}_\beta\gamma^\mu P_L b_\beta)$, can be related to $Q^c_2[L,L]$ and $Q^c_1[L,L]$ using Fierz identities.

[10] The authors of [251] have considered four-fermion operators at the high scale $\mu_{\rm KK}$. They found that when including the four-fermion operators the electromagnetic dipole coefficient $C_{7\gamma}(\mu_b)$ would increase by 5% on average for RS points with $y_\star = 3$.

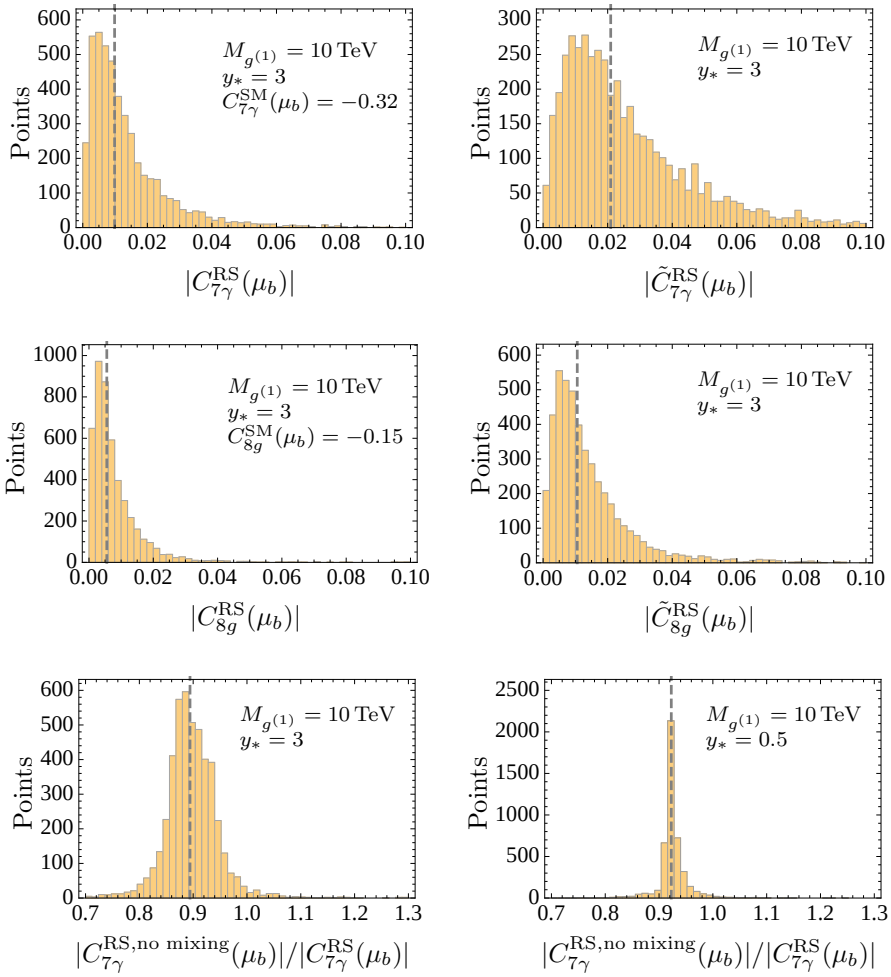

Figure 5.5: The upper four plots show the corrections in the RS model to the effective Wilson coefficients in the SM $C_{7\gamma}^{\text{SM}}(\mu_b) = -0.32$ [255] and $C_{8g}^{\text{SM}} = -0.15$ [255] at the B-meson scale $\mu_b = 4.8\,\text{GeV}$ for a set of RS points with $y_* = 3$ and $M_{g^{(1)}} = 10\,\text{TeV}$. The size of the corrections are equally distributed among the real and imaginary parts of the Wilson coefficients. The lower two plots show the amount of mixing of the chromo- into the electromagnetic dipole Wilson coefficients. Vertical dashed lines denote the median values of the corresponding distributions.

the B-meson scale are given by

$$\begin{aligned} C_{7\gamma}^{\text{RS}}(\mu_b) &= 0.475\, C_{7\gamma}^{\text{RS,KK}}(\mu_{\text{KK}}) + 0.123\, C_{8g}^{\text{RS,KK}}(\mu_{\text{KK}}) + 0.667\, C_{7\gamma}^{\text{RS,0}}(\mu_W) \\ &\quad + 0.092\, C_{8g}^{\text{RS,0}}(\mu_W)\,, \\ C_{8g}^{\text{RS}}(\mu_b) &= 0.522\, C_{8g}^{\text{RS,KK}}(\mu_{\text{KK}}) + 0.702\, C_{8g}^{\text{RS,0}}(\mu_W)\,. \end{aligned} \tag{5.56}$$

The numbers in front of the zero-mode and KK corrections have been calculated for $\mu_{\text{KK}} = 1\,\text{TeV}$, $\mu_b = 4.8\,\text{GeV}$ and $\mu_W = 80.385\,\text{GeV}$. In our numerical analysis we set $\mu_{\text{KK}} = M_{\text{KK}}$ for each RS point. We note that the numbers decrease by approximately 10% for the scale choice $\mu_b = 2.6$ which is sometimes used in the literature, e.g in the analysis of [251]. Relation (5.56) also holds for the chirality-flipped Wilson coefficients, since (massless) QCD is blind to the fermion chirality.

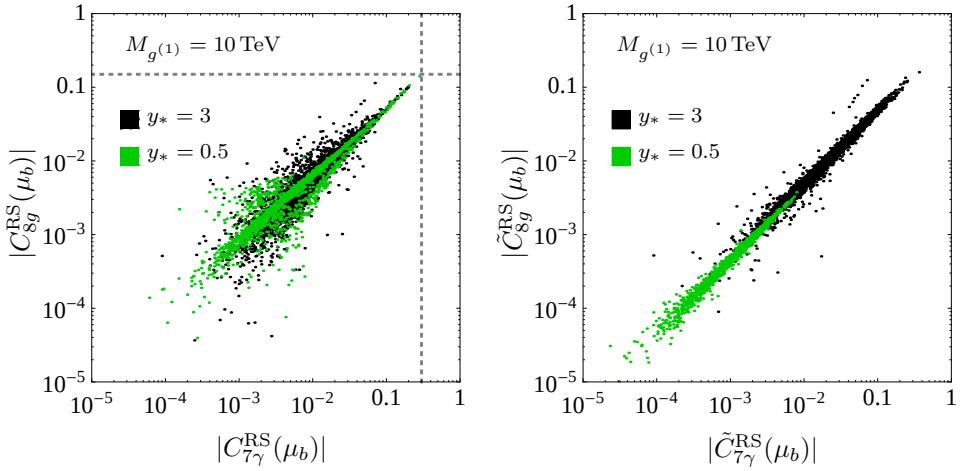

Figure 5.6: Left (right) is shown the approximate linear correlation between the RS corrections to the (flipped) electro- and chromomagnetic dipole coefficients for RS points with $y_* = 0.5, 3$ and $M_{g^{(1)}} = 10\,\text{TeV}$. The crossing of the vertical dashed lines in the left plot denotes the SM value $|C_{7\gamma,8g}^{\text{SM}}(\mu_b)|$. There is no correlation between $C_{7\gamma,8g}^{\text{RS}}(\mu_b)$ and their chirality-flipped counterparts.

The first four plots in Figure 5.5 show the RS corrections of the dipole Wilson coefficients at the B-meson scale for RS points with $y_* = 3$ and $M_{g^{(1)}} = 10\,\text{TeV}$. We see that the corrections to the SM Wilson coefficients $C_{7\gamma}^{\text{SM}}(\mu_b) = -0.32$ [255] and $C_{8g}^{\text{SM}}(\mu_b) \approx -0.15$ [255] lie in the few percent region. The dominant contributions to $C_{7\gamma}^{\text{RS}}(\mu_b)$ are given by the RG-evolved KK and zero-mode corrections of the electromagnetic dipole Wilson coefficients. The mixing of the chromomagnetic dipole coefficients into $C_{7\gamma}^{\text{RS}}(\mu_b)$ is shown in the lower two plots of Figure 5.5 for RS points with $y_\star = 0.5$ and 3. Here, $C_{7\gamma}^{\text{RS,no mixing}}(\mu_b)$ is obtained from (5.56) without including the contributions from the chromomagnetic dipole Wilson coefficients. Neglecting the mixing would decrease the Wilson coefficients at the level of 10%, which shows the relative importance of the mixing effects for the transition $b \to s\gamma$. We remark that $C_{7\gamma}^{\text{RS}}(\mu_b)$ and $C_{8g}^{\text{RS}}(\mu_b)$ are approximately linearly correlated, which can be seen in Figure 5.6. This is expected, since the main contributions arise from penguin diagrams containing $W^\pm$-boson modes, and they only differ by the factor $(\kappa_W^{7\gamma}+\kappa_{WW}^{7\gamma})/\kappa_W^{8g} = 1+Q_u = 5/3$. In general, we observe that the RS corrections for $y_\star = 3$ are larger in magnitude than for $y_\star = 0.5$. However, the difference in size is more pronounced in case of the chirality-flipped Wilson coefficients, since their corrections are more dominated by the RG-evolved KK contributions than by the zero-mode corrections.

5.3 Phenomenological implications

In the following we discuss observables that are sensitive to corrections to the loop-induced dipole Wilson coefficients. Therefore, we concentrate on the branching ratio of the inclusive B-meson decay $\bar{B} \to X_s\gamma$ and the time-dependent CP asymmetry in $\bar{B}_d^0 \to \bar{K}^{*0}\gamma$.[11]

[11] For further observables, we refer the reader to [199], which includes a discussion of the branching fraction for the leptonic inclusive decay $\bar{B} \to X_s l^+ l^-$, the direct CP asymmetry $A_{\text{CP}}^{b\to s\gamma}$ and the CP asymmetry difference $\Delta A_{\text{CP}}^{b\to s\gamma}$. However, $\text{Br}(\bar{B} \to X_s l^+ l^-)$ is mainly affected by RS corrections to the Wilson coefficients of the leptonic four-quark penguin operators, and is not sensitive to the dipole Wilson

Branching ratio of the inclusive decay $\bar{B} \to X_s\gamma$

We begin with the CP- and isospin-averaged $\bar{B} \to X_s\gamma$ branching ratio, which is one of the cleanest observables in B physics from a theoretical point of view. Measurements lead to the combined result[12] $\mathrm{Br}(\bar{B} \to X_s\gamma)_{\mathrm{exp}} = (3.43 \pm 0.21 \pm 0.07) \times 10^{-4}$ [256] for the branching ratio defined with a lower cut $E_\gamma \geq E_0 = 1.6\,\mathrm{GeV}$ on the photon energy in the meson rest frame. The SM prediction at NNLO reads $\mathrm{Br}(\bar{B} \to X_s\gamma)_{\mathrm{SM}} = (3.36 \pm 0.23) \times 10^{-4}$ [257] for $E_0 = 1.6\,\mathrm{GeV}$, showing that both values are compatible at the 1σ level. In order to estimate the effects of the RS model we use the approximate formula (for $E_\gamma \geq 1.6\,\mathrm{GeV}$) [254, 258]

$$\begin{aligned} \frac{\mathrm{Br}(\bar{B} \to X_s\gamma)}{\mathrm{Br}(\bar{B} \to X_s\gamma)_{\mathrm{SM}}} &= \frac{1}{|C_{7\gamma}^{\mathrm{SM}}(\mu_b)|^2 + N(E_\gamma)} \left[|C_{7\gamma}(\mu_b)|^2 + |\tilde{C}_{7\gamma}(\mu_b)|^2 + N(E_\gamma) \right] \\ &= 1 + 0.0032 \left[|C_{7\gamma}^{\mathrm{RS}}(\mu_b)|^2 + |\tilde{C}_{7\gamma}^{\mathrm{RS}}(\mu_b)|^2 \right] - 0.0020\,\mathrm{Re}\, C_{7\gamma}^{\mathrm{RS}}(\mu_b)\,, \end{aligned} \tag{5.57}$$

where $N(E_\gamma)$ in the first line is a non-perturbative correction and evaluates to $N(E_\gamma = 1.6\,\mathrm{GeV}) = 3.6 \times 10^{-3}$ at the minimum photon energy. The second line of (5.57) is obtained by using the SM value $C_{7\gamma}^{\mathrm{SM}}(\mu_b) = -0.32$ [255], while we neglect the contribution of the chirality-flipped Wilson coefficient $\tilde{C}_{7\gamma}^{\mathrm{SM}}(\mu_b)$ in the SM since it is suppressed by the ratio m_s/m_b. Note that the Wilson coefficients in (5.57) are evaluated at the B-meson scale $\mu_b \approx 4.8\,\mathrm{GeV}$.

The dominant correction to $\mathrm{Br}(\bar{B} \to X_s\gamma)_{\mathrm{SM}}$ stems from the last term in the second line of (5.57), which is proportional to $\mathrm{Re}\, C_{7\gamma}^{\mathrm{RS}}(\mu_b)$. The squared contributions (and in particular the chirality-flipped Wilson coefficient), have only a minor impact. Since the KK contributions are approximately proportional to y_*^2, the biggest effects can be expected for large values of y_*. In the left plot in Figure 5.7, we show the RS predictions for the branching ratio $\mathrm{Br}(\bar{B} \to X_s\gamma)$ as a function of the first KK gluon mass. The black (green) points are obtained with $y_* = 3\,(0.5)$. We see that the RS model with $y_\star = 0.5$ is completely compatible with the experimental data at 95% CL. If we require that at least 10% of the RS points lie within the experimental 2σ error margin, we can derive the lower bound $M_{g^{(1)}} \geq 3.4\,\mathrm{TeV}$ at 95% CL for $y_* = 3$. However, this bound cannot compete with the constraints coming from a tree-level analysis of the Peskin-Takeuchi parameters and from Higgs physics. Thus, $\mathrm{Br}(\bar{B} \to X_s\gamma)$ does not give any new constraint on the RS parameter space.[13]

Let us comment on two further constraints on the RS parameter space. First, we consider the CP-violating observable ϵ_K in kaon mixing, which can receive large corrections in the RS model due to a strong chiral enhancement of the four-quark operator $Q_4 = (\bar{d}_R s_L)(\bar{d}_L s_R)$, after performing the RG running from M_{KK} down to the kaon mass. When we impose the constraint that the RS prediction for ϵ_K lies in the 2σ region of the SM prediction we find that roughly 15% (1%) of the black (green) points in Figure 5.7 survive. The fraction of allowed points decreases with smaller values of

coefficients discussed in this thesis. Furthermore, $A_{\mathrm{CP}}^{b\to s\gamma}$ and $\Delta A_{\mathrm{CP}}^{b\to s\gamma}$ are plagued by large hadronic uncertainties, such that the RS parameter space cannot be constrained by those observables.

[12] This experimental result is the average value obtained by the Heavy Flavor Averaging Group (HFAG) in 2014. The first error is statistical, and the second one is systematic. Experimentally, there are two approaches to measure $\mathrm{Br}(\bar{B} \to X_s\gamma)$. While in the semi-inclusive approach one considers a sum of exclusive decay modes, in the fully-inclusive approach one measures the emitted photon but does not reconstruct X_s.

[13] It is reported in [259] that the future Belle II experiment has the potential to reduce the 1σ uncertainty on $\mathrm{Br}(\bar{B} \to X_s\gamma)$ from 13% of Belle in 2006 to 7% (6%) for a luminosity of $5\,\mathrm{ab}^{-1}$ ($50\,\mathrm{ab}^{-1}$). This will increase the potential to discover the impact of KK states on the decay $\bar{B} \to X_s\gamma$.

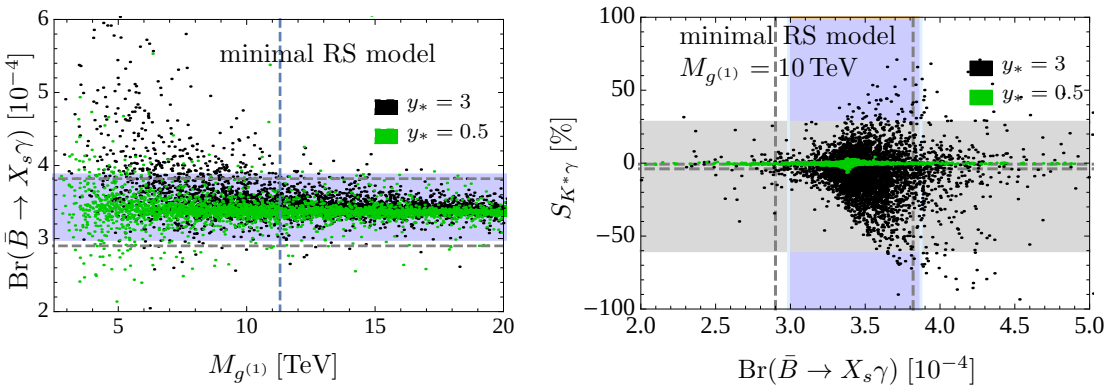

Figure 5.7: Left is shown the branching ratio of the radiative decay $\bar{B} \to X_s\gamma$ as a function of the first KK gluon mass $M_{g^{(1)}}$. The right plot shows the time-dependent CP asymmetry $S_{K^*\gamma}$ with respect to $\mathrm{Br}(\bar{B} \to X_s\gamma)$. In both plots the light gray and blue bands show the 2σ experimental error margins while the area between the horizontal dashed lines contains the SM prediction with 2σ uncertainty. The vertical dashed line in the left plot shows the lower bound on $M_{g^{(1)}}$ obtained from a tree-level analysis of the Peskin-Takeuchi parameters. All black (green) points represent possible RS scenarios with $y_* = 3\,(0.5)$. In case of the right plot the lightest KK gluon mass is fixed to $M_{g^{(1)}} = 10\,\mathrm{TeV}$.

y_*, since the RS corrections to ϵ_K are approximately proportional to $1/y_*^2$. Still, the shape of the distribution of points is not strongly affected, since ϵ_K is uncorrelated with the observables discussed in this paper. Secondly, we can discuss the impact of Higgs physics, where the strongest bounds arise from the signal rates of the Higgs decaying into pairs of electroweak gauge bosons. Details have been given in Section 4.4. Comparing with LHC data we find the condition $M_{g^{(1)}} \geq 11.3\,\mathrm{TeV} \times (y_*/3)$ at 95% CL, see (4.154). Applying this bound to the RS points with $M_{g^{(1)}} = 10\,\mathrm{TeV}$ would exclude the black points ($y_* = 3$) but still allow for the green points ($y_* = 0.5$).

Time-dependent CP asymmetry in $\bar{B}_d^0 \to \bar{K}^{*0}\gamma$

In the SM, the left-chiral structure of the weak interactions makes the emitted photon mainly left-handed in b decays ($b \to s\gamma_L$) and right-handed in $\bar{b}$ decays ($\bar{b} \to \bar{s}\gamma_R$). The reason for the helicity suppression of right-handed (left-handed) photons in b ($\bar{b}$) decays is that those decays require a chirality-flip on the external s-quark line, which implies that the chirality-flipped Wilson coefficient $\tilde{C}_{7\gamma}^{\mathrm{SM}}$ is m_s/m_b suppressed with respect to $C_{7\gamma}^{\mathrm{SM}}$. However, in new-physics scenarios like the RS model there can be chirality flips on internal fermion lines of a penguin diagram, such that the amplitude for a right-handed (left-handed) photon in b ($\bar{b}$) decays is no longer suppressed by m_s/m_b.

Experimentally, the photon helicity can be accessed indirectly by measuring the time-dependent CP asymmetry in exclusive $\bar{B}_d^0 \to \bar{K}^{*0}\gamma$ decays, which is defined by[14]

$$\frac{\Gamma(\bar{B}_d^0(t) \to \bar{K}^{*0}\gamma) - \Gamma(B_d^0(t) \to K^{*0}\gamma)}{\Gamma(\bar{B}_d^0(t) \to \bar{K}^{*0}\gamma) + \Gamma(B_d^0(t) \to K^{*0}\gamma)} = S_{K^*\gamma}\sin(\Delta m_B t) - C_{K^*\gamma}\cos(\Delta m_B t)\,. \quad (5.58)$$

Here, $S_{K^*\gamma}$ and $C_{K^*\gamma}$ indicate the mixing-induced and direct CP violation, and Δm_B denotes the mass difference between the heavier and the lighter neutral B-meson mass eigenstates. The mesons K^{*0} and $\bar{K}^{*0}$ can be observed via their decay into the CP

[14] We are interested in the CP asymmetries that follow from the interference of mixing and decay, which requires that both B_d^0 and $\bar{B}_d^0$ decay to the same exclusive final state $K^{*0}\gamma$, and that the photons produced in $B_d^0 \to K^{*0}\gamma$ and $\bar{B}_d^0 \to \bar{K}^{*0}\gamma$ must be a mixture of left- and right-handed helicities.

eigenstate $K_S^0\pi^0$, where K_S is the short-lived neutral Kaon. The helicity suppression can be measured by $S_{K^*\gamma}$, which to leading order is given by [260, 261]

$$S_{K^*\gamma} \approx \frac{2}{|C_{7\gamma}(\mu_b)|^2 + |\tilde{C}_{7\gamma}(\mu_b)|^2} \, \mathrm{Im}\left[e^{-i\phi_1} \, C_{7\gamma}(\mu_b) \, \tilde{C}_{7\gamma}(\mu_b)\right]. \tag{5.59}$$

This observable is sensitive to the chirality-flipped Wilson coefficient $\tilde{C}_{7\gamma}(\mu_b)$. The angle ϕ_1 is one of the three angles of the unitarity triangle diagram, and is defined via $\phi_1 \equiv \arg(-V_{td}V_{tb}^*/(V_{cd}V_{cb}^*))$. This phase appears in the description of $B^0 - \bar{B}^0$ mixing and has been measured in $B^0 \to J/\psi \, K_{S,L}^0$ decays to be $\sin\phi_1 = 0.682 \pm 0.019$ [256]. Due to the occurrence of $\tilde{C}_{7\gamma}(\mu_b)$ in the numerator of (5.59), the SM prediction for $S_{K^*\gamma}$ is suppressed by the ratio m_s/m_b and reads $S_{K^*\gamma}^{\mathrm{SM}} = (-2.3 \pm 1.6)\%$ [262].[15] The current experimental value $S_{K^*\gamma}^{\mathrm{exp}} = (-16 \pm 22)\%$ [256] still suffers from large uncertainties.[16]

The right plot of Figure 5.7 shows the asymmetry $S_{K^*\gamma}$ with respect to the branching ratio $\mathrm{Br}(\bar{B} \to X_s\gamma)$ by the black (green) points for $y_* = 3\,(0.5)$ and $M_{g^{(1)}} = 10\,\mathrm{TeV}$. Gray and blue bands denote the experimental values with the experimental 2σ error margins for $S_{K^*\gamma}$ and $\mathrm{Br}(\bar{B} \to X_s\gamma)$, respectively. Compared with the SM prediction the RS corrections can be significant due to the sensitivity of $S_{K^*\gamma}$ on the imaginary part of $\tilde{C}_{7\gamma}(\mu_b)$, which can receive large corrections in the RS model. On the other hand, the corrections are not significant when compared with the experimental result due to the large uncertainty. The RS model with $y_\star = 0.5$ is completely compatible with the experimental measurements. Requiring, in case of $y_\star = 3$, that at least 10% of the RS points lie within the experimental 2σ regions of $S_{K^*\gamma}$ and $\mathrm{Br}(\bar{B} \to X_s\gamma)$, we can derive the lower bound $M_{g^{(1)}} \geq 3.8\,\mathrm{TeV}$ at 95% CL. Again, this constraint cannot compete with the lower bound obtained from a tree-level analysis of the Peskin-Takeuchi parameters. However, according to [259] the future Belle II experiment can reduce the experimental 1σ error from 0.32 of Belle in 2006 to 0.10 (0.03) at an integrated luminosity of $5\,\mathrm{ab}^{-1}$ ($50\,\mathrm{ab}^{-1}$). This significant reduction of the error margins has the potential to find possible deviations from the SM prediction or to cut strongly into the RS parameter space.

[15] A naive estimation for $S_{K^*\gamma}$ in the SM is given by the formula $S_{K^*\gamma} \approx -2(m_s/m_b)\sin(2\phi_1)$ [263].

[16] The experimental value is the HFAG average of the BaBar [264] and Belle [265] results for the decay into the vector-meson resonance $K^{*0}(892)$, which has a mass of 892 MeV.

Conclusions

We have presented a comprehensive study of the Higgs-boson production and decay processes and the flavor-changing neutral current $b \to s\gamma$ in models with one warped extra dimension. All models considered in this work allow the gauge bosons and fermions to propagate into the bulk of the fifth dimension, while the Higgs sector is being localized on or near the infra-red brane. These so-called Randall-Sundrum models are well motivated, since they provide a geometrical solution for the gauge-hierarchy problem, the flavor puzzle and the smallness of flavor-changing neutral current processes. In case of our study of the Higgs-boson processes we have extended the results from the minimal to the custodial RS model. The latter version is less constrained by a tree-level analysis of the Peskin-Takeuchi parameters, i.e. the lower bound on the lightest KK gluon mass[17] is reduced at 95% CL from $M_{g^{(1)}} \geq 11.3\,\text{TeV}$ in the minimal model to $M_{g^{(1)}} \geq 4.9\,\text{TeV}$ in the model with custodial protection. However, both bounds already exclude the direct detection of heavy Kaluza-Klein resonances at current collider experiments. As a consequence this thesis has focused on the indirect search for hints of a warped extra dimension, especially via loop-induced processes, where possible new Kaluza-Klein states in the loops can lead to sizeable deviations from the SM expectations.

At the technical level we have performed the calculation of Feynman amplitudes in the 5D framework. Using 5D Feynman rules we have derived exact expressions for the amplitudes of the loop-induced processes of Higgs production via gluon fusion $gg \to h$, Higgs decay into two photons $h \to \gamma\gamma$ and the electromagnetic dipole transition $b \to s\gamma$ in terms of integrals over fermion and gauge-boson 5D propagators. The use of 5D propagators avoids the notion of infinite KK sums and has allowed us to obtain closed analytic expressions valid to all orders in an expansion of v^2/M_{KK}^2, where M_{KK} sets the mass scale for the lightest of the new KK resonances. We have calculated the boson and fermion propagators in a warped 5D space-time where we have worked in the mixed momentum-position representation. For the first time we have derived the W-boson 5D propagator in the custodial RS model valid for arbitrary values of the four-momentum. Furthermore, we have derived the fermion 5D propagator by retaining the full dependence on the Yukawa matrices, and by regularizing the profile of the Higgs vev by a square box of width η and height $1/\eta$ with $\eta \ll v|Y_q|/M_{\text{KK}}$.

The main conceptual result of this thesis has been to show that the amplitude of the fermion triangle diagram, contributing to the processes $gg \to h$ and $h \to \gamma\gamma$, does not smoothly interpolate between a Higgs-boson localized on and near the IR brane. Our analysis has led to a classification of different versions of the RS model according to the parametric relation of the characteristic width η of the Higgs-boson profile with respect to the two ratios $v|Y_q|/M_{\text{KK}}$ and $v|Y_q|/\Lambda_{\text{TeV}}$, where Λ_{TeV} is the value of the inherent UV cutoff near the IR brane. We have defined the *brane-localized Higgs scenario* for $\eta \ll v|Y_q|/\Lambda_{\text{TeV}}$, and the *narrow bulk-Higgs scenario* by $v|Y_q|/\Lambda_{\text{TeV}} \ll \eta \ll$

[17] We have used the convention to quote bounds on the mass of the first KK gluon resonance which is directly connected to the KK scale via the relation $M_{g^{(1)}} = 2.45\,M_{\text{KK}}$.

$v|Y_q|/M_{\rm KK}$. When one tries to interpolate between both scenarios one enters a transition region with $\eta \sim v|Y_q|/\Lambda_{\rm TeV}$, in which the contributions from certain higher-dimensional operators involving additional derivatives in the RS Lagrangian become unsuppressed, so that the effective field theory approach breaks down. Our 5D analysis has shown that the dominant new-physics contributions arise from KK states with masses of order of several times $M_{\rm KK}$, while in the narrow bulk-Higgs scenario there is another equally important contribution from states with masses of order v/η, which can resolve the "bulky nature" of the Higgs boson.

In case of the effective Higgs coupling to two gluons (hgg) we have shown that to good approximation the RS corrections scale proportional to $\mp y_\star^2 v^2/M_{\rm KK}^2$, where $y_\star$ sets the upper bound for the entries of the anarchic 5D Yukawa matrices such that $|(\boldsymbol{Y}_{u,d})_{ij}| \leq y_\star$. The negative (positive) sign in the brane-localized (narrow bulk-) Higgs scenario leads to a suppressed (enhanced) effective hgg coupling with respect to the SM prediction. Furthermore, we have addressed the question of the numerical impact of power-suppressed $|\Phi|^2(G^a_{\mu\nu})^2$ operators, which contribute to the hgg coupling at tree-level. We have shown that, irrespective of whether the Higgs sector is localized on the IR brane or lives in the bulk, one expects power corrections of similar size. We have argued that the resulting power corrections are likely to be numerically smaller than the RS loop effects. In case of the effective Higgs coupling to two photons ($h\gamma\gamma$) we have concentrated our analysis on the diagrams with bosonic fields propagating in the loops. We have shown that the relevant diagrams, calculated in the general R_ξ gauge, add up to a gauge-invariant result. Working in unitary gauge, we have derived an exact expression for the $h\gamma\gamma$ coupling in terms of an integral over the W-boson 5D propagator and the Higgs-boson profile. In contrast to the fermion triangle diagram, we have shown that the 5D loop diagrams with bosonic fields are insensitive to the precise details of the localization of the scalar sector on or near the IR brane. The tower of KK excitations of the W boson (including the Nambu-Goldstone fields) leads to a correction that is proportional to $-Lm_W^2/M_{\rm KK}^2$, where $L \approx 33.5$ denotes the *volume* of the RS space. In general, when switching from the minimal to the custodial RS model the contribution of the KK quarks increases by a factor of 4 (68/5) for the effective hgg ($h\gamma\gamma$) couplings, which is due to the larger KK-fermion multiplicity in the model with custodial protection. We have shown that the Higgs couplings hgg and $h\gamma\gamma$ are strongly anti-correlated. Moreover, we have studied the tree-level Higgs decay $h \to VV^*$ with the subsequent decay of the off-shell gauge boson into a pair of fermions. We have also calculated the RS corrections on the Higgs-strahlung and vector-boson fusion production processes and shown that to very good approximation they can be accounted for by the corrections to the on-shell hVV coupling. This analysis has included the effects of virtual KK gauge bosons, which have been shown to be subleading (in L) with respect to the contributions stemming from the modified hVV couplings.

In the phenomenological section we have compared the RS predictions for the tree-level $c_W, c_Z, c_t, c_b, c_\tau$ and loop-induced effective $c_g^{\rm eff}, c_\gamma^{\rm eff}$ Higgs couplings with fit results obtained from current experimental data of the LHC. The fit value for the Higgs coupling to top quarks $c_t = 1.42^{+0.23}_{-0.22}$ [219] imposes a strong constraint on $M_{g^{(1)}}$ since the RS corrections for c_t are always predicted to be reduced with respect to the SM value. As a consequence KK gluon masses are excluded in the range of $M_{g^{(1)}} < 12\,{\rm TeV} \times (y_\star/3)$ in the minimal and $M_{g^{(1)}} < 18\,{\rm TeV} \times (y_\star/3)$ in the custodial RS model at 99% CL. In order to elucidate the potential of future measurements at high-luminosity proton and lepton colliders we have compared the predicted new-physics effects on the relevant couplings with the sensitivities that can be reached at the LHC with $\sqrt{s} = 14\,{\rm TeV}$ and an integrated luminosity of $300\,{\rm fb}^{-1}$, and at the ILC with $\sqrt{s} = 1\,{\rm TeV}$ and an integrated luminosity

of $1000\,\text{fb}^{-1}$. At the ILC in particular, one will be able to probe KK gluon masses in the range over several tens of TeV from an analysis of the loop-induced Higgs couplings to gluons and photons. The analysis of the Higgs coupling to W bosons at the ILC will have an expected sensitivity to KK gluon masses of 11 TeV (16 TeV) in the minimal (custodial) RS model, which is independent of the realization of the Yukawa sector and hence the value of the parameter $y_\star$. Apart from the Higgs couplings we have also compared the modifications of the signal rates of the processes $pp \to h \to b\bar{b}$, $\tau^+\tau^-$, WW^*, ZZ^*, $\gamma\gamma$ with the latest data from the LHC. The strongest exclusion bounds originate from the Higgs decay rates into pairs of electroweak gauge bosons. In the minimal model we can exclude at 95% CL KK gluon masses lighter than $11.3\,\text{TeV} \times (y_\star/3)$ in the brane-Higgs case and $7.3\,\text{TeV} \times (y_\star/3)$ in the narrow bulk-Higgs scenario. Those bounds increase in the custodial model to $22.2\,\text{TeV} \times (y_\star/3)$ in the brane-Higgs case and $15.0\,\text{TeV} \times (y_\star/3)$ in the narrow bulk-Higgs scenario. We observe that the bounds on $M_{g^{(1)}}$ in the minimal (custodial) RS model are weaker (complementary or stronger) than those from the electroweak precision observables and rare flavor-changing processes. Thus, we find that while the implementation of the custodial symmetry can tame the tree-level effects on the Peskin-Takeuchi T parameter the bounds from Higgs physics undermine this original advantage. In general, our analysis has shown that Higgs physics provides very sensitive probes of virtual effects from heavy KK excitations. Consequently, improved precision measurements of the Higgs-boson couplings to SM particles in the future will provide a powerful tool to either find hints for the existence of a warped extra dimension or to exclude large portions of the RS parameter space.

At last, we have investigated the loop-induced electro- and chromomagnetic (quark) dipole coefficients $C_{7\gamma,8g}$ and $\tilde{C}_{7\gamma,8g}$ for the $b \to s\gamma$ and $b \to sg$ transitions in the minimal RS model with a brane-localized Higgs sector. We have derived integral expressions for all contributions arising at one-loop order using fermion and gauge-boson 5D propagators, where our final results involve one four-momentum and two extra-dimensional integrations. In addition, we have derived expressions in the KK-decomposed (4D) theory and shown analytically and numerically that the dipole Wilson coefficients coincide in both pictures, presenting a highly non-trivial cross-check of our calculations. We have shown that the dominant corrections of heavy KK resonances originate from the W-boson penguin diagrams. More precisely, when working in Feynman-'t Hooft gauge the dominant corrections stem from the parts of the diagrams which involve the scalar component of the 5D gauge-boson field and the charged Nambu-Goldstone bosons from the Higgs sector. For $y_\star \gtrsim 1$ the latter contributions dominate and the size of the corrections to the dipole Wilson coefficients increase proportionally to y_*^2. For the phenomenological analysis we have renormalization-group evolved the RS corrections of the dipole Wilson coefficients to the B-meson scale $\mu_b = 4.8\,\text{GeV}$, where we have taken into account the mixing of the chromo- and electromagnetic dipole operators. The mixing effects enhance the corrections to $C_{7\gamma}(\mu_b)$ at the level of 10%. For RS points with $M_{g^{(1)}} = 10\,\text{TeV}$ and $y_\star = 3$ one can obtain corrections to $C_{7\gamma}(\mu_b)$ and $C_{8g}(\mu_b)$ in the few percent region with respect to the SM values. Furthermore, we have shown that the RS corrections $C_{7\gamma}^{\text{RS}}(\mu_b)$ and $C_{8g}^{\text{RS}}(\mu_b)$ are linearly correlated. We have investigated the branching ratio of the inclusive decay $\bar{B} \to X_s\gamma$ and the time-dependent CP asymmetry $S_{K^*\gamma}$ in $\bar{B}_d^0 \to \bar{K}^{*0}\gamma$ decays, which are both sensitive on new-physics corrections to $C_{7\gamma}(\mu_b)$ and $\tilde{C}_{7\gamma}(\mu_b)$. For RS points with $y_\star = 0.5$, the predictions are in general compatible with the experimental measurements. In case of $y_\star = 3$, we can derive the lower bound $M_{g^{(1)}} \geq 3.8\,\text{TeV}$ if we require that at least 10% of the RS points lie inside the 2σ experimental error margins. However, in contrast to the bounds derived from the analysis of Higgs-boson

production and decay processes hard constraints on the RS parameter space could not be obtained.

A Summary of Feynman rules

In the following we present the Feynman rules of all vertices that are required for the calculations in Chapters 4 and 5. We consider the minimal RS model and distinguish between the rules in the 5D framework and the KK-decomposed (4D) theory. The general convention is that all particle momenta are flowing into the vertices and that amplitudes are denoted by the symbol $\mathcal{A}$.

5D framework

We begin with the vertices that couple two 5D quarks and one 5D boson. Each vertex is labelled by the extra-dimensional coordinate $t \in [\epsilon, 1]$. The corresponding amplitudes can be summarized by

$$\begin{aligned}
\mathcal{A}^{\{\bar{q}A_\mu q,\, \bar{q}_a G^c_\mu q_b,\, \bar{q}Z_\mu q,\, \bar{q}W^\pm_\mu q'\}} &= \left\{ iQ_q e_5,\; ig_{s,5}\, t^c_{ab},\; \frac{ig_5\, g^q_L}{c_w},\; \frac{ig_5}{\sqrt{2}} \right\} \gamma_\mu\, \boldsymbol{P}_B, \\
\mathcal{A}^{\{\,\bar{q}A_5 q,\, \bar{q}_a G^c_5 q_b,\, \bar{q}Z_5 q,\, \bar{q}W^\pm_5 q'\}} &= \left\{ Q_q e_5,\; g_{s,5}\, t^c_{ab},\; \frac{g_5\, g^q_L}{c_w},\; \frac{g_5}{\sqrt{2}} \right\} \left[\boldsymbol{V}_{B^\pm_5}(t) P_L + \tilde{\boldsymbol{V}}_{B^\pm_5}(t) P_R \right], \\
\mathcal{A}^{\bar{q}hq} &= \frac{-i}{\sqrt{2}}\, \delta^\eta(t-1) \left[\mathcal{M}^Y_q P_R + \mathcal{M}^{Y\dagger}_q P_L \right], \qquad \text{(A.1)}
\end{aligned}$$

where $\mathcal{M}^Y_q = \boldsymbol{Y}^C_q\, \boldsymbol{P}_{12} + \boldsymbol{Y}^{S\dagger}_q\, \boldsymbol{P}_{21}$, $Q_u = 2/3$, $Q_d = -1/3$ and $g^q_L = T^q_3 - Q_q s^2_w$. In the first two lines of (A.1) the subscript B of $\boldsymbol{P}_B$, $\boldsymbol{V}_{B^\pm_5}$ and $\tilde{\boldsymbol{V}}_{B^\pm_5}$ must be replaced by the corresponding bosonic label $B = A, G, Z, W$ on the left side.[1] The projector $\boldsymbol{P}_{ij}$ for $i, j = 1, 2$ is a 2×2 matrix with zero entries except for the ij-component, which equals 1. Furthermore, the structures $\boldsymbol{P}_B$ are given by $\boldsymbol{P}_A = \boldsymbol{P}_G = \mathbf{1}_{2\times 2}$, $\boldsymbol{P}_W = \boldsymbol{P}_+$ and $\boldsymbol{P}_Z = \boldsymbol{P}_+ + g^q_R/g^q_L\, \boldsymbol{P}_-$ with $\boldsymbol{P}_+ \equiv \mathrm{diag}(1,0)$, $\boldsymbol{P}_- \equiv \mathrm{diag}(0,1)$ and $g^q_R = -Q_q s^2_w$. The electromagnetic, $SU(2)_L$ and strong 5D gauge-boson couplings are denoted by e_5, g_5 and $g_{s,5}$. The weak mixing angle is defined via $c^2_w \equiv \cos^2\theta_w = g^2_5/(g^2_5 + g'^2_5)$ where g'_5 is the hypercharge 5D gauge coupling. The t-dependent functions in (A.1) are given by

$$\begin{aligned}
\boldsymbol{V}_{A_5}(t) &= \frac{\epsilon}{t}\, \mathbf{1}_{2\times 2}\,, & \tilde{\boldsymbol{V}}_{A_5}(t) &= -\boldsymbol{V}_{A_5}(t), \qquad \text{(A.2)} \\
\boldsymbol{V}_{W^+_5}(t) &= \frac{\epsilon}{t}\left[\boldsymbol{P}_W + \frac{\varrho M^2_{\mathrm{KK}}}{L\tilde{m}^2_W} \delta^\eta(t-1)\, \mathcal{M}^{Y\dagger}_{ud} \right], & \tilde{\boldsymbol{V}}_{W^+_5}(t) &= -\boldsymbol{V}_{W^+_5}(t)\big|_{\mathcal{M}^{Y\dagger}_{ud} \to -\mathcal{M}^Y_{du}}, \\
\boldsymbol{V}_{W^-_5}(t) &= \frac{\epsilon}{t}\left[\boldsymbol{P}_W + \frac{\varrho M^2_{\mathrm{KK}}}{L\tilde{m}^2_W} \delta^\eta(t-1)\, \mathcal{M}^{Y\dagger}_{du} \right], & \tilde{\boldsymbol{V}}_{W^-_5}(t) &= -\boldsymbol{V}_{W^-_5}(t)\big|_{\mathcal{M}^{Y\dagger}_{du} \to -\mathcal{M}^Y_{ud}}, \\
\boldsymbol{V}_{Z_5}(t) &= \frac{\epsilon}{t}\left[\boldsymbol{P}_Z + \left(1 - \frac{g^q_R}{g^q_L}\right) \frac{\varrho M^2_{\mathrm{KK}}}{L\tilde{m}^2_Z}\, \delta^\eta(t-1)\, \mathcal{M}^{Y\dagger}_{qq} \right], & \tilde{\boldsymbol{V}}_{Z_5}(t) &= -\boldsymbol{V}_{Z_5}(t)\big|_{\mathcal{M}^{Y\dagger}_{qq} \to -\mathcal{M}^Y_{qq}},
\end{aligned}$$

[1] The superscripts of $B^\pm_5$ are only relevant for $B = W$ and can be ignored otherwise.

where $\boldsymbol{V}_{G_5}(t) = \boldsymbol{V}_{A_5}(t)$, $\tilde{\boldsymbol{V}}_{G_5}(t) = \tilde{\boldsymbol{V}}_{A_5}(t)$ and $\mathcal{M}^Y_{qq'} \equiv \boldsymbol{Y}^C_q \boldsymbol{P}_{12} - \boldsymbol{Y}^{S\dagger}_{q'} \boldsymbol{P}_{21}$. The Nambu-Goldstone boson contributions from the Higgs sector are contained in the IR brane-localized terms, where we implement the regularized δ-function given in (1.58).

We continue with the Feynman rules for the triple gauge-boson vertices. We assume that some of the attached fields are photon and gluon zero modes, which are denoted by $A^{(0)}$ and $G^{(0)}$ below.[2] The corresponding amplitudes are then given by

$$\begin{aligned}
\mathcal{A}^{W^\pm_\beta(p)\, A^{(0)}_\alpha(q)\, W^\mp_\gamma(k)} &= \mp i e_5 \frac{2\pi}{L}\frac{1}{t}\Big[\eta_{\alpha\beta}(q-p)_\gamma + \eta_{\beta\gamma}(p-k)_\alpha + \eta_{\gamma\alpha}(k-q)_\beta\Big]\,, \\
\mathcal{A}^{W^\pm_5\, A^{(0)}_\alpha\, W^\mp_\gamma} &= \pm e_5\, \eta_{\alpha\gamma}\, \frac{2\pi M_{\rm KK}}{L}\left[\partial_t^{W^\pm_5} + \delta^\eta(t-1)\right]\frac{\epsilon}{t^2}\,, \\
\mathcal{A}^{W^\pm_5(p)\, A^{(0)}_\alpha\, W^\mp_5(k)} &= \pm(p-k)_\alpha\, i e_5\, \frac{2\pi}{L}\left[1 + \frac{M^2_{\rm KK}}{L\tilde{m}^2_W}\delta^\eta(t-1)\right]\frac{\epsilon^2}{t^3}\,, \\
\mathcal{A}^{G_{\beta,b}(p)\, G^{(0)}_{\alpha,a}(q)\, G_{\gamma,c}(k)} &= g_{s,5}\, f^{abc}\, \frac{2\pi}{L}\frac{1}{t}\Big[\eta_{\alpha\beta}(q-p)_\gamma + \eta_{\beta\gamma}(p-k)_\alpha + \eta_{\gamma\alpha}(k-q)_\beta\Big]\,, \\
\mathcal{A}^{G_{\beta,b}\, G^{(0)}_{\alpha,a}\, G_{5,c}} &= i g_{s,5}\, \eta_{\alpha\beta}\, f^{abc}\, \frac{2\pi M_{\rm KK}}{L}\, \partial_t^{G^c_5}\, \frac{\epsilon}{t^2}\,, \\
\mathcal{A}^{G_{5,b}(p)\, G^{(0)}_{\alpha,a}\, G_{5,c}(k)} &= g_{s,5}\, f^{abc}\, (p-k)_\alpha\, \frac{2\pi}{L}\, \frac{\epsilon^2}{t^3}\,,
\end{aligned} \tag{A.3}$$

where the incoming four-momenta p, q, k are only shown if they are necessary for the corresponding Feynman rule. The superscript of the t-derivatives indicates the field it should act on.

KK-decomposed (4D) theory

Working in the 4D framework, the amplitudes for the vertices coupling two quarks and one boson can be summarized by

$$\begin{aligned}
\mathcal{A}^{\{\bar{q}A_\mu q,\, \bar{q}_a G^c_\mu q_b,\, \bar{q}Z_\mu q,\, \bar{q}W^\pm_\mu q'\}} &= \left\{i Q_q e_5,\, i g_{s,5}\, t^c_{ab},\, \frac{i g_5\, g^q_L}{c_w},\, \frac{i g_5}{\sqrt{2}}\right\}\frac{\gamma_\mu}{\sqrt{2\pi r}}\left[V^B_{nmk}\, P_L + \tilde{V}^B_{nmk}\, P_R\right], \\
\mathcal{A}^{\{\,\bar{q}\varphi_A q,\, \bar{q}_a \varphi^c_G q_b,\, \bar{q}\varphi_Z q,\, \bar{q}\varphi^\pm_W q'\}} &= \left\{Q_q e_5,\, g_{s,5}\, t^c_{ab},\, \frac{g_5\, g^q_L}{c_w},\, \frac{g_5}{\sqrt{2}}\right\}\frac{1}{\sqrt{2\pi r}}\left[V^{\varphi_B}_{nmk}\, P_L + \tilde{V}^{\varphi_B}_{nmk}\, P_R\right], \\
\mathcal{A}^{\bar{q}hq} &= -i\left[(\tilde{\boldsymbol{g}}^q_h)_{nk}\, P_L + (\boldsymbol{g}^q_h)_{nk}\, P_R\right],
\end{aligned} \tag{A.4}$$

where n, m and k are the KK-mode numbers of the incoming anti-quarks, bosons and quarks. The label B on the right side must be replaced by the corresponding bosonic label on the left side. The vector and scalar overlap integrals for the neutral gauge bosons are given by ($B = A, G, Z$)

$$V^B_{nmk} = \sqrt{2\pi}\int_\epsilon^1 dt\, \chi^B_m(t)\, \mathcal{Q}^{(n)\dagger}_L(t)\, \boldsymbol{P}_B\, \mathcal{Q}^{(k)}_L(t)\,, \quad \tilde{V}^B_{nmk} = V^B_{nmk}|_{L\leftrightarrow R}\,, \tag{A.5}$$

$$V^{\varphi_B}_{nmk} = \sqrt{2\pi}\int_\epsilon^1 dt\, \frac{-kt\, \partial_t \chi^B_m(t)}{m_{B_m}}\, \mathcal{Q}^{(n)\dagger}_R(t)\, \boldsymbol{V}_{B_5}(t)\, \mathcal{Q}^{(k)}_L(t)\,, \quad \tilde{V}^{\varphi_B}_{nmk} = V^{\varphi_B}_{nmk}|_{L\leftrightarrow R,\, \boldsymbol{V}_{B_5}\to\tilde{\boldsymbol{V}}_{B_5}}\,,$$

[2] This assumption simplifies the Feynman rules and is also sufficient for the calculation of the processes considered in this thesis.

where the various functions $\boldsymbol{V}_{B_5}$, $\tilde{\boldsymbol{V}}_{B_5}$ are defined in (A.2). In case of the W boson we find the following overlap integrals

$$
\begin{aligned}
V^{W^+}_{nmk} &= \sqrt{2\pi}\int_\epsilon^1 dt\, \chi^W_m(t)\, \mathcal{U}^{(n)\dagger}_L(t)\, \boldsymbol{P}_W\, \mathcal{D}^{(k)}_L(t), \quad V^{W^-}_{nmk} = V^{W^+}_{nmk}\big|_{\mathcal{U}\leftrightarrow\mathcal{D}}, \quad \tilde{V}^{W^\pm}_{nmk} = V^{W^\pm}_{nmk}\big|_{L\leftrightarrow R}, \\
V^{\varphi^+_W}_{nmk} &= \sqrt{2\pi}\int_\epsilon^1 dt\, \frac{-kt\big[\partial_t\chi^W_m(t)\big]}{m_{W_m}}\, \mathcal{U}^{(n)\dagger}_R(t)\, \boldsymbol{V}_{W_5^+}(t)\, \mathcal{D}^{(k)}_L(t), \quad \tilde{V}^{\varphi^\pm_W}_{nmk} = V^{\varphi^\pm_W}_{nmk}\big|_{L\leftrightarrow R,\, \boldsymbol{V}_{W_5^\pm}\to\tilde{\boldsymbol{V}}_{W_5^\pm}}, \\
V^{\varphi^-_W}_{nmk} &= \sqrt{2\pi}\int_\epsilon^1 dt\, \frac{-kt\big[\partial_t\chi^W_m(t)\big]}{m_{W_m}}\, \mathcal{D}^{(n)\dagger}_R(t)\, \boldsymbol{V}_{W_5^-}(t)\, \mathcal{U}^{(k)}_L(t),
\end{aligned}
\tag{A.6}
$$

We can simplify the scalar overlap integrals by performing a partial t-integration noting that boundary terms at $t=\epsilon,1$ vanish, since we work with the regularised δ-function (1.58). We can apply the equation of motions for the quark profiles such that the terms with the δ-functions cancel. For instance, in case of the integral $V^{\varphi^+_W}_{nmk}$ we can use that

$$
\begin{aligned}
\partial_t\Big[\mathcal{U}^{(n)\dagger}_R(t)\, P_+\, \mathcal{D}^{(k)}_L(t)\Big] = {}& \frac{m_{u_n}}{M_{\rm KK}}\, \mathcal{U}^{(n)\dagger}_L(t)\, P_+\, \mathcal{D}^{(k)}_L(t) - \frac{m_{d_k}}{M_{\rm KK}}\, \mathcal{U}^{(n)\dagger}_R(t)\, P_+\, \mathcal{D}^{(k)}_R(t) \\
& - \varrho\, \delta^\eta(t-1)\, \mathcal{U}^{(n)\dagger}_R(t)\, M^{Y\dagger}_{ud}\, \mathcal{D}^{(k)}_L(t)\,,
\end{aligned}
\tag{A.7}
$$

where the last term in (A.7) cancels the δ-function appearing in $\boldsymbol{V}_{W_5^+}(t)$. Repeating the steps for the remaining cases we find

$$
\begin{aligned}
V^{\varphi_B}_{nmk} &= \frac{m_{q_n}}{m_{B_m}} V^B_{nmk} - \frac{m_{q_k}}{m_{B_m}} \tilde{V}^B_{nmk}\,, \quad \tilde{V}^{\varphi_B}_{nmk} = \frac{m_{q_n}}{m_{B_m}} \tilde{V}^B_{nmk} - \frac{m_{q_k}}{m_{B_m}} V^B_{nmk}\,, \quad (B = A, G, Z) \\
V^{\varphi^+_W}_{nmk} &= \frac{m_{u_n}}{m_{W_m}} V^{W^+}_{nmk} - \frac{m_{d_k}}{m_{W_m}} \tilde{V}^{W^+}_{nmk}\,, \quad \tilde{V}^{\varphi^+_W}_{nmk} = \frac{m_{u_n}}{m_{W_m}} \tilde{V}^{W^+}_{nmk} - \frac{m_{d_k}}{m_{W_m}} V^{W^+}_{nmk}\,, \\
V^{\varphi^-_W}_{nmk} &= \frac{m_{d_n}}{m_{W_m}} V^{W^-}_{nmk} - \frac{m_{u_k}}{m_{W_m}} \tilde{V}^{W^-}_{nmk}\,, \quad \tilde{V}^{\varphi^-_W}_{nmk} = \frac{m_{d_n}}{m_{W_m}} \tilde{V}^{W^-}_{nmk} - \frac{m_{u_k}}{m_{W_m}} V^{W^-}_{nmk}\,,
\end{aligned}
\tag{A.8}
$$

where all scalar overlap integrals can be expressed in terms of the vector overlap integrals. Concerning the Higgs-boson couplings to quarks in (A.4) the overlap integrals are given by $(q = u, d)$

$$
(\boldsymbol{g}^q_h)_{nk} = \frac{1}{\sqrt{2}} \int_\epsilon^1 dt\, \delta^\eta(t-1)\, \mathcal{Q}^{(n)\dagger}_L(t)\, \mathcal{M}^Y_q\, \mathcal{Q}^{(k)}_R(t)\,, \qquad (\tilde{\boldsymbol{g}}^q_h)_{nk} = \big[(\boldsymbol{g}^q_h)_{kn}\big]^\dagger\,. \tag{A.9}
$$

In the brane-localized Higgs scenario with $\boldsymbol{Y}^C_q = \boldsymbol{Y}^S_q$ we can perform the t-integration analytically and find

$$
(\boldsymbol{g}^q_h)_{nk} = \frac{1}{\sqrt{2}}\, \mathcal{Q}^{(n)\dagger}_L(1^-)\, \boldsymbol{P}_{12}\, \frac{2\boldsymbol{X}_q}{\sinh 2\boldsymbol{X}_q}\, \tilde{\boldsymbol{Y}}_q\, \mathcal{Q}^{(k)}_R(1^-)\,, \tag{A.10}
$$

where $\boldsymbol{X}_q = \varrho(\boldsymbol{Y}_q\boldsymbol{Y}_q^\dagger)^{1/2}$ and $\tilde{\boldsymbol{Y}}_q = (\tanh\boldsymbol{X}_q/\boldsymbol{X}_q)\boldsymbol{Y}_q$.

Next, we present selected Higgs-boson couplings to KK modes of the W boson and the photon. They read

$$
\begin{aligned}
\mathcal{A}^{W^{\pm(n)}_\beta\, h\, W^{\mp(k)}_\alpha} &= \frac{2i\tilde{m}^2_W}{v}\, 2\pi\, \chi^W_n(1)\, \chi^W_k(1)\, \eta_{\alpha\beta}\,, \\
\mathcal{A}^{\varphi^{\pm(n)}_W(p)\, h(q)\, W^{\mp(k)}_\alpha} &= \frac{\tilde{m}^2_W}{v\, m_{W_n}}\, (p-q)_\alpha\, 2\pi\, \chi^W_n(1)\, \chi^W_k(1)\,,
\end{aligned}
$$

$$\begin{aligned}
\mathcal{A}^{\varphi_W^{\pm(n)}\, h\, \varphi_W^{\mp(k)}} &= -\frac{i m_h^2}{v}\, \frac{\tilde{m}_W^2}{m_{W_n} m_{W_k}}\, 2\pi\, \chi_n^W(1)\, \chi_k^W(1)\,, \\
\mathcal{A}^{\varphi_W^{\pm(n)}\, h\, A_\beta^{(0)}\, W_\alpha^{\mp(k)}} &= \pm\frac{e_5}{\sqrt{2\pi r}}\, \frac{\tilde{m}_W^2}{v\, m_{W_n}}\, 2\pi\, \chi_n^W(1)\, \chi_k^W(1)\, \eta_{\alpha\beta}\,,
\end{aligned} \tag{A.11}$$

which are all non-diagonal in the KK-mode numbers.

Now, we consider important triple and quartic gauge-boson vertices. The corresponding amplitudes are given by

$$\begin{aligned}
\mathcal{A}^{W_\beta^{\pm(n)}(p)\, A_\alpha^{(0)}(q)\, W_\gamma^{\mp(k)}(k)} &= \mp\frac{i e_5}{\sqrt{2\pi r}}\Big[\eta_{\alpha\beta}(q-p)_\gamma + \eta_{\beta\gamma}(p-k)_\alpha + \eta_{\gamma\alpha}(k-q)_\beta\Big]\delta_{nk}\,, \\
\mathcal{A}^{\varphi_W^{\pm(n)}\, A_\alpha^{(0)}\, W_\beta^{\mp(k)}} &= \pm\frac{e_5}{\sqrt{2\pi r}}\, \eta_{\alpha\beta}\, m_{W_n}\, \delta_{nk}\,, \\
\mathcal{A}^{\varphi_W^{\pm(n)}(p)\, A_\alpha^{(0)}\, \varphi_W^{\mp(k)}(k)} &= \pm(p-k)_\alpha \frac{i e_5}{\sqrt{2\pi r}}\, \delta_{nk}\,, \\
\mathcal{A}^{W_\beta^{\pm(n)}\, W_\alpha^{\mp(k)}\, A_\gamma^{(0)} A_\delta^{(0)}} &= -\frac{e_5^2}{2\pi r}\Big[2\eta_{\beta\alpha}\eta_{\gamma\delta} - \eta_{\beta\gamma}\eta_{\alpha\delta} - \eta_{\beta\delta}\eta_{\alpha\gamma}\Big]\delta_{nk}\,, \\
\mathcal{A}^{\varphi_W^{\pm(n)}\, \varphi_W^{\mp(k)}\, A_\alpha^{(0)}\, A_\beta^{(0)}} &= \frac{2 i e_5^2}{2\pi r}\, \eta_{\alpha\beta}\, \delta_{nk}\,, \\
\mathcal{A}^{G_{\beta,b}^{(n)}(p)\, G_{\alpha,a}^{(0)}(q)\, G_{\gamma,c}^{(k)}(k)} &= \frac{g_{s,5}}{\sqrt{2\pi r}}\, f^{abc}\Big[\eta_{\alpha\beta}(q-p)_\gamma + \eta_{\beta\gamma}(p-k)_\alpha + \eta_{\gamma\alpha}(k-q)_\beta\Big]\delta_{nk}\,, \\
\mathcal{A}^{G_{\beta,b}^{(n)}\, G_{\alpha,a}^{(0)}\, \varphi_{G,c}^{(k)}} &= \frac{i g_{s,5}}{\sqrt{2\pi r}}\, \eta_{\alpha\beta}\, f^{abc}\, m_{G_n}\, \delta_{nk}\,, \\
\mathcal{A}^{\varphi_{G,b}^{(n)}(p)\, G_{\alpha,a}^{(0)}\, \varphi_{G,c}^{(k)}(k)} &= (p-k)_\alpha\, \frac{g_{s,5}}{\sqrt{2\pi r}}\, f^{abc}\, \delta_{nk}\,.
\end{aligned} \tag{A.12}$$

Due to the presence of photon (or gluon) zero-modes all vertices conserve the KK-mode number.

Finally, we present the relevant couplings involving ghost fields of the W boson, which are required for the calculation of the $h \to \gamma\gamma$ decay amplitude. They read

$$\begin{aligned}
\mathcal{A}^{c_W^{\pm(n)}\, h\, c_W^{\mp(k)}} &= -\xi\, \frac{i\tilde{m}_W^2}{v}\, 2\pi\, \chi_n^W(1)\, \chi_k^W(1)\,, \\
\mathcal{A}^{c_W^{\pm(n)}(p)\, A_\alpha^{(0)}\, c_W^{\mp(k)}} &= \mp\frac{i e_5}{\sqrt{2\pi r}}\, p_\alpha\, \delta_{nk}\,,
\end{aligned} \tag{A.13}$$

where ξ is the gauge-fixing parameter and $c_W^{\pm(n)}$ is the n^{th} KK-mode of the W-boson ghost.

B Loop functions

In the KK-decomposed (4D) theory the dipole Wilson coefficients in (5.37) involve the loop functions $I_{3,4}(x)$ and $I_{6-11}(x)$. They can be defined by the integral representations

$$
\begin{aligned}
I_3(x_m^n) &= \frac{m_m^2}{m_n^2}\left(\frac{1}{2} + m_m^2\int_0^\infty dk_E\,\frac{1}{k_E^2+m_n^2}\left[\frac{3k_E^2}{4}\partial_{k_E} + \frac{k_E^3}{4}\partial_{k_E}^2\right]\frac{1}{k_E^2+m_m^2}\right),\\
I_4(x_m^n) &= \frac{m_m^2}{m_n^2}\left(\frac{1}{12} + m_m^2\int_0^\infty dk_E\,\frac{1}{k_E^2+m_n^2}\left[\frac{k_E^2}{16}\partial_{k_E} - \frac{k_E^3}{16}\partial_{k_E}^2 - \frac{k_E^4}{48}\partial_{k_E}^3\right]\frac{1}{k_E^2+m_m^2}\right),\\
I_6(x_m^n) &= -\frac{1}{2} + m_m^2\int_0^\infty dk_E\frac{1}{k_E^2+m_n^2}\left[\frac{9k_E^2}{4}\partial_{k_E} + \frac{3k_E^3}{4}\partial_{k_E}^2\right]\frac{1}{k_E^2+m_m^2},\\
I_7(x_m^n) &= \frac{5}{12} + m_m^2\int_0^\infty dk_E\frac{1}{k_E^2+m_n^2}\left[-\frac{3k_E^2}{16}\partial_{k_E} + \frac{3k_E^3}{16}\partial_{k_E}^2 + \frac{k_E^4}{16}\partial_{k_E}^3\right]\frac{1}{k_E^2+m_m^2},\\
I_8(x_n^m) &= -\frac{1}{4} + m_m^2\int_0^\infty dk_E\frac{1}{k_E^2+m_n^2}\left[\frac{3k_E^2}{8}\partial_{k_E} - \frac{3k_E^3}{8}\partial_{k_E}^2\right]\frac{1}{k_E^2+m_m^2},\\
I_9(x_n^m) &= \frac{1}{6} + m_m^2\int_0^\infty dk_E\frac{1}{k_E^2+m_n^2}\left[-\frac{3k_E^2}{32}\partial_{k_E} + \frac{3k_E^3}{32}\partial_{k_E}^2 - \frac{k_E^4}{32}\partial_{k_E}^3\right]\frac{1}{k_E^2+m_m^2},\\
I_{10}(x_n^m) &= -\frac{1}{4} + m_m^2\int_0^\infty dk_E\frac{1}{k_E^2+m_n^2}\left[-\frac{3k_E^2}{8}\partial_{k_E} + \frac{3k_E^3}{8}\partial_{k_E}^2\right]\frac{1}{k_E^2+m_m^2},\\
I_{11}(x_n^m) &= \frac{1}{6} + m_m^2\int_0^\infty dk_E\frac{1}{k_E^2+m_n^2}\left[\frac{5k_E^2}{32}\partial_{k_E} - \frac{5k_E^3}{32}\partial_{k_E}^2 + \frac{k_E^4}{96}\partial_{k_E}^3\right]\frac{1}{k_E^2+m_m^2},
\end{aligned}
\tag{B.1}
$$

where $x_b^a \equiv m_a^2/m_b^2$. Note that the loop functions $I_{3,4,6,7}(x)$ and $I_{8-11}(x)$ have different arguments. The equations in (B.1) can be used to rewrite the dipole Wilson coefficients in the 5D framework, given by (5.8), (5.24) and (5.33), in terms of the corresponding expressions in the KK-decomposed theory in (5.37). Performing the momentum integrals in (B.1) the loop functions explicitly read

$$
\begin{aligned}
I_3(x) &= \frac{3-4x+x^2+2\ln x}{2(x-1)^3},\\
I_4(x) &= \frac{2+3x-6x^2+x^3+6x\ln x}{12(x-1)^4},\\
I_6(x) &= \frac{4-3x-x^3+6x\ln x}{2(x-1)^3},\\
I_7(x) &= \frac{8-38x+39x^2-14x^3+5x^4-18x^2\ln x}{12(x-1)^4},\\
I_8(x) &= \frac{1-12x+15x^2-4x^3-6x\ln x}{4(x-1)^3},
\end{aligned}
$$

$$
\begin{aligned}
I_9(x) &= \frac{4 - 49x + 78x^2 - 43x^3 + 10x^4 - 18x \ln x}{24(x-1)^4}\,, \\
I_{10}(x) &= \frac{1 + 6x - 9x^2 + 2x^3 + 6x \ln x}{4(x-1)^3}\,, \\
I_{11}(x) &= \frac{4 + 13x - 36x^2 + 23x^3 - 4x^4 - 6x(2x-3) \ln x}{24(x-1)^4}\,.
\end{aligned} \tag{B.2}
$$

Acknowledgements

First of all, I would like to thank Matthias for giving me the opportunity to work on a very interesting research topic. I am very thankful for his support and his guidance throughout my time as a diploma and PhD student. Furthermore, I would like to express my gratitude to him and the Graduate School *Symmetry Breaking in Fundamental Interactions* for allowing me to attend physics schools at various places around the world. Finally, I would like to thank the whole working group and in particular Christoph for the enjoyable time in discussing physics as well as non-physics related issues.

I dedicate this thesis to my family, in particular Karin, Michael and Lara and to my girlfriend Anna-Lisa, just for being herself.

My own contribution

In the following, I clarify which parts of my thesis are based on results that have been published in our four publications [A-D] (listed on the next page). Furthermore, I explain which results have been worked out by myself and are therefore my own contributions.

Chapter 1 serves as an introduction into the subject of my thesis. Therefore, the presented material is not based on my own work. The only exception is Section 1.4.5, which discusses the Higgs-sector localization in RS models, and which includes results that I have derived in [D].

Chapter 2 introduces different RS models. Sections 2.1, 2.2 and 2.4 discuss the minimal and custodial RS models, where the presented material is mainly based on [132, 149]. Section 2.3, which presents the extension of the minimal RS model to a bulk-Higgs sector, is based on my own work published in [D]. Section 2.5 explains the procedure to generate RS points, which is based on an updated and modified version of the algorithm first used in [132]. The last paragraph calculates the Peskin-Takeuchi parameters and is based on an updated analysis of [164].

Chapter 3 is dedicated to the warped 5D propagators. Sections 3.1 and 3.2 derive the bosonic 5D propagators. These propagators have already been obtained earlier in the literature, but I have derived them in the so-called t-notation. The only exception is the W-boson 5D propagator in the custodial RS model, which I have derived for the first time in an exact form valid for arbitrary four-momentum. This result has been published in [C]. Section 3.3 includes a comprehensive derivation of the fermion 5D propagator in the minimal and custodial RS models, while keeping the full dependence on the Yukawa interactions, and by working with three family generations. This section has been partly published in [A] and [D]. There exists only one earlier work [200], which has calculated the fermion 5D propagator in the minimal RS model for a brane-localized Higgs sector, and which has also kept the dependence on the Yukawa couplings. However, I have performed the derivation by regularizing the vacuum expectation value by a square box of width η and height $1/\eta$ with $\eta \ll v|Y_q|/M_{\rm KK}$, which has allowed me to obtain exact results in both the brane-localized and narrow bulk-Higgs scenarios. In addition, I have extended the results to the custodial RS model. Section 3.4 discusses the ultra-violet behavior of the fermion and gauge-boson 5D propagators in the minimal RS model, which has been published in [A].

Chapter 4 discusses Higgs physics in a warped extra dimension. Section 4.1 deals with the process $gg \to h$, where I have worked out the ideas of M. Neubert and performed all the calculations. This section is based on [D]. By working in the 5D framework, I have shown that the Feynman amplitude for the fermion triangle diagram does not smoothly interpolate between the brane- and narrow bulk-Higgs scenarios. Furthermore, I have shown that the disagreement of the results for the KK-tower contribution to the $gg \to h$ amplitude, between [149] and [209], can be resolved, once it is realized that the calculations had been performed in two different implementations of the Higgs

sector. Section 4.2 analyzes the process $h \to \gamma\gamma$ in the RS model and is based on [C]. I have performed all the calculations and analyses presented in this section, except for showing the R_ξ gauge invariance of the $h \to \gamma\gamma$ amplitude in the RS model, which has been done first by J. Hahn. Section 4.3 discusses the tree-level Higgs production and decay processes, which I have worked out by myself and which have been published in [B]. Section 4.4 includes the phenomenological implications, which are based on an updated and extended analysis of the one published in [B]. All numerical calculations and plots have been performed and created by myself, using *Mathematica* [186].

Chapter 5 includes a comprehensive investigation of the $b \to s\gamma$ transition in the minimal RS model, and by working in the 5D framework. This chapter is entirely based on [A], written mainly by myself. There are only two other works, [246] and [251], which have performed comprehensive calculations of the $b \to s\gamma$ transition in the 5D framework. However, in contrast to both works I have obtained integral expressions that are formally valid to all orders in $v^2/M_{\rm KK}^2$. Furthermore, I have shown that my results from the 5D calculation coincide analytically and numerically with the corresponding expressions in the KK-decomposed theory. Concerning the results in the KK-decomposed theory, I have benefited from earlier calculations performed by C. Schmell, which are contained in his doctoral thesis [247]. All numerical calculations, especially extensive have been the evaluation of the integral expressions for the dipole Wilson coefficients and the determination of the KK masses up to the fifth KK level, have been performed by myself, using *Mathematica* [186].

Appendix A includes the Feynman rules in the RS model, which I have derived in order to calculate all the amplitudes that are relevant for my thesis. They have been partly published in [A-D]. Appendix B contains the necessary loop functions for the $b \to s\gamma$ transition in the KK-decomposed theory, which have been published in [A].

[A] R. Malm, M. Neubert, C. Schmell, *Impact of Warped Extra Dimensions on the Dipole Coefficients in $b \to s\gamma$ Transitions*, JHEP 04, 042 (2016), arXiv:1509.02539 [hep-ph] .

[B] R. Malm, M. Neubert, C. Schmell, *Higgs Couplings and Phenomenology in a Warped Extra Dimension*, JHEP 02, 008 (2015), arXiv:1408.4456 [hep-ph] .

[C] J. Hahn, C. Hörner, R. Malm, M. Neubert, K. Novotny, C. Schmell, *Higgs Decay into Two Photons at the Boundary of a Warped Extra Dimension*, Eur. Phys. J. C74, 2857 (2014), arXiv:1312.5731 [hep-ph] .

[D] R. Malm, M. Neubert, K. Novotny, C. Schmell, *5D Perspective on Higgs Production at the Boundary of a Warped Extra Dimension*, JHEP 01, 173 (2014), arXiv:1303.5702 [hep-ph] .

Versicherung

Hiermit versichere ich gemäß § 12 Abs. 3e der Promotionsordnung des Fachbereichs 08, Physik, Mathematik und Informatik der Johannes Gutenberg-Universität Mainz vom 02.12.2013:

a) Ich habe die jetzt als Dissertation vorgelegte Arbeit selbständig verfasst. Es wurden ausschließlich die angegebenen Quellen und Hilfsmittel verwendet. Von der Ordnung zur Sicherung guter wissenschaftlicher Praxis in Forschung und Lehre und vom Verfahren zum Umgang mit wissenschaftlichem Fehlverhalten habe ich Kenntnis genommen.

b) Ich habe oder hatte die jetzt als Dissertation vorgelegte Arbeit nicht schon als Prüfungsarbeit für eine andere Prüfung eingereicht ***)**

~~Ich hatte die jetzt als Dissertation vorgelegte Arbeit als Prüfungsarbeit für folgende Prüfung eingereicht: *)~~

_____

(Bezeichnung der Prüfung)

_____

(Bezeichnung und Ort der Prüfungsstelle)

c) Ich hatte weder die jetzt als Dissertation vorgelegte Arbeit noch Teile davon an einer anderen Stelle als Dissertation eingereicht ***)**

~~Ich hatte die folgende Abhandlung mit anstehendem Ergebnis als Dissertation eingereicht *)~~

_____

(Titel der Abhandlung)

_____

(Fakultät bzw. Fachbereich und Hochschule)

_____

(Ergebnis bzw. Beurteilung)

02.05.2016
(Datum)

R. Mu(u
(Unterschrift)

) Nichtzutreffendes bitte streichen

18.03.2014/mm

Bibliography

[1] P. J. Mohr, B. N. Taylor, and D. B. Newell, Rev. Mod. Phys. **84**, 1527 (2012).

[2] R. Malm, M. Neubert, K. Novotny, and C. Schmell, JHEP **01**, 173 (2014), arXiv:1303.5702 [hep-ph] .

[3] S. Weinberg, *The Quantum Theory of Fields. Vol. 1: Foundations* (Cambridge University Press, 2005).

[4] M. E. Peskin and D. V. Schroeder, *An Introduction to Quantum Field Theory* (Westview Press, 1995).

[5] T. P. Cheng and L. F. Li, *Gauge Theory of Elementary Particle Physics* (Oxford Science Publications, 1984).

[6] A. J. Buras, in *Probing the Standard Model of Particle Interactions. Proceedings, Summer School in Theoretical Physics, NATO Advanced Study Institute, 68th session, Les Houches, France* (1998) pp. 281–539, arXiv:hep-ph/9806471 .

[7] M. Neubert, in *Physics in $D \geq 4$. Proceedings, Theoretical Advanced Study Institute in elementary particle physics, TASI 2004, Boulder, USA* (2005) pp. 149–194, arXiv:hep-ph/0512222 .

[8] B. Grinstein and M. Trott, Phys. Rev. **D76**, 073002 (2007), arXiv:0704.1505 [hep-ph] .

[9] A. G. Riess *et al.* (Supernova Search Team), Astron. J. **116**, 1009 (1998), arXiv:astro-ph/9805201 .

[10] S. Perlmutter *et al.* (Supernova Cosmology Project), Astrophys. J. **517**, 565 (1999), arXiv:astro-ph/9812133 .

[11] M. Trodden and S. M. Carroll, in *Progress in String Theory. Proceedings, Summer School, TASI 2003, Boulder, USA* (2004) pp. 703–793, arXiv:astro-ph/0401547 .

[12] P. A. R. Ade *et al.* (Planck), Astron. Astrophys. **571**, A16 (2014), arXiv:1303.5076 [astro-ph] .

[13] S. Weinberg, Phys. Rev. Lett. **43**, 1566 (1979).

[14] W. Buchmüller and D. Wyler, Nucl. Phys. **B268**, 621 (1986).

[15] R. Alonso, E. E. Jenkins, A. V. Manohar, and M. Trott, JHEP **04**, 159 (2014), arXiv:1312.2014 [hep-ph] .

[16] S. L. Glashow, Nucl. Phys. **22**, 579 (1961).

[17] S. Weinberg, Phys. Rev. Lett. **19**, 1264 (1967).

[18] A. Salam, *8th Nobel Symposium Lerum, Sweden, May 19-25, 1968*, Conf. Proc. **C680519**, 367 (1968).

[19] G. 't Hooft and M. J. G. Veltman, Nucl. Phys. **B44**, 189 (1972).

[20] M. Gell-Mann, Phys. Lett. **8**, 214 (1964).

[21] G. Zweig, CERN-TH-401 (1964).

[22] D. J. Gross and F. Wilczek, Phys. Rev. Lett. **30**, 1343 (1973).

[23] D. J. Gross and F. Wilczek, Phys. Rev. **D8**, 3633 (1973).

[24] D. J. Gross and F. Wilczek, Phys. Rev. **D9**, 980 (1974).

[25] H. D. Politzer, Phys. Rev. **D9**, 2174 (1974).

[26] G. Arnison *et al.* (UA1), Phys. Lett. **B122**, 103 (1983).

[27] M. L. Perl *et al.*, Phys. Rev. Lett. **35**, 1489 (1975).

[28] S. W. Herb *et al.*, Phys. Rev. Lett. **39**, 252 (1977).

[29] F. Abe *et al.* (CDF), Phys. Rev. Lett. **74**, 2626 (1995), arXiv:hep-ex/9503002 .

[30] G. Aad *et al.* (ATLAS), Phys. Lett. **B716**, 1 (2012), arXiv:1207.7214 [hep-ex] .

[31] S. Chatrchyan *et al.* (CMS), Phys. Lett. **B716**, 30 (2012), arXiv:1207.7235 [hep-ex] .

[32] S. Weinberg, Eur. Phys. J. **C34**, 5 (2004), arXiv:hep-ph/0401010 .

[33] P. W. Anderson, Phys. Rev. **130**, 439 (1963).

[34] F. Englert and R. Brout, Phys. Rev. Lett. **13**, 321 (1964).

[35] P. W. Higgs, Phys. Rev. Lett. **13**, 508 (1964).

[36] G. S. Guralnik, C. R. Hagen, and T. W. B. Kibble, Phys. Rev. Lett. **13**, 585 (1964).

[37] N. Cabibbo, Phys. Rev. Lett. **10**, 531 (1963).

[38] M. Kobayashi and T. Maskawa, Prog. Theor. Phys. **49**, 652 (1973).

[39] Y. Fukuda *et al.* (Super-Kamiokande), Phys. Rev. Lett. **81**, 1562 (1998), arXiv:hep-ex/9807003 .

[40] G. 't Hooft, Phys. Rev. Lett. **37**, 8 (1976).

[41] V. A. Kuzmin, V. A. Rubakov, and M. E. Shaposhnikov, Phys. Lett. **B155**, 36 (1985).

[42] V. A. Rubakov and M. E. Shaposhnikov, Usp. Fiz. Nauk **166**, 493 (1996), arXiv:hep-ph/9603208 .

[43] P. Sikivie, L. Susskind, M. B. Voloshin, and V. I. Zakharov, Nucl. Phys. **B173**, 189 (1980).

[44] M. J. G. Veltman, Acta Phys. Polon. **B8**, 475 (1977).

[45] M. J. G. Veltman, Nucl. Phys. **B123**, 89 (1977).

[46] M. E. Peskin and T. Takeuchi, Phys. Rev. **D46**, 381 (1992).

[47] N. Arkani-Hamed, D. P. Finkbeiner, T. R. Slatyer, and N. Weiner, Phys. Rev. **D79**, 015014 (2009), arXiv:0810.0713 [hep-ph] .

[48] A. D. Sakharov, Pisma Zh. Eksp. Teor. Fiz. **5**, 32 (1967).

[49] P. Minkowski, Phys. Lett. **B67**, 421 (1977).

[50] R. N. Mohapatra and G. Senjanovic, Phys. Rev. Lett. **44**, 912 (1980).

[51] T. Blum, A. Denig, I. Logashenko, E. de Rafael, B. Lee Roberts, T. Teubner, and G. Venanzoni, (2013), arXiv:1311.2198 [hep-ph] .

[52] H. Davoudiasl, H.-S. Lee, and W. J. Marciano, Phys. Rev. **D89**, 095006 (2014), arXiv:1402.3620 [hep-ph] .

[53] R. Pohl *et al.*, Nature **466**, 213 (2010).

[54] A. Antognini *et al.*, Science **339**, 417 (2013).

[55] A. Pich, in *37th International Conference on High Energy Physics (ICHEP 2014) Valencia, Spain* (2015) arXiv:1505.01813 [hep-ph] .

[56] The ATLAS Collaboration, *Search for resonances decaying to photon pairs in 3.2 fb^{-1} of pp collisions at $\sqrt{s}$ = 13 TeV with the ATLAS detector*, ATLAS-CONF-2015-081 (2015).

[57] The CMS Collaboration, *Search for new physics in high mass diphoton events in proton-proton collisions at $\sqrt{s}$ = 13 TeV*, CMS-PAS-EXO-15-004 (2015).

[58] L. D. Landau, Dokl. Akad. Nauk Ser. Fiz. **60**, 207 (1948).

[59] C.-N. Yang, Phys. Rev. **77**, 242 (1950).

[60] M. Bauer, C. Hoerner, and M. Neubert, (2016), arXiv:1603.05978 [hep-ph] .

[61] C. Csaki and L. Randall, (2016), arXiv:1603.07303 [hep-ph] .

[62] D. Buttazzo, G. Degrassi, P. P. Giardino, G. F. Giudice, F. Sala, A. Salvio, and A. Strumia, JHEP **12**, 089 (2013), arXiv:1307.3536 [hep-ph] .

[63] H. Georgi and S. L. Glashow, Phys. Rev. Lett. **32**, 438 (1974).

[64] G. F. Giudice, in *Kane, Gordon (ed.), Pierce, Aaron (ed.): Perspectives on LHC physics, pp. 155-178* (2008) arXiv:0801.2562 [hep-ph] .

[65] P. A. M. Dirac, Nature **139**, 323 (1937).

[66] P. A. M. Dirac, Proc. Roy. Soc. Lond. **A165**, 199 (1938).

[67] G. 't Hooft, C. Itzykson, A. Jaffe, H. Lehmann, P. K. Mitter, I. M. Singer, and R. Stora, NATO Sci. Ser. B **59**, pp.1 (1980).

[68] C. G. Bollini and J. J. Giambiagi, Nuovo Cim. **B12**, 20 (1972).

[69] G. 't Hooft, Nucl. Phys. **B61**, 455 (1973).

[70] G. Aad *et al.* (ATLAS, CMS), Phys. Rev. Lett. **114**, 191803 (2015), arXiv:1503.07589 [hep-ex] .

[71] G. Degrassi, S. Di Vita, J. Elias-Miro, J. R. Espinosa, G. F. Giudice, G. Isidori, and A. Strumia, JHEP **08**, 098 (2012), arXiv:1205.6497 [hep-ph] .

[72] V. Agrawal, S. M. Barr, J. F. Donoghue, and D. Seckel, Phys. Rev. **D57**, 5480 (1998), arXiv:hep-ph/9707380 .

[73] G. F. Giudice and R. Rattazzi, Nucl. Phys. **B757**, 19 (2006), arXiv:hep-ph/0606105 .

[74] K. A. Meissner and H. Nicolai, Phys. Lett. **B648**, 312 (2007), arXiv:hep-th/0612165 .

[75] S. Weinberg, Phys. Rev. Lett. **59**, 2607 (1987).

[76] K. A. Olive *et al.* (Particle Data Group), Chin. Phys. **C38**, 090001 (2014 and 2015 update).

[77] X. Qian and P. Vogel, Prog. Part. Nucl. Phys. **83**, 1 (2015), arXiv:1505.01891 [hep-ex] .

[78] B. Pontecorvo, Sov. Phys. JETP **7**, 172 (1958).

[79] B. Pontecorvo, Sov. Phys. JETP **26**, 984 (1968).

[80] Z. Maki, M. Nakagawa, and S. Sakata, Prog. Theor. Phys. **28**, 870 (1962).

[81] L. Wolfenstein, Phys. Rev. Lett. **51**, 1945 (1983).

[82] S. L. Glashow, J. Iliopoulos, and L. Maiani, Phys. Rev. D **2**, 1285 (1970).

[83] M. Bona *et al.* (Unitarity Triangle fit), JHEP **03**, 049 (2008), arXiv:0707.0636 [hep-ph] .

[84] S. P. Martin, *A Supersymmetry primer*, (1997), arXiv:hep-ph/9709356 .

[85] R. Haag, J. T. Lopuszanski, and M. Sohnius, Nucl. Phys. **B88**, 257 (1975).

[86] S. R. Coleman and J. Mandula, Phys. Rev. **159**, 1251 (1967).

[87] S. Dimopoulos and H. Georgi, Nucl. Phys. **B193**, 150 (1981).

[88] N. Seiberg, Phys. Lett. **B318**, 469 (1993), arXiv:hep-ph/9309335 .

[89] P. Fayet, Phys. Lett. **B64**, 159 (1976).

[90] H. Goldberg, Phys. Rev. Lett. **50**, 1419 (1983).

[91] J. R. Ellis, J. S. Hagelin, D. V. Nanopoulos, K. A. Olive, and M. Srednicki, Nucl. Phys. **B238**, 453 (1984).

[92] K. Inoue, A. Kakuto, H. Komatsu, and S. Takeshita, Prog. Theor. Phys. **67**, 1889 (1982).

[93] R. A. Flores and M. Sher, Annals Phys. **148**, 95 (1983).

[94] P. H. Chankowski, S. Pokorski, and J. Rosiek, Nucl. Phys. **B423**, 437 (1994), arXiv:hep-ph/9303309 .

[95] H. E. Haber and R. Hempfling, Phys. Rev. **D48**, 4280 (1993), arXiv:hep-ph/9307201 .

[96] R. Hempfling and A. H. Hoang, Phys. Lett. **B331**, 99 (1994), arXiv:hep-ph/9401219 .

[97] M. Carena, H. E. Haber, S. Heinemeyer, W. Hollik, C. E. M. Wagner, and G. Weiglein, Nucl. Phys. **B580**, 29 (2000), arXiv:hep-ph/0001002 .

[98] S. Dimopoulos and D. W. Sutter, Nucl. Phys. **B452**, 496 (1995), arXiv:hep-ph/9504415 .

[99] A. H. Chamseddine, R. L. Arnowitt, and P. Nath, Phys. Rev. Lett. **49**, 970 (1982).

[100] R. Barbieri, S. Ferrara, and C. A. Savoy, Phys. Lett. **B119**, 343 (1982).

[101] H. P. Nilles, M. Srednicki, and D. Wyler, Phys. Lett. **B120**, 346 (1983).

[102] E. Cremmer, P. Fayet, and L. Girardello, Phys. Lett. **B122**, 41 (1983).

[103] L. J. Hall, J. D. Lykken, and S. Weinberg, Phys. Rev. **D27**, 2359 (1983).

[104] S. K. Soni and H. A. Weldon, Phys. Lett. **B126**, 215 (1983).

[105] M. Dine, W. Fischler, and M. Srednicki, Nucl. Phys. **B189**, 575 (1981).

[106] S. Dimopoulos and S. Raby, Nucl. Phys. **B192**, 353 (1981).

[107] M. Dine and W. Fischler, Phys. Lett. **B110**, 227 (1982).

[108] C. R. Nappi and B. A. Ovrut, Phys. Lett. **B113**, 175 (1982).

[109] L. Alvarez-Gaume, M. Claudson, and M. B. Wise, Nucl. Phys. **B207**, 96 (1982).

[110] M. Dine and A. E. Nelson, Phys. Rev. **D48**, 1277 (1993), arXiv:hep-ph/9303230 .

[111] M. Dine, A. E. Nelson, Y. Nir, and Y. Shirman, Phys. Rev. **D53**, 2658 (1996), arXiv:hep-ph/9507378 .

[112] P. Bechtle, T. Plehn, and C. Sander, in *The Large Hadron Collider: Harvest of Run 1* (2015) pp. 421–462, arXiv:1506.03091 [hep-ex] .

[113] D. B. Kaplan, H. Georgi, and S. Dimopoulos, Phys. Lett. **B136**, 187 (1984).

[114] D. B. Kaplan and H. Georgi, Phys. Lett. **B136**, 183 (1984).

[115] H. Georgi, D. B. Kaplan, and P. Galison, Phys. Lett. **B143**, 152 (1984).

[116] H. Georgi and D. B. Kaplan, Phys. Lett. **B145**, 216 (1984).

[117] M. J. Dugan, H. Georgi, and D. B. Kaplan, Nucl. Phys. **B254**, 299 (1985).

[118] G. Panico and A. Wulzer, Lect. Notes Phys. **913**, 1 (2016), arXiv:1506.01961 [hep-ph] .

[119] K. Agashe, R. Contino, and A. Pomarol, Nucl. Phys. **B719**, 165 (2005), arXiv:hep-ph/0412089 .

[120] R. Contino, L. Da Rold, and A. Pomarol, Phys. Rev. **D75**, 055014 (2007), arXiv:hep-ph/0612048 .

[121] R. Contino, in *Physics of the large and the small, TASI 2009, Proceedings of the Theoretical Advanced Study Institute in Elementary Particle Physics, Boulder, Colorado* (2011) pp. 235–306, arXiv:1005.4269 [hep-ph] .

[122] G. F. Giudice, C. Grojean, A. Pomarol, and R. Rattazzi, JHEP **06**, 045 (2007), arXiv:hep-ph/0703164 .

[123] The ATLAS Collaboration (ATLAS), *Constraints on New Phenomena via Higgs Coupling Measurements with the ATLAS Detector*, ATLAS-CONF-2014-010 (2014).

[124] D. B. Kaplan, Nucl. Phys. **B365**, 259 (1991).

[125] L. Randall and R. Sundrum, Phys. Rev. Lett. **83**, 3370 (1999), arXiv:hep-ph/9905221 .

[126] L. Randall and M. D. Schwartz, JHEP **11**, 003 (2001), arXiv:hep-th/0108114 .

[127] A. Pomarol, Phys. Rev. Lett. **85**, 4004 (2000), arXiv:hep-ph/0005293 .

[128] K.-w. Choi, H. D. Kim, and I.-W. Kim, JHEP **11**, 033 (2002), arXiv:hep-ph/0202257 .

[129] W. D. Goldberger and I. Z. Rothstein, Phys. Rev. Lett. **89**, 131601 (2002), arXiv:hep-th/0204160 .

[130] K. Agashe, A. Delgado, and R. Sundrum, Nucl. Phys. **B643**, 172 (2002), arXiv:hep-ph/0206099 .

[131] W. D. Goldberger and M. B. Wise, Phys. Rev. Lett. **83**, 4922 (1999), arXiv:hep-ph/9907447 .

[132] S. Casagrande, F. Goertz, U. Haisch, M. Neubert, and T. Pfoh, JHEP **10**, 094 (2008), arXiv:0807.4937 [hep-ph] .

[133] R. Contino, Y. Nomura, and A. Pomarol, Nucl. Phys. **B671**, 148 (2003), arXiv:hep-ph/0306259 .

[134] J. M. Maldacena, Int. J. Theor. Phys. **38**, 1113 (1999), arXiv:hep-th/9711200 .

[135] T. Gherghetta, in *Physics of the large and the small, TASI 2009, proceedings of the Theoretical Advanced Study Institute in Elementary Particle Physics, Boulder, Colorado, USA* (2011) pp. 165–232, arXiv:1008.2570 [hep-ph] .

[136] E. Ponton, in *The Dark Secrets of the Terascale* (2013) pp. 283–374, arXiv:1207.3827 [hep-ph] .

[137] Y. Grossman and M. Neubert, Phys. Lett. **B474**, 361 (2000), arXiv:hep-ph/9912408 .

[138] C. Csaki, C. Delaunay, C. Grojean, and Y. Grossman, JHEP **10**, 055 (2008), arXiv:0806.0356 [hep-ph] .

[139] M. Bauer, S. Casagrande, L. Grunder, U. Haisch, and M. Neubert, Phys. Rev. **D79**, 076001 (2009), arXiv:0811.3678 [hep-ph] .

[140] M. Bauer, S. Casagrande, U. Haisch, and M. Neubert, JHEP **09**, 017 (2010), arXiv:0912.1625 [hep-ph] .

[141] M. Bauer, *On Flavor in Strongly Coupled Theories*, Ph.D. thesis, Johannes Gutenberg-University Mainz, Institute for Physics (2012).

[142] K. Agashe, G. Perez, and A. Soni, Phys. Rev. Lett. **93**, 201804 (2004), arXiv:hep-ph/0406101 .

[143] K. Agashe, G. Perez, and A. Soni, Phys. Rev. **D71**, 016002 (2005), arXiv:hep-ph/0408134 .

[144] C. Csaki, A. Falkowski, and A. Weiler, JHEP **09**, 008 (2008), arXiv:0804.1954 [hep-ph] .

[145] M. Blanke, A. J. Buras, B. Duling, S. Gori, and A. Weiler, JHEP **03**, 001 (2009), arXiv:0809.1073 [hep-ph] .

[146] M. Blanke, A. J. Buras, B. Duling, K. Gemmler, and S. Gori, JHEP **03**, 108 (2009), arXiv:0812.3803 [hep-ph] .

[147] M. Carena, E. Ponton, J. Santiago, and C. E. M. Wagner, Nucl. Phys. **B759**, 202 (2006), arXiv:hep-ph/0607106 .

[148] K. Agashe, R. Contino, L. Da Rold, and A. Pomarol, Phys. Lett. **B641**, 62 (2006), arXiv:hep-ph/0605341 .

[149] S. Casagrande, F. Goertz, U. Haisch, M. Neubert, and T. Pfoh, JHEP **09**, 014 (2010), arXiv:1005.4315 [hep-ph] .

[150] M. E. Albrecht, M. Blanke, A. J. Buras, B. Duling, and K. Gemmler, JHEP **09**, 064 (2009), arXiv:hep-ph/0903.2415 .

[151] R. Malm, *Mitigation of the ϵ_K Fine-tuning Problem in the Randall-Sundrum Model*, Master's thesis, Johannes Gutenberg-University Mainz, Institute for Physics (2012).

[152] M. Bauer, R. Malm, and M. Neubert, Phys. Rev. Lett. **108**, 081603 (2012), arXiv:1110.0471 [hep-ph] .

[153] J. Santiago, JHEP **12**, 046 (2008), arXiv:0806.1230 [hep-ph] .

[154] C. Csaki, A. Falkowski, and A. Weiler, Phys. Rev. **D80**, 016001 (2009), arXiv:0806.3757 [hep-ph] .

[155] C. Csaki, G. Perez, Z. Surujon, and A. Weiler, Phys. Rev. **D81**, 075025 (2010), arXiv:0907.0474 [hep-ph] .

[156] K. Agashe, A. Azatov, and L. Zhu, Phys. Rev. **D79**, 056006 (2009), arXiv:0810.1016 [hep-ph] .

[157] T. Gherghetta and A. Pomarol, Nucl. Phys. **B586**, 141 (2000), arXiv:hep-ph/0003129 .

[158] S. J. Huber, Nucl. Phys. **B666**, 269 (2003), arXiv:hep-ph/0303183 .

[159] B. Batell, T. Gherghetta, and D. Sword, Phys. Rev. **D78**, 116011 (2008), arXiv:0808.3977 [hep-ph] .

[160] J. A. Cabrer, G. von Gersdorff, and M. Quiros, New J. Phys. **12**, 075012 (2010), arXiv:0907.5361 [hep-ph] .

[161] J. A. Cabrer, G. von Gersdorff, and M. Quiros, Phys. Lett. **B697**, 208 (2011), arXiv:1011.2205 [hep-ph] .

[162] P. R. Archer, JHEP **09**, 095 (2012), arXiv:1204.4730 [hep-ph] .

[163] J. Hahn, C. Hörner, R. Malm, M. Neubert, K. Novotny, and C. Schmell, Eur. Phys. J. **C74**, 2857 (2014), arXiv:1312.5731 [hep-ph] .

[164] P. R. Archer, M. Carena, A. Carmona, and M. Neubert, JHEP **01**, 060 (2015), arXiv:1408.5406 [hep-ph] .

[165] H. Davoudiasl, J. L. Hewett, and T. G. Rizzo, Phys. Lett. **B473**, 43 (2000), arXiv:hep-ph/9911262 .

[166] A. Pomarol, Phys. Lett. **B486**, 153 (2000), arXiv:hep-ph/9911294 .

[167] C. Csaki, C. Grojean, J. Hubisz, Y. Shirman, and J. Terning, Phys. Rev. **D70**, 015012 (2004), arXiv:hep-ph/0310355 .

[168] S. J. Huber and Q. Shafi, Phys. Lett. **B498**, 256 (2001), arXiv:hep-ph/0010195 .

[169] F. del Aguila and J. Santiago, Phys. Lett. **B493**, 175 (2000), arXiv:hep-ph/0008143 .

[170] J. L. Hewett, F. J. Petriello, and T. G. Rizzo, JHEP **09**, 030 (2002), arXiv:hep-ph/0203091 .

[171] R. Barceló, S. Mitra, and G. Moreau, Eur. Phys. J. **C75**, 527 (2015), arXiv:1408.1852 [hep-ph] .

[172] J. A. Bagger, F. Feruglio, and F. Zwirner, Phys. Rev. Lett. **88**, 101601 (2002), arXiv:hep-th/0107128 .

[173] G. Cacciapaglia, C. Csaki, G. Marandella, and J. Terning, JHEP **02**, 036 (2007), arXiv:hep-ph/0611358 .

[174] P. Breitenlohner and D. Z. Freedman, Annals Phys. **144**, 249 (1982).

[175] G. Cacciapaglia, C. Csaki, G. Marandella, and J. Terning, Phys. Rev. **D75**, 015003 (2007), arXiv:hep-ph/0607146 [hep-ph] .

[176] M. Carena, E. Ponton, J. Santiago, and C. E. M. Wagner, Phys. Rev. **D76**, 035006 (2007), arXiv:hep-ph/0701055 .

[177] G. Burdman and L. Da Rold, JHEP **11**, 025 (2008), arXiv:0809.4009 [hep-ph] .

[178] A. D. Medina, N. R. Shah, and C. E. M. Wagner, Phys. Rev. **D76**, 095010 (2007), arXiv:0706.1281 [hep-ph] .

[179] The ATLAS Collaboration, *A search for $t\bar{t}$ resonances in the lepton plus jets final state with ATLAS using 14 fb^{-1} of pp collisions at $\sqrt{s}$ = 8 TeV*, ATLAS-CONF-2013-052 (2013).

[180] The CMS Collaboration, *Search for $t\bar{t}$ resonances in semileptonic final state*, CMS-PAS-B2G-12-006 (2012).

[181] The ATLAS Collaboration, *Studies of sensitivity to new dilepton and ditop resonances with an upgraded ATLAS detector at a high-luminosity LHC*, Tech. Rep. ATL-PHYS-PUB-2013-003 (2013).

[182] K. Agashe, H. Davoudiasl, G. Perez, and A. Soni, Phys. Rev. **D76**, 036006 (2007), arXiv:hep-ph/0701186 [hep-ph] .

[183] G. Aad *et al.* (ATLAS), Phys. Rev. **D92**, 032004 (2015), arXiv:1504.05511 [hep-ex] .

[184] The CMS Collaboration, *Search for high-mass diphoton resonances in pp collisions at $\sqrt{s} = 8$ TeV with the CMS detector*, CMS-PAS-EXO-12-045 (2015).

[185] K. Agashe *et al.*, in *Warped Extra Dimensional Benchmarks for Snowmass 2013* (2013) arXiv:1309.7847 [hep-ph] .

[186] Wolfram Research, Inc., *Mathematica, Version 10.0, Champaign, Illinois*, (2014).

[187] J. Charles *et al.*, Phys. Rev. **D91**, 073007 (2015), arXiv:1501.05013 [hep-ph] .

[188] M. Carena, A. Delgado, E. Ponton, T. M. P. Tait, and C. E. M. Wagner, Phys. Rev. **D68**, 035010 (2003), arXiv:hep-ph/0305188 .

[189] M. Carena, A. Delgado, E. Ponton, T. M. P. Tait, and C. E. M. Wagner, Phys. Rev. **D71**, 015010 (2005), arXiv:hep-ph/0410344 .

[190] C. Csaki, J. Erlich, and J. Terning, Phys. Rev. **D66**, 064021 (2002), arXiv:hep-ph/0203034 .

[191] K. Agashe, A. Delgado, M. J. May, and R. Sundrum, JHEP **08**, 050 (2003), arXiv:hep-ph/0308036 .

[192] A. Delgado and A. Falkowski, JHEP **05**, 097 (2007), arXiv:hep-ph/0702234 .

[193] M. Baak, J. Cúth, J. Haller, A. Hoecker, R. Kogler, K. Mönig, M. Schott, and J. Stelzer (Gfitter Group), Eur. Phys. J. **C74**, 3046 (2014), arXiv:1407.3792 [hep-ph] .

[194] H. Davoudiasl, G. Perez, and A. Soni, Phys. Lett. **B665**, 67 (2008), arXiv:0802.0203 [hep-ph] .

[195] The ATLAS Collaboration, *Physics at a High-Luminosity LHC with ATLAS*, ATL-PHYS-PUB-2013-007 (2013), arXiv:1307.7292 [hep-ex] .

[196] R. Contino and A. Pomarol, JHEP **11**, 058 (2004), arXiv:hep-th/0406257 .

[197] M. Puchwein and Z. Kunszt, Annals Phys. **311**, 288 (2004), arXiv:hep-th/0309069 .

[198] C. Csaki, Y. Grossman, P. Tanedo, and Y. Tsai, Phys. Rev. **D83**, 073002 (2011), arXiv:1004.2037 [hep-ph] .

[199] R. Malm, M. Neubert, and C. Schmell, JHEP **04**, 042 (2016), arXiv:1509.02539 [hep-ph] .

[200] F. Goertz, *Warped Extra Dimensions: Flavor, Precision Tests and Higgs Physics*, Ph.D. thesis, Johannes Gutenberg-University Mainz, Institute for Physics (2011), arXiv:1112.6387 [hep-ph] .

[201] R. Malm, M. Neubert, and C. Schmell, JHEP **02**, 008 (2015), arXiv:1408.4456 [hep-ph] .

[202] A. Djouadi and G. Moreau, Phys. Lett. **B660**, 67 (2008), arXiv:0707.3800 [hep-ph] .

[203] A. Falkowski, Phys. Rev. **D77**, 055018 (2008), arXiv:0711.0828 [hep-ph] .

[204] A. Azatov and J. Galloway, Phys. Rev. **D85**, 055013 (2012), arXiv:1110.5646 [hep-ph] .

[205] G. Cacciapaglia, A. Deandrea, and J. Llodra-Perez, JHEP **06**, 054 (2009), arXiv:0901.0927 [hep-ph] .

[206] C. Bouchart and G. Moreau, Phys. Rev. **D80**, 095022 (2009), arXiv:0909.4812 [hep-ph] .

[207] M. Carena, S. Casagrande, F. Goertz, U. Haisch, and M. Neubert, JHEP **08**, 156 (2012), arXiv:1204.0008 [hep-ph] .

[208] G. Bhattacharyya and T. S. Ray, Phys. Lett. **B675**, 222 (2009), arXiv:0902.1893 [hep-ph] .

[209] A. Azatov, M. Toharia, and L. Zhu, Phys. Rev. **D82**, 056004 (2010), arXiv:1006.5939 [hep-ph] .

[210] A. Azatov, M. Toharia, and L. Zhu, Phys. Rev. **D80**, 035016 (2009), arXiv:0906.1990 [hep-ph] .

[211] C. Delaunay, J. F. Kamenik, G. Perez, and L. Randall, JHEP **01**, 027 (2013), arXiv:1207.0474 [hep-ph] .

[212] F. Goertz, U. Haisch, and M. Neubert, Phys. Lett. **B713**, 23 (2012), arXiv:1112.5099 [hep-ph] .

[213] M. Beneke and M. Neubert, Nucl. Phys. **B651**, 225 (2003), arXiv:hep-ph/0210085 .

[214] A. Djouadi, Phys. Rept. **459**, 1 (2008), arXiv:hep-ph/0503173 .

[215] M. Beneke, P. Dey, and J. Rohrwild, JHEP **08**, 010 (2013), arXiv:1209.5897 [hep-ph] .

[216] W. J. Marciano, C. Zhang, and S. Willenbrock, Phys. Rev. **D85**, 013002 (2012), arXiv:1109.5304 [hep-ph] .

[217] W.-Y. Keung and W. J. Marciano, Phys. Rev. **D30**, 248 (1984).

[218] J. R. Andersen *et al.* (LHC Higgs Cross Section Working Group), *Handbook of LHC Higgs Cross Sections: 3. Higgs Properties*, (2013), 10.5170/CERN-2013-004, arXiv:1307.1347 [hep-ph] .

[219] The ATLAS and CMS Collaborations, *Measurements of the Higgs boson production and decay rates and constraints on its couplings from a combined ATLAS and CMS analysis of the LHC pp collision data at $\sqrt{s}$ = 7 and 8 TeV*, ATLAS-CONF-2015-044 (2015).

[220] M. E. Peskin, *Comparison of LHC and ILC Capabilities for Higgs Boson Coupling Measurements*, (2012), arXiv:1207.2516 [hep-ph] .

[221] H. Baer, T. Barklow, K. Fujii, Y. Gao, A. Hoang, S. Kanemura, J. List, H. E. Logan, A. Nomerotski, M. Perelstein, *et al.*, (2013), arXiv:1306.6352 [hep-ph] .

[222] M. Klute, R. Lafaye, T. Plehn, M. Rauch, and D. Zerwas, Europhys. Lett. **101**, 51001 (2013), arXiv:1301.1322 [hep-ph] .

[223] D. M. Asner *et al.*, in *Community Summer Study 2013: Snowmass on the Mississippi (CSS2013) Minneapolis, MN, USA* (2013) arXiv:1310.0763 [hep-ph] .

[224] J. Tian and K. Fujii (ILD), *Proceedings, 2013 European Physical Society Conference on High Energy Physics (EPS-HEP 2013)*, PoS **EPS-HEP2013**, 316 (2013), arXiv:1311.6528 [hep-ph] .

[225] G. Aad *et al.* (ATLAS), Phys. Lett. **B726**, 120 (2013), arXiv:1307.1432 [hep-ex] .

[226] V. Khachatryan *et al.* (CMS), Phys. Rev. **D92**, 012004 (2015), arXiv:1411.3441 [hep-ex] .

[227] V. Khachatryan *et al.* (CMS), Eur. Phys. J. **C75**, 212 (2015), arXiv:1412.8662 [hep-ex] .

[228] V. Khachatryan *et al.* (CMS), Phys. Lett. **B736**, 64 (2014), arXiv:1405.3455 [hep-ex] .

[229] G. Aad *et al.* (ATLAS), Eur. Phys. J. **C75**, 335 (2015), arXiv:1503.01060 [hep-ex] .

[230] J. Brod, U. Haisch, and J. Zupan, JHEP **11**, 180 (2013), arXiv:1310.1385 [hep-ph] .

[231] J. Baron *et al.* (ACME), Science **343**, 269 (2014), arXiv:1310.7534 [physics.atom-ph] .

[232] F. Bishara, Y. Grossman, R. Harnik, D. J. Robinson, J. Shu, and J. Zupan, JHEP **04**, 084 (2014), arXiv:1312.2955 [hep-ph] .

[233] A. Denner, S. Heinemeyer, I. Puljak, D. Rebuzzi, and M. Spira, Eur. Phys. J. **C71**, 1753 (2011), arXiv:1107.5909 [hep-ph] .

[234] G. Aad *et al.* (ATLAS), JHEP **01**, 069 (2015), arXiv:1409.6212 [hep-ex] .

[235] G. Aad *et al.* (ATLAS), JHEP **04**, 117 (2015), arXiv:1501.04943 [hep-ex] .

[236] G. Aad *et al.* (ATLAS), JHEP **08**, 137 (2015), arXiv:1506.06641 [hep-ex] .

[237] G. Aad *et al.* (ATLAS), Phys. Rev. **D91**, 012006 (2015), arXiv:1408.5191 [hep-ex] .

[238] G. Aad *et al.* (ATLAS), Phys. Rev. **D90**, 112015 (2014), arXiv:1408.7084 [hep-ex] .

[239] V. Khachatryan *et al.* (CMS), Phys. Rev. **D92**, 032008 (2015), arXiv:1506.01010 [hep-ex] .

[240] S. Chatrchyan *et al.* (CMS), JHEP **05**, 104 (2014), arXiv:1401.5041 [hep-ex] .

[241] S. Chatrchyan *et al.* (CMS), JHEP **01**, 096 (2014), arXiv:1312.1129 [hep-ex] .

[242] S. Chatrchyan *et al.* (CMS), Phys. Rev. **D89**, 092007 (2014), arXiv:1312.5353 [hep-ex] .

[243] V. Khachatryan *et al.* (CMS), Eur. Phys. J. **C74**, 3076 (2014), arXiv:1407.0558 [hep-ex] .

[244] T. A. Collaboration (ATLAS), *Search for the $b\bar{b}$ decay of the Standard Model Higgs boson in associated W/ZH production with the ATLAS detector*, ATLAS-CONF-2013-079 (2013).

[245] K. Agashe, A. E. Blechman, and F. Petriello, Phys. Rev. **D74**, 053011 (2006), arXiv:hep-ph/0606021 .

[246] M. Blanke, B. Shakya, P. Tanedo, and Y. Tsai, JHEP **08**, 038 (2012), arXiv:1203.6650 [hep-ph] .

[247] C. Schmell, *Hunting for Warped Extra Dimensions via Loop-Induced Processes*, Ph.D. thesis, Johannes Gutenberg-University Mainz, Institute for Physics (2014).

[248] P. Biancofiore, P. Colangelo, and F. De Fazio, Phys. Rev. **D89**, 095018 (2014), arXiv:1403.2944 [hep-ph] .

[249] K. Agashe, A. Azatov, Y. Cui, L. Randall, and M. Son, JHEP **06**, 196 (2015), arXiv:1412.6468 [hep-ph] .

[250] M. Beneke, P. Moch, and J. Rohrwild, Nucl. Phys. **B** (2015), 10.1016/j.nuclphysb.2016.02.037, arXiv:1508.01705 [hep-ph] .

[251] P. Moch and J. Rohrwild, Nucl. Phys. **B902**, 142 (2016), arXiv:1509.04643 [hep-ph] .

[252] M. Beneke, P. Moch, and J. Rohrwild, *Proceedings, International Conference on Flavor Physics and Mass Generation*, Int. J. Mod. Phys. **A29**, 1444011 (2014), arXiv:1404.7157 [hep-ph] .

[253] P. Moch and J. Rohrwild, J. Phys. **G41**, 105005 (2014), arXiv:1405.5385 [hep-ph] .

[254] A. J. Buras, L. Merlo, and E. Stamou, JHEP **08**, 124 (2011), arXiv:1105.5146 [hep-ph] .

[255] C. Greub and P. Liniger, Phys. Rev. **D63**, 054025 (2001), arXiv:hep-ph/0009144 .

[256] Y. Amhis *et al.* (Heavy Flavor Averaging Group), *Averages of b-hadron, c-hadron, and τ-lepton properties as of summer 2014*, (2014), arXiv:1412.7515 [hep-ex] .

[257] M. Misiak *et al.*, Phys. Rev. Lett. **114**, 221801 (2015), arXiv:1503.01789 [hep-ph] .

[258] C. Niehoff, P. Stangl, and D. M. Straub, JHEP **01**, 119 (2016), arXiv:1508.00569 [hep-ph] .

[259] T. Aushev *et al.*, *Physics at Super B Factory*, (2010), arXiv:1002.5012 [hep-ex] .

[260] P. Ball and R. Zwicky, Phys. Lett. **B642**, 478 (2006), arXiv:hep-ph/0609037 .

[261] W. Altmannshofer, P. Paradisi, and D. M. Straub, JHEP **04**, 008 (2012), arXiv:1111.1257 [hep-ph] .

[262] Y. Amhis *et al.* (Heavy Flavor Averaging Group), *Averages of b-hadron, c-hadron, and τ-lepton properties as of early 2012*, (2012), arXiv:1207.1158 [hep-ex] .

[263] D. Atwood, T. Gershon, M. Hazumi, and A. Soni, Phys. Rev. **D71**, 076003 (2005), arXiv:hep-ph/0410036 [hep-ph] .

[264] B. Aubert *et al.* (BaBar), Phys. Rev. **D78**, 071102 (2008), arXiv:0807.3103 [hep-ex] .

[265] Y. Ushiroda *et al.* (Belle), *Proceedings of the 33rd International Conference on High Energy Physics (ICHEP '06)*, Phys. Rev. **D74**, 111104 (2006), arXiv:hep-ex/0608017 [hep-ex] .